

# FACTS

## Modelling and Simulation in Power Networks

Enrique Acha

Claudio R. Fuerte-Esquivel

Hugo Ambriz-Perez

Cesar Angeles-Camacho

 WILEY



POWEREN.IR

**FACTS**





# FACTS

## *Modelling and Simulation in Power Networks*

**Enrique Acha**

*University of Glasgow, UK*

**Claudio R. Fuerte-Esquivel**

*Universidad Michoacana, MEXICO*

**Hugo Ambriz-Pérez**

*Comisión Federal de Electricidad, MEXICO*

**César Angeles-Camacho**

*University of Glasgow, UK*



JOHN WILEY & SONS, LTD

Copyright © 2004 John Wiley & Sons Ltd, The Atrium, Southern Gate, Chichester,  
West Sussex PO19 8SQ, England

Telephone (+44) 1243 779777

Email (for orders and customer service enquiries): [cs-books@wiley.co.uk](mailto:cs-books@wiley.co.uk)  
Visit our Home Page on [www.wileyeurope.com](http://www.wileyeurope.com) or [www.wiley.com](http://www.wiley.com)

All Rights Reserved. No part of this publication may be reproduced, stored in a retrieval system or transmitted in any form or by any means, electronic, mechanical, photocopying, recording, scanning or otherwise, except under the terms of the Copyright, Designs and Patents Act 1988 or under the terms of a licence issued by the Copyright Licensing Agency Ltd, 90 Tottenham Court Road, London W1T 4LP, UK, without the permission in writing of the Publisher. Requests to the Publisher should be addressed to the Permissions Department, John Wiley & Sons Ltd, The Atrium, Southern Gate, Chichester, West Sussex PO19 8SQ, England, or emailed to [permreq@wiley.co.uk](mailto:permreq@wiley.co.uk), or faxed to (+44) 1243 770620.

This publication is designed to provide accurate and authoritative information in regard to the subject matter covered. It is sold on the understanding that the Publisher is not engaged in rendering professional services. If professional advice or other expert assistance is required, the services of a competent professional should be sought.

#### ***Other Wiley Editorial Offices***

John Wiley & Sons Inc., 111 River Street, Hoboken, NJ 07030, USA

Jossey-Bass, 989 Market Street, San Francisco, CA 94103-1741, USA

Wiley-VCH Verlag GmbH, Boschstr. 12, D-69469 Weinheim, Germany

John Wiley & Sons Australia Ltd, 33 Park Road, Milton, Queensland 4064, Australia

John Wiley & Sons (Asia) Pte Ltd, 2 Clementi Loop #02-01, Jin Xing Distripark, Singapore 129809

John Wiley & Sons Canada Ltd, 22 Worcester Road, Etobicoke, Ontario, Canada M9W 1L1

Wiley also publishes its books in a variety of electronic formats. Some content that appears in print may not be available in electronic books.

#### ***British Library Cataloguing in Publication Data***

A catalogue record for this book is available from the British Library

ISBN 0-470-85271-2

Typeset in 10/12 Times by Thomson Press (India) Ltd, New Delhi  
Printed and bound in Great Britain by Antony Rowe Ltd, Chippenham, Wiltshire  
This book is printed on acid-free paper responsibly manufactured from sustainable forestry in which at least two trees are planted for each one used for paper production.

To Our Beloved Families



# Contents

<b>Preface</b>	<b>xiii</b>
<b>1 Introduction</b>	<b>1</b>
1.1 Background	1
1.2 Flexible Alternating Current Transmission Systems	2
1.3 Inherent Limitations of Transmission Systems	3
1.4 FACTS Controllers	3
1.5 Steady-state Power System Analysis	6
References	6
<b>2 Modelling of FACTS Controllers</b>	<b>9</b>
2.1 Introduction	9
2.2 Modelling Philosophy	11
2.3 Controllers Based on Conventional Thyristors	11
2.3.1 The Thyristor-controlled Reactor	12
2.3.2 The Static VAR Compensator	16
2.3.3 The Thyristor-controlled Series Compensator	18
2.3.3.1 Thyristor-controlled Series Capacitor Equivalent Circuit	19
2.3.3.2 Steady-state Current and Voltage Equations	20
2.3.3.3 Thyristor-controlled Series Capacitor Fundamental Frequency Impedance	24
2.4 Power Electronic Controllers Based on Fully Controlled Semiconductor Devices	28
2.4.1 The Voltage Source Converter	29
2.4.1.1 Pulse-width Modulation Control	30
2.4.1.2 Principles of Voltage Source Converter Operation	33
2.4.2 The Static Compensator	34
2.4.3 The Solid State Series Compensator	35
2.4.4 The Unified Power Flow Controller	36
2.4.5 The High-voltage Direct-current Based on Voltage Source Converters	38
2.5 Control Capabilities of Controllers Based on Voltage Source Converters	40
2.6 Summary	41
References	41
<b>3 Modelling of Conventional Power Plant</b>	<b>43</b>
3.1 Introduction	43
3.2 Transmission Line Modelling	44
3.2.1 The Voltage-drop Equation	45
3.2.1.1 Calculation of Lumped RLC Parameters	45
3.2.1.2 Shunt Admittances	47
3.2.1.3 Internal Impedances	47
3.2.1.4 Ground Return Impedances	48
3.2.2 Ground Wires	50
3.2.3 Bundle Conductors	51

3.2.4	Double Circuit Transmission Lines	54
3.2.5	The Per-unit System	55
3.2.6	Transmission-line Program: Basic Parameters	56
3.2.7	Numerical Example of Transmission Line Parameter Calculation	59
3.2.8	Long Line Effects	60
3.2.9	Transmission Line Transpositions	62
3.2.10	Transmission Line Program: Distributed Parameters	63
3.2.11	Numerical Example of Long Line Parameter Calculation	66
3.2.12	Symmetrical Components and Sequence Domain Parameters	67
3.2.13	Transmission Line Program: Sequence Parameters	69
3.2.14	Numerical Example of Sequence Parameter Calculation	69
3.3	Power Transformer Modelling	70
3.3.1	Single-phase Transformers	70
3.3.2	Simple Tap-changing Transformer	72
3.3.3	Advanced Tap-changing Transformer	73
3.3.4	Three-phase Transformers	75
3.3.4.1	Star–Star Connection	76
3.3.4.2	Delta–Delta Connection	78
3.3.4.3	Star–Delta Connection	78
3.3.5	Sequence Domain Parameters	79
3.4	Rotating Machinery Modelling	82
3.4.1	Machine Voltage Equation	83
3.5	System Load	86
3.6	Summary	89
	References	90
<b>4</b>	<b>Conventional Power Flow</b>	<b>93</b>
4.1	Introduction	93
4.2	General Power Flow Concepts	93
4.2.1	Basic Formulation	94
4.2.2	Variables and Bus Classification	97
4.3	Power Flow Solution Methods	97
4.3.1	Early Power Flow Algorithms	97
4.3.2	The Newton–Raphson Algorithm	98
4.3.3	State Variable Initialisation	101
4.3.4	Generator Reactive Power Limits	101
4.3.5	Linearised Frame of Reference	102
4.3.6	Newton–Raphson Computer Program in Matlab <sup>®</sup> Code	104
4.3.7	The Fast Decoupled Algorithm	111
4.3.8	Fast Decoupled Computer Program in Matlab <sup>®</sup> Code	112
4.3.9	A Benchmark Numerical Example	115
4.4	Constrained Power Flow Solutions	119
4.4.1	Load Tap-changing Transformers	119
4.4.1.1	State Variable Initialisation and Limit Checking	121
4.4.1.2	Load Tap Changer Computer Program in Matlab <sup>®</sup> Code	122
4.4.1.3	Test Case of Voltage Magnitude Control with Load Tap-changing	127
4.4.1.4	Combined Voltage Magnitude Control by Means of Generators and Load Tap Changers	130
4.4.1.5	Control Coordination between One Load Tap Changer and One Generator	130
4.4.2	Phase-shifting Transformer	132
4.4.2.1	State Variable Initialisation and Limit Checking	134
4.4.2.2	Phase-shifter Computer Program in Matlab <sup>®</sup> Code	135
4.4.2.3	Test Cases for Phase-shifting Transformers	140

4.5	Further Concepts in Power Flows	144
4.5.1	Sparsity-oriented Solutions	144
4.5.2	Truncated Adjustments	145
4.5.2.1	Test Case of Truncated Adjustments Involving Three Load Tap-changing Transformers	145
4.5.3	Special Load Tap Changer Configurations	147
4.5.3.1	Test Case of Sensitivity Factors in Parallel Load Tap-changing Operation	148
4.6	Summary	149
	References	150
<b>5</b>	<b>Power Flow Including FACTS Controllers</b>	<b>153</b>
5.1	Introduction	153
5.2	Power Flow Solutions Including FACTS Controllers	154
5.3	Static VAR Compensator	155
5.3.1	Conventional Power Flow Models	155
5.3.2	Shunt Variable Susceptance Model	158
5.3.3	Static VAR Compensator Computer Program in Matlab <sup>®</sup> Code	159
5.3.4	Firing-angle Model	162
5.3.5	Static VAR Compensator Firing-angle Computer Program in Matlab <sup>®</sup> Code	162
5.3.6	Integrated Transformer Firing-angle Model	166
5.3.7	Nodal Voltage Magnitude Control using Static VAR Compensators	167
5.3.8	Control Coordination between Reactive Sources	168
5.3.9	Numerical Example of Voltage Magnitude Control using One Static VAR Compensator	168
5.4	Thyristor-controlled Series Compensator	171
5.4.1	Variable Series Impedance Power Flow Model	171
5.4.2	Thyristor-controlled Series Compensator Computer Program in Matlab <sup>®</sup> Code	173
5.4.3	Numerical Example of Active Power Flow Control using One Thyristor-controlled Series Compensator: Variable Series Compensator Model	178
5.4.4	Firing-angle Power Flow Model	180
5.4.5	Thyristor-controlled Series Compensator Firing-angle Computer Program in Matlab <sup>®</sup> Code	182
5.4.6	Numerical Example of Active Power Flow Control using One Thyristor-controlled Series Compensator: Firing-angle Model	187
5.4.7	Numerical Properties of the Thyristor-controlled Series Compensator Power Flow Model	189
5.5	Static Synchronous Compensator	191
5.5.1	Power Flow Model	191
5.5.2	Static Compensator Computer Program in Matlab <sup>®</sup> Code	192
5.5.3	Numerical Example of Voltage Magnitude Control using One Static Compensator	198
5.6	Unified Power Flow Controller	200
5.6.1	Power Flow Model	201
5.6.2	Unified Power Flow Controller Computer Program in Matlab <sup>®</sup> Code	203
5.6.3	Numerical Example of Power Flow Control using One Unified Power Flow Controller	213
5.7	High-voltage Direct-current-based Voltage Source Converter	216
5.7.1	Power Equations	217
5.7.2	High-voltage Direct-current-based Voltage Source Converter Computer Program in Matlab <sup>®</sup> Code	218
5.7.3	Numerical Example of Power Flow Control using One HVDC-VSC	225

5.7.3.1	HVDC-VSC Back-to-back Model	225
5.7.3.2	HVDC-VSC Full Model	225
5.8	Effective Initialisation of FACTS Controllers	227
5.8.1	Controllers Represented by Shunt Synchronous Voltage Sources	227
5.8.2	Controllers Represented by Shunt Admittances	227
5.8.3	Controllers Represented by Series Reactances	227
5.8.4	Controllers Represented by Series Synchronous Voltage Sources	228
5.9	Summary	228
	References	229
<b>6</b>	<b>Three-phase Power Flow</b>	<b>231</b>
6.1	Introduction	231
6.2	Power Flow in the Phase Frame of Reference	232
6.2.1	Power Flow Equations	233
6.2.2	Newton–Raphson Power Flow Algorithm	234
6.2.3	Matlab <sup>®</sup> Code of a Power Flow Program in the Phase Frame of Reference	236
6.2.4	Numerical Example of a Three-phase Network	244
6.3	Static VAR Compensator	249
6.3.1	Variable Susceptance Model	250
6.3.2	Firing-angle Model	251
6.3.3	Numerical Example: Static VAR Compensator Voltage Magnitude Balancing Capability	252
6.4	Thyristor-controlled Series Compensator	253
6.4.1	Variable Susceptance Model	253
6.4.2	Firing-angle Model	255
6.4.3	Numerical Example: Power Flow Control using One Thyristor-controlled Series Compensator	257
6.5	Static Compensator	257
6.5.1	Static Compensator Three-phase Numerical Example	260
6.6	Unified Power Flow Controller	261
6.6.1	Numerical Example of Power Flow Control using One Unified Power Flow Controller	264
6.7	Summary	264
	References	265
<b>7</b>	<b>Optimal Power Flow</b>	<b>267</b>
7.1	Introduction	267
7.2	Optimal Power Flow using Newton’s Method	268
7.2.1	General Formulation	268
7.2.1.1	Variables	268
7.2.1.2	Objective Function	269
7.2.1.3	Equality Constraints	269
7.2.1.4	Inequality Constraints	270
7.2.2	Application of Newton’s Method to Optimal Power Flow	270
7.2.3	Linearised System Equations	271
7.2.4	Optimality Conditions for Newton’s Method	272
7.2.5	Conventional Power Plant Modelling in Optimal Power Flow	272
7.2.5.1	Transmission Lines	273
7.2.5.2	Shunt Elements	274
7.2.5.3	Synchronous Generators	275
7.2.6	Handling of Inequality Constraints	275
7.2.6.1	Handling of Inequality Constraints on Variables	275
7.2.6.2	Handling of Inequality Constraints on Functions	277

7.3	Implementation of Optimal Power Flow using Newton's Method	278
7.3.1	Initial Conditions in Optimal Power Flow Solutions	279
7.3.2	Active Power Schedule	279
7.3.3	Lagrange Multipliers	280
7.3.4	Penalty Weighting Factors	280
7.3.5	Conjugated Variables	280
7.3.6	An Optimal Power Flow Numerical Example	281
7.4	Power System Controller Representation in Optimal Power Flow Studies	283
7.5	Load Tap-changing Transformer	283
7.5.1	Load Tap-changing Lagrangian Function	283
7.5.2	Linearised System of Equations	284
7.5.3	Load Tap-changing Transformer Test Cases	285
7.6	Phase-shifting Transformer	286
7.6.1	Lagrangian Function	286
7.6.2	Linearised System of Equations	287
7.6.3	Phase-shifting Transformer Test Cases	289
7.6.3.1	Case 1: No Active Power Flow Regulation	289
7.6.3.2	Case 2: Active Power Flow Regulation at LakePS	290
7.7	Static VAR Compensator	291
7.7.1	Lagrangian Function	291
7.7.2	Linearised System of Equations	292
7.7.3	Static VAR Compensator Test Cases	293
7.7.3.1	Firing-angle Model	293
7.7.3.2	Susceptance Model	295
7.8	Thyristor-controlled Series Compensator	296
7.8.1	Lagrangian Function	296
7.8.2	Linearised System of Equations	297
7.8.3	Thyristor-controlled Series Compensator Test Cases	299
7.9	Unified Power Flow Controller	301
7.9.1	Unified Power Flow Controller Lagrangian Function	301
7.9.2	Direct-current Link Lagrangian Function	301
7.9.3	Unified Power Flow Controller Power Flow Constraints	302
7.9.4	Linearised System of Equations	302
7.9.5	Unified Power Flow Controller Test Cases	305
7.9.6	Unified Power Flow Controller Operating Modes	307
7.10	Summary	307
	References	308

<b>8</b>	<b>Power Flow Tracing</b>	<b>311</b>
8.1	Introduction	311
8.2	Basic Assumptions	312
8.3	Mathematical Justification of the Proportional Sharing Principle	313
8.4	Dominions	315
8.4.1	Dominion Contributions to Active Power Flows	317
8.4.2	Dominion Contributions to Reactive Power Flows	319
8.4.3	Dominion Contributions to Loads and Sinks	320
8.5	Tracing Algorithm	321
8.6	Numerical Examples	322
8.6.1	Simple Radial Network	322
8.6.2	Simple Meshed Network: Active Power	324
8.6.3	Meshed Network with FACTS Controllers: Reactive Power	329
8.6.4	Large Network	331
8.6.5	Tracing the Power Output of a Wind Generator	331
8.6.5.1	The Wind Generator Model	335
8.6.5.2	Numerical Example	336

8.7 Summary	339
References	340
<b>Appendix A: Jacobian Elements for FACTS Controllers in Positive Sequence Power Flow</b>	<b>343</b>
A.1 Tap-changing Transformer	343
A.2 Thyristor-controlled Series Compensator	344
A.3 Static Synchronous Compensator	345
A.4 Unified Power Flow Controller	345
A.5 High-voltage Direct-current-based Voltage Source Converter	347
<b>Appendix B: Gradient and Hessian Elements for Optimal Power Flow Newton's Method</b>	<b>349</b>
B.1 First and Second Partial Derivatives for Transmission Lines	349
B.1.1 The Gradient Vector	349
B.1.2 The Matrix <b>W</b>	350
B.2 Phase Shifter Transformer	352
B.3 Static VAR Compensator	355
B.4 Thyristor-controlled Series Compensator	356
B.5 Unified Power Flow Controller	357
<b>Appendix C: Matlab<sup>®</sup> Computer Program for Optimal Power Flow Solutions using Newton's Method</b>	<b>365</b>
<b>Index</b>	<b>399</b>





[PowerEn.ir](http://PowerEn.ir)

# Preface

Flexible alternating-current transmission systems (FACTS) is a recent technological development in electrical power systems. It builds on the great many advances achieved in high-current, high-power semiconductor device technology, digital control and signals conditioning. From the power systems engineering perspective, the wealth of experience gained with the commissioning and operation of high-voltage direct-current (HVDC) links and static VAR compensator (SVC) systems, over many decades, in many parts of the globe, may have provided the driving force for searching deeper into the use of emerging power electronic equipment and techniques, as a means of alleviating long-standing operational problems in both high-voltage transmission and low-voltage distribution systems. A large number of researchers have contributed to the rapid advancement of the FACTS technology, but the names N.G. Hingorani and L. Gyugyi stand out prominently. Their work on FACTS, synthesised in their book, *Understanding FACT – Concepts and Technology of Flexible AC Transmission Systems* (Institute of Electronic and Electrical Engineers, New York, 2000), is a source of learning and inspiration.

Following universal acceptance of the FACTS technology and the commissioning of a vast array of controllers in both high-voltage transmission and low voltage distribution systems, research attention turned to the steady-state and dynamic interaction of FACTS controllers with the power network. The research community responded vigorously, lured by the novelty of the technology, turning out a very healthy volume of advanced models and high-quality simulations and case studies. Most matters concerning steady-state modelling and simulations of FACTS controllers are well agreed on, and the goal of our current book: *FACTS: Modelling and Simulation in Power Networks*, is to provide a coherent and systematic treatise of the most popular FACTS models, their interaction with the power network, and the main steady-state operational characteristics.

The overall aims and objectives of the FACTS philosophy are outlined in Chapter 1. The inherent limitations exhibited by high-voltage transmission systems, which are inflexible and overdesigned, are brought to attention as a means of explaining the background against which the FACTS technology developed and took hold. The most promising FACTS controllers and their range of steady-state applicability are described in this chapter.

Chapters 2 and 3 provide a thorough grounding on the mathematical representation of the most popular FACTS controllers and power plant components. The models are derived from first principles: by encapsulating the main steady-state operational characteristics and physical structure of the actual equipment, advanced power system models are developed in phase coordinates. As a by-product, more restrictive models are then derived, which are suitable for positive sequence power system analysis. Software written in Matlab<sup>®</sup> code is given for the most involved aspects of power plant modelling, such as transmission Line parameter calculation.

The power flow method is the most basic system analysis tool with which to assess the steady-state operation of a power system. It has been in existence for almost half a century, having reached quite a sophisticated level of development, in terms of both computational efficiency and modelling flexibility. The Newton–Raphson method is the *de facto* standard for solving the nonlinear power equations, which describe the power systems, owing to its reliability towards convergence. Chapter 4 covers the theory of positive sequence power flow in depth, and makes extensions to incorporate cases of adjusted solutions using two conventional power system controllers. This serves as a preamble to the material presented in Chapter 5, where a wide range of positive sequence power flow models of FACTS controllers are developed. Test cases and software written in Matlab<sup>®</sup> code is provided for each controller to enable the reader to gain ample experience with the various models provided. Furthermore, suitable coding of the Jacobian elements given in Appendix A enables more general FACTS power flow computer programs than those given in Chapter 5.

The concepts used in the study of positive sequence power flow in Chapters 4 and 5 are extended in Chapter 6 to address the more involved topic of three-phase power flow. The first part deals with the Newton–Raphson in-phase coordinates using simplified representations of conventional power plant components. Software written in Matlab<sup>®</sup> code is provided to enable the solution of small and medium-size three-phase power systems. Advanced models of conventional power plants are not included in the Matlab<sup>®</sup> function given in this chapter but their incorporation is a straightforward programming exercise. The second half of Chapter 6 addresses the modelling of three-phase controllers within the context of the power flow Newton–Raphson method, where the voltage and power flow balancing capabilities of shunt and series FACTS controllers, respectively, are discussed.

The topic of optimal power flow is covered in depth in Chapter 7. Building on the ground covered in Chapters 4 and 5, the theory of positive sequence power flow is blended with advanced optimisation techniques to incorporate economic and security aspects of power system operation. The optimisation method studied in this chapter is Newton’s method, which exhibits strong convergence and fits in well with the modelling philosophy developed throughout the book. Both conventional plant equipment and FACTS controller representations are accommodated with ease within the frame of reference provided by Newton’s method. To facilitate the extension of a conventional optimal power flow computer program to include FACTS representation, Appendix B gives the Hessian and gradient elements for all the FACTS controllers presented in Chapter 7. Software written in Matlab<sup>®</sup> code is provided in Appendix C to carry out non-FACTS optimal power flow solutions of small and medium-size power systems. The timely issue of power flow tracing is presented in Chapter 8. The method is based on the principle of proportional sharing and yields unambiguous information on the contribution of each generator to each transmission Line power flow and load in the system. Several application examples are presented in the chapter.

## **ACKNOWLEDGEMENTS**

The preparation of the book is a testimony to international collaboration, overcoming fixed work commitments, continental distances, and widely differing time zones to bring the project to fruition: we would like to thank our respective families for the time that we were kindly spared throughout the duration of the project. In this tenor, we would also like to acknowledge the unstinting support of our colleagues in the Power Engineering Group at the

University of Glasgow. The research work underpinning most of the new modelling concepts and methods presented in this book were carried out at the University of Glasgow by the authors over a period of more than 10 years. We would like to thank Mr Colin Tan Soon Guan and Dr Jesus Rico Melgoza for their early contribution to the research project. It is fair to say that the dream was only made possible by the generous support of the role model for all research councils in the world, the Consejo Nacional de Ciencia y Tecnología (CONACYT), México. The dream goes on . . . thanks CONACYT.

We are grateful to the staff of John Wiley & Sons, particularly Kathryn Sharples, Simone Taylor, and Susan Barclay for their patience and continuous encouragement throughout the preparation of the manuscript.



# 1

## Introduction

### 1.1 BACKGROUND

The electricity supply industry is undergoing a profound transformation worldwide. Market forces, scarcer natural resources, and an *everincreasing* demand for electricity are some of the drivers responsible for such an unprecedented change. Against this background of rapid evolution, the expansion programmes of many utilities are being thwarted by a variety of well-founded, environmental, land-use, and regulatory pressures that prevent the licensing and building of new transmission lines and electricity generating plants. An in-depth analysis of the options available for maximising existing transmission assets, with high levels of reliability and stability, has pointed in the direction of power electronics. There is general agreement that novel power electronics equipment and techniques are potential substitutes for conventional solutions, which are normally based on electromechanical technologies that have slow response times and high maintenance costs (Hingorani and Gyugyi, 2000; Song and Johns, 1999).

An electrical power system can be seen as the interconnection of generating sources and customer loads through a network of transmission lines, transformers, and ancillary equipment. Its structure has many variations that are the result of a legacy of economic, political, engineering, and environmental decisions. Based on their structure, power systems can be broadly classified into meshed and longitudinal systems. Meshed systems can be found in regions with a high population density and where it is possible to build power stations close to load demand centres. Longitudinal systems are found in regions where large amounts of power have to be transmitted over long distances from power stations to load demand centres.

Independent of the structure of a power system, the power flows throughout the network are largely distributed as a function of transmission line impedance; a transmission line with low impedance enables larger power flows through it than does a transmission line with high impedance. This is not always the most desirable outcome because quite often it gives rise to a myriad of operational problems; the job of the system operator is to intervene to try to achieve power flow redistribution, but with limited success. Examples of operating problems to which unregulated active and reactive power flows may give rise are: loss of system stability, power flow loops, high transmission losses, voltage limit violations, an inability to utilise transmission line capability up to the thermal limit, and cascade tripping.

In the long term, such problems have traditionally been solved by building new power plants and transmission lines, a solution that is costly to implement and that involves long construction times and opposition from pressure groups. It is envisaged that a new solution to such operational problems will rely on the upgrading of existing transmission corridors by using the latest power electronic equipment and methods, a new technological thinking that comes under the generic title of FACTS – an acronym for flexible alternating current transmission systems.

## **1.2 FLEXIBLE ALTERNATING CURRENT TRANSMISSION SYSTEMS**

In its most general expression, the FACTS concept is based on the substantial incorporation of power electronic devices and methods into the high-voltage side of the network, to make it electronically controllable (IEEE/CIGRÉ, 1995).

Many of the ideas upon which the foundation of FACTS rests evolved over a period of many decades. Nevertheless, FACTS, an integrated philosophy, is a novel concept that was brought to fruition during the 1980s at the Electric Power Research Institute (EPRI), the utility arm of North American utilities (Hingorani and Gyugyi, 2000). FACTS looks at ways of capitalising on the many breakthroughs taking place in the area of high-voltage and high-current power electronics, aiming at increasing the control of power flows in the high-voltage side of the network during both steady-state and transient conditions. The new reality of making the power network electronically controllable has started to alter the way power plant equipment is designed and built as well as the thinking and procedures that go into the planning and operation of transmission and distribution networks. These developments may also affect the way energy transactions are conducted, as high-speed control of the path of the energy flow is now feasible. Owing to the many economical and technical benefits it promised, FACTS received the uninstinctive support of electrical equipment manufacturers, utilities, and research organisations around the world (Song and Johns, 1999).

Several kinds of FACTS controllers have been commissioned in various parts of the world. The most popular are: load tap changers, phase-angle regulators, static VAR compensators, thyristor-controlled series compensators, interphase power controllers, static compensators, and unified power flow controllers (IEEE/CIGRÉ, 1995).

It was recognised quite early on the development programme of the FACTS technology that, in order to determine the effectiveness of such controllers; on a networkwide basis, it would be necessary to upgrade most of the system analysis tools with which power engineers plan and operate their systems. Some of the tools that have received research attention and, to a greater or lesser extent, have reached a high degree of modelling sophistication are:

- positive sequence power flow;
- three-phase power flow;
- optimal power flow;
- state estimation;
- transient stability;
- dynamic stability;
- electromagnetic transients;
- power quality.

This book covers in breadth and depth the modelling and simulation methods required for a thorough study of the steady-state operation of electrical power systems with FACTS controllers. The first three application areas, which are clearly defined within the realm of steady-state operation, are addressed in the book. The area of FACTS state estimation is still under research and no definitive models or simulation methods have emerged, as yet. A great deal of research progress has been made on the modelling and simulation of FACTS controllers for transient and dynamic stability, electromagnetic transients, and power quality, but the simulation tools required to conduct studies in such application areas are not really suited to conduct steady-state power systems analysis, and they are not covered in this book.

### **1.3 INHERENT LIMITATIONS OF TRANSMISSION SYSTEMS**

The characteristics of a given power system evolve with time, as load grows and generation is added. If the transmission facilities are not upgraded sufficiently the power system becomes vulnerable to steady-state and transient stability problems, as stability margins become narrower (Hingorani and Gyugyi, 2000).

The ability of the transmission system to transmit power becomes impaired by one or more of the following steady-state and dynamic limitations (Song and Johns, 1999):

- angular stability;
- voltage magnitude;
- thermal limits;
- transient stability;
- dynamic stability.

These limits define the maximum electrical power to be transmitted without causing damage to transmission lines and electric equipment. In principle, limitations on power transfer can always be relieved by the addition of new transmission and generation facilities. Alternatively, FACTS controllers can enable the same objectives to be met with no major alterations to system layout. The potential benefits brought about by FACTS controllers include reduction of operation and transmission investment cost, increased system security and reliability, increased power transfer capabilities, and an overall enhancement of the quality of the electric energy delivered to customers (IEEE/CIGRÉ, 1995).

### **1.4 FACTS CONTROLLERS**

Power flow control has traditionally relied on generator control, voltage regulation by means of tap-changing and phase-shifting transformers, and reactive power plant compensation switching. Phase-shifting transformers have been used for the purpose of regulating active power in alternating current (AC) transmission networks. In practice, some of them are permanently operated with fixed angles, but in most cases their variable tapping facilities are actually made use of.

Series reactors are used to reduce power flow and short-circuit levels at designated locations of the network. Conversely, series capacitors are used to shorten the electrical length of lines, hence increasing the power flow. In general, series compensation is switched on and off according to load and voltage conditions. For instance, in longitudinal power

systems, series capacitive compensation is bypassed during minimum loading in order to avoid transmission line overvoltages due to excessive capacitive effects in the system. Conversely, series capacitive compensation is fully utilised during maximum loading, aiming at increasing the transfer of power without subjecting transmission lines to overloads.

Until recently, these solutions served well the needs of the electricity supply industry. However, deregulation of the industry and difficulties in securing new ‘rights of way’ have created the momentum for adopting new, radical technological developments based on high-voltage, high-current solid-state controllers (Hingorani and Gyugyi, 2000). A few years ago, in partnership with manufacturers and research organisations, the supply industry embarked on an ambitious programme to develop a new generation of power electronic-based plant components (Song and Johns, 1999). The impact of such developments has already made inroads in all three areas of the business, namely, generation, transmission, and distribution.

Early developments of the FACTS technology were in power electronic versions of the phase-shifting and tap-changing transformers. These controllers together with the electronic series compensator can be considered to belong to the first generation of FACTS equipment. The unified power flow controller, the static compensator, and the interphase power controller are more recent developments. Their control capabilities and intended function are more sophisticated than those of the first wave of FACTS controllers. They may be considered to belong to a second generation of FACTS equipment. Shunt-connected thyristor-switched capacitors and thyristor-controlled reactors, as well as high-voltage direct-current (DC) power converters, have been in existence for many years, although their operational characteristics resemble those of FACTS controllers.

A number of FACTS controllers have been commissioned. Most of them perform a useful role during both steady-state and transient operation, but some are specifically designed to operate only under transient conditions, for instance, Hingorani’s subsynchronous resonance (SSR) damper.

FACTS controllers intended for steady-state operation are as follows (IEEE/CIGRÉ, 1995):

- Thyristor-controlled phase shifter (PS): this controller is an electronic phase-shifting transformer adjusted by thyristor switches to provide a rapidly varying phase angle.
- Load tap changer (LTC): this may be considered to be a FACTS controller if the tap changes are controlled by thyristor switches.
- Thyristor-controlled reactor (TCR): this is a shunt-connected, thyristor-controlled reactor, the effective reactance of which is varied in a continuous manner by partial conduction control of the thyristor valve.
- Thyristor-controlled series capacitor (TCSC): this controller consists of a series capacitor paralleled by a thyristor-controlled reactor in order to provide smooth variable series compensation.
- Interphase power controller (IPC): this is a series-connected controller comprising two parallel branches, one inductive and one capacitive, subjected to separate phase-shifted voltage magnitudes. Active power control is set by independent or coordinated adjustment of the two phase-shifting sources and the two variable reactances. Reactive power control is independent of active power.
- Static compensator (STATCOM): this is a solid-state synchronous condenser connected in shunt with the AC system. The output current is adjusted to control either the nodal voltage magnitude or the reactive power injected at the bus.

- Solid-state series controller (SSSC): this controller is similar to the STATCOM but it is connected in series with the AC system. The output current is adjusted to control either the nodal voltage magnitude or the reactive power injected at one of the terminals of the series-connected transformer.
- Unified power flow controller (UPFC): this consists of a static synchronous series compensator (SSSC) and a STATCOM, connected in such a way that they share a common DC capacitor. The UPFC, by means of an angularly unconstrained, series voltage injection, is able to control, concurrently or selectively, the transmission line impedance, the nodal voltage magnitude, and the active and reactive power flow through it. It may also provide independently controllable shunt reactive compensation.

Power electronic and control technology have been applied to electric power systems for several decades. HVDC links and static VAR compensators are mature pieces of technology:

- Static VAR compensator (SVC): this is a shunt-connected static source or sink of reactive power.
- High-voltage direct-current (HVDC) link: this is a controller comprising a rectifier station and an inverter station, joined either back-to-back or through a DC cable. The converters can use either conventional thyristors or the new generation of semiconductor devices such as gate turn-off thyristors (GTOs) or insulated gate bipolar transistors (IGBTs).

The application of FACTS controllers to the solution of steady-state operating problems is outlined in Table 1.1.

**Table 1.1** The role of FACTS (flexible alternating current transmission systems) controllers in power system operation

Operating problem	Corrective action	FACTS controller
Voltage limits:		
Low voltage at heavy load	Supply reactive power	STATCOM, SVC,
High voltage at low load	Absorb reactive power	STATCOM, SVC, TCR
High voltage following an outage	Absorb reactive power; prevent overload	STATCOM, SVC, TCR
Low voltage following an outage	Supply reactive power; prevent overload	STATCOM, SVC
Thermal limits:		
Transmission circuit overload	Reduce overload	TCSC, SSSC, UPFC, IPC, PS
Tripping of parallel circuits	Limit circuit loading	TCSC, SSSC, UPFC, IPC, PS
Loop flows:		
Parallel line load sharing	Adjust series reactance	IPC, SSSC, UPFC, TCSC, PS
Postfault power flow sharing	Rearrange network or use thermal limit actions	IPC, TCSC, SSSC, UPFC, PS
Power flow direction reversal	Adjust phase angle	IPC, SSSC, UPFC, PS

## 1.5 STEADY-STATE POWER SYSTEM ANALYSIS

In order to assist power system engineers to assess the impact of FACTS equipment on transmission system performance, it has become necessary to write new power system software or to upgrade existing software (Ambriz-Pérez, 1998; Fuerte-Esquivel, 1997). This has called for the development of a new generation of mathematical models for transmission systems and FACTS controllers, which had to be blended together, coded, and extensively verified. This has been an area of intense research activity, which has given rise to a copious volume of publications. Many aspects of FACTS modelling and simulation have reached maturity, and we believe that the time is ripe for such an important and large volume of information to be put together in a coherent and systematic fashion. This book aims to achieve such a role in the area of steady-state operation of FACTS-upgraded power systems.

From the operational point of view, FACTS technology is concerned with the ability to control, in an adaptive fashion, the path of the power flows throughout the network, where before the advent of FACTS, high-speed control was very restricted. The ability to control the line impedance and the nodal voltage magnitudes and phase angles at both the sending and the receiving ends of key transmission lines, with almost no delay, has significantly increased the transmission capabilities of the network while considerably enhancing the security of the system. In this context, power flow computer programs with FACTS controller modelling capability have been very useful tools for system planners and system operators to evaluate the technical and economical benefits of a wide range of alternative solutions offered by the FACTS technology.

Arguably, power flow analysis – also termed load flow analysis in the parlance of power systems engineers – is the most popular analysis tool used by planning and operation engineers today for the purpose of steady-state power system assessment. The reliable solution of real-life transmission and distribution networks is not a trivial matter, and Newton–Raphson-type methods, with their strong convergence characteristics, have proved most successful (Fuerte-Esquivel, 1997). Extensive research has been carried out over the past 10 years in order to implement FACTS models into Newton–Raphson-type power flow programs. This book offers a thorough grounding on the theory and practice of positive sequence power flow and three-phase power flow. In many practical situations, it is desirable to include economical and operational considerations into the power flow formulation, so that optimal solutions, within constrained solution spaces, can be obtained. This is the object of optimal power flow algorithms (Ambriz-Pérez, 1998), a topic also covered in the book.

## REFERENCES

- Ambriz-Pérez, H., 1998, *Flexible AC Transmission Systems Modelling in Optimal Power Flows Using Newton's Method*, PhD thesis, Department of Electronics and Electrical Engineering, University of Glasgow, Glasgow.
- Fuerte-Esquivel, C.R., 1997, *Steady State Modelling and Analysis of Flexible AC Transmission Systems*, PhD thesis, Department of Electronics and Electrical Engineering, University of Glasgow, Glasgow.

- Hingorani, N.G., Gyugyi, L., 2000, *Understanding FACTS: Concepts and Technology of Flexible AC Transmission Systems*, Institute of Electrical and Electronic Engineers, New York.
- IEEE/CIGRÉ (Institute of Electrical and Electronic Engineers/Conseil International des Grands Réseaux Electriques), 1995, *FACTS Overview*, special issue, 95TP108, IEEE Service Centre, Piscata-way, NJ.
- Song, Y.H., Johns, A.T., 1999, *Flexible AC Transmission Systems (FACTS)*, Institution of Electrical Engineers, London.



# 2

## Modelling of FACTS Controllers

### 2.1 INTRODUCTION

Two kinds of emerging power electronics applications in power systems are already well defined: (1) bulk active and reactive power control and (2) power quality improvement (Hingorani and Gyugyi, 2000). The first application area is known as FACTS, where the latest power electronic devices and methods are used to control the high-voltage side of the network electronically (Hingorani, 1993). The second application area is custom power, which focuses on low-voltage distribution and is a technology created in response to reports of poor power quality and reliability of supply affecting factories, offices, and homes. It is expected that when widespread deployment of the technology takes place, the end-user will see tighter voltage regulation, minimum power interruptions, low harmonic voltages, and acceptance of rapidly fluctuating and other nonlinear loads in the vicinity (Hingorani, 1995).

The one-line diagram shown in Figure 2.1 illustrates the connection of power plants in an interconnected transmission system, where the boundary between the high-voltage transmission and the low-voltage distribution is emphasised. The former benefits from the installation of FACTS equipment whereas the latter benefits from the installation of custom power equipment.

To a greater or lesser extent, high-voltage transmission systems are highly meshed. For many decades the trend has been towards interconnection, linking generators and loads into large integrated systems. The motivation has been to take advantage of load diversity, enabling a better utilisation of primary energy resources.

From the outset, interconnection was aided by breakthroughs in high-current, high-power semiconductor valve technology (Arrillaga, 1998). Thyristor-based high-voltage direct-current (HVDC) converter installations provided a means for interconnecting power systems with different operating frequencies – e.g. 50/60 Hz, for interconnecting power systems separated by the sea and for interconnecting weak and strong power systems (Hingorani, 1996). The most recent development in HVDC technology is the HVDC system based on solid-state voltage source converters, which enables independent, fast control of active and reactive powers (McMurray, 1987).

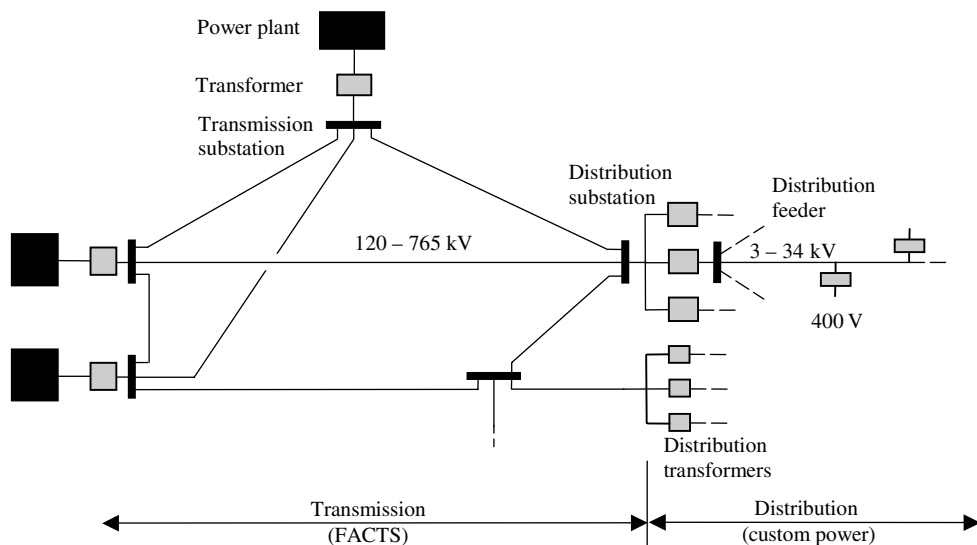


**Figure 2.1** A simplified one-line diagram of a power system. Redrawn, with permission, from N.G. Hingorani, 'Introducing Custom Power', *IEEE Spectrum* 32(6) 41–48, © 1995 IEEE

Power electronics is a ubiquitous technology that has affected every aspect of electrical power networks, not just HVDC transmission but also alternating current (AC) transmission, distribution, and utilisation. Deregulated markets are imposing further demands on generating plants, increasing their wear and tear and the likelihood of generator instabilities of various kinds. To help to alleviate such problems, power electronic controllers have recently been developed to enable generators to operate more reliably in the new marketplace. The thyristor-controlled series compensator (TCSC) is used to mitigate subsynchronous resonances (SSRs) and to damp power system oscillations (Larsen *et al.*, 1992). However, it may be argued that the primary function of the TCSC, like that of its mechanically controlled counterpart, the series capacitor bank, is to reduce the electrical length of the compensated transmission line. Hence, the aim is still to increase power transfers significantly, but with increased transient stability margins. With reference to the schematic network of Figure 2.1, the TCSC is deployed on the FACTS side.

For most practical purposes the thyristor-based static VAR compensator (SVC) has made the rotating synchronous compensator redundant, except where an increase in the short-circuit level is required along with fast-acting reactive power support (Miller, 1982). However, as power electronic technology continues to develop further, the replacement of the SVC by a new breed of static compensators based on the use of voltage source converters (VSCs) is looming. They are known as STATCOMs (static compensators) and provide all the functions that the SVC can provide but at a higher speed (IEEE/CIGRÉ, 1995); it is more compact and requires only a fraction of the land required by an SVC installation. The STATCOM is essentially a VSC interfaced to the AC system through a shunt-connected transformer. The VSC is the basic building block of the new generation of

power electronic controllers that have emerged from the FACTS and custom power initiatives (Hingorani and Gyugyi, 2000). In high-voltage transmission, the most popular FACTS equipment are: the STATCOM, the unified power flow controller (UPFC) and the HVDC-VSC. At the low-voltage distribution level, the SVC provides the core of the following custom power equipment: the distribution STATCOM, the dynamic voltage restorer, and active filters.

## **2.2 MODELLING PHILOSOPHY**

The remit of this book is the study of models and procedures with which to assess the steady-state operation of electrical power systems at the fundamental frequency. The power system application tool is termed ‘power flows’, and the most popular variants of the tool are presented in this book; namely, positive sequence power flow (Stagg and El-Abiad, 1968), optimal power flow (Wood and Wollenberg, 1984), and three-phase power flow (Arrillaga and Arnold, 1990). The first two applications deal with cases of balanced operation, for nonoptimal and optimal solutions, respectively. The third application deals with unbalanced operation induced by imbalances present either in plant components or in system load. In this book, all three applications incorporate representation of conventional power plant components and FACTS controllers.

The modelling of FACTS controllers in both the phase domain and the sequence domain is addressed in this chapter, and Chapter 3 deals with the representation of conventional power plant components in both domains. All models are developed from first principles, with strong reference to the physical structure of the equipment. Such an approach is amenable to flexible models useful for assessing the operation of plant components in network-wide applications, taking due care of equipment design imbalances, which are naturally present in all power plant equipment. However, if such imbalances are small and can be neglected in the study, then simpler models of plant components become readily available, in the form of sequence domain models.

It should be kept in mind that, in this book, the interest is in steady-state analysis at the fundamental frequency, and the models developed reflect this fact. They are not suitable for assessing the periodic steady-state operation of power systems (Acha and Madrigal, 2001) or their dynamic or transient operation (Kundur, 1994).

## **2.3 CONTROLLERS BASED ON CONVENTIONAL THYRISTORS**

Power electronic circuits using conventional thyristors have been widely used in power transmission applications since the early 1970s (Arrillaga, 1998). The first applications took place in the area of HVDC transmission, but shunt reactive power compensation using fast controllable inductors and capacitors soon gained general acceptance (Miller, 1982). More recently, fast-acting series compensators using thyristors have been used to vary the electrical length of key transmission lines, with almost no delay, instead of the classical series capacitor, which is mechanically controlled. In distribution system applications, solid-state transfer switches using thyristors are being used to enhance the reliability of supply to critical customer loads (Anaya-Lara and Acha, 2002).

In this section, the following three thyristor-based controllers receive attention: the thyristor-controlled reactor (TCR), the SVC and the TCSC. The operational characteristic of each one of these controllers is studied with particular reference to steady-state operation.

### 2.3.1 The Thyristor-controlled Reactor

The main components of the basic TCR are shown in Figure 2.2(a). The controllable element is the antiparallel thyristor pair, Th1 and Th2, which conducts on alternate half-cycles of the supply frequency. The other key component is the linear (air-core) reactor of inductance  $L$  (Miller, 1982). The thyristor circuit symbol is shown in Figure 2.2(b).

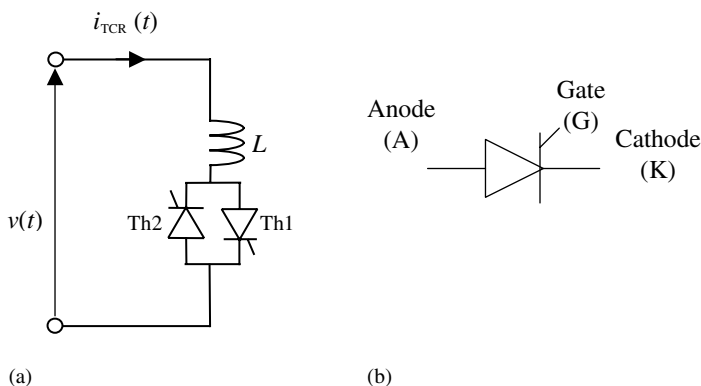


**Figure 2.2** Thyristor-based circuit: (a) Basic thyristor-controlled reactor (TCR); (b) thyristor circuit symbol.

The overall action of the thyristor controller on the linear reactor is to enable the reactor to act as a controllable susceptance, in the inductive sense, which is a function of the firing angle  $\alpha$ . However, this action is not trouble free, since the TCR achieves its fundamental frequency steady-state operating point at the expense of generating harmonic distortion, except for the condition of full conduction.

First, consider the condition when no harmonic distortion is generated by the TCR, which takes place when the thyristors are gated into conduction, precisely at the peaks of the supply voltage. The reactor conducts fully, and one could think of the thyristor controller as being short-circuited. The reactor contains little resistance and the current is essentially sinusoidal and inductive, lagging the voltage by almost  $90^\circ (\pi/2)$ . This is illustrated in Figure 2.3(a), where a fundamental frequency period of the voltage and current are shown.

It should be mentioned that this condition corresponds to a firing angle  $\alpha$  of  $\pi/2$ , which is the current zero-crossing measured with reference to the voltage zero-crossing. The relationship between the firing angle  $\alpha$  and the conduction angle  $\sigma$  is given by

$$\sigma = 2(\pi - \alpha). \quad (2.1)$$

Partial conduction is achieved with firing angles in the range:  $\pi/2 < \alpha < \pi$ , in radians. This is illustrated in Figures 2.3(b)–2.3(d), where TCR currents, as a function of the firing angle,

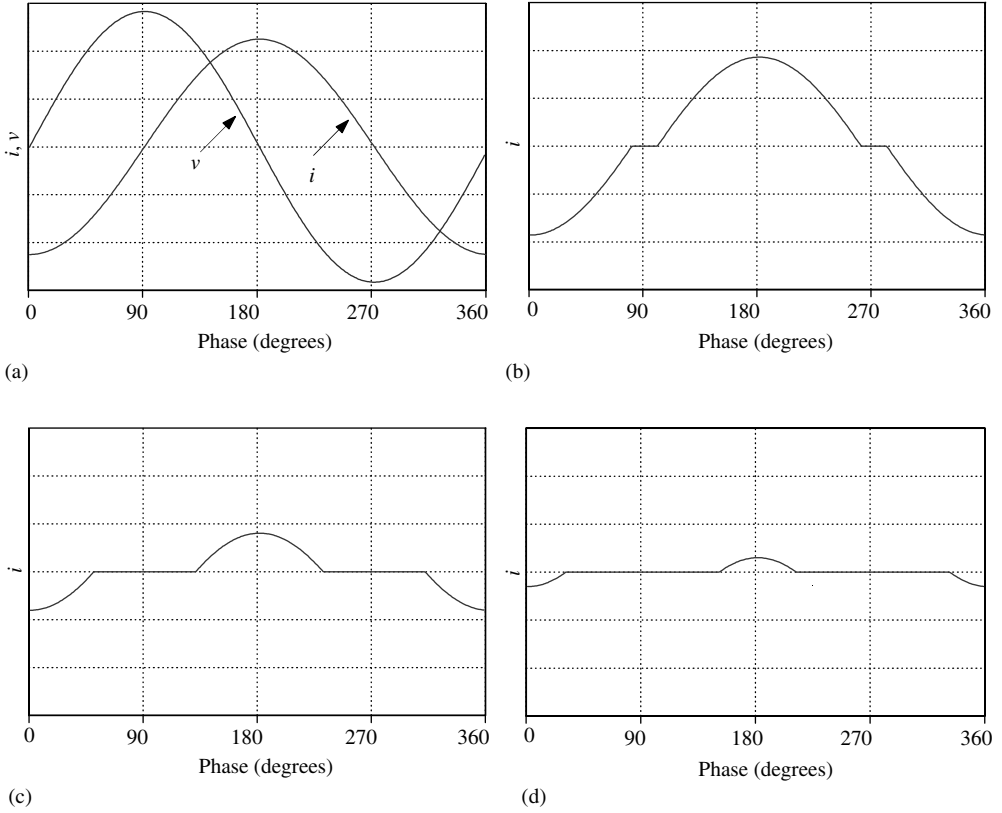


**Figure 2.3** Current waveforms in the basic thyristor-controlled reactor: (a)  $\alpha = 90^\circ$ ,  $\sigma = 180^\circ$ ; (b)  $\alpha = 100^\circ$ ,  $\sigma = 160^\circ$ ; (c)  $\alpha = 130^\circ$ ,  $\sigma = 100^\circ$ ; (d)  $\alpha = 150^\circ$ ,  $\sigma = 60^\circ$ ; for convenience, angles are given in degrees. Note:  $i$ , current;  $v$ , voltage;  $\alpha$ , firing angle;  $\sigma$ , conduction angle. Reproduced by permission of John Wiley & Sons Inc. from T.J.E Miller, 1982, *Reactive Power Control in Electric Systems*

are shown. Increasing the value of firing angle above  $\pi/2$  causes the TCR current waveform to become nonsinusoidal, with its fundamental frequency component reducing in magnitude. This, in turn, is equivalent to an increase in the inductance of the reactor, reducing its ability to draw reactive power from the network at the point of connection.

For the voltage condition shown in Figure 2.2(a), with  $v(t) = \sqrt{2} V \sin \omega t$ , the TCR instantaneous current  $i_{\text{TCR}}(t)$  is given by

$$i_{\text{TCR}}(t) = \frac{1}{L} \int_{\alpha}^{\omega t} \sqrt{2} V \sin \omega t \, dt = \frac{\sqrt{2} V}{\omega L} (\cos \alpha - \cos \omega t) \tag{2.2}$$

in the interval  $\alpha \leq \omega t \leq (\alpha + \sigma)$ , and is zero otherwise.  $V$  is the root mean square (rms) voltage, and  $\omega = 2\pi f$ , where  $f$  is the operating frequency.

Using Fourier analysis, an expression for the fundamental frequency current,  $I_{\text{TCRf1}}$ , is found:

$$I_{\text{TCRf1}} = \frac{V}{j\omega L \pi} [2(\pi - \alpha) + \sin 2\alpha]. \tag{2.3}$$

If the firing angles of Th1 and Th2 are balanced, no even harmonics are generated, and the rms value of the  $h$ th odd harmonic current is given by

$$I_{TCR\ h} = \frac{4V}{j\omega L\pi} \left[ \frac{\sin(h+1)\alpha}{2(h+1)} + \frac{\sin(h-1)\alpha}{2(h-1)} - \cos\alpha \frac{\sin h\alpha}{h} \right], \quad (2.4)$$

where  $h = 3, 5, 7, 9, 11, 13, \dots$

Power system TCR installations are three-phase and use filters and other harmonic cancellation arrangements to prevent the harmonic currents from reaching the high-voltage side of the network. Also, the TCR inductors will have a small resistive component. By way of example, Figure 2.4 shows a three-phase, delta-connected TCR. This topology uses six groups of thyristor and is commonly known as a six-pulse TCR.

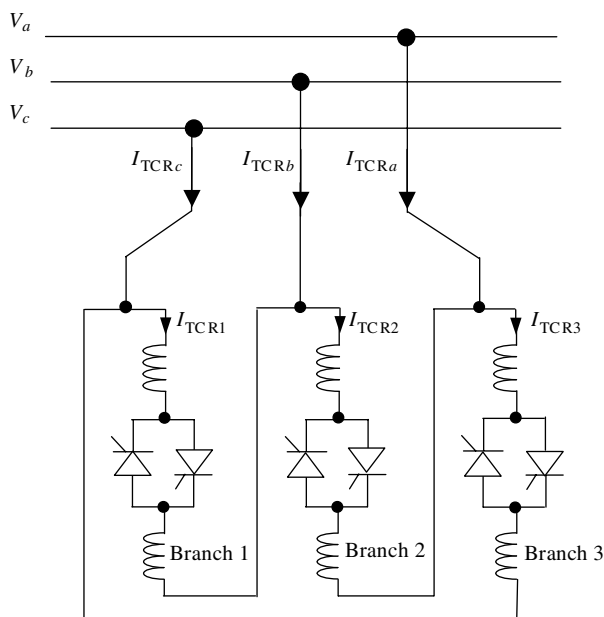


Figure 2.4 Three-phase thyristor-controlled reactor

In this arrangement, and under balanced operating conditions, the triplet harmonic currents generated by the three TCR branches do not reach the external network, only harmonic orders  $h = 5, 7, 11, 13, \dots$ . Moreover, if the TCR is split into two units of equal rating and connected to the low-voltage side of a transformer having two secondary windings, one connected in star and the other in delta, then cancellation of harmonic orders  $h = 5$ , and  $h = 7$  is achieved. The alternative arrangement is termed a twelve-pulse TCR. The lowest harmonic orders reaching the primary winding of the transformer are  $h = 11, 13, \dots$ , which are normally removed by using tuned filters (Miller, 1982).

We would assume in the ensuing analysis that suitable harmonic cancellation measures are in place, as we are concerned only with fundamental frequency operation and parameters. However, neither balanced operation nor balanced TCR designs will be

assumed a priori. It is not difficult to see from Equation (2.3) that a part of it may be interpreted as the equivalent susceptances of the basic TCR shown in Figure 2.2, which is a function of the controllable parameters  $\alpha$ . Accordingly, Equation (2.3) may be expressed by

$$I_{\text{TCR}} = -jB_{\text{TCR}}V, \quad (2.5)$$

where

$$B_{\text{TCR}} = \frac{2(\pi - \alpha) + \sin 2\alpha}{\omega L\pi}, \quad (2.6)$$

and the subscript f1, which indicates fundamental frequency current, has been dropped for convenience.

The three-phase nodal admittance representation of a TCR may be obtained by resorting to linear transformations. For instance, using the result in Equation (2.5), the case of the six-pulse TCR shown in Figure 2.4 will have the following primitive parameters:

$$\begin{bmatrix} I_{\text{TCR}1} \\ I_{\text{TCR}2} \\ I_{\text{TCR}3} \end{bmatrix} = \begin{bmatrix} -jB_{\text{TCR}1} & 0 & 0 \\ 0 & -jB_{\text{TCR}2} & 0 \\ 0 & 0 & -jB_{\text{TCR}3} \end{bmatrix} \begin{bmatrix} V_1 \\ V_2 \\ V_3 \end{bmatrix}, \quad (2.7)$$

and connectivity matrices for phases  $a, b, c$ :

$$\begin{bmatrix} V_1 \\ V_2 \\ V_3 \end{bmatrix} = \frac{(\pi/6)}{\sqrt{3}} \begin{bmatrix} 1 & -1 & 0 \\ 0 & 1 & -1 \\ -1 & 0 & 1 \end{bmatrix} \begin{bmatrix} V_a \\ V_b \\ V_c \end{bmatrix}, \quad (2.8)$$

$$\begin{bmatrix} I_{\text{TCR}a} \\ I_{\text{TCR}b} \\ I_{\text{TCR}c} \end{bmatrix} = \frac{(-\pi/6)}{\sqrt{3}} \begin{bmatrix} 1 & 0 & -1 \\ -1 & 1 & 0 \\ 0 & -1 & 1 \end{bmatrix} \begin{bmatrix} I_{\text{TCR}1} \\ I_{\text{TCR}2} \\ I_{\text{TCR}3} \end{bmatrix}. \quad (2.9)$$

Substituting Equation (2.8) into Equation (2.7), and the intermediate result into Equation (2.9), we obtain the following phase domain equivalent circuit for the six-pulse TCR:

$$\begin{bmatrix} I_{\text{TCR}a} \\ I_{\text{TCR}b} \\ I_{\text{TCR}c} \end{bmatrix} = \frac{1}{3} \begin{bmatrix} -j(B_{\text{TCR}1} + B_{\text{TCR}3}) & jB_{\text{TCR}1} & jB_{\text{TCR}3} \\ jB_{\text{TCR}1} & -j(B_{\text{TCR}1} + B_{\text{TCR}2}) & jB_{\text{TCR}2} \\ jB_{\text{TCR}3} & jB_{\text{TCR}2} & -j(B_{\text{TCR}2} + B_{\text{TCR}3}) \end{bmatrix} \begin{bmatrix} V_a \\ V_b \\ V_c \end{bmatrix}. \quad (2.10)$$

As a special condition, if all three branches in the TCR have equal equivalent susceptances ( $B_{\text{TCR}1} = B_{\text{TCR}2} = B_{\text{TCR}3} = B_{\text{TCR}}$ ), something that is possible to achieve by careful design, Equation (2.10) simplifies to

$$\begin{bmatrix} I_{\text{TCR}a} \\ I_{\text{TCR}b} \\ I_{\text{TCR}c} \end{bmatrix} = \frac{1}{3} \begin{bmatrix} -j2B_{\text{TCR}} & jB_{\text{TCR}} & jB_{\text{TCR}} \\ jB_{\text{TCR}} & -j2B_{\text{TCR}} & jB_{\text{TCR}} \\ jB_{\text{TCR}} & jB_{\text{TCR}} & -j2B_{\text{TCR}} \end{bmatrix} \begin{bmatrix} V_a \\ V_b \\ V_c \end{bmatrix}. \quad (2.11)$$

In this situation, an alternative representation becomes feasible, using the frame of reference afforded by the concept of symmetrical components. Three sequence components are associated with three-phase circuits, namely zero (0), positive (1), and negative (2) sequences. The transformation from phase coordinates to sequence coordinates involves

applying the matrix of symmetrical components  $\mathbf{T}_S$  and its inverse to Equation (2.11), leading to the following result:

$$\begin{bmatrix} I_{\text{TCR}(0)} \\ I_{\text{TCR}(1)} \\ I_{\text{TCR}(2)} \end{bmatrix} = \begin{bmatrix} 0 & 0 & 0 \\ 0 & -jB_{\text{TCR}} & 0 \\ 0 & 0 & -jB_{\text{TCR}} \end{bmatrix} \begin{bmatrix} V_{(0)} \\ V_{(1)} \\ V_{(2)} \end{bmatrix}. \quad (2.12)$$

The operation required to transform a three-phase quantity into sequence quantities is explained in detail in Section 3.2.12.

As expected, no zero sequence current can flow in this circuit owing to the delta-connected nature of the TCR. The positive sequence (1) and negative sequence (2) circuits present equal impedances (susceptances) to their respective current flows. Also, it is shown in Equation (2.12) that no couplings exist between sequences. It should be remarked that this would not have been the case if symmetrical components had been applied to Equation (2.10) as opposed to Equation (2.11). The reason is that the admittance matrix of Equation (2.10) is not necessarily a balanced one, since the condition  $B_{\text{TCR}1} \neq B_{\text{TCR}2} \neq B_{\text{TCR}3}$  may exist.

Nevertheless, if equal equivalent admittances may be assumed in the six-pulse TCR then the positive sequence representation becomes

$$I_{\text{TCR}(1)} = -jB_{\text{TCR}}V_{(1)}. \quad (2.13)$$

This representation matches the behaviour of the basic (single-phase) TCR shown in Figure 2.2(a) and given by Equation (2.5).

### 2.3.2 The Static VAR Compensator

In its simplest form, the SVC consists of a TCR in parallel with a bank of capacitors. From an operational point of view, the SVC behaves like a shunt-connected variable reactance, which either generates or absorbs reactive power in order to regulate the voltage magnitude at the point of connection to the AC network. It is used extensively to provide fast reactive power and voltage regulation support. The firing angle control of the thyristor enables the SVC to have almost instantaneous speed of response.

A schematic representation of the SVC is shown in Figure 2.5, where a three-phase, three-winding transformer is used to interface the SVC to a high-voltage bus. The transformer has two identical secondary windings: one is used for the delta-connected, six-pulse TCR and the other for the star-connected, three-phase bank of capacitors, with its star point floating. The three transformer windings are also taken to be star-connected, with their star points floating.

The modelling of one TCR branch has been dealt with in Section 2.3.1, and attention is now dedicated to a bank of capacitors. The admittances of both branches of the SVC will then combine quite straightforwardly.

The nodal admittance of the capacitor bank, in phase coordinates, may be expressed with explicit representation of the star point, which is not grounded. However, it is more advantageous to perform a Kron reduction to obtain a reduced equivalent, where only the parameters of phases  $a$ ,  $b$ , and  $c$  are represented explicitly.

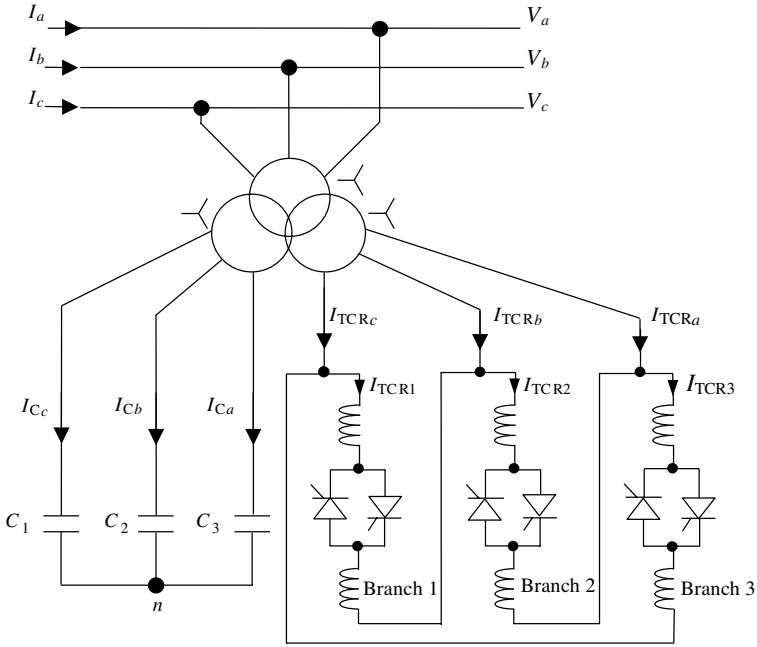


**Figure 2.5** Representation of a three-phase static VAR compensator (SVC) comprising fixed capacitors and thyristor-controlled reactors (TCRs)

In the most general case, when  $B_{C1} \neq B_{C2} \neq B_{C3}$ , and after having performed Kron's reduction, the reduced equivalent model of the bank of capacitors is:

$$\begin{bmatrix} I_{Ca} \\ I_{Cb} \\ I_{Cc} \end{bmatrix} = \begin{bmatrix} j\left(B_{C1} - \frac{B_{C1}^2}{\Delta B_C}\right) & -j\frac{B_{C2}B_{C1}}{\Delta B_C} & -j\frac{B_{C3}B_{C1}}{\Delta B_C} \\ -j\frac{B_{C1}B_{C2}}{\Delta B_C} & j\left(B_{C2} - \frac{B_{C2}^2}{\Delta B_C}\right) & -j\frac{B_{C3}B_{C2}}{\Delta B_C} \\ -j\frac{B_{C1}B_{C3}}{\Delta B_C} & -j\frac{B_{C2}B_{C3}}{\Delta B_C} & j\left(B_{C3} - \frac{B_{C3}^2}{\Delta B_C}\right) \end{bmatrix} \begin{bmatrix} V_a \\ V_b \\ V_c \end{bmatrix}, \quad (2.14)$$

where

$$\left. \begin{aligned} \Delta B_C &= B_{C1} + B_{C2} + B_{C3}, \\ B_{C1} &= \omega C_1, \\ B_{C2} &= \omega C_2, \\ B_{C3} &= \omega C_3. \end{aligned} \right\} \quad (2.15)$$

Kron's reduction is a technique used to eliminate mathematically, specific rows and columns in a matrix equation. It is explained in detail in Section 3.2.3.

If all three branches in the bank of capacitors have equal equivalent susceptances ( $B_{C1} = B_{C2} = B_{C3} = B_C$ ), Equation (2.14) simplifies to:

$$\begin{bmatrix} I_{Ca} \\ I_{Cb} \\ I_{Cc} \end{bmatrix} = \frac{1}{3} \begin{bmatrix} j2B_C & -jB_C & -jB_C \\ -jB_C & j2B_C & -jB_C \\ -jB_C & -jB_C & j2B_C \end{bmatrix} \begin{bmatrix} V_a \\ V_b \\ V_c \end{bmatrix}. \quad (2.16)$$

Three-phase models of the SVC in phase coordinates can now be formed with ease. The most general expression for the six-pulse SVC would be the case when Equations (2.10) and (2.14) are added together, giving rise to a model where design imbalances in the SVC may be accounted for.

A more constrained, but still very useful, model is the case when Equations (2.11) and (2.16) are used as the constituent parts of the SVC model:

$$\begin{aligned} \begin{bmatrix} I_{SVCa} \\ I_{SVCb} \\ I_{SVCc} \end{bmatrix} &= \begin{bmatrix} I_{Ca} \\ I_{Cb} \\ I_{Cc} \end{bmatrix} + \begin{bmatrix} I_{TCRa} \\ I_{TCRb} \\ I_{TCRc} \end{bmatrix} \\ &= \frac{1}{3} \begin{bmatrix} j2(B_C - B_{TCR}) & -j(B_C - B_{TCR}) & -j(B_C - B_{TCR}) \\ -j(B_C - B_{TCR}) & j2(B_C - B_{TCR}) & -j(B_C - B_{TCR}) \\ -j(B_C - B_{TCR}) & -j(B_C - B_{TCR}) & j2(B_C - B_{TCR}) \end{bmatrix} \begin{bmatrix} V_a \\ V_b \\ V_c \end{bmatrix}. \end{aligned} \quad (2.17)$$

It is clear that alternative models, of varying functionality, can also be formed. For instance, combination of Equations (2.10) and (2.16) leads to an SVC model where the three branches of the TCR may have different equivalent inductances but the three capacitances of the bank are equal. Use of Equations (2.11) and (2.14) have the opposite functionality effect in the SVC model.

In any case, only the SVC model given by Equation (2.17) is suitable for deriving a representation in the frame of reference of symmetrical components. Applying the matrix of symmetrical components  $T_S$  and its inverse to Equation (2.17) leads to the following result:

$$\begin{bmatrix} I_{SVC(0)} \\ I_{SVC(1)} \\ I_{SVC(2)} \end{bmatrix} = \begin{bmatrix} 0 & 0 & 0 \\ 0 & j(B_C - B_{TCR}) & 0 \\ 0 & 0 & j(B_C - B_{TCR}) \end{bmatrix} \begin{bmatrix} V_{(0)} \\ V_{(1)} \\ V_{(2)} \end{bmatrix}. \quad (2.18)$$

Similar to the TCR, no zero sequence current can flow in the SVC circuit as the star point of the bank of capacitors is not grounded. The positive sequence and negative sequence circuits contain equal impedances. However, for cases of balanced operation and balanced SVC designs only the positive sequence representation is of interest:

$$I_{SVC(1)} = jB_{SVC}V_{(1)}, \quad (2.19)$$

where

$$\left. \begin{aligned} B_{SVC} &= B_C - B_{TCR} = \frac{1}{X_C X_L} \left\{ X_L - \frac{X_C}{\pi} [2(\pi - \alpha) + \sin 2\alpha] \right\}, \\ X_L &= \omega L, \\ X_C &= \frac{1}{\omega C}. \end{aligned} \right\} \quad (2.20)$$

It should be remarked that the positive sequence model of the SVC should also serve the purpose of representing a single-phase SVC.

### 2.3.3 The Thyristor-controlled Series Compensator

TCSCs vary the electrical length of the compensated transmission line with little delay. This characteristic enables the TCSC to be used to provide fast active power flow regulation. It

also increases the stability margin of the system and has proved very effective in damping SSR and power oscillations (Larsen *et al.*, 1992).

In principle, the steady-state response of the TCSC may be calculated by solving the differential equations that describe its electrical performance, using a suitable numeric integration method. Alternatively, the TCSC differential equations may be expressed in algebraic form and then a phasorial method used to solve them. The former approach involves the integration of the differential equations over many cycles until the transient response dies out. This solution method is rich in information as the full evolution of the response is captured, from transient inception to steady-state operation, but it suffers from excessive computational overheads, particularly when solving lightly damped circuits. Two different solution flavours emerge from the phasorial approach. (1) the TCSC steady-state operation may be determined very efficiently by using fundamental and harmonic frequency phasors, neatly arranged in the harmonic domain frame of reference (Acha and Madrigal, 2001). The method yields full information for the fundamental and harmonic frequency TCSC parameters but no transient information is available. (2) Alternatively, a nonlinear equivalent impedance expression is derived for the TCSC and solved by iteration (Fuerte-Esquivel, Acha, and Ambriz-Pérez, 2000a). The solution method is accurate and converges very robustly towards the solution, but it only yields information for the fundamental frequency steady-state solution. This is precisely the approach taken in power flow studies, the application topic covered in this book.

### 2.3.3.1 Thyristor-controlled series capacitor equivalent circuit

A basic TCSC module consists of a TCR in parallel with a fix capacitor. An actual TCSC comprises one or more modules. Figure 2.6 shows the layout of one phase of the TCSC installed in the Slatt substation (Kinney, Mittelstadt, and Suhrbier, 1994).

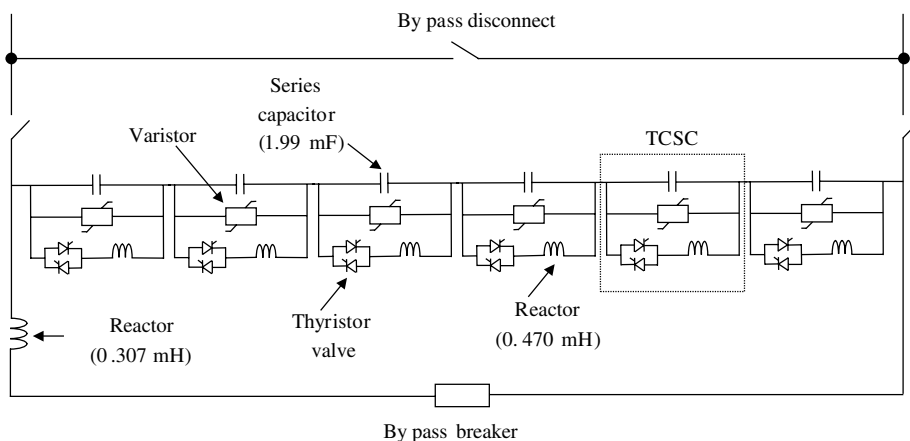


**Figure 2.6** Physical structure of one phase of a thyristor-controlled series capacitor (TCSC). Reproduced, with permission, from S.J. Kinney, W.A. Mittelstadt, and R.W. Suhrbier, ‘Test Results and Initial Operating Experience for the BPA 500 kV Thyristor Controlled Series Capacitor: Design, Operation, and Fault Test Results, Northcon 95’, in *IEEE Technical Conference and Workshops Northcon 95, Portland, Oregon, USA, October 1995*, pp. 268–273, © 1995 IEEE

The TCR achieves its fundamental frequency operating state at the expense of generating harmonic currents, which are a function of the thyristor conduction angle. Nevertheless, contrary to the SVC application where the harmonic currents generated by the TCR tend to escape towards the network, in the TCSC application the TCR harmonic currents are trapped inside the TCSC because of the low impedance of the capacitor compared with the network equivalent impedance. This is, at least, the case for a well-designed TCSC operating in capacitive mode. Measurements conducted in the Slatt and the Kayenta TCSC systems support this observation. For instance, the Kayenta system generates at its terminals, a maximum total harmonic distortion (THD) voltage of 1.5% when operated in capacitive mode and firing at an angle of  $147^\circ$  (Christl *et al.*, 1992). It should be noted that there is little incentive for operating the TCSC in inductive mode as this would increase the electrical length of the compensated transmission line, with adverse consequences on stability margins, and extra losses.

For the purpose of fundamental frequency power system studies, a complex TCSC topology, such as the single-phase branch shown in Figure 2.6, may be taken to consist of one equivalent TCR paralleled by one equivalent capacitor, as illustrated schematically in Figure 2.7. The surge arrester is not represented as this is a representation intended for steady-state operation, but the existence of a loop current is emphasised.

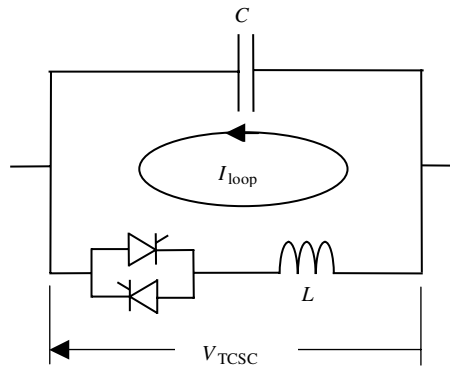


**Figure 2.7** Thyristor-controlled series capacitor (TCSC) equivalent circuit. Reproduced with permission from C.R. Fuerte-Esquivel, E. Acha, and H. Ambriz-Pérez, 'A Thyristor Controlled Series Compensator Model for the Power Flow Solution of Practical Power Networks', *IEEE Trans. Power Systems* **15**(1) 58–64, © 2000 IEEE

This equivalent circuit has an associated equivalent reactance, which is a function of the thyristor gating signals. Expressions for the various electrical parameters in the TCSC equivalent circuit are derived in the following two sections.

### 2.3.3.2 Steady-state current and voltage equations

The TCSC current equations may be obtained with reference to the circuit shown in Figure 2.8, using Laplace theory. This electric circuit represents, in simple terms, the

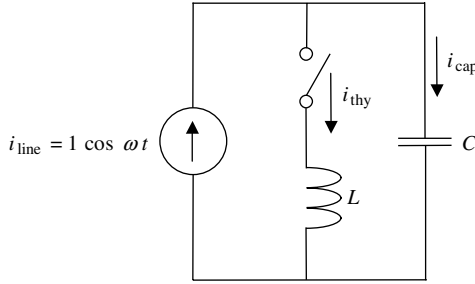


**Figure 2.8** Thyristor-controlled series capacitor (TCSC) electric circuit. Reproduced with permission from C.R. Fuerte-Esquivel, E. Acha, and H. Ambriz-Pérez, ‘A Thyristor Controlled Series Compensator Model for the Power Flow Solution of Practical Power Networks’, *IEEE Trans. Power Systems* **15**(1) 58–64, © 2000 IEEE

topology of a TCR in parallel with a capacitor branch, just before the thyristor fires on. The thyristor is represented as an ideal switch, and the contribution of the external network is assumed to be in the form of a sinusoidal current source. The current pulse through the thyristor, which exhibits a degree of asymmetry right up to the point when the steady-state is reached, is shown schematically in Figure 2.9. The time reference, termed the ‘original time reference’ (OR), is taken at the positive-going zero-crossing of the voltage across

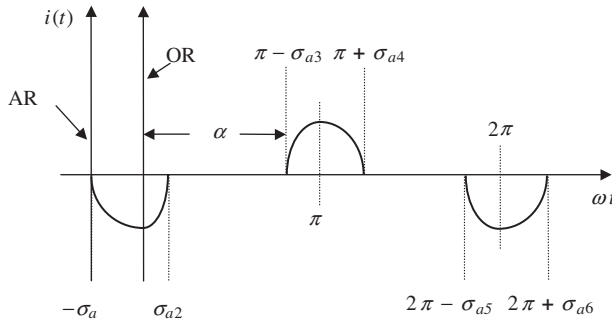


**Figure 2.9** Thyristor-controlled series capacitor (TCSC) asymmetrical thyristor current. Note: AR, auxiliary time reference; OR, original time reference. Reproduced with permission from C.R. Fuerte-Esquivel, E. Acha, and H. Ambriz-Pérez, ‘A Thyristor Controlled Series Compensator Model for the Power Flow Solution of Practical Power Networks’, *IEEE Trans. Power Systems* **15**(1) 58–64, © 2000 IEEE

the inductive reactance of the TCSC. It is useful at this stage to introduce an ‘auxiliary time reference’ (AR) in addition to the OR, which is taken at a time when the thyristor starts to conduct.

Expressing the line current given in the circuit of Figure 2.8,  $i_{\text{line}} = \cos \omega t$ , in terms of the auxiliary reference plane (AR),

$$i_{\text{line}} = \cos(\omega t - \sigma_a) = \cos \omega t \cos \sigma_a + \sin \omega t \sin \sigma_a, \tag{2.21}$$

where  $\sigma_a$ , equal to  $\pi - \alpha$ , is the firing advance angle, and  $\alpha$  is the firing angle with the capacitor voltage positive-going, zero-crossing as reference.

Applying Kirchhoff's current law to the circuit of Figure 2.8, we obtain

$$i_{\text{line}} = i_{\text{thy}} + i_{\text{cap}}. \quad (2.22)$$

During the conduction period the voltage across the TCSC inductive and capacitive reactances have equal values,

$$L \frac{di_{\text{thy}}}{dt} = \frac{1}{C} \int i_{\text{cap}} dt + V_{\text{cap}}^+, \quad (2.23)$$

where  $V_{\text{cap}}^+$  is the voltage across the capacitor when the thyristor turns on.

Expressing Equations (2.21)–(2.23) in the Laplace domain, we obtain

$$I_{\text{line}} = \cos\left(\sigma_a \frac{s}{s^2 + \omega^2}\right) + \sin\left(\sigma_a \frac{\omega}{s^2 + \omega^2}\right), \quad (2.24)$$

$$I_{\text{line}} = I_{\text{thy}} + I_{\text{cap}}, \quad (2.25)$$

$$I_{\text{cap}} = s^2 LC I_{\text{thy}} - CV_{\text{cap}}^+, \quad (2.26)$$

where  $s$  is the Laplace operator.

Substituting Equations (2.24) and (2.26) into Equation (2.25), we obtain the current through the thyristor in the Laplace domain:

$$I_{\text{thy}} = \omega_0^2 \frac{s}{(s^2 + \omega_0^2)(s^2 + \omega^2)} \cos(\sigma_a) + \omega_0^2 \frac{1}{(s^2 + \omega_0^2)(s^2 + \omega^2)} \omega \sin(\sigma_a) + \frac{\omega_0^2 CV_{\text{cap}}^+}{s^2 + \omega_0^2}. \quad (2.27)$$

The corresponding expression in the time domain is readily established from the above equation:

$$i_{\text{thy}} = A \cos(\omega t - \sigma_a) - A \cos \sigma_a \cos \omega_0 t - B \sin \sigma_a \sin \omega_0 t + DV_{\text{cap}}^+ \sin \omega_0 t, \quad (2.28)$$

where

$$A = \frac{\omega_0^2}{\omega_0^2 - \omega^2}, \quad (2.29)$$

$$B = \frac{\omega_0 \omega}{\omega_0^2 - \omega^2}, \quad (2.30)$$

$$D = \omega_0 C, \quad (2.31)$$

$$\omega_0^2 = \frac{1}{LC}. \quad (2.32)$$

In order to make Equation (2.28) valid for the range  $[-\sigma_a, \sigma_{a2}]$  in Figure 2.9, it is necessary to shift the equation to the original time reference, OR, by adding  $\sigma_a/\omega$  to the time variable, to give

$$i_{\text{thy}} = A \cos\left[\omega\left(t + \frac{\sigma_a}{\omega}\right) - \sigma_a\right] - A \cos \sigma_a \cos \omega_0\left(t + \frac{\sigma_a}{\omega}\right) - B \sin \sigma_a \sin \omega_0\left(t + \frac{\sigma_a}{\omega}\right) + DV_{\text{cap}}^+ \sin \omega_0\left(t + \frac{\sigma_a}{\omega}\right). \quad (2.33)$$

After some arduous algebra, we have,

$$i_{thy} = A \cos \omega t + (-A \cos \sigma_a \cos \varpi \sigma_a - B \sin \sigma_a \sin \varpi \sigma_a + D V_{cap}^+ \sin \varpi \sigma_a) \cos \omega_0 t \\ + (A \cos \sigma_a \sin \varpi \sigma_a - B \sin \sigma_a \cos \varpi \sigma_a + D V_{cap}^+ \cos \varpi \sigma_a) \sin \omega_0 t, \quad (2.34)$$

where

$$\varpi = \frac{\omega_0}{\omega}. \quad (2.35)$$

Equation (2.34) is valid in the range  $-\sigma_a < \omega t < \sigma_{a2}$ , and contains the transient and steady-state components. One further consideration is added to this result to yield the desired expression for the thyristor current in steady-state, which is reached when the current pulse in Figure 2.9 becomes symmetrical (i.e.  $\sigma_a = \sigma_{a2}$ ). Such a condition takes place when the capacitor voltage,  $V_{cap}^+$ , reaches such a level that the coefficient of the sinusoidal term,  $\sin \omega_0 t$ , takes a value of zero. At this point in time the capacitor voltage becomes

$$V_{cap}^+ = \frac{B}{D} \sin(\sigma_a) - \frac{A}{D} \cos(\sigma_a) \tan(\varpi \sigma_a). \quad (2.36)$$

The expression for the steady-state thyristor current is obtained by substituting Equation (2.36) into Equation (2.34), to give

$$i_{thy} = A \cos(\omega t) - A \frac{\cos \sigma_a}{\cos(\varpi \sigma_a)} \cos(\varpi \omega t). \quad (2.37)$$

With reference to Figure 2.9, when the steady-state is reached

$$\sigma_a = \sigma_{a2} = \sigma_{a3} = \sigma_{a4} = \sigma_{a5} = \sigma_{a6}. \quad (2.38)$$

A similar equation to Equation (2.37), valid for the interval  $(\pi - \sigma_a) < \omega t < (\pi + \sigma_a)$ , may be obtained by assuming that a second firing pulse, in Figure 2.9, takes place  $\pi$  radians just after the first pulse, producing a current flow through the thyristor with opposite polarity to the current given by Equation (2.37):

$$i_{thy} = A \cos(\omega t) + A \frac{\cos(\sigma_a)}{\cos(\varpi \sigma_a)} \cos[\varpi(\omega t - \pi)]. \quad (2.39)$$

For completeness, in the interval  $\sigma_a < \omega t < (\pi - \sigma_a)$ :

$$i_{thy} = 0. \quad (2.40)$$

Expressions for the voltage across the TCSC capacitor during the conduction period  $v_{cap}^{on}$  are obtained by substituting Equations (2.37) and (2.39) into:

$$v_{cap}^{on} = L \frac{d i_{thy}}{d t}. \quad (2.41)$$

The combined solution of Equations (2.37), (2.39), and (2.41) gives the voltages across the capacitor in the intervals  $-\sigma_a < \omega t < \sigma_a$ , and  $(\pi - \sigma_a) < \omega t < (\pi + \sigma_a)$ :

$$v_{cap}^{on} = -A X_L \sin(\omega t) + A \left[ \frac{\varpi X_L \cos(\sigma_a)}{\cos(\varpi \sigma_a)} \right] \sin(\varpi \sigma_a), \quad (2.42)$$

$$v_{cap}^{on} = -A X_L \sin(\omega t) - A \left[ \frac{\varpi X_L \cos(\sigma_a)}{\cos(\varpi \sigma_a)} \right] \sin[\varpi(\omega t - \pi)], \quad (2.43)$$

where  $X_L$  is the inductive reactance defined by the product  $\omega L$ .

When the thyristor is not conducting, the circuit in Figure 2.8 reduces to a capacitor in series with a direct current (DC) voltage source, which represents the capacitor voltage at the time of thyristor commutation,

$$v_{\text{cap}}^{\text{off}} = \frac{1}{C} \int_{\alpha}^{\omega t} \cos(\omega t) dt + V_{\text{cap}}^{\text{on-off}}, \quad (2.44)$$

where  $V_{\text{cap}}^{\text{on-off}}$  is the voltage across the capacitor just at the time when the thyristor is turned off (i.e.  $\sigma_a/\omega$ ). This value is readily obtained from Equation (2.42), to be

$$V_{\text{cap}}^{\text{on-off}} = -A X_L \sin(\sigma_a) + A \varpi X_L \cos(\sigma_a) \tan(\varpi \sigma_a). \quad (2.45)$$

Substitution of Equation (2.45) into Equation (2.44) enables the solution of  $v_{\text{cap}}^{\text{off}}$  in the intervals  $-\sigma_a < \omega t < \sigma_a$ , and  $(\pi - \sigma_a) < \omega t < (\pi + \sigma_a)$ :

$$v_{\text{cap}}^{\text{off}} = X_C [\sin(\omega t) - \sin \sigma_a] - A X_L [\sin \sigma_a - \varpi \cos \sigma_a \tan \varpi \sigma_a], \quad (2.46)$$

$$v_{\text{cap}}^{\text{off}} = X_C [\sin(\omega t) + \sin \sigma_a] + A X_L (\sin \sigma_a - \varpi \cos \sigma_a \tan \varpi \sigma_a), \quad (2.47)$$

where  $X_C$  is the inductive reactance defined by  $1/\omega C$ .

Typical TCSC voltage and current waveforms are shown in Figures 2.10(a) and 2.10(b). They correspond to the TCSC installed at the Kayenta substation (Christl *et al.*, 1992), with the thyristors fired at angles of  $150^\circ$  and having an inductive reactance of  $2.6 \Omega$  and an capacitive reactance of  $15 \Omega$ , at a base frequency of 60 Hz.

### 2.3.3.3 Thyristor-controlled series capacitor fundamental frequency impedance

As illustrated by the TCSC waveforms shown in Figures 2.10(a) and 2.10(b), the inductor current is nonsinusoidal but periodic, and it is said to contain harmonic distortion. If the interest is the study of the TCSC at only the fundamental frequency then it becomes necessary to apply Fourier analysis to a full period of the inductor current, say Equations (2.37), (2.39), and (2.40), in order to obtain its expression at the fundamental frequency.

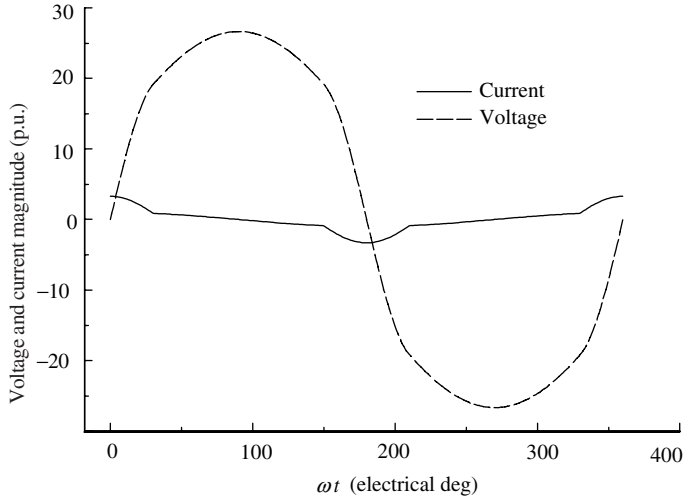
With reference to Figure 2.10(b), it is clear that the TCSC thyristor current has even and quarter-wave symmetry. Hence, the fundamental frequency component can be obtained by solving Equation (2.37) only:

$$\begin{aligned} I_{\text{thy}(1)} &= \frac{4}{\pi} \int_0^{\sigma_a} \left[ A \cos(\omega t) - A \frac{\cos(\sigma_a)}{\cos(\omega \sigma_a)} \cos(\varpi \omega t) \right] \cos(\omega t) d\omega t \\ &= A \left[ \frac{2\sigma_a + \sin(2\sigma_a)}{\pi} \right] - \frac{4A \cos^2(\sigma_a)}{\varpi^2 - 1} \left[ \frac{\varpi \tan(k \sigma_a) - \tan(\sigma_a)}{\pi} \right]. \end{aligned} \quad (2.48)$$

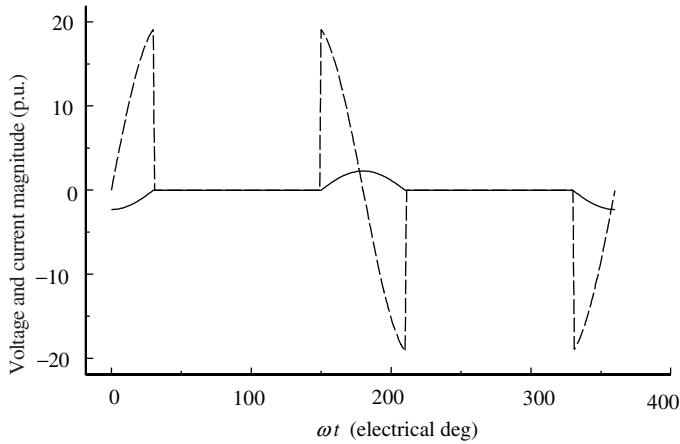
The thyristor current at the fundamental frequency may be expressed as

$$i_{\text{thy}(1)} = I_{\text{thy}(1)} \cos(\omega t). \quad (2.49)$$

By recognising that the fundamental frequency voltage across the TCSC module,  $V_{\text{TCSC}(1)}$ , equals the fundamental frequency voltage across the capacitor, and that the ideal current source representing the external circuit is taken to be sinusoidal, an expression for



(a)



(b)

**Figure 2.10** Voltage and current waveforms in (a) thyristor-controlled series capacitor the (TCSC) capacitor and (b) the TCSC inductor

the TCSC fundamental frequency impedance may be determined:

$$Z_{TCSC(1)} = \frac{V_{TCSC(1)}}{I_{line}} = \frac{-jX_C I_{cap(1)}}{I_{line}} \tag{2.50}$$

Moreover, the TCSC contains no resistance and the line current splits between the currents flowing in the capacitive and inductive branches:

$$X_{TCSC(1)} = \frac{-jX_C (\cos \omega t - I_{thy(1)} \cos \omega t)}{\cos \omega t} = -jX_C [1 + I'_{thy(1)}] \tag{2.51}$$

where  $X_{\text{TCSC}(1)}$  is the TCSC equivalent reactance at the fundamental frequency, and  $I'_{\text{thy}(1)}$  has the form of  $I_{\text{thy}(1)}$  in Equation (2.48) but is a dimensionless parameter as it has been divided by a unitary current.

The TCSC equivalent reactance is as a function of its capacitive and inductive parameters, and the firing angle:

$$X_{\text{TCSC}(1)} = -X_C + C_1 \{2(\pi - \alpha) + \sin[2(\pi - \alpha)]\} + C_2 \cos^2(\pi - \alpha) \{\varpi \tan[\varpi(\pi - \alpha)] - \tan(\pi - \alpha)\}, \quad (2.52)$$

where

$$X_{LC} = \frac{X_C X_L}{X_C - X_L}, \quad (2.53)$$

$$C_1 = \frac{X_C + X_{LC}}{\pi}, \quad (2.54)$$

$$C_2 = -\frac{4X_{LC}^2}{X_L \pi}. \quad (2.55)$$

The poles of Equation (2.52) are:

$$\alpha = \pi - \frac{(2n - 1)(LC)^{1/2} \pi \omega}{2}, \quad \text{for } n = 1, 2, 3 \dots \quad (2.56)$$

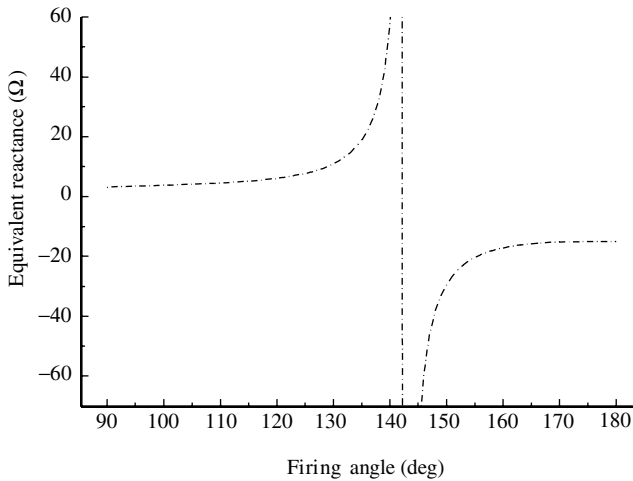


**Figure 2.11** Thyristor-controlled series capacitor (TCSC) fundamental frequency impedance

The TCSC capacitive and inductive reactance values should be chosen carefully in order to ensure that just one resonant point is present in the range of  $\pi/2$  to  $\pi$ . Figure 2.11 shows the TCSC fundamental frequency reactance, as a function of the firing angle, for the TCSC installed at the Kayenta substation (Christl *et al.*, 1992).

For the purpose of power flow studies, the TCSC may be adequately represented by the equivalent reactance in Equation (2.52), which enables a straightforward representation of the TCSC in the form of a nodal transfer admittance matrix. This is derived with reference

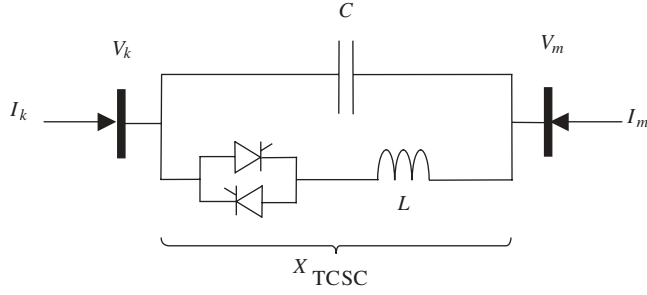


**Figure 2.12** Single-phase thyristor-controlled series capacitor (TCSC) comprising an equivalent capacitor and a thyristor-controlled reactor (TCR) in parallel. Reproduced with permission from C.R. Fuerte-Esquivel, E. Acha, and H. Ambriz-Pérez, ‘A Thyristor Controlled Series Compensator Model for the Power Flow Solution of Practical Power Networks’, *IEEE Trans. Power Systems* **15**(1) 58–64, © 2000 IEEE

to the equivalent circuit in Figure 2.12, where it is assumed that the TCSC is connected between buses  $k$  and  $m$ .

The transfer admittance matrix relates the nodal currents injections,  $I_k$  and  $I_m$ , to the nodal voltages,  $V_k$  and  $V_m$ , via the variable TCSC reactance shown in the equivalent circuit of Figure 2.12:

$$\begin{bmatrix} I_k \\ I_m \end{bmatrix} = \begin{bmatrix} -\frac{1}{jX_{TCSC}} & \frac{1}{jX_{TCSC}} \\ \frac{1}{jX_{TCSC}} & -\frac{1}{jX_{TCSC}} \end{bmatrix} \begin{bmatrix} V_k \\ V_m \end{bmatrix}. \tag{2.57}$$

In three-phase TCSC installations, three independent modules, possibly of the form shown in Figure 2.6, may be used, one for each phase. For modelling and simulation purposes, it is assumed that no electromagnetic couplings exist between the TCSC units making up the three-phase module. This enables a straightforward extension of the single-phase TCSC transfer admittance, given by Equation (2.57), to model the three-phase TCSC:

$$\begin{bmatrix} I_{TCSCak} \\ I_{TCSCbk} \\ I_{TCSCck} \\ I_{TCSCam} \\ I_{TCSCbm} \\ I_{TCSCcm} \end{bmatrix} = \begin{bmatrix} -\frac{1}{jX_{TCSC1}} & 0 & 0 & \frac{1}{jX_{TCSC1}} & 0 & 0 \\ 0 & -\frac{1}{jX_{TCSC2}} & 0 & 0 & \frac{1}{jX_{TCSC2}} & 0 \\ 0 & 0 & -\frac{1}{jX_{TCSC3}} & 0 & 0 & \frac{1}{jX_{TCSC3}} \\ \frac{1}{jX_{TCSC1}} & 0 & 0 & -\frac{1}{jX_{TCSC1}} & 0 & 0 \\ 0 & \frac{1}{jX_{TCSC2}} & 0 & 0 & -\frac{1}{jX_{TCSC2}} & 0 \\ 0 & 0 & \frac{1}{jX_{TCSC3}} & 0 & 0 & -\frac{1}{jX_{TCSC3}} \end{bmatrix} \begin{bmatrix} V_{TCSCak} \\ V_{TCSCbk} \\ V_{TCSCck} \\ V_{TCSCam} \\ V_{TCSCbm} \\ V_{TCSCcm} \end{bmatrix} \tag{2.58}$$

where subscripts 1, 2, and 3 are used to indicate that the three single-phase units may take different values owing to either different design parameters or unequal thyristor firing pulses.

If the three single-phase TCSC units have identical reactance values, say  $X_{TCSC}$ , then it is possible to transform the TCSC phase domain model into the sequence domain frame of reference. Owing to the decoupled nature of Equation (2.58), the positive, negative, and zero sequence models are identical and have the same form as Equation (2.57), the representation of the single-phase TCSC.

### 2.4 POWER ELECTRONIC CONTROLLERS BASED ON FULLY CONTROLLED SEMICONDUCTOR DEVICES

Modern power system controllers based on power electronic converters are capable of generating reactive power with no need for large reactive energy storage elements, such as in SVC systems. This is achieved by making the currents circulate through the phases of the AC system with the assistance of fast switching devices (Hingorani and Gyugyi, 2000).

The semiconductor devices employed in the new generation of power electronic converters are of the fully controlled type, such as the insulated gate bipolar transistor (IGBT) and the gate turn-off thyristor (GTO). Their respective circuit symbols are shown in Figure 2.13 (Mohan, Undeland, and Robbins, 1995).

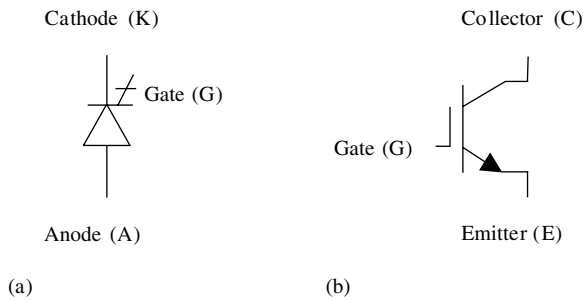


**Figure 2.13** Circuit symbols for: (a) gate turn-off thyristor and (b) insulated gate bipolar transistor. Reproduced by permission of John Wiley & Sons Inc. from N. Mohan, T.M. Undeland, and W.P. Robbins, 1995, *Power Electronics: Converter Applications and Design*, 2nd edn

The GTO is a more advanced version of the conventional thyristor, with a similar switched-on characteristic but with the ability to switch off at a time different from when the forward current falls naturally below the holding current level. Such added functionality has enabled new application areas in industry to be developed, even at bulk power transmission where nowadays it is possible to redirect active power at the megawatt level. However, there is room for improvement in GTO construction and design, where still large negative pulses are required to turn them off. At present, the maximum switching frequency attainable is in the order of 1 kHz (Mohan, Undeland, and Robbins, 1995).

The IGBT is one of the most well-developed members of the family of power transistors. It is the most popular device used in the area of AC and DC motor drives, reaching power

levels of a few hundred kilowatts. Power converters aimed at power systems applications are beginning to make use of IGBTs owing to their increasing power-handling capability and relatively low conduction losses. Further progress is expected in IGBT and GTO technology and applications (Hingorani, 1998).

In DC–AC converters that use fully controlled semiconductors rather than conventional thyristors, the DC input can be either a voltage source (typically a capacitor) or a current source (typically a voltage source in series with an inductor). With reference to this basic operational principle, converters can be classified as either voltage source converters (VSCs) or current source converters. For economic and performance reasons, most reactive power controllers are based on the VSC topology. The availability of modern semiconductors with relatively high voltage and current ratings, such as GTOs or IGBTs, has made the concepts of reactive compensation based on switching converters a certainty, even for substantial high-power applications.

A number of power system controllers that use VSCs as their basic building block are in operation in various parts of the world. The most popular are: STATCOMs, solid-state series controllers (SSSCs), the UPFC, and the HVDC-VSC (IEEE/CIGRÉ, 1995).

### 2.4.1 The Voltage Source Converter

There are several VSC topologies currently in use in actual power system operation and some others that hold great potential, including: the single-phase full bridge (H-bridge); the conventional three-phase, two-level converter; and the three-phase, three-level converter based on the neutral-point-clamped converter. Other VSC topologies are based on combinations of the neutral-point-clamped topology and multilevel-based systems. Common aims of these topologies are: to minimise the operating frequency of the semiconductors inside the VSC and to produce a high-quality sinusoidal voltage waveform with minimum or no filtering requirements. By way of example, the topology of a conventional two-level VSC using IGBT switches is illustrated in Figure 2.14.

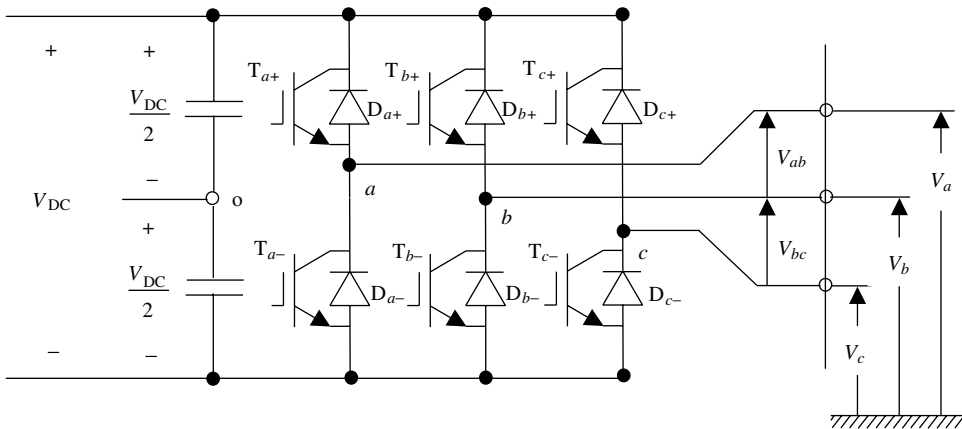


**Figure 2.14** Topology of a three-phase, two-level voltage source converter (VSC) using insulated gate bipolar transistors

The VSC shown in Figure 2.14 comprises six IGBTs, with two IGBTs placed on each leg. Moreover, each IGBT is provided with a diode connected antiparallel to make provisions for possible voltage reversals due to external circuit conditions. Two equally sized capacitors are placed on the DC side to provide a source of reactive power.

Although not shown in the circuit of Figure 2.14, the switching control module is an integral component of the VSC (Mohan, Undeland, and Robbins, 1995). Its task is to control the switching sequence of the various semiconductor devices in the VSC, aiming at producing an output voltage waveform, that is as near to a sinusoidal waveform as possible, with high power controllability and minimum switching loss.

Current VSC switching strategies aimed at utility applications may be classified into two main categories (Raju, Venkata, and Sastry, 1997):

- **Fundamental frequency switching:** the switching of each semiconductor device is limited to one turn-on and one turn-off per power cycle. The basic VSC topology shown in Figure 2.14, with fundamental frequency switching, yields a quasi-square-wave output, which has an unacceptable high harmonic content. It is current practice to use several six-pulse VSCs, arranged to form a multipulse structure, to achieve better waveform quality and higher power ratings (Hingorani and Gyugyi, 2000).
- **Pulse-width modulation (PWM):** this control technique enables the switches to be turned on and off at a rate considerably higher than the fundamental frequency. The output waveform is chopped and the width of the resulting pulses is modulated. Undesirable harmonics in the output waveform are shifted to the higher frequencies, and filtering requirements are much reduced. Over the years, various PWM control techniques have been published, but the sinusoidal PWM scheme remains one of the most popular owing to its simplicity and effectiveness (Mohan, Undeland, and Robbins, 1995).

From the viewpoint of utility applications, both switching techniques are far from perfect. The fundamental frequency switching technique requires complex transformer arrangements to achieve an acceptable level of waveform distortion. Such a drawback is offset by its high semiconductor switch utilization and low switching losses; and it is, at present, the switching technique used in high-voltage, high-power applications. The PWM technique incurs high switching loss, but it is envisaged that future semiconductor devices will reduce this by a significant margin, making PWM the universally preferred switching technique, even for high-voltage and extra-high-voltage transmission applications.

### 2.4.1.1 *Pulse-width modulation control*

The basic PWM control method can be explained with reference to Figure 2.15, in which a sinusoidal fundamental frequency signal is compared with a high-frequency triangular signal, producing a square-wave signal, which serves the purpose of controlling the firing of the individual valves of a given converter topology, such as the one shown in Figure 2.14. The sinusoidal and triangular signals, and their associated frequencies, are termed reference and carrier signals and frequencies, respectively. By varying the amplitude of the sinusoidal signal against the fixed amplitude of the carrier signal, which is normally kept at 1 p.u., the amplitude of the fundamental component of the resulting control signal varies linearly. In Figures 2.15(a)–2.15(c), the carrier frequency  $f_c$  is taken to be 9 times the desired frequency  $f_1$ .

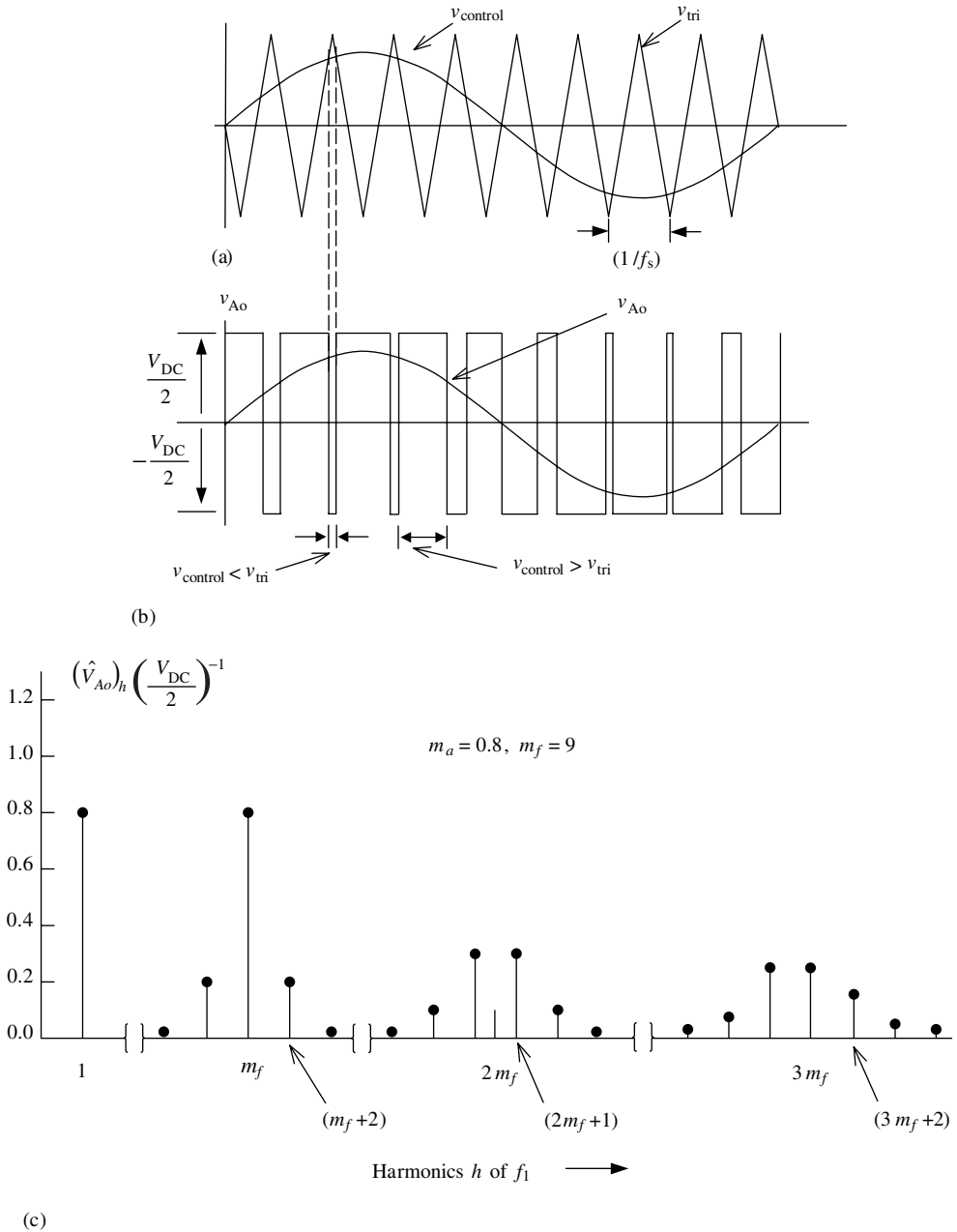


**Figure 2.15** Operation of a pulse-width modulator: (a) comparison of a sinusoidal fundamental frequency with a high-frequency triangular signal; (b) resulting train of square-wave signals; (c) harmonic voltage spectrum. Reproduced by permission of John Wiley & Sons Inc. from N. Mohan, T.M. Undeland, and W.P Robbins, 1995, *Power Electronics: Converter Applications and Design*, 2nd edn

The width of the square wave is modulated in a sinusoidal manner, and the fundamental and harmonic components can be determined by means of Fourier analysis. To determine the magnitude and frequency of the resulting fundamental and harmonic terms, it is useful to use the concept of amplitude modulation ratio,  $m_a$ , and frequency modulation ratio,  $m_f$ :

$$m_a = \frac{\hat{V}_{\text{control}}}{\hat{V}_{\text{tri}}}, \tag{2.59}$$

$$m_f = \frac{f_s}{f_1}, \tag{2.60}$$

where  $\hat{V}_{\text{control}}$  is the peak amplitude of the sinusoidal (control) signal and  $\hat{V}_{\text{tri}}$  is the peak amplitude of the triangular (carrier) signal, which, for most practical purposes, is kept constant.

With reference to the ‘one-leg’ converter shown in Figure 2.16, corresponding to one leg of the three-phase converter of Figure 2.14, the switches  $T_{a+}$  and  $T_{a-}$  are controlled by straightforward comparison of  $v_{\text{control}}$  and  $v_{\text{tri}}$ , resulting in the following output voltages:

$$v_{ao} = \begin{cases} \frac{1}{2} V_{\text{DC}} & \text{when } T_{a+} \text{ is on in response to } v_{\text{control}} > v_{\text{tri}}, \\ -\frac{1}{2} V_{\text{DC}} & \text{when } T_{a-} \text{ is on in response to } v_{\text{control}} < v_{\text{tri}}. \end{cases} \tag{2.61}$$

The output voltage  $v_{ao}$  fluctuates between  $-V_{\text{DC}}/2$  and  $V_{\text{DC}}/2$ , as  $T_{a-}$  and  $T_{a+}$  are never off simultaneously, and is independent of the direction of  $i_o$ .

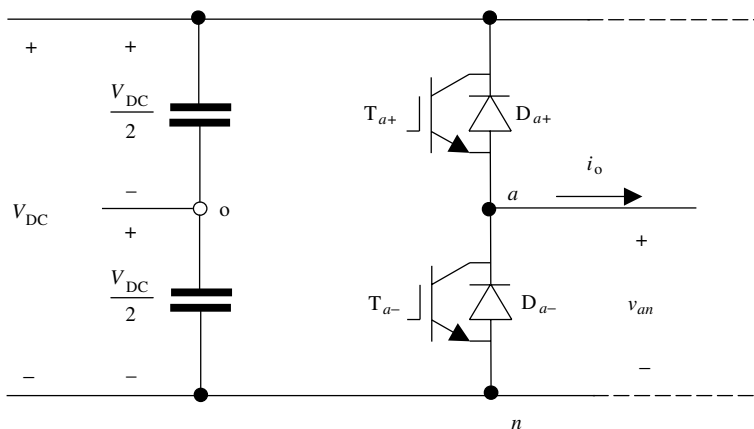


**Figure 2.16** ‘One leg’ voltage source converter (VSC). Reproduced by permission of John Wiley & Sons Inc. from N. Mohan, T.M. Undeland, and W.P. Robbins, 1995, *Power Electronics: Converter Applications and Designs*, 2nd edn

The voltage  $v_{ao}$  and its fundamental frequency component are shown in Figure 2.15(b), for the case of  $m_f = 9$  and  $m_a = 0.8$ . The corresponding harmonic voltage spectrum, in normalised form, is shown in Figure 2.15(c). This is a case of linear voltage control, where  $m_a < 1$ , but this is not the only possibility. Two other forms of voltage control exist, namely, overmodulation and square-wave modulation. The former takes place in the region  $1 < m_a < 3.24$  and the latter applies when  $m_a > 3.24$  (Mohan, Undeland, and Robbins, 1995).

Only the case of linear voltage control ( $m_a < 1$ ) is of interest in this section. The peak amplitude of the fundamental frequency component is  $m_a$  multiplied by  $V_{\text{DC}}/2$ , and the

harmonics appear as sidebands, centred around the switching frequency and its multiples, following a well-defined pattern given by:

$$f_h = (\beta m_f \pm \kappa) f_1. \tag{2.62}$$

Harmonic terms exist only for odd values of  $\beta$  with even values of  $\kappa$ . Conversely, even values of  $\beta$  combine with odd values of  $\kappa$ . Moreover, the harmonic  $m_f$  should be an odd integer in order to prevent the appearance of even harmonic terms in  $v_{a0}$ .

### 2.4.1.2 Principles of voltage source converter operation

The interaction between the VSC and the power system may be explained in simple terms, by considering a VSC connected to the AC mains through a loss-less reactor, as illustrated in the single-line diagram shown in Figure 2.17(a). The premise is that the amplitude and the

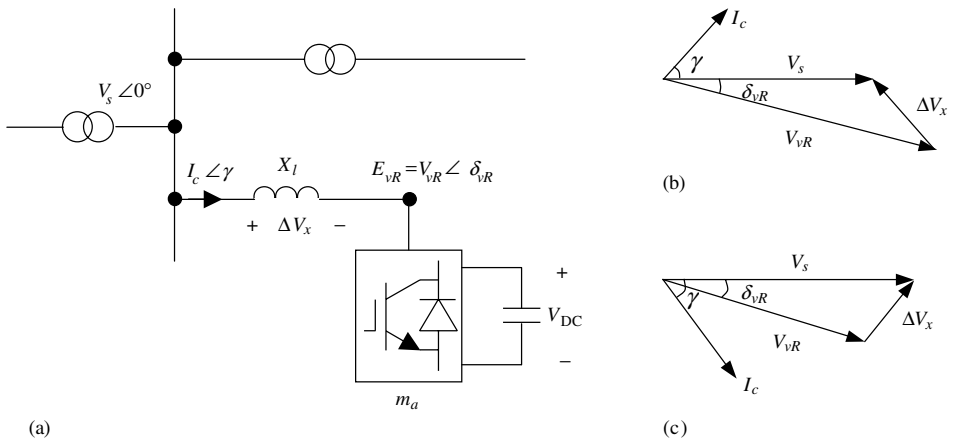


**Figure 2.17** Basic operation of a voltage source converter (VSC): (a) VSC connected to a system bus. Space vector representation for (b) lagging operation and (c) leading operation

phase angle of the voltage drop,  $\Delta V_x$ , across the reactor,  $X_l$ , can be controlled, defining the amount and direction of active and reactive power flows through  $X_l$ . The voltage at the supply bus is taken to be sinusoidal, of value  $V_s \angle 0^\circ$ <sup>(1)</sup>, and the fundamental frequency component of the SVC AC voltage is taken to be  $V_{vR} \angle \delta_{vR}$ . The positive sequence fundamental frequency vector representation is shown in Figures 2.17(b) and 2.17(c) for leading and lagging VAR compensation, respectively.

According to Figure 2.17, for both leading and lagging VAR, the active and the reactive powers can be expressed as

$$\left. \begin{aligned} P &= \frac{V_s V_{vR}}{X_l} \sin \delta_{vR}, \\ Q &= \frac{V_s^2}{X_l} - \frac{V_s V_{vR}}{X_l} \cos \delta_{vR}. \end{aligned} \right\} \tag{2.63}$$

<sup>(1)</sup>Note on notation:  $V \angle \delta$  is a single complex number having a magnitude of  $V$  and a phase angle  $\delta$ .

With reference to Figure 2.17 and Equation (2.63), the following observations are derived:

- The VSC output voltage  $V_{vR}$  lags the AC voltage source  $V_s$  by an angle  $\delta_{vR}$ , and the input current lags the voltage drop across the reactor  $\Delta V_x$  by  $\pi/2$ .
- The active power flow between the AC source and the VSC is controlled by the phase angle  $\delta_{vR}$ . Active power flows into the VSC from the AC source for lagging  $\delta_{vR}$  ( $\delta_{vR} > 0$ ) and flows out of the VSC from the AC source for leading  $\delta_{vR}$  ( $\delta_{vR} < 0$ ).
- The reactive power flow is determined mainly by the magnitude of the voltage source,  $V_s$ , and the VSC output fundamental voltage,  $V_{vR}$ . For  $V_{vR} > V_s$ , the VSC generates reactive power and consumes reactive power when  $V_{vR} < V_s$ .

The DC capacitor voltage  $V_{DC}$  is controlled by adjusting the active power flow that goes into the VSC. During normal operation, a small amount of active power must flow into the VSC to compensate for the power losses inside the VSC, and  $\delta_{vR}$  is kept slightly larger than  $0^\circ$  (lagging).

The various power system controllers that use the VSC as their basic building block are addressed below with reference to key steady-state operational characteristics and their impact on system voltage and power flow control.

### 2.4.2 The Static Compensator

The STATCOM consists of one VSC and its associated shunt-connected transformer. It is the static counterpart of the rotating synchronous condenser but it generates or absorbs reactive power at a faster rate because no moving parts are involved. In principle, it performs the same voltage regulation function as the SVC but in a more robust manner because, unlike the SVC, its operation is not impaired by the presence of low voltages (IEEE/CIGRÉ, 1995).

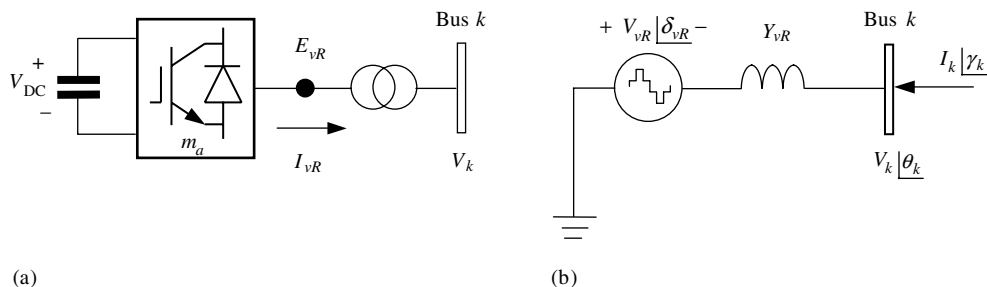


**Figure 2.18** Static compensator (STATCOM) system: (a) voltage source converter (VSC) connected to the AC network via a shunt-connected transformer; (b) shunt solid-state voltage source

A schematic representation of the STATCOM and its equivalent circuit are shown in Figures 2.18(a) and 2.18(b), respectively. The equivalent circuit corresponds to the Thevenin equivalent as seen from bus  $k$ , with the voltage source  $E_{vR}$  being the fundamental frequency component of the VSC output voltage, resulting from the product of  $V_{DC}$  and  $m_a$ .

In steady-state fundamental frequency studies the STATCOM may be represented in the same way as a synchronous condenser, which in most cases is the model of a synchronous

generator with zero active power generation. A more flexible model may be realised by representing the STATCOM as a variable voltage source  $E_{vR}$ , for which the magnitude and phase angle may be adjusted, using a suitable iterative algorithm, to satisfy a specified voltage magnitude at the point of connection with the AC network. The shunt voltage source of the three-phase STATCOM may be represented by:

$$E_{vR}^\rho = V_{vR}^\rho (\cos \delta_{vR}^\rho + j \sin \delta_{vR}^\rho), \quad (2.64)$$

where  $\rho$  indicates phase quantities,  $a$ ,  $b$ , and  $c$ .

The voltage magnitude,  $V_{vR}^\rho$ , is given maximum and minimum limits, which are a function of the STATCOM capacitor rating. However,  $\delta_{vR}^\rho$  may take any value between 0 and  $2\pi$  radians.

With reference to the equivalent circuit shown in Figure 2.18(b), and assuming three-phase parameters, the following transfer admittance equation can be written:

$$[\mathbf{I}_k] = [\mathbf{Y}_{vR} \quad -\mathbf{Y}_{vR}] \begin{bmatrix} \mathbf{V}_k \\ \mathbf{E}_{vR} \end{bmatrix}, \quad (2.65)$$

where

$$\mathbf{I}_k = [I_k^a \angle \gamma_k^a \quad I_k^b \angle \gamma_k^b \quad I_k^c \angle \gamma_k^c]^t, \quad (2.66)$$

$$\mathbf{V}_k = [V_k^a \angle \theta_k^a \quad V_k^b \angle \theta_k^b \quad V_k^c \angle \theta_k^c]^t, \quad (2.67)$$

$$\mathbf{E}_{vR} = [V_{vRk}^a \angle \delta_{vRk}^a \quad V_{vRk}^b \angle \delta_{vRk}^b \quad V_{vRk}^c \angle \delta_{vRk}^c]^t, \quad (2.68)$$

$$\mathbf{Y}_{vR} = \begin{bmatrix} Y_{vRk}^a & 0 & 0 \\ 0 & Y_{vRk}^b & 0 \\ 0 & 0 & Y_{vRk}^c \end{bmatrix}. \quad (2.69)$$

### 2.4.3 The Solid State Series Compensator

For the purpose of steady-state operation, the SSSC performs a similar function to the static phase shifter; it injects voltage in quadrature with one of the line end voltages in order to regulate active power flow. However, the SSSC is a far more versatile controller than the phase shifter because it does not draw reactive power from the AC system; it has its own reactive power provisions in the form of a DC capacitor. This characteristic makes the SSSC capable of regulating not only active but also reactive power flow or nodal voltage magnitude. This functionality is addressed further in Section 2.5. A schematic representation of the SSSC and its equivalent circuit are shown in Figures 2.19(a) and 2.19(b), respectively.

The series voltage source of the three-phase SSSC may be represented by

$$E_{cR}^\rho = V_{cR}^\rho (\cos \delta_{cR}^\rho + j \sin \delta_{cR}^\rho), \quad (2.70)$$

where  $\rho$  indicates phase quantities,  $a$ ,  $b$ , and  $c$ .

The magnitude and phase angle of the SSSC model are adjusted by using any suitable iterative algorithm to satisfy a specified active and reactive power flow across the SSSC. Similar to the STATCOM, maximum and minimum limits will exist for the voltage

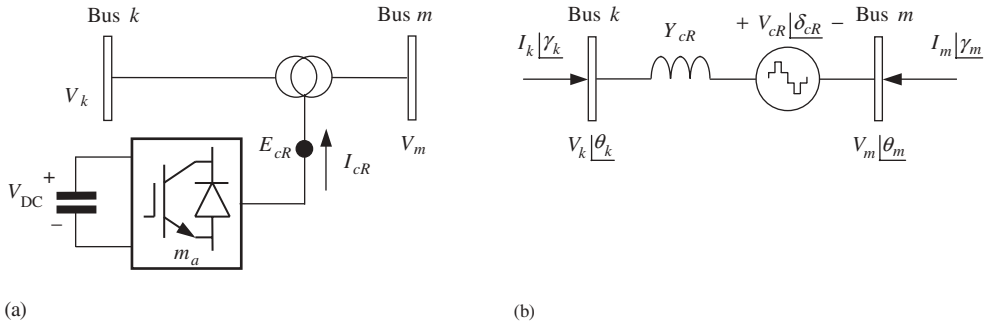


**Figure 2.19** Solid state series compensator (SSSC) system: (a) voltage source converter (VSC) connected to the AC network using a series transformer and (b) series solid state voltage source

magnitude  $V_{cR}$ , which are a function of the SSSC capacitor rating; the voltage phase angle  $\delta_{cR}$  can take any value between 0 and  $2\pi$  radians. The control capabilities of the SSSC are addressed in Section 2.5.

Based on the equivalent circuit shown in Figure 2.19(b), and assuming three-phase parameters, the following transfer admittance equation can be written:

$$\begin{bmatrix} \mathbf{I}_k \\ \mathbf{I}_m \end{bmatrix} = \begin{bmatrix} \mathbf{Y}_{cR} & -\mathbf{Y}_{cR} & -\mathbf{Y}_{cR} \\ -\mathbf{Y}_{cR} & \mathbf{Y}_{cR} & \mathbf{Y}_{cR} \end{bmatrix} \begin{bmatrix} \mathbf{V}_k \\ \mathbf{V}_m \\ \mathbf{E}_{cR} \end{bmatrix}. \quad (2.71)$$

In addition to parameters used in Equations (2.66)–(2.69) the following quantities are defined:

$$\mathbf{I}_m = [I_m^a \angle \gamma_m^a \quad I_m^b \angle \gamma_m^b \quad I_m^c \angle \gamma_m^c]^t, \quad (2.72)$$

$$\mathbf{V}_m = [V_m^a \angle \theta_m^a \quad V_m^b \angle \theta_m^b \quad V_m^c \angle \theta_m^c]^t, \quad (2.73)$$

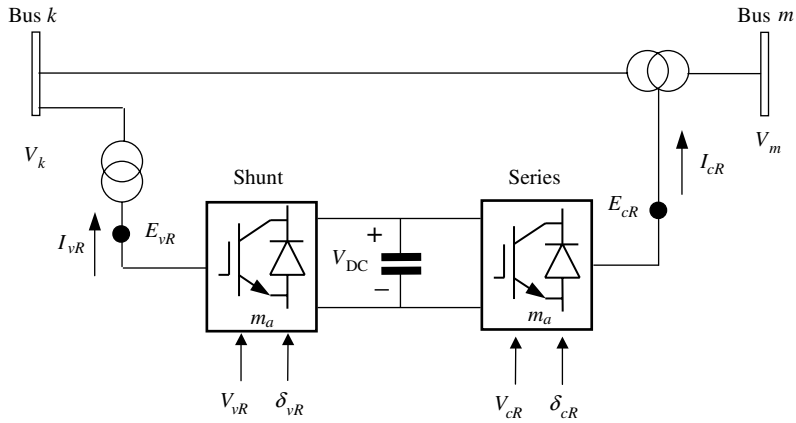
$$\mathbf{E}_{cR} = [V_{cR}^a \angle \delta_{cR}^a \quad V_{cR}^b \angle \delta_{cR}^b \quad V_{cR}^c \angle \delta_{cR}^c]^t, \quad (2.74)$$

$$\mathbf{Y}_{cR} = \begin{bmatrix} Y_{cRk}^a & 0 & 0 \\ 0 & Y_{cRk}^b & 0 \\ 0 & 0 & Y_{cRk}^c \end{bmatrix}. \quad (2.75)$$

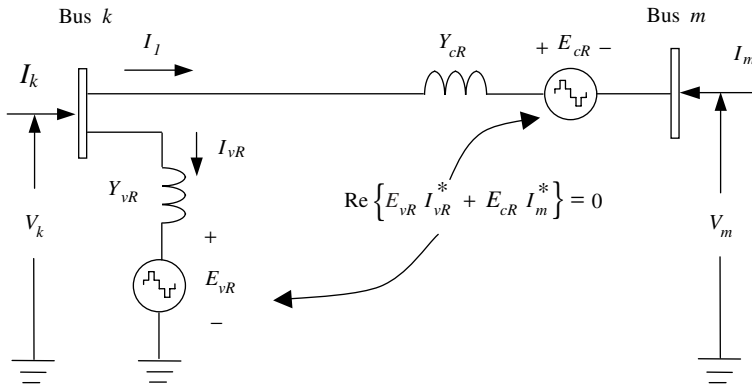
### 2.4.4 The Unified Power Flow Controller

The UPFC may be seen to consist of two VSCs sharing a common capacitor on their dc side and a unified control system. A simplified schematic representation of the UPFC is given in Figure 2.20(a), together with its equivalent circuit, in Figure 2.20(b) (Nabavi-Niaki and Iravani, 1996).

The UPFC allows simultaneous control of active power flow, reactive power flow, and voltage magnitude at the UPFC terminals. Alternatively, the controller may be set to control one or more of these parameters in any combination or to control none of them (Fuerte-Esquivel, Acha, and Ambriz-Pérez, 2000b).



(a)



(b)

**Figure 2.20** Unified power flow controller (UPFC) system: (a) two back-to-back voltage source converters (VSCs), with one VSC connected to the AC network using a shunt transformer and the second VSC connected to the AC network using a series transformer; (b) equivalent circuit based on solid-state voltage sources. Redrawn, with permission, from A. Nabavi-Niaki and M.R. Iravani, ‘Steady-state and Dynamic Models of Unified Power Flow Controller (UPFC) for Power System Studies’, *IEEE Trans. Power Systems* **11**(4) 1937–1943, © 1996 IEEE

The active power demanded by the series converter is drawn by the shunt converter from the AC network and supplied to bus  $m$  through the DC link. The output voltage of the series converter is added to the nodal voltage, at say bus  $k$ , to boost the nodal voltage at bus  $m$ . The voltage magnitude of the output voltage  $V_{cR}$  provides voltage regulation, and the phase angle  $\delta_{cR}$  determines the mode of power flow control (Hingorani and Gyugyi, 2000).

In addition to providing a supporting role in the active power exchange that takes place between the series converter and the AC system, the shunt converter may also generate or absorb reactive power in order to provide independent voltage magnitude regulation at its point of connection with the AC system.

The UPFC equivalent circuit shown in Figure 2.20(b) consists of a shunt-connected voltage source, a series-connected voltage source, and an active power constraint equation, which links the two voltage sources. The two voltage sources are connected to the AC system through inductive reactances representing the VSC transformers. In a three-phase UPFC, suitable expressions for the two voltage sources and constraint equation would be:

$$E_{vR}^\rho = V_{vR}^\rho (\cos \delta_{vR}^\rho + j \sin \delta_{vR}^\rho), \quad (2.76)$$

$$E_{cR}^\rho = V_{cR}^\rho (\cos \delta_{cR}^\rho + j \sin \delta_{cR}^\rho), \quad (2.77)$$

$$\text{Re}\{-E_{vR}^\rho I_{vR}^{*\rho} + E_{cR}^\rho I_m^{*\rho}\} = 0. \quad (2.78)$$

where  $\rho$  indicates phase quantities,  $a$ ,  $b$ , and  $c$ .

Similar to the shunt and series voltage sources used to represent the STATCOM and the SSSC, respectively, the voltage sources used in the UPFC application would also have limits.

Based on the equivalent circuit shown in Figure 2.20(b), and assuming three-phase parameters, the following transfer admittance equation can be written:

$$\begin{bmatrix} \mathbf{I}_k \\ \mathbf{I}_m \end{bmatrix} = \begin{bmatrix} (\mathbf{Y}_{cR} + \mathbf{Y}_{vR}) & -\mathbf{Y}_{cR} & -\mathbf{Y}_{cR} & -\mathbf{Y}_{vR} \\ -\mathbf{Y}_{cR} & \mathbf{Y}_{cR} & \mathbf{Y}_{cR} & \mathbf{0} \end{bmatrix} \begin{bmatrix} \mathbf{V}_k \\ \mathbf{V}_m \\ \mathbf{E}_{cR} \\ \mathbf{E}_{vR} \end{bmatrix}, \quad (2.79)$$

where all the parameters have been defined in Equations (2.66)–(2.69) and (2.72)–(2.75).

### 2.4.5 The High-voltage Direct-current Based on Voltage Source Converters

The HVDC-VSC comprises two VSCs, one operating as a rectifier and the other as an inverter. The two converters are connected either back-to-back or joined together by a DC cable, depending on the application. Its main function is to transmit constant DC power from the rectifier to the inverter station, with high controllability. A schematic representation of the HVDC-VSC and its equivalent circuit are shown in Figures 2.21(a) and 2.21(b), respectively.

One VSC controls DC voltage and the other the transmission of active power through the DC link. Assuming loss-less converters, the active power flow entering the DC system must equal the active power reaching the AC system at the inverter end minus the transmission losses in the DC cable. During normal operation, both converters have independent reactive power control (Asplund, 2000).

The HVDC-VSC system is suitably represented by two shunt-connected voltage sources linked together by an active power constraint equation. Each voltage source is connected to the AC system by means of its transformer reactance. Suitable expressions for the three-phase voltage sources and the linking power equation are:

$$E_{vR1}^\rho = V_{vR1}^\rho (\cos \delta_{vR1}^\rho + j \sin \delta_{vR1}^\rho), \quad (2.80)$$

$$E_{vR2}^\rho = V_{vR2}^\rho (\cos \delta_{vR2}^\rho + j \sin \delta_{vR2}^\rho), \quad (2.81)$$

$$\text{Re}\{-E_{vR1}^\rho I_{vR1}^{*\rho} + E_{vR2}^\rho I_m^{*\rho}\} = 0, \quad (2.82)$$

where  $\rho$  indicates phase quantities,  $a$ ,  $b$ , and  $c$ .

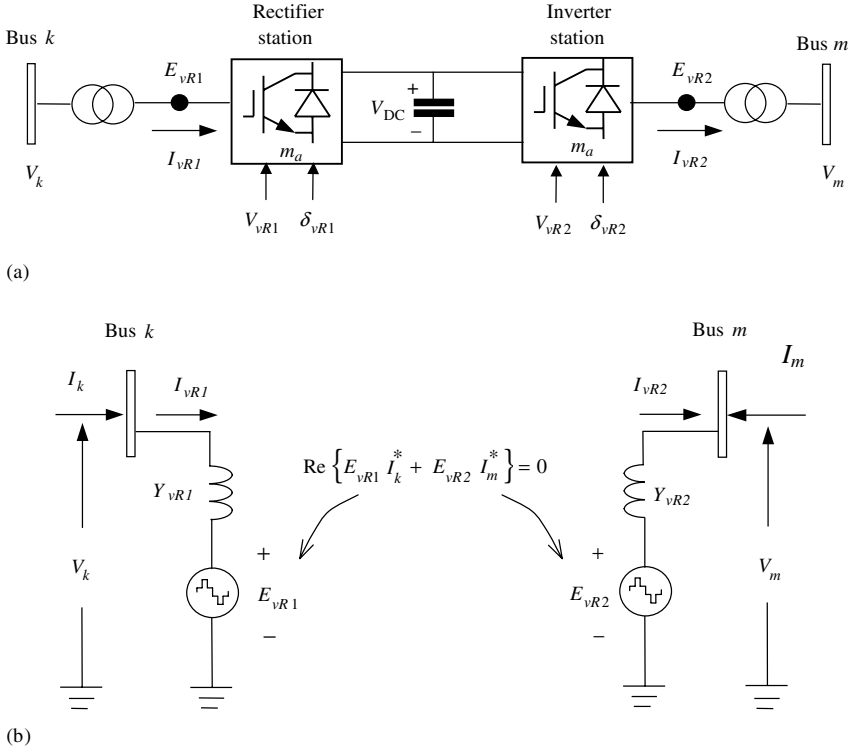


**Figure 2.21** High-voltage direct-current based on voltage source converter (HVDC-VSC) system: (a) the VSC at the sending end performs the role of rectifier, and the VSC at the receiving end performs the role of inverter; (b) equivalent circuit

In this application, the two shunt voltage sources used to represent the rectifier and inverter stations have the following voltage magnitudes and phase angles limits:

$$\begin{aligned}
 V_{vR \min 1}^\rho &< V_{vR1}^\rho < V_{vR \max 1}^\rho, \\
 0 &< \delta_{vR1}^\rho < 2\pi, \\
 V_{vR \min 2}^\rho &< V_{vR2}^\rho < V_{vR \max 2}^\rho, \\
 0 &< \delta_{vR2}^\rho < 2\pi.
 \end{aligned}$$

Based on the equivalent circuit shown in Figure 2.21(b), and assuming three-phase parameters, the following transfer admittance equation can be written:

$$\begin{bmatrix} \mathbf{I}_k \\ \mathbf{I}_m \end{bmatrix} = \begin{bmatrix} \mathbf{Y}_{vR1} & -\mathbf{Y}_{vR1} & \mathbf{0} & \mathbf{0} \\ \mathbf{0} & \mathbf{0} & \mathbf{Y}_{vR2} & -\mathbf{Y}_{vR2} \end{bmatrix} \begin{bmatrix} \mathbf{V}_k \\ \mathbf{E}_{vR1} \\ \mathbf{V}_m \\ \mathbf{E}_{vR2} \end{bmatrix}, \quad (2.83)$$

where all the parameters have been defined in Equations (2.66)–(2.69) and (2.72)–(2.75).

## 2.5 CONTROL CAPABILITIES OF CONTROLLERS BASED ON VOLTAGE SOURCE CONVERTERS

To a greater or lesser extent, the three ‘series’ VSC-based controllers, namely the SSSC, the UPFC, and the HVDC-VSC, share similar power system control capabilities. They are able to regulate either nodal voltage magnitude or injection of reactive power at one of its terminals, and active power flow through the controller. The UPFC and the HVDC-VSC employ two converters and are able to regulate nodal voltage magnitude with one of them and reactive power injection with the other. From the perspective of fundamental frequency power system studies, there is little difference between the control flexibility afforded by the three controllers, except that the UPFC and HVDC-SVC do it more robustly than does the SSSC. The individual control functions are illustrated in Figure 2.22, with reference to the operating regions of the SSSC.

The equivalent circuit of the SSSC shown Figure 2.19(b) is used as the basis for the analysis. The voltage magnitude of  $V_m|\theta_m$  can be controlled at a specified value by injecting an in-phase or antiphase voltage increment  $\Delta V_{cR}|\delta_{cR} = \theta_m$ , as illustrated in Figure 2.22(a). Notice that for the purpose of drawing the phasor diagrams in Figure 2.22, the phase angle  $\theta_m$  is taken to have a value of  $0^\circ$ . Series reactive compensation can be achieved by injecting a complex voltage,  $\Delta V_{cR}|\delta_{cR} = \gamma_m \pm 90^\circ$ , which is in quadrature with the line current,  $I_m|\gamma_m$ , as illustrated in Figure 2.22(b). Pure phase-angle control is also possible, as shown in Figure 2.22(c), by injecting an angular quantity,  $1|\pm\delta_{cR}$ , to the otherwise unaffected voltage,  $V_m|\theta_m$ . Furthermore, all three functions can be applied simultaneously by injecting an incremental complex voltage  $\Delta V_{cR}|\delta_{cR}$  to  $V_m|\theta_m$ , as shown in Figure 2.22(d), a characteristic that adds unrivalled flexibility in power system operation.

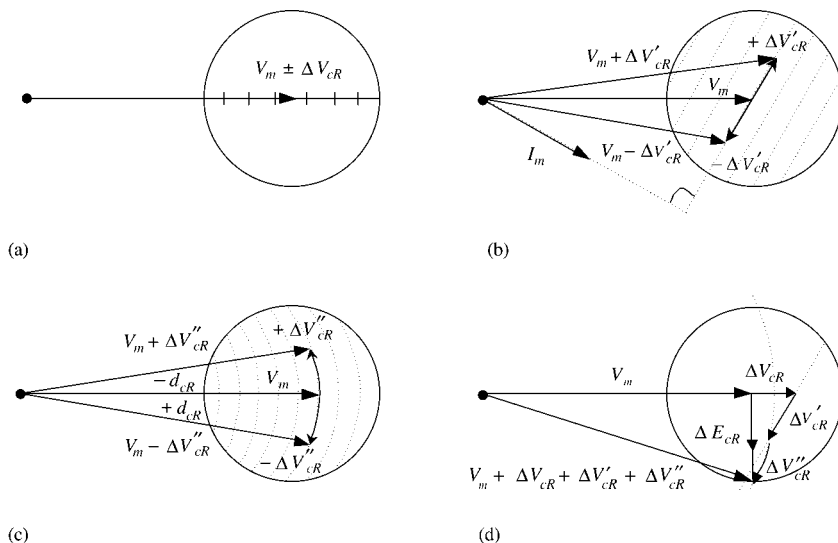


**Figure 2.22** Phasor diagram illustrating the general concept of: (a) magnitude voltage control, (b) impedance line compensation, (c) phase-angle regulation, and (d) simultaneous control. Redrawn, with permission, from Institute of Electrical and Electronic Engineers/Conseil International des Grands Réseaux Électrique, *FACTS Overview*, © 1995 IEEE

## 2.6 SUMMARY

This chapter has presented an overview of the most salient characteristics of the power electronic equipment currently used in the electricity supply industry for the purpose of voltage regulation, active and reactive power flow control, and power quality enhancement. The emphasis has been on steady-state operation, and a distinction has been made between power electronic equipment, which uses conventional power semiconductor devices (i.e. thyristors) and the new generation of power system controllers, which use fully controllable semiconductor devices such as GTOs and IGBTs. The latter devices work well with fast switching control techniques, such as the sinusoidal PWM control scheme, and, from the power system perspective, operate like voltage sources, having an almost delay-free response. Equipment based on thyristors have a slower speed of response, greater than one cycle of the fundamental frequency, and use phase control as opposed to PWM control. From the power system perspective, thyristor-based controllers behave like controllable reactances as opposed to voltage sources.

The TCR, SVC, and TCSC belong to the category of thyristor-based equipment. The STATCOM, SSSC, UPFC, and HVDC-VSC use the VSC as their basic building block. It has been emphasised that all these power electronic controllers produce harmonic distortion, which is an undesirable side-effect, as part of their normal operation. The various means of harmonic cancellation open to system engineers have been mentioned, such as switching control, multilevel configurations, three-phase connections, and, as a last resort, filtering equipment. The remit of this book is not power system harmonics; hence, it is assumed that harmonic distortion is effectively contained at source. The mathematical modelling conducted for the various power electronic controllers addressed in the chapter reflect this fact. The emphasis has been on deriving flexible models in the form of nodal admittance matrices that use the frame of reference of the phases, which is a frame of reference closely associated with the physical structure of the actual power system plant. A major strength of this frame of reference is that all design and operational imbalances present in the power system are incorporated quite straightforwardly in the model. Nevertheless, it is acknowledged that very often it is desirable to reduce the comprehensiveness of the power system solution and to carry out the study in the frame of reference of the sequences rather than in that of the phases. This has the advantage of speedier calculations, but key information becomes unavailable since sequence domain modelling tacitly assumes that no imbalances are present in the plant being modelled. When such an assumption is incorporated in the phase domain nodal admittance models, it yields simpler models expressed in the frame of reference of the sequences.

The phase domain nodal admittance models are used in Chapter 6 as the basis for developing the power flow equations of three-phase power systems. Similarly, the sequence domain nodal admittance models are used to develop in Chapter 5 the power flow equations of positive sequence power systems.

## REFERENCES

Acha, E., Madrigal, M., 2001, *Power System Harmonics: Computer Modelling and Analysis*, John Wiley & Sons, Chichester.

- Anaya-Lara, O., Acha, E., 2002, Modelling and Analysis of Custom Power Systems by PSCAD/EMTDC', *IEEE Trans. Power Delivery* **7**(1) 266–272.
- Arrillaga, J., 1998, *High Voltage Direct Current Transmission*, 2nd edn, Institution of Electrical Engineers, London.
- Arrillaga, J., Arnold, C.P., 1990, *Computer Analysis of Power Systems*, John Wiley & Sons, Chichester.
- Asplund, G., 2000, Application of HVDC Light to Power System Enhancement', IEEE Winter Meeting, Session on Development and Application of Self-commutated Converters in Power Systems, Singapore, January 2000.
- Christl, N., Hedin R., Sadek, K., Lutzberger, P., Krause, P.E., McKenna, S.M., Montoya, A.H., Torgerson, D., 1992, 'Advanced Series Compensation (ASC) with Thyristor Controlled Impedance', International Conference on Large High Voltage Electric Systems (CIGRÉ), Paper 14/37/38-05, Paris, September 1992.
- Fuerte-Esquivel, C.R., Acha, E., Ambriz-Pérez, H., 2000a, 'A Thyristor Controlled Series Compensator Model for the Power Flow Solution of Practical Power Networks', *IEEE Trans. Power Systems* **15**(1) 58–64.
- Fuerte-Esquivel, C.R., Acha, E., Ambriz-Pérez, H., 2000b, 'A Comprehensive UPFC Model for the Quadratic Load Flow Solution of Power Networks', *IEEE Trans. Power Systems* **15**(1) 102–109.
- Hingorani, N.G., 1993, 'Flexible AC Transmission Systems', *IEEE Spectrum* **30**(4) 41–48.
- Hingorani, N.G., 1995, 'Introducing Custom Power', *IEEE Spectrum* **32**(6) 41–48.
- Hingorani, N.G., 1996, 'High Voltage DC Transmission: a Power Electronics work-horse', *IEEE Spectrum*, Vol. 33, No. 4, April 1996, pp. 63–72.
- Hingorani, N.G., 1998, 'High Power Electronics and Flexible AC Transmission Systems', *IEEE Power Engineering Review* (July) 3–4.
- Hingorani, N.G., Gyugyi, L., 2000 *Understanding FACTS Concepts and Technology of Flexible AC Transmission Systems*, Institute of Electrical and Electronic Engineers, New York.
- IEEE/CIGRÉ (Institute of Electrical and Electronic Engineers/Conseil International des Grands Réseaux Électriques) *FACTS Overview*, Special Issue, 95TP108, IEEE Service Center, Piscataway, NJ.
- Kinney, S.J., Mittelstadt, W.A., Suhrbier, R.W., 1995, 'Test Results and Initial Operating Experience for the BPA 500 kV Thyristor Controlled Series Capacitor: Design, Operation, and Fault Test Results, Northcon 95', in *IEEE Technical Conference and Workshops Northcon 95, Portland, Oregon, USA, October 1995*, IEEE, New York, pp. 268–273.
- Kundur, P., 1994, *Power System Stability and Control*, McGraw-Hill, New York.
- Larsen, E.V., Bowler, C., Damsky, B., Nilsson, S., 1992, 'Benefits of Thyristor Controlled Series Compensation', International Conference on Large High Voltage Electric Systems (CIGRÉ), Paper 14/37/38-04, Paris, September 1992.
- McMurray, W., 1987, 'Feasibility of GTO Thyristors in a HVDC Transmission System', EPRI EL-5332, Project 2443-5, Final Report, August 1987, Electric Power Research Institute.
- Miller, T.J.E., 1982, *Reactive Power Control in Electric Systems*, John Wiley Interscience, Chichester.
- Mohan, N., Undeland, T.M., Robbins, W.P., 1995, *Power Electronics: Converter Applications and Design*, 2nd edn, John Wiley & Sons, Chichester.
- Nabavi-Niaki, A., Irvani, M.R., 1996, 'Steady-state and Dynamic Models of Unified Power Flow Controller (UPFC) for Power System Studies', *IEEE Trans. Power Systems* **11**(4) 1937–1943.
- Raju, N.R., Venkata, S.S., Sastry, V.V., 1997, 'The Use of Decoupled Converters to Optimise the Power Electronics of Shunt and Series AC System Controllers', *IEEE Trans. Power Delivery* **12**(2) 895–900.
- Stagg, G.W., El-Abiad, H., 1968, *Computer Methods in Power Systems Analysis*, McGraw-Hill, New York.
- Wood, A.J., Wollenberg, B., 1984, *Power Generation, Operation and Control*, 2nd edn, John Wiley & Sons, Chichester.

# 3

## Modelling of Conventional Power Plant



### 3.1 INTRODUCTION

The conventional elements of an electrical power system are: generators, transformers, transmission lines, cables, loads, banks of capacitors, nonlinear inductors, and protection and control equipment. These elements are suitably interconnected to enable the generation of electricity in sufficient quantity to meet system demand at any one point in time. The operational objective is to transmit the electricity to the load centres at minimum production cost, maximum reliability, and minimum transmission loss (Elgerd, 1982).

For most practical purposes, the electrical power network may be divided into four subsystems, namely, generation, transmission, distribution, and utilisation. Transmission networks operate at high voltages, typically in the range 500–132 kV, although even higher voltages are used in parts of North America (Weedy, 1987). Conversely, electricity is produced at relatively low voltages, in the range of 25–11 kV, and step-up transformers are used at the generator substation to increase the voltage up to transmission levels. In contrast, step-down transformers are used to reduce the high voltages used in transmission systems to levels that are appropriate for industrial, commercial, and residential applications. In the United Kingdom, a typical voltage level used in distribution networks is 33 kV; and industrial and residential consumers are fed at 11 kV and 415 V or 240 V.

Three-phase synchronous generators are used to produce most of the electricity consumed worldwide (Grainger and Stevenson, 1994) and, except for a small percentage which is transported in direct current (DC) form using high-voltage direct-current (HVDC) links, all electricity is brought to the points of demand using alternating current (AC) three-phase transmission lines and cables. This point deserves further analysis because quite often the generating stations are located far away from where the load sites are, and long-distance transmission becomes necessary (Shlash, 1974). More often than not, long-distance transmission circuits consist of more than one three-phase circuit, and contain series and shunt compensation to enable stable operation. Nevertheless, it has long been recognised that remote generating stations, which are mostly of the hydroelectric type, are only weakly interconnected and that the nonuniform nature of their rotors (i.e. saliency) increases the overall system unbalance. It should also be remarked that the windings of

three-phase transformers can be connected in a variety of ways to suit specific requirements and that transformer connections should be modelled explicitly when system imbalances cannot be ignored in power system studies (Hesse, 1966). The bulk load points associated with transmission systems may be taken to be highly balanced, but such an assumption is no longer valid in low-voltage distribution systems, where load points may be highly unbalanced owing to an abundance of individual single-phase loads within a distribution load point.

The application tool used to assess the steady-state operation of power systems exhibiting a considerable degree of geometric unbalance or load unbalance is known as three-phase power flow (Chen and Dillon, 1974; Laughton, 1968; Wasley and Shlash, 1974a). In this application, all operations are carried out on a per-phase basis, and all power plant components making up the power system are modelled in the frame of reference of the phases (Chen *et al.*, 1990; Harker and Arrillaga, 1979). However, if system geometric imbalances may be taken to be insignificant and system load is balanced then there is much numerical advantage to be gained by representing all power plant components in the frame of reference of the sequences as opposed to that of the phases. In this situation, a positive sequence power flow solution can be carried out, as opposed to the full blown three-phase solution.

### 3.2 TRANSMISSION LINE MODELLING

High-voltage and extra-high-voltage transmission lines consist of a group of phase conductors, which are responsible for transmitting the electrical energy. All power network transmission lines are located at a finite distance from the earth’s surface and may use the ground as a return path. Accordingly, it becomes necessary to take this effect into account when calculating transmission-line parameters (Anderson, 1973). High-voltage transmission lines may contain several conductors per phase (bundle conductors) and ground wires, and distribution lines may include a neutral wire as a return path. Transmission and primary distribution circuits may be responsible for introducing considerable geometric imbalances, even at the fundamental frequency, depending on their electrical distance (Acha and Madrigal, 2001; Arrillaga *et al.*, 1997).

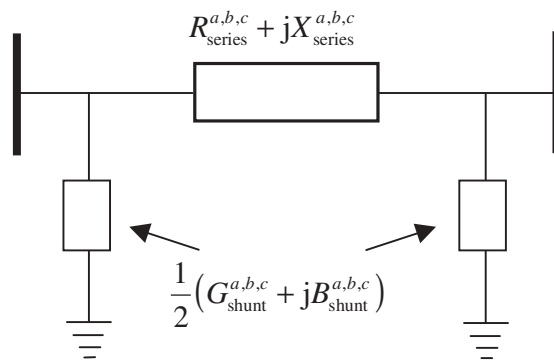


Figure 3.1 Transmission line representation in the form of an equivalent  $\pi$ -circuit

In power system studies it is current practice to model the inductive and resistive effects of multiconductor transmission lines as a series impedance matrix, and the capacitive effects as a shunt admittance matrix. The overall transmission line model can then be represented by either a nominal  $\pi$ -circuit or an equivalent  $\pi$ -circuit, as shown in Figure 3.1, if the electrical length of the line is sufficient to merit the extra work involved in calculating it.

### 3.2.1 The Voltage-drop Equation

The phase conductors of a three-phase transmission line, with ground as the return path and negligible capacitive effects, are illustrated schematically in Figure 3.2. If the circuit terminal conditions enable current to flow in conductors  $a, b, c$ , and in the ground return path, the voltage-drop equation of the transmission line shown in Figure 3.2, at a given frequency, may be expressed in matrix form as follows:

$$\begin{bmatrix} V_a \\ V_b \\ V_c \end{bmatrix} = \begin{bmatrix} R_{aa-g} + j\omega L_{aa-g} & R_{ab-g} + j\omega L_{ab-g} & R_{ac-g} + j\omega L_{ac-g} \\ R_{ba-g} + j\omega L_{ba-g} & R_{bb-g} + j\omega L_{bb-g} & R_{bc-g} + j\omega L_{bc-g} \\ R_{ca-g} + j\omega L_{ca-g} & R_{cb-g} + j\omega L_{cb-g} & R_{cc-g} + j\omega L_{cc-g} \end{bmatrix} \begin{bmatrix} I_a \\ I_b \\ I_c \end{bmatrix} + \begin{bmatrix} V'_a \\ V'_b \\ V'_c \end{bmatrix}, \quad (3.1)$$

the subscript  $g$  indicating that the ground return effect has been included.

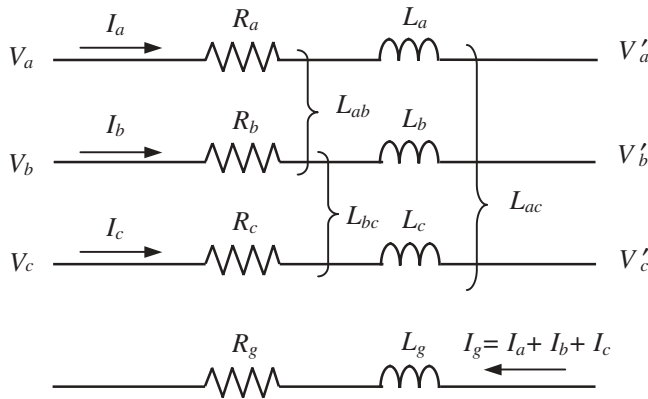


**Figure 3.2** Phase conductors of a three-phase transmission line

#### 3.2.1.1 Calculation of lumped RLC parameters

The computation of three-phase transmission line parameters becomes cumbersome by the existence of inductive and capacitive couplings between conductors, and between conductors and ground (Anderson, 1973). Moreover, resistances and self and mutual inductances vary nonlinearly with frequency and, together with the capacitive effects, vary nonlinearly with the electrical distance of the line (Acha and Madrigal, 2001; Arrillaga et al., 1997).

In fundamental frequency power system applications, it is normal practice to calculate the inductive and capacitive effects of the transmission line independently and then to combine

them together to give the final transmission-line representation. Once the resistances, inductances, and capacitances associated with a particular transmission line configuration have been determined, a transmission-line model in the form of a  $\pi$ -circuit, or any other alternative representation, become feasible.

The series impedance matrix  $\mathbf{Z}_{series}$  of a multiconductor transmission line, which takes account of geometric imbalances and frequency dependency but not long-line effects, may be assumed to consist of the following components:

$$\mathbf{Z}_{series} = \mathbf{Z}_{internal} + \mathbf{Z}_{geometric} + \mathbf{Z}_{ground}. \tag{3.2}$$

In Equation (3.2),  $\mathbf{Z}_{internal}$  is the impedance inside the conductors,  $\mathbf{Z}_{ground}$  is the impedance contribution of the ground return path, and  $\mathbf{Z}_{geometric}$  is the impedance contribution from the magnetic fluxes in the air surrounding the conductors. For most practical purposes, the parameters  $\mathbf{Z}_{geometric}$  may be taken to be linear functions of the potential coefficients  $\mathbf{P}$ . Unlike  $\mathbf{Z}_{internal}$ , the parameters  $\mathbf{Z}_{ground}$ ,  $\mathbf{Z}_{geometric}$ , and  $\mathbf{P}$  are a function of the physical geometry of the conductor's arrangement in the tower. The capacitive effects are incorporated in the shunt admittance matrix  $\mathbf{Y}_{shunt}$ , which is a linear function of  $\mathbf{P}$ . Shunt parameters are addressed in Section 3.2.1.2.

If the surfaces of the conductors and the earth beneath the conductors may be assumed to be equipotential surfaces then the standard method of images may be used to calculate the potential coefficients  $\mathbf{P}$ .

The method of images allows the conducting plane to be replaced by a fictitious conductor located at the mirror image of the actual conductors. Figure 3.3 shows the case when phase conductors  $a$ ,  $b$ , and  $c$  above ground have been replaced by three equivalent conductors and their images (Anderson, 1973).

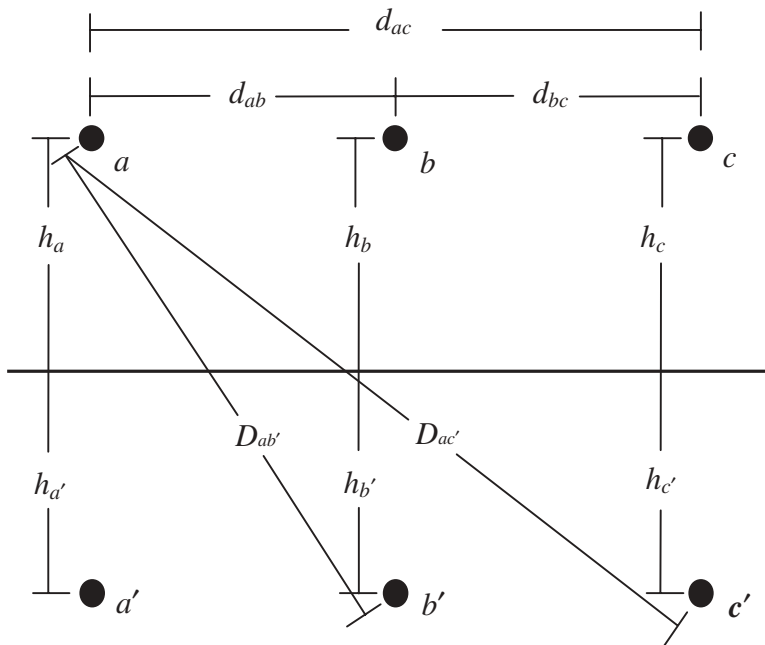


Figure 3.3 Line geometry and its image

The self-potential coefficient of an overhead conductor is solely a function of the height of the conductor above ground, say  $h$ , and the external radius of the conductor, say  $r_{\text{ext}}$ . In contrast, the mutual potential coefficient between two conductors is a function of the separation between the two conductors,  $d$ , and the separation between one conductor and the image of the second conductor,  $D$ . For the three conductors in the transmission line shown in Figure 3.3, the matrix of potential coefficients is

$$\mathbf{P} = \begin{bmatrix} \ln\left(\frac{2h_a}{r_{\text{ext } a}}\right) & \ln\left(\frac{D_{ab}}{d_{ab}}\right) & \ln\left(\frac{D_{ac}}{d_{ac}}\right) \\ \ln\left(\frac{D_{ba}}{d_{ba}}\right) & \ln\left(\frac{2h_b}{r_{\text{ext } b}}\right) & \ln\left(\frac{D_{bc}}{d_{bc}}\right) \\ \ln\left(\frac{D_{ca}}{d_{ca}}\right) & \ln\left(\frac{D_{cb}}{d_{cb}}\right) & \ln\left(\frac{2h_c}{r_{\text{ext } c}}\right) \end{bmatrix}. \quad (3.3)$$

It should be noted that potential coefficients are dimensionless and reciprocal.

The geometric impedance matrix for the circuit of Figure 3.3 is

$$\mathbf{Z}_{\text{geometric}} = j \frac{\omega \mu_0}{4\pi} \mathbf{P} \Omega \text{ km}^{-1}, \quad (3.4)$$

where  $\mathbf{Z}_{\text{geometric}}$  varies linearly with the base frequency  $f$ ,  $\omega = 2\pi f$ , and the permeability of free space is  $\mu_0 = 4\pi \times 10^{-4} \text{ H km}^{-1}$ .

### 3.2.1.2 Shunt admittances

Shunt admittance parameters vary linearly with frequency and are completely defined by the inverse potential coefficients (Anderson, 1973). The matrix of shunt admittance parameters for the circuit of Figure 3.3 is

$$\mathbf{Y}_{\text{shunt}} = j\omega 2\pi\epsilon_0 \mathbf{P}^{-1} \text{ S km}^{-1}, \quad (3.5)$$

where  $\epsilon_0$ , equal to  $8.85 \times 10^{-9} \text{ F km}^{-1}$ , is the permittivity of free space.

### 3.2.1.3 Internal impedances

It has long been recognised that the internal resistance and inductance of conductors vary with frequency in a nonlinear manner. The reason for this effect is attributed mainly to the nonuniform distribution of current flow over the full area available, with current tending to flow on the surface. This trend increases with frequency and is termed the ‘skin effect’. The overall effect is an increase in resistance and a decrease in internal inductance (Arrillaga *et al.*, 1997).

In power systems applications, the established formula for evaluating the impedance of an annular conductor, at a given frequency, uses the Bessel functions of zero order, first kind, and second kind and their derivatives, which are solved, within specified accuracy, using their associated infinite series. However, at power frequencies, the skin effect is negligibly small and there is little error in calculating the internal impedance of conductors by assuming that the magnetic field inside the conductor is confined to an area lying between the external radius,  $r_{\text{ext}}$ , of the conductor and the geometric mean radius (gmr),  $r_{\text{gmr}}$ , of the conductor (Grainger and Stevenson, 1994).

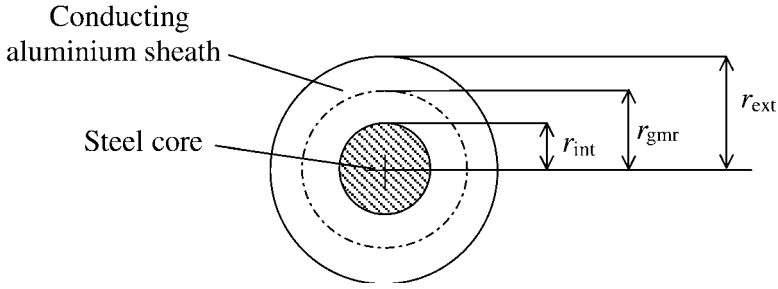


**Figure 3.4** Cross-section of a power conductor

As illustrated in Figure 3.4, the gmr lies between the external and internal radii of the conductor. The gmr is normally measured and made available by the manufacturer. An approximated, frequency-independent relationship is given by

$$r_{\text{gmr}} = e^{-1/4} r_{\text{ext}}. \quad (3.6)$$

If the frequency of interest is low enough for the skin effect to be of no consequence, then the concept of potential coefficients can be applied to calculate the internal impedance of conductors. For the three conductors in Figure 3.3, the matrix of internal potential coefficients is,

$$\mathbf{P}_{\text{internal}} = \begin{bmatrix} \ln\left(\frac{r_{\text{ext}1}}{r_{\text{gmr}1}}\right) & 0 & 0 \\ 0 & \ln\left(\frac{r_{\text{ext}2}}{r_{\text{gmr}2}}\right) & 0 \\ 0 & 0 & \ln\left(\frac{r_{\text{ext}3}}{r_{\text{gmr}3}}\right) \end{bmatrix}. \quad (3.7)$$

Hence, the conductor impedance matrix for this circuit is

$$\mathbf{Z}_{\text{internal}} = \mathbf{R}_{\text{ac}} + j \frac{\omega \mu_0}{4\pi} \mathbf{P}_{\text{internal}} \Omega \text{ km}^{-1}, \quad (3.8)$$

where  $\mathbf{R}_{\text{ac}}$  is a diagonal matrix with entries corresponding to the AC power frequency resistances (50 or 60 Hz) of the various conductors in the transmission circuit.

### 3.2.1.4 Ground return impedances

The impedance of the ground return path varies nonlinearly with frequency and exhibits an effect similar to that of the skin effect in conductors, where the effective area available for the current to flow reduces with frequency.

The problem of current-carrying wires above a flat earth of homogeneous conductivity, and the related issue of transmission-line parameter calculation, received a great deal of research attention almost a century ago. It was J.R. Carson who in 1926 published a comprehensive solution to the problem. The solution involves an infinite integral that cannot be solved analytically or in closed form. However, the integral is conveniently expressed by a set of infinite series that show good convergence characteristics for most problems encountered in the areas of electromagnetic fields, propagation characteristics, and magnetic

induction effects caused by power lines. Ever since, and perhaps because of the existence of the infinite series, the solution published by Carson has been extensively used by power engineers worldwide.

As the need arises to calculate ground impedances for a wide spectrum of frequencies, and also because of the uncertainty in the available data, in particular regarding ground conductivity, the tendency is to go for simpler formulations aiming at a reduction in computing time while keeping the accuracy at a reasonable level. Recent formulations use the concept of a complex mirroring surface beneath the ground. Rigorous mathematical analyses have shown these formulations to be good physical and mathematical approximations to Carson’s solution.

The most popular equations in power system applications are those attributed to C. Dubanton (Deri *et al.*, 1981). The reason is their simplicity and good accuracy for the whole span of frequencies for which Carson’s equations are valid. With reference to Figure 3.5, the equations for calculating the self-impedance of conductor *l* and the mutual impedance between conductors *l* and *m* take the following form:

$$Z_{ll} = j \frac{\omega\mu_0}{2\pi} \ln \left[ \frac{2(h_l + p)}{r_{ext\ l}} \right] \Omega \text{ km}^{-1}, \tag{3.9}$$

$$Z_{lm} = j \frac{\omega\mu_0}{2\pi} \ln \left\{ \frac{[(h_l + h_m + 2p)^2 + d_{lm}^2]^{1/2}}{[(h_l - h_m)^2 + d_{lm}^2]^{1/2}} \right\} \Omega \text{ km}^{-1}, \tag{3.10}$$

where *p*, equal to  $(j\omega\mu_0\sigma_g)^{1/2}$ , is the complex depth beneath the ground at which the mirroring surface is located.

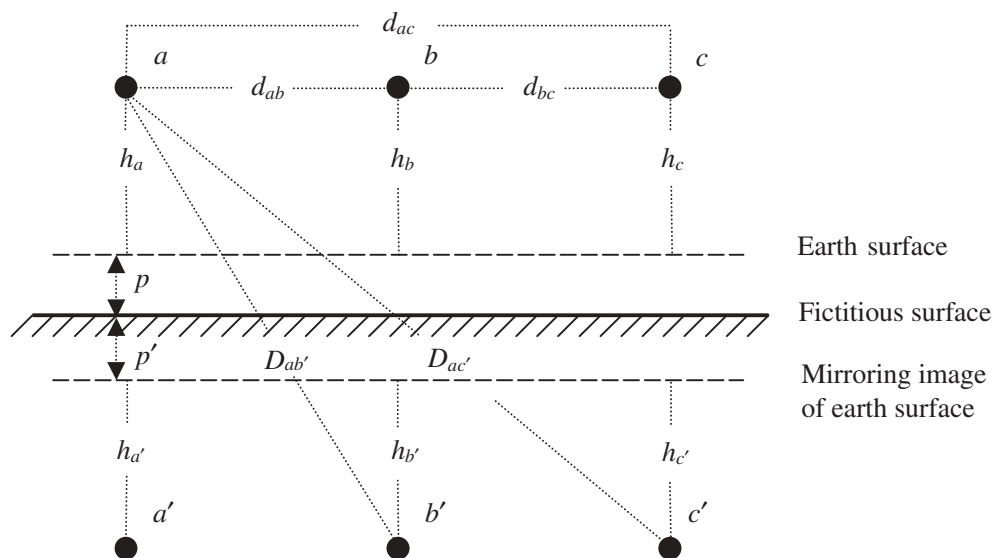


Figure 3.5 Line geometry showing the complex depth

It should be noted that the use of Equations (3.9) and (3.10) yields combined information of  $\mathbf{Z}_{\text{geometric}} + \mathbf{Z}_{\text{ground}}$ . Moreover, if the transmission-line parameters are intended for power frequency applications (50 or 60 Hz) then the skin effect inside the conductors can be ignored and Equation (3.9) can be combined with Equation (3.8) to take account of the impedance contribution from  $\mathbf{Z}_{\text{internal}}$ :

$$Z_{ll} = R_{ac\ l} + j \frac{\omega \mu_0}{2\pi} \ln \left[ \frac{2(h_l + p)}{r_{\text{gmr}\ l}} \right] \Omega \text{ km}^{-1}. \quad (3.11)$$

In summary, for the purpose of low-frequency power applications, Equations (3.10) and (3.11) may be used to calculate the individual elements of Equation (3.1). The impedance parameters include geometric imbalances and ground return effects but no full frequency dependency.

### 3.2.2 Ground Wires

Using the same notation as in Section 3.2.1, we may express the voltage-drop equation of a three-phase transmission line with two ground wires,  $w$  and  $v$ , as follows (Anderson, 1973):

$$\begin{bmatrix} V_a \\ V_b \\ V_c \\ V_w \\ V_v \end{bmatrix} = \begin{bmatrix} Z_{aa-g} & Z_{ab-g} & Z_{ac-g} & Z_{aw-g} & Z_{av-g} \\ Z_{ba-g} & Z_{bb-g} & Z_{bc-g} & Z_{bw-g} & Z_{bv-g} \\ Z_{ca-g} & Z_{cb-g} & Z_{cc-g} & Z_{cw-g} & Z_{cv-g} \\ Z_{wa-g} & Z_{wb-g} & Z_{wc-g} & Z_{ww-g} & Z_{wv-g} \\ Z_{va-g} & Z_{vb-g} & Z_{vc-g} & Z_{vw-g} & Z_{vv-g} \end{bmatrix} \begin{bmatrix} I_a \\ I_b \\ I_c \\ I_w \\ I_v \end{bmatrix} + \begin{bmatrix} V'_a \\ V'_b \\ V'_c \\ V'_w \\ V'_v \end{bmatrix}. \quad (3.12)$$

It is assumed that the individual impedance elements are calculated by using Equations (3.10) and (3.11). In compact notation, we have,

$$\Delta \mathbf{V}_{abc} = \mathbf{A} \mathbf{I}_{abc} + \mathbf{B} \mathbf{I}_{wv}, \quad (3.13)$$

$$\Delta \mathbf{V}_{wv} = \mathbf{C} \mathbf{I}_{abc} + \mathbf{D} \mathbf{I}_{wv}, \quad (3.14)$$

where

$$\left. \begin{aligned} \Delta \mathbf{V}_{abc} &= \begin{bmatrix} V_a - V'_a \\ V_b - V'_b \\ V_c - V'_c \end{bmatrix}, & \mathbf{I}_{abc} &= \begin{bmatrix} I_a \\ I_b \\ I_c \end{bmatrix}, \\ \Delta \mathbf{V}_{wv} &= \begin{bmatrix} V_w - V'_w \\ V_v - V'_v \end{bmatrix}, & \mathbf{I}_{wv} &= \begin{bmatrix} I_w \\ I_v \end{bmatrix}, \end{aligned} \right\} \quad (3.15)$$

$$\begin{aligned} \mathbf{A} &= \begin{bmatrix} Z_{aa-g} & Z_{ab-g} & Z_{ac-g} \\ Z_{ba-g} & Z_{bb-g} & Z_{bc-g} \\ Z_{ca-g} & Z_{cb-g} & Z_{cc-g} \end{bmatrix}, & \mathbf{B} &= \begin{bmatrix} Z_{aw-g} & Z_{av-g} \\ Z_{bw-g} & Z_{bv-g} \\ Z_{cw-g} & Z_{cv-g} \end{bmatrix}, \\ \mathbf{C} &= \begin{bmatrix} Z_{wa-g} & Z_{wb-g} & Z_{wc-g} \\ Z_{va-g} & Z_{vb-g} & Z_{vc-g} \end{bmatrix}, & \mathbf{D} &= \begin{bmatrix} Z_{ww-g} & Z_{wv-g} \\ Z_{vw-g} & Z_{vv-g} \end{bmatrix}. \end{aligned} \quad (3.16)$$

As it is normal practice to connect ground wires to earth at both ends of every transmission span,  $\Delta \mathbf{V}_{wv} = \mathbf{0}$ , and it is possible to simplify Equation (3.12) to

$$\Delta \mathbf{V}_{abc} = \mathbf{A} \mathbf{I}_{abc} + \mathbf{B} \mathbf{I}_{wv}, \tag{3.17}$$

$$\mathbf{0} = \mathbf{C} \mathbf{I}_{abc} + \mathbf{D} \mathbf{I}_{wv}. \tag{3.18}$$

Solving Equation (3.18) for  $\mathbf{I}_{wv}$ ,

$$\mathbf{I}_{wv} = -\mathbf{D}^{-1} \mathbf{C} \mathbf{I}_{abc}, \tag{3.19}$$

and substitution of Equation (3.19) into Equation (3.17) yields

$$\Delta \mathbf{V}_{abc} = [\mathbf{A} - \mathbf{B} \mathbf{D}^{-1} \mathbf{C}] \mathbf{I}_{abc} = \mathbf{Z}_{abc-wv-g} \mathbf{I}_{abc}, \tag{3.20}$$

where

$$\mathbf{Z}_{abc-wv-g} = \mathbf{A} - \mathbf{B} \mathbf{D}^{-1} \mathbf{C}. \tag{3.21}$$

Equation (3.20) can be written in expanded form as

$$\begin{bmatrix} \Delta V_a \\ \Delta V_b \\ \Delta V_c \end{bmatrix} = \begin{bmatrix} Z_{aa-wv-g} & Z_{ab-wv-g} & Z_{ac-wv-g} \\ Z_{ba-wv-g} & Z_{bb-wv-g} & Z_{bc-wv-g} \\ Z_{ca-wv-g} & Z_{cb-wv-g} & Z_{cc-wv-g} \end{bmatrix} \begin{bmatrix} I_a \\ I_b \\ I_c \end{bmatrix}. \tag{3.22}$$

The reduced equivalent matrix Equation (3.22) is fully equivalent to matrix Equation (3.12), where the ground wires have been mathematically eliminated. For most system analysis purposes, Equation (3.22) provides a suitable representation for transmission lines with ground wires. Symmetrical components can be applied to Equation (3.22), and it is therefore preferred over Equation (3.12).

### 3.2.3 Bundle Conductors

The use of more than one conductor per phase (i.e. bundle conductors) reduces the equivalent transmission-line impedance and allows for an increase in power transmission. It also allows for a reduction in corona loss and radio interference owing to a reduction in conductor-surface voltage gradients.

For cases of transmission lines of 400 kV and above it is standard practice to have four bundle conductors per phase, whereas for 230 kV lines, only three or two bundle conductors per phase are required. These arrangements are shown in Figures 3.6(a), 3.6(b), and 3.6(c), respectively (Grainger and Stevenson, 1994).

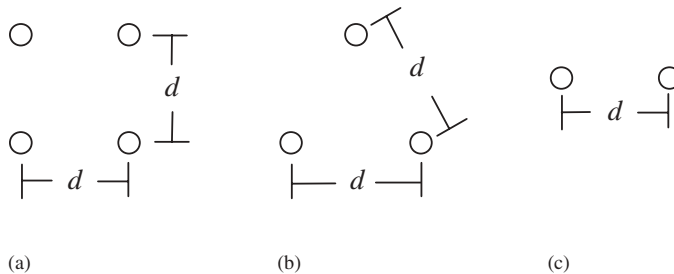


**Figure 3.6** Typical arrangements of bundle conductors: (a) four, (b) three, and (c) two bundle conductors (open circles)

In power system studies the interest is rarely on individual conductors but, rather, on the individual phases. Hence, steps are taken to find reduced equivalents that involve only one conductor per phase. The equivalent conductors correctly account for the original configuration but keep essential information only.

The bundle-conductor reduction may be achieved in a number of ways. Use of the concept of an equivalent geometric mean radius (GMR),  $R_{gmr}$  is one of them, and, although it is a frequency-independent method, it yields reasonably accurate solutions, particularly at power frequencies.

For cases of two, three, and four bundle conductors per phase, the following relations are used to calculate the equivalent GMR:

$$R_{gmr} = (r_{gmr} \times d)^{1/2}, \tag{3.23}$$

$$R_{gmr} = (r_{gmr} \times d \times d)^{1/3}, \tag{3.24}$$

$$R_{gmr} = (r_{gmr} \times d \times d \times \sqrt{2}d)^{1/4}. \tag{3.25}$$

In this case, the equivalent phase resistance is simply obtained by dividing the resistance of one of the original phase conductors in the bundle by the number of conductors in the bundle. This simple approach takes the very practical view that all conductors in the bundle are equal and that they are at the same potential.

A more rigorous approach, which includes frequency dependency for the reduction of the series impedance matrix, involves matrix reduction using Kron’s method (Anderson, 1973). In this situation, all conductor impedances are calculated explicitly and, after a suitable manipulation of terms in the impedance matrix, the mathematical elimination of bundle conductors is carried out. The actual elimination is the same process as that for the matrix reduction given by Equations (3.17)–(3.21) in the elimination of ground wires.

To illustrate the elimination procedure used when bundle conductors are present, take the case of a three-phase transmission line ( $a, b, c$ ) with two conductors per phase (1, 2) and no ground wires. Using similar notation as in Sections 3.2.1 and 3.2.2, the matrix of series impedance parameters representing such a transmission line would be:

$$\begin{bmatrix} \Delta V_{a1} \\ \Delta V_{b1} \\ \Delta V_{c1} \\ \Delta V_{a2} \\ \Delta V_{b2} \\ \Delta V_{c2} \end{bmatrix} = \begin{bmatrix} Z_{a1a1-g} & Z_{a1b1-g} & Z_{a1c1-g} & Z_{a1a2-g} & Z_{a1b2-g} & Z_{a1c2-g} \\ Z_{b1a1-g} & Z_{b1b1-g} & Z_{b1c1-g} & Z_{b1a2-g} & Z_{b1b2-g} & Z_{b1c2-g} \\ Z_{c1a1-g} & Z_{c1b1-g} & Z_{c1c1-g} & Z_{c1a2-g} & Z_{c1b2-g} & Z_{c1c2-g} \\ Z_{a2a1-g} & Z_{a2b1-g} & Z_{a2c1-g} & Z_{a2a2-g} & Z_{a2b2-g} & Z_{a2c2-g} \\ Z_{b2a1-g} & Z_{b2b1-g} & Z_{b2c1-g} & Z_{b2a2-g} & Z_{b2b2-g} & Z_{b2c2-g} \\ Z_{c2a1-g} & Z_{c2b1-g} & Z_{c2c1-g} & Z_{c2a2-g} & Z_{c2b2-g} & Z_{c2c2-g} \end{bmatrix} \begin{bmatrix} I_{a1} \\ I_{b1} \\ I_{c1} \\ I_{a2} \\ I_{b2} \\ I_{c2} \end{bmatrix}. \tag{3.26}$$

The individual elements of Equation (3.26) are calculated by using Equations (3.10) and (3.11). In compact notation, we have,

$$\begin{bmatrix} \Delta \mathbf{V}_{abc1} \\ \Delta \mathbf{V}_{abc2} \end{bmatrix} = \begin{bmatrix} \mathbf{Z}_{abc11} & \mathbf{Z}_{abc12} \\ \mathbf{Z}_{abc21} & \mathbf{Z}_{abc22} \end{bmatrix} \begin{bmatrix} \mathbf{I}_{abc1} \\ \mathbf{I}_{abc2} \end{bmatrix}. \tag{3.27}$$

If it is assumed that the two conductors in the bundle are at equal potential, then the row and column corresponding to one of the conductors in the bundle, say 2, is mathematically eliminated. There are three main steps involved in the elimination process:

- Step 1: The voltage equality constraint  $\Delta \mathbf{V}_{abc2} - \Delta \mathbf{V}_{abc1} = \mathbf{0}$  is incorporated into Equation (3.27):

$$\begin{bmatrix} \Delta \mathbf{V}_{abc1} \\ \Delta \mathbf{V}_{abc2} - \Delta \mathbf{V}_{abc1} = \mathbf{0} \end{bmatrix} = \begin{bmatrix} \mathbf{Z}_{abc11} & \mathbf{Z}_{abc12} \\ \mathbf{Z}_{abc21} - \mathbf{Z}_{abc11} & \mathbf{Z}_{abc22} - \mathbf{Z}_{abc12} \end{bmatrix} \begin{bmatrix} \mathbf{I}_{abc1} \\ \mathbf{I}_{abc2} \end{bmatrix}. \quad (3.28)$$

- Step 2: matrix symmetry is restored. This is achieved by adding and subtracting the terms  $\mathbf{Z}_{abc11} \mathbf{I}_{abc2}$  and  $(\mathbf{Z}_{abc21} - \mathbf{Z}_{abc11}) \mathbf{I}_{abc2}$  in rows 1 and 2, respectively:

$$\begin{bmatrix} \Delta \mathbf{V}_{abc1} \\ \mathbf{0} \end{bmatrix} = \begin{bmatrix} \mathbf{Z}_{abc11} & \mathbf{Z}_{abc12} - \mathbf{Z}_{abc11} \\ \mathbf{Z}_{abc21} - \mathbf{Z}_{abc11} & (\mathbf{Z}_{abc22} + \mathbf{Z}_{abc11} - \mathbf{Z}_{abc12} - \mathbf{Z}_{abc21}) \end{bmatrix} \begin{bmatrix} \mathbf{I}_{abc1} + \mathbf{I}_{abc2} \\ \mathbf{I}_{abc2} \end{bmatrix}. \quad (3.29)$$

- Step 3: the actual matrix reduction is carried out. This is fully equivalent to that given by Equations (3.17)–(3.21) used for the mathematical elimination of ground wires:

$$\Delta \mathbf{V}_{abc-b} = \mathbf{Z}_{abc-b-g} \mathbf{I}_{abc-b}, \quad (3.30)$$

where

$$\left. \begin{aligned} \mathbf{Z}_{abc-b-g} &= \mathbf{A} - \mathbf{B}\mathbf{D}^{-1}\mathbf{C}, \\ \mathbf{A} &= \mathbf{Z}_{abc11}, \\ \mathbf{B} &= \mathbf{Z}_{abc12} - \mathbf{Z}_{abc11}, \\ \mathbf{C} &= \mathbf{Z}_{abc21} - \mathbf{Z}_{abc11}, \\ \mathbf{D} &= \mathbf{Z}_{abc22} + \mathbf{Z}_{abc11} - \mathbf{Z}_{abc12} - \mathbf{Z}_{abc21}, \\ \Delta \mathbf{V}_{abc-b} &= \Delta \mathbf{V}_{abc1}, \\ \mathbf{I}_{abc-b} &= \mathbf{I}_{abc1} + \mathbf{I}_{abc2}. \end{aligned} \right\} \quad (3.31)$$

As illustrated in Figure 3.7, the current  $\mathbf{I}_{abc-b}$  may be interpreted as the phase current just before it splits into the individual currents  $\mathbf{I}_{abc1}$  and  $\mathbf{I}_{abc2}$  in the bundle.

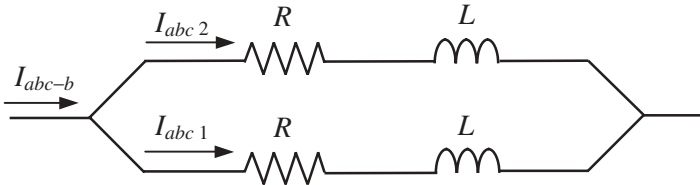


**Figure 3.7** Currents in a two-bundle conductor

An alternative, more elegant approach than that carried out in steps 1 and 2 is achieved by applying the following set of transformation matrices:

$$\mathbf{T}_b = \begin{bmatrix} \mathbf{1} & -\mathbf{1} \\ \mathbf{0} & \mathbf{1} \end{bmatrix} \quad \text{and} \quad \mathbf{T}'_b = \begin{bmatrix} \mathbf{1} & \mathbf{0} \\ -\mathbf{1} & \mathbf{1} \end{bmatrix} \quad (3.32)$$

to the impedance matrix in Equation (3.27), that is,

$$\begin{bmatrix} \mathbf{1} & \mathbf{0} \\ -\mathbf{1} & \mathbf{1} \end{bmatrix} \begin{bmatrix} \mathbf{Z}_{abc11} & \mathbf{Z}_{abc12} \\ \mathbf{Z}_{abc21} & \mathbf{Z}_{abc22} \end{bmatrix} \begin{bmatrix} \mathbf{1} & -\mathbf{1} \\ \mathbf{0} & \mathbf{1} \end{bmatrix}. \quad (3.33)$$

This operation yields the same result as Equation (3.30). In Equations (3.32) and (3.33),  $\mathbf{1}$  is a  $3 \times 3$  unit matrix, and the superscript  $t$  indicates the transpose of the matrix.

In the more general case, when there are  $n$  conductors per phase, the transformation matrix  $\mathbf{T}_b$  may have the following form:

$$\mathbf{T}_b = \begin{bmatrix} \mathbf{1} & -\mathbf{1} & \dots & -\mathbf{1} \\ \mathbf{0} & \mathbf{1} & \dots & \mathbf{0} \\ \vdots & \vdots & \ddots & \vdots \\ \mathbf{0} & \mathbf{0} & \dots & \mathbf{1} \end{bmatrix}. \tag{3.34}$$

Independent of the procedure used to determine the reduced equivalent matrix Equation (3.30), this can be written in expanded form as

$$\begin{bmatrix} \Delta V_{a-b} \\ \Delta V_{b-b} \\ \Delta V_{c-b} \end{bmatrix} = \begin{bmatrix} Z_{aa-b} & Z_{ab-b} & Z_{ac-b} \\ Z_{ba-b} & Z_{bb-b} & Z_{bc-b} \\ Z_{ca-b} & Z_{cb-b} & Z_{cc-b} \end{bmatrix} \begin{bmatrix} I_{a-b} \\ I_{b-b} \\ I_{c-b} \end{bmatrix}. \tag{3.35}$$

### 3.2.4 Double Circuit Transmission Lines

Often two or more three-phase transmission lines are operated in parallel (Anderson, 1973; Grainger and Stevenson, 1994). A common arrangement is to place two three-phase circuits in the same tower, as shown in Figure 3.8. In this case, the magnetic interaction between the phase conductors of both three-phase circuits can be represented by the following

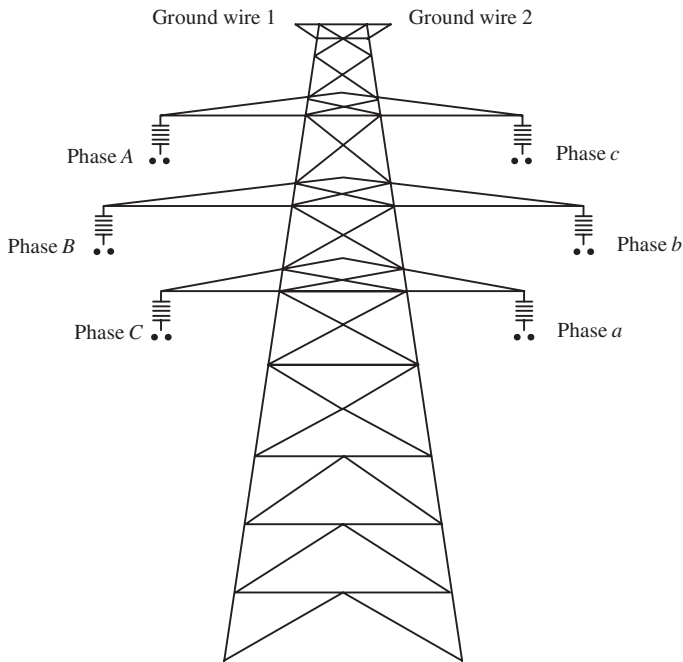


Figure 3.8 Double circuit, three-phase transmission line

impedance matrix equation:

$$\begin{bmatrix} \Delta V_a \\ \Delta V_b \\ \Delta V_c \\ \Delta V_A \\ \Delta V_B \\ \Delta V_C \end{bmatrix} = \begin{bmatrix} Z_{aa-g} & Z_{ab-g} & Z_{ac-g} & Z_{aA-g} & Z_{aB-g} & Z_{aC-g} \\ Z_{ba-g} & Z_{bb-g} & Z_{bc-g} & Z_{bA-g} & Z_{bB-g} & Z_{bC-g} \\ Z_{ca-g} & Z_{cb-g} & Z_{cc-g} & Z_{cA-g} & Z_{cB-g} & Z_{cC-g} \\ Z_{Aa-g} & Z_{Ab-g} & Z_{Ac-g} & Z_{AA-g} & Z_{AB-g} & Z_{AC-g} \\ Z_{Ba-g} & Z_{Bb-g} & Z_{Bc-g} & Z_{BA-g} & Z_{BB-g} & Z_{BC-g} \\ Z_{Ca-g} & Z_{Cb-g} & Z_{Cc-g} & Z_{CA-g} & Z_{CB-g} & Z_{CC-g} \end{bmatrix} \begin{bmatrix} I_a \\ I_b \\ I_c \\ I_A \\ I_B \\ I_C \end{bmatrix}. \quad (3.36)$$

It is assumed here that neither ground wires nor bundle conductors are present in the double circuit transmission line; alternatively, it is assumed they have been mathematically eliminated by using the methods discussed in Sections 3.2.2 and 3.2.3, respectively. It is also assumed that the individual elements of Equation (3.36) were calculated by using Equation (3.11) and (3.10).

### 3.2.5 The Per-unit System

Transmission-line parameters as calculated by Equations (3.10) and (3.11) are given in ohms per kilometre. However, when dealing with transmission lines at the system level, there are several advantages to be gained by expressing the line parameters in a uniform units system, termed the per-unit system.

Moreover, equipment manufacturers also specify the equipment characteristics in either percentage or per-unit values with respect to their nominal values. This is a simple mechanism that enables the electrical power network to be analysed as a single entity regardless of the voltage level at which the equipment operates.

The following electrical parameters are handled in per-unit values: voltage, current, power, and impedance. In each case, the corresponding per-unit value is the ratio of the actual value to a base value; that is,

$$\text{per-unit value} = \frac{\text{actual value}}{\text{base value}}. \quad (3.37)$$

The per-unit (p.u.) value is dimensionless by virtue of the base and actual values sharing the same units. It is common practice to specify the voltage,  $V_{\text{Base}}$ , and power,  $S_{\text{Base}}$ , to be the primary base values, from which the base current and impedance can be derived. In single-phase systems:

$$I_{\text{Base}} = \frac{S_{\text{Base}}}{V_{\text{Base}}} \text{ A}, \quad (3.38)$$

$$Z_{\text{Base}} = \frac{V_{\text{Base}}^2}{S_{\text{Base}}} \Omega. \quad (3.39)$$

In three-phase systems, the total power,  $S_{3\phi}$ , and the line-to-line voltage,  $V_{\text{LL}}$ , are readily available, and the following relations apply:

$$I_{\text{Base}} = \frac{S_{3\phi} \text{ Base}}{\sqrt{3} V_{\text{LL Base}}} \text{ A}, \quad (3.40)$$

$$Z_{\text{Base}} = \frac{V_{\text{LL Base}}^2}{S_{3\phi} \text{ Base}} \Omega. \quad (3.41)$$

Based on Equation (3.37), the per-unit parameters are:

$$\begin{aligned} S_{\text{p.u.}} &= \frac{S}{S_{\text{Base}}}, & V_{\text{p.u.}} &= \frac{V}{V_{\text{Base}}}, \\ I_{\text{p.u.}} &= \frac{I}{I_{\text{Base}}}, & Z_{\text{p.u.}} &= \frac{Z}{Z_{\text{Base}}}. \end{aligned} \quad (3.42)$$

It should be noted that the transmission line shunt admittances in Equation (3.5) are converted into per-unit values by using:

$$Y_{\text{p.u.}} = YZ_{\text{Base}}. \quad (3.43)$$

The transmission-line shunt admittance is sometimes referred to as ‘charging MVAR’,  $Q_{\text{sh}}$ . In some application programs, such as power flows, is actually supplied in terms of MVAR as opposed to Siemens (S) or  $\Omega^{-1}$ . There is no difficulty in transforming  $Q_{\text{sh}}$  into an equivalent per-unit shunt admittance if it is assumed that a voltage value of 1 p.u. exists at both ends of the transmission line:

$$Y_{\text{p.u.}} = \frac{Q_{\text{sh p.u.}}}{V_{\text{p.u.}}^2} = Q_{\text{sh p.u.}}. \quad (3.44)$$

Conversely, the information given by a transmission-line parameter program for the shunt admittance can also be expressed as a charging admittance under the assumption of a 1 p.u. voltage.

In high-voltage transmission studies, a base power of 100 MVA is normally selected for the whole system. In contrast, selection of the base voltage is not unique; instead, as many base voltages are selected as are required to match the number of voltage levels in the network under study. Having said that, it is important to mention that in some application studies, such as positive sequence power flows, it is not uncommon to have only one base voltage being selected. This is owing to the fact that the generating plant is modelled as injections of active and reactive power at the high-voltage bus of the generator transformer. Also, it is normal to conduct a detailed study for only one voltage level of the network, say 400 kV, with contributions from other parts of the network, operating at different voltage, treated as either bulk power supply points or loads.

### 3.2.6 Transmission-line Program: Basic Parameters

A computer program for the calculation of transmission line parameters is given in Program 3.1.<sup>(1)</sup> The program is general, as far as the number of conductors in the transmission line is concerned, and caters for up to four bundle conductors per phase and any number of earth wires.

PROGRAM 3.1 Program written in Matlab<sup>®</sup> to calculate transmission-line parameters

```
***- - - - Main Program
```

```
TransmissionLineData;
```

<sup>(1)</sup>Note<sup>®</sup>: in Matlab<sup>®</sup> it is possible to write very long lines, up to 600 characters. Continuation lines are possible and are indicated by the use of three periods at the end of the previous line. This convention has been adopted in this copy.

```

[ZSeries, YShunt] = ShortLine(nphc, ngw, nb, bsep, resis, rdext, gmr, ...
x, y, f, sigmag, vbase, sbase)

%End main Program

function [ZSeries, YShunt] = ShortLine(nphc, ngw, nb, bsep, ...
resis, rdext, gmr, x, y, f, sigmag, vbase, sbase)

[RAD, GMR, RES] = BundleReduction(nphc, ngw, nb, bsep, rdext, gmr, resis);
[YShunt] = PotCoeff(nphc, RAD, x, y, f);
[ZSeries] = Dubanton(nphc, ngw, GMR, RES, x, y, f, sigmag);
[ZSeries] = GroundWireReduction(nphc, ngw, ZSeries);
[ZSeries, YShunt] = PerUnit(nphc, ZSeries, YShunt, vbase, sbase);

function [RAD, GMR, RES] = BundleReduction(nphc, ngw, nb, bsep, rdext, ...
gmr, resis);
for ii = 1: nphc + ngw
    if nb(ii) == 1
        RAD(ii) = rdext(ii);
        GMR(ii) = gmr(ii);
    elseif nb(ii) == 2
        RAD(ii) = sqrt(rdext(ii)*bsep(ii));
        GMR(ii) = sqrt(gmr(ii)*bsep(ii));
    elseif nb(ii) == 3
        RAD(ii) = exp(log(rdext(ii)*bsep(ii)*bsep(ii))/3);
        GMR(ii) = exp(log(gmr(ii)*bsep(ii)*bsep(ii))/3);
    elseif nb(ii) == 4
        RAD(ii) = sqrt(sqrt(rdext(ii)*bsep(ii)*bsep(ii)*bsep(ii)...
        *sqrt(2)));
        GMR(ii) = sqrt(sqrt(gmr(ii)*bsep(ii)*bsep(ii)*bsep(ii)*sqrt(2)));
    end
    RES(ii) = resis(ii)/nb(ii);
end

function [YShunt] = PotCoeff(nphc, RAD, x, y, f);
[YShunt] = zeros(nphc, nphc);
omega = 2*pi*f;
eps = 8.854*1e-9;
for ii = 1: nphc
    for jj = 1: nphc
        if ( ii == jj )
            YShunt(ii, ii) = log(2*y(ii)/RAD(ii));
        else
            YShunt(ii, jj) = log( sqrt( ( x(ii) - x(jj) )^2 + ...
            ( y(ii) + y(jj) )^2 ) / sqrt( ( x(ii) - x(jj) )^2 + ...

```

```

        ( y(ii)-y(jj) )^2 ) );
    end
end
end
YShunt = i*2*pi*omega*eps*inv(YShunt);

function [ZSeries] = Dubanton(nphc,ngw,GMR,RES,x,y,f,sigmag)
[ZSeries] = zeros(nphc+ngw,nphc+ngw);
mnu = 4*pi*1e-7;
omega = (0+(2*pi*f)*i);
pe = 1/sqrt(omega*mnu*sigmag);
for ii = 1: nphc + ngw
    for jj = 1: nphc + ngw
        if( ii == jj )
            ZSeries(ii,ii) = 1000*( RES(ii) + omega*mnu*...
                log((y(ii)+y(jj)+2*pe)/GMR(ii))/(2*pi) );
        else
            ZSeries(ii,jj) = 1000*omega*mnu*...
                log( sqrt((x(ii)-x(jj))^2+(y(ii)+y(jj)+2*pe)^2) /...
                    sqrt((x(ii)-x(jj))^2+(y(ii)-y(jj))^2) ))/(2*pi);
        end
    end
end
end

function [ZSeries] = GroundWireReduction(nphc,ngw,ZSeries)
for ii = nphc + 1: nphc + ngw
    ZSeries(ii,ii) = 1/ZSeries(ii,ii);
    for jj = 1: nphc + ngw
        if( ii ~= jj )
            ZSeries(jj,ii) = ZSeries(jj,ii)*ZSeries(ii,ii);
            for kk = 1: nphc + ngw
                if( kk ~= ii )
                    ZSeries(jj,kk) = ZSeries(jj,kk) -ZSeries(jj,ii)*...
                        ZSeries(ii,kk);
                    if ( jj == nphc + ngw)
                        ZSeries(ii,kk) = -ZSeries(ii,ii)*ZSeries(ii,kk);
                    end
                end
            end
        end
    end
end
end
end
end

if ngw > 0
    for jj = 1: nphc + ngw -1
        ZSeries(nphc+ngw,jj) = -ZSeries(nphc+ngw,nphc+ngw)*...
            ZSeries(nphc+ngw,jj);
    end
end

```

```

    ZSeries = ZSeries(1:nphc,1:nphc);
end

function [ZSeries,YShunt] = PerUnit(nphc,ZSeries,YShunt,vbase,sbase)
zbase = vbase*vbase/sbase;
for ii = 1:nphc
    for jj = 1:nphc
        ZSeries(ii,jj) = ZSeries(ii,jj)/zbase;
        YShunt(ii,jj) = YShunt(ii,jj)*zbase;
    end
end
end

```

### 3.2.7 Numerical Example of Transmission Line Parameter Calculation

The basic parameters of a 500 kV, three-phase transmission line of flat configuration are calculated using the Matlab<sup>®</sup> function `ShortLine` given in Section 3.2.6. There are four (bundle) conductors per phase and no ground wires in the tower (Arrillaga *et al.*, 1986).

The series impedance and the shunt admittance matrices are calculated in ohms per kilometres and in per-unit values using a base power of 100 MVA.

Function `TransmissionLineData`, to read data for the 500 kV, three-phase transmission line of flat configuration, is as follows:

```

%transmission line.
%
%nphc = number of phase conductors
%ngw = number of ground wires
%
nphc = 3 ; ngw = 0 ;
%
%Individual Conductors Data
%resis = resistance in ohms per meter
%rdext = external radius in meters
%gmr = geometrical mean radius in meters
%nb = number of bundle conductors per phase -1 to 4
%bsep = separation between conductors in the bundle in meters
%x,y = conductor's co-ordinates in the tower in meters
%
resis(1) = 0.1379/1000 ; rdext(1) = 1.049/100 ; gmr(1) = 0.817/100 ;
nb(1) = 4 ; bsep(1) = 0.46 ; x(1) = 12.65 ; y(1) = 27.50 ;
resis(2) = 0.1379/1000 ; rdext(2) = 1.049/100 ; gmr(2) = 0.817/100 ;
nb(2) = 4 ; bsep(2) = 0.46 ; x(2) = 0 ; y(2) = 27.50 ;
resis(3) = 0.1379/1000 ; rdext(3) = 1.049/100 ; gmr(3) = 0.817/100 ;
nb(3) = 4 ; bsep(3) = 0.46 ; x(3) = -12.65 ; y(3) = 27.50 ;
%

```

```

%General Data
%f = frequency
%sigmag = ground's conductivity
%vbase = base voltage
%sbase = base power
%
f = 50 ; sigmag = 0.01 ; vbase = 500 ; sbase = 100 ;
%
%End of function TransmissionLineData

```

The series impedance and the shunt admittance matrices in ohms per kilometre are:

$$\mathbf{Z}_{abc} = \begin{bmatrix} 0.0815 + j0.5435 & 0.0470 + j0.2774 & 0.0470 + j0.2339 \\ 0.0470 + j0.2774 & 0.0815 + j0.5435 & 0.0470 + j0.2774 \\ 0.0470 + j0.2339 & 0.0470 + j0.2774 & 0.0815 + j0.5435 \end{bmatrix} \Omega \text{ km}^{-1},$$

$$\mathbf{Y}_{abc} = \begin{bmatrix} j3.359 & -j0.809 & -j0.305 \\ -j0.809 & j3.527 & -j0.809 \\ -j0.305 & -j0.809 & j3.359 \end{bmatrix} \mu\text{S km}^{-1}.$$

The geometric imbalances inherent in this transmission line, due to its flat configuration, are reflected in the fact that not all mutual reactances have the same value, that is,  $X_{ab} \neq X_{ac}$ . Similar effects can be observed in the mutual values of  $\mathbf{Y}_{abc}$ . Also, The resistive effects shown in the mutual elements of  $\mathbf{Z}_{abc}$  are entirely due to the ground return effects. As expected, this effect is not present in  $\mathbf{Y}_{abc}$  since capacitive effects are not a function of ground return.

With reference to a base voltage of 500 kV and 100 MVA, the series impedance and shunt admittance matrices in per-unit values are:

$$\mathbf{Z}_{abc} = 10^{-3} \times \begin{bmatrix} 0.0326 + j0.2174 & 0.0188 + j0.1110 & 0.0188 + j0.0935 \\ 0.0188 + j0.1110 & 0.0326 + j0.2174 & 0.0188 + j0.1110 \\ 0.0188 + j0.0935 & 0.0188 + j0.1110 & 0.0326 + j0.2174 \end{bmatrix} \text{ p.u.},$$

$$\mathbf{Y}_{abc} = 10^{-3} \times \begin{bmatrix} j8.398 & -j2.024 & -j0.762 \\ -j2.024 & j8.816 & -j2.024 \\ -j0.762 & -j2.024 & j8.398 \end{bmatrix} \text{ p.u.}$$

### 3.2.8 Long-line Effects

The transmission line models required for long-distance transmission applications are more involved than those covered in Section 3.2.4, which are only suitable to represent short to medium-distance transmission lines (Grainger and Stevenson, 1994). In actual applications, however, it is not common practice to see transmission lines of more than 300 km without series compensation, which fall within the category of medium-distance transmission lines for the purpose of fundamental frequency operation.

However, in some special cases it is desirable to incorporate long-line effects into the transmission line parameters (Bowman and McNamee, 1964). A case in point would

be studies relating to placement and sizing of shunt and series compensation of long-distance transmission. At frequency applications higher than the fundamental frequency, it is certainly mandatory to incorporate long-line effects since the electrical distance increases rapidly with frequency (Acha and Madrigal, 2001; Arrillaga *et al.*, 1997). Even transmission lines of only a few tens of kilometres may be seen as a very long line at 1 kHz.

Calculation of multiconductor transmission line parameters, including long-line effects, requires the use of formulations derived from the wave propagation equation. This introduces a degree of extra complexity as these formulations invariably involve square roots and circular and hyperbolic functions of matrices. Several options are available to carry out such nonconventional matrix operations, but perhaps the best known method is to simply apply suitable eigenvector techniques to the relevant transmission line parameter matrices (Wedephol, 1963). This enables all calculations to be performed in the frame of reference of the modes and then referred back to the frame of reference of the phases.

Arguably, the best known formulation derived from the wave propagation equation is the ‘ABCD’ parameter formulation:

$$\begin{bmatrix} \mathbf{V}_S \\ \mathbf{I}_S \end{bmatrix} = \begin{bmatrix} \mathbf{A} & \mathbf{B} \\ \mathbf{C} & \mathbf{D} \end{bmatrix} \begin{bmatrix} \mathbf{V}_R \\ -\mathbf{I}_R \end{bmatrix}, \quad (3.45)$$

where

$$\left. \begin{aligned} \mathbf{A} &= \mathbf{T}_v \times \mathbf{Diag}(\cosh \gamma_m l) \times \mathbf{T}_v^{-1}, \\ \mathbf{B} &= \mathbf{T}_v \times \mathbf{Diag}(z_m \times \sinh \gamma_m l) \times \mathbf{T}_i^{-1}, \\ \mathbf{C} &= \mathbf{T}_i \times \mathbf{Diag}(y_m \times \sinh \gamma_m l) \times \mathbf{T}_v^{-1}, \\ \mathbf{D} &= \mathbf{T}_i \times \mathbf{Diag}(\cosh \gamma_m l) \times \mathbf{T}_i^{-1}. \end{aligned} \right\} \quad (3.46)$$

In Equations (3.46), **Diag** is a diagonal matrix;  $m$  is the subscript for modes 0,  $\alpha$ , and  $\beta$ ;  $l$  is the length of the line;  $\mathbf{T}_v$  and  $\mathbf{T}_i$  are transformation matrices made up of the eigenvectors of the matrix products  $\mathbf{ZY}$  and  $\mathbf{YZ}$ , respectively; and  $\mathbf{Z}$  and  $\mathbf{Y}$  are lumped transmission-line parameters as calculated by the Matlab<sup>®</sup> computer program given in Section 3.2.6.

The modal parameters for the propagation constant,  $\gamma_m$ , and the characteristic impedance and admittance,  $z_m$ , and  $y_m$ , in Equations (3.46) are calculated by first making  $\mathbf{Z}$  and  $\mathbf{Y}$  diagonal:

$$\left. \begin{aligned} \mathbf{Z}_m &= \mathbf{T}_v^{-1} \mathbf{Z} \mathbf{T}_i, \\ \mathbf{Y}_m &= \mathbf{T}_i^{-1} \mathbf{Y} \mathbf{T}_v, \end{aligned} \right\} \quad (3.47)$$

and then performing the following operations:

$$\gamma_m = \begin{bmatrix} (z_0 y_0)^{1/2} & 0 & 0 \\ 0 & (z_\alpha y_\alpha)^{1/2} & 0 \\ 0 & 0 & (z_\beta y_\beta)^{1/2} \end{bmatrix}, \quad (3.48)$$

$$z_m = \frac{1}{y_m} = \begin{bmatrix} (z_0 y_0^{-1})^{1/2} & 0 & 0 \\ 0 & (z_\alpha y_\alpha^{-1})^{1/2} & 0 \\ 0 & 0 & (z_\beta y_\beta^{-1})^{1/2} \end{bmatrix}. \quad (3.49)$$

Alternative formulations, derived from the wave propagation equation, are available that may present advantages in certain applications. The two obvious ones are the impedance

and the admittance representations:

$$\begin{bmatrix} \mathbf{V}_S \\ \mathbf{V}_R \end{bmatrix} = \begin{bmatrix} \mathbf{Z}' & \mathbf{Z}'' \\ \mathbf{Z}'' & \mathbf{Z}' \end{bmatrix} \begin{bmatrix} \mathbf{I}_S \\ \mathbf{I}_R \end{bmatrix}, \tag{3.50}$$

$$\begin{bmatrix} \mathbf{I}_S \\ \mathbf{I}_R \end{bmatrix} = \begin{bmatrix} \mathbf{Y}' & \mathbf{Y}'' \\ \mathbf{Y}'' & \mathbf{Y}' \end{bmatrix} \begin{bmatrix} \mathbf{V}_S \\ \mathbf{V}_R \end{bmatrix}, \tag{3.51}$$

where

$$\left. \begin{aligned} \mathbf{Z}' &= \mathbf{T}_v \times \mathbf{Diag}(z_m \times \coth \gamma_m l) \times \mathbf{T}_i^{-1}, \\ \mathbf{Z}'' &= \mathbf{T}_v \times \mathbf{Diag}(z_m \times \operatorname{csch} \gamma_m l) \times \mathbf{T}_i^{-1}, \\ \mathbf{Y}' &= \mathbf{T}_i \times \mathbf{Diag}(y_m \times \coth \gamma_m l) \times \mathbf{T}_v^{-1}, \\ \mathbf{Y}'' &= -\mathbf{T}_i \times \mathbf{Diag}(y_m \times \operatorname{csch} \gamma_m l) \times \mathbf{T}_v^{-1}. \end{aligned} \right\} \tag{3.52}$$

### 3.2.9 Transmission Line Transpositions

High-voltage transmission lines may contain considerable geometric asymmetry, which in turn causes voltage imbalances at the far end of the line, and transpositions are often used as a means of balancing the overall impedances of the line (Anderson, 1973; Arrillaga *et al.*, 1986).

A three-phase transmission line, with a full set of transpositions, consists of three *RLC* subsystems, as shown in Figure 3.9, where each section can be viewed as a  $\pi$ -circuit. Alternatively, if each section is expressed in terms of its ABCD parameters then an equivalent result can be obtained for the overall transmission line by cascading the

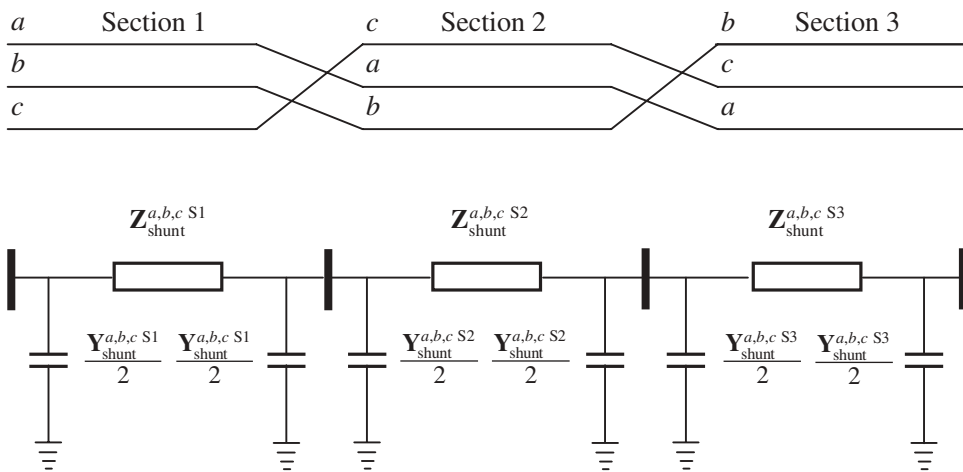


Figure 3.9 Transposed transmission line representation and corresponding  $\pi$  sections

individual elements (Anderson, 1973):

$$\left. \begin{aligned} \begin{bmatrix} \mathbf{V}_S \\ \mathbf{I}_S \end{bmatrix} &= \begin{bmatrix} \mathbf{A}_1 & \mathbf{B}_1 \\ \mathbf{C}_1 & \mathbf{D}_1 \end{bmatrix} \times \begin{bmatrix} \mathbf{A}_2 & \mathbf{B}_2 \\ \mathbf{C}_2 & \mathbf{D}_2 \end{bmatrix} \times \begin{bmatrix} \mathbf{A}_3 & \mathbf{B}_3 \\ \mathbf{C}_3 & \mathbf{D}_3 \end{bmatrix} \begin{bmatrix} \mathbf{V}_R \\ -\mathbf{I}_R \end{bmatrix}, \\ \begin{bmatrix} \mathbf{V}_S \\ \mathbf{I}_S \end{bmatrix} &= \begin{bmatrix} \mathbf{A} & \mathbf{B} \\ \mathbf{C} & \mathbf{D} \end{bmatrix} \begin{bmatrix} \mathbf{V}_R \\ -\mathbf{I}_R \end{bmatrix}. \end{aligned} \right\} \quad (3.53)$$

Notice that the voltages and currents at the receiving end of section 1 are the voltages and current at the sending end of section 2, and so on. Notice also in Figure 3.9 that the phase conductors in sections 1, 2, and 3 occupy different positions in the tower, following the sense of rotation ( $a, b, c$ ), ( $c, a, b$ ), and ( $b, c, a$ ).

Cascading is also useful for calculating equivalent ABCD parameters of transmission lines that contain not just transpositions but also shunt and series passive compensation. The ABCD parameters of the series capacitive compensators are:

$$\begin{bmatrix} \mathbf{V}_S \\ \mathbf{I}_S \end{bmatrix} = \begin{bmatrix} \mathbf{1} & \mathbf{Z} \\ \mathbf{0} & \mathbf{1} \end{bmatrix} \begin{bmatrix} \mathbf{V}_R \\ -\mathbf{I}_R \end{bmatrix}, \quad (3.54)$$

where  $\mathbf{1}$  and  $\mathbf{0}$  are the unit and zero matrices, and  $\mathbf{Z} = \mathbf{Diag}(1/j\omega C)$ . Similarly, the ABCD parameters of the shunt compensator are:

$$\begin{bmatrix} \mathbf{V}_S \\ \mathbf{I}_S \end{bmatrix} = \begin{bmatrix} \mathbf{1} & \mathbf{0} \\ \mathbf{Y} & \mathbf{1} \end{bmatrix} \begin{bmatrix} \mathbf{V}_R \\ -\mathbf{I}_R \end{bmatrix}, \quad (3.55)$$

where  $\mathbf{Y} = \mathbf{Diag}(j\omega C)$  and  $\mathbf{Y} = \mathbf{Diag}(1/j\omega L)$  for capacitive and inductive shunt compensation, respectively.

### 3.2.10 Transmission Line Program: Distributed Parameters

In Program 3.2, Program 3.1 is expanded to incorporate long-line effects and discontinuities along the length of the line such as passive shunt and series compensation. The expansion is neatly accommodated, leaving the code unchanged, and all added modelling functionality is coded in two new functions, namely `LongLineData` and `LongLine`.

PROGRAM 3.2 Program written in Matlab<sup>®</sup> to calculate transmission line parameters, including long-line effects and passive shunt and series compensation

```

%***- - - - Main Program

TransmissionLineData;

LongLineData;
[ZSeries, YShunt, Z012, Y012] = ShortLine(nphc, ngw, nb, bsep, resis, ...
rdext, gmr, x, y, f, sigmag, vbase, sbase);

[ZPhase, YPhase] = LongLine(nphc, nsections, length, ZSeries, YShunt, ...
ZSe, Ysh);

%End main Program

function [ZPhase, YPhase] = LongLine(nphc, nsect, length, ZSeries, ...
YShunt, ZSe, YSh)

```

```

AUX = eye(nphc*2);
[TV, ZY] = eig(ZSeries*YShunt);
[TI, YZ] = eig(YShunt*ZSeries);
ZModal = inv(TV)*ZSeries*TI;
YModal = inv(TI)*YShunt*TV;
kk = 1;
for ll = 1: nsect
    if ( length(ll) > 0 )
        [ABCD] = ABCDLine(ll, nphc, length, ZModal, YModal, TV, TI);
    else
        [ABCD] = ABCDComp(kk, nphc, ZSe, YSh);
        kk = kk + 1;
    end
    AUX = AUX*ABCD;
end
ABCD = AUX;

A = ABCD(1:nphc, 1:nphc);
B = ABCD(1:nphc, nphc+1:nphc*2);
C = ABCD(nphc+1:nphc*2, 1:nphc);
D = ABCD(nphc+1:nphc*2, nphc+1:nphc*2);

ZPhase(1:nphc, 1:nphc) = A*inv(C);
ZPhase(1:nphc, nphc+1:nphc*2) = -B + A*inv(C)*D;
ZPhase(nphc+1:nphc*2, 1:nphc) = inv(C);
ZPhase(nphc+1:nphc*2, nphc+1:nphc*2) = inv(C)*D;

YPhase = inv(ZPhase);

%End LongLine function

function [ABCD] = ABCDLine(ll, nphc, length, ZModal, YModal, TV, TI);
Modal = zeros(nphc, nphc);
for ii = 1: nphc
    gamma = sqrt(ZModal(ii, ii)*YModal(ii, ii));
    gammar = real(gamma*length(ll));
    gammai = imag(gamma*length(ll));
    fact1 = sinh(gammar);
    fact2 = cosh(gammar);
    fact3 = sin(gammai);
    fact4 = cos(gammai);
    Modal(ii, ii) = ((fact2*fact4)+(fact1*fact3)*i);
end
ABCD(1:nphc, 1:nphc) = TV*Modal*inv(TV);

for ii = 1: nphc
    gamma = sqrt(ZModal(ii, ii)*YModal(ii, ii));
    gammar = real(gamma*length(ll));
    gammai = imag(gamma*length(ll));

```

```

    fact1 = sinh(gammar);
    fact2 = cosh(gammar);
    fact3 = sin(gammai);
    fact4 = cos(gammai);
    Modal(ii,ii) = sqrt(ZModal(ii,ii)/YModal(ii,ii))*...
    (fact1*fact4+fact2*fact3*i);

end

ABCD(1:nphc,nphc+1:nphc*2) = TV*Modal*inv(TI);

for ii = 1:nphc

    gamma = sqrt(ZModal(ii,ii)*YModal(ii,ii));
    gammar = real(gamma*length(l1));
    gammai = imag(gamma*length(l1));
    fact1 = sinh(gammar);
    fact2 = cosh(gammar);
    fact3 = sin(gammai);
    fact4 = cos(gammai);
    Modal(ii,ii) = sqrt(YModal(ii,ii)/ZModal(ii,ii))*...
    (fact1*fact4+fact2*fact3*i);

end

ABCD(nphc+1:nphc*2,1:nphc) = TI*Modal*inv(TV);

for ii = 1:nphc

    gamma = sqrt(ZModal(ii,ii)*YModal(ii,ii));
    gammar = real(gamma*length(l1));
    gammai = imag(gamma*length(l1));
    fact1 = sinh(gammar);
    fact2 = cosh(gammar);
    fact3 = sin(gammai);
    fact4 = cos(gammai);
    Modal(ii,ii) = (fact2*fact4+fact1*fact3*i);
end

ABCD(nphc+1:nphc*2,nphc+1:nphc*2) = TI*Modal*inv(TI);

%End ABCDLine function

function [ABCD] = ABCDComp(kk,nphc,ZSe,YSh)
One = eye(nphc) ;
ABCD(1:nphc,1:nphc) = One ;
ABCD(1:nphc,nphc+1:nphc*2) = ZSe(:, :, kk) ;
ABCD(nphc+1:nphc*2,1:nphc) = YSh(:, :, kk) ;
ABCD(nphc+1:nphc*2,nphc+1:nphc*2) = YSh(:, :, kk)*ZSe(:, :, kk) + One ;

%End ABCDComp function

```

### 3.2.11 Numerical Example of Long Line Parameter Calculation

The parameters of the transmission line in Section 3.2.7 are calculated for the case when the line is 500 km long. The Matlab<sup>®</sup> function `LongLine` and the data given below, in `LongLineData`, are used to such effect.

Function `LongLineData`, to read data for the 500 kV, three-phase transmission line of flat configuration is as follows:

```
%transmission line of Example 1, to include long-line effects and passive
%shunt and series compensation. The line is 500 km long and contains no
%compensation.
%
%Transmission Line Data
%
%nsections = number of sections in the transmission line
%length = total length of transmission line
%
nsections = 1 ;
length(1) = 500 ;
%
%Compensating Plant Data
%
ZSe(:, :, 1) = [ 0 0 0 ; 0 0 0 ; 0 0 0 ] ;
YSh(:, :, 1) = [ 0 0 0 ; 0 0 0 ; 0 0 0 ] ;
%
%End of function LongLineData
```

In this example, the self and mutual admittances  $\mathbf{Y}'$  and  $\mathbf{Y}''$  of the transfer admittance matrix of Equation (3.51), are:

$$\mathbf{Y}' = \begin{bmatrix} 1.6428 - j11.4850 & -0.6708 + j4.7380 & -0.1371 + j2.9077 \\ -0.6708 + j4.7380 & 1.9417 - j12.7038 & -0.6708 + j4.7380 \\ -0.1371 + j2.9077 & -0.6708 + j4.7380 & 1.6428 - j11.4850 \end{bmatrix} \text{ p.u.},$$

$$\mathbf{Y}'' = \begin{bmatrix} -1.6336 + j13.6479 & 0.6713 - j5.2450 & 0.1400 - j3.0994 \\ 0.6713 - j5.2450 & -1.9327 + j14.9702 & 0.6713 - j5.2450 \\ 0.1400 - j3.0994 & 0.6713 - j5.2450 & -1.6336 + j13.6479 \end{bmatrix} \text{ p.u.}$$

These parameters were calculated by using accurate expressions derived from the wave propagation equation. An alternative, approximated, solution, involving the lumped parameters calculated with Matlab<sup>®</sup> function `ShortLine` and the nodal-based equations

$$\mathbf{Y}' = (\mathbf{Z}_{abc} \times \text{length})^{-1} + \frac{1}{2} \mathbf{Y}_{abc} \times \text{length},$$

and

$$\mathbf{Y}'' = -(\mathbf{Z}_{abc} \times \text{length})^{-1},$$

is as follows:

$$\mathbf{Y}' = \begin{bmatrix} 1.6379 - j10.8189 & -0.6711 + j4.5699 & -0.1387 + j2.8400 \\ -0.6711 + j4.5699 & 1.9369 - j12.0023 & -0.6711 + j4.5699 \\ -0.1387 + j2.8400 & -0.6711 + j4.5699 & 1.6379 - j10.8189 \end{bmatrix} \text{ p.u.,}$$

$$\mathbf{Y}'' = \begin{bmatrix} -1.6379 + j12.9184 & 0.6711 - j5.0759 & 0.1387 - j3.0306 \\ 0.6711 - j5.0759 & -1.9369 + j14.2064 & 0.6711 - j5.0759 \\ 0.1387 - j3.0306 & 0.6711 - j5.0759 & -1.6379 + j12.9184 \end{bmatrix} \text{ p.u.}$$

It is interesting to notice that even for this relatively long-distance transmission line, little difference exists between the conductances of the accurate and the approximated solutions. However, the absolute error in the susceptances is around 5%.

### 3.2.12 Symmetrical Components and Sequence Domain Parameters

If Equation (3.1), or its more involved counterparts Equations (3.22) and (3.35), can be assumed to be perfectly balanced then they can be replaced by the following impedance matrix equation (Chen and Dillon, 1974):

$$\begin{bmatrix} \Delta V_a \\ \Delta V_b \\ \Delta V_c \end{bmatrix} = \begin{bmatrix} Z & M & M \\ M & Z & M \\ M & M & Z \end{bmatrix} \begin{bmatrix} I_a \\ I_b \\ I_c \end{bmatrix}. \quad (3.56)$$

Such a representation is easily transformed into the sequence domain frame of reference by using the matrix of symmetrical components and its inverse:

$$\mathbf{T}_s = \begin{bmatrix} 1 & 1 & 1 \\ 1 & h^2 & h \\ 1 & h & h^2 \end{bmatrix} \quad \text{and} \quad \mathbf{T}_s^{-1} = \frac{1}{3} \begin{bmatrix} 1 & 1 & 1 \\ 1 & h & h^2 \\ 1 & h^2 & h \end{bmatrix}, \quad (3.57)$$

where  $h = 1\angle 120^\circ$ , and  $h^2 = 1\angle 240^\circ$ .

Equation (3.56), written in compact notation, is subjected to the following treatment,

$$\mathbf{T}_s^{-1} \Delta \mathbf{V}_{abc} = \mathbf{T}_s^{-1} \mathbf{Z}_{abc} \mathbf{T}_s \mathbf{T}_s^{-1} \mathbf{I}_{abc}. \quad (3.58)$$

This yields the sequence domain representation of Equation (3.56),

$$\Delta \mathbf{V}_{012} = \mathbf{Z}_{012} \mathbf{I}_{012}. \quad (3.59)$$

The subscripts 0, 1, and 2 stand for zero, positive, and negative sequence components, respectively. The following relationships exist between the terms in Equations (3.58) and (3.59):

$$\left. \begin{aligned} \Delta \mathbf{V}_{012} &= \mathbf{T}_s^{-1} \Delta \mathbf{V}_{abc}, \\ \mathbf{I}_{012} &= \mathbf{T}_s^{-1} \mathbf{I}_{abc}, \\ \mathbf{Z}_{012} &= \mathbf{T}_s^{-1} \mathbf{Z}_{abc} \mathbf{T}_s. \end{aligned} \right\} \quad (3.60)$$

Furthermore, Equation (3.59), in expanded form, is

$$\begin{bmatrix} \Delta V_0 \\ \Delta V_1 \\ \Delta V_2 \end{bmatrix} = \begin{bmatrix} Z_0 & 0 & 0 \\ 0 & Z_1 & 0 \\ 0 & 0 & Z_2 \end{bmatrix} \begin{bmatrix} I_0 \\ I_1 \\ I_2 \end{bmatrix}, \quad (3.61)$$

where

$$\left. \begin{aligned} Z_0 &= Z + 2M, \\ Z_1 &= Z - M, \\ Z_2 &= Z - M. \end{aligned} \right\} \quad (3.62)$$

This is a useful result that enables the calculation of the zero, positive, and negative sequence impedances from known self and mutual impedances.

The reverse problem – that where the self and mutual impedances of a perfectly balanced transmission line are to be determined from known sequence impedances – is of great practical interest. Suitable equations can be derived from Equations (3.62):

$$\left. \begin{aligned} Z &= \frac{1}{3}(Z_0 + 2Z_1), \\ M &= \frac{1}{3}(Z_0 - Z_1). \end{aligned} \right\} \quad (3.63)$$

However, it should be remarked that if Equation (3.1) cannot be assumed to be perfectly balanced then the use of symmetrical components does not yield a decoupled matrix equation and the use of symmetrical components is of limited value.

To a limited extent this problem arises when the perfectly balanced counterpart of matrix Equation (3.36) is represented in the sequence domain. If Equation (3.36) can be assumed to be perfectly balanced then it is replaced by the following matrix equation:

$$\begin{bmatrix} \Delta V_a \\ \Delta V_b \\ \Delta V_c \\ \Delta V_A \\ \Delta V_B \\ \Delta V_C \end{bmatrix} = \begin{bmatrix} Z & M & M & M & M & M \\ M & Z & M & M & M & M \\ M & M & Z & M & M & M \\ M & M & M & Z & M & M \\ M & M & M & M & Z & M \\ M & M & M & M & M & Z \end{bmatrix} \begin{bmatrix} I_a \\ I_b \\ I_c \\ I_A \\ I_B \\ I_C \end{bmatrix}. \quad (3.64)$$

Using compact notation to represent Equation (3.64), and applying symmetrical components,

$$\begin{bmatrix} \mathbf{T}_s^{-1} & \mathbf{0} \\ \mathbf{0} & \mathbf{T}_s^{-1} \end{bmatrix} \begin{bmatrix} \Delta \mathbf{V}_{abc} \\ \Delta \mathbf{V}_{ABC} \end{bmatrix} = \begin{bmatrix} \mathbf{T}_s^{-1} & \mathbf{0} \\ \mathbf{0} & \mathbf{T}_s^{-1} \end{bmatrix} \begin{bmatrix} \mathbf{Z} & \mathbf{M} \\ \mathbf{M} & \mathbf{Z} \end{bmatrix} \begin{bmatrix} \mathbf{T}_s & \mathbf{0} \\ \mathbf{0} & \mathbf{T}_s \end{bmatrix} \begin{bmatrix} \mathbf{T}_s^{-1} & \mathbf{0} \\ \mathbf{0} & \mathbf{T}_s^{-1} \end{bmatrix} \begin{bmatrix} \mathbf{I}_{abc} \\ \mathbf{I}_{ABC} \end{bmatrix}, \quad (3.65)$$

we obtain the following result:

$$\begin{bmatrix} \Delta \mathbf{V}'_{012} \\ \Delta \mathbf{V}_{012} \end{bmatrix} = \begin{bmatrix} \mathbf{Z}_{012} & \mathbf{M}_{012} \\ \mathbf{M}_{012} & \mathbf{Z}_{012} \end{bmatrix} \begin{bmatrix} \mathbf{I}_{012} \\ \mathbf{I}'_{012} \end{bmatrix}. \quad (3.66)$$

Equation (3.66) in expanded form is written as

$$\begin{bmatrix} \Delta V_0 \\ \Delta V_1 \\ \Delta V_2 \\ \Delta V'_0 \\ \Delta V'_1 \\ \Delta V'_2 \end{bmatrix} = \begin{bmatrix} Z + 2M & 0 & 0 & 3M & 0 & 0 \\ 0 & Z - M & 0 & 0 & 0 & 0 \\ 0 & 0 & Z - M & 0 & 0 & 0 \\ 3M & 0 & 0 & Z + 2M & 0 & 0 \\ 0 & 0 & 0 & 0 & Z - M & 0 \\ 0 & 0 & 0 & 0 & 0 & Z - M \end{bmatrix} \begin{bmatrix} I_0 \\ I_1 \\ I_2 \\ I'_0 \\ I'_1 \\ I'_2 \end{bmatrix}, \quad (3.67)$$

where the sequence domain voltages and currents corresponding to circuit two are primed to differentiate them from those in circuit one. Also, note the impedance coupling between the two zero sequence circuits.

### 3.2.13 Transmission Line Program: Sequence Parameters

Computer Program 3.1 is expanded in Program 3.3 to incorporate sequence parameter calculations. The new function, `SequenceImpedance`, is added to the code given in the program. No additional input data are required.

PROGRAM 3.3 Program written in Matlab<sup>®</sup> to calculate transmission-line sequence parameters

```

%***- - - - Main Program

TransmissionLineData;

[ZSeries,YShunt] = ShortLine(nphc,ngw,nb,bsep,resis,rdext,gmr,...
x,y,f, sigmag,vbase,sbase)

[Z012,Y012] = SequenceImpedance(ZSeries,YShunt);

%End main Program

function [Z012,Y012] = SequenceImpedance(ZSeries,YShunt)
TS(1,1) = 1;
TS(1,2) = 1;
TS(1,3) = 1;
TS(2,1) = 1;
TS(2,2) = -0.5-sqrt(3)*0.5*i;
TS(2,3) = -0.5+sqrt(3)*0.5*i;
TS(3,1) = 1;
TS(3,2) = -0.5+sqrt(3)*0.5*i;
TS(3,3) = -0.5-sqrt(3)*0.5*i;
ST = inv(TS);
Z012 = ST*ZSeries*TS;
Y012 = ST*YShunt*TS;

```

### 3.2.14 Numerical Example of Sequence Parameter Calculation

The positive, negative, and zero sequence parameters of the transmission line in Section 3.2.7 are:

$$\mathbf{Z}_{012} = 10^{-3} \times \begin{bmatrix} 0.0702 + j0.4277 & 0.0050 - j0.0029 & -0.0050 - j0.0029 \\ -0.0050 - j0.0029 & 0.0138 + j0.1122 & -0.0101 + j0.0058 \\ 0.0050 - j0.0029 & 0.0101 + j0.0058 & 0.0138 + j0.1122 \end{bmatrix} \text{ p.u.},$$

$$\mathbf{Y}_{012} = \begin{bmatrix} j0.0053 & -0.0002 + j0.0001 & 0.0002 + j0.0001 \\ 0.0002 + j0.0001 & j0.0101 & 0.0008 - j0.0005 \\ -0.0002 + j0.0001 & -0.0008 - j0.0005 & j0.0101 \end{bmatrix} \text{ p.u.}$$

As expected,  $\mathbf{Z}_{012}$  and  $\mathbf{Y}_{012}$  are diagonally dominant and the values on the diagonal correspond to zero, positive, and negative sequence parameters, respectively. It is important to notice that no full decoupling of the sequences is possible because of the inherent geometric imbalances exhibited by the transmission line used in this test case; it is a transmission line of flat configuration and contains no line transpositions.

### 3.3 POWER TRANSFORMER MODELLING

Power transformers are essential plant components of the power system. In general, they provide the interface between sections of the network with different rating voltages, for example a generating plant and the transmission network, a static VAR compensation (SVC) and the transmission network. Transformers consist of two or three copper windings per phase and one or more iron cores. They are normally contained in metallic enclosures (i.e. tanks), and are immersed in high-grade oil for insulation purposes (Grainger and Stevenson, 1994).

From the modelling point of view, it is convenient to separate the electric circuit, formed by the copper windings, from the magnetic circuit, formed by the iron core. The reactances of the windings can be found from short-circuit tests, and the iron-core reactances can be found from open-circuit tests. The three-phase windings of power transformers may be connected in a number of ways, but in high-voltage transmission the most popular connections are: (1) star–star, (2) delta–delta, and (3) star–delta. Furthermore, the star point can be either solidly grounded, grounded through an earthing impedance, or it may be floating.

In power transformers the magnetising current usually represents only a small percentage of the load current. However, this current is rich in harmonics, and a detailed representation of the magnetic circuit is mandatory in studies involving harmonic frequencies. In fundamental frequency studies, such as power flows, this requirement is not as severe and it is waived in most cases, unless the study is aimed at conducting an accurate assessment of power system losses (Acha and Madrigal, 2001; Arrillaga *et al.*, 1997).

#### 3.3.1 Single-phase Transformers

The starting point for developing comprehensive power flow transformer models is the schematic representation of the basic two-winding transformer shown in Figure 3.10. The windings contain resistance but it is assumed that the core does not saturate and exhibits no hysteresis.

The two transformer windings, termed primary (p) and secondary (s) windings contain  $N_p$  and  $N_s$  turns, respectively. The voltages and currents existing in both windings are related by a matrix of short-circuit (sc) impedance parameters, as given by the following

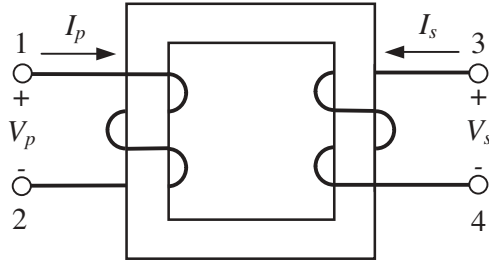


**Figure 3.10** Two-winding transformer

expression:

$$\begin{bmatrix} V_p \\ V_s \end{bmatrix} = \begin{bmatrix} Z_{scp} & Z_{scm} \\ Z_{scm} & Z_{scs} \end{bmatrix} \begin{bmatrix} I_p \\ I_s \end{bmatrix} \tag{3.68}$$

where

$$\left. \begin{aligned} Z_{scp} &= R_p + jX_{scp}, \\ Z_{scs} &= R_s + jX_{scs}, \\ Z_{scm} &= jX_{scm}. \end{aligned} \right\} \tag{3.69}$$

These parameters are obtained by measurements of the actual transformer, where  $R_p$  and  $R_s$  are the resistances of the primary and secondary windings, respectively. The reactances  $X_{scp}$ ,  $X_{scs}$ , and  $X_{scm}$  are short-circuit reactances obtained by exciting two terminals of the transformer shown in Figure 3.10, at reduced voltage, and short circuiting the other two. The ratio of excitation voltage to short-circuit current gives the relevant short-circuit reactance:

$$X_{scp} = \frac{E_{12}}{I_{34}}, \quad X_{scs} = \frac{E_{34}}{I_{12}}, \quad X_{scm} = \frac{E_{13}}{I_{24}}. \tag{3.70}$$

From the point of view of system analysis there are advantages in expressing the short-circuit impedance matrix of Equation (3.68) in admittance form:

$$\begin{bmatrix} I_p \\ I_s \end{bmatrix} = \begin{bmatrix} Y_{scp} & -Y_{scm} \\ -Y_{scm} & Y_{scs} \end{bmatrix} \begin{bmatrix} V_p \\ V_s \end{bmatrix}, \tag{3.71}$$

where

$$\left. \begin{aligned} Y_{scp} &= \frac{Z_{scs}}{Z_{scp}Z_{scs} - Z_{scm}^2}, \\ Y_{scs} &= \frac{Z_{scp}}{Z_{scp}Z_{scs} - Z_{scm}^2}, \\ Y_{scm} &= \frac{Z_{scm}}{Z_{scp}Z_{scs} - Z_{scm}^2}. \end{aligned} \right\} \tag{3.72}$$

It is observed that up to three short-circuit tests may be required to characterise the matrices of short-circuit parameters. However, the primary and secondary short-circuit admittances are almost the same when expressed in per-unit values, say  $Y_{sc}$ . Owing to the strong magnetic coupling afforded by iron cores, the mutual admittance between primary and

secondary windings can also be taken to have a value of  $Y_{sc}$ . Hence, the transformer short-circuit admittance matrix, in per units, is:

$$\begin{bmatrix} I_p \\ I_s \end{bmatrix} = \begin{bmatrix} Y_{sc} & -Y_{sc} \\ -Y_{sc} & Y_{sc} \end{bmatrix} \begin{bmatrix} V_p \\ V_s \end{bmatrix}. \tag{3.73}$$

### 3.3.2 Simple Tap-changing Transformer

The effect of expressing the transformer parameters in the per-unit system is to transform the original voltage ratio  $N_p : N_s$  into a unity voltage ratio 1 : 1. This enables a simple equivalent circuit consisting of the short-circuit admittance  $Y_{sc}$  connected between the primary bus (p) and the secondary bus (s) to describe adequately the system performance of the two-winding transformer.

However, power transformers are often fitted with a tap-changing mechanism to enable a degree of voltage magnitude regulation at one of the transformer terminals. This is achieved by injecting a small variable voltage magnitude in phase (added or subtracted) with the voltage magnitude at the output winding. Such transformers are termed load tap-changing (ltc) transformers and play an important role in power flow studies. The representation of an ltc transformer may be achieved by the series connection of the short-circuit admittance representing a per-unit transformer and an ideal transformer with taps ratio  $T : 1$  (Laughton, 1968). This arrangement is shown in Figure 3.11.

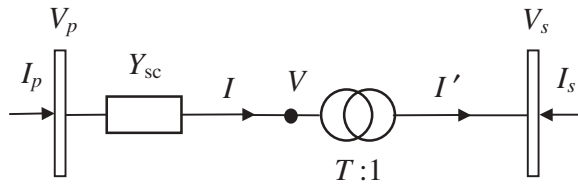


Figure 3.11 Simple tap-changing transformer

The following relationships exist in the ideal transformer,

$$\frac{V}{V_s} = \frac{T}{1}, \quad \text{and} \quad \frac{T}{1} = \frac{I'}{I}. \tag{3.74}$$

The current across the admittance  $Y_{sc}$  is:

$$I = Y_{sc}(V_p - V) = Y_{sc}(V_p - TV_s) = I_p. \tag{3.75}$$

Also,

$$I' = TI = Y_{sc}(TV_p - T^2V_s) = -I_s. \tag{3.76}$$

Combining Equations (3.75) and (3.76) in matrix form gives:

$$\begin{bmatrix} I_p \\ I_s \end{bmatrix} = \begin{bmatrix} Y_{sc} & -TY_{sc} \\ -TY_{sc} & T^2Y_{sc} \end{bmatrix} \begin{bmatrix} V_p \\ V_s \end{bmatrix}. \tag{3.77}$$

### 3.3.3 Advanced Tap-changing Transformer

Following the same line of reasoning, a comprehensive power system transformer model is derived for a single-phase three-winding transformer (Acha, Ambriz-Pérez, and Fuerte-Esquivel, 2000). Each winding is represented as the series combination of a short-circuit admittance and an ideal transformer. Furthermore, each winding is provided with a complex tap-changing mechanism to allow for tap-changing and phase-shifting facilities. Moreover, the magnetising branch of the transformer is included to account for the core losses. Figure 3.12 shows the equivalent circuit of the three-winding transformer.

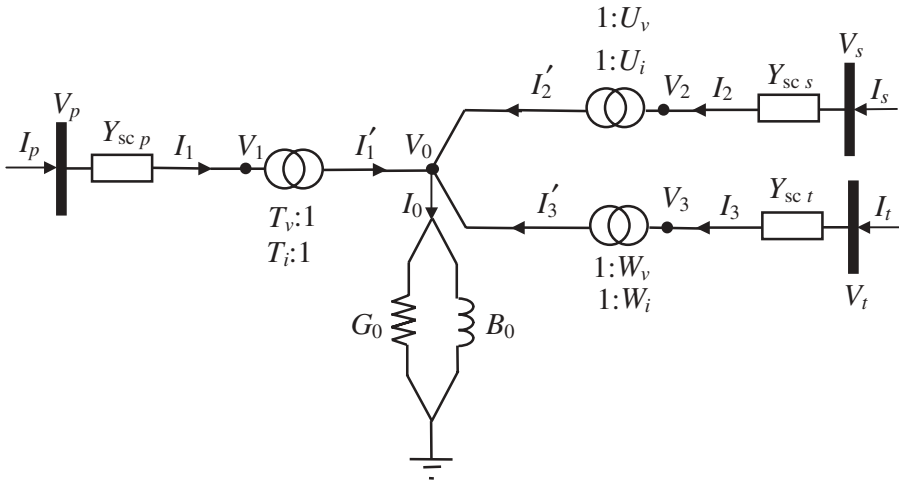


**Figure 3.12** Comprehensive tap-changing transformer. Reproduced, with permission, from E. Acha, H. Ambriz-Pérez, and C.R. Fuerte-Esquivel, ‘Advanced Transformer Control Modelling in an Optimal Power Flow using Newton’s Method’, *IEEE Trans. Power Systems* **15**(1) 290–298, © 2000 IEEE

The primary winding is represented as an ideal transformer having complex tap ratios  $T_v : 1$  and  $T_i : 1$  in series with the admittance  $Y_{sc p}$ , where  $T_v = T_i^* = t + j\alpha = T\angle\phi_t$ . The symbol \* denotes the conjugate operation. The secondary winding is represented as an ideal transformer having complex tap ratios  $U_v : 1$  and  $U_i : 1$  in series with the admittance  $Y_{sc s}$ , where  $U_v = U_i^* = u + j\beta = U\angle\phi_u$ . Similarly, the ideal transformer in the tertiary winding has complex tap ratios  $W_v : 1$  and  $W_i : 1$  in series with an admittance  $Y_{sc t}$ , where  $W_v = W_i^* = w + j\gamma = W\angle\phi_w$ . It is assumed here that  $Y_{sc p}$ ,  $Y_{sc s}$  and  $Y_{sc t}$  are the short-circuit admittances of the primary, secondary, and tertiary windings, respectively. The magnetising branch of the transformer is represented by the admittance  $Y_0 = G_0 + jB_0$ .

The resistive path of the magnetising branch is directly related to the iron losses, and its conductance  $G_0$  draws a current that varies linearly with the voltage across the magnetising branch. However, in the inductive path the relationship between the current and the voltage is dictated by the rms  $V$ - $I$  characteristic, which under saturating conditions becomes non-linear.

The following relationships exist in the ideal primary, secondary, and tertiary transformers:

$$\frac{V_1}{V_0} = \frac{T_v}{1}, \quad \text{and} \quad \frac{T_i}{1} = \frac{I'_1}{I_1}, \quad (3.78)$$

$$\frac{V_2}{V_0} = \frac{U_v}{1}, \quad \text{and} \quad \frac{U_i}{1} = \frac{I'_2}{I_2}, \quad (3.79)$$

$$\frac{V_3}{V_0} = \frac{W_v}{1}, \quad \text{and} \quad \frac{W_i}{1} = \frac{I'_3}{I_3}. \quad (3.80)$$

The currents across the admittances  $Y_{scp}$ ,  $Y_{scs}$ , and  $Y_{sct}$  are, respectively,

$$I_1 = Y_{scp}(V_p - V_1) = Y_{scp}(V_p - T_v V_0) = I_p, \quad (3.81)$$

$$I_2 = Y_{scs}(V_s - V_2) = Y_{scs}(V_s - U_v V_0) = I_s, \quad (3.82)$$

$$I_3 = Y_{sct}(V_t - V_3) = Y_{sct}(V_t - W_v V_0) = I_t, \quad (3.83)$$

and at the centre of the transformer the following relationship holds:

$$0 = I'_1 + I'_2 + I'_3 - I_0 = T_i I_1 + U_i I_2 + W_i I_3 - I_0. \quad (3.84)$$

Substituting Equations (3.81)–(3.83) into Equation (3.84) gives:

$$0 = -T_v^* Y_{scp} V_p - U_v^* Y_{scs} V_s - W_v^* Y_{sct} V_t + (T_v^2 Y_{scp} + U_v^2 Y_{scs} + W_v^2 Y_{sct} + Y_0) V_0. \quad (3.85)$$

Putting Equations (3.81)–(3.83) and (3.85) in matrix form gives:

$$\begin{bmatrix} I_p \\ I_s \\ I_t \\ 0 \end{bmatrix} = \begin{bmatrix} Y_{scp} & 0 & 0 & -T_v Y_{scp} \\ 0 & Y_{scs} & 0 & -U_v Y_{scs} \\ 0 & 0 & Y_{sct} & -W_v Y_{sct} \\ -T_v^* Y_{scp} & -U_v^* Y_{scs} & -W_v^* Y_{sct} & T_v^2 Y_{scp} + U_v^2 Y_{scs} + W_v^2 Y_{sct} + Y_0 \end{bmatrix} \begin{bmatrix} V_p \\ V_s \\ V_t \\ V_0 \end{bmatrix}. \quad (3.86)$$

Equation (3.86) represents the transformer shown in Figure 3.12. However, it is possible to find a reduced equivalent matrix that still models the transformer correctly while retaining only the external buses  $p$ ,  $s$ , and  $t$ . This is done by means of Gaussian elimination:

$$\begin{bmatrix} I_p \\ I_s \\ I_t \end{bmatrix} = \frac{1}{\Delta} \begin{bmatrix} U_v^2 Y_{scp} Y_{scs} + W_v^2 Y_{scp} Y_{sct} + Y_{scp} Y_0 & -T_v U_v^* Y_{scp} Y_{scs} \\ -T_v^* U_v Y_{scp} Y_{scs} & T_v^2 Y_{scs} Y_{scp} + W_v^2 Y_{scs} Y_{sct} + Y_{scs} Y_0 \\ -T_v^* W_v Y_{scp} Y_{sct} & -U_v^* W_v Y_{scs} Y_{sct} \\ -T_v W_v^* Y_{scp} Y_{sct} & -U_v W_v^* Y_{scs} Y_{sct} \\ T_v^2 Y_{sct} Y_{scp} + U_v^2 Y_{sct} Y_{scs} + Y_{sct} Y_0 & \end{bmatrix} \begin{bmatrix} V_p \\ V_s \\ V_t \end{bmatrix}, \quad (3.87)$$

where

$$\Delta = T_v^2 Y_{scp} + U_v^2 Y_{scs} + W_v^2 Y_{sct} + Y_0.$$

The nodal admittance representation of a two-winding transformer can be easily obtained by introducing simplifying assumptions in Equation (3.87). For instance, when the tertiary winding does not exist, the row and column corresponding to this bus become redundant and they are removed from Equation (3.87). Moreover, the tap ratios  $W_v$  and  $W_i$  become zero. Hence, the nodal admittance matrix equation representing the two-winding transformer is arrived at:

$$\begin{bmatrix} I_p \\ I_s \end{bmatrix} = \frac{1}{\Delta} \begin{bmatrix} U_v^2 Y_{scp} Y_{scs} + Y_{scp} Y_0 & -T_v U_v^* Y_{scp} Y_{scs} \\ -T_v^* U_v Y_{scp} Y_{scs} & T_v^2 Y_{scs} Y_{scp} + Y_{scs} Y_0 \end{bmatrix} \begin{bmatrix} V_p \\ V_s \end{bmatrix}, \quad (3.88)$$

where

$$\Delta = T_v^2 Y_{scp} + U_v^2 Y_{scs} + Y_0.$$

It must be noted that owing to the flexibility of the two-winding transformer model in Equation (3.88), it is possible to assemble a transformer model that represents the transformer circuit shown in Figure 3.12 by using three of these two-winding transformer models. An example of how this can be achieved is shown elsewhere (see Acha, Ambriz-Pérez, and Fuerte-Esquivel, 2000).

Transformer models with more constrained tapping arrangements can also be derived from Equation (3.88). For instance, take the case of the tap-changing transformer shown in Figure 3.11, represented by Equation (3.77). Such a representation can be derived from Equation (3.88) by including no magnetising branch,  $Y_0 = 0$ , and a nominal tapping position for the secondary winding,  $U_v = 1$ . Moreover, the tapping position of the primary winding is real as opposed to complex,  $T_v = T$ , and the short-circuit admittance is assumed to be all on the primary side,  $Y_{scs} = 0$  and  $Y_{scp} = Y_{sc}$ . The latter consideration requires application of L'Hopital differentiation rule with respect to  $Y_{scs}$ .

A further strength of the transformer model in Equation (3.88) is that, owing to the complex nature of their taps, it represents rather well the system behaviour of a phase-shifting (PS) two-winding transformer. This is more easily appreciated if it is assumed that in Equation (3.88) both complex taps have unit magnitudes:

$$\left. \begin{aligned} T_v &= 1 \angle \phi_t = \cos \phi_t + j \sin \phi_t, \\ U_v &= 1 \angle \phi_v = \cos \phi_v + j \sin \phi_v. \end{aligned} \right\} \quad (3.89)$$

Hence,

$$\begin{bmatrix} I_p \\ I_s \end{bmatrix} = \frac{1}{Y_{scp} + Y_{scs} + Y_0} \begin{bmatrix} Y_{scp}(Y_{scs} + Y_0) \\ -Y_{scp}(\cos \phi_t - j \sin \phi_t) \times Y_{scs}(\cos \phi_u + j \sin \phi_u) \\ -Y_{scp}(\cos \phi_t + j \sin \phi_t) \times Y_{scs}(\cos \phi_u - j \sin \phi_u) \\ Y_{scs}(Y_{scp} + Y_0) \end{bmatrix} \begin{bmatrix} V_p \\ V_s \end{bmatrix}. \quad (3.90)$$

This is a comprehensive model of a PS transformer that yields very flexible power flow and optimal power flow PS models, as will be shown in Chapters 4 and 7, respectively.

### 3.3.4 Three-phase Transformers

Based on nodal analysis, quite general models for multiwindings, multiphase transformers can be derived (Chen and Dillon, 1974; Laughton, 1968). The essence of the method is to transform the short-circuit parameters of the transformer windings, suitably arranged in a

matrix of primitive parameters  $\mathbf{Y}_{\psi\psi}$ , into nodal parameters  $\mathbf{Y}_{\alpha\alpha}$ . This is done with the help of appropriate connectivity matrices, namely,  $\mathbf{C}_{\alpha\psi}$  and  $\mathbf{C}_{\psi\alpha}$ . The connectivity matrices relate the voltages and currents in the unconnected transformer windings to the phase voltages and currents when the three-phase transformer is actually connected.

The primitive and nodal parameters are related by the following matrix expression:

$$\mathbf{Y}_{\alpha\alpha} = \mathbf{C}_{\alpha\psi} \mathbf{Y}_{\psi\psi} \mathbf{C}_{\psi\alpha}. \tag{3.91}$$

The primitive parameters of three identical single-phase transformers, for which the terminals between transformers are not connected in any way but contain off-nominal tapping facilities on the primary winding, have the following arrangement:

$$\left. \begin{aligned} \begin{bmatrix} I_1 \\ I_2 \end{bmatrix} &= \begin{bmatrix} Y_{sc} & -T_v Y_{sc} \\ -T_v^* Y_{sc} & T_v^2 Y_{sc} \end{bmatrix} \begin{bmatrix} V_1 \\ V_2 \end{bmatrix}, \\ \begin{bmatrix} I_3 \\ I_4 \end{bmatrix} &= \begin{bmatrix} Y_{sc} & -T_v Y_{sc} \\ -T_v^* Y_{sc} & T_v^2 Y_{sc} \end{bmatrix} \begin{bmatrix} V_3 \\ V_4 \end{bmatrix} \Rightarrow \begin{bmatrix} I_1 \\ I_2 \\ I_3 \\ I_4 \\ I_5 \\ I_6 \end{bmatrix} = \begin{bmatrix} Y_{sc} & -T_v Y_{sc} & 0 & 0 & 0 & 0 \\ -T_v^* Y_{sc} & T_v^2 Y_{sc} & 0 & 0 & 0 & 0 \\ 0 & 0 & Y_{sc} & -T_v Y_{sc} & 0 & 0 \\ 0 & 0 & -T_v^* Y_{sc} & T_v^2 Y_{sc} & 0 & 0 \\ 0 & 0 & 0 & 0 & Y_{sc} & -T_v Y_{sc} \\ 0 & 0 & 0 & 0 & -T_v^* Y_{sc} & T_v^2 Y_{sc} \end{bmatrix} \begin{bmatrix} V_1 \\ V_2 \\ V_3 \\ V_4 \\ V_5 \\ V_6 \end{bmatrix}, \\ \begin{bmatrix} I_5 \\ I_6 \end{bmatrix} &= \begin{bmatrix} Y_{sc} & -T_v Y_{sc} \\ -T_v^* Y_{sc} & T_v^2 Y_{sc} \end{bmatrix} \begin{bmatrix} V_5 \\ V_6 \end{bmatrix}. \end{aligned} \right\} \tag{3.92}$$

In general, these matrix equations may be expressed in compact form:

$$\mathbf{I}_{\psi} = \mathbf{Y}_{\psi\psi} \mathbf{V}_{\psi}. \tag{3.93}$$

The three single-phase transformers, when suitably connected, electrically speaking, may serve the purpose of transforming three-phase voltages and currents. The assembly is termed a ‘three-phase bank’. Each single-phase unit in the bank is closely associated with one phase of the three-phase system. Depending on the electrical connection and operating conditions, there may be currents from more than one phase circulating in one single-phase unit at any one time, but there are not flux interactions between windings of different units.

Quite a different situation prevails in multilimb transformers, where all windings of the three-phase unit are magnetically coupled. The primitive admittance matrix equation of the two-winding, three-phase transformers is a full matrix, and up to 21 short-circuit tests may be required to define fully this primitive admittance matrix. In the remainder of this chapter only the three-phase bank will be addressed.

The three most popular three-phase transformer connections found in high-voltage transmission are addressed below, namely the star–star, delta–delta, and star–delta. To determine their nodal admittance matrix models, one requires information of the matrix of primitive parameters,  $\mathbf{Y}_{\psi\psi}$ , and the relevant connectivity matrices,  $\mathbf{C}_{\alpha\psi}$  and  $\mathbf{C}_{\psi\alpha}$ .

### 3.3.4.1 Star-star connection

The three-phase connection is shown in Figure 3.13 when the windings are connected in star–star configuration, with both star points grounded through admittances,  $Y_N$  and  $Y_n$ , respectively.

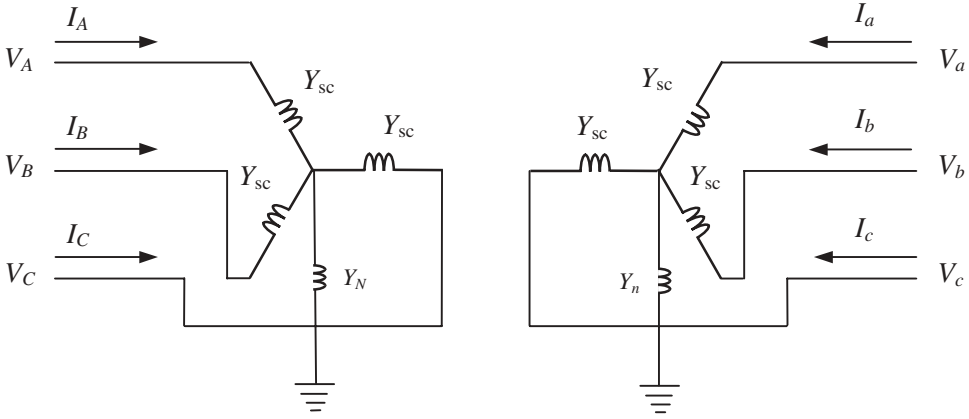


**Figure 3.13** Star–star connection

The transformation matrix, which relates the voltages existing in the unconnected transformer to the voltages in the connected three-phase transformer shown in Figure 3.13, is given explicitly in Equation (3.94):

$$\begin{bmatrix} V_1 \\ V_2 \\ V_3 \\ V_4 \\ V_5 \\ V_6 \\ V_7 \\ V_8 \end{bmatrix} = \begin{bmatrix} 1 & 0 & 0 & 0 & 0 & 0 & -1 & 0 \\ 0 & 0 & 0 & 1 & 0 & 0 & 0 & -1 \\ 0 & 1 & 0 & 0 & 0 & 0 & -1 & 0 \\ 0 & 0 & 0 & 0 & 1 & 0 & 0 & -1 \\ 0 & 0 & 1 & 0 & 0 & 0 & -1 & 0 \\ 0 & 0 & 0 & 0 & 0 & 1 & 0 & -1 \\ 0 & 0 & 0 & 0 & 0 & 0 & 1 & 0 \\ 0 & 0 & 0 & 0 & 0 & 0 & 0 & 1 \end{bmatrix} \begin{bmatrix} V_A \\ V_B \\ V_C \\ V_a \\ V_b \\ V_c \\ V_N \\ V_n \end{bmatrix} \tag{3.94}$$

In compact form, we have,

$$\mathbf{V}_\psi = \mathbf{C}_{\psi/\alpha} \mathbf{V}_\alpha \tag{3.95}$$

The nodal matrix representation of this transformer connection is obtained by substituting Equations (3.92) and (3.94) into Equation (3.91):

$$\begin{bmatrix} I_A \\ I_B \\ I_C \\ I_a \\ I_b \\ I_c \\ I_N \\ I_n \end{bmatrix} = \begin{bmatrix} Y_{sc} & 0 & 0 & -T_v Y_{sc} & 0 & 0 & -Y_{sc} & T_v Y_{sc} \\ 0 & Y_{sc} & 0 & 0 & -T_v Y_{sc} & 0 & -Y_{sc} & T_v Y_{sc} \\ 0 & 0 & Y_{sc} & 0 & 0 & -T_v Y_{sc} & -Y_{sc} & T_v Y_{sc} \\ -T_v^* Y_{sc} & 0 & 0 & T_v^2 Y_{sc} & 0 & 0 & T_v^* Y_{sc} & -T_v^2 Y_{sc} \\ 0 & -T_v^* Y_{sc} & 0 & 0 & T_v^2 Y_{sc} & 0 & T_v^* Y_{sc} & -T_v^2 Y_{sc} \\ 0 & 0 & -T_v^* Y_{sc} & 0 & 0 & T_v^2 Y_{sc} & T_v^* Y_{sc} & -T_v^2 Y_{sc} \\ -Y_{sc} & -Y_{sc} & -Y_{sc} & T_v Y_{sc} & T_v Y_{sc} & T_v Y_{sc} & 3Y_{sc} + Y_N & -3T_v Y_{sc} \\ T_v^* Y_{sc} & T_v^* Y_{sc} & T_v^* Y_{sc} & -T_v^2 Y_{sc} & -T_v^2 Y_{sc} & -T_v^2 Y_{sc} & -3T_v^* Y_{sc} & 3T_v^2 Y_{sc} + Y_n \end{bmatrix} \begin{bmatrix} V_A \\ V_B \\ V_C \\ V_a \\ V_b \\ V_c \\ V_N \\ V_n \end{bmatrix} \tag{3.96}$$

If both star points  $N$  and  $n$  are solidly grounded then the nodal voltages  $V_N$  and  $V_n$  become zero. Hence, the rows and columns corresponding to bus  $N$  and bus  $n$  become redundant and

are deleted from matrix Equation (3.96):

$$\begin{bmatrix} I_A \\ I_B \\ I_C \\ I_a \\ I_b \\ I_c \end{bmatrix} = \begin{bmatrix} Y_{sc} & 0 & 0 & -T_v Y_{sc} & 0 & 0 \\ 0 & Y_{sc} & 0 & 0 & -T_v Y_{sc} & 0 \\ 0 & 0 & Y_{sc} & 0 & 0 & -T_v Y_{sc} \\ -T_v^* Y_{sc} & 0 & 0 & T_v^2 Y_{sc} & 0 & 0 \\ 0 & -T_v^* Y_{sc} & 0 & 0 & T_v^2 Y_{sc} & 0 \\ 0 & 0 & -T_v^* Y_{sc} & 0 & 0 & T_v^2 Y_{sc} \end{bmatrix} \begin{bmatrix} V_A \\ V_B \\ V_C \\ V_a \\ V_b \\ V_c \end{bmatrix} \quad (3.97)$$

### 3.3.4.2 Delta-delta connection

This transformer connection is shown in Figure 3.14. In the delta connection the following relationships exist between the voltages and currents in the connected and unconnected circuits:

$$\mathbf{V}_\psi = \frac{1}{\sqrt{3}} \mathbf{C}_{\psi\alpha} \mathbf{V}_\alpha, \quad (3.98)$$

$$\sqrt{3} \mathbf{I}_\alpha = \mathbf{C}_{\alpha\psi} \mathbf{I}_\psi. \quad (3.99)$$

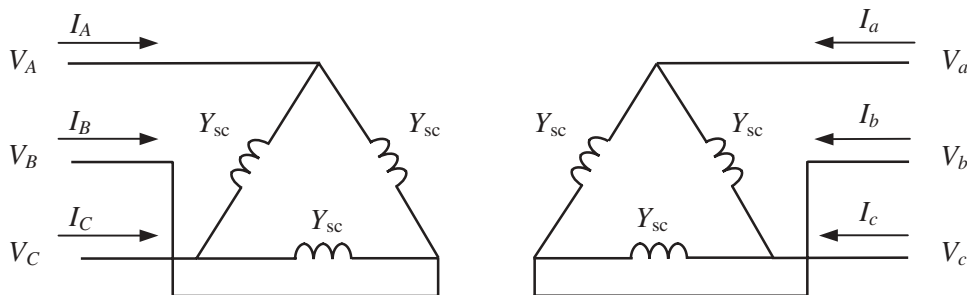


Figure 3.14 Delta-delta connection

The relevant connectivity matrices for this transformer connection are set up and, upon substitution in Equation (3.91), the following nodal admittance matrix is arrived at:

$$\begin{bmatrix} I_A \\ I_B \\ I_C \\ I_a \\ I_b \\ I_c \end{bmatrix} = \frac{1}{3} \begin{bmatrix} 2Y_{sc} & -Y_{sc} & -Y_{sc} & -2T_v Y_{sc} & T_v Y_{sc} & T_v Y_{sc} \\ -Y_{sc} & 2Y_{sc} & -Y_{sc} & T_v Y_{sc} & -2T_v Y_{sc} & T_v Y_{sc} \\ -Y_{sc} & -Y_{sc} & 2Y_{sc} & T_v Y_{sc} & T_v Y_{sc} & -2T_v Y_{sc} \\ -2T_v^* Y_{sc} & T_v^* Y_{sc} & T_v^* Y_{sc} & 2T_v^2 Y_{sc} & -T_v^2 Y_{sc} & -T_v^2 Y_{sc} \\ T_v^* Y_{sc} & -2T_v^* Y_{sc} & T_v^* Y_{sc} & -T_v^2 Y_{sc} & 2T_v^2 Y_{sc} & -T_v^2 Y_{sc} \\ T_v^* Y_{sc} & T_v^* Y_{sc} & -2T_v^* Y_{sc} & -T_v^2 Y_{sc} & -T_v^2 Y_{sc} & 2T_v^2 Y_{sc} \end{bmatrix} \begin{bmatrix} V_A \\ V_B \\ V_C \\ V_a \\ V_b \\ V_c \end{bmatrix} \quad (3.100)$$

### 3.3.4.3 Star-delta connection

This transformer connection is shown in Figure 3.15 for the case when the star point is solidly grounded. Following a similar procedure to that used to derive the nodal admittance

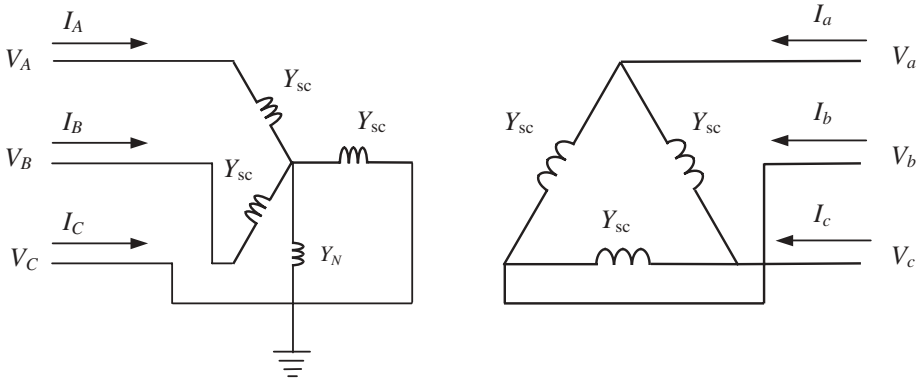


Figure 3.15 Star-delta connection

matrices of the star-star and delta-delta connections, the nodal matrix representation of this transformer connection is:

$$\begin{bmatrix} I_A \\ I_B \\ I_C \\ I_a \\ I_b \\ I_c \end{bmatrix} = \begin{bmatrix} Y_{sc} & 0 & 0 & -T_v Y_{sc}/\sqrt{3} & T_v Y_{sc}/\sqrt{3} & 0 \\ 0 & Y_{sc} & 0 & 0 & -T_v Y_{sc}/\sqrt{3} & T_v Y_{sc}/\sqrt{3} \\ 0 & 0 & Y_{sc} & T_v Y_{sc}/\sqrt{3} & 0 & -T_v Y_{sc}/\sqrt{3} \\ -T_v^* Y_{sc}/\sqrt{3} & 0 & T_v^* Y_{sc}/\sqrt{3} & 2T_v^2 Y_{sc}/3 & -T_v^2 Y_{sc}/3 & -T_v^2 Y_{sc}/3 \\ T_v^* Y_{sc}/\sqrt{3} & -T_v^* Y_{sc}/\sqrt{3} & 0 & -T_v^2 Y_{sc}/3 & 2T_v^2 Y_{sc}/3 & -T_v^2 Y_{sc}/3 \\ 0 & T_v^* Y_{sc}/\sqrt{3} & -T_v^* Y_{sc}/\sqrt{3} & -T_v^2 Y_{sc}/3 & -T_v^2 Y_{sc}/3 & 2T_v^2 Y_{sc}/3 \end{bmatrix} \begin{bmatrix} V_A \\ V_B \\ V_C \\ V_a \\ V_b \\ V_c \end{bmatrix} \tag{3.101}$$

### 3.3.5 Sequence Domain Parameters

Transformer parameters are also amenable to representation in the frame of reference of the sequences (Chen and Dillon, 1974). The matrix of symmetrical components and its inverse, given in Equations (3.57), are used to such effect. This requires that the order of all matrices involved in the exercise be a multiple of three. This characteristic is met by matrices representing the star-star connected transformer with both star points solidly grounded, the delta-delta transformer, and the star-delta transformer with the star point solidly grounded. It should be noted that the symmetrical components transform given in Equations (3.57) cannot directly be applied to cases of star-connected windings, where one or two star points are not grounded or are grounded through earthing impedances. In such cases, Kron's reductions are applied first to find out reduced equivalent representations which are a function only of phase terminals. This follows the spirit of the procedure presented in Section 3.2.2 for the elimination of transmission line ground wires.

A generic, compact representation of Equations (3.97), (3.100), and (3.101) corresponding to the star-star, delta-delta, and star-delta connections may be expressed as:

$$\begin{bmatrix} \mathbf{I}_{ABC} \\ \mathbf{I}_{abc} \end{bmatrix} = \begin{bmatrix} \mathbf{Y}_I & -\mathbf{Y}_{II} \\ -\mathbf{Y}_{III} & \mathbf{Y}_{IV} \end{bmatrix} \begin{bmatrix} \mathbf{V}_{ABC} \\ \mathbf{V}_{abc} \end{bmatrix}, \tag{3.102}$$

where the order of matrices  $\mathbf{Y}_I, \mathbf{Y}_{II}, \mathbf{Y}_{III}, \mathbf{Y}_{IV}$  is  $3 \times 3$  and suitable for direct treatment by the matrix of symmetrical components, to enable representation in the frame of reference of the sequences. This is achieved by applying the following symmetrical component operations:

$$\left. \begin{aligned} \mathbf{Y}_i &= \mathbf{T}_S^{-1} \mathbf{Y}_I \mathbf{T}_S, \\ \mathbf{Y}_{ii} &= \mathbf{T}_S^{-1} \mathbf{Y}_{II} \mathbf{T}_S, \\ \mathbf{Y}_{iii} &= \mathbf{T}_S^{-1} \mathbf{Y}_{III} \mathbf{T}_S, \\ \mathbf{Y}_{iv} &= \mathbf{T}_S^{-1} \mathbf{Y}_{IV} \mathbf{T}_S. \end{aligned} \right\} \quad (3.103)$$

Table 3.1 shows matrices  $\mathbf{Y}_i, \mathbf{Y}_{ii}, \mathbf{Y}_{iii},$  and  $\mathbf{Y}_{iv}$  in explicit form, for the star–star, delta–delta, and star–delta transformer connections.

**Table 3.1** Transformer sequence domain admittances

Matrix type	Star–star	Delta–delta	Star–delta
$\mathbf{Y}_i$	$\begin{bmatrix} Y_{sc} & 0 & 0 \\ 0 & Y_{sc} & 0 \\ 0 & 0 & Y_{sc} \end{bmatrix}$	$\begin{bmatrix} 0 & 0 & 0 \\ 0 & Y_{sc} & 0 \\ 0 & 0 & Y_{sc} \end{bmatrix}$	$\begin{bmatrix} Y_{sc} & 0 & 0 \\ 0 & Y_{sc} & 0 \\ 0 & 0 & Y_{sc} \end{bmatrix}$
$\mathbf{Y}_{ii}$	$\begin{bmatrix} T_v Y_{sc} & 0 & 0 \\ 0 & T_v Y_{sc} & 0 \\ 0 & 0 & T_v Y_{sc} \end{bmatrix}$	$\begin{bmatrix} 0 & 0 & 0 \\ 0 & T_v Y_{sc} & 0 \\ 0 & 0 & T_v Y_{sc} \end{bmatrix}$	$\begin{bmatrix} 0 & 0 & 0 \\ 0 & T_v Y_{sc} \angle 30^\circ & 0 \\ 0 & 0 & T_v Y_{sc} \angle -30^\circ \end{bmatrix}$
$\mathbf{Y}_{iii}$	$\begin{bmatrix} T_v^* Y_{sc} & 0 & 0 \\ 0 & T_v^* Y_{sc} & 0 \\ 0 & 0 & T_v^* Y_{sc} \end{bmatrix}$	$\begin{bmatrix} 0 & 0 & 0 \\ 0 & T_v^* Y_{sc} & 0 \\ 0 & 0 & T_v^* Y_{sc} \end{bmatrix}$	$\begin{bmatrix} 0 & 0 & 0 \\ 0 & T_v^* Y_{sc} \angle -30^\circ & 0 \\ 0 & 0 & T_v^* Y_{sc} \angle 30^\circ \end{bmatrix}$
$\mathbf{Y}_{iv}$	$\begin{bmatrix} T_v^2 Y_{sc} & 0 & 0 \\ 0 & T_v^2 Y_{sc} & 0 \\ 0 & 0 & T_v^2 Y_{sc} \end{bmatrix}$	$\begin{bmatrix} 0 & 0 & 0 \\ 0 & T_v^2 Y_{sc} & 0 \\ 0 & 0 & T_v^2 Y_{sc} \end{bmatrix}$	$\begin{bmatrix} 0 & 0 & 0 \\ 0 & T_v^2 Y_{sc} & 0 \\ 0 & 0 & T_v^2 Y_{sc} \end{bmatrix}$

The sequence domain representation of a transformer, in compact form, is:

$$\begin{bmatrix} \mathbf{I}_{012p} \\ \mathbf{I}_{012s} \end{bmatrix} = \begin{bmatrix} \mathbf{Y}_i^{(i)} & -\mathbf{Y}_i^{(ii)} \\ -\mathbf{Y}_i^{(iii)} & \mathbf{Y}_i^{(iv)} \end{bmatrix} \begin{bmatrix} \mathbf{V}_{012p} \\ \mathbf{V}_{012s} \end{bmatrix}, \quad (3.104)$$

where the subscripts 0, 1, and 2 refer to zero, positive, and negative sequence quantities, respectively. It has been emphasised in various points.

Careful examination of the sequence domain parameters indicates that three independent transfer admittance matrix equations, leading to three independent circuits, are generated for a three-phase transformer. This is more easily realised if the transformer taps are taken to be

real as opposed to complex, yielding symmetrical matrix equations and, hence, reciprocal circuits. The star–star, delta–delta, and star–delta connections share the same positive and negative sequence equivalent circuits, given in Figure 3.16.

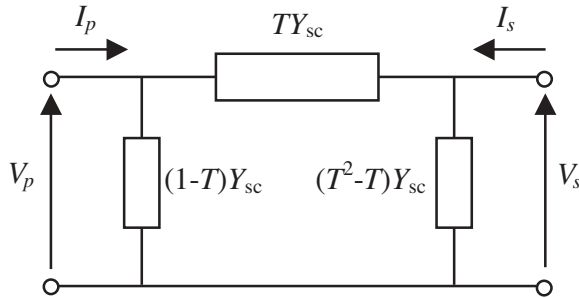


**Figure 3.16** Positive and negative sequence equivalent circuit for the star–star, delta–delta, and star–delta connections

In contrast, the zero sequence equivalent circuits for the three connections differ from one another. The equivalent circuits are shown in Figures 3.17(a), 3.17(b), and 3.17(c) for the star–star, delta–delta, and star–delta connections, respectively.

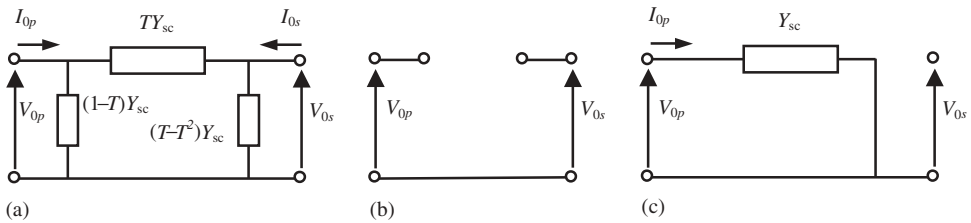


**Figure 3.17** Zero sequence equivalent circuits for: (a) star–star, (b) delta–delta, and (c) star–delta connections

It should be noted that for the star–delta transformer connection the primary and secondary terminals of the zero sequence equivalent circuit are not electrically connected. However, the primary terminal contains an admittance  $Y_{sc}$  connected between this terminal and the reference. It is also interesting to note that the positive and negative transfer admittances contain an asymmetrical phase shift of  $30^\circ$  between the primary and secondary terminals giving rise to nonreciprocal equivalent circuits. The asymmetrical phase shift is entirely attributable to the star–delta connection and it is present even when no taps are available in the transformer. It is common practice in application studies, such as positive sequence power flow and sequence domain-based fault levels to ignore the phase shift during the calculations and then to account for it during the analysis of results.

### 3.4 ROTATING MACHINERY MODELLING

In general, synchronous machines are grouped into two main types, according to their rotor structure: round rotor and salient pole machines (Grainger and Stevenson, 1994). Steam turbine driven generators (turbogenerators) work at high speed and have cylindrical rotors. The rotor carries a DC excited field winding. Hydro units work at low speed and have salient pole rotors. They normally have damper windings in addition to the field winding. Damper windings consist of bars placed in slots on the pole faces and connected together at both ends. Turbogenerators contain no damper windings but the solid steel of the rotor offers a path for eddy currents, which have similar damping effects.

For simulation purposes, the currents circulating in the solid steel or in the damping windings can be treated as currents circulating in two closed circuits. Accordingly, a three-phase synchronous machine may be assumed to have three stator windings and three rotor windings. This is illustrated in Figure 3.18, where all six windings are magnetically coupled.

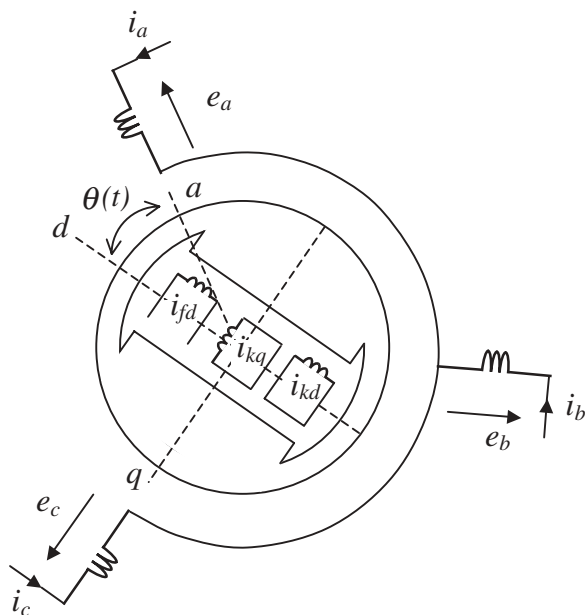


**Figure 3.18** Schematic representation of a three-phase synchronous generator. Redrawn by permission of the Institution of Electrical Engineers from R.G. Wasley and M.A. Shlash, 'Steady-state Phase-variable Model of the Synchronous Machine for Use in 3-phase Load-flow Studies', *Proceedings of the IEEE* **121**(10) 1155–1164 © 1974 IEEE

The relative position of the rotor with respect to the stator is given by the angle  $\theta$  between the rotor's direct axis and the stator's phase  $a$  axis, termed the  $d$  axis and  $a$  axis, respectively. In the stator, the axis of phases  $a$ ,  $b$ , and  $c$  are displaced from each other by 120 electrical degrees. In the rotor, the  $d$  axis is magnetically centred in the north pole of the machine. A

second axis, located 90 electrical degrees behind the  $d$  axis is termed the quadrature axis or  $q$  axis.

Three main control systems directly affect the turbine-generator set, namely the boiler's firing control, the governor control, and the excitation system control. The excitation system consists of the exciter and absolute value rectifier (AVR). The latter regulates the generator terminal voltage by controlling the amount of current supplied to the field winding by the exciter. For the purpose of steady-state analysis, it is assumed that the three control systems act in an idealised manner, enabling the synchronous generator to produce constant power output, to run at synchronous speed, and to regulate voltage magnitude at the generator's terminal with no delay and up to its reactive power design limits.

### 3.4.1 Machine Voltage Equation

The objective of this section is to derive a steady-state expression for the stator three-phase voltages and currents of the synchronous generator (Wasley and Shlash, 1974b). The rotor emfs (electromagnetic forces) and saliency are accounted for in the resulting voltage equation, which may form the basis for connecting the machine model to a given three-phase bus of an unbalanced power system representation.

With reference to Figure 3.18, using stator and rotor quantities expressed in frames of reference attached to their respective physical circuits, namely stator and rotor circuits, the instantaneous voltages of the machine may be expressed as:

$$\mathbf{v} = \mathbf{R}\mathbf{i} + p\mathbf{L}\mathbf{i}, \quad (3.105)$$

where  $\mathbf{R}$  and  $\mathbf{L}$  are the machine resistance and inductance matrices, respectively, and  $p$  is the time derivative operator.

Furthermore, expanding Equation (3.105) into stator and rotor subsets, we obtain:

$$\begin{bmatrix} \mathbf{v}_s \\ \mathbf{v}_r \end{bmatrix} = \begin{bmatrix} \mathbf{R}_s & \mathbf{0} \\ \mathbf{0} & \mathbf{R}_r \end{bmatrix} \begin{bmatrix} \mathbf{i}_s \\ \mathbf{i}_r \end{bmatrix} + \omega_r \begin{bmatrix} \mathbf{G}_{ss} & \mathbf{G}_{sr} \\ \mathbf{G}'_{sr} & \mathbf{0} \end{bmatrix} \begin{bmatrix} \mathbf{i}_s \\ \mathbf{i}_r \end{bmatrix} + \begin{bmatrix} \mathbf{L}_{ss} & \mathbf{L}_{sr} \\ \mathbf{L}'_{sr} & \mathbf{L}_{rr} \end{bmatrix} \begin{bmatrix} p\mathbf{i}_s \\ p\mathbf{i}_r \end{bmatrix}, \quad (3.106)$$

where  $\mathbf{G} = d\mathbf{L}/d\theta$ ;  $\omega_r$ , equal to  $d\theta/dt$ , is the rotor speed; and  $\theta = \omega_r t + \delta$ .

The submatrix coefficients  $\mathbf{L}$ ,  $\mathbf{G}$ , and  $\mathbf{R}$  are:

$$\mathbf{L}_{ss} = \begin{bmatrix} L_{aa0} + L_{a2} \cos(2\theta) & -L_{ab0} - L_{a2} \cos(2\theta + 60) & -L_{ab0} - L_{a2} \cos(2\theta - 60) \\ -L_{ab0} - L_{a2} \cos(2\theta + 60) & L_{aa0} + L_{a2} \cos(2\theta + 120) & -L_{ab0} - L_{a2} \cos(2\theta - 180) \\ -L_{ab0} - L_{a2} \cos(2\theta - 60) & -L_{ab0} - L_{a2} \cos(2\theta - 180) & L_{aa0} + L_{a2} \cos(2\theta - 120) \end{bmatrix}, \quad (3.107)$$

$$\mathbf{L}_{sr} = \begin{bmatrix} L_{af} \cos(\theta) & L_{af} \cos(\theta) & -L_{af} \sin(\theta) \\ L_{af} \cos(\theta - 120) & L_{af} \cos(\theta - 120) & -L_{af} \sin(\theta - 120) \\ L_{af} \cos(\theta + 120) & L_{af} \cos(\theta + 120) & -L_{af} \sin(\theta + 120) \end{bmatrix}, \quad (3.108)$$

$$\mathbf{L}_{rr} = \begin{bmatrix} L_{fd} & L_{mkd} & 0 \\ L_{mkd} & L_{kd} & 0 \\ 0 & 0 & L_{kq} \end{bmatrix}, \quad (3.109)$$

$$\mathbf{G}_{ss} = \begin{bmatrix} -2L_{a2} \sin(2\theta) & 2L_{a2} \sin(2\theta + 60) & 2L_{a2} \sin(2\theta - 60) \\ 2L_{a2} \sin(2\theta + 60) & -2L_{a2} \sin(2\theta + 120) & 2L_{a2} \sin(2\theta - 180) \\ 2L_{a2} \sin(2\theta - 60) & 2L_{a2} \sin(2\theta - 180) & -2L_{a2} \sin(2\theta - 120) \end{bmatrix}, \quad (3.110)$$

$$\mathbf{G}_{sr} = \begin{bmatrix} -L_{af} \sin(\theta) & -L_{af} \sin(\theta) & -L_{af} \cos(\theta) \\ -L_{af} \sin(\theta - 120) & -L_{af} \sin(\theta - 120) & -L_{af} \cos(\theta - 120) \\ -L_{af} \sin(\theta + 120) & -L_{af} \sin(\theta + 120) & -L_{af} \cos(\theta + 120) \end{bmatrix}, \quad (3.111)$$

$$\mathbf{R}_r = \begin{bmatrix} R_a & 0 & 0 \\ 0 & R_b & 0 \\ 0 & 0 & R_c \end{bmatrix}, \quad (3.112)$$

$$\mathbf{R}_r = \begin{bmatrix} R_{fd} & 0 & 0 \\ 0 & R_{kd} & 0 \\ 0 & 0 & R_{kq} \end{bmatrix}. \quad (3.113)$$

Since the rotor circuits are represented by a field winding on the  $d$  axis and two short-circuited damper windings on the  $d$  axis and  $q$  axis, respectively, the rotor voltage vector may be written as

$$\mathbf{v}_r = \begin{bmatrix} v_{fd} \\ 0 \\ 0 \end{bmatrix}, \quad (3.114)$$

where  $v_{fd}$  is the applied direct field voltage.

For the purpose of steady-state analysis, it will be assumed that the applied direct field voltage equals the voltage drop across the field resistance owing to the DC component of the field current and that additional voltages from  $R_f i_f$  can be neglected. Using such a simplification, the relevant part of Equation (3.106) is solved for  $\mathbf{p}\mathbf{i}_r$ :

$$\mathbf{p}\mathbf{i}_r = -\mathbf{L}_{rr}^{-1} [\omega \mathbf{G}_{rs} \mathbf{i}_s + \mathbf{L}_{rs} \mathbf{p}\mathbf{i}_s]. \quad (3.115)$$

Assuming the following set of unbalanced stator currents:

$$\mathbf{i}_s = \begin{bmatrix} I_1 \sin(\omega t + \beta_1) \\ I_2 \sin(\omega t + \beta_2) \\ I_3 \sin(\omega t + \beta_3) \end{bmatrix}, \quad (3.116)$$

and the fact that the rotor runs at synchronous speed (i.e.  $\omega_r = \omega$ ), we have,

$$\mathbf{p}\mathbf{i}_r = -\omega \mathbf{L}_{af} \mathbf{L}_{rr}^{-1} \sum_{m=1}^3 \begin{bmatrix} I_m \cos(\psi_m) \\ I_m \cos(\psi_m) \\ -I_m \sin(\psi_m) \end{bmatrix}, \quad (3.117)$$

where

$$\left. \begin{aligned} \psi_1 &= 2\omega t + \delta + \beta_1, \\ \psi_2 &= 2\omega t + \delta + \beta_2 - 120, \\ \psi_3 &= 2\omega t + \delta + \beta_3 + 120. \end{aligned} \right\} \quad (3.118)$$

The expression for  $\mathbf{p}\mathbf{i}_r$  can be further simplified by substituting the inverse relation of Equation (3.109) into Equation (3.117):

$$\mathbf{p}\mathbf{i}_r = \sum_{m=1}^3 \begin{bmatrix} k_1 I_m \cos(\psi_m) \\ -k_2 I_m \cos(\psi_m) \\ k_2 I_m \sin(\psi_m) \end{bmatrix}, \quad (3.119)$$

where

$$\left. \begin{aligned} k_1 &= -\frac{\omega L_{af}}{L_{fd}} \left[ 1 - \frac{L_{mkd}}{L_{kd}} \right], \\ k_2 &= \frac{\omega L_{af}}{L_{kd}}. \end{aligned} \right\} \quad (3.120)$$

It should be mentioned that the following practical simplifications have been made while substituting the inverse relation of Equation (3.109) into Equation (3.117):  $L_{fd}$  is much greater than  $L_{mkd}$ , and  $L_{kq} = L_{kd}$ .

Equation (3.119) is now integrated:

$$\mathbf{i}_r = \frac{1}{2\omega} \sum_{m=1}^3 \begin{bmatrix} k_1 I_m \sin(\psi_m) \\ -k_2 I_m \sin(\psi_m) \\ -k_2 I_m \cos(\psi_m) \end{bmatrix} + \begin{bmatrix} i_{fd} \\ 0 \\ 0 \end{bmatrix}, \quad (3.121)$$

where  $i_{fd}$  is the DC component of the field current.

Inspection of Equation (3.118) and (3.121) reveals that the presence of negative sequence currents at the machine terminals gives rise to rotor currents of double the supply frequency. In contrast, positive sequence currents are associated with zero frequency rotor currents, other than the direct field current. Also, owing to balanced machine design considerations, there is no contribution from zero sequence currents:

Substituting Equations (3.119) and (3.121) into Equation (3.106) we obtain a reduced expression for the stator voltage vector:

$$\begin{aligned} \begin{bmatrix} v_a \\ v_b \\ v_c \end{bmatrix} &= \begin{bmatrix} R_a & 0 & 0 \\ 0 & R_b & 0 \\ 0 & 0 & R_c \end{bmatrix} \begin{bmatrix} I_1 \sin(\omega t + \beta_1) \\ I_2 \sin(\omega t + \beta_2) \\ I_3 \sin(\omega t + \beta_3) \end{bmatrix} + \omega L_{aa0} \begin{bmatrix} 1 & -1 & -1 \\ -1 & 1 & -1 \\ -1 & -1 & 1 \end{bmatrix} \begin{bmatrix} I_1 \cos(\omega t + \beta_1) \\ I_2 \cos(\omega t + \beta_2) \\ I_3 \cos(\omega t + \beta_3) \end{bmatrix} \\ &+ \frac{(k_1 - 2k_2)L_{af}}{4} \begin{bmatrix} \cos(\omega t + \beta_1) & \cos(\omega t + \beta_2 - 120) & \cos(\omega t + \beta_3 + 120) \\ \cos(\omega t + \beta_1 + 120) & \cos(\omega t + \beta_2) & \cos(\omega t + \beta_3 - 120) \\ \cos(\omega t + \beta_1 - 120) & \cos(\omega t + \beta_2 + 120) & \cos(\omega t + \beta_3) \end{bmatrix} \begin{bmatrix} I_1 \\ I_2 \\ I_3 \end{bmatrix} \\ &- \frac{\omega L_{a2}}{2} \begin{bmatrix} \cos(\omega t - \beta_1 + 2\delta) & -\cos(\omega t - \beta_2 + 2\delta + 60) & -\cos(\omega t - \beta_3 + 2\delta - 60) \\ -\cos(\omega t - \beta_1 + 2\delta + 60) & \cos(\omega t - \beta_2 + 2\delta + 120) & -\cos(\omega t - \beta_3 + 2\delta - 180) \\ -\cos(\omega t - \beta_1 + 2\delta - 60) & -\cos(\omega t - \beta_2 + 2\delta - 180) & \cos(\omega t - \beta_3 + 2\delta - 120) \end{bmatrix} \\ &\times \begin{bmatrix} I_1 \\ I_2 \\ I_3 \end{bmatrix} - \omega L_{af} i_{fd} \begin{bmatrix} \sin(\omega t) \\ \sin(\omega t + \delta - 120) \\ \sin(\omega t + \delta + 120) \end{bmatrix}. \end{aligned} \quad (3.122)$$

The last term in Equation (3.122) may be interpreted as an array of rotor emfs. Moreover, taking the stator *a* phase as reference,

$$\begin{bmatrix} v_a \\ v_b \\ v_c \end{bmatrix} = \begin{bmatrix} V_1 \sin(\omega t) \\ V_2 \sin(\omega t + \alpha_2) \\ V_3 \sin(\omega t + \alpha_3) \end{bmatrix}. \quad (3.123)$$

It is seen that a root mean square (rms) form of Equation (3.122) may be established very readily. Also, by negating the stator currents to correspond to generator operating conditions, we have

$$\mathbf{E}_S = [\mathbf{R}_S + j(\mathbf{X}_1 + \mathbf{X}_2)]\mathbf{I}_S + j\mathbf{X}_3\mathbf{I}_S^* + \mathbf{V}_S, \quad (3.124)$$

where

$$\mathbf{X}_1 = \omega \begin{bmatrix} L_{aa0} & -L_{ab0} & -L_{ab0} \\ -L_{ab0} & L_{aa0} & -L_{ab0} \\ -L_{ab0} & -L_{ab0} & L_{aa0} \end{bmatrix}, \quad (3.125)$$

$$\mathbf{X}_2 = \frac{L_{af}(k_1 - 2k_2)}{4} \begin{bmatrix} 1 & h^2 & h \\ h & 1 & h^2 \\ h^2 & h & 1 \end{bmatrix}, \quad (3.126)$$

$$\mathbf{X}_3 = -\frac{\omega L_{a2} e^{j2\delta}}{2} \begin{bmatrix} 1 & h^2 & h \\ h^2 & h & 1 \\ h & 1 & h^2 \end{bmatrix}. \quad (3.127)$$

It is observed that the term  $L_{af}(k_1 - 2k_2)/4$  reduces to  $-\omega L_{af}^2/4L_{fd}$  if damper windings are not present.

As a means of evaluating the reactance elements in Equation (3.124), it is noted that the usually available *dq0* reactances of the machine may be used in the following expressions:

$$\left. \begin{aligned} \omega L_{aa0} &= \frac{1}{3}(X_d + X_q + X_0), \\ \omega L_{ab0} &= \frac{1}{6}(X_d + X_q - 2X_0), \\ \omega L_{a2} &= \frac{1}{3}(X_d - X_q). \end{aligned} \right\} \quad (3.128)$$

Equation (3.124) includes the effect of machine saliency through matrix  $\mathbf{X}_3$ , where  $(X_d - X_q)$  expresses the degree of saliency. Notice that if saliency can be ignored (i.e.  $X_d = X_q$ ) matrix  $\mathbf{X}_3$  plays no role in machine performance. Also,  $\mathbf{X}_3$  is dependent on external circuit conditions through the machine angle  $\delta$ . Matrix  $\mathbf{X}_2$  contributes negative sequence impedance, impairing the balanced behaviour of the machine.

### 3.5 SYSTEM LOAD

In general, power system loads can be classified into rotating and static loads (Weedy, 1987). A third category corresponds to power electronic-based loads. Rotating loads consist mainly of induction and synchronous motors, and their steady-state operation is affected by

voltage and frequency variations in the supply. Power electronic-based loads are also affected by voltage and frequency variations in the supply. There is general agreement that such loads are more difficult to operate because, in addition to being susceptible to supply variations, they inject harmonic current distortion back into the supply point (Acha and Madrigal, 2001).

Detailed representation of a synchronous motor load in a three-phase power flow study requires use of Equation (3.124), with changed signs to reflect the motoring action. An expression of comparable detail can be derived for the induction motor load. However, owing to the large number and diversity of loads that exist in power networks, it is preferable to group loads and to treat them as bulk load points. It is only very important loads that are singled out for detailed representation. It is interesting to note that a group of rotating loads operating at constant torque may be adequately represented as a static load that exhibits the characteristic of a constant current sink (Weedy, 1987).

In steady-state applications, most system loads are adequately represented by a three-phase power sink, which may be connected either in a star or delta configuration, depending on requirements (Chen and Dillon, 1974). Figure 3.19(a) shows the schematic representation of a star-connected load with the star point solidly grounded, whereas Figure 3.19(b) shows a schematic representation of a delta-connected load.

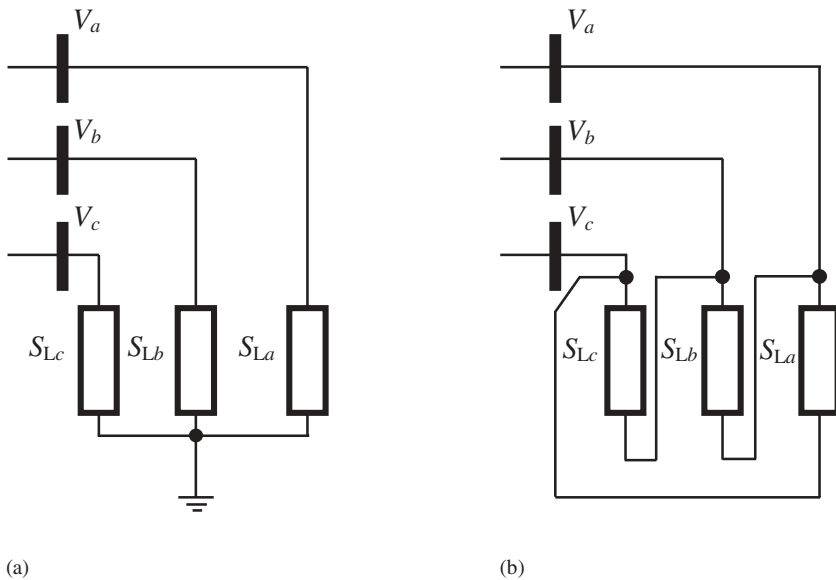


**Figure 3.19** System load representation: (a) star-connected load with star point solidly grounded and (b) delta-connected load

In three-phase power flow studies it is normal to represent bulk power load points as complex powers per phase, on a per-unit basis:

$$\left. \begin{aligned} S_{La} &= P_{La} + jQ_{La}, \\ S_{Lb} &= P_{Lb} + jQ_{Lb}, \\ S_{Lc} &= P_{Lc} + jQ_{Lc}. \end{aligned} \right\} \quad (3.129)$$

Refinements can be applied to the above equations to make the power characteristic more responsive to voltage performance:

$$\left. \begin{aligned} S'_{La} &= P_{La} \left[ \frac{1}{V_a} \right]^\alpha + jQ_{La} \left[ \frac{1}{V_a} \right]^\beta, \\ S'_{Lb} &= P_{Lb} \left[ \frac{1}{V_b} \right]^\alpha + jQ_{Lb} \left[ \frac{1}{V_b} \right]^\beta, \\ S'_{Lc} &= P_{Lc} \left[ \frac{1}{V_c} \right]^\alpha + jQ_{Lc} \left[ \frac{1}{V_c} \right]^\beta. \end{aligned} \right\} \quad (3.130)$$

In Equations (3.130),  $\alpha$  and  $\beta$  take values in the range 0–2 and  $V_a$ ,  $V_b$ , and  $V_c$  are the per-unit three-phase nodal voltage magnitudes at the load point. Notice that when  $\alpha = \beta = 0$  the complex power expressions in Equations (3.130) coincide with those in Equations (3.129). However, if  $\alpha = \beta = 1$ , Equations (3.130) resemble complex current characteristics more than complex power characteristics. Also, if  $\alpha = \beta = 2$ , the complex powers in Equations (3.130) would behave like complex admittances.

The admittance-like characteristic in Equations (3.130) may be expressed in matrix form for both kinds of load connections, star and delta, respectively:

$$\begin{bmatrix} S_{La}/V_a^2 & 0 & 0 \\ 0 & S_{Lb}/V_b^2 & 0 \\ 0 & 0 & S_{Lc}/V_c^2 \end{bmatrix}, \quad (3.131)$$

$$\frac{1}{3} \begin{bmatrix} S_{La}/V_a^2 + S_{Lb}/V_b^2 & -S_{Lb}/V_b^2 & -S_{La}/V_a^2 \\ -S_{Lb}/V_b^2 & S_{Lb}/V_b^2 + S_{Lc}/V_c^2 & -S_{Lc}/V_c^2 \\ -S_{La}/V_a^2 & -S_{Lc}/V_c^2 & S_{Lc}/V_c^2 + S_{La}/V_a^2 \end{bmatrix}. \quad (3.132)$$

Moreover, if it is assumed that the load powers and voltage magnitudes are taken to be balanced,  $S_{La} = S_{Lb} = S_{Lc} = S_L$ , and  $V_a = V_b = V_c = V$ , then application of the following symmetrical component operation,  $\mathbf{Y}_{012} = \mathbf{T}_S^{-1} \mathbf{Y}_{abc} \mathbf{T}_S$ , leads to the load model representation for zero, positive, and negative (0, 1, 2) sequences:

$$\begin{bmatrix} S_L/V^2 & 0 & 0 \\ 0 & S_L/V^2 & 0 \\ 0 & 0 & S_L/V^2 \end{bmatrix}, \quad (3.133)$$

$$\begin{bmatrix} 0 & 0 & 0 \\ 0 & S_L/V^2 & 0 \\ 0 & 0 & S_L/V^2 \end{bmatrix}. \quad (3.134)$$

Notice that no zero sequence loads exist for the case of a three-phase delta-connected load, only positive and negative sequences.

As an extension of the above result, the positive, negative, and zero sequence expression of a star-connected load with its star point solidly grounded may be expressed as

$$S'_{L(1)} = S'_{L(2)} = S'_{L(0)} = P_L \left[ \frac{1}{V} \right]^\alpha + jQ_L \left[ \frac{1}{V} \right]^\beta, \quad (3.135)$$

whereas for the case of a delta-connected load we have

$$S'_{L(1)} = S'_{L(2)} = P_L \left[ \frac{1}{V} \right]^\alpha + jQ_L \left[ \frac{1}{V} \right]^\beta, \quad \text{and} \quad S'_{L(0)} = 0. \quad (3.136)$$

It should be remarked that the exponents  $\alpha$  and  $\beta$  are not confined to integer values and that a wide range of load characteristics can be achieved by judicious selection of  $\alpha$  and  $\beta$ , depending on the group of loads present in the study.

Also, a three-phase delta connected load can always be transformed into an equivalent star circuit by using a delta–star transformation. However, notice that the transformation will generate an extra bus in the form of the star point, which yields no physical meaning.

### 3.6 SUMMARY

The chapter has addressed the mathematical modelling of the most common elements found in conventional electrical power systems, namely, transmission lines, transformers, generators, loads, and shunt and series passive compensation. The tools and methods covered in the book are limited to fundamental frequency steady-state phenomena, and the modelling approach followed in this chapter reflects this fact. Notwithstanding this, the overall modelling philosophy is quite general in the sense that all plant component models are formulated in the frame of reference of the phases, which is closely associated with the physical structure of the equipment and its actual steady-state electrical operation. It is shown throughout the chapter that simpler models do exist to represent a given plant component but that these models are based on the assumption of perfect geometric balance conditions. These models are realised with the help of the symmetrical component transform, leading to plant component representation in the frame of reference of the sequences.

Multiphase transmission line parameters are calculated with great accuracy, incorporating all key effects that affect fundamental frequency operation such as geometric imbalances, ground return loops, and even long-line effects. Practical transmission lines include several conductors per phase and ground wires as well as more than one three-phase circuit sharing the same right of way, giving rise to a large number of electromagnetically coupled conductors. The chapter has presented a methodology for handling all these effects in a systematic and efficient manner. A comprehensive computer program in Matlab<sup>®</sup> has been written to calculate multiconductor transmission line parameters.

Three-phase power transformers have been modelled in the frame of reference of the phases, with particular reference to complex off-nominal tapping positions. This caters for the possibility of the transformer acting as a tap changer or as a phase shifter. The most popular transformer connections used in high-voltage transmission have been addressed and, under the assumption of perfect geometric conditions, transformer models in the frame of reference of the sequences have been derived. The thrust of these models is fundamental frequency, steady-state operation, and there is little loss of accuracy in representing the three-phase transformer as a three-phase bank of transformers. A detailed model of the synchronous generator, based on its physical windings arrangement, has been presented.

The effects of saliency and the generator load angle are explicitly represented in the model. This model also serves the purpose of representing a synchronous motor, by suitable modification of signs to conform to motoring action. Static loads suitable for bulk load representation have also received attention.

The models of conventional power plant components developed in this chapter interface quite naturally with the models of FACTS components developed in Chapter 2. Together, they provide a very sophisticated tool with which to represent power system networks containing a vast array of power electronic controllers of various kinds. These are the power systems that may be in operation tomorrow. Two different modelling flavours emerge from this modelling exercise, the frame of reference of the phases and the frame of reference of the sequences, each one having its own time and space. Chapters 4, 5, and 7, dealing with positive sequence power flow and optimal power flow, use the positive sequence models derived in this and Chapter 2. Chapter 6 covers the topic of three-phase power flow and uses the comprehensive models developed in the frame of reference of the phases.

## REFERENCES

- Acha, E., Madrigal, M., 2001, *Power System Harmonics: Computer Modelling and Analysis*, John Wiley & Sons, Chichester.
- Acha, E., Ambriz-Pérez, H., Fuerte-Esquivel, C.R., 2000, 'Advanced Transformer Control Modelling in an Optimal Power Flow using Newton's Method', *IEEE Trans. Power Systems* **15**(1) 290–298.
- Anderson, P.M., 1973, *Analysis of Power Systems*, Iowa State University Press, Ames IA.
- Arrillaga, J., Acha, E., Densem, T.J., Bodger, P.S., 1986, 'Ineffectiveness of Transmission Line Transpositions at Harmonic Frequencies', *Proceedings of the IEE: Part C* **133**(2) 99–104.
- Arrillaga, J., Smith, B.C., Watson, N.R., Wood, A.R., 1997, *Power System Harmonic Analysis*, John Wiley & Sons, Chichester.
- Bowman, W.I., McNamee, J.M., 1964, 'Development of Equivalent PI and T Matrix Circuits for Long Untransposed Transmission Lines', *IEEE Trans. Power Apparatus and Systems* **PAS-84**(6) 625–632.
- Carson, J.R., 1926, 'Wave Propagation in Overhead Wires with Ground Return', *Bell System Technical Journal*, **5** (October) 539–554.
- Chen, M.S., Dillon, W.E. 1974, 'Power System Modelling', *Proceeding of the IEE* **62**(7) 901–915.
- Chen, B.K., Chen, M.S., Shoults, R.R., Liang, C.C., 1990, 'Hybrid Three-phase Load Flow', *IEE Proceedings on Generation, Transmission and Distribution: Part C* **137**(3) 177–185.
- Deri, A., Tevan, G., Semlyen, A., Castanheira, A., 1981, 'The Complex Ground Return Plane, Simplified Model for Homogeneous and Multi-layer Earth Return', *IEEE Trans. Power Apparatus and Systems*, **PAS-100**(8) 3686–3693.
- Elgerd, O.I., 1982, *Electric Energy System Theory: An Introduction*, McGraw-Hill, New York.
- Grainger, J.J., Stevenson, W.D., 1994, *Power System Analysis*, McGraw-Hill, New York.
- Harker, B.J., Arrillaga, J., 1979, '3-Phase a.c./d.c. Load Flows', *Proceedings of the IEE* **126**(12) 1275–1281.
- Hesse, M.H., 1966, 'Circulating Currents in Paralleled Untransposed Multicircuit Lines', *IEEE Trans. Power Apparatus and Systems*, **PAS-85**(7) 802–820.
- Loughton, M.A., 1968, 'Analysis of Unbalanced Polyphase Networks by the Method of Phase Coordinates', *Proceedings of the IEE* **115**(8) 1163–1172.

- Shlash, M.A., 1974, *Three-Phase Analysis of Unbalanced Power System Networks*, PhD thesis, Department of Electrical Engineering and Electronics, University of Manchester Institute of Science and Technology, Manchester, UK.
- Wasley, R.G., Shlash, M.A., 1974a, 'Newton–Raphson Algorithm for 3-Phase Load Flow', *Proceedings of the IEE* **121**(7) 630–638.
- Wasley, R.G., Shlash, M.A., 1974b, 'Steady-state Phase-variable Model of the Synchronous Machine for Use in 3-phase Load-flow Studies', *Proceedings of the IEE* **121**(10) 1155–1164.
- Wedephol, L.M., 1963, 'Application of Matrix Methods to the Solution of Travelling Wave Phenomena in Poly-Phase Systems', *Proceedings of the IEE* **110**(12) 2200–2212.
- Weedy, B.M., 1987, *Electric Power Systems*, John Wiley & Sons, Chichester.



# 4



## Conventional Power Flow

### 4.1 INTRODUCTION

The main aim of a modern electrical power system is to satisfy continuously the electrical power contracted by all customers. This is a problem of great engineering complexity where the following operational policies must be observed: (1) nodal voltage magnitudes and system frequency must be kept within narrow boundaries; (2) the alternating current (AC) voltage and current waveforms must remain largely sinusoidal; (3) transmission lines must be operated well below their thermal and stability limits; and (4) even short-term interruptions must be kept to a minimum. Moreover, because of the very competitive nature of the electricity supply business in an era of deregulation and open access, transmission costs must be kept as low as possible.

To a large extent, several of these key issues in power system operation may be assessed quite effectively by resorting to power flow and derived studies (Arrillaga and Arnold, 1990; Grainger and Stevenson, 1994; Stagg and El-Abiad, 1968; Wood and Wollenberg, 1984). The main objective of a power flow study is to determine the steady-state operating condition of the electrical power network. The steady-state may be determined by finding out, for a given set of loading conditions, the flow of active and reactive powers throughout the network and the voltage magnitudes and phase angles at all buses of the network.

Expansion, planning and daily operation of power systems relies on extensive power flow studies (Kundur, 1994; Weedy, 1987). The information conveyed by such studies indicates whether or not the nodal voltage magnitudes and active and reactive power flows in transmission lines and transformers are within prescribed operating limits. If voltage magnitudes are outside bounds in one or more points of the network, then appropriate action is taken in order to regulate such voltage magnitudes. Similarly, if the study predicts that the power flow in a given transmission line is beyond the power carrying capacity of the line, then control action is taken.

### 4.2 GENERAL POWER FLOW CONCEPTS

The power flow problem, is solved to determine the steady-state complex voltages at all buses of the network, from which the active and reactive power flows in every transmission

line and transformer are calculated (Stagg and El-Abiad, 1968). The set of equations representing the power system are nonlinear. For most practical purposes, all power flow methods exploit the well-conformed nodal properties of the power network and equipment. In its most basic form, these equations are derived by assuming that a perfect symmetry exists between the phases of the three-phase power system (Arrillaga and Arnold, 1990). Owing to the nonlinear nature of the power flow equations, the numerical solution is reached by iteration (Grainger and Stevenson, 1994).

#### 4.2.1 Basic Formulation

A popular approach to assess the steady-state operation of a power system is to write equations stipulating that at a given bus the generation, load, and powers exchanged through the transmission elements connecting to the bus must add up to zero. This applies to both active power and reactive power. These equations are termed ‘mismatch power equations’ and at bus  $k$  they take the following form:

$$\Delta P_k = P_{Gk} - P_{Lk} - P_k^{\text{cal}} = P_k^{\text{sch}} - P_k^{\text{cal}} = 0, \quad (4.1)$$

$$\Delta Q_k = Q_{Gk} - Q_{Lk} - Q_k^{\text{cal}} = Q_k^{\text{sch}} - Q_k^{\text{cal}} = 0. \quad (4.2)$$

The terms  $\Delta P_k$  and  $\Delta Q_k$  are the mismatch active and reactive powers at bus  $k$ , respectively.  $P_{Gk}$  and  $Q_{Gk}$  represent, respectively, the active and reactive powers injected by the generator at bus  $k$ . For the purpose of the power flow solutions it is assumed that these variables can be controlled by the power plant operator.  $P_{Lk}$  and  $Q_{Lk}$  represent the active and reactive powers drawn by the load at bus  $k$ , respectively. Under normal operation the customer has control of these variables, and in the power flow formulation they are assumed to be known variables.

In principle, at least, the generation and the load at bus  $k$  may be measured by the electric utility and, in the parlance of power system engineers, their net values are known as the scheduled active and reactive powers:

$$P_k^{\text{sch}} = P_{Gk} - P_{Lk}, \quad (4.3)$$

$$Q_k^{\text{sch}} = Q_{Gk} - Q_{Lk}. \quad (4.4)$$

The transmitted active and reactive powers,  $P_k^{\text{cal}}$  and  $Q_k^{\text{cal}}$ , are functions of nodal voltages and network impedances and are computed using the power flow equations. Provided the nodal voltages throughout the power network are known to a good degree of accuracy then the transmitted powers are easily and accurately calculated. In this situation, the corresponding mismatch powers are zero for any practical purpose and the power balance at each bus of the network is satisfied. However, if the nodal voltages are not known precisely then the calculated transmitted powers will have only approximated values and the corresponding mismatch powers are not zero. The power flow solution takes the approach of successively correcting the calculated nodal voltages and, hence, the calculated transmitted powers until values accurate enough are arrived at, enabling the mismatch powers to be zero or fairly close to zero. In modern power flow computer programs, it is normal for all mismatch equations to satisfy a tolerance as tight as  $1e-12$  before the iterative solution can be considered successful. Upon convergence, the nodal voltage magnitudes and angles yield useful information about the steady-state operating conditions of the power system and are known as state variables.

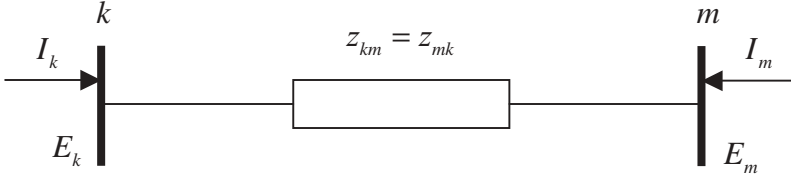


**Figure 4.1** Equivalent impedance

In order to develop suitable power flow equations, it is necessary to find relationships between injected bus currents and bus voltages. Based on Figure 4.1 the injected complex current at bus  $k$ , denoted by  $I_k$ , may be expressed in terms of the complex bus voltages  $E_k$  and  $E_m$  as follows:

$$I_k = \frac{1}{z_{km}} (E_k - E_m) = y_{km} (E_k - E_m). \quad (4.5)$$

Similarly for bus  $m$ ,

$$I_m = \frac{1}{z_{mk}} (E_m - E_k) = y_{mk} (E_m - E_k). \quad (4.6)$$

The above equations can be written in matrix form as,

$$\begin{bmatrix} I_k \\ I_m \end{bmatrix} = \begin{bmatrix} y_{km} & -y_{km} \\ -y_{mk} & y_{mk} \end{bmatrix} \begin{bmatrix} E_k \\ E_m \end{bmatrix}, \quad (4.7)$$

or

$$\begin{bmatrix} I_k \\ I_m \end{bmatrix} = \begin{bmatrix} Y_{kk} & Y_{km} \\ Y_{mk} & Y_{mm} \end{bmatrix} \begin{bmatrix} E_k \\ E_m \end{bmatrix}, \quad (4.8)$$

where the bus admittances and voltages can be expressed in more explicit form:

$$Y_{ij} = G_{ij} + jB_{ij}, \quad (4.9)$$

$$E_i = V_i e^{j\theta_i} = V_i (\cos \theta_i + j \sin \theta_i), \quad (4.10)$$

where  $i = k, m$ , and  $j = k, m$ .

The complex power injected at bus  $k$  consists of an active and a reactive component and may be expressed as a function of the nodal voltage and the injected current at the bus:

$$\begin{aligned} S_k &= P_k + jQ_k = E_k I_k^* \\ &= E_k (Y_{kk} E_k + Y_{km} E_m)^*, \end{aligned} \quad (4.11)$$

where  $I_k^*$  is the complex conjugate of the current injected at bus  $k$ .

The expressions for  $P_k^{\text{cal}}$  and  $Q_k^{\text{cal}}$  can be determined by substituting Equations (4.9) and (4.10) into Equation (4.11), and separating into real and imaginary parts:

$$P_k^{\text{cal}} = V_k^2 G_{kk} + V_k V_m [G_{km} \cos(\theta_k - \theta_m) + B_{km} \sin(\theta_k - \theta_m)], \quad (4.12)$$

$$Q_k^{\text{cal}} = -V_k^2 B_{kk} + V_k V_m [G_{km} \sin(\theta_k - \theta_m) - B_{km} \cos(\theta_k - \theta_m)]. \quad (4.13)$$

For specified levels of power generation and power load at bus  $k$ , and according to Equations (4.1) and (4.2), the mismatch equations may be written down as

$$\Delta P_k = P_{Gk} - P_{Lk} - \{V_k^2 G_{kk} + V_k V_m [G_{km} \cos(\theta_k - \theta_m) + B_{km} \sin(\theta_k - \theta_m)]\} = 0, \tag{4.14}$$

$$\Delta Q_k = Q_{Gk} - Q_{Lk} - \{-V_k^2 B_{kk} + V_k V_m [G_{km} \sin(\theta_k - \theta_m) - B_{km} \cos(\theta_k - \theta_m)]\} = 0. \tag{4.15}$$

Similar equations may be obtained for bus  $m$  simply by exchanging subscripts  $k$  and  $m$  in Equations (4.14) and (4.15).

It should be remarked that Equations (4.12) and (4.13) represent only the powers injected at bus  $k$  through the  $i$ th transmission element, that is,  $P_k^{i\text{ cal}}$  and  $Q_k^{i\text{ cal}}$ . However, a practical power system will consist of many buses and many transmission elements. This calls for Equations (4.12) and (4.13) to be expressed in more general terms, with the net power flow injected at bus  $k$  expressed as the summation of the powers flowing at each one of the transmission elements terminating at this bus. This is illustrated in Figures 4.2(a) and 4.2(b) for cases of active and reactive powers, respectively.

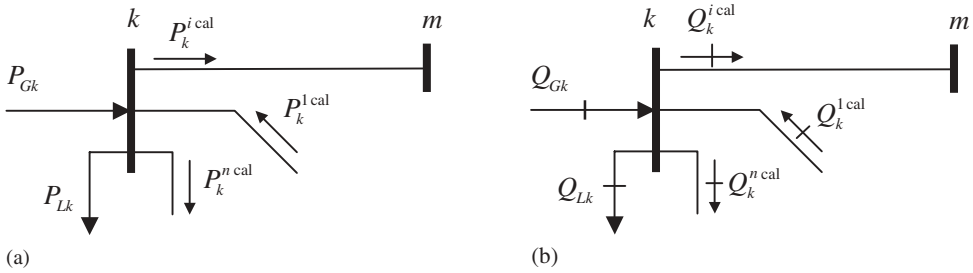


**Figure 4.2** Power balance at bus  $k$ : (a) active power, and (b) reactive power

The generic net active and reactive powers injected at bus  $k$  are:

$$P_k^{\text{cal}} = \sum_{i=1}^n P_k^{i\text{ cal}}, \tag{4.16}$$

$$Q_k^{\text{cal}} = \sum_{i=1}^n Q_k^{i\text{ cal}}, \tag{4.17}$$

where  $P_k^{i\text{ cal}}$  and  $Q_k^{i\text{ cal}}$  are computed by using Equations (4.12) and (4.13), respectively.

As an extension, the generic power mismatch equations at bus  $k$  are:

$$\Delta P_k = P_{Gk} - P_{Lk} - \sum_{i=1}^n P_k^{i\text{ cal}} = 0, \tag{4.18}$$

$$\Delta Q_k = Q_{Gk} - Q_{Lk} - \sum_{i=1}^n Q_k^{i\text{ cal}} = 0. \tag{4.19}$$

## 4.2.2 Variables and Bus Classification

In conventional power flow theory each bus is described by four variables: net active power, net reactive powers, voltage magnitude, and voltage phase angle.

Since there are only two equations per bus, two out of the four variables must be specified in each bus in order to have a solvable problem. From a purely mathematical viewpoint, any two variables can be specified; however, in engineering terms, the choice is based on which variables at the bus can be physically controlled through the availability of a nearby controller (Elgerd, 1982; Kundur, 1994; Weedy, 1987; Wood and Wollenberg, 1984). In the broadest sense, one can think of voltage magnitudes and phase angles as state variables, and active and reactive powers as control variables.

Busess are classified according to which two out of the four variables are specified:

- Load  $PQ$  bus: no generator is connected to the bus, hence the control variables  $P_G$  and  $Q_G$  are zero. Furthermore, the active and reactive powers drawn by the load  $P_L$  and  $Q_L$  are known from available measurements. In these types of buses the net active power and net reactive power are specified, and  $V$  and  $\theta$  are computed.
- Generator  $PV$  bus: a generating source is connected to the bus; the nodal voltage magnitude  $V$  is maintained at a constant value by adjusting the field current of the generator and hence it generates or absorbs reactive power. Moreover, the generated active power  $P_G$  is also set at a specified value. The other two quantities  $\theta$  and  $Q_G$  are computed. Constant voltage operation is possible only if the generator reactive power design limits are not violated, that is,  $Q_{G \min} < Q_G < Q_{G \max}$ .
- Generator  $PQ$  bus: if the generator cannot provide the necessary reactive power support to constrain the voltage magnitude at the specified value then the reactive power is fixed at the violated limit and the voltage magnitude is freed. In this case, the generated active power  $P_G$  and reactive power  $Q_G$  are specified, and the nodal voltage magnitude  $V$  and phase angle  $\theta$  are computed.
- Slack (swing) bus: one of the generator buses is chosen to be the slack bus where the nodal voltage magnitude,  $V_{\text{slack}}$ , and phase angle,  $\theta_{\text{slack}}$ , are specified. There is only one slack bus in the power system and the function of a slack generator is to produce sufficient power to provide for any unmet system load and for system losses, that are not known in advance of the power flow calculation. The voltage phase angle at the slack bus  $\theta_{\text{slack}}$  is chosen as the reference against which all other voltage phase angles in the system are measured. It is normal to fix its value to zero.

## 4.3 POWER FLOW SOLUTION METHODS

### 4.3.1 Early Power Flow Algorithms

From the mathematical modelling point of view, a power flow solution consists of solving the set of nonlinear, algebraic equations that describe the electrical power network under steady-state conditions. Over the years, several approaches have been put forward for the solution of the power flow equations. Early approaches were based on loop equations and numerical methods using Gauss-type solutions. The method was laborious because the network loops had to be specified beforehand by the systems engineer. Improved techniques saw the introduction of nodal analysis in favour of loop analysis, leading to a considerable

reduction in data preparation. Nevertheless, reliability towards convergence was still the main concern. Further developments led to the introduction of the Gauss–Seidel method with acceleration factors. The appeal of this generation of power flow methods is their minimum storage requirements and the fact that they are easy to comprehend and to code in the form of computer programs. The drawback is that these algorithms exhibit poor convergence characteristics when applied to the solution of networks of realistic size (Elgerd, 1982). Power flow solutions based on the nodal impedance matrix were briefly experimented with (Brown, 1975), but problems with computer storage and speed became insurmountable issues at the time. To overcome such limitations, the Newton–Raphson method and derived formulations were developed in the early 1970s and have since become firmly established throughout the power system industry (Peterson and Scott Meyer, 1971; Stott, 1974; Stott and Alsac, 1978; Tinney and Hart, 1967).

### 4.3.2 The Newton–Raphson Algorithm

In large-scale power flow studies the Newton–Raphson method has proved most successful owing to its strong convergence characteristics (Peterson and Scott Meyer, 1971; Tinney and Hart, 1967). This approach uses iteration to solve the following set of nonlinear algebraic equations:

$$\left. \begin{aligned} f_1(x_1, x_2, \dots, x_N) &= 0, \\ f_2(x_1, x_2, \dots, x_N) &= 0, \\ &\vdots \\ f_N(x_1, x_2, \dots, x_N) &= 0, \end{aligned} \right\}, \text{ or } \mathbf{F}(\mathbf{X}) = \mathbf{0} \tag{4.20}$$

where  $\mathbf{F}$  represents the set of  $n$  nonlinear equations, and  $\mathbf{X}$  is the vector of  $n$  unknown state variables.

The essence of the method consists of determining the vector of state variables  $\mathbf{X}$  by performing a Taylor series expansion of  $\mathbf{F}(\mathbf{X})$  about an initial estimate  $\mathbf{X}^{(0)}$ :

$$\mathbf{F}(\mathbf{X}) = \mathbf{F}(\mathbf{X}^{(0)}) + \mathbf{J}(\mathbf{X}^{(0)}) (\mathbf{X} - \mathbf{X}^{(0)}) + \text{higher-order terms}, \tag{4.21}$$

where  $\mathbf{J}(\mathbf{X}^{(0)})$  is a matrix of first-order partial derivatives of  $\mathbf{F}(\mathbf{X})$  with respect to  $\mathbf{X}$ , termed the Jacobian, evaluated at  $\mathbf{X} = \mathbf{X}^{(0)}$ .

This expansion lends itself to a suitable formulation for calculating the vector of state variables  $\mathbf{X}$  by assuming that  $\mathbf{X}^{(1)}$  is the value computed by the algorithm at iteration 1 and that this value is sufficiently close to the initial estimate  $\mathbf{X}^{(0)}$ . Based on this premise, all high-order derivative terms in Equation (4.21) may be neglected. Hence,

$$\underbrace{\begin{bmatrix} f_1(\mathbf{X}^{(1)}) \\ f_2(\mathbf{X}^{(1)}) \\ \vdots \\ f_n(\mathbf{X}^{(1)}) \end{bmatrix}}_{\mathbf{F}(\mathbf{X}^{(1)})} \approx \underbrace{\begin{bmatrix} f_1(\mathbf{X}^{(0)}) \\ f_2(\mathbf{X}^{(0)}) \\ \vdots \\ f_n(\mathbf{X}^{(0)}) \end{bmatrix}}_{\mathbf{F}(\mathbf{X}^{(0)})} + \underbrace{\begin{bmatrix} \frac{\partial f_1(\mathbf{X})}{\partial x_1} & \frac{\partial f_1(\mathbf{X})}{\partial x_2} & \dots & \frac{\partial f_1(\mathbf{X})}{\partial x_n} \\ \frac{\partial f_2(\mathbf{X})}{\partial x_1} & \frac{\partial f_2(\mathbf{X})}{\partial x_2} & \dots & \frac{\partial f_2(\mathbf{X})}{\partial x_n} \\ \vdots & \vdots & \ddots & \vdots \\ \frac{\partial f_n(\mathbf{X})}{\partial x_1} & \frac{\partial f_n(\mathbf{X})}{\partial x_2} & \dots & \frac{\partial f_n(\mathbf{X})}{\partial x_n} \end{bmatrix}}_{\mathbf{J}(\mathbf{X}^{(0)})} \bigg|_{\mathbf{X}=\mathbf{X}^{(0)}} \underbrace{\begin{bmatrix} X_1^{(1)} - X_1^{(0)} \\ X_2^{(1)} - X_2^{(0)} \\ \vdots \\ X_n^{(1)} - X_n^{(0)} \end{bmatrix}}_{\mathbf{X}^{(1)} - \mathbf{X}^{(0)}}. \tag{4.22}$$

In compact form, and generalising the above expression for the case of iteration ( $i$ ),

$$\mathbf{F}(\mathbf{X}^{(i)}) \approx \mathbf{F}(\mathbf{X}^{(i-1)}) + \mathbf{J}(\mathbf{X}^{(i-1)}) (\mathbf{X}^{(i)} - \mathbf{X}^{(i-1)}), \quad (4.23)$$

where  $i = 1, 2, \dots$ . Furthermore, if it is assumed that  $\mathbf{X}^{(i)}$  is sufficiently close to the solution  $\mathbf{X}^{(*)}$  then  $\mathbf{F}(\mathbf{X}^{(i)}) \approx \mathbf{F}(\mathbf{X}^{(*)}) = \mathbf{0}$ . Hence, Equation (4.23) becomes

$$\mathbf{F}(\mathbf{X}^{(i-1)}) + \mathbf{J}(\mathbf{X}^{(i-1)}) (\mathbf{X}^{(i)} - \mathbf{X}^{(i-1)}) = \mathbf{0}, \quad (4.24)$$

and, solving for  $\mathbf{X}^{(i)}$ ,

$$\mathbf{X}^{(i)} = \mathbf{X}^{(i-1)} - \mathbf{J}^{-1}(\mathbf{X}^{(i-1)}) \mathbf{F}(\mathbf{X}^{(i-1)}) \quad (4.25)$$

The iterative solution can be expressed as a function of the correction vector  $\Delta \mathbf{X}^{(i)} = \mathbf{X}^{(i)} - \mathbf{X}^{(i-1)}$ ,

$$\Delta \mathbf{X}^{(i)} = -\mathbf{J}^{-1}(\mathbf{X}^{(i-1)}) \mathbf{F}(\mathbf{X}^{(i-1)}), \quad (4.26)$$

and the initial estimates are updated using the following relation:

$$\mathbf{X}^{(i)} = \mathbf{X}^{(i-1)} + \Delta \mathbf{X}^{(i)}. \quad (4.27)$$

The calculations are repeated as many times as required using the most up-to-date values of  $\mathbf{X}$  in equation (4.26). This is done until the mismatches  $\Delta \mathbf{X}$  are within a prescribed small tolerance (i.e.  $1e-12$ ).

In order to apply the Newton–Raphson method to the power flow problem, the relevant equations must be expressed in the form of Equation (4.26), where  $\mathbf{X}$  represents the set of unknown nodal voltage magnitudes and phase angles. The power mismatch equations  $\Delta \mathbf{P}$  and  $\Delta \mathbf{Q}$  are expanded around a base point  $(\theta^{(0)}, \mathbf{V}^{(0)})$  and, hence, the power flow Newton–Raphson algorithm is expressed by the following relationship:

$$\underbrace{\begin{bmatrix} \Delta \mathbf{P} \\ \Delta \mathbf{Q} \end{bmatrix}}_{\mathbf{F}(\mathbf{X}^{(i-1)})} = - \underbrace{\begin{bmatrix} \frac{\partial \mathbf{P}}{\partial \theta} & \frac{\partial \mathbf{P}}{\partial \mathbf{V}} \mathbf{V} \\ \frac{\partial \mathbf{Q}}{\partial \theta} & \frac{\partial \mathbf{Q}}{\partial \mathbf{V}} \mathbf{V} \end{bmatrix}}_{\mathbf{J}(\mathbf{X}^{(i-1)})} \underbrace{\begin{bmatrix} \Delta \theta \\ \frac{\Delta \mathbf{V}}{\mathbf{V}} \end{bmatrix}}_{\Delta \mathbf{X}^{(i)}}. \quad (4.28)$$

The various matrices in the Jacobian may consists of up to  $(nb - 1) \times (nb - 1)$  elements of the form:

$$\left. \begin{array}{l} \frac{\partial P_k}{\partial \theta_m}, \quad \frac{\partial P_k}{\partial V_m} V_m, \\ \frac{\partial Q_k}{\partial \theta_m}, \quad \frac{\partial Q_k}{\partial V_m} V_m, \end{array} \right\} \quad (4.29)$$

where  $k = 1, \dots, nb$ , and  $m = 1, \dots, nb$  but omitting the *slack* bus entries.

Also, the rows and columns corresponding to reactive power and voltage magnitude for *PV* buses are discarded. Furthermore, when buses  $k$  and  $m$  are not directly linked by a transmission element, the corresponding  $k$ – $m$  entry in the Jacobian is null. Owing to the low degree of connectivity that prevails in practical power systems, the Jacobians of power flows are highly sparse. An additional characteristic is that they are symmetric in structure but not in value (Zollenkoff, 1970).

It must be pointed out that the correction terms  $\Delta V_m$  are divided by  $V_m$  to compensate for the fact that Jacobian terms  $(\partial P_k / \partial V_m) V_m$  and  $(\partial Q_k / \partial V_m) V_m$  are multiplied by  $V_m$ . It is shown in the derivative terms given below that this artifice yields useful simplifying calculations.

Consider the  $l$ th element connected between buses  $k$  and  $m$  in Figure 4.1, for which self and mutual Jacobian terms are given below.

For  $k \neq m$ :

$$\frac{\partial P_{k,l}}{\partial \theta_{m,l}} = V_k V_m [G_{km} \sin(\theta_k - \theta_m) - B_{km} \cos(\theta_k - \theta_m)], \quad (4.30)$$

$$\frac{\partial P_{k,l}}{\partial V_{m,l}} V_{m,l} = V_k V_m [G_{km} \cos(\theta_k - \theta_m) + B_{km} \sin(\theta_k - \theta_m)], \quad (4.31)$$

$$\frac{\partial Q_{k,l}}{\partial \theta_{m,l}} = -\frac{\partial P_{k,l}}{\partial V_{m,l}} V_{m,l}, \quad (4.32)$$

$$\frac{\partial Q_{k,l}}{\partial V_{m,l}} V_{m,l} = \frac{\partial P_{k,l}}{\partial \theta_{m,l}}. \quad (4.33)$$

For  $k = m$ :

$$\frac{\partial P_{k,l}}{\partial \theta_{k,l}} = -Q_k^{\text{cal}} - V_k^2 B_{kk}, \quad (4.34)$$

$$\frac{\partial P_{k,l}}{\partial V_{k,l}} V_{k,l} = P_k^{\text{cal}} + V_k^2 G_{kk}, \quad (4.35)$$

$$\frac{\partial Q_{k,l}}{\partial \theta_{k,l}} = P_k^{\text{cal}} - V_k^2 G_{kk}, \quad (4.36)$$

$$\frac{\partial Q_{k,l}}{\partial V_{k,l}} V_{k,l} = Q_k^{\text{cal}} - V_k^2 B_{kk}. \quad (4.37)$$

In general, for a bus  $k$  containing  $n$  transmission elements  $l$ , the bus self-elements take the following form:

$$\frac{\partial P_k}{\partial \theta_k} = \sum_{l=1}^n \frac{\partial P_{k,l}}{\partial \theta_{k,l}}, \quad (4.38)$$

$$\frac{\partial P_k}{\partial V_k} V_k = \sum_{l=1}^n \frac{\partial P_{k,l}}{\partial V_{k,l}} V_{k,l}, \quad (4.39)$$

$$\frac{\partial Q_k}{\partial \theta_k} = \sum_{l=1}^n \frac{\partial Q_{k,l}}{\partial \theta_{k,l}}, \quad (4.40)$$

$$\frac{\partial Q_k}{\partial V_k} V_k = \sum_{l=1}^n \frac{\partial Q_{k,l}}{\partial V_{k,l}} V_{k,l}. \quad (4.41)$$

The mutual elements given by Equations (4.30)–(4.33) remain the same whether we have one transmission element or  $n$  transmission elements terminating at bus  $k$ .

After the voltage magnitudes and phase angles have been calculated by iteration, active and reactive power flows throughout the transmission system are determined quite straightforwardly.

An important point to bear in mind is that the mismatch power equations  $\Delta P$  and  $\Delta Q$  of the slack bus are not included in Equation (4.28) and the unknown variables  $P_{\text{slack}}$  and  $Q_{\text{slack}}$  are computed once the system power flows and power losses have been determined. Also,  $Q_G$  in  $PV$  buses are calculated in each iteration in order to check if the generators are within reactive power limits. However, the mismatch reactive power equations  $\Delta Q$  of  $PV$  buses are not included in Equation (4.28). Details of this computation are given in the next section.

One of the main strengths of the Newton–Raphson method is its reliability towards convergence. For most practical situations, and provided the state variables,  $X^{(0)}$ , are suitably initialised, the method is said to exhibit a quadratic convergence characteristic; for example,

$$\begin{aligned} f(X^{(1)}) &= 1e - 1, \\ f(X^{(2)}) &= 1e - 2, \\ f(X^{(3)}) &= 1e - 4, \\ f(X^{(4)}) &= 1e - 8, \end{aligned}$$

for the maximum mismatch. Contrary to non-Newton–Raphson solutions, such a characteristic is independent of the size of the network being solved and the number and kinds of control equipment present in the power system. Aspects that may dent its quadratic convergence performance are reactive power limit violations in generator  $PV$  buses and extreme loading conditions.

### 4.3.3 State Variable Initialisation

The effectiveness of the Newton–Raphson method to achieve feasible iterative solutions is dependent upon the selection of suitable initial values for all the state variables involved in the study.

The power flow solution of networks that contain only conventional plant components is normally started with voltage magnitudes of 1 p.u. (per unit) at all  $PQ$  buses. The slack and  $PV$  buses are given their specified values, which remain constant throughout the iterative solution if no generator reactive power limits are violated. The initial voltage phase angles are selected to be 0 at all buses.

### 4.3.4 Generator Reactive Power Limits

Even though the mismatch reactive power equation  $\Delta Q_k$  of  $PV$  bus  $k$  is not required in Equation (4.28), solution of Equation (4.17) for the  $PV$  bus is still carried out at each iterative step to assess whether or not the calculated reactive power  $Q_k^{\text{cal}}$  is within the generator reactive power limits:

$$Q_{G \min k} < Q_{Gk} < Q_{G \max k}. \quad (4.42)$$

If either of the following conditions occur during the iterative process:

$$\left. \begin{aligned} Q_k^{\text{cal}} &\geq Q_{G \max k}, \\ Q_k^{\text{cal}} &\leq Q_{G \min k}, \end{aligned} \right\} \quad (4.43)$$

bus  $k$  becomes a generator  $PQ$  bus with either of the following mismatch power equations incorporated in Equation (4.28):

$$\left. \begin{aligned} \Delta Q_k &= Q_{G \max k} - Q_{Lk} - Q_k^{\text{cal}}, \\ \Delta Q_k &= Q_{G \min k} - Q_{Lk} - Q_k^{\text{cal}}, \end{aligned} \right\} \quad (4.44)$$

depending on the violated limit, together with the relevant Jacobian entries. The nodal voltage magnitude at bus  $k$  is allowed to vary and  $V_k$  becomes a state variable.

It should be remarked that bus  $k$  may revert to being a generator  $PV$  bus at some point during the iterative process if better estimates of  $Q_k^{\text{cal}}$ , calculated with more accurate nodal voltages, indicate that the reactive power requirements at bus  $k$  can, after all, be met by the generator connected at bus  $k$ . Hence, reactive power limit checking is carried out at each iteration. Programming wisdom indicates that limit checking should start after the first or second iteration, since nodal voltage values computed at the beginning of the iterative process may be quite inaccurate leading to misleading reactive power requirements. The switching of buses from  $PV$  to  $PQ$  and vice versa impose additional numerical demands on the iterative solution and retard convergence.

### 4.3.5 Linearised Frame of Reference

In order to illustrate how network components may be processed in the linearised frame of reference afforded by the Newton–Raphson method (Fuerte-Esquivel *et al.*, 1998) consider the simple three-bus system shown in Figure 4.3. Bus 1 is selected to be the slack bus and bus 2 is a generator bus. Bus 3 contains no generation and becomes a load bus. A transformer and a transmission line link buses 1 and 2 and buses 2 and 3, respectively. One shunt element and one load are connected at bus 3.

The concept of ‘power balance at a node’ may be used to great effect to account for bus power injections in the Newton–Raphson solution. At a given bus, the power balance is obtained by adding the contribution of each plant component connected to that bus.

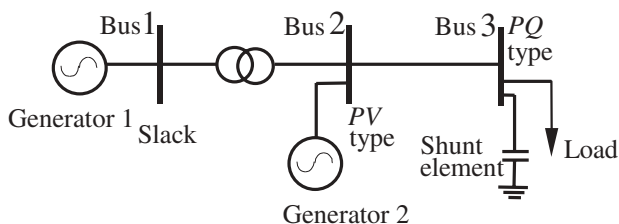


**Figure 4.3** Three-bus network. Redrawn, with permission, from C.R. Fuerte-Esquivel, E. Acha, S.G. Tan, and J.J. Rico, ‘Efficient Object Oriented Power System Software for the Analysis of Large-scale Networks Containing FACTS Controlled Branches’, *IEEE Trans. Power Systems* 3(2) 464–472, © 1998 IEEE

This is illustrated in Figure 4.4 with reference to Figure 4.3. The contribution of all three buses is shown in this example for completeness, but it should be remembered that in actual calculations active and reactive power mismatch entries are not required for the slack bus. Likewise, the reactive power mismatch entry is not required for the generator *PV* bus.

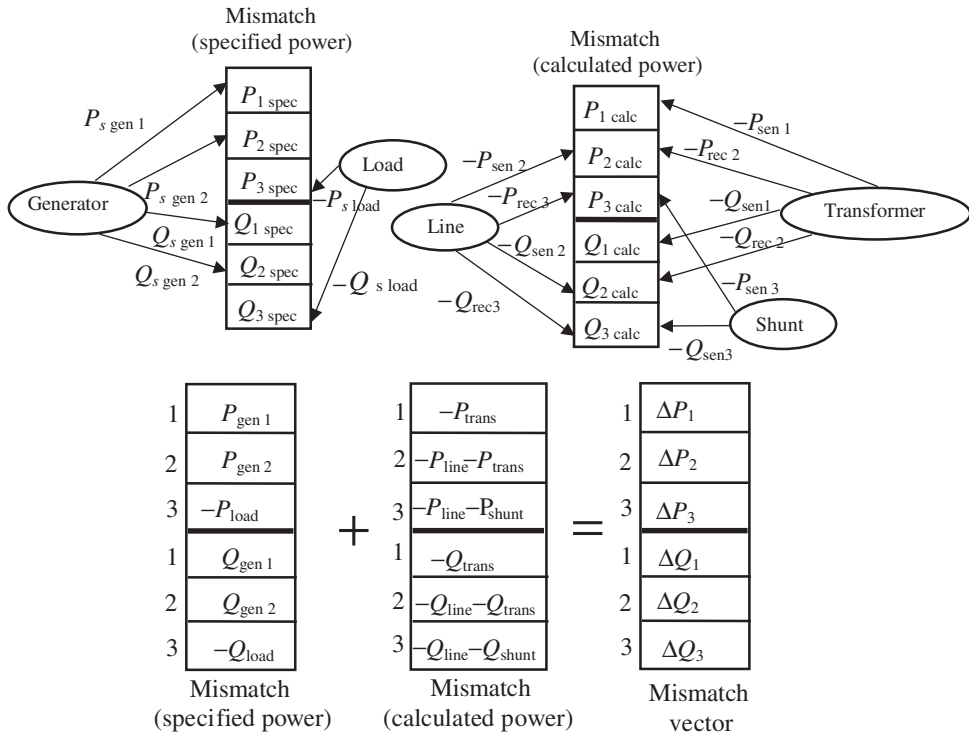


**Figure 4.4** Power mismatch vector; subscripts ‘sen’ and ‘rec’ indicate the sending and receiving ends. Reproduced, with permission, from C.R. Fuerte-Esquivel, E. Acha, S.G. Tan, and J.J. Rico, ‘Efficient Object Oriented Power System Software for the Analysis of Large-scale Networks Containing FACTS Controlled Branches’, *IEEE Trans. Power Systems* 3(2) 464–472, © 1998 IEEE

The construction of the Jacobian matrix is slightly more involved owing to the need to evaluate self and mutual Jacobian terms, and finding their location in the matrix. Nevertheless, the basic procedure illustrated above, based on superposition, will also apply to the formation of the Jacobian. For each plant component, relevant Jacobian equations are chosen based on the type of buses to which the plant component is connected. These buses determine the location of the individual Jacobian terms in the overall Jacobian structure. The contributions of the line, transformer, and shunt components to the Jacobian are shown in Figure 4.5. It should be noted that entries for the slack bus and the reactive power entry of the generator bus are not considered in the Jacobian structure.

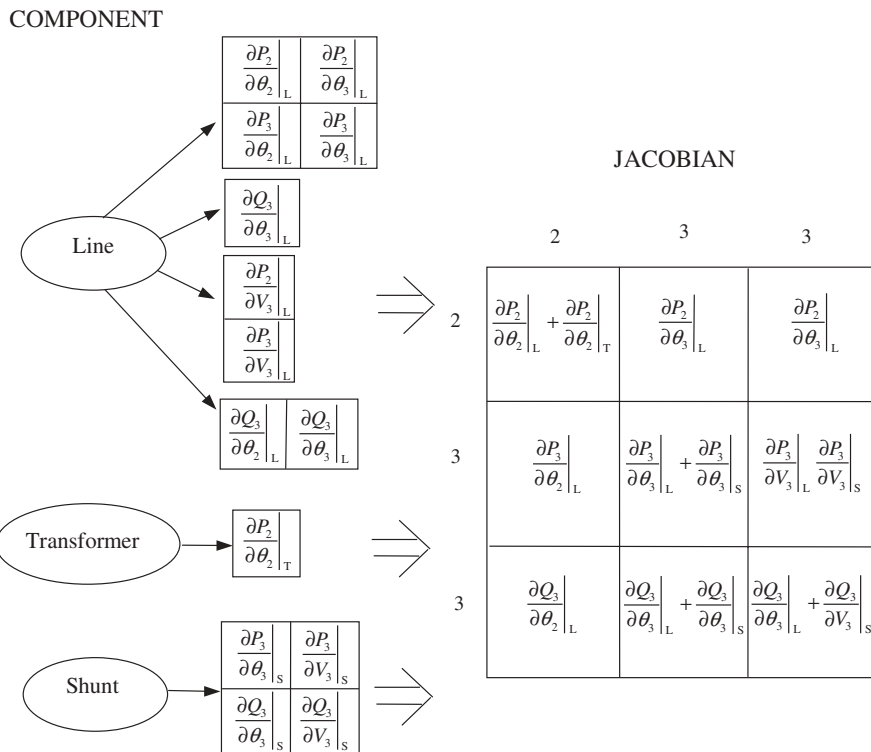


**Figure 4.5** Jacobian structure. Reproduced, with permission, from C.R. Fuerte-Esquivel, E. Acha, S.G. Tan, and J.J. Rico, ‘Efficient Object Oriented Power System Software for the Analysis of Large-scale Networks Containing FACTS Controlled Branches’, *IEEE Trans. Power Systems* 3(2) 464–472, © 1998 IEEE

### 4.3.6 Newton-Raphson Computer Program in Matlab® Code

A computer program suitable for the power flow solution of small and medium-sized power systems is given in Program 4.1. The program is general, as far as the topology of the network is concerned, and caters for any number of *PV* and *PQ* buses. Moreover, any bus in the network may be designated to be the slack bus. Provisions are made for generator reactive limit checking and to accommodate fix shunt compensation. No transformers are represented in this base program and no sparsity techniques (Zollenkoff, 1970) are incorporated.

PROGRAM 4.1 A program written in Matlab® to calculate positive sequence power flows using the Newton–Raphson method

```

%***- - - Main Program

PowerFlowsData; %Read system data

[YR,YI] = YBus(tlsend,tlrec,tlresis,tlreac,tlsuscep,tlcond,shbus,...
shresis,shreac,ntl,nbb,nsh);
    
```

```

[VM,VA,it] = NewtonRaphson(nmax,tol,itmax,ngn,nld,nbb,bustype,...
genbus,loadbus,PGEN,QGEN,QMAX,QMIN,PLOAD,QLOAD,YR,YI,VM,VA);

[PQsend,PQrec,PQloss,PQbus] = PQflows(nbb,ngn,ntl,nld,genbus,...
loadbus,tlsend,tlrec,tlresis,tlreac,tlcond,tlsuscep,PLOAD,...
QLOAD,VM,VA);

it %Iteration number
VM %Nodal voltage magnitude (p.u.)
VA = VA*180/pi %Nodal voltage phase angle(Deg)
PQsend %Sending active and reactive powers (p.u.)
PQrec %Receiving active and reactive powers (p.u.)

%End Main Program

%Build up admittance matrix
function [YR,YI] = YBus(tlsend,tlrec,tlresis,tlreac,tlsuscep,...
tlcond,shbus,shresis,shreac,ntl,nbb,nsh);
YR=zeros(nbb,nbb);
YI=zeros(nbb,nbb);
% Transmission lines contribution
for kk = 1: ntl
    ii = tlsend(kk);
    jj = tlrec(kk);
    denom = tlresis(kk)^2+tlreac(kk)^2;
    YR(ii,ii) = YR(ii,ii) + tlresis(kk)/denom + 0.5*tlcond(kk);
    YI(ii,ii) = YI(ii,ii) - tlreac(kk)/denom + 0.5*tlsuscep(kk);
    YR(ii,jj) = YR(ii,jj) - tlresis(kk)/denom;
    YI(ii,jj) = YI(ii,jj) + tlreac(kk)/denom;
    YR(jj,ii) = YR(jj,ii) - tlresis(kk)/denom;
    YI(jj,ii) = YI(jj,ii) + tlreac(kk)/denom;
    YR(jj,jj) = YR(jj,jj) + tlresis(kk)/denom + 0.5*tlcond(kk);
    YI(jj,jj) = YI(jj,jj) - tlreac(kk)/denom + 0.5*tlsuscep(kk);
end
% Shunt elements contribution
for kk = 1: nsh
    ii = shbus(kk);
    denom = shresis(kk)^2+shreac(kk)^2;
    YR(ii,ii) = YR(ii,ii) + shresis(kk)/denom;
    YI(ii,ii) = YI(ii,ii) - shreac(kk)/denom;
end
% End of function YBus

%Carry out iterative solution using the Newton-Raphson method
function [VM,VA,it] = NewtonRaphson(nmax,tol,itmax,ngn,nld,nbb,...
bustype, genbus, loadbus, PGEN, QGEN, QMAX, QMIN, PLOAD, QLOAD, YR, YI, VM, VA)

```

## 106 CONVENTIONAL POWER FLOW

```
% GENERAL SETTINGS
D = zeros(1, nmax);
flag = 0;
it = 1;

% CALCULATE NET POWERS
[PNET, QNET] = NetPowers(nbb, ngn, nld, genbus, loadbus, PGEN, QGEN, ...
PLOAD, QLOAD);

while ( it < itmax & flag==0 )
    % CALCULATED POWERS
    [PCAL, QCAL] = CalculatedPowers(nbb, VM, VA, YR, YI);

    % CHECK FOR POSSIBLE GENERATOR'S REACTIVE POWERS LIMITS VIOLATIONS
    [QNET, bustype] = GeneratorsLimits(ngn, genbus, bustype, QGEN, QMAX, ...
QMIN, QCAL, QNET, QLOAD, it, VM, nld, loadbus);

    % POWER MISMATCHES
    [DPQ, DP, DQ, flag] = PowerMismatches(nmax, nbb, tol, bustype, flag, PNET, ...
QNET, PCAL, QCAL);

    % JACOBIAN FORMATION
    [JAC] = NewtonRaphsonJacobian(nmax, nbb, bustype, PCAL, QCAL, VM, VA, ...
YR, YI);

    % SOLVE FOR THE STATE VARIABLES VECTOR
    D = JAC\DPQ';

    % UPDATE STATE VARIABLES
    [VA, VM] = StateVariablesUpdates(nbb, D, VA, VM);

    it = it + 1;
end
% End function Newton-Raphson

%Function to calculate the net scheduled powers
function [PNET, QNET] = NetPowers(nbb, ngn, nld, genbus, loadbus, PGEN, ...
QGEN, PLOAD, QLOAD);
% CALCULATE NET POWERS
PNET = zeros(1, nbb);
QNET = zeros(1, nbb);
for ii = 1: ngn
    PNET(genbus(ii)) = PNET(genbus(ii)) + PGEN(ii);
    QNET(genbus(ii)) = QNET(genbus(ii)) + QGEN(ii);
end
for ii = 1: nld
    PNET(loadbus(ii)) = PNET(loadbus(ii)) - PLOAD(ii);
```

```

    QNET(loadbus(ii)) = QNET(loadbus(ii)) - QLOAD(ii);
end
%End function NetPowers

%Function to calculate injected bus powers
function [PCAL,QCAL] = CalculatedPowers(nbb,VM,VA,YR,YI)
% Include all entries
PCAL = zeros(1,nbb);
QCAL = zeros(1,nbb);
for ii = 1:nbb
    PSUM = 0;
    QSUM = 0;
    for jj = 1:nbb
        PSUM = PSUM + VM(ii)*VM(jj)*(YR(ii,jj)*cos(VA(ii)-VA(jj)) +...
            YI(ii,jj)*sin(VA(ii)-VA(jj)));
        QSUM = QSUM + VM(ii)*VM(jj)*(YR(ii,jj)*sin(VA(ii)-VA(jj)) -...
            YI(ii,jj)*cos(VA(ii)-VA(jj)));
    end
    PCAL(ii) = PSUM;
    QCAL(ii) = QSUM;
end
%End of functionCalculatePowers

%Function to check whether or not solution is within generators limits
function [QNET,bustype] = GeneratorsLimits(ngn,genbus,bustype,QGEN,...
QMAX,QMIN,QCAL,QNET, QLOAD, it, VM, nld, loadbus)
% CHECK FOR POSSIBLE GENERATOR'S REACTIVE POWERS LIMITS VIOLATIONS
if it > 2
    flag2 = 0;
    for ii = 1:ngn
        jj = genbus(ii);
        if (bustype(jj) == 2)
            if ( QCAL(jj) > QMAX(ii) )
                QNET(genbus(ii)) = QMAX(ii);
                bustype(jj) = 3;
                flag2 = 1;
            elseif ( QCAL(jj) < QMIN(ii) )
                QNET(genbus(ii)) = QMIN(ii);
                bustype(jj) = 3;
                flag2 = 1;
            end
        end
        if flag2 == 1
            for ii = 1:nld
                if loadbus(ii) == jj
                    QNET(loadbus(ii)) = QNET(loadbus(ii)) - QLOAD(ii)
                end
            end
        end
    end
end
end

```

```

    end
    end
    end
%End function Generatorslimits

%Function to compute power mismatches
function [DPQ,DP,DQ,flag] = PowerMismatches(nmax,nbb,tol,bustype,...
flag,PNET,QNET,PCAL,QCAL);
% POWER MISMATCHES
DPQ = zeros(1,nmax);
DP = zeros(1,nbb);
DQ = zeros(1,nbb);
DP = PNET - PCAL;
DQ = QNET - QCAL;
% To remove the active and reactive powers contributions of the slack
% bus and reactive power of all PV buses
for ii = 1:nbb
    if (bustype(ii) == 1 )
        DP(ii) = 0;
        DQ(ii) = 0;
    elseif (bustype(ii) == 2 )
        DQ(ii) = 0;
    end
end
% Re-arrange mismatch entries
kk = 1;
for ii = 1:nbb
    DPQ(kk) = DP(ii);
    DPQ(kk+1) = DQ(ii);
    kk = kk + 2;
end
% Check for convergence
for ii = 1:nbb*2
    if ( abs(DPQ) < tol)
        flag = 1;
    end
end
%End function PowerMismatches

%Function to built the Jacobian matrix
function [JAC] = NewtonRaphsonJacobian(nmax,nbb,bustype,PCAL,QCAL,...
VM,VA,YR,YI);
% JACOBIAN FORMATION
% Include all entries
JAC = zeros(nmax,nmax);
iii = 1;

```

```

for ii = 1: nbb
    jjj = 1;
    for jj = 1: nbb
        if ii == jj
            JAC(iii, jjj) = -QCAL(ii) - VM(ii)^2*YI(ii, ii);
            JAC(iii, jjj+1) = PCAL(ii) + VM(ii)^2*YR(ii, ii);
            JAC(iii+1, jjj) = PCAL(ii) - VM(ii)^2*YR(ii, ii);
            JAC(iii+1, jjj+1) = QCAL(ii) - VM(ii)^2*YI(ii, ii);
        else
            JAC(iii, jjj) = VM(ii)*VM(jj)*(YR(ii, jj)*sin(VA(ii)-VA(jj))...
            -YI(ii, jj)*cos(VA(ii)-VA(jj)));
            JAC(iii+1, jjj) = -VM(ii)*VM(jj)*(YI(ii, jj)*sin(VA(ii)...
            -VA(jj))+YR(ii, jj)*cos(VA(ii)-VA(jj)));
            JAC(iii, jjj+1) = -JAC(iii+1, jjj);
            JAC(iii+1, jjj+1) = JAC(iii, jjj);
        end
        jjj = jjj + 2;
    end
    iii = iii + 2;
end
% Delete the voltage magnitude and phase angle equations of the slack
% bus and voltage magnitude equations corresponding to PV buses
for kk = 1: nbb
    if (bustype(kk) == 1)
        ii = kk*2-1;
        for jj = 1: 2*nbb
            if ii == jj
                JAC(ii, ii) = 1;
            else
                JAC(ii, jj) = 0;
                JAC(jj, ii) = 0;
            end
        end
    end
    if (bustype(kk) == 1) | (bustype(kk) == 2)
        ii = kk*2;
        for jj = 1: 2*nbb
            if ii == jj
                JAC(ii, ii) = 1;
            else
                JAC(ii, jj) = 0;
                JAC(jj, ii) = 0;
            end
        end
    end
end
%End of function NewtonRaphsonJacobian

```

```

%Function to update state variables
function [VA,VM] = StateVariablesUpdates(nbb,D,VA,VM)
iii = 1;
for ii = 1: nbb
    VA(ii) = VA(ii) + D(iii);
    VM(ii) = VM(ii) + D(iii+1)*VM(ii);
    iii = iii + 2;
end
%End function StateVariableUpdating

%Function to calculate the power flows
function [PQsend,PQrec,PQloss,PQbus] = PQflows(nbb,ngn,ntl,nld,...
genbus,loadbus,tlsend,tlrec,tlresis,tlreac,tlcond,tl suscep,PLOAD,...
QLOAD,VM,VA);
PQsend = zeros(1,ntl);
PQrec = zeros(1,ntl);
% Calculate active and reactive powers at the sending and receiving
% ends of transmission lines
for ii = 1: ntl
    Vsend = ( VM(tlsend(ii))*cos(VA(tlsend(ii))) + ...
    VM(tlsend(ii))*sin(VA(tlsend(ii)))*i );
    Vrec = ( VM(tlrec(ii))*cos(VA(tlrec(ii))) + ...
    VM(tlrec(ii))*sin(VA(tlrec(ii)))*i );
    tlimped = tlresis(ii) + tlreac(ii)*i;
    current = (Vsend - Vrec) / tlimped + Vsend*( tlcond(ii) + ...
    tl suscep(ii)*i )*0.5 ;
    PQsend(ii) = Vsend*conj(current);
    current = (Vrec - Vsend) / tlimped + Vrec*( tlcond(ii) + ...
    tl suscep(ii)*i )*0.5 ;
    PQrec(ii) = Vrec*conj(current);
    PQloss(ii) = PQsend(ii) + PQrec(ii);
end
% Calculate active and reactive powers injections at buses
PQbus = zeros(1,nbb);
for ii = 1: ntl
    PQbus(tlsend(ii)) = PQbus(tlsend(ii)) + PQsend(ii);
    PQbus(tlrec(ii)) = PQbus(tlrec(ii)) + PQrec(ii);
end

% Make corrections at generator buses, where there is load, in order to
% get correct generators contributions
for ii = 1: nld
    jj = loadbus(ii);
    for kk = 1: ngn
        ll = genbus(kk);

```

```

if jj == 11
    PQbus(jj) = PQbus(jj) + ( PLOAD(ii) + QLOAD(ii)*i );
end
end
end
end
%End function PQflows

```

### 4.3.7 The Fast Decoupled Algorithm

It was demonstrated in the late 1970s that the storage and computing requirements of the Newton–Raphson method could be reduced very significantly by introducing a series of well-substantiated, simplifying, assumptions in Equation (4.28). These assumptions are based on physical properties exhibited by electrical power systems, in particular in high-voltage transmission systems.

The resulting formulation is no longer a Newton–Raphson method but a derived formulation described as ‘fast decoupled’ (Stott, 1974; Stott and Alsac, 1978). The power mismatch equations of both methods are identical but their Jacobians are quite different; the Jacobian elements of the Newton–Raphson method are voltage-dependent whereas those of the fast decoupled method are voltage-independent (i.e. constant parameters). Moreover, the number of Jacobian entries used in the fast decoupled method is only half of those used in the Newton–Raphson method. The trade-off lies in the weakening of the strong convergence characteristic exhibited by the Newton–Raphson method; the convergence characteristics of the fast decoupled method are linear as opposed to quadratic.

For a typical power flow problem, where convergence to a tight tolerance is mandatory, the 6 iterations normally taken by the Newton–Raphson method to converge will increase to 25 iterations and above when the fast decoupled method is employed. In fact, the number of iterations taken by the fast decoupled method may be influenced by the size of the system being solved, how loaded the system is, the number of power system controllers, and the ratio of resistance to reactance in the transmission elements – although there are simple programming artifices to circumvent this problem. However, an asset of the fast decoupled method is that one of its iterations only takes a fraction of the time required by one of the Newton–Raphson method iterations. Hence, in power flow studies of high-voltage networks with a small number of system controllers, the use of the fast decoupled method may be advantageous.

With a view to developing the fast decoupled formulation, simplifications will be introduced into the Jacobian of Equation (4.28). It has been observed that, during normal operation, incremental changes in voltage magnitude produce almost no change in active power flow and that, likewise, incremental changes in voltage phase angle produce almost no change in reactive power flow. Hence, the following Jacobian elements may be assumed to be zero:

$$\left[ \frac{\partial \mathbf{P}}{\partial \mathbf{V}} \mathbf{V} \right], \quad \text{and} \quad \left[ \frac{\partial \mathbf{Q}}{\partial \boldsymbol{\theta}} \right]. \quad (4.45)$$

Accordingly, the overall problem stated in Equation (4.28) reduces to the following two subproblems:

$$\underbrace{[\Delta \mathbf{P}]}_{\mathbf{F}_1(\mathbf{x}_1^{(i-1)})} = - \underbrace{\left[ \frac{\partial \mathbf{P}}{\partial \boldsymbol{\theta}} \right]}_{\mathbf{J}_1(\mathbf{x}_1^{(i-1)})} \underbrace{[\Delta \boldsymbol{\theta}]}_{\Delta \mathbf{x}_1^{(i)}}, \quad (4.46)$$

$$\underbrace{[\Delta \mathbf{Q}]}_{\mathbf{F}_2(\mathbf{x}_2^{(i-1)})} = - \underbrace{\left[ \frac{\partial \mathbf{Q}}{\partial \mathbf{V}} \mathbf{V} \right]}_{\mathbf{J}_2(\mathbf{x}_2^{(i-1)})} \underbrace{\left[ \frac{\Delta \mathbf{V}}{\mathbf{V}} \right]}_{\Delta \mathbf{x}_2^{(i)}}. \quad (4.47)$$

Further simplifying assumptions pertaining to high-voltage transmission networks, which are relevant to the problem at hand, are as follows:

- $X \gg R$  in all transmission lines and transformers of the network.
- The difference in voltage phase angles between two adjacent buses is small and hence the following relations apply:  $\sin(\theta_k - \theta_m) = \theta_k - \theta_m$ , and  $\cos(\theta_k - \theta_m) = 1$ .
- The nodal voltage magnitudes are close to 1 p.u. at every bus.
- Current flows in shunt-connected elements may be grouped together with the equivalent loads and generator currents.

Incorporating these assumptions in the Jacobian elements of Equations (4.46) and (4.47) we obtain the following set of equations:

$$\underbrace{[\Delta \mathbf{P}]}_{\mathbf{F}_1(\mathbf{x}_1^{(i-1)})} = - [\mathbf{B}'] \underbrace{[\Delta \boldsymbol{\theta}]}_{\Delta \mathbf{x}_1^{(i)}}, \quad (4.48)$$

$$\underbrace{[\Delta \mathbf{Q}]}_{\mathbf{F}_2(\mathbf{x}_2^{(i-1)})} = - [\mathbf{B}''] \underbrace{[\Delta \mathbf{V}]}_{\Delta \mathbf{x}_2^{(i)}}, \quad (4.49)$$

where  $\mathbf{B}'$  corresponds almost exactly to the negative of the imaginary part of the nodal admittance matrix. Owing to the requirements of the power flow problem, the row and column corresponding to the slack bus is not included in  $\mathbf{B}'$ . Matrices  $\mathbf{B}'$  and  $\mathbf{B}''$  are identical if no generator buses exist in the system. However, in the more general case, when generator buses do exist in the system then the row and column corresponding to each generator bus are removed from matrix  $\mathbf{B}''$ .

Equations (4.48) and (4.49) are very simple compared with that of the full Newton–Raphson method given by Equation (4.28). Matrices  $\mathbf{B}'$  and  $\mathbf{B}''$  are symmetric in structure and, provided no phase-shifting transformers are present in the system, they are also symmetric in value. These matrices are inverted only once, during the first iteration, and then remain constant throughout the iterative process. This is in contrast to with the Newton–Raphson method, where the Jacobian is evaluated and inverted (factorised; Zollenkoff, 1970) at each iteration.

### 4.3.8 Fast Decoupled Computer Program in Matlab® Code

Program 4.2 is fully equivalent to the Newton–Raphson power flow program given in Section 4.3.6 (Program 4.1). The functions `PowerFlowsData`, `YBus` and `PQflows` are also

used here. The function `FastDecoupled` replaces `NewtonRaphson`, with the new function using all the functions called by `NewtonRaphson` except for `NewtonRaphsonJacobian`, which is replaced with `FastDecoupledJacobian`.

PROGRAM 4.2 Program written in Matlab® to calculate positive sequence power flows by means of the fast decoupled method.

```
% - - - Main Program

PowerFlowsData; %Function to read data

% Form the bus admittance matrix
[YR, YI] = YBus(tlsend, tlrec, tlresis, tlreac, tlsuscep, tlcond, shbus, ...
shresis, shreac, ntl, nbb, nsh);

[VM, VA, it] = FastDecoupled(nmax, tol, itmax, ngn, nld, nbb, bustype, ...
genbus, loadbus, PGEN, QGEN, QMAX, QMIN, PLOAD, QLOAD, YR, YI, VM, VA);

[PQsend, PQrec, PQloss, PQbus] = PQflows(nbb, ngn, ntl, nld, genbus, ...
loadbus, tlsend, tlrec, tlresis, tlreac, tlcond, tlsuscep, PLOAD, QLOAD, ...
VM, VA);

it %Iteration number
VM %Nodal voltage magnitude (p.u.)
VA = VA*180/pi %Nodal voltage phase angle(Deg)
PQsend %Sending active and reactive powers (p.u.)
PQrec %Receiving active and reactive powers (p.u.)

% End of Main Program

% Fast Decoupled function
function [VM, VA, it] = FastDecoupled(nmax, tol, itmax, ngn, nld, nbb, ...
bustype, genbus, loadbus, PGEN, QGEN, QMAX, QMIN, PLOAD, QLOAD, YR, YI, VM, VA);

% GENERAL SETTINGS
flag = 0;
B1 = zeros(nbb, nbb);
B2 = zeros(nbb, nbb);
% CALCULATE NET POWERS
[PNET, QNET] = NetPowers(nbb, ngn, nld, genbus, loadbus, PGEN, QGEN, PLOAD, ...
QLOAD);

% BEGINNING OF ITERATIVE LOOP

it = 1;
while ( it < itmax & flag==0 )
```

```

% CALCULATED POWERS
[PCAL,QCAL] = CalculatedPowers(nbb,VM,VA,YR,YI);

% CHECK FOR POSSIBLE GENERATOR'S REACTIVE POWERS LIMITS VIOLATIONS
[QNET,bustype] = GeneratorsLimits(ngn,genbus,bustype,QGEN,QMAX,...
QMIN,QCAL,QNET, QLOAD, it, VM, nld, loadbus);

% POWER MISMATCHES
[DPQ,DP,DQ,flag] = PowerMismatches(nmax,nbb,tol,bustype,flag,PNET,...
QNET,PCAL,QCAL);

% OBTAIN INVERTED JACOBIANS DURING THE FIRST ITERATION
[B1,B2] = FastDecoupledJacobian(nbb,bustype,DP,DQ,YI,B1,B2,it);
% SOLVE FOR THE STATE VARIABLES VECTOR
DVA = B1*DP';
DVM = B2*DQ';
% Re-arrange state variables entries
kk = 1;
for ii = 1: nbb
    D(kk) = DVA(ii);
    D(kk+1) = DVM(ii);
    kk = kk + 2;
end

% UPDATE THE STATE VARIABLES VALUES
[VA,VM] = StateVariablesUpdating(nbb,D,VA,VM,it);

it = it + 1;
end
% End of function FastDecoupled

%Form the Jacobian for the Fast Decoupled Method
function [B1,B2] = FastDecoupledJacobian(nbb,bustype,DP,DQ,YI,...
B1,B2,it);
DVA = zeros(nbb);
DVM = zeros(nbb);
if ( it == 1 )
    % Include all entries
    B1 = zeros(nbb,nbb);
    B2 = zeros(nbb,nbb);
    B1 = -YI;
    B2 = -YI;
    % Delete the voltage magnitude and phase angle equations of the slack
    % bus and voltage magnitude equations corresponding to PV buses
    for ii = 1: nbb
        if (bustype(ii) == 1)
            for jj = 1: nbb

```

```

    if ii == jj
        B1(ii,ii) = 1;
        B2(ii,ii) = 1;
    else
        B1(ii,jj) = 0;
        B1(jj,ii) = 0;
        B2(ii,jj) = 0;
        B2(jj,ii) = 0;
    end
end
end
if (bustype(ii) == 1) | (bustype(ii) == 2)
    for jj = 1:nbb
        if ii == jj
            B2(ii,ii) = 1;
        else
            B2(ii,jj) = 0;
            B2(jj,ii) = 0;
        end
    end
end
end
end
B1 = inv(B1);
B2 = inv(B2);
end
% End of FastdecoupledJacobian Function

```

### 4.3.9 A Benchmark Numerical Example

A small network (Stagg and El-Abiad, 1968) is used to illustrate the power flow solutions given by the Newton–Raphson and the fast decoupled methods. As shown in Figure 4.6, this is a five-bus network containing two generators and seven transmission lines. The data are given in function `PowerFlowsData`, suitable for use with either the Newton–Raphson or the fast decoupled Matlab<sup>®</sup> programs. The power flow results are superimposed on the one-line diagram of the network, and the bus voltages are given in Table 4.1.

Function `PowerFlowsData`, to read data for the five-bus test network, is as follows:

```

%The following convention is used for the four types of buses available
%in conventional power flow studies:
%bustype = 1 is slack or swing bus
%bustype = 2 is generator PV bus
%bustype = 3 is load PQ bus
%bustype = 4 is generator PQ bus
%
%The five buses in the network shown in Figure 4.6 are numbered for the
% purpose of the power flow solution, as follows:

```

```

%North = 1
%South = 2
%Lake = 3
%Main = 4
%Elm = 5
%
%Bus data
%nbb = number of buses
%bustype = type of bus
%VM = nodal voltage magnitude
%VA = nodal voltage phase angle
nbb = 5 ;
bustype(1) = 1 ; VM(1) = 1.06 ; VA(1) = 0 ;
bustype(2) = 2 ; VM(2) = 1 ; VA(2) = 0 ;
bustype(3) = 3 ; VM(3) = 1 ; VA(3) = 0 ;
bustype(4) = 3 ; VM(4) = 1 ; VA(4) = 0 ;
bustype(5) = 3 ; VM(5) = 1 ; VA(5) = 0 ;
%
%Generator data
%ngn = number of generators
%genbus = generator bus number
%PGEN = scheduled active power contributed by the generator
%QGEN = scheduled reactive power contributed by the generator
%QMAX = generator reactive power upper limit
%QMIN = generator reactive power lower limit
ngn = 2 ;
genbus(1) = 1 ; PGEN(1) = 0 ; QGEN(1) = 0 ; QMAX(1) = 5 ; QMIN(1) = -5 ;
genbus(2) = 2 ; PGEN(2) = 0.4 ; QGEN(2) = 0 ; QMAX(2) = 3 ; QMIN(2) = -3 ;
%
%Transmission line data
%ntl = number of transmission lines
%tlsend = sending end of transmission line
%tlrec = receiving end of transmission line
%tlresis = series resistance of transmission line
%tlreac = series reactance of transmission line
%tlcond = shunt conductance of transmission line
%tlsuscep = shunt susceptance of transmission line
ntl = 7 ;
tlsend(1) = 1 ; tlrec(1) = 2 ; tlresis(1) = 0.02 ; tlreac(1) = 0.06 ;
tlcond(1) = 0 ; tlsuscep(1) = 0.06 ;
tlsend(2) = 1 ; tlrec(2) = 3 ; tlresis(2) = 0.08 ; tlreac(2) = 0.24 ;
tlcond(2) = 0 ; tlsuscep(2) = 0.05 ;
tlsend(3) = 2 ; tlrec(3) = 3 ; tlresis(3) = 0.06 ; tlreac(3) = 0.18 ;
tlcond(3) = 0 ; tlsuscep(3) = 0.04 ;
tlsend(4) = 2 ; tlrec(4) = 4 ; tlresis(4) = 0.06 ; tlreac(4) = 0.18 ;
tlcond(4) = 0 ; tlsuscep(4) = 0.04 ;

```

```

tlsend(5) = 2 ; tlrec(5) = 5 ; tlresis(5) = 0.04 ; tlreac(5) = 0.12 ;
tlcond(5) = 0 ; tlsuscep(5) = 0.03 ;
tlsend(6) = 3 ; tlrec(6) = 4 ; tlresis(6) = 0.01 ; tlreac(6) = 0.03 ;
tlcond(6) = 0 ; tlsuscep(6) = 0.02 ;
tlsend(7) = 4 ; tlrec(7) = 5 ; tlresis(7) = 0.08 ; tlreac(7) = 0.24 ;
tlcond(7) = 0 ; tlsuscep(7) = 0.05 ;
%
%Shunt data
%nsh = number of shunt elements
%shbus = shunt element bus number
%shresis = resistance of shunt element
%shreac = reactance of shunt element:
%+ve for inductive reactance and -ve for capacitive reactance
nsh = 0 ;
shbus(1) = 0 ; shresis(1) = 0 ; shreac(1) = 0 ;
%
%Load data
%nld = number of load elements
%loadbus = load element bus number
%PLOAD = scheduled active power consumed at the bus
%QLOAD = scheduled reactive power consumed at the bus
nld = 4 ;
loadbus(1) = 2 ; PLOAD(1) = 0.2 ; QLOAD(1) = 0.1 ;
loadbus(2) = 3 ; PLOAD(2) = 0.45 ; QLOAD(2) = 0.15 ;
loadbus(3) = 4 ; PLOAD(3) = 0.4 ; QLOAD(3) = 0.05 ;
loadbus(4) = 5 ; PLOAD(4) = 0.6 ; QLOAD(4) = 0.1 ;

%General parameters
%itmax = maximum number of iterations permitted before the iterative
%process is terminated - protection against infinite iterative loops
%tol = criterion tolerance to be met before the iterative solution is
%successfully brought to an end
itmax = 100;
tol = 1e-12;
nmax = 2*nbb;
%End of function PowerFlowsData

```

As expected, the Newton–Raphson and the fast decoupled methods yield practically the same results when the power flow problem is solved to a prescribed tolerance of  $1e-12$ . The former method takes 6 iterations to converge whereas the latter takes 27 iterations. However, it should be mentioned that one iteration of the fast decoupled method executes much faster than one iteration of the Newton–Raphson method; no inversion (refactorisation) of the Jacobian is required at each iterative step of the fast decoupled.

It can be observed from the results presented in Table 4.1 that all nodal voltages are within accepted voltage magnitude limits (i.e.  $100 \pm 6\%$  in the UK). The largest power flow

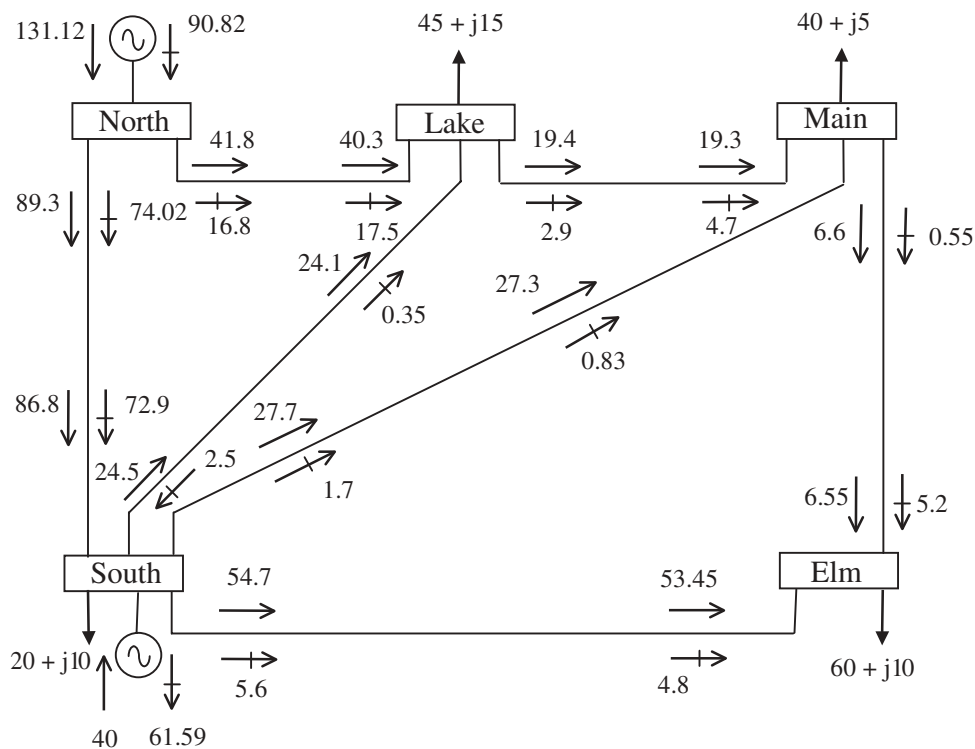


**Figure 4.6** The five-bus test network, and the power flow results. From G.W. Stagg and A.H. El-Abiad, *Computer Methods in Power System Analysis*, © 1968 McGraw-Hill. Reproduced by permission of The McGraw-Hill Companies

**Table 4.1** Nodal voltages of original network

Nodal voltage	Network bus				
	North	South	Lake	Main	Elm
Magnitude (p.u.)	1.06	1.00	0.987	0.984	0.972
Phase angle (deg)	0.00	-2.06	-4.64	-4.96	-5.77

takes place in the transmission line connecting the two generator buses: 89.3 MW, and 74.02 MVAR leave North, and 86.8 MW and 72.9 MVAR arrive at South. This is also the transmission line that incurs higher active power loss (i.e. 2.5 MW). The active power system loss is 6.12 MW.

The operating conditions demand a large amount of reactive power generation by the generator connected at North (i.e. 90.82 MVAR). This amount is well in excess of the reactive power drawn by the system loads (i.e. 40 MVAR). The generator at South draws the excess of reactive power in the network (i.e. 61.59 MVAR). This amount includes the net reactive power produced by several of the transmission lines.

## 4.4 CONSTRAINED POWER FLOW SOLUTIONS

The handling of *PV* buses in power flow algorithms may fall within the category of constrained power flow solutions – generators regulate nodal voltage magnitude by supplying or absorbing reactive power up to their design limits. Load tap-changing and phase-shifting transformers are used to regulate nodal voltage magnitude and active power flow, respectively. They also give rise to constrained power flow solutions. Suitable power flow models of tap-changing and phase-shifting transformers are developed in this section.

### 4.4.1 Load Tap-changing Transformers

The power flow models for load tap-changing (LTC) transformers addressed in this section are based on the two-winding, single-phase transformer model presented in Section 3.3.3, which is quite a general one. The model makes provisions for complex taps on both the primary and the secondary windings, and the magnetising branch of the transformer is included to account for core losses.

However, the LTC model does not require complex taps, and Equation (3.89) simplifies to the following expression:

$$\begin{bmatrix} I_k \\ I_m \end{bmatrix} = \frac{1}{T_k^2 Y_k + U_m^2 Y_m + Y_0} \begin{bmatrix} U_m^2 Y_k Y_m + Y_k Y_0 & -T_k U_m Y_k Y_m \\ -T_k U_m Y_k Y_m & T_k^2 Y_k Y_m + Y_m Y_0 \end{bmatrix} \begin{bmatrix} V_k \\ V_m \end{bmatrix}. \quad (4.50)$$

It is assumed in this expression that the primary and secondary sides of the transformer are connected to bus  $k$  and bus  $m$ , respectively. This is with a view to developing LTC models aimed at systems applications. Also, the subscript *sc* is dropped in the transformer admittance terms.

Comprehensive bus power injection equations for the LTC transformer may be derived based on Equation (4.50), but this involves very arduous algebra. Simpler expressions may be derived if a number of practical assumptions are introduced in this equation. For instance, it may be assumed that the tap-changing facility is only on the primary side ( $U_m = 1$ ); the impedance is all on the primary side ( $Y_m = 0$ ); and the impact of the magnetising branch is negligibly small in the power flow solution ( $Y_0 = 0$ ). Incorporating these simplifying assumptions in Equation (4.50) we obtain an expression that is compatible with Equation (3.78):

$$\begin{bmatrix} I_k \\ I_m \end{bmatrix} = \begin{bmatrix} Y_k & -T_k Y_k \\ -T_k Y_k & T_k^2 Y_k \end{bmatrix} \begin{bmatrix} V_k \\ V_m \end{bmatrix} = \begin{bmatrix} Y_{kk} & T_k Y_{km} \\ T_k Y_{mk} & T_k^2 Y_{mm} \end{bmatrix} \begin{bmatrix} V_k \\ V_m \end{bmatrix}. \quad (4.51)$$

Power flow equations at both ends of the transformer are derived, where  $T_k$  is allowed to vary within design rating values ( $T_k \min < T_k < T_k \max$ ):

$$P_k = V_k^2 G_{kk} + T_k V_k V_m [G_{km} \cos(\theta_k - \theta_m) + B_{km} \sin(\theta_k - \theta_m)], \quad (4.52)$$

$$Q_k = -V_k^2 B_{kk} + T_k V_k V_m [G_{km} \sin(\theta_k - \theta_m) - B_{km} \cos(\theta_k - \theta_m)], \quad (4.53)$$

$$P_m = T_k^2 V_m^2 G_{mm} + T_k V_m V_k [G_{mk} \cos(\theta_m - \theta_k) + B_{mk} \sin(\theta_m - \theta_k)], \quad (4.54)$$

$$Q_m = -T_k^2 V_m^2 B_{mm} + T_k V_m V_k [G_{mk} \sin(\theta_m - \theta_k) - B_{mk} \cos(\theta_m - \theta_k)], \quad (4.55)$$

where

$$\begin{aligned} Y_{kk} &= Y_{mm} = G_{kk} + jB_{kk} = Y_k, \\ Y_{km} &= Y_{mk} = G_{km} + jB_{km} = -Y_k. \end{aligned} \quad (4.56)$$

The set of linearised power flow equations for the nodal power injections, Equations (4.52)–(4.55), assuming that the load tap changer (LTC) is controlling nodal voltage magnitude at its sending end (bus  $k$ ), may be written as:

$$\begin{bmatrix} \Delta P_k \\ \Delta P_m \\ \Delta Q_k \\ \Delta Q_m \end{bmatrix}^{(i)} = \begin{bmatrix} \frac{\partial P_k}{\partial \theta_k} & \frac{\partial P_k}{\partial \theta_m} & \frac{\partial P_k}{\partial T_k} T_k & \frac{\partial P_k}{\partial V_m} V_m \\ \frac{\partial P_m}{\partial \theta_k} & \frac{\partial P_m}{\partial \theta_m} & \frac{\partial P_m}{\partial T_k} T_k & \frac{\partial P_m}{\partial V_m} V_m \\ \frac{\partial Q_k}{\partial \theta_k} & \frac{\partial Q_k}{\partial \theta_m} & \frac{\partial Q_k}{\partial T_k} T_k & \frac{\partial Q_k}{\partial V_m} V_m \\ \frac{\partial Q_m}{\partial \theta_k} & \frac{\partial Q_m}{\partial \theta_m} & \frac{\partial Q_m}{\partial T_k} T_k & \frac{\partial Q_m}{\partial V_m} V_m \end{bmatrix}^{(i)} \begin{bmatrix} \Delta \theta_k \\ \Delta \theta_m \\ \frac{\Delta T_k}{T_k} \\ \frac{\Delta V_m}{V_m} \end{bmatrix}^{(i)}. \quad (4.57)$$

The tap variable  $T_k$  is adjusted, within limits, to constrain the voltage magnitude at bus  $k$  at a specified value  $V_k$ . For this mode of operation  $V_k$  is maintained constant at the target value.

The Jacobian elements in matrix Equation (4.57) are given as follows:

$$\frac{\partial P_k}{\partial \theta_k} = -\frac{\partial P_k}{\partial \theta_m} = -Q_k - V_k^2 B_{kk}, \quad (4.58)$$

$$\frac{\partial P_k}{\partial T_k} T_k = \frac{\partial P_k}{\partial V_m} V_m = P_k - V_k^2 G_{kk}, \quad (4.59)$$

$$\frac{\partial Q_k}{\partial \theta_k} = -\frac{\partial Q_k}{\partial \theta_m} = P_k - V_k^2 G_{kk}, \quad (4.60)$$

$$\frac{\partial Q_k}{\partial T_k} T_k = \frac{\partial Q_k}{\partial V_m} V_m = Q_k + V_k^2 B_{kk}, \quad (4.61)$$

$$\frac{\partial P_m}{\partial \theta_m} = -\frac{\partial P_m}{\partial \theta_k} = -Q_m - T_k^2 V_m^2 B_{mm}, \quad (4.62)$$

$$\frac{\partial P_m}{\partial V_m} V_m = \frac{\partial P_m}{\partial T_k} T_k = P_m + T_k^2 V_m^2 G_{mm}, \quad (4.63)$$

$$\frac{\partial Q_m}{\partial \theta_m} = -\frac{\partial Q_m}{\partial \theta_k} = P_m - T_k^2 V_m^2 G_{mm}, \quad (4.64)$$

$$\frac{\partial Q_m}{\partial V_m} V_m = \frac{\partial Q_m}{\partial T_k} T_k = Q_m - T_k^2 V_m^2 B_{mm}. \quad (4.65)$$

If nodal voltage magnitude control by the LTC takes place on its receiving end (bus  $m$ ) as opposed to the sending end (bus  $k$ ), the second and third columns in Equation (4.57) are interchanged, and Jacobian elements similar to Equations (4.58)–(4.65) are derived and used as entries in Equation (4.57). Also, note that in the state variables vector  $\Delta T_k$  and  $\Delta V_k$  commute places.

At the end of each iteration,  $i$ , the tap controller is updated using the following relation:

$$T_k^{(i)} = T_k^{(i-1)} + \left( \frac{\Delta T_k}{T_k} \right)^{(i)} T_k^{(i-1)}. \quad (4.66)$$

The implementation of the LTC model within the power flow algorithm benefits from the introduction of a controlled bus, termed the *PVT* bus. It resembles a generator *PV* bus but here the voltage control is exerted by an LTC as opposed to a generator. The nodal voltage magnitude and the bus active and reactive powers are specified, whereas the LTC tap  $T_k$  is handled as a state variable. If  $T_k$  is within limits, the specified voltage is attained and the controlled bus remains *PVT*. However, if  $T_k$  goes out of limits,  $T_k$  is fixed at the violated limit and the bus becomes *PQ*.

It should be remarked that a more comprehensive set of nodal power equations may be derived for the two-winding transformer by basing the power equation derivations on Equation (4.50) as opposed to Equation (4.51). There is no need to assume that the transformer impedance is all placed on the primary side. Also, the effect of the magnetising admittance may be included in the nodal power equations of the LTC transformer. Alternatively, it may be assumed that the tap-changing facility is on the secondary side as opposed to the primary side, in which case  $T_k = 1$ , and  $U_{m \min} < U_m < U_{m \max}$ .

#### 4.4.1.1 State variable initialisation and limit checking

Further to the recommendations given in Section 4.3.3 for initialising the nodal voltage magnitudes and phase angles of power flow solutions of networks that contain only conventional plat components, it is normal to select the initial tapping position of LTCs to be at their nominal value. Hence,  $T_k = 1$  and  $U_m = 1$  are used for cases of two-winding LTCs.

The status of LTC taps is checked at each iterative step to assess whether or not the LTC is still operating within limits and capable of regulating voltage magnitude. For an LTC regulating nodal voltage magnitude at bus  $k$  with tapping facilities in the primary winding

$$T_{k \min} < T_k < T_{k \max}. \quad (4.67)$$

If either of the following conditions occur during the iterative process:

$$\begin{aligned} T_k^{(i+1)} + \Delta T_k^{(i)} &\geq T_{k \max}, \\ T_k^{(i+1)} + \Delta T_k^{(i)} &\leq T_{k \min}, \end{aligned} \quad (4.68)$$

bus  $k$  becomes a *PQ* bus and the tap is fixed at the violated limit. The nodal voltage magnitude at bus  $k$  is allowed to vary and  $V_k$  replaces  $T_k$  as the state variable. The tap-changing transformer works as a conventional transformer, and the set of linearised power flow equations is given as follows:

$$\begin{bmatrix} \Delta P_k \\ \Delta P_m \\ \Delta Q_k \\ \Delta Q_m \end{bmatrix}^{(i)} = \begin{bmatrix} \frac{\partial P_k}{\partial \theta_k} & \frac{\partial P_k}{\partial \theta_m} & \frac{\partial P_k}{\partial V_k} V_k & \frac{\partial P_k}{\partial V_m} V_m \\ \frac{\partial P_m}{\partial \theta_k} & \frac{\partial P_m}{\partial \theta_m} & \frac{\partial P_m}{\partial V_k} V_k & \frac{\partial P_m}{\partial V_m} V_m \\ \frac{\partial Q_k}{\partial \theta_k} & \frac{\partial Q_k}{\partial \theta_m} & \frac{\partial Q_k}{\partial V_k} V_k & \frac{\partial Q_k}{\partial V_m} V_m \\ \frac{\partial Q_m}{\partial \theta_k} & \frac{\partial Q_m}{\partial \theta_m} & \frac{\partial Q_m}{\partial V_k} V_k & \frac{\partial Q_m}{\partial V_m} V_m \end{bmatrix}^{(i)} \begin{bmatrix} \Delta \theta_k \\ \Delta \theta_m \\ \frac{\Delta V_k}{V_k} \\ \frac{\Delta V_m}{V_m} \end{bmatrix}^{(i)}. \quad (4.69)$$

Checking of LTC taps limits normally starts after the first or second iteration since nodal voltage values computed at the beginning of the iterative process may be quite inaccurate, leading to misleading LTC tapping requirements.

Similar criteria would apply if the LTC tapping facilities were on the secondary winding, with  $U_m$  and  $T_k$  changing roles in Equation (4.50). Moreover, relevant power equations and Jacobian elements, equivalent to Equations (4.52)–(4.55) and (4.58)–(4.65), are derived. The linearised Equation (4.57) is modified accordingly.

#### 4.4.1.2 Load tap changer computer program in Matlab<sup>®</sup> code

Program 4.3 incorporates LTC transformer representation within the Newton–Raphson power flow program given in Section 4.3.6. The functions `PowerFlowsData`, `YBus`, and `PQflows` are also used here. In the main LTC Newton–Raphson program, the function `LTCPowerFlowsData` is added to read LTC data, `LTCNewtonRaphson` replaces `NewtonRaphson`, and `LTCPQflows` is used to calculate power flows and losses in the LTC transformer.

Function `LTCNewtonRaphson` borrows the following functions from `NewtonRaphson`: `NetPowers`; `CalculatedPowers`; `GeneratorsLimits`; `PowerMismatches`; `NewtonRaphsonJacobian`; and `StateVariablesUpdates`. Furthermore, four new functions are added to cater for LTC representation, namely: `LTCCalculatedPowers`; `LTCUpdates`; `LTCLimits`; and `LTCNewtonRaphsonJacobian`.

PROGRAM 4.3 Program written in Matlab<sup>®</sup> to incorporate load tap-changing representation within the Newton–Raphson power flow algorithm.

```
%- - - Main LTC Program

PowerFlowsData; %Function to read network data

LTCPowerFlowsData; %Function to read LTC data

[YR, YI] = YBus(tlsend, tlrec, tlresis, tlreac, tlsuscep, tlcond, shbus, ...
shresis, shreac, ntl, nbb, nsh);

[VM, VA, it, Tap] = LTCNewtonRaphson(tol, itmax, ngn, nld, nbb, bustype, ...
genbus, loadbus, PGEN, QGEN, QMAX, QMIN, PLOAD, QLOAD, YR, YI, VM, VA, NLTC, ...
LTCsend, LTCrece, Rltc, Xltc, Tap, TapHi, TapLo, Bus, LTCVM);

[PQsend, PQrec, PQloss, PQbus] = PQflows(nbb, ngn, ntl, nld, genbus, ...
loadbus, tlsend, tlrec, tlresis, tlreac, tlcond, tlsuscep, PLOAD, QLOAD, ...
VM, VA);

[LTCPQsend, LTCPQrece] = LTCPQflows(NLTC, LTCsend, LTCrece, Rltc, Xltc, ...
Tap, VM, VA);

it %Iteration number
VM %Nodal voltage magnitude (p.u.)
```

```

VA = VA*180/pi %Nodal voltage phase angle(Deg)
PQsend %Sending active and reactive powers (p.u.)
PQrec %Receiving active and reactive powers (p.u.)
Tap %Final transformer tap position

% End of Main LTCNewtonRaphson PROGRAM

function [VM,VA,it,Tap] = LTCNewtonRaphson(tol,itmax,ngn,nld,nbb,...
bustype,genbus,loadbus,PGEN,QGEN,QMAX,QMIN,PLOAD,QLOAD,YR,YI,VM,...
VA,NLTC,LTCsend,LTCrec,Rltc,Xltc,Tap,TapHi,TapLo,Bus,LTCVM);
% GENERAL SETTINGS
flag = 0;
it = 1;
% CALCULATE NET POWERS
[PNET,QNET] = NetPowers(nbb,ngn,nld,genbus,loadbus,PGEN,QGEN,PLOAD,...
QLOAD);

while (it <= itmax & flag==0)

% CALCULATED POWERS
[PCAL,QCAL] = CalculatedPowers(nbb,VM,VA,YR,YI);

% CALCULATED LTC POWERS
[PCAL,QCAL,ltcPCAL,ltcQCAL] = LTCCalculatedPowers(NLTC,LTCsend,...
LTCrec,Tap,Rltc,Xltc,VM,VA,PCAL,QCAL);

% POWER MISMATCHES
[DPQ,DP,DQ,flag] = PowerMismatches(nbb,tol,bustype,flag,PNET,QNET,...
PCAL,QCAL);
% Check for convergence
if flag == 1
    break
end
% JACOBIAN FORMATION
[JAC] = NewtonRaphsonJacobian(nbb,bustype,PCAL,QCAL,VM,VA,YR,YI);

% LTC JACOBIAN UPDATING
[JAC] = LTCNewtonRaphsonJacobian(bustype,LTCsend,LTCrec,NLTC,Tap,...
Bus,Rltc,Xltc,ltcPCAL,ltcQCAL,VM,VA,JAC);

```

## 124 CONVENTIONAL POWER FLOW

```

% SOLVE FOR THE STATE VARIABLES VECTOR
D = JAC\DPQ';

% UPDATE STATE VARIABLES
[VA,VM] = StateVariablesUpdates(nbb,D,VA,VM);

% UPDATE LTC TAPs
[VM, Tap] = LTCUpdates(VM,D,bustype,NLTC,LTCsend,LTCrec, Tap, Bus, ...
LTCVM);

% CHECK FOR POSSIBLE LTC TAPs' LIMITS VIOLATIONS
[ Tap,bustype] = LTCLimits(bustype,NLTC, Tap, TapHi, TapLo, LTCsend, ...
LTCrec);

it = it + 1;
end

function [PCAL,QCAL,ltcPCAL,ltcQCAL] = LTCCalculatedPowers(NLTC, ...
LTCsend,LTCrec,ltctap,Rltc,Xltc,VM,VA,PCAL,QCAL)

for ii = 1: NLTC
    kk = (ii-1)*2+1;
    % Calculate LTC admittances
    denom = Rltc(ii)^2+Xltc(ii)^2;
    YRS = Rltc(ii)/denom;
    YIS = -Xltc(ii)/denom;
    YRM = -Rltc(ii)/denom;
    YIM = Xltc(ii)/denom;

    A1 = VA(LTCsend(ii))-VA(LTCrec(ii));
    A2 = VA(LTCrec(ii))-VA(LTCsend(ii));
    % Calculate LTC powers
    ltcPCAL(kk) = VM(LTCsend(ii))^2*YRS + ltctap(ii)*VM(LTCsend(ii))*...
VM(LTCrec(ii))*(YRM*cos(A1) + YIM*sin(A1));
    ltcQCAL(kk) = -VM(LTCsend(ii))^2*YIS + ltctap(ii)*VM(LTCsend(ii))*...
VM(LTCrec(ii))*(YRM*sin(A1) - YIM*cos(A1));

    ltcPCAL(kk+1) = (VM(LTCrec(ii))*ltctap(ii))^2*YRS + ltctap(ii)*...
VM(LTCsend(ii))*VM(LTCrec(ii))*(YRM*cos(A2)+YIM*sin(A2));
    ltcQCAL(kk+1) = - (VM(LTCrec(ii))*ltctap(ii))^2*YIS + ltctap(ii)*...
VM(LTCsend(ii))*VM(LTCrec(ii))*(YRM*sin(A2)-YIM*cos(A2));

    % Update calculated powers PCAL and QCAL
    PCAL(LTCsend(ii)) = PCAL(LTCsend(ii)) + ltcPCAL(kk);
    QCAL(LTCsend(ii)) = QCAL(LTCsend(ii)) + ltcQCAL(kk);

    PCAL(LTCrec(ii)) = PCAL(LTCrec(ii)) + ltcPCAL(kk+1);

```

```

    QCAL(LTCrec(ii)) = QCAL(LTCrec(ii)) + ltcQCAL(kk+1);
end

function [JAC] = LTCNewtonRaphsonJacobian(bustype,LTCsend,LTCrec,...
NLTC, Tap, Bus, Rltc, Xltc, ltcPCAL, ltcQCAL, VM, VA, JAC)
% LTC JACOBIAN MODIFICATION
for ii = 1: NLTC
    ind = Bus(ii)-LTCsend(ii);
    JAC(:,2*Bus(ii)) = 0.0;
    for nn = 1: 2
        % Calculate LTC admittances
        denom = Rltc(ii)^2+Xltc(ii)^2;
        YRS = Rltc(ii)/denom;
        YIS = - Xltc(ii)/denom;
        % Calculate LTC Jacobian entries
        JKK(1,1) = - (VM(LTCsend(ii))^2)*YIS;
        JKK(1,2) = (VM(LTCsend(ii))^2)*YRS;
        JKK(2,1) = - (VM(LTCsend(ii))^2)*YRS;
        JKK(2,2) = - (VM(LTCsend(ii))^2)*YIS;

        JKM(1,1) = ltcQCAL((ii-1)*2+nn) + (VM(LTCsend(ii))^2)*YIS;
        JKM(1,2) = ltcPCAL((ii-1)*2+nn) + (VM(LTCsend(ii))^2)*YRS;
        JKM(2,1) = - (ltcPCAL((ii-1)*2+nn) + (VM(LTCsend(ii))^2)*YRS);

        if ind == 0
            JKM(2,2) = -(-ltcQCAL((ii-1)*2+nn) + (VM(LTCsend(ii))^2)*YIS);
        else
            JKM(2,2) = ltcQCAL((ii-1)*2+nn) + (VM(LTCsend(ii))^2)*YIS;
        end

        if ((bustype(LTCsend(ii)) == 4) & (Bus(ii) == LTCsend(ii)))
            JKK(1,2) = (ltcPCAL((ii-1)*2+nn) + (VM(LTCsend(ii))^2)*YRS);
            if (nn == 2)
                JKK(2,2) = -(-ltcQCAL((ii-1)*2+nn) + (VM(LTCsend(ii))^2)*YIS);
            else
                JKK(2,2) = ltcQCAL((ii-1)*2+nn) + (VM(LTCsend(ii))^2)*YIS;
                JKM(2,1) = - (ltcPCAL((ii-1)*2+nn) + ...
                    (VM(LTCsend(ii))^2)*YRS);
                JKM(2,2) = (ltcQCAL((ii-1)*2+nn) + ...
                    (VM(LTCsend(ii))^2)*YIS);
            end
        end
    end
end

% Add LTC contribution to system JAC

```

```

if ( (bustype(LTCsend(ii))==2) & (bustype(LTCrec(ii))>2))
    JKK(1,2) = 0;
    JKK(2,1) = 0;
    JKK(2,2) = 0;
    if nn == 1
        JKM(2,1) = 0;
        JKM(2,2) = 0;
    else
        JKM(1,2) = 0;
        JKM(2,2) = 0;
    end
elseif ( (bustype(LTCsend(ii))==1) & (bustype(LTCrec(ii))>2))
    JKK = zeros;
    JKM = zeros;
    JMK = zeros;
end

kk = 2*LTCsend(ii)-1;
mm = 2*LTCrec(ii)-1;
JAC(kk:kk+1, kk:kk+1) = JAC(kk:kk+1, kk:kk+1) + JKK;
JAC(kk:kk+1, mm:mm+1) = JAC(kk:kk+1, mm:mm+1) + JKM;
send = LTCsend(ii);
LTCsend(ii) = LTCrec(ii);
LTCrec(ii) = send;
VM(LTCsend(ii)) = VM(LTCsend(ii))*Tap(ii);
end
end

function [VM, Tap] = LTCUpdates(VM, D, bustype, NLTC, LTCsend, LTCrec, Tap, ...
Bus, LTCVM)
for ii = 1: NLTC
    if ( (bustype(LTCsend(ii)) == 4) & (Bus(ii) == LTCsend(ii)))
        Tap(ii) = Tap(ii) + (D(2*LTCsend(ii))*Tap(ii));
        VM(LTCsend(ii)) = LTCVM(ii);
    elseif ( (bustype(LTCrec(ii)) == 4) & (Bus(ii) == LTCrec(ii)) )
        Tap(ii) = Tap(ii) + D(2*LTCrec(ii))*Tap(ii);
        VM(LTCrec(ii)) = LTCVM(ii);
    end
end

function [Tap, bustype] = LTCLimits(bustype, NLTC, Tap, TapHi, TapLo, ...
LTCsend, LTCrec)
% CHECK FOR POSSIBLE LTCS' TAPS LIMITS VIOLATIONS
for ii = 1: NLTC
    for kk = 1: 2

```

```

if (bustype(LTCsend(ii)) == 4)
    if ( Tap(ii) > TapHi(ii) )
        Tap(ii) = TapHi(ii);
        bustype(LTCsend(ii)) = 3;
    elseif (Tap(ii) < TapLo(ii))
        Tap(ii) = TapLo(ii);
        bustype(LTCsend(ii)) = 3;
    end
end
LTCsend(ii) = LTCrec(ii);
end
end

function [LTCPQsend,LTCPQrec] = LTCPQflows(NLTC,LTCsend,LTCrec,Rltc,...
Xltc, Tap, VM, VA)
for ii = 1: NLTC
    % Calculate LTC admittances
    denom = Rltc(ii)^2+Xltc(ii)^2;
    YRS = Rltc(ii)/denom;
    YIS = -Xltc(ii)/denom;
    YRM = -Rltc(ii)/denom;
    YIM = Xltc(ii)/denom;
    for jj = 1 : 2
        A1 = VA(LTCsend(ii))-VA(LTCrec(ii));
        % Calculate LTC powers
        ltcPCAL = VM(LTCsend(ii))^2*YRS + Tap(ii)*VM(LTCsend(ii))*
VM(LTCrec(ii))*(YRM*cos(A1) + YIM*sin(A1));
        ltcQCAL = -VM(LTCsend(ii))^2*YIS + Tap(ii)*VM(LTCsend(ii))*
VM(LTCrec(ii))*(YRM*sin(A1) - YIM*cos(A1));
        if jj == 1
            LTCPQsend = ltcPCAL + j*ltcQCAL;
        else
            LTCPQrec = ltcPCAL + j*ltcQCAL;
        end
        send = LTCsend(ii);
        LTCsend(ii) = LTCrec(ii);
        LTCrec(ii) = send;
    end
end
end

```

#### 4.4.1.3 Test case of voltage magnitude control with load tap-changing

The original five-bus network described in Section 4.3.9 is modified to include one LTC in series with the transmission line connected between bus Lake and bus Main. An additional bus, termed Lakefa, is used to connect the LTC as shown in Figure 4.7. The LTC is used to

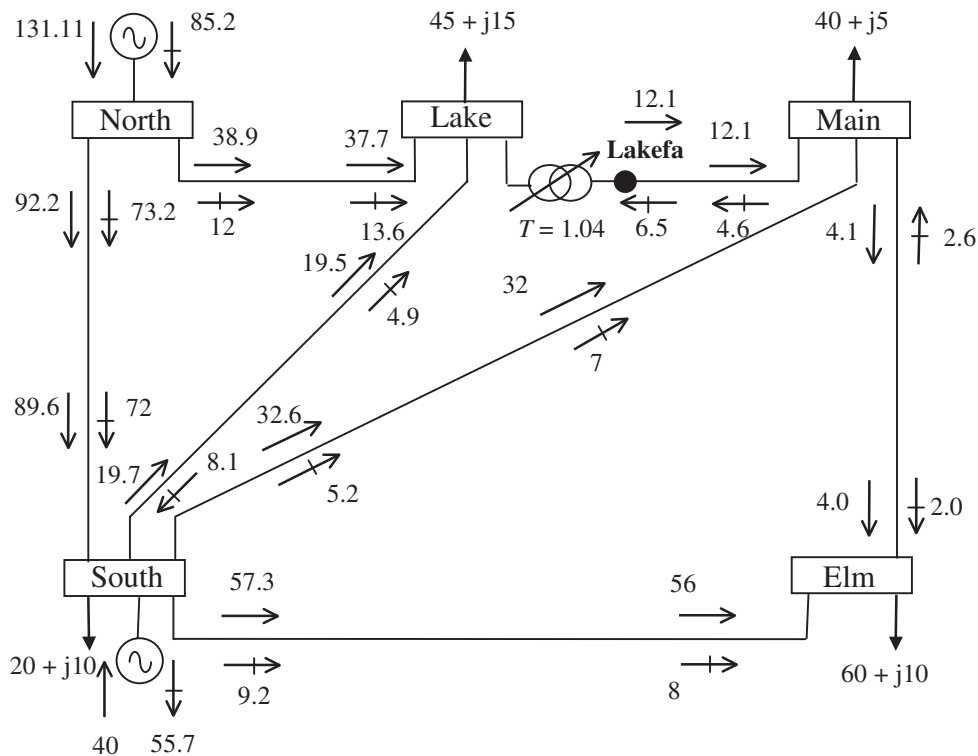


Figure 4.7 Modified test network and power flow results

maintain the voltage magnitude at Lake at 1 p.u. The initial condition of the tap is set to a nominal value (i.e.  $T = 1$ ). The winding impedance contains no resistance, and an inductive reactance of 0.1 p.u.

The data given in function `PowerFlowsData` in Section 4.3.9 is modified to accommodate the inclusion of the LTC. The transmission line originally connected between Lake and Main is now connected between Lakefa (bus 6) and Main (bus 4). Only the modified code lines are shown here:

```
%The convention used for the types of buses available in power flow
%studies is expanded to include nodal voltage control by LTC:
%bustype = 5

nbb = 6 ;
bustype(3) = 5 ; VM(1) = 1 ; VA(1) = 0 ;
bustype(6) = 3 ; VM(1) = 1 ; VA(1) = 0 ;

tlsend(6) = 6 ; tlrec(6) = 4 ; tlresis(6) = 0.01 ; tlreac(6) = 0.03 ;
tlcond(6) = 0 ; tlsuscep(6) = 0.02 ;
```

Function `LTCPowerFlowsData` is as follows:

```
%This function is used exclusively to enter LTC data:
% Load Tap Changing transformers data
% NLTC: Number of LTC's
% LTCsend: Sending end bus
% LTCrec: Receiving end bus
% Rltc: LTC winding resistance
% Xltc: LTC winding reactance
% Tap: Initial value of LTC tap
% TapHi: Higher value of LTC tap
% TapLo: Lower value of LTC tap
% Bus: Controlled bus
% LTCVM: Target voltage magnitude at LTC bus

NLTC = 1 ;
LTCsend(1) = 3 ; LTCrec(1) = 6 ; Rltc(1) = 0 ; Xltc(1) = 0.1 ;
Tap(1) = 1 ; TapHi(1) = 1.5 ; TapLo(1) = 0.5 ; Bus(1) = 3 ; LTCVM(1) = 1 ;
```

Convergence is obtained in 5 iterations to a power mismatch tolerance of  $1e-12$ . The power flow results are shown in Figure 4.7. The nodal voltages are given in Table 4.2. It should be noted that the LTC upholds the target value of 1 p.u. voltage magnitude at Lake with a tap setting of  $T = 1.04$ .

**Table 4.2** Nodal voltages in the modified network

Nodal voltage	System bus					
	North	South	Lake	Lakefa	Main	Elm
Magnitude (p.u.)	1.060	1.000	1.000	0.969	0.969	0.966
Phase angle (deg)	0.00	-2.16	-4.41	-5.13	-5.99	-5.99

It is interesting to note that the voltages at Main and Elm deteriorate compared with the case when no voltage regulation takes place at Lake; the base case presented in Section 4.3.9. It is also interesting to note that the LTC achieves its voltage regulation objective at the expense of consuming reactive power; it draws 10 MVAR from the system. There is a general redistribution of reactive power flows throughout the network owing to the inclusion of the LTC and its control action; however, the net amount of active and reactive power generated or absorbed by the two generators changes little (i.e. 171.11 MVA and 29.5 MVAR). The system active power loss is 6.11 MW. To show the prowess of the Newton–Raphson method towards convergence, in Table 4.3 we give the maximum absolute power mismatches in the system buses, which are shown to decrease quadratically towards zero.

**Table 4.3** Maximum absolute power mismatches

Iteration	$\Delta P$	$\Delta Q$
1	$6.0e-1$	$1.2e-1$
2	$2.4e-2$	$2.5e-2$
3	$1.5e-4$	$7.5e-4$
4	$1.5e-8$	$1.6e-7$
5	0	0

#### 4.4.1.4 Combined voltage magnitude control by means of generators and load tap changers

The option of controlling nodal voltage magnitude by adjusting LTCs and generators in a combined fashion is a practical operating situation; such controls are prioritised. It is normal to choose the generator as the first regulating component, holding the associated LTC taps at their initial condition so long as the generator’s reactive limits are not reached. If the generator hits one of its reactive limits then the master LTC tap becomes active and the bus is converted to *PVT*; the bus becomes controlled by the LTC as opposed to the generator.

The control of nodal voltage magnitude by the generator has higher priority. If the set of LTCs associated with a given generator are controlling buses different from the generator bus and the generator reaches one of its reactive limits then the LTC is switched to control the generator bus so that it changes to a *PVT* bus. The previous *PVT* bus controlled by the LTC is converted to a *PQ* bus in the absence of another LTC available to regulate that bus. These control actions are shown schematically in Figure 4.8.

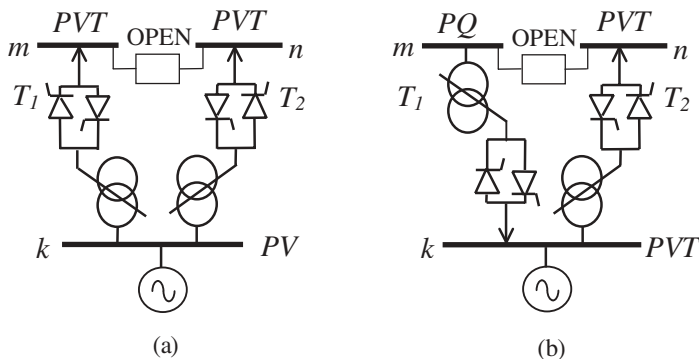


**Figure 4.8** Control of nodal voltage magnitude using: (a) one generator and two load tap changers (LTCs) and (b) two LTCs after the generator violates one of its reactive limits

#### 4.4.1.5 Control coordination between one load tap changer and one generator

This test case serves to illustrate the situation where the voltage magnitude at a given bus is controlled by one generator and one LTC. The five-bus network is modified to include one

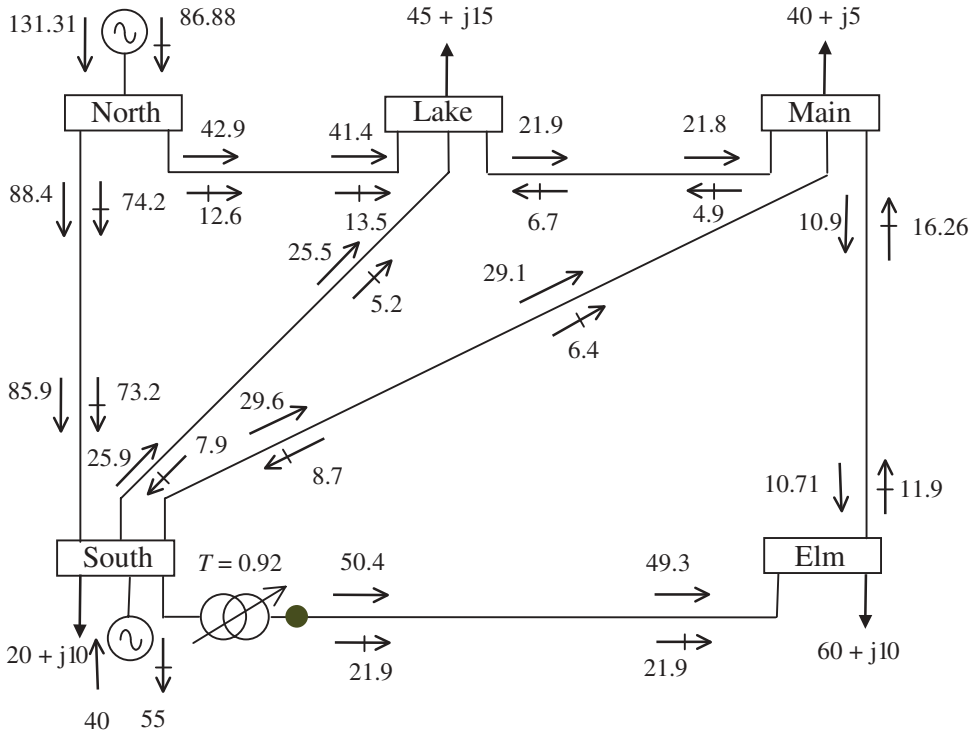


**Figure 4.9** Control coordination between the generator and load tap changer at South

LTC, as shown in Figure 4.9. The minimum reactive power limit of the generator connected at South is specified to be  $-55$  MVAR. The LTC tap, located on the primary winding, is used to control voltage magnitude when the generator violates its minimum reactive power limit.

The LTC works as a conventional transformer, with the tap fixed at the value given by the initial condition for as long as the generator operates within its reactive limits. The initial condition of the tap is set to a nominal value (i.e.  $T = 1$ ). The winding impedance contains no resistance and an inductive reactance of  $0.1$  p.u. Once the generator violates reactive limits the LTC becomes active. The controlled bus is *PV* when controlled by the generator and then changes to *PVT* when controlled by the LTC.

For the condition when the target voltage magnitude at South is  $1$  p.u. the generator violates its minimum reactive power limit, and voltage magnitude control switches to the LTC. Convergence is obtained in  $7$  iterations. The power flow results are shown in Figure 4.9.

The nodal voltages are very similar to the base case presented in Section 4.3.9. The value of LTC tap required to achieve  $1$  p.u. voltage magnitude at South is  $0.92$ . As expected, the LTC achieves its operating point at the expense of consuming reactive power. However, in this case it draws only  $2.9$  MVAR from the system. The system active power loss increases to  $6.31$  MW.

#### 4.4.2 Phase-shifting Transformer

A flexible power flow model for the phase-shifting transformer is described in this section. It is derived from the two-winding, single-phase transformer model presented by Section 3.3.4, which contains complex taps on both the primary and secondary windings.

Comprehensive bus power injection equations for the phase shifter may be derived with reference to Equation (3.91). However, simpler expressions may be derived if some practical assumptions are introduced at this stage. For instance, it is reasonable to assume that the phase-changing facility is only on the primary side, (i.e.  $\phi_u = 0$ ); the primary and secondary windings admittances may be combined together [ $Y = Y_{scp}Y_{scs}/(Y_{scp} + Y_{scs})$ ]; and the impact of the magnetising branch is negligibly small in the power flow solution ( $Y_0 = 0$ ):

$$\begin{bmatrix} I_k \\ I_m \end{bmatrix} = \begin{bmatrix} Y & -Y(\cos \phi + j \sin \phi) \\ -Y(\cos \phi - j \sin \phi) & Y \end{bmatrix} \begin{bmatrix} V_k \\ V_m \end{bmatrix} = \begin{bmatrix} Y_{kk} & Y_{km} \\ Y_{mk} & Y_{mm} \end{bmatrix} \begin{bmatrix} V_k \\ V_m \end{bmatrix}. \quad (4.70)$$

Similar to the power flow LTC model, it is assumed in this expression that the primary and secondary sides of the transformer are connected to bus  $k$  and bus  $m$ , respectively. Also, the subscripts  $sc$  and  $u$  are dropped in the admittance term and in the phase angle  $\phi$ , respectively.

Based on Equation (4.70), equations for the nodal power injections of the phase-shifting transformer, where  $\phi$  is allowed to vary within design rating values ( $\phi_{\min} < \phi < \phi_{\max}$ ), are as follows:

$$P_k = V_k^2 G_{kk} + V_k V_m [G_{km} \cos(\theta_k - \theta_m) + B_{km} \sin(\theta_k - \theta_m)], \quad (4.71)$$

$$Q_k = -V_k^2 B_{kk} + V_k V_m [G_{km} \sin(\theta_k - \theta_m) - B_{km} \cos(\theta_k - \theta_m)], \quad (4.72)$$

$$P_m = V_m^2 G_{mm} + V_m V_k [G_{mk} \cos(\theta_m - \theta_k) + B_{mk} \sin(\theta_m - \theta_k)], \quad (4.73)$$

$$Q_m = -V_m^2 B_{mm} + V_m V_k [G_{mk} \sin(\theta_m - \theta_k) - B_{mk} \cos(\theta_m - \theta_k)], \quad (4.74)$$

where

$$\left. \begin{aligned} Y_{kk} &= G_{kk} + jB_{kk} = Y, \\ Y_{mm} &= G_{mm} + jB_{mm} = Y, \\ Y_{km} &= G_{km} + jB_{km} = -Y(\cos \phi + j \sin \phi), \\ Y_{mk} &= G_{mk} + jB_{mk} = -Y(\cos \phi - j \sin \phi). \end{aligned} \right\} \quad (4.75)$$

Alternatively, substituting Equations (4.75) into Equations (4.71)–(4.74) leads to the following more explicit expressions:

$$P_k = V_k^2 G - V_k V_m [G \cos(\theta_k - \theta_m - \phi) + B \sin(\theta_k - \theta_m - \phi)], \quad (4.76)$$

$$Q_k = -V_k^2 B - V_k V_m [G \sin(\theta_k - \theta_m - \phi) - B \cos(\theta_k - \theta_m - \phi)], \quad (4.77)$$

$$P_m = V_m^2 G - V_m V_k [G \cos(\theta_m - \theta_k + \phi) + B \sin(\theta_m - \theta_k + \phi)], \quad (4.78)$$

$$Q_m = -V_m^2 B - V_m V_k [G \sin(\theta_m - \theta_k + \phi) - B \cos(\theta_m - \theta_k + \phi)]. \quad (4.79)$$

If the phase-shifting transformer is used to control the active power flowing through it at a specified value then the Jacobian is enlarged to accommodate one additional equation. In

this situation  $\phi$  enters as an extra state variable in the Jacobian equation. If the control is exerted at the sending end (bus  $k$ ) of the phase shifter then  $P_{km}^{\phi ps}$  is the target power to be regulated.

The set of linearised power flow equations for the phase-shifting transformer is,

$$\begin{bmatrix} \Delta P_k \\ \Delta P_m \\ \Delta Q_k \\ \Delta Q_m \\ \Delta P_{km}^{\phi ps} \end{bmatrix}^{(i)} = \begin{bmatrix} \frac{\partial P_k}{\partial \theta_k} & \frac{\partial P_k}{\partial \theta_m} & \frac{\partial P_k}{\partial V_k} V_k & \frac{\partial P_k}{\partial V_m} V_m & \frac{\partial P_k}{\partial \phi} \\ \frac{\partial P_m}{\partial \theta_k} & \frac{\partial P_m}{\partial \theta_m} & \frac{\partial P_m}{\partial V_k} V_k & \frac{\partial P_m}{\partial V_m} V_m & \frac{\partial P_m}{\partial \phi} \\ \frac{\partial Q_k}{\partial \theta_k} & \frac{\partial Q_k}{\partial \theta_m} & \frac{\partial Q_k}{\partial V_k} V_k & \frac{\partial Q_k}{\partial V_m} V_m & \frac{\partial Q_k}{\partial \phi} \\ \frac{\partial Q_m}{\partial \theta_k} & \frac{\partial Q_m}{\partial \theta_m} & \frac{\partial Q_m}{\partial V_k} V_k & \frac{\partial Q_m}{\partial V_m} V_m & \frac{\partial Q_m}{\partial \phi} \\ \frac{\partial P_{km}^{\phi}}{\partial \theta_k} & \frac{\partial P_{km}^{\phi}}{\partial \theta_m} & \frac{\partial P_{km}^{\phi}}{\partial V_k} V_k & \frac{\partial P_{km}^{\phi}}{\partial V_m} V_m & \frac{\partial P_{km}^{\phi}}{\partial \phi} \end{bmatrix}^{(i)} \begin{bmatrix} \Delta \theta_k \\ \Delta \theta_m \\ \frac{\Delta V_k}{V_k} \\ \frac{\Delta V_m}{V_m} \\ \Delta \phi_{ps} \end{bmatrix}^{(i)}, \quad (4.80)$$

where  $\Delta P_{km}^{\phi ps}$ , given by

$$\Delta P_{km}^{\phi ps} = P_{km}^{\phi, reg} - P_{km}^{\phi ps},$$

is the active power flow mismatch for the phase shifter;  $P_{km}^{\phi ps}$  is the calculated power as given by Equation (4.76);  $\Delta \phi_{ps}$ , given by

$$\Delta \phi_{ps} = \phi^{(i)} - \phi^{(i-1)},$$

is the incremental change in the phase shifter angle at the  $i$ th iteration.

The Jacobian elements in matrix Equation (4.80) are as follows:

$$\frac{\partial P_k}{\partial \theta_k} = -\frac{\partial P_k}{\partial \theta_m} = -\frac{\partial Q_k}{\partial V_m} V_m = -\frac{\partial P_k}{\partial \phi} = -Q_k - V_k^2 B, \quad (4.81)$$

$$\frac{\partial P_k}{\partial V_k} V_k = P_k + V_k^2 G, \quad (4.82)$$

$$\frac{\partial Q_k}{\partial \theta_k} = -\frac{\partial Q_k}{\partial \theta_m} = \frac{\partial P_k}{\partial V_m} V_m = -\frac{\partial Q_k}{\partial \phi} = P_k - V_k^2 G, \quad (4.83)$$

$$\frac{\partial Q_k}{\partial V_k} V_k = Q_k - V_k^2 B, \quad (4.84)$$

$$\frac{\partial P_m}{\partial \theta_m} = -\frac{\partial P_m}{\partial \theta_k} = -\frac{\partial Q_m}{\partial V_k} V_k = \frac{\partial P_m}{\partial \phi} = -Q_m - V_m^2 B, \quad (4.85)$$

$$\frac{\partial P_m}{\partial V_m} V_m = P_m + V_m^2 G, \quad (4.86)$$

$$\frac{\partial Q_m}{\partial \theta_m} = -\frac{\partial Q_m}{\partial \theta_k} = \frac{\partial P_m}{\partial V_k} V_k = \frac{\partial Q_m}{\partial \phi} = P_m - V_m^2 G, \quad (4.87)$$

$$\frac{\partial Q_m}{\partial V_m} V_m = Q_m - V_m^2 B. \quad (4.88)$$

It should be noted that since  $P_{km}^{\phi_{PS}} = P_k$ , the following relationships hold true and simplify the evaluation of the Jacobian matrix,

$$\frac{\partial P_{km}^{\phi}}{\partial \theta_k} = \frac{\partial P_k}{\partial \theta_k}, \quad (4.89)$$

$$\frac{\partial P_{km}^{\phi}}{\partial \theta_m} = \frac{\partial P_k}{\partial \theta_m}, \quad (4.90)$$

$$\frac{\partial P_{km}^{\phi}}{\partial V_k} V_k = \frac{\partial P_k}{\partial V_k} V_k, \quad (4.91)$$

$$\frac{\partial P_{km}^{\phi}}{\partial V_m} V_m = \frac{\partial P_k}{\partial V_m} V_m, \quad (4.92)$$

$$\frac{\partial P_{km}^{\phi}}{\partial \phi} = \frac{\partial P_k}{\partial \phi}. \quad (4.93)$$

At the end of each iterative step,  $i$ , the phase angle  $\phi$  is updated by using the following relation:

$$\phi^{(i)} = \phi^{(i-1)} + \Delta\phi_{PS}^{(i)} \quad (4.94)$$

It should be noted that a more comprehensive power flow phase-shifter model may be obtained by basing the power derivations on Equation (3.91) as opposed to Equation (4.70). For instance, the effect of the magnetising admittance may be included in the nodal power equations of the transformer. Also, it may be considered that the phase-shifting facility is on the secondary side as opposed to the primary side, in which case  $\phi_r = 0$  and  $\phi_{u \min} < \phi_u < \phi_{u \max}$ . The associated Jacobian elements have the same form as Equations (4.81)–(4.93).

#### 4.4.2.1 State variable initialisation and limit checking

Similar to the case with LTCs, it is normal to initialise the tapping positions of phase-shifting transformers at their nominal values. Hence,  $\phi_r = 0$  and  $\phi_u = 0$  are used for cases of two-winding phase shifters.

The status of phase-shifter taps is checked at each iterative step to assess whether or not they are still within limits and capable of regulating active power flow. For a phase shifter connected between buses  $k$  and  $m$ , and regulating active power flow at bus  $k$  with tapping facilities available in the primary winding, we may write:

$$\phi_{\min} < \phi < \phi_{\max}. \quad (4.95)$$

If either of the following conditions occur during the iterative process:

$$\begin{aligned} \phi^{(i+1)} + \Delta\phi^{(i)} &\geq \phi_{\max}, \\ \phi^{(i+1)} + \Delta\phi^{(i)} &\leq \phi_{\min}, \end{aligned} \quad (4.96)$$

the tap is fixed at the violated limit. The active power flow in branch  $k$ – $m$  is allowed to vary, and  $\phi$  is removed from the state variable vector. It becomes a constant parameter within the

nodal admittance matrix of the phase-shifting transformer in Equation (4.70). Checking of phase-shifter tap limits starts from iteration 1.

#### 4.4.2.2 Phase-shifter computer program in Matlab® code

Program 4.4 incorporates phase-shifting transformer representation within the Newton–Raphson power flow program given in Section 4.3.6. The functions `PowerFlowsData`, `YBus`, and `PQflows` are also used here.

In the main phase-shifter Newton–Raphson program, the function `PSPowerFlowsData` is added to read phase-shifter data, `PSNewtonRaphson` replaces `NewtonRaphson`, and `PSPQflows` is used to calculate power flows and losses in the phase-shifting transformer.

Function `PSNewtonRaphson` uses the following functions from `NewtonRaphson`: `NetPowers`; `CalculatedPowers`; `GeneratorsLimits`; `PowerMismatches`; `NewtonRaphsonJacobian`; and `StateVariablesUpdates`. Furthermore, five new functions are added to cater for phase shifters representation; namely: `PSCalculatedPowers`; `PSUpdates`; `PSNewtonRaphsonJacobian`; `PSPowerMismatches`; and `PSLimits`.

PROGRAM 4.4 Program written in Matlab® to incorporate phase-shifter representation within the Newton–Raphson power flow algorithm.

```
%- - - Main PS Program

PowerFlowsData; %Function to read network data

PSPowerFlowsData; %Function to read PS data

[YR, YI] = YBus(tlsend, tlrec, tlresis, tlreac, tlsuscep, tlcond, shbus, ...
shresis, shreac, ntl, nbb, nsh);

[VM, VA, Tap, it] = PSNewtonRaphson(nmax, tol, itmax, ngn, nld, nbb, ...
bustype, genbus, loadbus, PGEN, QGEN, QMAX, QMIN, PLOAD, QLOAD, YR, YI, VM, ...
VA, NPS, PSsend, PSrec, Rps, Xps, Tap, TapHi, TapLo, Bus, psP);

[PQsend, PQrec, PQloss, PQbus] = PQflows(nbb, ngn, ntl, nld, genbus, ...
loadbus, tlsend, tlrec, tlresis, tlreac, tlcond, tlsuscep, PLOAD, QLOAD, ...
VM, VA);

[PQPSsend, PQPSrec, PQPSloss] = PSPQflows(VM, VA, NPS, PSsend, PSrec, Rps, ...
Xps, Tap);

it %Iteration number
VM %Nodal voltage magnitude (p.u.)
VA = VA*180/pi %Nodal voltage phase angle(Deg)
PQsend %Sending active and reactive powers (p.u.)
PQrec %Receiving active and reactive powers (p.u.)
```

## 136 CONVENTIONAL POWER FLOW

```
Tap      %Final transformer phase-shifting position
% End of Main PSNewtonRaphson Function

function [VM,VA, Tap, it] = PSNewtonRaphson(nmax,tol,itmax,ngn,nld,...
nbb,bustype,genbus,loadbus,PGEN,QGEN,QMAX,QMIN,PLOAD,QLOAD,YR,YI,...
VM,VA,NPS,PSsend,PSrec,Rps,Xps, Tap, TapHi, TapLo, Bus, psP);

% GENERAL SETTINGS
flag = 0;
it = 1;
% CALCULATE NET POWERS
[PNET,QNET] = NetPowers(nbb,ngn,nld,genbus,loadbus,PGEN,QGEN,PLOAD,...
QLOAD);

while (it < itmax & flag==0)
    % CALCULATED POWERS
    [PCAL,QCAL] = CalculatedPowers(nbb,VM,VA,YR,YI);
    % CALCULATED PS POWERS
    [PCAL,QCAL,psPCAL,psQCAL] = PS CalculatedPowers(VM,VA,PCAL,QCAL,...
    PSsend, PSrec,NPS, Tap, Rps, Xps);

% POWER MISMATCHES
[DPQ,DP,DQ,flag] = PowerMismatches(nmax,nbb,tol,bustype,flag,PNET,...
QNET,PCAL,QCAL);

% PS POWER MISMATCHES
[DPQ,flag] = PS PowerMismatches(nbb,DPQ,flag,tol,NPS,PSsend,PSrec,Bus,...
psP,psPCAL);

%Check for convergence
if flag == 1
    break
end

% JACOBIAN FORMATION
[JAC] = NewtonRaphsonJacobian(nmax,nbb,bustype,PCAL,QCAL,VM,VA,...
YR,YI);

% PS JACOBIAN UPDATING
[JAC] = PSNewtonRaphsonJacobian(nbb,VM,VA,JAC,NPS,PSsend,PSrec, Tap,...
Bus,Rps,Xps,psPCAL,psQCAL);
```

```

% SOLVE FOR THE STATE VARIABLES VECTOR
D = JAC\DPQ';

% UPDATE STATE VARIABLES
[VA,VM] = StateVariablesUpdates(nbb,D,VA,VM);

% UPDATE PS TAPS
[Tap] = PSUpdates(nbb,D,NPS,Tap);

% CHECK FOR PS TAPS LIMITS VIOLATIONS
[Tap,Bus] = PSLimits(NPS,Tap,TapHi,TapLo,Bus);

    it = it + 1;

end

function [PCAL,QCAL,psPCAL,psQCAL] = PSCalculatedPowers(VM,VA,PCAL,...
QCAL, PSsend,PSrec,NPS,Tap,Rps,Xps)
for ii = 1:NPS
    % Calculate PS admittances
    denom = Rps(ii)^2+Xps(ii)^2;
    YR = Rps(ii)/denom;
    YI = - Xps(ii)/denom;
    % Calculate PS powers
    for nn = 1:2
        kk = (ii-1)*2+nn;
        A1=VA(PSsend(ii))-VA(PSrec(ii))-Tap(ii);
        psPCAL(kk) = (VM(PSsend(ii))^2)*YR - VM(PSsend(ii))*VM(PSrec(ii))...
        * (YR*cos(A1)+YI*sin(A1));
        psQCAL(kk) = -(VM(PSsend(ii))^2)*YI - VM(PSsend(ii))*VM(PSrec(ii))...
        * (YR*sin(A1)-YI*cos(A1));

        % Update calculated powers PCAL and QCAL
        PCAL(PSsend(ii)) = PCAL(PSsend(ii)) + psPCAL(kk);
        QCAL(PSsend(ii)) = QCAL(PSsend(ii)) + psQCAL(kk);

        send = PSsend(ii);
        PSsend(ii) = PSrec(ii);
        PSrec(ii) = send;
        Tap(ii)=-Tap(ii);
    end
end

function [DPQ,flag] = PSPowerMismatches(nbb,DPQ,flag,tol,NPS,PSsend,...
PSrec,Bus,psP,psPCAL);

```

```

% ADD PS POWER MISMATCHES TO DPQ
ll = 1;
for ii = 1:NPS
    if (PSsend(ii) == Bus(ii))
        DPQ(ii+2*nbb) = psP(ii) - psPCAL(ii);
    elseif (PSrec(ii) == Bus(ii))
        DPQ(ii+2*nbb) = psP(ii) + psPCAL(ll+1);
    end
    if (Bus(ii) == 0)
        DPQ(ii+2*nbb) = 0;
    end
    ll = ll + 2;
end
% Check for convergence
if (flag == 1)
    for ll = 2*nbb+1 : 2*nbb + NPS
        if (abs(DPQ) < tol)
            flag = 1;
        else
            flag = 0;
        end
    end
end
end

```

```

function [JAC] = PSNewtonRaphsonJacobian(nbb,VM,VA,JAC,NPS,PSsend,...
PSrec, Tap, Bus, Rps, Xps, psPCAL, psQCAL)
% PS JACOBIAN MODIFICATION
for ii = 1:NPS
    nn = (ii-1)*2+1;
    pp = 2*nbb+ii;

    % Calculate PS admittances
    denom = Rps(ii)^2+Xps(ii)^2;
    YR = Rps(ii)/denom;
    YI = -Xps(ii)/denom;

    % Calculate PS Jacobian entries
    for kk1 = 1: 2
        kk = 2*PSsend(ii)-1;
        mm = 2*PSrec(ii)-1;
        nn = (ii-1)*2+kk1;

        JKK(1,1) = -(VM(PSsend(ii))^2)*YI;
        JKK(1,2) = (VM(PSsend(ii))^2)*YR;
        JKK(2,1) = -(VM(PSsend(ii))^2)*YR;
        JKK(2,2) = -(VM(PSsend(ii))^2)*YI;
    end
end

```

```

JKM(1,1) = psQCAL(nn) + (VM(PSsend(ii))^2)*YI;
JKM(1,2) = psPCAL(nn) - (VM(PSsend(ii))^2)*YR;
JKM(2,1) = -psPCAL(nn) + (VM(PSsend(ii))^2)*YR;
JKM(2,2) = psQCAL(nn) + (VM(PSsend(ii))^2)*YI;

% Add PS contribution to system JAC
JAC(kk:kk+1, kk:kk+1) = JAC(kk:kk+1, kk:kk+1) + JKK;
JAC(kk:kk+1, mm:mm+1) = JAC(kk:kk+1, mm:mm+1) + JKM;

send = PSsend(ii);
PSsend(ii) = PSrec(ii);
PSrec(ii) = send;
end
kk = 2*PSsend(ii)-1;
mm = 2*PSrec(ii)-1;
nn = (ii-1)*2+1;
JKE(1) = psQCAL(nn) + (VM(PSsend(ii))^2)*YI;
JKE(2) = -psPCAL(nn) + (VM(PSsend(ii))^2)*YR;
JEK(1) = -psQCAL(nn) - (VM(PSsend(ii))^2)*YI;
JEK(2) = psPCAL(nn) + (VM(PSsend(ii))^2)*YR;

JME(1) = -psQCAL(nn+1) - (VM(PSrec(ii))^2)*YI;
JME(2) = psPCAL(nn+1) - (VM(PSrec(ii))^2)*YR;
JEM(1) = psQCAL(nn) + (VM(PSsend(ii))^2)*YI;
JEM(2) = psPCAL(nn) - (VM(PSsend(ii))^2)*YR;
JE(1) = psQCAL(nn) + (VM(PSsend(ii))^2)*YI;

if (Bus(ii) ~= 0)
    JAC(kk:kk+1, pp) = JAC(kk:kk+1, pp) + JKE';
    JAC(mm:mm+1, pp) = JAC(mm:mm+1, pp) + JME';
    JAC(pp, kk:kk+1) = JAC(pp, kk:kk+1) + JEK;
    JAC(pp, mm:mm+1) = JAC(pp, mm:mm+1) + JEM;
    JAC(pp, pp) = JAC(pp, pp) + JE(1);
else
    JAC(1:pp, pp) = zeros;
    JAC(pp, 1:pp) = zeros;
    JAC(pp, pp) = 1;
end
end

function [Tap] = PSUpdates(nbb, D, NPS, Tap)
for ii = 1: NPS
    Tap(ii) = Tap(ii) + D(ii+nbb*2);
end

function [Tap, Bus] = PSLimits(NPS, Tap, TapHi, TapLo, Bus)
% CHECK FOR POSSIBLE PS TAPS' LIMITS VIOLATIONS

```

```

for ii = 1:NPS
    if (Bus(ii) ~= 0)
        if (Tap(ii) > TapHi(ii))
            Tap(ii) = TapHi(ii);
            Bus(ii) = 0;
        elseif (Tap(ii) < TapLo(ii))
            Tap(ii) = TapLo(ii);
            Bus(ii) = 0;
        end
    end
end
end

```



```

function[PQPSsend,PQPSrec,PQPSloss] = PSPQflows(VM,VA,NPS,PSsend,...
PSrec,Rps,Xps,Tap)
%
PQPSsend = zeros(1,NPS);
PQPSrec = zeros(1,NPS);
% Calculate active and reactive powers at the sending and reciving ends of
% Phase shifter transformers
for ii = 1:NPS
    Vsend = (VM(PSsend(ii))*cos(VA(PSsend(ii))) + ...
    VM(PSsend(ii))*sin(VA(PSsend(ii)))*i);
    Vrec = (VM(PSrec(ii))*cos(VA(PSrec(ii))) + ...
    VM(PSrec(ii))*sin(VA(PSrec(ii)))*i);
    Zself = (Rps(ii) + Xps(ii)*i);
    Ymutual = -(cos(Tap(ii)) + sin(Tap(ii))*i)/Zself;

    current = Vsend/Zself + Vrec*Ymutual;
    PQPSsend(ii) = Vsend*conj(current);
    Ymutual = -(cos(Tap(ii)) - sin(Tap(ii))*i)/Zself;
    current = Vsend*Ymutual + Vrec/Zself;
    PQPSrec(ii) = Vrec*conj(current);
    PQPSloss(ii) = PQPSsend(ii) + PQPSrec(ii);
end
end

```

#### 4.4.2.3 Test cases for phase-shifting transformers

The PSNewtonRaphson power flow function is used to solve two test cases. The first case corresponds to a straightforward active power flow control in a phase-shifter-upgraded transmission line. The second case is an assessment of the power flow feasibility region of a two phase-shifting transformer system.

##### *Active power flow*

The five-bus network is modified to include one phase-shifting transformer in series with the transmission line connecting bus Lake and bus Main. The phase shifter is used to maintain

active power flowing from Lakefa towards Main at 40 MW. This bus is added to enable connection of the phase shifter. The initial value of the complex tap is set to the nominal value (i.e.  $1/0^\circ$ ). The winding contains no resistance, and an inductive reactance of 0.1 p.u.

The data given in function `PowerFlowsData` in Section 4.3.9 is modified to accommodate for the inclusion of the phase shifter. The transmission line originally connected between Lake and Main is now connected between Lakefa (bus 6) and Main (bus 4). Only the modified code lines are shown here:

```
nbb = 6 ;
bustype(6) = 4 ; VM(1) = 1 ; VA(1) = 0 ;

tlsend(6) = 6 ; tlrec(6) = 4 ; tlresis(6) = 0.01 ; tlreac(6) = 0.03 ;
tlcond(6) = 0 ; tlsuscep(6) = 0.02 ;
```

Function `PSPowerFlowsData` is as follows:

```
% Phase-Shifting Transformers Data

% NPS: number of PS's
% PSsend: Sending end bus
% PSrec: Receiving end bus
% Rps: PS winding resistance
% Xps: PS windding reactance
% Tap: Initial value of PS tap
% TapHi: Higher value of PS tap
% TapLo: Lower value of PS tap
% Bus: Controlled bus
% psP: Target active power at Bus
NPS = 1;
PSsend(1) = 3 ; PSrec(1) = 6 ; Rps(1) = 0 ; Xps(1) = 0.1 ;
Tap(1) = 0 ; TapHi(1) = 10*pi/180 ; TapLo(1) = -10*pi/180 ;
Bus(1) = 6 ; psP(1) = 0.4 ;
nmax = nmax + NPS;
```

Convergence is obtained in 5 iterations to a power mismatch tolerance of  $1e-12$ . The phase shifter upholds its target value. The power flow results are shown in Figure 4.10. The nodal voltages are given in Table 4.4. The maximum absolute power mismatches of the system buses and phase shifter are shown in Table 4.5.

As expected, the nodal voltage magnitudes do not change compared with the base case presented in Section 4.3.9. However, the voltage phase angle difference between Lake and Main does increase in value to reflect the larger amount of active power flowing through this transmission line, which increases from 19.4 MW to 40 MW. This is slightly more than a twofold increase in transmitted power, and the phase angle difference changes from  $-0.32^\circ$  to  $-2.74^\circ$ .

The value of tap required to achieve the 40 MW flow through the phase shifter is  $-5.83^\circ$ . The phase shifter achieves its operating point at the expense of consuming 1.7 MVAR. The system active power loss is 6.6 MW.

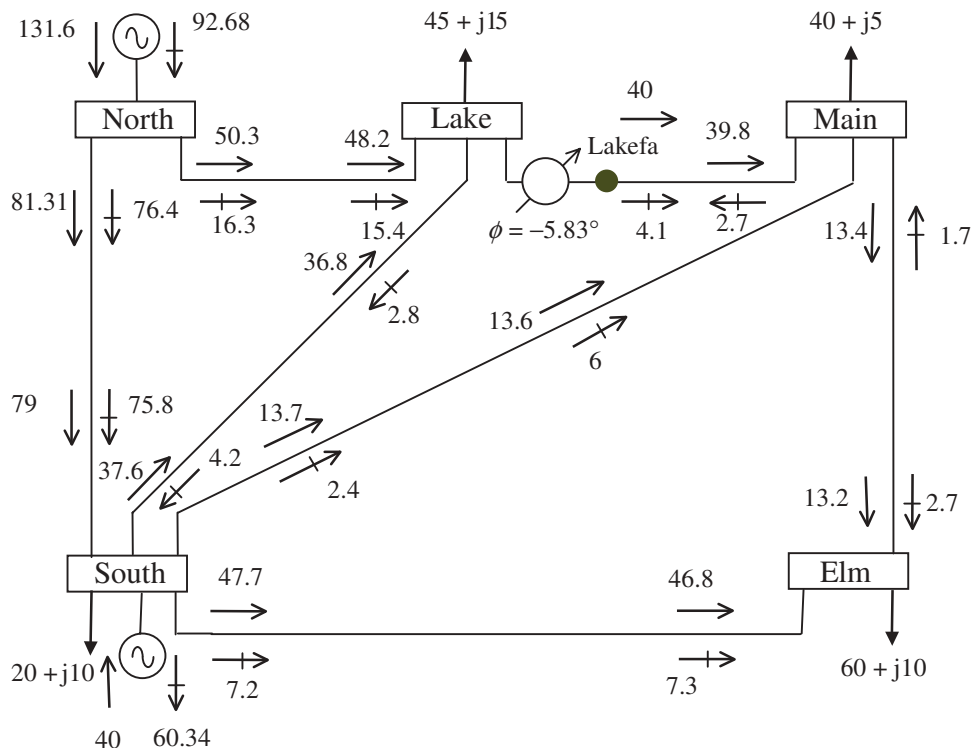


Figure 4.10 Modified test network and power flow results

Table 4.4 Nodal voltages of the modified network

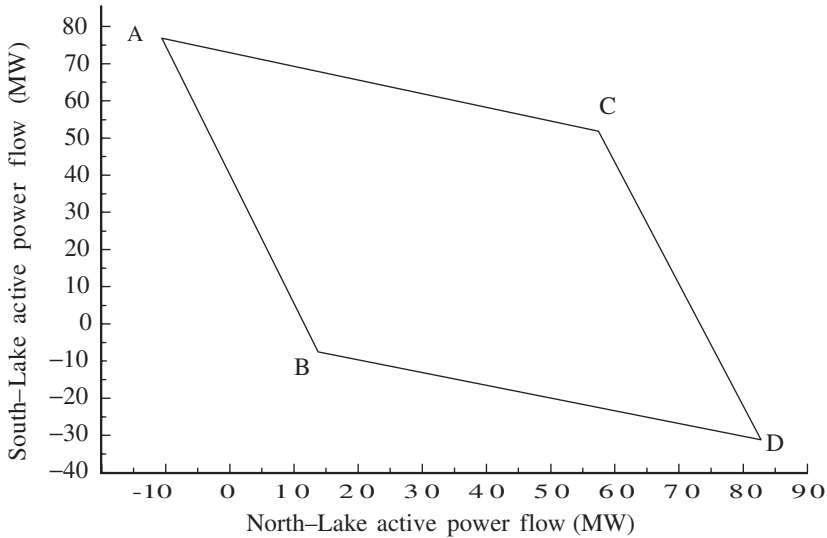
Nodal voltage	System buses					
	North	South	Lake	Lakefa	Main	Elm
Magnitude (p.u.)	1.06	1.000	0.984	0.987	0.984	0.972
Phase angle (deg)	0.00	-1.77	-5.8	-2.33	-3.06	-4.95

Table 4.5 Maximum absolute mismatches

Iteration	Bus		
	$\Delta P$	$\Delta Q$	Phase shifter $\Delta\phi$
1	$6.0e-1$	$1.2e-1$	$4e-1$
2	$2.1e-2$	$3.7e-2$	$8e-3$
3	$9.6e-5$	$1.8e-4$	$9.3e-5$
4	$3.6e-9$	$5.3e-9$	$4.7e-9$
5	0	0	0

### Feasible active power control region

When two or more phase-shifting transformers are close together, electrically speaking, they may interact with each other. The amount of active power flow controlled by these series controllers is confined to a region in which the phase angle controllers operate within limits and where the solution of the power flow equations exists. Figure 4.11 shows the feasible



**Figure 4.11** Feasible region of active power flow control for PS1 and PS2

active power flow control region when phase shifters PS1 and PS2 are connected in series with the transmission lines connecting North-Lake and South-Lake, respectively. The range of phase angle variation is specified to be  $\pm 10^\circ$ . The following combinations of phase angles give the boundaries:

- Point A:  $\phi_{PS1} = 10^\circ$ , and  $\phi_{PS2} = -10^\circ$ ;
- Point B:  $\phi_{PS1} = 10^\circ$ , and  $\phi_{PS2} = 10^\circ$ ;
- Point C:  $\phi_{PS1} = -10^\circ$ , and  $\phi_{PS2} = -10^\circ$ ;
- Point D:  $\phi_{PS1} = -10^\circ$ , and  $\phi_{PS2} = 10^\circ$ .

Extensive power flow simulations verify the feasibility region shown in Figure 4.11 for this example. For instance, simulations are presented in Table 4.6, where the phase shifter parameters, initial conditions, and control targets are given.

As expected, all the power flows specified inside the feasible region are successfully upheld (Cases 1–3). Power flows specified outside the feasibility region lead to phase-shifter limits violations; these are indicated by an asterisk. The size of the feasible active power control region is a function of the phase angle controller range; as the range increases so too does the sizes of the regions.

**Table 4.6** Feasible active power flow control by PS1 and PS2

Case	Iteration	Final phase angle value (deg)		Active power flow North-Lake (MW)		Active power flow South-Lake (MW)	
		$\phi_{PS1}$	$\phi_{PS2}$	Specified	Final	Specified	Final
1	4	-5.64	-3.62	50	50	30	30
2	4	8.7	8.78	-5	-5	70	70
3	4	-7.6	6.62	70	70	-15	-15
4	7	10*	0.96	-5	2.2	30	30
5	7	-10*	-4.87	70	66.7	30	30
6	6	5.2	10*	30	30	-20	-13.5
7	7	-7.87	-10*	50	50	70	54
8	9	10*	10*	-10	13.8	-30	-7.6

\*Phase-shifter limit violation.

## 4.5 FURTHER CONCEPTS IN POWER FLOWS

### 4.5.1 Sparsity-oriented Solutions

When dealing with large-scale electrical power systems, the formation of actual matrices is not desirable because of the exorbitant processing times associated with their numerical solution. Instead, the Jacobian and nodal admittance matrices of the power system are stored

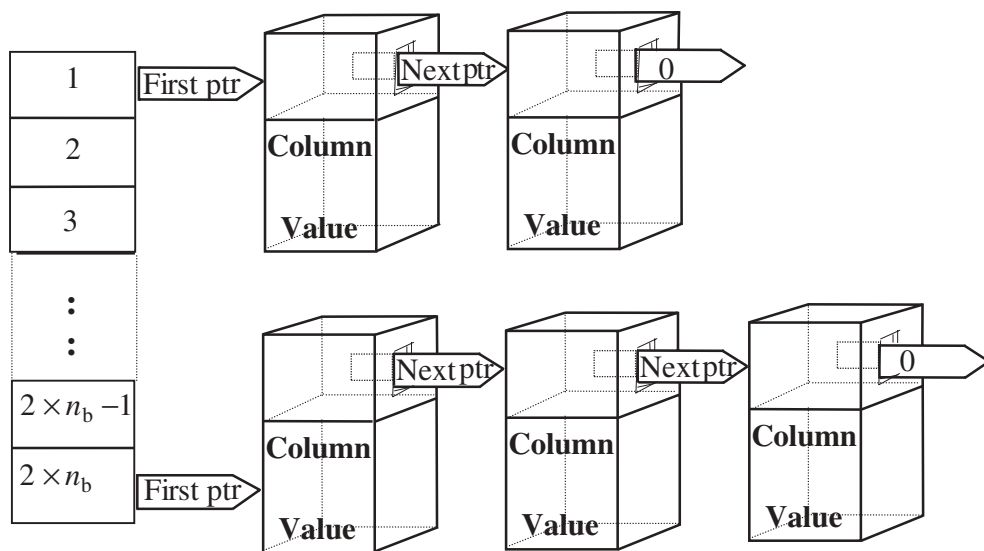


**Figure 4.12** Linked lists for storing a sparse Jacobian matrix. Note: ptr, pointer. Redrawn, with permission, from C.R. Fuerte-Esquivel, E. Acha, S.G. Tan, and J.J. Rico, ‘Efficient Object Oriented Power System Software for the Analysis of Large-scale Networks Containing FACTS Controlled Branches’, *IEEE Trans. Power Systems* 3(2) 464–472, © 1998 IEEE

and processed in vector form, where only nonzero elements are explicitly handled. In computer languages with no linked list facilities several one-dimensional arrays and skilful programming schemes are required in order to obtain efficient power flow analysis solutions. In modern programming languages such as C++, programming efforts are greatly reduced owing to the existence of pointers and structures.

In theory, C++ allows sparsity techniques to be implemented following a rather purist object-oriented programming (OOP) approach. However, this programming philosophy incurs excessive cpu overheads. Alternatively, a more efficient OOP approach may be adopted where sparsity is implemented using an array of pointers pointing to structures. Structures allow the encapsulation, in a single variable, of all the information associated with a sparse coefficient (e.g. value, column, and pointer to next element). Pointers are used to move from one structure to another. This is illustrated in Figure 4.12 for the case of a system containing  $n_b$  buses.

An array of pointers is created, the size of which equals the number of rows in the matrix. Each element points to the address of the start of a list. Moreover, one list is created for each row. In the case of conventional power flows, where storage locations are kept for the slack bus, an array of pointers of size equal to  $2 \times (n_b - 1)$  is created, where  $n_b$  is the number of buses in the network. Each list consists of an array of structures used to store information associated with off-diagonal Jacobian elements. The information associated with diagonal elements is stored in a separate array of structures.

## 4.5.2 Truncated Adjustments

The Newton–Raphson algorithm may perform poorly when solving large-scale power systems that are either heavily loaded or contain a substantial number of power system controllers in close proximity, such as LTCs and phase shifters. In such circumstances, large increments in the state variables may take place during the iterative solution, with this in turn inducing large  $\Delta P$  and  $\Delta Q$  residual terms. The result may be poor convergence, or more seriously, divergent solutions.

Such unwanted problems can be avoided quite effectively by limiting the size of correction, with the actual computed adjustments being replaced by truncated adjustments. This is a straightforward software solution to a common problem when dealing with utility-size power systems.

### 4.5.2.1 Test case of truncated adjustments involving three load tap-changing transformers

The AEP30 test network (Freris and Sasson, 1968) modified to assess the impact of truncated LTC solutions. The network contains two generators and four synchronous condensers. Transformers connected between buses 4–12, 6–10, and 27–28 are taken to be LTC transformers. The nodal voltage magnitudes at buses 4, 6, and 12 are controlled at 1, 1, and 1.04 p.u., respectively, using the primary taps of the three LTCs. The transformer connected between buses 6–9 is taken to be a phase shifter with a fix tap on the primary winding of  $1\angle -3.75^\circ$ .

To show the effectiveness of truncated solutions, two types of adjustments are carried out:

- Truncation of the size of correction (TA);
- Use of full correction (NTA).

Adjusted solutions are achieved in 6 iterations to a power mismatch tolerance of  $1e-12$ . However, the algorithm fails to reach convergence if the state variable increments are not truncated. This is illustrated in Figure 4.13, where maximum active and reactive power mismatches for both kinds of adjustments are shown.

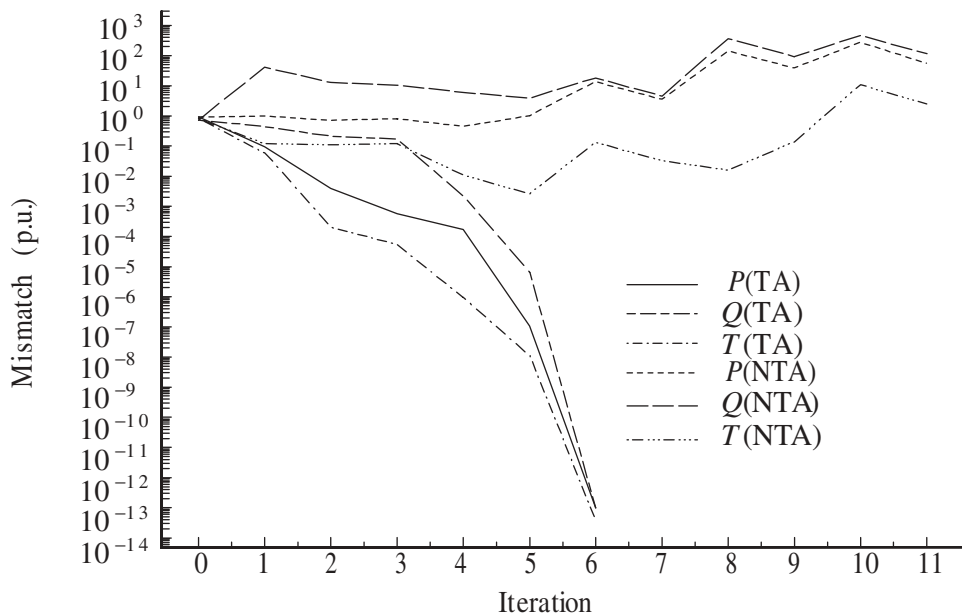


Figure 4.13 Convergence profile as a function of power mismatch

The final LTC parameters are shown in Table 4.7. It is assumed in the study that none of the LTCs violates tap limits. The active and reactive powers generated by the two synchronous generators (GE) and four synchronous condensers (CO) are shown in Table 4.8, where it is shown that one generator and two condensers hit their upper reactive power limits.

Table 4.7 Final settings of power system controllers

Controller	Magnitude (p.u.)	Angle (deg)
LTC 4–12	0.9013	0.00
LTC 6–10	0.8821	0.00
LTC 27–28	1.0667	0.00
PS 6–9	1.0000	-3.75

Note: LTC, load tap changer; PS, phase shifter.

**Table 4.8** Power generation

Source	Active power (MW)	Reactive power (MVAR)
GE-1	261.29	- 3.1
GE-2	40.0	50.0*
CO-5	0.0	40.0*
CO-8	0.0	40.0*
CO-11	0.0	13.17
CO-13	0.0	- 2.27

\* Violation reactive power limit.  
 Note: GE, generator; CO, condenser.

### 4.5.3 Special Load Tap Changer Configurations

Groups of LTCs may be operated in a coordinated fashion enabling more general control strategies than those afforded by a single LTC. Series and parallel LTC configurations are the most obvious possibilities. The series condition occurs when one or more LTCs regulate the nonregulated terminal of another LTC. This situation is shown in Figure 4.14(a), in which LTC 1 regulates bus  $k$ , and LTC 2 regulates bus  $m$ . The parallel condition occurs when bus  $k$  is regulated by two or more LTCs, as shown in Figure 4.14(b). It must be noted that buses  $m$  and  $n$  may not necessarily be electrically connected.

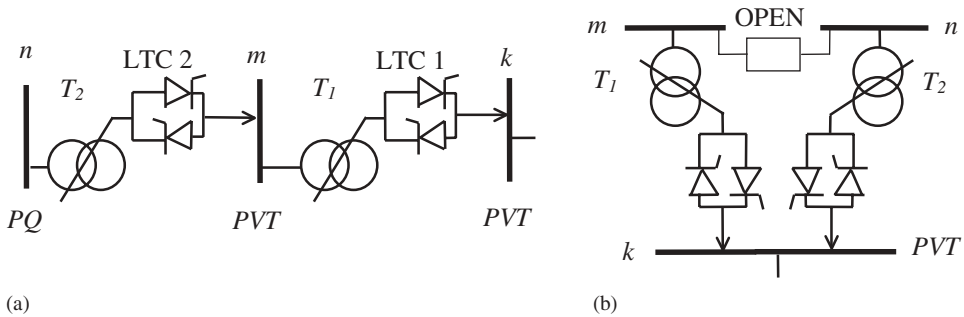


**Figure 4.14** Control configurations: (a) series and, (b) parallel. Reproduced, with permission, from C.R. Fuerte-Esquivel, E. Acha, S.G. Tan, and J.J. Rico, ‘Efficient Object Oriented Power System Software for the Analysis of Large-scale Networks Containing FACTS Controlled Branches’, *IEEE Trans. Power Systems* 3(2) 464–472, © 1998 IEEE

The parallel condition does not belong to the category of single criterion control, where only one control variable is adjusted in order to maintain another dependent variable at a specified value. When two or more LTCs are controlling one nodal voltage magnitude multiple solutions become a possibility because the number of unknown variables is greater than the number of equations. An entire group of parallel LTCs may be treated as a single control criterion if they are started from the same tapping initial condition. One equation and

one variable corresponding to the common tap position may be sufficient to describe the group performance. This Equation is linearised with respect to the common tap and incorporated in the overall Jacobian Equation (4.57).

From the LTC set, the LTC that draws less reactive power is selected to be the master, and its tapping position becomes the master tapping position. Since the various LTCs in the group may have the same tapping position but different tap limits, it may be appropriate to consider the following options:

- If an LTC different from the master hits one of its limits, the tapping position is fixed at the offending limit and the LTC is removed from the linearised system of equations.
- If the master LTC hits a limit, it follows the same treatment as a slave LTC. Moreover, a new master is selected from the remaining active LTCs. If no active LTC remains following limit violation by the master then the bus becomes  $PQ$ .

A sensitivity factor,  $\alpha$ , may be used when the various LTCs in the parallel set have different tapping positions;  $\alpha$  refers the slave tap position to the master tap position.

Assuming a group of  $n_p$  LTCs operating in parallel, and taking  $T_k$  to be the master position, the sensitivity factor is calculated as:

$$\alpha_p = \frac{T_k}{T_p}, \quad p = 1, \dots, n_p. \quad (4.97)$$

The expression used for computing the Jacobian entry for the master tap position is also used for the other LTCs in the group. The tap is adjusted by using Equation (4.97), where each LTC in the group has its own adjusting pattern and where the sensitivity factor is taken into account:

$$T_p^{(i)} = T_p^{(i-1)} + \left( \frac{\Delta T_k}{T_k} \right)^{(i)} T_p^{(i-1)}, \quad p = 1, \dots, n_p. \quad (4.98)$$

An alternative adjusting strategy is given by Equation (4.98), where equal corrections are given to all the LTCs in the group:

$$T_p^{(i)} = T_p^{(i-1)} + \left( \frac{\Delta T_k}{T_k} \right)^{(i)} \alpha_p^{(i)} T_p^{(i-1)}, \quad p = 1, \dots, n_p. \quad (4.99)$$

#### 4.5.3.1 Test case of sensitivity factors in parallel load tap-changing operation

The AEP30 test system (Freris and Sasson, 1968) is modified to include four LTCs. The nodal voltage magnitude at bus 6 is kept at 1.01 p.u. with LTCs 6–9 and 6–10 exerting parallel control in bus 6. The voltage magnitude at buses 4 and 27 are controlled at 1.01 p.u. and 1 p.u. by LTCs 4–12 and 27–28, respectively. The transformers reactance and off-nominal tap values given in (Freris and Sasson, 1968) are taken to be on the secondary and primary windings, respectively. The primary windings of the four transformers are assumed connected to buses 6, 4, and 27, respectively.

**Table 4.9** Initial position of load tap changer (LTC) taps

Case	LTC 6–9	LTC 6–10	LTC 4–12	LTC 27–28
1	0.978	0.969	0.932	0.968
2	1.1	1.1	1.1	1.1
3	1.0	1.0	1.0	1.0
4	0.9	0.9	0.9	0.9
5	1.0	0.9	1.0	1.0

Following on the discussion started in Section 4.5.3, the adjustment of the two LTCs operating in parallel is carried out by using: (1) sensitivity factors and (2) equal updating of taps. A comparison is made for the various cases given in Table 4.9. The number of iterations taken to obtain the solution as well as the final tapping values required to maintain the nodal voltage magnitudes at the specified values are given in Table 4.10.

As expected, both adjusting methods give the same solution for a specified LTC initial condition. However, the use of sensitivity factors guarantees better results in terms of the number of iterations required to get to the solution, compared with the case in which identical tapping updates is carried out.

**Table 4.10** Final position of load tap changer (LTC) taps: (a) updating using sensitivity factors and (b) equal updating

Case	Iteration	Tap position			
		LTC 6–9	LTC 6–10	LTC 4–12	LTC 27–28
(a)					
1	5	0.976	0.967	0.915	0.998
2	5	0.974	0.974	0.915	0.998
3	5	0.974	0.974	0.915	0.998
4	5	0.974	0.974	0.915	0.998
5	5	1.008	0.907	0.913	0.995
(b)					
1	6	0.976	0.967	0.915	0.998
2	5	0.974	0.974	0.915	0.998
3	5	0.974	0.974	0.915	0.998
4	5	0.974	0.974	0.915	0.998
5	10	1.008	0.908	0.913	0.995

## 4.6 SUMMARY

In this chapter we have addressed the basic theory of power flows. Building upon elementary concepts afforded by circuit theory and complex algebra, we have derived

equations for active and reactive powers injections at a bus. Owing to the idiosyncrasies of the electrical power network, the mathematical model that describes its operation during steady-state is nonlinear. Furthermore, for most practical situations, the power network is a very large-scale system. Hence, solution of the nonlinear set of equations, which must be reached by iteration, requires a robust and efficient numerical technique. For several decades the Newton–Raphson method, with its quadratic convergence characteristic, has proved invaluable in solving the power flow problem. The additional burden imposed on the numerical solution by the many constraint actions resulting from the various power system controllers in the network does not impair the ability of the Newton–Raphson method to converge in a quadratic fashion. Derived Newton–Raphson formulations, such as the fast decoupled method, also possess strong convergence characteristics. Both methods have been explained in full detail in this chapter. The calculated power equations, mismatch powers, and Jacobian terms all have been derived from first principles. The relevant equations making up the Newton–Raphson and fast decoupled methods have been coded in Matlab<sup>®</sup> and the programs used to solve a classical test case. The test system is small and yet it provides sufficient realism and flexibility for the reader to explore different loading scenarios, active power generator schedules, and transmission-line parameters. This is something we certainly encourage the user to do.

The material presented in this chapter progressed to tackle the most specialised issue of constrained power flow solutions. To this end, flexible models of tap-changing and phase-shifting transformers were developed from first principles. Together with the generator, these two power controllers are capable of providing automatic regulation at specific points of the network provided their design limits are not exceeded. The generator and the tap-changing transformer provide voltage magnitude regulation whereas the phase-shifting transformer provides active power regulation. Inclusion of such regulating characteristics within the power flow solution is a matter of great engineering importance. However, they introduce additional complexity in power flow theory and may impose an extra burden on the numerical solution. We believe that sufficient breadth and depth was provided in the second part of this chapter to make accessible the concepts associated with constrained power flow solutions. This is in preparation for the widespread constrained solutions associated with the various FACTS controllers presented in the next chapter.

## REFERENCES

- Arrillaga, J., Arnold, C.P., 1990, *Computer Analysis of Power Systems*, John Wiley & Sons, Chichester.
- Brown, H.E., 1975, *Solution of Large Networks by Matrix Methods*, John Wiley & Sons, Chichester.
- Elgerd, O., 1982, *Electric Energy System Theory: An Introduction*, McGraw-Hill, New York.
- Freris, L.L., Sasson, A.M., 1968, ‘Investigation of the Load-flow Problem’, *Proceedings of the IEE, Part C* **115**(10), 1459–1470.
- Fuerte-Esquivel, C.R., Acha, E., Tan, S.G., Rico, J.J., 1998, ‘Efficient Object Oriented Power System Software for the Analysis of Large-scale Networks Containing FACTS Controlled Branches’, *IEEE Trans. Power System* **3**(2) 464–472.
- Grainger, J.J., Stevenson, W.D., 1984, *Power System Analysis*, McGraw-Hill, New York.
- Kundur, P.P., 1994, *Power System Stability and Control*, McGraw-Hill, New York.

- Peterson, N.M., Scott Meyer, W., 1974, 'Automatic Adjustment of Transformer and Phase Shifter Taps in the Newton Power Flow', *IEEE Trans. Power Apparatus and Systems* **PAS-90**(1) 103–108.
- Stagg, G.W., El-Abiad, A.H., 1968, *Computer Methods in Power System Analysis*, McGraw-Hill, New York.
- Stott, B., 1974, 'Review of Load-flow Calculation Methods', *IEEE Proceedings* **62**(July) 916–929.
- Stott, B., Alsac, O., 1978, 'Fast Decoupled Load Flow', *IEEE Trans. Power Apparatus and Systems* **PAS-93**, 859–862.
- Tinney, W.F., Hart, C.E., 1967, 'Power Flow Solution by Newton's Method', *IEEE Trans. Power Apparatus and Systems* **PAS-86**(11) 1449–1460.
- Weedy, B.M., 1987, *Electric Power Systems*, John Wiley & Sons, Chichester.
- Wood, A.J., Wollenberg, B.F., 1984, *Power Generation, Operation and Control*, John Wiley & Sons, Chichester.
- Zollenkoff, K., 1970, 'Bifactorization: Basic Computational Algorithm and Programming Techniques', in J.K. Reid (ed.), *Large Sparse Sets of Linear Equations*, Academic Press, Oxford, pp. 75–96.



# 5

## Power Flow Including FACTS Controllers

### 5.1 INTRODUCTION

FACTS controllers narrow the gap between the noncontrolled and the controlled power system mode of operation, by providing additional degrees of freedom to control power flows and voltages at key locations of the network (Hingorani and Gyugyi, 2000). Key objectives of the technology are: to increase transmission capacity allowing secure loading of the transmission lines up to their thermal capacities; to enable better utilisation of available generation; and to contain outages from spreading to wider areas (Song and Johns, 1999).

In order to determine the effectiveness of this new generation of power systems controllers on a network-wide basis, it has become necessary to upgrade most of the analysis tools on which power engineers rely to plan and to operate their systems (IEEE/CIGRÉ, 1995). For the purpose of steady-state network assessment, power flow solutions are probably the most popular kind of computer-based calculations carried out by planning and operation engineers. The reliable solution of power flows in real-life transmission and distribution networks is not a trivial matter and, over the years, owing to its very practical nature, many calculation methods have been put forward to solve this problem. Among them, Newton–Raphson type methods, with their strong convergence characteristics, have proved the most successful and have been embraced by industry (Tinney and Hart, 1967).

In preparation for the material covered in this chapter, in Chapter 4 we provided a thorough grounding on conventional power flow theory with particular reference to the Newton–Raphson method. Similar material can also be found in many of the excellent power system analysis books that address the subject (Arrillaga and Arnold, 1990; Grainger and Stevenson, 1994; Kundur, 1994). The aim of this chapter is to introduce a systematic and coherent way to study models and methods for the representation of FACTS controllers in power flow studies. This aspect of power flow theory has not been covered in existing textbooks in the breadth and depth that the importance and complexity of the subject demands (Fuerte-Esquivel *et al.*, 1998). It should be emphasised that the material presented in this chapter is a distillation of the wealth of research contributions on the subject that have

been published over recent years (Ambriz-Pérez, Acha, and Fuerte-Esquivel, 2000; Fuerte-Esquivel and Acha, 1996, 1997; Fuerte-Esquivel, Acha, and Ambriz-Pérez, 2000a, 2000b, 2000c; Nabavi-Niaki and Iravani, 1996; Noroozian and Andersson, 1993). It is in this respect that the chapter gives an up-to-date and authoritative account of the power flow models and methods of power electronics-based controllers currently available in the power transmission industry.

## 5.2 POWER FLOW SOLUTIONS INCLUDING FACTS CONTROLLERS

The technical literature is populated with clever and elegant solutions for accommodating models of controllable plant in Newton–Raphson power flow algorithms; load tap-changing (ltc) and phase-shifting transformers are early examples of such work. The modelling approach used to represent controllable equipment can be broadly classified into two main categories, namely, sequential and simultaneous solution methods. The former approach is amenable to easier implementations in Newton–Raphson algorithms. However, its major drawback is that the bus voltage magnitudes and angles are the only state variables that are calculated in true Newton fashion, and a subproblem is formulated for updating the state variables of the controllable devices at the end of each iteration. Such an approach yields no quadratic convergence (Acha, 1993; Chang and Brandwajn, 1988).

Alternatively, the unified approach combines the state variables describing controllable equipment with those describing the network in a single frame of reference for unified, iterative solutions using the Newton–Raphson algorithm (Ambriz-Pérez, Acha, and Fuerte-Esquivel, 2000; Fuerte-Esquivel and Acha, 1996, 1997; Fuerte-Esquivel, Acha, and Ambriz-Pérez, 2000a, 2000b, 2000c; Fuerte-Esquivel *et al.*, 1998). The method retains Newton’s quadratic convergence characteristics.

The unified approach blends the alternating-current (AC) network and power system controller state variables in a single system of simultaneous equations:

$$\begin{aligned} f(X_{nAC}, R_{nF}) &= 0, \\ g(X_{nAC}, R_{nF}) &= 0, \end{aligned} \tag{5.1}$$

where  $X_{nAC}$  stands for the AC network state variables, namely, nodal voltage magnitudes and phase angles, and  $R_{nF}$  stands for the power system controller state variables.

The increase in the dimensions of the Jacobian, compared with the case when there are no power system controllers, is proportional to the number and kind of such controllers. In very general terms, the structure of the modified Jacobian is shown in Figure 5.1.

Building upon the basic principles of steady-state operation and modelling of FACTS controllers described in Chapter 2 and the power flow theory detailed in Chapter 4, key aspects of modelling implementation of FACTS controllers are presented in this chapter, within the context of the Newton–Raphson power flow algorithm. The FACTS controllers that receive attention are:

- Static VAR compensator (SVC);
- Thyristor-controlled series compensator (TCSC);
- Static compensator (STATCOM);
- Unified power flow controller (UPFC);
- High-voltage direct-current-based voltage source converter (HVDC-VSC).

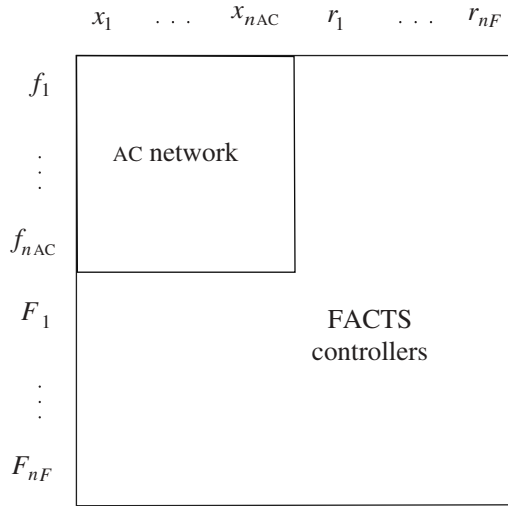


**Figure 5.1** Augmented Jacobian

### 5.3 STATIC VAR COMPENSATOR

Conventional and advanced power flow models of SVCs are presented in this section. The advanced models depart from the conventional generator-type representation (Erinmez, 1986; IEEE SSCWG, 1995) of the SVC and are based instead on the *variable shunt susceptance* concept. In the latter case, the SVC state variables are combined with the nodal voltage magnitudes and angles of the network in a single frame of reference for unified, iterative solutions using the Newton–Raphson method. Two models are presented in this category (Ambriz-Pérez, Acha, and Fuerte-Esquivel, 2000), namely, the variable shunt susceptance model and the firing-angle model. Moreover, a compound transformer and SVC model based on the SVC firing-angle representation is also given.

#### 5.3.1 Conventional Power Flow Models

Early SVC models for power flow analysis treat the SVC as a generator behind an inductive reactance (Erinmez, 1986; IEEE SSCWG, 1995). The reactance accounts for the SVC voltage-regulation characteristic.

A simpler representation assumes that the SVC slope is zero; an assumption that may be acceptable as long as the SVC operates within its design limits, but one which may lead to gross errors if the SVC is operating close to its limits (Kundur, 1994). This point is illustrated in Figure 5.2 with reference to the upper characteristic when the system is operating under low loading conditions. If the slope is taken to be zero then the generator will violate its minimum limit, point  $A_{X_{SL}=0}$ . However, the generator will operate well within limits if the SVC voltage–current slope is taken into account at, point A.

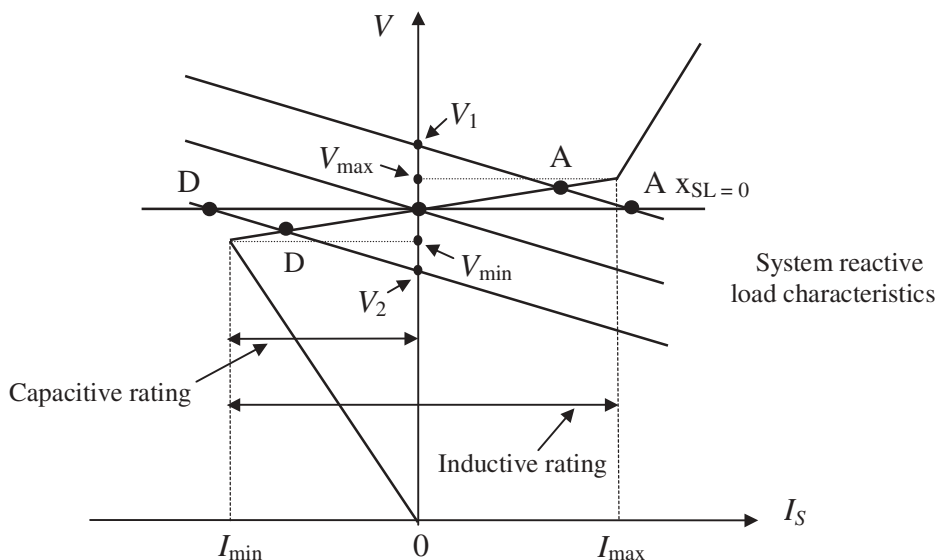


**Figure 5.2** Static VAR compensator and power system voltage–current characteristics. From P.P. Kundur, *Power System Stability and Control*, © 1994 McGraw-Hill. Reproduced by permission of The McGraw-Hill Companies

The reasons for including the SVC voltage–current slope in power flow studies are compelling. The slope can be represented by connecting the SVC model to an auxiliary bus coupled to the high-voltage bus by an inductive reactance consisting of the transformer reactance and the SVC slope, in per unit (p.u.) on the SVC base. The auxiliary bus is represented as a *PV* bus and the high-voltage bus is taken to be *PQ*. This model is shown schematically in Figure 5.3(a). Alternatively, the SVC coupling transformer may be represented explicitly as shown in Figure 5.3(b).

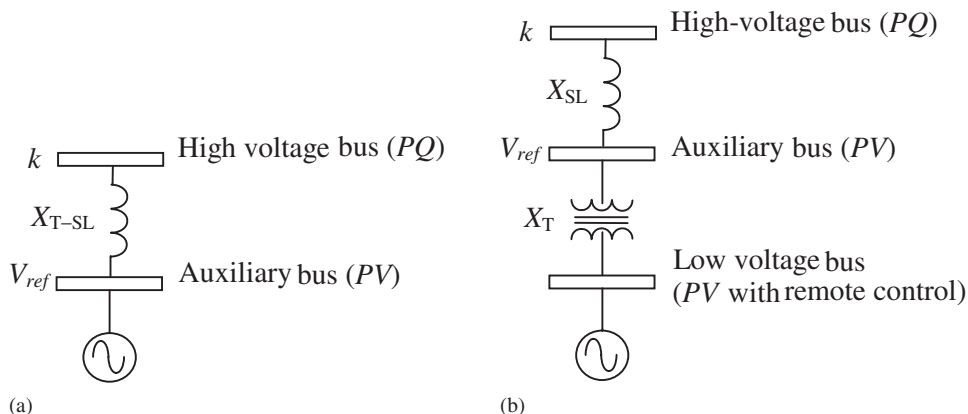


**Figure 5.3** Conventional static VAR compensator power flow models: (a) slope representation and (b) slope and coupling transformer representation

These SVC representations are quite straightforward but are invalid for operation outside the limits (IEEE SSCWG, 1995). In such cases, it becomes necessary to change the SVC representation to a fixed reactive susceptance, given by

$$B_{SVC} = -\frac{Q_{lim}}{V_{SVC}^2}, \tag{5.2}$$

where  $V_{SVC}$  is the newly freed voltage due to the reactive power limit  $Q_{lim}$  being exceeded.

The combined generator–susceptance representation yields accurate results. However, a drawback of such a representation is that both models use a different number of buses. The generator uses two or three buses, as shown in Figure 5.3, whereas the fixed susceptance uses only one bus. In Newton–Raphson power flow solutions such a difference in the number of buses required to represent the same plant component may lead to Jacobian reordering and redimensioning during the iterative solution. Also, extensive checking becomes necessary in order to verify whether or not the SVC has returned to operation within limits at any stage of the iterative solution.

It should be remarked that for operation outside limits the SVC must be modelled as a susceptance and not as a generator set at its violated limit,  $Q_{lim}$ . Ignoring this point will lead to inaccurate results. The reason is that the amount of reactive power drawn by the SVC is given by the product of the fixed susceptance,  $B_{fix}$ , and the nodal voltage magnitude,  $V_k$ . Since  $V_k$  is a function of network operating conditions, the amount of reactive power drawn by the fixed susceptance model differs from the reactive power drawn by the generator model; that is,

$$Q_{lim} \neq -B_{fix}V_k^2. \tag{5.3}$$

This point is exemplified in Figure 5.4, where the reactive power output of the generator is set at 100 MVAR. This value is constant as it is voltage-independent. The result given by the

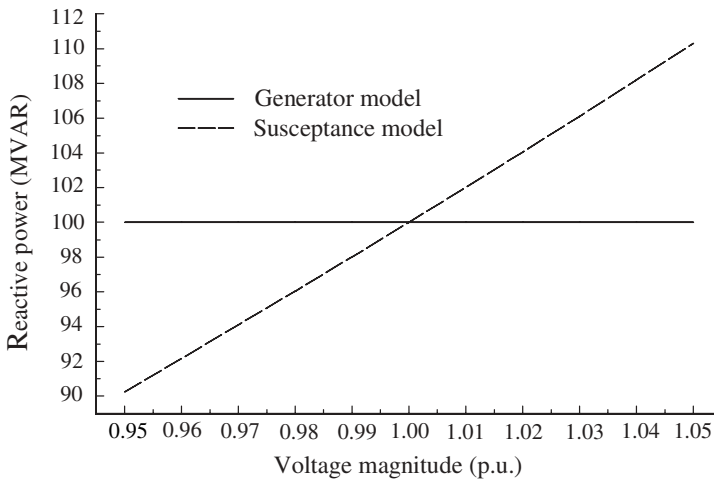


**Figure 5.4** Comparison of reactive power drawn by the generator and susceptance models. Reproduced, with permission, from H. Ambriz-Pérez, E. Acha, and C.R. Fuerte-Esquivel, ‘Advanced SVC Models for Newton–Raphson Load Flow and Newton Optimal Power Flow Studies’, *IEEE Trans. Power Systems* **15**(1) 129–136, © 2000 IEEE

constant susceptance model varies with nodal voltage magnitude. The voltage range considered is 0.95–1.05 p.u. The susceptance value, on a 100 MVA base, is of 1 p.u.

### 5.3.2 Shunt Variable Susceptance Model

In practice the SVC can be seen as an adjustable reactance with either firing-angle limits or reactance limits (Ambriz-Pérez, Acha, and Fuerte-Esquivel, 2000). The equivalent circuit shown in Figure 5.5 is used to derive the SVC nonlinear power equations and the linearised equations required by Newton’s method.

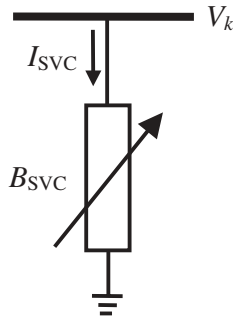


**Figure 5.5** Variable shunt susceptance. Reproduced, with permission, from H. Ambriz-Pérez, E. Acha, and C.R. Fuerte-Esquivel, ‘Advanced SVC Models for Newton–Raphson Load Flow and Newton Optimal Power Flow Studies’, *IEEE Trans. Power Systems* **15**(1) 129–136, © 2000 IEEE

With reference to Figure 5.5, the current drawn by the SVC is

$$I_{SVC} = jB_{SVC} V_k, \tag{5.4}$$

and the reactive power drawn by the SVC, which is also the reactive power injected at bus  $k$ , is

$$Q_{SVC} = Q_k = -V_k^2 B_{SVC}. \tag{5.5}$$

The linearised equation is given by Equation (5.6), where the equivalent susceptance  $B_{SVC}$  is taken to be the state variable:

$$\begin{bmatrix} \Delta P_k \\ \Delta Q_k \end{bmatrix}^{(i)} = \begin{bmatrix} 0 & 0 \\ 0 & Q_k \end{bmatrix}^{(i)} \begin{bmatrix} \Delta \theta_k \\ \Delta B_{SVC}/B_{SVC} \end{bmatrix}^{(i)}. \tag{5.6}$$

At the end of iteration  $(i)$ , the variable shunt susceptance  $B_{SVC}$  is updated according to

$$B_{SVC}^{(i)} = B_{SVC}^{(i-1)} + \left( \frac{\Delta B_{SVC}}{B_{SVC}} \right)^{(i)} B_{SVC}^{(i-1)}. \tag{5.7}$$

The changing susceptance represents the total SVC susceptance necessary to maintain the nodal voltage magnitude at the specified value.

Once the level of compensation has been computed then the thyristor firing angle can be calculated. However, the additional calculation requires an iterative solution because the SVC susceptance and thyristor firing angle are nonlinearly related.

### 5.3.3 Static VAR Compensator Computer Program in Matlab<sup>®</sup> Code

Program 5.1 incorporates the SVC representation, modelled as a variable shunt susceptance model, within the Newton–Raphson power flow program given in Section 4.3.6. The functions `PowerFlowsData`, `YBus`, and `PQflows` are also used here. In the main SVC Newton–Raphson program, the function `SVCBData` is added to read the SVC data, `SVCNewtonRaphson` replaces `NewtonRaphson`, and `SVCPCflows` is used to calculate power flows and losses in the SVC.

Function `SVCNewtonRaphson` borrows the following functions from `NewtonRaphson`: `NetPowers`; `CalculatedPowers`; `GeneratorsLimits`; `PowerMismatches`; `NewtonRaphsonJacobian`; and `StateVariablesUpdates`. Furthermore, four new functions are added to cater for the SVC representation: `SVCCalculatedPowers`; `SVCUpdates`; `SVCLimits`; and `SVCNewtonRaphsonJacobian`.

Program 5.1 Program written in Matlab<sup>®</sup> to incorporate static VAR compensator (SVC) variable shunt susceptance model within the Newton–Raphson power flow algorithm

```
% - - - Main SVC Program

PowerFlowsData; %Function to read network data

SVCBData; %Function to read Static VAR Compensator data

[YR, YI] = YBus(tlsend, tlrec, tlresis, tlreac, tlsuscep, tlcond, ntl, nbb);

[VM, VA, it, B] = SVCNewtonRaphson(tol, itmax, ngn, nld, nbb, bustype, ...
genbus, loadbus, PGEN, QGEN, QMAX, QMIN, PLOAD, QLOAD, YR, YI, VM, VA, NSVC, ...
SVCsend, B, BLo, BHi, TarVol, VSta);

[PQsend, PQrec, PQloss, PQbus] = PQflows(nbb, ngn, ntl, nld, genbus, loadbus,
tlsend, tlrec, tlresis, tlreac, tlcond, tlsuscep, PLOAD, QLOAD, VM, VA);

[QSVC] = SVCQpower(VM, NSVC, SVCsend, B);

%Print results
it           %Number of iterations
VM           %Nodal voltage magnitude (p.u)
VA=VA*180/pi %Nodal voltage phase angles (Deg)
QSVC        %Final reactive power (p.u.)
B           %Final susceptance (p.u)

%End of MAIN FOR SVC SHUT VARIABLE SUSCEPTANCE
```

```

function [VM,VA,it,B] = SVCNewtonRaphson(tol,itmax,ngn,nld,nbb,...
bustype, genbus,loadbus,PGEN,QGEN,QMAX,QMIN,PLOAD,QLOAD,YR,YI,...
VM,VA,NSVC,SVCsend,B,BLo,BHi,TarVol,VSta);

% GENERAL SETTINGS
flag = 0;
it = 1;

% CALCULATE NET POWERS
[PNET,QNET] = NetPowers(nbb,ngn,nld,genbus,loadbus,PGEN,QGEN,...
PLOAD,QLOAD);

while (it < itmax & flag==0)

    % CALCULATED POWERS
    [PCAL,QCAL] = CalculatedPowers(nbb,VM,VA,YR,YI);

    %SVC CALCULATED POWER
    [QCAL] = SVCCalculatePower(QCAL,VM,NSVC,SVCsend,B)

    % POWER MISMATCHES
    [DPQ,DP,DQ,flag] = PowerMismatches(nbb,tol,bustype,flag,PNET,...
QNET,PCAL,QCAL);
    if flag == 1
        break
    end
    % JACOBIAN FORMATION
    [JAC] = NewtonRaphsonJacobian(nbb,bustype,PCAL,QCAL,DPQ,VM,VA,...
YR,YI);
    % MODIFICATION THE JACOBIAN FOR SVC
    [JAC] = SVCJacobian(JAC,VM,NSVC,SVCsend,B,VSta);

    % SOLVE JOCOBIAN
    D = JAC\DPQ';

    % UPDATE THE STATE VARIABLES VALUES, WITH TRUNCATED CORRECTIONS
    % IF NECESSARY (VM increments < +-0.1 p.u. and VA increments < +- 5 deg)
    [VA,VM] = StateVariablesUpdating(nbb,D,VA,VM,it);

    % UPDATE THE SVC VARIABLES
    [VM,B] = SVCUpdating(VM,D,NSVC,SVCsend,B,BLo,BHi,TarVol,VSta);

```

```

%CHECK SUSCEPTANCE FOR LIMITS
[B] = SVCLimits(NSVC,B,BLo,BHi);

it = it + 1;

end

%Function to calculate injected bus powers by the SVC function
[QCAL]= SVCCalculatePower(QCAL,VM,NSVC,SVCsend,B);
for ii = 1 : NSVC
    QCAL(SVCsend(ii))=QCAL(SVCsend(ii))-VM(SVCsend(ii))^2*B(ii);
end

%Function to upgrade the Jacobian matrix with SVC elements
function [JAC] = SVCJacobian(JAC,VM,NSVC,SVCsend,B,VSta);
for ii = 1 : NSVC

    if (VSta(ii) == 1)
        %Delete the voltage magnitud for the SVC bus
        JAC( : , 2*SVCsend(ii) ) = 0;

        JAC(2*SVCsend(ii)-1,2*SVCsend(ii)-1) = ...
        JAC(2*SVCsend(ii)- 1,2*SVCsend(ii)-1)- ...
        VM(SVCsend(ii))^2*B(ii);
        JAC(2*SVCsend(ii),2*SVCsend(ii))= - VM(SVCsend(ii))^2*B(ii);
    end
end

%Function to update SVC state variable
function [VM,B] = SVCUpdating(VM,D,NSVC,SVCsend,B,BLo,BHi,TarVol,...
VSta);
for ii = 1 : NSVC

    if (VSta(ii) == 1)
        % Adjust the Voltage Magnitud target
        VM(SVCsend(ii)) = TarVol(ii);
        % Truncation
        value = B(ii)*D(2*SVCsend(ii));
        value2 = D(2*SVCsend(ii));
        if (value > 0.1)
            value2 = 0.1/B(ii);
        elseif (value < -0.1)
            value2 = -0.1/B(ii);
        end
        B(ii) = B(ii) + B(ii)*value2;
    end
end
end

```

```

%Function to check the susceptance limits
function [B] = SVCLimits(NSVC,B,BLo,BHi);
% Check susceptance limits in SVC
for ii = 1 : NSVC
    if (B(ii) > BHi(ii))
        B(ii) = BHi(ii);
    elseif (B(ii) < BLo(ii))
        B(ii) = BLo(ii);
    end
end

%Function to calculate the reactive power in SVC
function [Q SVC] = SVCQpower(VM,NSVC,SVCsend,B);
for ii = 1 : NSVC
    Q SVC(ii) = -VM(SVCsend(ii))^2*B(ii);
end

```

### 5.3.4 Firing-angle Model

An alternative SVC model, which circumvents the additional iterative process, consists in handling the thyristor-controlled reactor (TCR) firing angle  $\alpha$  as a state variable in the power flow formulation (Ambriz-Pérez, Acha, and Fuerte-Esquivel, 2000). The variable  $\alpha$  will be designated here as  $\alpha_{\text{SVC}}$ , to distinguish it from the TCR firing angle  $\alpha$  used in the TCSC model.

The positive sequence susceptance of the SVC, given by Equation (2.20), is used in Equation (5.5):

$$Q_k = \frac{-V_k^2}{X_C X_L} \left\{ X_L - \frac{X_C}{\pi} [2(\pi - \alpha_{\text{SVC}}) + \sin(2\alpha_{\text{SVC}})] \right\}. \quad (5.8)$$

From Equation (5.8), the linearised SVC equation is given as

$$\begin{bmatrix} \Delta P_k \\ \Delta Q_k \end{bmatrix}^{(i)} = \begin{bmatrix} 0 & 0 \\ 0 & \frac{2V_k^2}{\pi X_L} [\cos(2\alpha_{\text{SVC}}) - 1] \end{bmatrix}^{(i)} \begin{bmatrix} \Delta \theta_k \\ \Delta \alpha_{\text{SVC}} \end{bmatrix}^{(i)}. \quad (5.9)$$

At the end of iteration  $(i)$ , the variable firing angle  $\alpha_{\text{SVC}}$  is updated according to

$$\alpha_{\text{SVC}}^{(i)} = \alpha_{\text{SVC}}^{(i-1)} + \Delta \alpha_{\text{SVC}}^{(i)}. \quad (5.10)$$

### 5.3.5 Static VAR Compensator Firing-angle Computer Program in Matlab® Code

Program 5.2 incorporates the SVC firing-angle (SVC-FA) model within the Newton-Raphson power flow program given in Section 4.3.6. The functions `PowerFlowsData`, `YBus`, and `PQflows` are also used here. In the main SVC-FA Newton-Raphson program, the

function `SVCFAData` is added to read the SVC-FA data, `SVCFANewtonRaphson` replaces `NewtonRaphson`, and `SVCFAPOflows` is used to calculate power flows and losses in the SVC-FA model.

Function `SVCFANewtonRaphson` borrows the following functions from `NewtonRaphson`: `NetPowers`; `CalculatedPowers`; `PowerMismatches`; `NewtonRaphsonJacobian`; and `StateVariablesUpdates`. Furthermore, four new functions are added to cater for the SVC-FA representation, namely: `SVCFACalculatedPowers`; `SVCFAUpdates`; `SVCFALimits`; and `SVCFANewtonRaphsonJacobian`.

**PROGRAM 5.2** Program written in Matlab<sup>®</sup> to incorporate the static VAR compensator firing-angle (SVC-FA) model within the Newton–Raphson power flow algorithm

```
% - - - Main SVC-FA Program

PowerFlowsData; %Function to read network data

SVCFAData; %Function to read SVC-FA data

[YR, YI] = YBus(tlsend, tlrec, tlresis, tlreac, tlsuscep, tlcond, ntl, nbb);

[VM, VA, it, FA] = SVCFANewtonRaphson(tol, itmax, ngn, nld, nbb, bustype, ...
genbus, loadbus, PGEN, QGEN, QMAX, QMIN, PLOAD, QLOAD, YR, YI, VM, VA, NSVC, ...
SVCsend, FA, Xc, Xl, FALo, FAHi, TarVol, VSta);

[PQsend, PQrec, PQloss, PQbus] = PQflows(nbb, ngn, ntl, nld, genbus, ...
loadbus, tlsend, tlrec, tlresis, tlreac, tlcond, tlsuscep, PLOAD, QLOAD, ...
VM, VA);

[QSVC, B] = SVCFAQpower(VM, NSVC, SVCsend, FA, Xc, Xl);

%Print online results
it           %Number of iterations
VM           %Nodal voltage magnitude (p.u)
VA=VA*180/pi %Nodal voltage phase angles (Deg)
QSVC        %Final reactive power value(p.u.)
B           %Final susceptance value (p.u.)
FA=FA*180/pi %Final firing angle value (Deg)

%End of MAIN SVC-FA PROGRAM

function [VM, VA, it, FA] = SVCFANewtonRaphson(tol, itmax, ngn, nld, nbb, ...
bustype, genbus, loadbus, PGEN, QGEN, QMAX, QMIN, PLOAD, QLOAD, YR, YI, VM, ...
VA, NSVC, SVCsend, FA, Xc, Xl, FALo, FAHi, TarVol, VSta);

% GENERAL SETTINGS
flag = 0;
it = 1;
```

## 164 POWER FLOW INCLUDING FACTS CONTROLLERS

```
% CALCULATE NET POWERS
[PNET,QNET] = NetPowers(nbb,ngn,nld,genbus,loadbus,PGEN,QGEN,...
PLOAD,QLOAD);

while ( it < itmax & flag==0 )
    % CALCULATED POWERS
    [PCAL,QCAL] = CalculatedPowers(nbb,VM,VA,YR,YI);

    %SVC CALCULATED POWER
    [QCAL,B] = SVCFACalculatePower(QCAL,VM,NSVC,SVCsend,FA,Xc,Xl);

    % POWER MISMATCHES
    [DPQ,DP,DQ,flag] = PowerMismatches(nbb,tol,bustype,flag,PNET,QNET,...
PCAL,QCAL);

    % JACOBIAN FORMATION
    [JAC]=NewtonRaphsonJacobian(nbb,bustype,PCAL,QCAL,DPQ,VM,...
VA,YR,YI);

    % SVC-FA JACOBIAN UPDATING
    [JAC]=SVCFAJacobian(JAC,VM,NSVC,SVCsend,FA,Xl,B,VSta);

    % SOLVE FOR THE STATE VARIABLES VECTOR
    D = JAC\DPQ';

    % UPDATE THE STATE VARIABLES
    [VA,VM] = StateVariablesUpdating(nbb,D,VA,VM,it);

    % UPDATE THE SVC-FA VARIABLES
    [VM,FA] = SVCFAUpdating(VM,D,NSVC,SVCsend,FA,FALo,FAHi,TarVol,...
VSta);

    %CHECK SVC-FA FIRING ANGLE FOR LIMITS VIOLATIONS
    [FA] = SVCFALimits(NSVC,FA,FALo,FAHi);

    it = it + 1;

end

%Function to calculate injected bus powers by the SVC-FA
function [QCAL,B] = SVCFACalculatePower(QCAL,VM,NSVC,SVCsend,FA,...
Xc,Xl);
for ii = 1 : NSVC
    FA(ii) = FA(ii)*pi/180;
```

```

B(ii) = (2*(pi-FA(ii)) + sin(2*FA(ii)))*Xc(ii)/pi;
B(ii) = (Xl(ii) - B(ii))/(Xc(ii)*Xl(ii));

QCAL(SVCsend(ii))=QCAL(SVCsend(ii))-VM(SVCsend(ii))^2*B(ii);
end

%Function to add up the SVC-FA elements to Jacobian matrix function
[JAC] = SVCFAJacobian(JAC,VM,NSVC,SVCsend,FA,Xl,B,VSta);
for ii = 1 : NSVC
    if VSta(ii) == 1
        %Delete the voltage magnitud for the SVC bus
        JAC(:,2*SVCsend(ii))=0;
        % Element add by the SVC to the Jacobian
        FA(ii)=FA(ii)*pi/180;
        JAC(2*SVCsend(ii)-1,2*SVCsend(ii)-1) = JAC(2*SVCsend(ii)-1,2*...
        SVCsend(ii)-1) - VM(SVCsend(ii))^2*B(ii);
        JAC(2*SVCsend(ii),2*SVCsend(ii))= 2*VM(SVCsend(ii))^2*...
        (cos(2*FA(ii))-1)/(Xl(ii)*pi);
    end
end

%Function to update SVC-FA state variable
function[VM,FA]=SVCFAUpdating(VM,D,NSVC,SVCsend,FA,FALo,FAHi,...
TarVol,VSta);
for ii = 1 : NSVC
    if (VSta(ii) == 1)
        % Adjust the Volatge Magnitud target
        VM(SVCsend(ii)) = TarVol(ii);
        % Truncation
        value = D(2*SVCsend(ii));
        if (value > 0.5236)
            value = 0.5236;
        elseif (value < -0.5236)
            value = -0.5236;
        end
        FA(ii) = FA(ii) + value*180/pi;
        if (FA(ii)<0.0)
            FA(ii) = FA(ii)*(-1);
        end
    end
end

%Function to check the firing angle limits
function [FA] = SVCFALimits(NSVC,FA,FALo,FAHi);
%Check SVC-FA Limits
for ii = 1 : NSVC
    if (FA(ii) > FAHi(ii))

```

```

    FA(ii) = FAHi(ii);
elseif (FA(ii) < FALo(ii))
    FA(ii) = FALo(ii);
end
end

%Function to calculate the reactive power in SVC
function [Q SVC, B] = SVCFAQpower(VM, NSVC, SVCsend, FA, Xc, Xl);
for ii = 1 : NSVC
    FA(ii) = FA(ii)*pi/180;
    B(ii) = (2*(pi-FA(ii)) + sin(2*FA(ii)))*Xc(ii)/pi;
    B(ii) = (Xl(ii) - B(ii))/(Xc(ii)*Xl(ii));
    Q SVC(ii)=-VM(SVCsend(ii))^2*B(ii);
end

```

### 5.3.6 Integrated Transformer Firing-angle Model

The SVC firing angle model is extended in this section to include the explicit representation of the step-down transformer (Fuerte-Esquivel, Acha, and Ambriz-Pérez, 2000a). Both components are combined to form a single model, which allows for direct voltage magnitude control at the high-voltage side of the transformer without compromising the quadratic convergence characteristics of the Newton–Raphson method.

The total admittance of the combined SVC–transformer set,  $Y_{T-SVC}$ , as seen from the high-voltage side of the transformer, consists of the series combination of admittances  $Y_T$  and  $Y_{SVC}$ , as shown schematically in Figure 5.6.

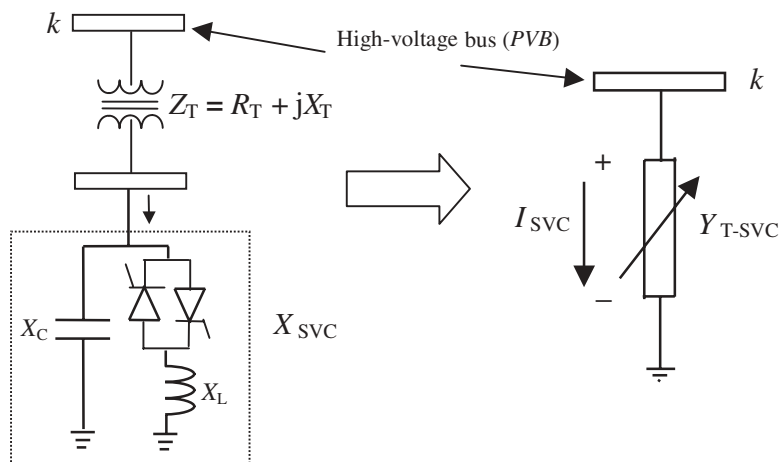


**Figure 5.6** Combined static VAR compensator–transformer representation. Reproduced, with permission, from C.R. Fuerte-Esquivel, E. Acha, and H. Ambriz-Pérez, ‘Integrated SVC and Step-down Transformer Model for Newton–Raphson Load Flow Studies’, *IEEE Power Engineering Review* 20(2) 45–46, © 2000 IEEE

It should be noted that the equivalent admittance,  $Y_{T-SVC}$ , is a function of the SVC firing angle:

$$Y_{T-SVC}(\alpha_{SVC}) = \frac{Y_T Y_{SVC}}{Y_T + Y_{SVC}}. \quad (5.11)$$

The admittance of the combined variable shunt compensator is given by

$$Y_{T-SVC} = G_{T-SVC} + jB_{T-SVC}, \quad (5.12)$$

where

$$G_{T-SVC} = \frac{R_T}{R_T^2 + X_{Eq}^2}, \quad (5.13)$$

$$B_{T-SVC} = -\frac{X_{Eq}}{R_T^2 + X_{Eq}^2}, \quad (5.14)$$

$$X_{Eq} = X_T + X_{SVC}, \quad (5.15)$$

$$X_{SVC} = \frac{X_C X_{TCR}}{X_C - X_{TCR}}, \quad (5.16)$$

$$X_{TCR} = \frac{\pi X_L}{2(\pi - \alpha_{SVC}) + \sin(2\alpha_{SVC})}. \quad (5.17)$$

The linearised power flow equations are given as

$$\begin{bmatrix} \Delta P_k \\ \Delta Q_k \end{bmatrix}^{(i)} = \begin{bmatrix} 0 & V_k^2 \frac{\partial G_{T-SVC}}{\partial \alpha_{SVC}} \\ 0 & -V_k^2 \frac{\partial B_{T-SVC}}{\partial \alpha_{SVC}} \end{bmatrix}^{(i)} \begin{bmatrix} \Delta \theta_k \\ \Delta \alpha_{SVC} \end{bmatrix}^{(i)}, \quad (5.18)$$

where the Jacobian terms in explicit form are:

$$\frac{\partial G_{T-SVC}}{\partial \alpha_{SVC}} = -\frac{R_T}{D^2} \frac{\partial D}{\partial \alpha_{SVC}}, \quad (5.19)$$

$$\frac{\partial B_{T-SVC}}{\partial \alpha_{SVC}} = \frac{1}{D_T^2} \left( -D \frac{\partial X_{SVC}}{\partial \alpha_{SVC}} + X_{Eq} \frac{\partial D}{\partial \alpha_{SVC}} \right), \quad (5.20)$$

$$\frac{\partial D}{\partial \alpha_{SVC}} = 2X_{Eq} \frac{\partial X_{SVC}}{\partial \alpha_{SVC}}, \quad (5.21)$$

$$\frac{\partial X_{SVC}}{\partial \alpha_{SVC}} = \frac{2X_{SVC}^2}{\pi X_L} (1 - \cos 2\alpha_{SVC}), \quad (5.22)$$

$$D = R_T^2 + X_{Eq}^2. \quad (5.23)$$

At the end of iteration  $(i)$ , the firing angle  $\alpha_{SVC}$  is updated according to

$$\alpha_{SVC}^{(i)} = \alpha_{SVC}^{(i-1)} + \Delta \alpha_{SVC}^{(i)}. \quad (5.24)$$

### 5.3.7 Nodal Voltage Magnitude Control using Static VAR Compensators

The SVC connecting bus is a voltage-controlled bus where the voltage magnitude and active and reactive powers are specified and either the SVC firing angle,  $\alpha_{SVC}$ , or the SVC

equivalent susceptance,  $B_{SVC}$ , are handled as state variables. This bus is defined to be *PVB*-type. If  $\alpha_{SVC}$  or  $B_{SVC}$  are within limits, the specified voltage magnitude is attained and the controlled bus remains *PVB*. However, if  $\alpha_{SVC}$  or  $B_{SVC}$  go outside the limits then these variables are fixed at the violated limit and the bus becomes *PQ*. This is, of course, in the absence of any other controller capable of providing reactive power control at the bus.

The reactive power mismatch values at the controlled buses are used to check whether or not the SVC is operating within limits, a process that starts just after the reactive power mismatch at the controlled bus is less than a specified tolerance; a value of  $1e-3$  p.u. is normally used.

### 5.3.8 Control Coordination between Reactive Sources

The use of different kinds of reactive power sources to control voltage magnitude at a given bus calls for a prioritisation of reactive power sources in order to have a single control criterion. Synchronous generators are normally selected to be the regulating plant components with the highest priority, holding all the other reactive power sources fixed at their initial values as long as the generators operate within limits. If all the generators connected to the bus violate their reactive power limits then other kinds of reactive power sources become activated (e.g. SVC). In such a case, the generators' reactive powers are set at their violated limits and the bus is transformed from *PV* to *PVB*. The control sequence is shown schematically in Figure 5.7.

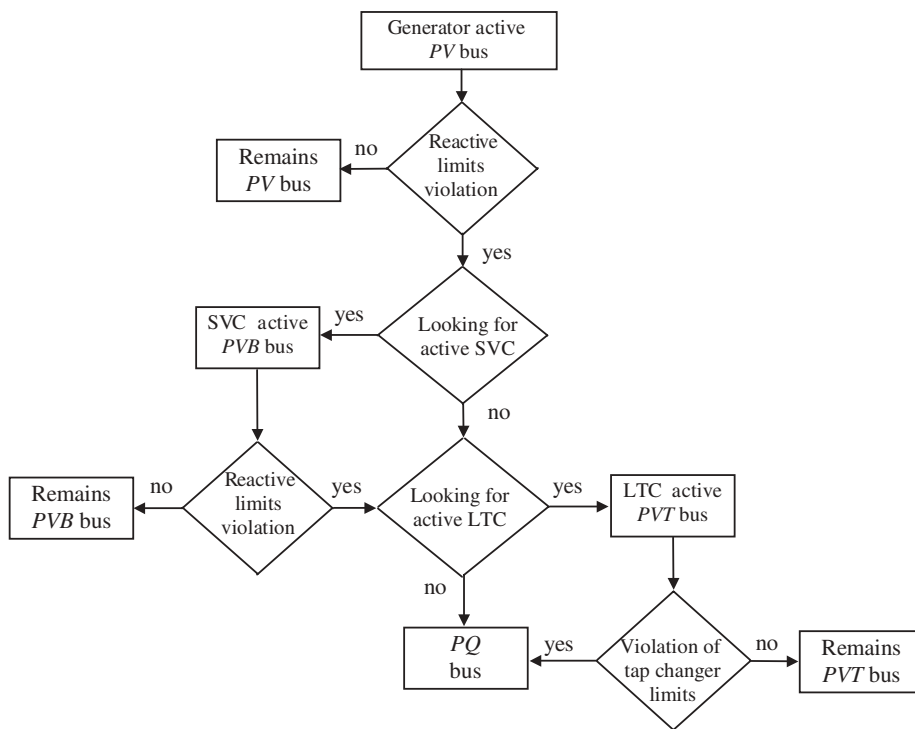


**Figure 5.7** Coordination between nodal voltage magnitude controllers. Note: LTC, load tap charger; SVC, static VAR compensator

### 5.3.9 Numerical Example of Voltage Magnitude Control using One Static VAR Compensator

The five-bus network (see Figure 5.8) is modified to examine the voltage-control capabilities of the SVC models. The generators are set to control voltage magnitudes at the Slack bus (North) and the PV bus (South) at 1.06 p.u. and 1 p.u., respectively. One SVC is placed at Lake to keep voltage magnitude at that bus at 1 p.u.

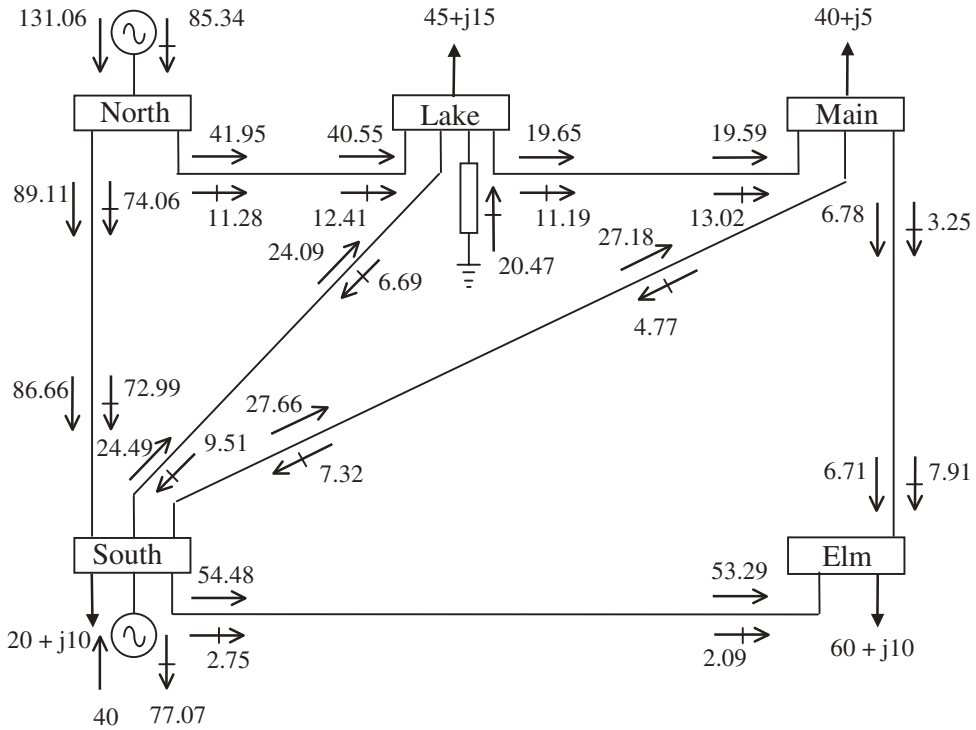


**Figure 5.8** Power flow results in the five-bus network with one static VAR compensator

In order to compare the various SVC models, three different power flow simulations are carried out. First, the SVC susceptance model is used to attain the specified voltage magnitude. The other two simulations are for the firing-angle model and for the integrated transformer–firing-angle model, respectively. The aim in all cases is to achieve 1 p.u. voltage magnitude at Lake.

The SVC inductive and capacitive reactances are taken to be 0.288 p.u. and 1.07 p.u., respectively. The SVC firing angle is set initially at 140°, a value that lies on the capacitive region of the SVC characteristic. The SVC transformer impedance is  $Z_T = j0.11$  p.u.

In all three cases, the SVC upholds its target value and, as expected, identical power flows and bus voltages are obtained. Power flows are shown in Figure 5.8, and nodal voltages are given in Table 5.1. Moreover, the three SVC models contribute the same amount of reactive power to the system.

**Table 5.1** Nodal voltages of modified network

Nodal voltage	Network bus				
	North	South	Lake	Main	Elm
Magnitude (p.u.)	1.06	1	1	0.994	0.975
Phase angle (deg)	0	-2.05	-4.83	-5.11	-5.80

Convergence is achieved in 5 iterations, satisfying a prespecified tolerance of  $1e-12$  for all the variables involved. The SVC susceptance values and firing-angle values are shown in Table 5.2 for each step of the iterative process. It should be noted that the final firing-angle solutions for the firing-angle model and the combined transformer-firing-angle model differ slightly because of the inclusion of the reactance of the transformer in the latter model.

**Table 5.2** Static VAR compensator state variables

Iteration	Susceptance model	Firing-angle model		Transformer-firing angle model	
	$B_{SVC}$ (p.u.)	$B_{SVC}$ (p.u.)	$\alpha_{SVC}$ (deg)	$B_{SVC}$ (p.u.)	$\alpha_{T-SVC}$ (deg)
1	0.1	0.4798	140	0.5066	140
2	0.1679	0.1038	130.23	0.1166	130.48
3	0.2047	0.2013	132.47	0.2029	132.40
4	0.2047	0.2047	132.55	0.2047	132.44
5	0.2047	0.2047	132.55	0.2047	132.44

The SVC data for both variable shunt susceptance and firing angle are given in function `SVCBData` and `SVCFAData`, respectively; function `PowerFlowsData` remains as the original:

Function `SVCBData` is as follows:

```
%This function is used exclusively to enter data for:
% STATIC VAR COMPENSATION
% VARIABLE SHUNT SUSCEPTANCE MODEL

% NSVC : Number of SVC's
% SVCsend : Compensated bus
% B : Initial SVC's susceptance value (p.u.)
% BLo : Lower limit of variable susceptance (p.u.)
% BHi : Higher limit of variable susceptance (p.u.)
% TarVol : Target nodal voltage magnitude to be controlled by SVC (p.u.)
% VSta : Indicate control status for nodal voltage magnitude: 1 is on and 0
% is off

NSVC=1;
SVCsend(1)=3; B(1)=0.02; BLo(1)=-0.25; BHi=0.25;
TarVol(1)=1.0; VSta(1)=1;
```

Function SVCFADData is as follows:

```
%This function is used exclusively to enter data for:
% STATIC VAR COMPENSATION
% FIRING ANGLE MODEL

% NSVC : Number of SVC's
% SVCsend : Compensated bus
% Xc : Capacitive reactance (p.u.)
% Xl : Inductive reactance (p.u.)
% FA : Initial SVC's firing angle value (Deg)
% FALo : Lower limit of firing angle (Deg)
% BHi : Higher limit of firing angle (Deg)
% TarVol : Target nodal voltage magnitude to be controlled by SVC (p.u.)
% VSta : Indicate the status to get control over voltage magnitude nodal : 1
% is on; 0 is off

NSVC=1;
SVCsend(1)=3; Xc(1)=1.07; Xl(1)=0.288; FA(1)=140; FALo(1)=90;
FAHi(1)=180; TarVol(1)=1.0; VSta(1)=1;
```

The SVC injects 20.5 MVAR into Lake and keeps the nodal voltage magnitude at 1 p.u. The action of the SVC results in an overall improved voltage profile. The SVC generates reactive power in excess of the local demand, which stands at 15 MVAR and, compared with the base case, there is an almost fourfold export increase of reactive power to Main. Also, there is an export of reactive power to South via transmission line Lake–South, with the larger amount of reactive power available at the bus being absorbed by the synchronous generator. It draws 77.1 MVAR as opposed to 61.59 MVAR in the base case.

## 5.4 THYRISTOR-CONTROLLED SERIES COMPENSATOR

Two alternative power flow models to assess the impact of TCSC equipment in network-wide applications are presented in this section (Ambriz-Pérez, Acha, and Fuerte-Esquivel, 2000; Fuerte-Esquivel and Acha, 1996). The simpler TCSC model exploits the concept of a *variable series reactance*. The series reactance is adjusted automatically, within limits, to satisfy a specified amount of active power flows through it. The more advanced model uses directly the TCSC reactance–firing-angle characteristic, given in the form of a nonlinear relation. The TCSC firing angle is chosen to be the state variable in the Newton–Raphson power flow solution.

### 5.4.1 Variable Series Impedance Power Flow Model

The TCSC power flow model presented in this section is based on the simple concept of a variable series reactance, the value of which is adjusted automatically to constrain the power flow across the branch to a specified value. The amount of reactance is determined efficiently using Newton's method. The changing reactance  $X_{TCSC}$ , shown in Figures 5.9(a) and 5.9(b), represents the equivalent reactance of all the series-connected modules making up the TCSC, when operating in either the inductive or the capacitive regions.



**Figure 5.9** Thyristor-controlled series compensator equivalent circuit: (a) inductive and (b) capacitive operative regions

The transfer admittance matrix of the variable series compensator shown in Figure 5.9 is given by

$$\begin{bmatrix} I_k \\ I_m \end{bmatrix} = \begin{bmatrix} jB_{kk} & jB_{km} \\ jB_{mk} & jB_{mm} \end{bmatrix} \begin{bmatrix} V_k \\ V_m \end{bmatrix}. \tag{5.25}$$

For inductive operation, we have

$$\left. \begin{aligned} B_{kk} = B_{mm} &= -\frac{1}{X_{TCSC}}, \\ B_{km} = B_{mk} &= \frac{1}{X_{TCSC}}, \end{aligned} \right\} \tag{5.26}$$

and for capacitive operation the signs are reversed.

The active and reactive power equations at bus  $k$  are:

$$P_k = V_k V_m B_{km} \sin(\theta_k - \theta_m), \tag{5.27}$$

$$Q_k = -V_k^2 B_{kk} - V_k V_m B_{km} \cos(\theta_k - \theta_m). \tag{5.28}$$

For the power equations at bus  $m$ , the subscripts  $k$  and  $m$  are exchanged in Equations (5.27) and (5.28).

In Newton–Raphson solutions these equations are linearised with respect to the series reactance. For the condition shown in Figure 5.9, where the series reactance regulates the amount of active power flowing from bus  $k$  to bus  $m$  at a value  $P_{km}^{reg}$ , the set of linearised power flow equations is:

$$\begin{bmatrix} \Delta P_k \\ \Delta P_m \\ \Delta Q_k \\ \Delta Q_m \\ \Delta P_{km}^{X_{TCSC}} \end{bmatrix} = \begin{bmatrix} \frac{\partial P_k}{\partial \theta_k} & \frac{\partial P_k}{\partial \theta_m} & \frac{\partial P_k}{\partial V_k} V_k & \frac{\partial P_k}{\partial V_m} V_m & \frac{\partial P_k}{\partial X_{TCSC}} X_{TCSC} \\ \frac{\partial P_m}{\partial \theta_k} & \frac{\partial P_m}{\partial \theta_m} & \frac{\partial P_m}{\partial V_k} V_k & \frac{\partial P_m}{\partial V_m} V_m & \frac{\partial P_m}{\partial X_{TCSC}} X_{TCSC} \\ \frac{\partial Q_k}{\partial \theta_k} & \frac{\partial Q_k}{\partial \theta_m} & \frac{\partial Q_k}{\partial V_k} V_k & \frac{\partial Q_k}{\partial V_m} V_m & \frac{\partial Q_k}{\partial X_{TCSC}} X_{TCSC} \\ \frac{\partial Q_m}{\partial \theta_k} & \frac{\partial Q_m}{\partial \theta_m} & \frac{\partial Q_m}{\partial V_k} V_k & \frac{\partial Q_m}{\partial V_m} V_m & \frac{\partial Q_m}{\partial X_{TCSC}} X_{TCSC} \\ \frac{\partial P_{km}^{X_{TCSC}}}{\partial \theta_k} & \frac{\partial P_{km}^{X_{TCSC}}}{\partial \theta_m} & \frac{\partial P_{km}^{X_{TCSC}}}{\partial V_k} V_k & \frac{\partial P_{km}^{X_{TCSC}}}{\partial V_m} V_m & \frac{\partial P_{km}^{X_{TCSC}}}{\partial X_{TCSC}} X_{TCSC} \end{bmatrix} \begin{bmatrix} \Delta \theta_k \\ \Delta \theta_m \\ \frac{\Delta V_k}{V_k} \\ \frac{\Delta V_m}{V_m} \\ \frac{\Delta X_{TCSC}}{X_{TCSC}} \end{bmatrix}, \tag{5.29}$$

where  $\Delta P_{km}^{X_{TCSC}}$

$$\Delta P_{km}^{X_{TCSC}} = P_{km}^{reg} - P_{km}^{X_{TCSC}, cal},$$

is the active power flow mismatch for the series reactance;  $\Delta X_{TCSC}$ , given by

$$\Delta X_{TCSC} = X_{TCSC}^{(i)} - X_{TCSC}^{(i-1)},$$

is the incremental change in series reactance; and  $P_{km}^{X_{TCSC}, cal}$  is the calculated power as given by Equation (5.27). The Jacobian elements for the series reactance are given in Appendix A, Section A.2.

The state variable  $X_{TCSC}$  of the series controller is updated at the end of each iterative step according to

$$X_{TCSC}^{(i)} = X_{TCSC}^{(i-1)} + \left( \frac{\Delta X_{TCSC}}{X_{TCSC}} \right)^{(i)} X_{TCSC}^{(i-1)}. \quad (5.30)$$

#### 5.4.2 Thyristor-controlled Series Compensator Computer Program in Matlab<sup>®</sup> Code

Program 5.3 incorporates the TCSC variable series reactance model within the Newton–Raphson power flow program. The functions `PowerFlowsData`, `YBus`, and `PQflows` are also used here. In the main TCSC Newton–Raphson program, the function `TCSCPowerFlowsData` is added to read the TCSC data, `TCSCNewtonRaphson` replaces `NewtonRaphson`, and `TCSCPQflows` is used to calculate power flows and losses in the TCSC model.

**PROGRAM 5.3** Program written in Matlab<sup>®</sup> to incorporate the thyristor-controlled series compensator (TCSC) variable reactance model within the Newton–Raphson power flow algorithm

```
% - - - Main TCSC variable reactance

PowerFlowsData; %Function to read network data

TCSCData; %Function to read TCSC variable series reactance

[YR, YI] = YBus(tlsend, tlrec, tlresis, tlreac, tlsuscep, tlcond, ntl, nbb);

[VM, VA, it, X] = TCSCNewtonRaphson(tol, itmax, ngn, nld, nbb, bustype, ...
genbus, loadbus, PGEN, QGEN, QMAX, QMIN, PLOAD, QLOAD, YR, ...
YI, VM, VA, NTCSC, TCSCsend, TCSCrec, X, XLo, XHi, Flow, Psp, PSta);
```

## 174 POWER FLOW INCLUDING FACTS CONTROLLERS

```
[PQsend,PQrec,PQloss,PQbus] = PQflows(nbb,ngn,ntl,nld,genbus,...  
loadbus,tlsend,tlrec,tlresis,tlreac,tlcond,tlsuscep,PLOAD,QLOAD,...  
VM,VA);
```

```
[Ptcsc,Qtcsc] = TCSCPQflows(nbb,VA,VM,NTCSC,TCSCsend,TCSCrec,X);
```

```
%Print results
```

```
it           %Number of iterations  
VM           %Nodal voltage magnitude (p.u)  
VA=VA*180/pi %Nodal voltage phase angles (Deg)  
Ptcsc       %Active power flow in TCSC (p.u.)  
Qtcsc       %Reactive power flow in TCSC (p.u.)  
X           %Final reactance value (p.u.)
```

```
%End of TCSC MAIN PROGRAM
```

```
%Carry out iterative solution using the Newton-Raphson method  
function [VM,VA,it,X] = TCSCNewtonRaphson(tol,itmax,ngn,nld,nbb,...  
bustype, genbus,loadbus,PGEN,QGEN,QMAX,QMIN,PLOAD,QLOAD,YR,YI,...  
VM,VA,NTCSC, TCSCsend,TCSCrec,X,XLo,XHi,Flow,Psp,PSta);
```

```
% GENERAL SETTINGS
```

```
flag = 0;  
it = 1;
```

```
% CALCULATE NET POWERS
```

```
[PNET,QNET]=NetPowers(nbb,ngn,nld,genbus,loadbus,PGEN,QGEN,...  
PLOAD,QLOAD);
```

```
while ( it < itmax & flag==0 )
```

```
    % CALCULATED POWERS
```

```
    [PCAL,QCAL]=CalculatedPowers(nbb,VM,VA,YR,YI);
```

```
    % CALCULATED TCSC POWERS
```

```
    [TCSC_PQsend,TCSC_PQrec,PCAL,QCAL]=TCSCCalculatedpower(nbb,VA,...  
VM,NTCSC,TCSCsend,TCSCrec,X,PCAL,QCAL);
```

```
    % POWER MISMATCHES
```

```
    [DPQ,DP,DQ,flag]=PowerMismatches(nbb,tol,bustype,flag,PNET,QNET,...  
PCAL,QCAL);
```

```

% TCSC POWER MISMATCHES
[DPQ,flag]=TCSCPowerMismatches(flag,tol,nbb,DPQ,VM,VA,NTCSC,...
TCSCsend,TCSCrec,X,Flow,it,Psp,PSta);

%Check for convergence
if flag == 1
    break
end

% JACOBIAN FORMATION
[JAC]=NewtonRaphsonJacobian(nbb,bustype,PCAL,QCAL,DPQ,VM,VA,...
YR,YI);

% MODIFICATION THE JACOBIAN FOR TCSC
[JAC]=TCSCJacobian(nbb,JAC,VM,VA,NTCSC,TCSCsend,TCSCrec,X,...
Flow,PSta,it);

% SOLVE JOCOBIAN
D = JAC\DPQ';
% UPDATE THE STATE VARIABLES VALUES, WITH TRUNCATED CORRECTIONS IF
% NECESSARY (VM increments < +-0.1 p.u. and VA inrements < +- 5 deg)
[VA,VM]=StateVariablesUpdating(nbb,D,VA,VM,it);

% UPDATE THE TCSC VARIABLES
[X]=TCSCUpdating(it,nbb,D,NTCSC,X,PSta);

%CHECK IMPEDANCE FOR LIMITS
[X]=TCSCLimits(NTCSC,X,XLo,XHi,PSta);

it = it + 1;
end

%Function to calculate injected bus powers by the TCSC
function [TCSC_PQsend,TCSC_PQrec,PCAL,QCAL] = TCSCCalculatedpower...
(nbb,VA, VM,NTCSC,TCSCsend,TCSCrec,X,PCAL,QCAL);
for ii = 1 : NTCSC
    Bmm = - 1/X(ii);
    Bmk = 1/X(ii);
    for kk = 1 : 2
        A = VA(TCSCsend(ii))-VA(TCSCrec(ii));
        Pcal = VM(TCSCsend(ii))*VM(TCSCrec(ii))*Bmk*sin(A);
        Qcal = - VM(TCSCsend(ii))^2*Bmm - VM(TCSCsend(ii))*...
VM(TCSCrec(ii))*Bmk*cos(A);
        PCAL(TCSCsend(ii)) = PCAL(TCSCsend(ii)) + Pcal;
        QCAL(TCSCsend(ii)) = QCAL(TCSCsend(ii)) + Qcal;
        if kk == 1
            TCSC_PQsend(ii) = Pcal + j*Qcal;
        end
    end
end

```

```

else
    TCSC_PQrec(ii) = Pcal + j*Qcal;
end
send = TCSCsend(ii);
TCSCsend(ii) = TCSCrec(ii);
TCSCrec(ii) = send;
end
end

%Function to compute power mismatches with TCSC
function [DPQ,flag] = TCSCPowerMismatches(flag,tol,nbb,DPQ,VM,VA,...
NTCSC, TCSCsend,TCSCrec,TCSCX,Flow,it,TCSC_P,PSta);
if it > 1
    for ii = 1 : NTCSC
        if PSta(ii) == 1
            Bmk = 1/TCSCX(ii);
            for kk = 1 : 2
                A = VA(TCSCsend(ii)) - VA(TCSCrec(ii));
                Pcal = VM(TCSCsend(ii))*VM(TCSCrec(ii))*Bmk*sin(A);
                if (Flow(ii) == 1 & kk == 1) | (Flow(ii) == -1 & kk == 2)
                    DPQ(1, 2*nbb + ii) = TCSC_P(ii) - Pcal;
                    break;
                end
                send = TCSCsend(ii);
                TCSCsend(ii) = TCSCrec(ii);
                TCSCrec(ii) = send;
            end
        else
            DPQ(1, 2*nbb + ii) = 0;
        end
    end
end
end

%Function to add the TCSC elements to Jacobian matrix
function [JAC] = TCSCJacobian(nbb,JAC,VM,VA,NTCSC,TCSCsend,...
TCSCrec,X,Flow, PSta,it);
for ii = 1 : NTCSC
    Bmm = - 1/X(ii);
    Bmk = 1/X(ii);
    for kk = 1 : 2
        A = VA(TCSCsend(ii))-VA(TCSCrec(ii));
        Hkm = - VM(TCSCsend(ii))*VM(TCSCrec(ii))*Bmm*cos(A);
        Nkm = VM(TCSCsend(ii))*VM(TCSCrec(ii))*Bmm*sin(A);

        JAC(2*TCSCsend(ii)-1, 2*TCSCsend(ii)-1) = JAC(2*TCSCsend(ii)-1,...
2*TCSCsend(ii)-1) - VM(TCSCsend(ii))^2*Bmm;
    end
end

```

```
JAC(2*TCSCsend(ii)-1, 2*TCSCrec(ii)-1) = JAC(2*TCSCsend(ii)-1,...
2*TCSCrec(ii)-1) - Hkm;
JAC(2*TCSCsend(ii)-1, 2*TCSCrec(ii)) = JAC(2*TCSCsend(ii)-1,...
2*TCSCrec(ii)) - Nkm;
JAC(2*TCSCsend(ii), 2*TCSCsend(ii)) = JAC(2*TCSCsend(ii),...
2*TCSCsend(ii)) - VM(TCSCsend(ii))^2*Bmm;
JAC(2*TCSCsend(ii), 2*TCSCrec(ii)-1) = JAC(2*TCSCsend(ii),...
2*TCSCrec(ii)-1) + Nkm;
JAC(2*TCSCsend(ii), 2*TCSCrec(ii)) = JAC(2*TCSCsend(ii),...
2*TCSCrec(ii)) - Hkm;
if it > 1
    if PSta(ii) == 1
        if (Flow(ii) == 1 & kk == 1) | (Flow(ii) == -1 & kk == 2)
            JAC(2*nbb + ii, 2*TCSCsend(ii)-1) = Hkm;
            JAC(2*nbb + ii, 2*TCSCsend(ii)) = - Nkm;
            JAC(2*nbb + ii, 2*TCSCrec(ii)-1) = - Hkm;
            JAC(2*nbb + ii, 2*TCSCrec(ii)) = - Nkm;
            JAC(2*nbb + ii, 2*nbb + ii) = + Nkm;
        end
        JAC(2*TCSCsend(ii)-1, 2*nbb + ii) = Nkm;
        JAC(2*TCSCsend(ii), 2*nbb + ii) = Hkm - VM(TCSCsend(ii))^2*Bmk;
    else
        JAC(2*nbb + ii, 2*nbb + ii) = 1;
    end
end
send = TCSCsend(ii);
TCSCsend(ii) = TCSCrec(ii);
TCSCrec(ii) = send;
end
end
```

```
%Function to update TCSC state variable
function [X]= TCSCUpdating(it,nbb,D,NTCSC,X,PSta);
if it > 1
    for ii = 1 : NTCSC
        if PSta(ii) == 1
            X(ii) = X(ii) + D(2*nbb + ii,1)*X(ii);
        end
    end
end
end
```

```
%Function to check the impedance limits
function [X] = TCSCLimits(NTCSC,X,XLo,XHi,PSta);
for ii = 1 : NTCSC
    % Check impedance Limits
    if X(ii) < XLo(ii) | X(ii) > XHi(ii)
```

```

PSta(ii) = 0;
if X(ii) < XLo(ii)
    X(ii) = XLo(ii);
elseif X(ii) > XHi(ii)
    X(ii) = XHi(ii);
end
end
end

%Function to calculate power flows in TCSC controller
function [Ptcsc,Qtcsc] = TCSCPQflows(nbb,VA,VM,NTCSC,TCSCsend,...
TCSCrec,TCSCX);
for ii = 1 : NTCSC
    Bmk = 1/TCSCX(ii);
    Bmm = -1/TCSCX(ii);
    for kk = 1 : 2
        A = VA(TCSCsend(ii)) - VA(TCSCrec(ii));
        Ptcsc(ii,kk) = VM(TCSCsend(ii))*VM(TCSCrec(ii))*Bmk*sin(A);
        Qtcsc(ii,kk) = - VM(TCSCsend(ii))^2*Bmm - M(TCSCsend(ii))*VM...
(TCSCrec(ii))*Bmk*cos(A);
        send = TCSCsend(ii);
        TCSCsend(ii) = TCSCrec(ii);
        TCSCrec(ii) = send;
    end
end
end

```

### 5.4.3 Numerical Example of Active Power Flow Control using One Thyristor-controlled Series Compensator: Variable Series Compensator Model

The original five-bus network is modified to include one TCSC to compensate the transmission line connected between Lake and Main. An extra bus, termed Lakefa, is used to connect the TCSC, as shown in Figure 5.10.

The TCSC is used to maintain active power flowing from Lakefa towards Main at 21 MW. The starting value of the TCSC is set at 50 % of the value of the transmission-line inductive reactance (i.e.  $X = 0.015$  p.u.). Convergence is obtained in 6 iterations to a power mismatch tolerance of  $1e-12$ . The TCSC upholds the target value of 21 MW, which is achieved with 70 % series capacitive compensation of the transmission line Lake–Main.

The power flow results are shown in Figure 5.10, and the nodal voltages are given in Table 5.3. As expected, nodal voltage magnitudes and reactive power flows do not change appreciably compared with the base case. It should be noticed that transmission line Lake–Main may not be the best candidate for series capacitive compensation since an increase of 8.2 % in active power has been achieved at the expense of 70 % compensation.

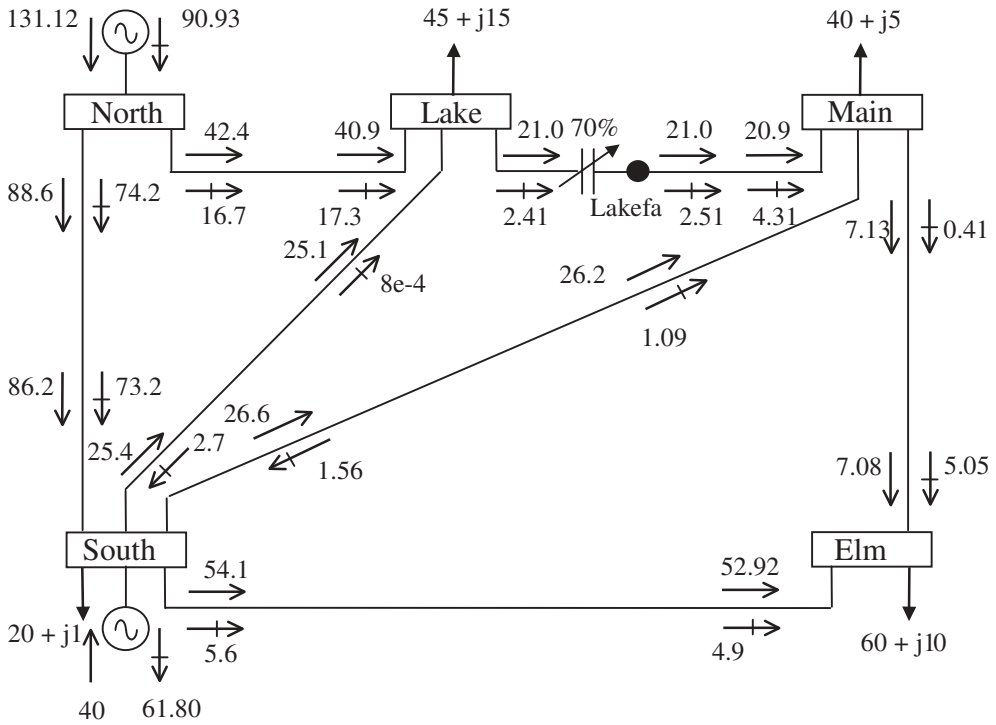


**Figure 5.10** Power flow results of the five-bus network with one thyristor-controlled series compensator

**Table 5.3** Bus voltages of the modified network

Nodal voltage	Network bus				
	North	South	Lake	Main	Elm
Magnitude (p.u.)	1.06	1	0.987	0.988	0.984
Phase angle (deg)	0	-2.04	-4.72	-4.46	-4.81

The data given in function `PowerFlowsData` (Section 4.3.9) is modified to accommodate the inclusion of the TCSC. The transmission line originally connected between Lake and Main is now connected between Lakefa (bus 6) and Main (bus 4). Only the modified code lines are shown here:

Function `PowerFlowsData` is as follows:

**%Modifications to enter data for the TCSC:**

```
nbb=6;
bustype(6)=3; VM(6)=1; VA(6)=0;
tlsend(6)=6; tlrec(6)=4; tlresis(6)=0.01; tlreac(6)=0.03;
tlcond(6)=0; tlsuscep6)=0.02;
```

Additionally, the function TCSCData is used for entering the TCSC data:

```
% This function is used exclusively to enter data for:
% THYRISTOR CONTROLLED SERIES COMPENSATOR reactance variable

% NTCSC : Number of TCSC's
% TCSCsend : Sending bus
% TCSCrec : Receiving bus
% X : TCSC's reactance
% XLo : Lower reactance limit
% XHi : Higher reactance limit
% Flow : Power flow direction: 1 is for sending to receiving bus; -1
% indicates opposite direction
% Psp : Active power flow to be controlled
% PSta : Indicates control status for active power: 1 is on and 0 is off

NTCSC=1;
TCSCsend(1)=3; TCSCrec(1)=6; X(1)=-0.015; XLo(1)=-0.05;
XHi(1)=0.05;
Flow(1)=1; Psp(1)=0.21; PSta(1)=1;
```

### 5.4.4 Firing-angle Power Flow Model

The model presented in Section 5.4.1 uses the concept of an equivalent series reactance to represent the TCSC. Once the value of reactance is determined using Newton's method then the associated firing angle  $\alpha_{TCSC}$  can be calculated. Of course, this makes engineering sense only in cases when all the modules making up the TCSC have identical design characteristics and are made to operate at equal firing angles. If this is the case, the computation of the firing angle is carried out. However, such calculation involves an iterative solution since the TCSC reactance and firing angle are nonlinearly related. One way to avoid the additional iterative process is to use the alternative TCSC power flow model presented in this section.

The fundamental frequency equivalent reactance  $X_{TCSC(1)}$  of the TCSC module shown in Figure 5.11 is (Fuerte-Esquivel, Acha, and Ambriz-Pérez, 2000):

$$X_{TCSC(1)} = -X_C + C_1\{2(\pi - \alpha) + \sin[2(\pi - \alpha)]\} - C_2 \cos^2(\pi - \alpha)\{\varpi \tan[\varpi(\pi - \alpha)] - \tan(\pi - \alpha)\}, \quad (5.31)$$

where

$$C_1 = \frac{X_C + X_{LC}}{\pi}, \quad (5.32)$$

$$C_2 = \frac{4X_{LC}^2}{X_L\pi}, \quad (5.33)$$

$$X_{LC} = \frac{X_C X_L}{X_C - X_L}, \quad (5.34)$$

$$\varpi = \left(\frac{X_C}{X_L}\right)^{1/2}. \quad (5.35)$$

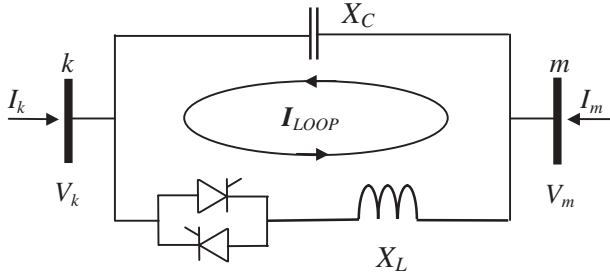


**Figure 5.11** Thyristor-controlled series compensator module. Reproduced, with permission, from C.R. Fuerte-Esquivel, E. Acha, and H. Ambriz-Pérez, 'A Thyristor Controlled Series Compensator Model for the Power Flow Solution of Practical Power Networks', *IEEE Trans. Power Systems* **15**(1) 58–64, © 2000 IEEE

The equivalent reactance  $X_{\text{TCSC}(1)}$  in Equation (5.31) replaces  $X_{\text{TCSC}}$  in Equations (5.26) and (5.25), and the TCSC active and reactive power equations at bus  $k$  are

$$P_k = V_k V_m B_{km}(f_1) \sin(\theta_k - \theta_m), \quad (5.36)$$

$$Q_k = -V_k^2 B_{kk}(f_1) - V_k V_m B_{km}(f_1) \cos(\theta_k - \theta_m), \quad (5.37)$$

where

$$B_{kk(1)} = -B_{km(1)} = B_{\text{TCSC}(1)}. \quad (5.38)$$

For equations at bus  $m$ , exchange subscripts  $k$  and  $m$  in Equations (5.36) and (5.37).

For the case when the TCSC controls active power flowing from bus  $k$  to bus  $m$ , at a specified value, the set of linearised power flow equations is:

$$\begin{bmatrix} \Delta P_k \\ \Delta P_m \\ \Delta Q_k \\ \Delta Q_m \\ \Delta P_{km}^{\alpha\text{TCSC}} \end{bmatrix} = \begin{bmatrix} \frac{\partial P_k}{\partial \theta_k} & \frac{\partial P_k}{\partial \theta_m} & \frac{\partial P_k}{\partial V_k} V_k & \frac{\partial P_k}{\partial V_m} V_m & \frac{\partial P_k}{\partial \alpha} \\ \frac{\partial P_m}{\partial \theta_k} & \frac{\partial P_m}{\partial \theta_m} & \frac{\partial P_m}{\partial V_k} V_k & \frac{\partial P_m}{\partial V_m} V_m & \frac{\partial P_m}{\partial \alpha} \\ \frac{\partial Q_k}{\partial \theta_k} & \frac{\partial Q_k}{\partial \theta_m} & \frac{\partial Q_k}{\partial V_k} V_k & \frac{\partial Q_k}{\partial V_m} V_m & \frac{\partial Q_k}{\partial \alpha} \\ \frac{\partial Q_m}{\partial \theta_k} & \frac{\partial Q_m}{\partial \theta_m} & \frac{\partial Q_m}{\partial V_k} V_k & \frac{\partial Q_m}{\partial V_m} V_m & \frac{\partial Q_m}{\partial \alpha} \\ \frac{\partial P_{km}^{\alpha\text{TCSC}}}{\partial \theta_k} & \frac{\partial P_{km}^{\alpha\text{TCSC}}}{\partial \theta_m} & \frac{\partial P_{km}^{\alpha\text{TCSC}}}{\partial V_k} V_k & \frac{\partial P_{km}^{\alpha\text{TCSC}}}{\partial V_m} V_m & \frac{\partial P_{km}^{\alpha\text{TCSC}}}{\partial \alpha\text{TCSC}} \end{bmatrix} \begin{bmatrix} \Delta \theta_k \\ \Delta \theta_m \\ \frac{\Delta V_k}{V_k} \\ \frac{\Delta V_m}{V_m} \\ \Delta \alpha\text{TCSC} \end{bmatrix}, \quad (5.39)$$

where  $\Delta P_{km}^{\alpha\text{TCSC}}$ , given by

$$\Delta P_{km}^{\alpha\text{TCSC}} = P_{km}^{\text{reg}} - P_{km}^{\alpha\text{TCSC}, \text{cal}},$$

is the active power flow mismatch for the TCSC module;  $\Delta\alpha_{\text{TCSC}}$ , given by

$$\Delta\alpha_{\text{TCSC}} = \alpha_{\text{TCSC}}^{(i+1)} - \alpha_{\text{TCSC}}^{(i)},$$

is the incremental change in the TCSC firing angle at the  $i$ th iteration; and  $P_{km}^{\alpha_{\text{TCSC}}, \text{cal}}$  is the calculated power as given by Equation (5.36). The Jacobian elements for the series reactance, as a function of the firing angle  $\alpha_{\text{TCSC}}$ , are given in Appendix A, Section A.2.

#### 5.4.5 Thyristor-controlled Series Compensator Firing-angle Computer Program in Matlab<sup>®</sup> Code

Program 5.4 incorporates the thyristor-controlled series compensator firing-angle (TCSC-FA) variable series reactance model within the Newton–Raphson power flow program. The functions PowerFlowsData, YBus, and PQflows are also used here. In the main TCSC-FA Newton–Raphson program, the function TCSCFAData is added to read the TCSC-FA data, TCSCFANewtonRaphson replaces NewtonRaphson, and TCSCFAPQflows is used to calculate power flows and losses in the TCSC model.

PROGRAM 5.4 Program written in Matlab<sup>®</sup> to incorporate the thyristor-controlled series compensator firing-angle (TCSC-FA) model within the Newton–Raphson power flow algorithm

```
% - - - Main TCSC-FA Program

PowerFlowsData; %Function to read network data

TCSCFAData; % Function to read TCSC-FA data

[YR, YI]=YBus(tlsend, tlrec, tlresis, tlreac, tlsuscep, tlcond, ntl, nbb);

[VM, VA, it, FA, X]=TCSCFANewtonRaphson(tol, itmax, ngn, nld, nbb, ...
bustype, genbus, loadbus, PGEN, QGEN, QMAX, QMIN, PLOAD, QLOAD, YR, YI, VM, ...
VA, NTCSCFA, TCSCFAsend, TCSCFArec, Xc, Xl, FA, FALo, FAHi, Flow, PSta, Psp);

[PQsend, PQrec, PQloss, PQbus]=PQflows(nbb, ngn, ntl, nld, genbus, ...
loadbus, tlsend, tlrec, tlresis, tlreac, tlcond, tlsuscep, PLOAD, QLOAD, ...
VM, VA);

[Ptcsc, Qtcsc]=TCSCPQpower(VA, VM, NTCSCFA, TCSCFAsend, TCSCFArec, X);

%Print results
it           %Number of iterations
VM           %Nodal voltage magnitude (p.u)
VA=VA*180/pi %Nodal voltage phase angles (deg)
Ptcsc       %Active power flow in TCSC (p.u.)
Qtcsc       %Reactive power flow in TCSC (p.u.)
X           %Final reactance value (p.u.)
FA         %Final firing angle value (deg)

% End of MAIN TCSC-FA PROGRAM
```

```

%Carry out iterative solution using the Newton–Raphson method
[VM,VA,it,FA,X] = TCSCFANewtonRaphson(tol,itmax,ngn,nld,nbb,...
bustype,genbus,loadbus,PGEN,QGEN,QMAX,QMIN,PLOAD,QLOAD,YR,YI,VM,...
VA,NTCSCFA,TCSCFAsend,TCSCFArec,Xc,Xl,FA,FALo,FAHi,Flow,PSta,Psp);

% GENERAL SETTINGS

flag = 0;
it = 1;

% CALCULATE NET POWERS
[PNET,QNET]=NetPowers(nbb,ngn,nld,genbus,loadbus,PGEN,QGEN,...
PLOAD,QLOAD);

while ( it < itmax & flag==0 )

    % CALCULATED POWERS
    [PCAL,QCAL]=CalculatedPowers(nbb,VM,VA,YR,YI);

    %TCSC CALCULATED POWER
    [PCAL,QCAL,X]=TCSCFACalculatePower(PCAL,QCAL,VM,VA,NTCSCFA,...
TCSCFAsend,TCSCFArec,FA,Xc,Xl,Flow,PSta,Psp);

    % POWER MISMATCHES
    [DPQ,DP,DQ,flag]=PowerMismatches(nbb,tol,bustype,flag,PNET,QNET,...
PCAL,QCAL);

    % TCSC POWER MISMATCHES
    [DPQ,flag]=TCSCFAPowerMismatches(flag,tol,nbb,DPQ,VM,VA,NTCSCFA,...
TCSCFAsend,TCSCFArec,X,Flow,it,Psp,PSta);

    %Check for convergence
    if flag == 1
        break
    end

    % JACOBIAN FORMATION
    [JAC]=NewtonRaphsonJacobian(nbb,bustype,PCAL,QCAL,DPQ,VM,VA,...
YR,YI);

    % MODIFICATION JACOBIAN FOR TCSC-FA -it calculates the TCSC
    % equivalent reactance
    [JAC]=TCS CFAJacobian(it,nbb,JAC,VM,VA,NTCSCFA,TCSCFAsend,...
TCSCFArec,FA,Xc,Xl,Flow,PSta,Psp,X);
    % SOLVE JOCOBIAN
    D = JAC\DPQ';

```

```

% UPDATE THE STATE VARIABLES VALUES, WITH TRUNCATED CORRECTIONS IF
% NECESSARY (VM increments < +-0.1 p.u. and VA increments < +- 5 deg)
[VA,VM] = StateVariablesUpdating(nbb,D,VA,VM,it);
% UPDATE THE TCSC-FA VARIABLES
[FA] = TCSCFAUpdating(it,nbb,D,NTCSCFA,FA,PSta);

%CHECK IMPEDANCE LIMITS
[FA] = TCSCFALimits(NTCSCFA,FA,FALo,FAHi,PSta);

it = it + 1;
end

```

```

%Function to calculate injected bus powers by TCSC-FA
function [PCAL,QCAL,X] = TCSCFACalculatePower(PCAL,QCAL,VM,VA,...
NTCSC,TCSCFAsend,TCSCFArec,FA,Xc,Xl,Flow,PSta,Psp);
for ii = 1 : NTCSC
    % Calculate Equivalent Reactance TCSCX
    Xlc = Xc(ii)*Xl(ii)/(Xc(ii)-Xl(ii));
    w = sqrt(Xc(ii)/Xl(ii));
    C1 = (Xc(ii) + Xlc)/pi;
    C2 = 4*Xlc^2/(Xl(ii)*pi);
    Ang = pi - FA(ii)*pi/180;

    X(ii) = -Xc(ii) + C1*(2*Ang + sin(2*Ang)) - C2*cos(Ang)^2*...
    (w*tan(w*Ang)-tan(Ang));

    Bmm = - 1/X(ii);
    Bmk = 1/X(ii);
    for kk = 1 : 2
        A = VA(TCSCFAsend(ii))-VA(TCSCFArec(ii));
        Pcal = VM(TCSCFAsend(ii))*VM(TCSCFArec(ii))*Bmk*sin(A);
        Qcal = - VM(TCSCFAsend(ii))^2*Bmm - VM(TCSCFAsend(ii))*VM...
        (TCSCFArec(ii))*Bmk*cos(A);
        PCAL(TCSCFAsend(ii)) = PCAL(TCSCFAsend(ii)) + Pcal;
        QCAL(TCSCFAsend(ii)) = QCAL(TCSCFAsend(ii)) + Qcal;
        if kk == 1
            TCSC_PQsend(ii) = Pcal + j*Qcal;
        else
            TCSC_PQrec(ii) = Pcal + j*Qcal;
        end
        send = TCSCFAsend(ii);
        TCSCFAsend(ii) = TCSCFArec(ii);
        TCSCFArec(ii) = send;
    end
end
end

```

```
%Function to compute power mismatches with TCSC-FA
function [DPQ,flag] = TCSCFAPowerMismatches(flag,tol,nbb,DPQ,VM,VA,...
NTCSCFA,TCSCFAsend,TCSCFArec,X,Flow,it,Psp,PSta);
if it > 1
    for ii = 1 : NTCSCFA
        if PSta(ii) == 1
            Bmk = 1/X(ii);
            for kk = 1 : 2
                A = VA(TCSCFAsend(ii)) - VA(TCSCFArec(ii));
                Pcal = VM(TCSCFAsend(ii))*VM(TCSCFArec(ii))*Bmk*sin(A);
                if ( Flow == 1 && kk == 1 ) | ( Flow == -1 && kk == 2 )
                    DPQ(1, 2*nbb + ii) = Psp(ii) - Pcal;
                    break;
                end
                send = TCSCFAsend(ii);
                TCSCFAsend(ii) = TCSCFArec(ii);
                TCSCFArec(ii) = send;
            end
        else
            DPQ(1, 2*nbb + ii) = 0;
        end
    end
end
end
```

```
%Function to add the TCSC-FA elements to Jacobian matrix
function [JAC] = TCSCFAJacobian(it,nbb,JAC,VM,VA,NTCSCFA,...
TCSCFAsend,TCSCFArec,FA,Xc,Xl,Flow,PSta,Psp,X);
for ii = 1 : NTCSCFA
    % Calculate Equivalent Reactance TCSCX
    Xlc = Xc(ii)*Xl(ii)/(Xc(ii)-Xl(ii));
    w = sqrt(Xc(ii)/Xl(ii));
    C1 = (Xc(ii) + Xlc)/pi;
    C2 = 4*Xlc^2/(Xl(ii)*pi);
    Ang = pi - FA(ii)*pi/180;

    TCSCX = -Xc(ii) + C1*(2*Ang + sin(2*Ang)) - C2*cos(Ang)^2*(w*tan...
(w*Ang)-tan(Ang));
```

```
%Calculate Reactance Derivative
A1 = FA(ii)*pi/180;
DTCSCX1 = - 2*C1*(1 + cos(2*Ang));
DTCSCX2 = C2*(w^2*(cos(Ang)^2/cos(w*Ang)^2));
DTCSCX3 = - C2*(w*tan(w*Ang)*sin(2*Ang));
DTCSCX4 = C2*(tan(Ang)*sin(2*Ang)-1);

DTCSCX = DTCSCX1 + DTCSCX2 + DTCSCX3 + DTCSCX4;
```

```

Bmm = - 1/TCSCX;
Bmk = 1/TCSCX;

for kk = 1 : 2
    A = VA(TCSCFAsend(ii))-VA(TCSCFArec(ii));
    Hkm = - VM(TCSCFAsend(ii))*VM(TCSCFArec(ii))*Bmm*cos(A);
    Nkm = VM(TCSCFAsend(ii))*VM(TCSCFArec(ii))*Bmm*sin(A);

    JAC(2*TCSCFAsend(ii)-1,2*TCSCFAsend(ii)-1) = JAC(2*TCSCFA...
    send(ii)-1,2*TCSCFAsend(ii)-1) - VM(TCSCFAsend(ii))^2*Bmm;
    JAC(2*TCSCFAsend(ii)-1,2*TCSCFArec(ii)-1) = JAC(2*TCSCFA...
    send(ii)-1,2*TCSCFArec(ii)-1) - Hkm;
    JAC(2*TCSCFAsend(ii)-1,2*TCSCFArec(ii)) = JAC(2*TCSCFA...
    send(ii)-1,2*TCSCFArec(ii)) - Nkm;
    JAC(2*TCSCFAsend(ii),2*TCSCFAsend(ii)) = JAC(2*TCSCFA...
    send(ii),2*TCSCFAsend(ii)) - VM(TCSCFAsend(ii))^2*Bmm;
    JAC(2*TCSCFAsend(ii),2*TCSCFArec(ii)-1) = JAC(2*TCSCFA...
    send(ii),2*TCSCFArec(ii)-1) + Nkm;
    JAC(2*TCSCFAsend(ii),2*TCSCFArec(ii)) = JAC(2*TCSCFA...
    send(ii),2*TCSCFArec(ii)) - Hkm;

    if it > 1
        if PSta(ii) == 1
            A = VA(TCSCFAsend(ii))-VA(TCSCFArec(ii));
            Ekm = -VM(TCSCFAsend(ii))*VM(TCSCFArec(ii))*sin(A)*Bmk^2*...
            DTSCSX;
            Fkm = - ((VM(TCSCFAsend(ii))^2 - VM(TCSCFAsend(ii))*VM...
            (TCSCFArec(ii))*cos(A))*Bmk^2*DTSCSX;
            if (Flow(ii) == 1 & kk == 1) | (Flow(ii) == -1 & kk == 2)
                Hkm = - VM(TCSCFAsend(ii))*VM(TCSCFArec(ii))*Bmk*cos(A);
                Nkm = VM(TCSCFAsend(ii))*VM(TCSCFArec(ii))*Bmk*sin(A);

                JAC(2*nbb + ii, 2*TCSCFAsend(ii)-1) = - Hkm;
                JAC(2*nbb + ii, 2*TCSCFAsend(ii)) = Nkm;
                JAC(2*nbb + ii, 2*TCSCFArec(ii)-1) = Hkm;
                JAC(2*nbb + ii, 2*TCSCFArec(ii)) = Nkm;
                JAC(2*nbb + ii, 2*nbb + ii) = Ekm;
            end
            JAC(2*TCSCFAsend(ii)-1, 2*nbb + ii) = Ekm;
            JAC(2*TCSCFAsend(ii), 2*nbb + ii) = Fkm;
        else
            JAC(2*nbb + ii, 2*nbb + ii) = 1;
        end
    end
end

```

```

    send = TCSCFAsend(ii);
    TCSCFAsend(ii) = TCSCFArec(ii);
    TCSCFArec(ii) = send;
end
end

%Function to update TCSC-FA state variables
function [FA] = TCSCFA_Updating(it,nbb,D,NTCSCFA,FA,PSta);
if it > 1
    for ii = 1 : NTCSCFA
        if PSta(ii) == 1
            FA(ii) = FA(ii) + D(2*nbb + ii,1)*180/pi;
        end
    end
end
end

%Function to calculate the power flows in TCSC-FA controller
function [PQTCSSEND,PQTCSCREC] = TCSCFPQpower(VA,VM,NTCSCFA,...
TCSCFAsend,TCSCFArec,X);
for ii = 1 : NTCSCFA
    Bmk = 1/X(ii);
    Bmm = -1/X(ii);
    for kk = 1 : 2
        A = VA(TCSCFAsend(ii)) - VA(TCSCFArec(ii));
        Ptcsc = VM(TCSCFAsend(ii))*VM(TCSCFArec(ii))*Bmk*sin(A);
        Qtcsc = - VM(TCSCFAsend(ii))^2*Bmm -...
M(TCSCFAsend(ii))*VM(TCSCFArec(ii))*Bmk*cos(A);
        if kk == 1
            PQTCSSEND(ii,kk) = Ptcsc + Qtcsc*i;
        else
            PQTCSCREC(ii,kk-1) = Ptcsc + Qtcsc*i;
        end
        send = TCSCFAsend(ii);
        TCSCFAsend(ii) = TCSCFArec(ii);
        TCSCFArec(ii) = send;
    end
end
end

```

#### 5.4.6 Numerical Example of Active Power Flow Control using One Thyristor-controlled Series Compensator: Firing-angle Model

Similar to the numerical example presented in Section 5.4.3, a TCSC is included in the five-bus network to compensate the transmission line connected between Lake and Main. The controller is used to maintain the active power flowing towards Main at 21 MW.

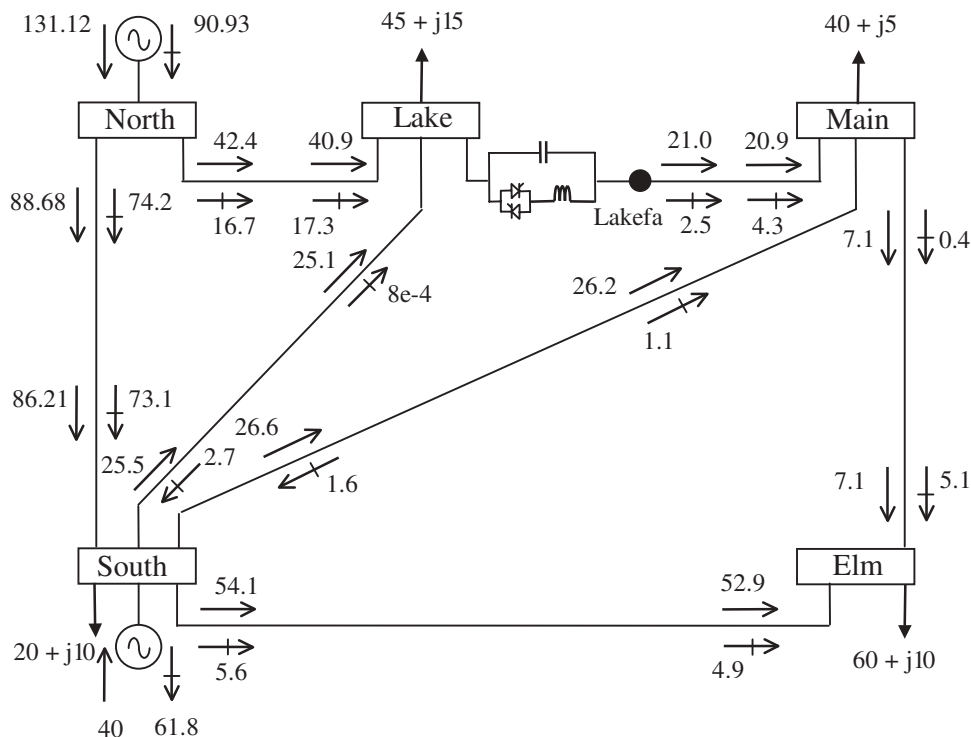


**Figure 5.12** Five-bus network with one thyristor-controlled series compensator, and power flow results

The initial value of firing angle is set at  $145^\circ$ , and convergence is obtained in 7 iterations to a power mismatch tolerance of  $1e-12$ . The TCSC upholds the target value of 21 MW. The power flow results are shown in Figure 5.12. As expected, the calculated TCSC equivalent reactances using the firing-angle model and the variable series reactance model agree with each other. Also, the nodal voltages are the same as those given in Table 5.3.

The maximum absolute power mismatches in the system buses and TCSC are shown in Figure 5.12. The TCSC characteristic is highly nonlinear, a fact that shows in the results in Table 5.4 where the nonquadratic convergent pattern of  $\Delta P$  and  $\Delta Q$  is evident, particularly up to the 4th iteration.

The data given in function `PowerFlowsData` (Section 4.3.9) are modified to accommodate for the inclusion of the TCSC-FA in the same way as described in Section 5.4.3. Additionally, the function `TCSCFAdata` is used for entering TCSC-FA model data:

```
% THYRISTOR CONTROLLED SERIES COMPENSATOR
% FIRING ANGLE MODEL

% NTCSCFA : Number of TCSC's
% TCSCFAend : Sending bus
```

```

% TCSCFArec : Receiving bus
% Xc : TCSC's reactance (p.u.)
% Xl : TCSC's inductance (p.u)
% FA : Initial firing angle (deg)
% FALo : Firing angle lower limit (deg)
% FAHi : Firing angle higher limit (deg)
% Flow : Power flow direction: 1 is for sending to receiving bus; -1
% indicates opposite direction
% Psp : Active power flow to be controlled (p.u.)
% PSta : Indicate the control status for active power: 1 is on; 0 is off

NTCSCFA=1;
TCSCFAsend(1)=3; TCSCFArec(1)=6; Xc(1)=9.375e-3; Xl(1)=1.625e-3;
FA(1)=145; FALo(1)=90; FAHi(1)=180;
Flow(1)=1; PSta(1)=1; Psp(1)=0.21;
    
```

**Table 5.4** Maximum absolute power mismatches in the system buses and thyristor-controlled series compensator (TCSC)

Iteration	Nodal power mismatches		TCSC mismatches and parameters		
	$\Delta P$	$\Delta Q$	$\Delta P_{km}^{\alpha_{TCSC}}$	$\alpha_{TCSC}$ (deg)	$X_{TCSC(f)}$ (p.u.)
1	6e-1	1.2e-1	2.1e-1	145	-0.0518
2	2.1e-2	1.6e-2	2e-2	145	-0.0518
3	7.8e-2	2.4e-3	7.8e-2	146.26	-0.0341
4	3.6e-3	7.7e-3	3.6e-3	148.46	-0.0222
5	1e-4	2.2e-4	1.1e-4	148.66	-0.0216
6	1.1e-8	4.3e-8	1.1e-8	148.66	-0.0216
7	1e-16	1e-16	1e-16	148.66	-0.0216

### 5.4.7 Numerical Properties of the Thyristor-controlled Series Compensator Power Flow Model

The performance of the TCSC mathematical model is affected by the number of internal resonant points exhibited by the TCSC in the range 90° to 180°. The resonant points (poles) of Equation (5.31) are determined by the following expression (Fuerte-Esquivel, Acha, and Ambriz-Pérez, 2000b):

$$\alpha_{TCSC} = \pi \left[ 1 - \frac{(2n - 1)\omega(LC)^{1/2}}{2} \right], \quad \text{where } n = 1, 2, 3, \dots \quad (5.40)$$

Although in theory a TCSC can have  $n$  resonant points, in practice a well-designed TCSC scheme will only have one resonant peak within its range of operation. By way of example, Figure 5.13 shows the fundamental frequency reactance as a function of  $\alpha_{TCSC}$  for the Kayenta TCSC installation. The rated inductive and capacitive reactances of this TCSC

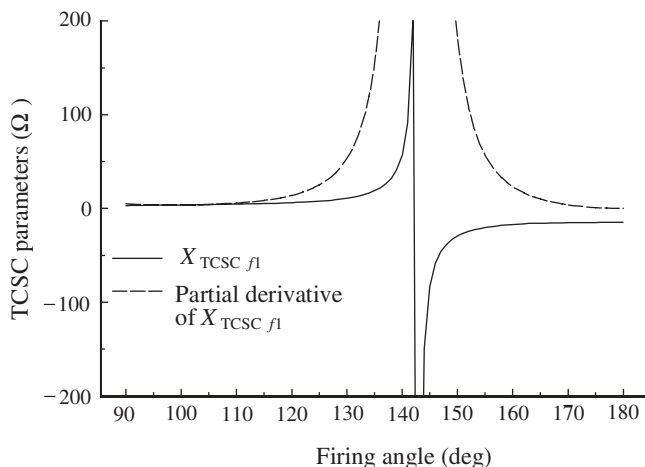


**Figure 5.13** Profiles of  $X_{TCSC(1)}$  and  $\partial X_{TCSC(1)}/\partial \alpha_{TCSC}$  as a function of firing angle,  $\alpha_{TCSC}$ . Reproduced, with permission, from C.R. Fuerte-Esquivel, E. Acha, and H. Ambriz-Pérez, 'A Thyristor Controlled Series Compensator Model for the Power Flow Solution of Practical Power Networks' *IEEE Trans. Power Systems* **15**(1) 58–64, © 2000 IEEE

are  $2.6\Omega$  and  $15\Omega$ , respectively, at a base frequency of 60Hz. The corresponding susceptance profile is shown in Figure 5.14. The partial derivatives of both parameters are also shown in these figures for completeness.

The TCSC exhibits a resonant point at  $\alpha_{TCSC} = 142.81^\circ$ , as shown in Figure 5.14. This pole defines the transition from the inductive to the capacitive operating region, as the firing angle value increases.

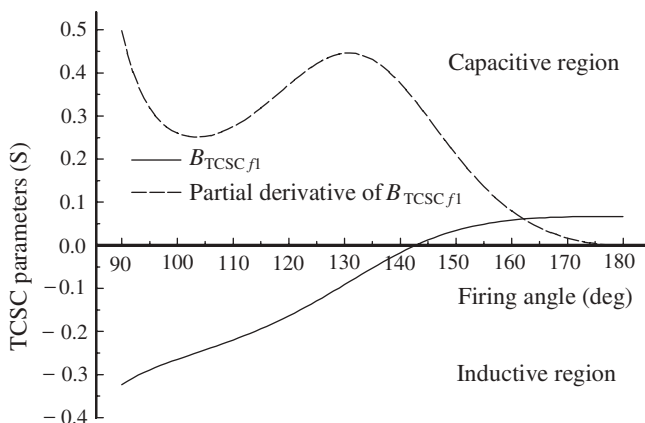


**Figure 5.14** Profiles of  $B_{TCSC(1)}$  and  $\partial B_{TCSC(1)}/\partial \alpha_{TCSC}$  as a function of firing angle. Reproduced, with permission, from C.R. Fuerte-Esquivel, E. Acha, and H. Ambriz-Pérez, 'A Thyristor Controlled Series Compensator Model for the Power Flow Solution of Practical Power Networks', *IEEE Trans. Power Systems* **15**(1) 58–64, © 2000 IEEE

It should be noted that both  $X_{TCSC(1)}$  and  $\partial X_{TCSC(1)} / \partial \alpha_{TCSC}$  present large variations in magnitude in response to small variations in firing angle near the resonant point. This intrinsic characteristic of the TCSC causes the power equations and Jacobian to be ill-conditioned if operation of the TCSC takes place too close to the resonant point.

### 5.5 STATIC SYNCHRONOUS COMPENSATOR

Following on the discussion of the STATCOM operational characteristics in Chapter 2, it is reasonable to expect that for the purpose of positive sequence power flow analysis the STATCOM will be well represented by a synchronous voltage source with maximum and minimum voltage magnitude limits. The synchronous voltage source represents the fundamental Fourier series component of the switched voltage waveform at the AC converter terminal of the STATCOM (Hingorani and Gyugyi, 2000; Song and Johns, 1999).

The bus at which the STATCOM is connected is represented as a *PVS* bus, which may change to a *PQ* bus in the event of limits being violated. In such a case, the generated or absorbed reactive power would correspond to the violated limit. Unlike the SVC, the STATCOM is represented as a voltage source for the full range of operation, enabling a more robust voltage support mechanism. The STATCOM equivalent circuit shown in Figure 5.15 is used to derive the mathematical model of the controller for inclusion in power flow algorithms.

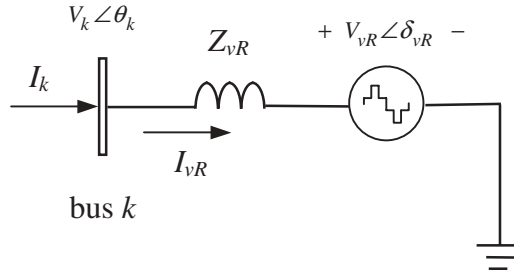


Figure 5.15 Static compensator (STATCOM) equivalent circuit

#### 5.5.1 Power Flow Model

The power flow equations for the STATCOM are derived below from first principles and assuming the following voltage source representation:

$$E_{vR} = V_{vR}(\cos \delta_{vR} + j \sin \delta_{vR}). \tag{5.41}$$

Based on the shunt connection shown in Figure 5.15, the following may be written:

$$S_{vR} = V_{vR} I_{vR}^* = V_{vR} Y_{vR}^* (V_{vR}^* - V_k^*). \tag{5.42}$$

After performing some complex operations, the following active and reactive power equations are obtained for the converter and bus  $k$ , respectively:

$$P_{vR} = V_{vR}^2 G_{vR} + V_{vR} V_k [G_{vR} \cos(\delta_{vR} - \theta_k) + B_{vR} \sin(\delta_{vR} - \theta_k)], \quad (5.43)$$

$$Q_{vR} = -V_{vR}^2 B_{vR} + V_{vR} V_k [G_{vR} \sin(\delta_{vR} - \theta_k) - B_{vR} \cos(\delta_{vR} - \theta_k)], \quad (5.44)$$

$$P_k = V_k^2 G_{vR} + V_k V_{vR} [G_{vR} \cos(\theta_k - \delta_{vR}) + B_{vR} \sin(\theta_k - \delta_{vR})], \quad (5.45)$$

$$Q_k = -V_k^2 B_{vR} + V_k V_{vR} [G_{vR} \sin(\theta_k - \delta_{vR}) - B_{vR} \cos(\theta_k - \delta_{vR})]. \quad (5.46)$$

Using these power equations, the linearised STATCOM model is given below, where the voltage magnitude  $V_{vR}$  and phase angle  $\delta_{vR}$  are taken to be the state variables:

$$\begin{bmatrix} \Delta P_k \\ \Delta Q_k \\ \Delta P_{vR} \\ \Delta Q_{vR} \end{bmatrix} = \begin{bmatrix} \frac{\partial P_k}{\partial \theta_k} & \frac{\partial P_k}{\partial V_k} V_k & \frac{\partial P_k}{\partial \delta_{vR}} & \frac{\partial P_k}{\partial V_{vR}} V_{vR} \\ \frac{\partial Q_k}{\partial \theta_k} & \frac{\partial Q_k}{\partial V_k} V_k & \frac{\partial Q_k}{\partial \delta_{vR}} & \frac{\partial Q_k}{\partial V_{vR}} V_{vR} \\ \frac{\partial P_{vR}}{\partial \theta_k} & \frac{\partial P_{vR}}{\partial V_k} V_k & \frac{\partial P_{vR}}{\partial \delta_{vR}} & \frac{\partial P_{vR}}{\partial V_{vR}} V_{vR} \\ \frac{\partial Q_{vR}}{\partial \theta_k} & \frac{\partial Q_{vR}}{\partial V_k} V_k & \frac{\partial Q_{vR}}{\partial \delta_{vR}} & \frac{\partial Q_{vR}}{\partial V_{vR}} V_{vR} \end{bmatrix} \begin{bmatrix} \Delta \theta_k \\ \frac{\Delta V_k}{V_k} \\ \Delta \delta_{vR} \\ \frac{\Delta V_{vR}}{V_{vR}} \end{bmatrix}. \quad (5.47)$$

The Jacobian elements in Equation (5.47) are given in explicit form in Appendix A, Section A.3.

### 5.5.2 Static Compensator Computer Program in Matlab® Code

Program 5.5 incorporates the STATCOM model within the Newton–Raphson power flow program. The functions `PowerFlowsData`, `YBus`, and `PQflows` are also used here. In the main STATCOM Newton–Raphson program, the function `SSCData` is added to read the STATCOM data, `SSCNewtonRaphson` replaces `NewtonRaphson`, and `SSCPQflows` is used to calculate power flows and losses in the STATCOM.

**PROGRAM 5.5** Program written in Matlab® to incorporate the static compensator (STATCOM) within the Newton–Raphson power flow algorithm

```
% - - - Main STATCOM Program

PowerFlowsData; %Function to read network data

SSCData; %Function to read the STATCOM data

[YR, YI] = YBus(tlsend, tlrec, tlresis, tlreac, tlsuscep, tlcond, ntl, nbb);
[VM, VA, it, Vvr, Tvr] = SSCNewtonRaphson(tol, itmax, ngn, nld, nbb, ...
bustype, genbus, loadbus, PGEN, QGEN, QMAX, QMIN, PLOAD, QLOAD, YR, YI, VM, ...
```

```

VA,NSSC,SSCsend, Xvr,TarVol,VSta,Psp,PSta,Qsp,QSta,Vvr,Tvr,VvrHi,...
VvrLo);
[PQsend,PQrec,PQloss,PQbus] = PQflows(nbb,ngn,ntl,nld,genbus,...
loadbus,tlsend,tlrec,tlresis,tlreac,tlcond,tlsuscep,PLOAD,QLOAD,...
VM,VA);

```

```

[Psend,Qsend,PSSC,QSSC] = SSCPQPowers(VM,VA,NSSC,SSCsend,Xvr,Vvr,...
Tvr);

```

```

%Print results
it                %Number of iterations
VM                %Nodal voltage magnitude (p.u)
VA=VA*180/pi      %Nodal voltage phase angles (Deg)
Vvr              %Final voltage magnitude source (p.u.)
Tvr=Tvr*180/pi   %Final voltage phase angle source (Deg)
PQsend=Psend + j*Qsend %Active and reactive powers in bus (p.u.)
PQSSC=PSSC + j*QSSC   %Active and reactive powers in STACOM (p.u.)

```

```

% End of MAIN STATCOM PROGRAM

```

```

%Carry out iterative solution using the Newton-Raphson method
[VM,VA,it,Vvr,Tvr] = SSCNewtonRaphson(tol,itmax,ngn,nld,nbb,...
bustype,genbus,loadbus,PGEN,QGEN,QMAX,QMIN,PLOAD,QLOAD,YR,YI,VM,...
VA,NSSC,SSCsend, Xvr,TarVol,VSta,Psp,PSta,Qsp,QSta,Vvr,Tvr,VvrHi,...
VvrLo);

```

```

% GENERAL SETTINGS
flag = 0;
it = 1;

```

```

% CALCULATE NET POWERS
[PNET,QNET] = NetPowers(nbb,ngn,nld,genbus,loadbus,PGEN,QGEN,...
PLOAD,QLOAD);

```

```

while ( it < itmax & flag==0 )

```

```

    % CALCULATED POWERS
    [PCAL,QCAL] = CalculatedPowers(nbb,VM,VA,YR,YI);

```

```

    %STATCOM CALCULATED POWERS
    [PCAL,QCAL,PSSC,QSSC] = SSCCalculatePowers(PCAL,QCAL,VM,VA,NSSC,...
SSCsend,Vxr,Vvr,Tvr);

```

POWER MISMATCHES

```
[DPQ,DP,DQ,flag] = PowerMismatches(nbb,tol,bustype,flag,PNET,QNET,...
PCAL,QCAL);
```

%STATCOM POWER MISMATCHES

```
[DPQ] = SSCMismatches(DPQ,nbb,VM,VA,NSSC,SSCsend,Xvr,VSta,Psp,...
PSta,Qsp,QSta,Vvr,Tvr);
```

% JACOBIAN FORMATION

```
[JAC] = NewtonRaphsonJacobian(nbb,bustype,PCAL,QCAL,DPQ,VM,VA,...
YR,YI);
```

% STATCOM JACOBIAN

```
[JAC] = SSCJacobian(nbb,JAC,VM,VA,NSSC,SSCsend,Xvr,TarVol,VSta,...
Psp,PSta,Qsp,QSta,Vvr,Tvr);
```

% SOLVE FOR THE STATE VARIABLES VECTOR

```
D = JAC\DPQ';
```

% UPDATE THE STATE VARIABLES VALUES, WITH TRUNCATED CORRECTIONS IF

% NECESSARY (VM increments < +0.1 p.u. and VA increments < +- 5 deg)

```
[VA,VM] = StateVariablesUpdating(nbb,D,VA,VM,it);
```

%UPDATE STATCOM STATE VARIABLES

```
[VM,Vvr,Tvr] = SSCUpdating(nbb,D,VM,VA,NSSC,SSCsend,TarVol,VSta,...
Psp,Vvr,Tvr);
```

%CHECK VOLTAGE MAGNITUDE LIMITS

```
[Vvr] = SSCLimits(NSSC,Vvr,VvrHi,VvrLo);
```

```
it = it + 1;
```

end

%Function to calculate injected bus powers by the STATCOM

```
function [PCAL,QCAL,PSSC,QSSC] = SSCCalculatePowers(PCAL,QCAL,VM,...
VA,NSSC,SSCsend,Xvr,Vvr,Tvr);
```

```
for ii = 1 : NSSC
```

```
    B(ii)=1/Xvr(ii);
```

```
    A1 = Tvr(ii)-VA(SSCsend(ii));
```

```
    A2 = VA(SSCsend(ii))-Tvr(ii);
```

```
    PCAL(SSCsend(ii)) = PCAL(SSCsend(ii)) + VM(SSCsend(ii))*Vvr(ii)*...
    (B(ii)*sin(A2));
```

```
    QCAL(SSCsend(ii)) = QCAL(SSCsend(ii)) + VM(SSCsend(ii))^2*B(ii) - ...
    Vvr(ii)*VM(SSCsend(ii))*(B(ii)*cos(A2));
```

```

PSSC(ii) = Vvr(ii)*VM(SSCsend(ii))*(B(ii)*sin(A1));
QSSC(ii) = - Vvr(ii)^2*B(ii) + Vvr(ii)*VM(SSCsend(ii))*(B(ii)...
*cos(A1));

end

```

```

%Function to compute power mismatches for the STATCOM
function [DPQ] = SSCMismatches(DPQ,nbb,VM,VA,NSSC,SSCsend,Xvr,...
VSta,Psp, PSta,Qsp,QSta,Vvr,Tvr);
for ii = 1 : NSSC
    B(ii)=1/Xvr(ii);
    A1 = Tvr(ii)-VA(SSCsend(ii));
    A2 = VA(SSCsend(ii))-Tvr(ii);

    Pcal = VM(SSCsend(ii))*Vvr(ii)*(B(ii)*sin(A2));
    Qcal = - VM(SSCsend(ii))^2*B(ii) + Vvr(ii)*VM(SSCsend(ii))*(B(ii)*...
cos(A2));

    DPQ(2*(nbb + ii)-1) = Pcal - Psp(ii);

```

```

    if (QSta(ii) == 1)
        DPQ(2*(nbb + ii)) = Qcal - Qsp(ii);
    else
        DPQ(2*(nbb + ii)) = 0;
    end
end

```

```

%Function to add the STATCOM elements to Jacobian matrix
function [JAC] = SSCJacobian(nbb,JAC,VM,VA,NSSC,SSCsend,Xvr,TarVol,...
VSta,Psp,PSta,Qsp,QSta,Vvr,Tvr);
for ii = 1 : NSSC
    B(ii)=1/Xvr(ii);
    if VSta(ii) == 1
        JAC(:, 2*SSCsend(ii) )=0;
    end
    JAC(2*(nbb + ii)-1,2*(nbb + ii)-1) = 1;
    JAC(2*(nbb + ii),2*(nbb + ii)) = 1;
    A1 = Tvr(ii)-VA(SSCsend(ii));
    A2 = VA(SSCsend(ii))-Tvr(ii);

    Pcal = - VM(SSCsend(ii))*Vvr(ii)*( + B(ii)*sin(A2));
    DQcal = Vvr(ii)*VM(SSCsend(ii))*(B(ii)*cos(A2));
    Pssc = - Vvr(ii)*VM(SSCsend(ii))*(B(ii)*sin(A1));
    DQssc = Vvr(ii)*VM(SSCsend(ii))*(B(ii)*cos(A1));

```

```

JAC(2*SSCsend(ii)-1,2*SSCsend(ii)-1) = JAC(2*SSCsend(ii)-1,...
2*SSCsend(ii)-1) + VM(SSCsend(ii))^2*B(ii);
JAC(2*SSCsend(ii),2*SSCsend(ii)-1) = JAC(2*SSCsend(ii),2*SSC...
send(ii)-1) - Pcal;
if (QSta(ii) == 1)
    JAC(2*SSCsend(ii)-1,2*SSCsend(ii)) = JAC(2*SSCsend(ii)-1,...
    2*SSCsend(ii)) - Pcal;
    JAC(2*SSCsend(ii),2*SSCsend(ii)) = JAC(2*SSCsend(ii),2*SSC...
    send(ii)) + VM(SSCsend(ii))^2*B(ii);
else
    JAC(2*SSCsend(ii)-1,2*SSCsend(ii)) = JAC(2*SSCsend(ii)-1,...
    2*SSCsend(ii)) - Pssc;
    JAC(2*SSCsend(ii),2*SSCsend(ii)) = JAC(2*SSCsend(ii),2*SSC...
    send(ii)) - DQssc;
end
if (PSta(ii) == 1)
    JAC(2*(nbb + ii)-1,2*SSCsend(ii)-1) = JAC(2*(nbb + ii)-1, 2*SSC...
    send(ii)-1) + DQcal;
    JAC(2*SSCsend(ii)-1,2*(nbb + ii)-1) = JAC(2*SSCsend(ii)-1,...
    2*(nbb + ii)-1) - DQssc;
    JAC(2*SSCsend(ii),2*(nbb + ii)-1) = JAC(2*SSCsend(ii),...
    2*(nbb + ii)-1) - Pssc;
    JAC(2*(nbb + ii)-1,2*(nbb + ii)-1) = - DQssc;
    if (QSta == 1)
        JAC(2*(nbb+ii),2*(nbb+ii)-1) = JAC(2*(nbb+ii),2*(nbb+ii)-1) - ...
        Pssc;
        JAC(2*(nbb + ii)-1,2*SSCsend(ii)) = JAC(2*(nbb + ii)-1,2*SSC...
        send(ii)) - Pcal;
    else
        JAC(2*(nbb + ii),2*(nbb + ii)-1) = 0.0;
        JAC(2*(nbb + ii)-1,2*SSCsend(ii)) = JAC(2*(nbb + ii)-1,2*SSC...
        send(ii)) + Pssc;
    end
else
    JAC(2*(nbb + ii)-1,2*(nbb + ii)-1) = 1.0;
end
if (QSta(ii) == 1)
    JAC(2*(nbb + ii),2*SSCsend(ii)-1) = JAC(2*(nbb + ii),2*SSCsend...
    (ii)-1) - Pcal;
    JAC(2*(nbb + ii),2*SSCsend(ii)) = JAC(2*(nbb + ii),2*SSCsend(ii))...
    + DQcal;
    JAC(2*SSCsend(ii)-1,2*(nbb + ii)) = JAC(2*SSCsend(ii)-1,2*...
    (nbb + ii)) + Pssc;
    JAC(2*SSCsend(ii),2*(nbb + ii)) = JAC((nbb + ii),2*...
    (nbb + ii)) - DQcal;
    JAC(2*(nbb + ii),2*(nbb + ii)) = -2*Vvr(ii)^2*B(ii) + DQssc;
if (PSta(ii) == 1)

```

```

    JAC(2*(nbb + ii)-1,2*(nbb + ii)) = JAC(2*(nbb + ii)-1,2*(nbb + ii)) - Pssc;
else
    JAC(2*(nbb + ii)-1,2*(nbb + ii)) = 0.0;
end
else
    JAC(2*(nbb + ii),2*(nbb + ii)) = 1.0;
end
end
end

```

```

%Function to update STATCOM state variable
function [VM,Vvr,Tvr] = SSCUpdating(nbb,D,VM,VA,NSSC,SSCsend,...
TarVol,VSta, Psp,Vvr,Tvr);
for ii = 1 : NSSC
    if (VSta(ii) == 1)
        % Adjust the Volatge Magnitud target
        Vvr(ii) = Vvr(ii) + Vvr(ii)*D(2*SSCsend(ii));
        VM(SSCsend(ii)) = TarVol(ii);
        if (Psp(ii) == 0)
            Tvr(ii) = VA(SSCsend(ii));
        else
            Tvr(ii) = Tvr(ii) + D(2*(nbb + ii)-1);
        end
    else
        Vvr(ii) = Vvr(ii) + Vvr(ii)*D(2*(nbb + ii));
        Tvr(ii) = VA(SSCsend(ii));
    end
end

```

```

%Function to check source voltages limits in the STATCOM
function [Vvr] = SSCLimits(NSSC,Vvr,VvrHi,VvrLo);
for ii = 1 : NSSC
    %Check STATCOM Vvr Limits
    if (Vvr(ii) > VvrHi(ii))
        Vvr(ii) = VvrHi(ii);
    elseif (Vvr(ii) < VvrLo(ii))
        Vvr(ii) = VvrLo(ii);
    end
end
end

```

```

%Function to calculate the power flows in the STATCOM
function [Psend,Qsend,PSSC,QSSC] = SSCPQPowers(VM,VA,NSSC,SSCsend,...
Xvr,Vvr,Tvr);
for ii = 1 : NSSC
    B(ii)=1/Xvr;
    A1 = Tvr(ii)-VA(SSCsend(ii));
    A2 = VA(SSCsend(ii))-Tvr(ii);

```

```

Psend(ii) = VM(SSCsend(ii))*Vvr(ii)*(B(ii)*sin(A2));
Qsend(ii) = - VM(SSCsend(ii))^2*B(ii) + Vvr(ii)*VM(SSCsend(ii))*...
(B(ii)*cos(A2));

PSSC(ii) = Vvr(ii)*VM(SSCsend(ii))*(B(ii)*sin(A1));
QSSC(ii) = - Vvr(ii)^2*B(ii) + Vvr(ii)*VM(SSCsend(ii))*(B(ii)*...
cos(A1));
end
    
```

### 5.5.3 Numerical Example of Voltage Magnitude Control using One Static Compensator

The five-bus network is modified to include one STATCOM connected at Lake, to maintain the nodal voltage magnitude at 1 p.u. The source impedance is  $X_{vR} = 0.1$  p.u. The power flow solution is shown in Figure 5.16 whereas the nodal voltage magnitudes and phase angles are given in Table 5.5. Convergence is achieved in five iterations to a power mismatch tolerance of  $1e-12$ . Function `SSCData` is used to enter STATCOM data, and function `PowerFlowsData` remain unchanged.

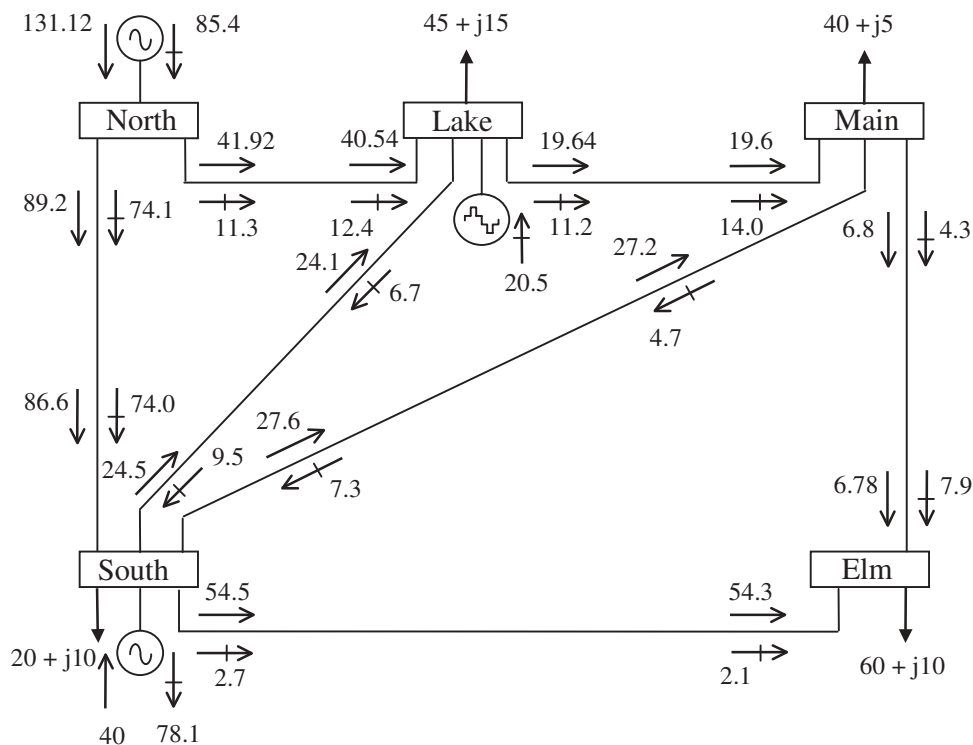


Figure 5.16 STATCOM-upgraded test network and power flow results

**Table 5.5** Bus voltages of the STATCOM-upgraded network

Nodal voltage	Network bus				
	North	South	Lake	Main	Elm
Magnitude (p.u.)	1.06	1	1	0.994	0.975
Phase angle (deg)	0	-2.05	-4.83	-5.11	-5.8

Function SSCData is as follows:

```
%This function is used exclusively to enter data for:
% STATIC SYNCHRONOUS COMPENSATOR (STATCOM)

% NSSC : Number of STATCOM's
% SSCsend: STATCOM's bus
% Xvr : Converter's reactance (p.u.)
% TarVol: Target nodal voltage magnitude (p.u.)
% VSta : Indicate the control status over nodal voltage magnitude: 1 is
% on; 0 is off
% Psp : Target active power flow (p.u.)
% PSta : Indicate the control status over active power: 1 is on; 0 is off
% Qsp : Target reactive power flow (p.u.)
% QSta : Indicate the control status over reactive power: 1 is on; 0 is off
% Vvr : Initial condition for the source voltage magnitude (p.u.)
% Tvr : Initial condition for the source voltage angle (deg)
% VvrHi : Lower limit source voltage magnitude (p.u.)
% VvrLo : higher limit source voltage magnitude (p.u.)

NSSC = 1;
SSCsend(1)=3; Xvr(1)=10; TarVol(1)=1.0; VSta(1)=1;
Psp(1)=0.0; PSta(1)=1; Qsp(1)=0.0; QSta(1)=0;
Vvr(1)=1.0; Tvr(1)=0.0; VvrHi(1)=1.1; VvrLo(1)=0.9;
```

The power flow result indicates that the STATCOM generates 20.5 MVAR in order to keep the voltage magnitude at 1 p.u. at Lake bus. The STATCOM parameters associated with this amount of reactive power generation are  $V_{vR} = 1.0205$  p.u. and  $\delta_{vR} = -4.83^\circ$ . Use of the STATCOM results in an improved network voltage profile, except at Elm, which is too far away from Lake to benefit from the influence of the STATCOM.

The slack generator reduces its reactive power generation by almost 6% compared with the base case, and the reactive power exported from North to Lake reduces by more than 30%. The largest reactive power flow takes place in the transmission line connecting North and South, where 74.1 MVAR leaves North and 74 MVAR arrives at South. In general, more reactive power is available in the network than in the base case, and the generator connected at South increases its share of reactive power absorption compared with the base case. As expected, active power flows are only marginally affected by the STATCOM installation.

### 5.6 UNIFIED POWER FLOW CONTROLLER

The basic principle of UPFC operation has been discussed in Chapter 2. It follows from that discussion that an equivalent circuit consisting of two coordinated synchronous voltage sources should represent the UPFC adequately for the purpose of fundamental frequency steady-state analysis. Such an equivalent circuit is shown in Figure 5.17. The synchronous voltage sources represent the fundamental Fourier series component of the switched voltage waveforms at the AC converter terminals of the UPFC (Hingorani and Gyugyi, 2000; Song and Johns, 1999).

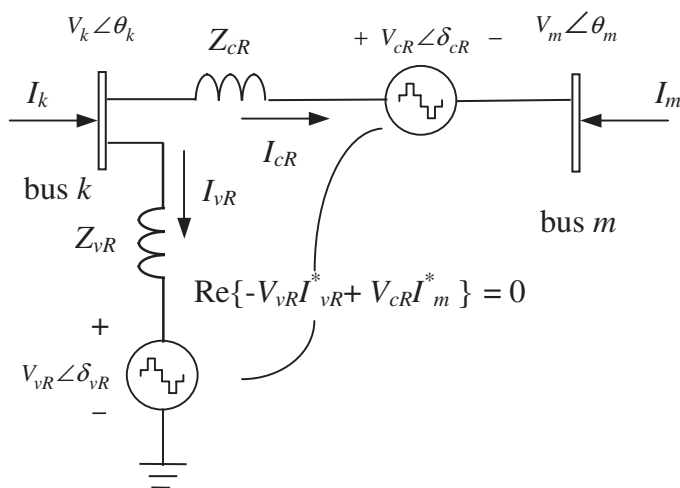


Figure 5.17 Unified power flow controller equivalent circuit

The UPFC voltage sources are:

$$E_{vR} = V_{vR}(\cos \delta_{vR} + j \sin \delta_{vR}), \tag{5.48}$$

$$E_{cR} = V_{cR}(\cos \delta_{cR} + j \sin \delta_{cR}), \tag{5.49}$$

where  $V_{vR}$  and  $\delta_{vR}$  are the controllable magnitude ( $V_{vR\min} \leq V_{vR} \leq V_{vR\max}$ ) and phase angle ( $0 \leq \delta_{vR} \leq 2\pi$ ) of the voltage source representing the shunt converter. The magnitude  $V_{cR}$  and phase angle  $\delta_{cR}$  of the voltage source representing the series converter are controlled between limits ( $V_{cR\min} \leq V_{cR} \leq V_{cR\max}$ ) and ( $0 \leq \delta_{cR} \leq 2\pi$ ), respectively.

The phase angle of the series-injected voltage determines the mode of power flow control. If  $\delta_{cR}$  is in phase with the nodal voltage angle  $\theta_k$ , the UPFC regulates the terminal voltage. If  $\delta_{cR}$  is in quadrature with respect to  $\theta_k$ , it controls active power flow, acting as a phase shifter. If  $\delta_{cR}$  is in quadrature with the line current angle then it controls active power flow, acting as a variable series compensator. At any other value of  $\delta_{cR}$ , the UPFC operates as a combination of voltage regulator, variable series compensator, and phase shifter. The magnitude of the series-injected voltage determines the amount of power flow to be controlled.

### 5.6.1 Power Flow Model

Based on the equivalent circuit shown in Figure 5.17 and Equations (5.48) and (5.49), the active and reactive power equations are (Fuerte-Esquivel and Acha, 1997; Fuerte-Esquivel, Acha, and Ambriz-Pérez, 2000c), at bus  $k$ :

$$\begin{aligned} P_k &= V_k^2 G_{kk} + V_k V_m [G_{km} \cos(\theta_k - \theta_m) + B_{km} \sin(\theta_k - \theta_m)] \\ &\quad + V_k V_{cR} [G_{km} \cos(\theta_k - \delta_{cR}) + B_{km} \sin(\theta_k - \delta_{cR})] \\ &\quad + V_k V_{vR} [G_{vR} \cos(\theta_k - \delta_{vR}) + B_{vR} \sin(\theta_k - \delta_{vR})], \end{aligned} \quad (5.50)$$

$$\begin{aligned} Q_k &= -V_k^2 B_{kk} + V_k V_m [G_{km} \sin(\theta_k - \theta_m) - B_{km} \cos(\theta_k - \theta_m)] \\ &\quad + V_k V_{cR} [G_{km} \sin(\theta_k - \delta_{cR}) - B_{km} \cos(\theta_k - \delta_{cR})] \\ &\quad + V_k V_{vR} [G_{vR} \sin(\theta_k - \delta_{vR}) - B_{vR} \cos(\theta_k - \delta_{vR})]; \end{aligned} \quad (5.51)$$

at bus  $m$ :

$$\begin{aligned} P_m &= V_m^2 G_{mm} + V_m V_k [G_{mk} \cos(\theta_m - \theta_k) + B_{mk} \sin(\theta_m - \theta_k)] \\ &\quad + V_m V_{cR} [G_{mm} \cos(\theta_m - \delta_{cR}) + B_{mm} \sin(\theta_m - \delta_{cR})], \end{aligned} \quad (5.52)$$

$$\begin{aligned} Q_m &= -V_m^2 B_{mm} + V_m V_k [G_{mk} \sin(\theta_m - \theta_k) - B_{mk} \cos(\theta_m - \theta_k)] \\ &\quad + V_m V_{cR} [G_{mm} \sin(\theta_m - \delta_{cR}) - B_{mm} \cos(\theta_m - \delta_{cR})]; \end{aligned} \quad (5.53)$$

series converter:

$$\begin{aligned} P_{cR} &= V_{cR}^2 G_{mm} + V_{cR} V_k [G_{km} \cos(\delta_{cR} - \theta_k) + B_{km} \sin(\delta_{cR} - \theta_k)] \\ &\quad + V_{cR} V_m [G_{mm} \cos(\delta_{cR} - \theta_m) + B_{mm} \sin(\delta_{cR} - \theta_m)], \end{aligned} \quad (5.54)$$

$$\begin{aligned} Q_{cR} &= -V_{cR}^2 B_{mm} + V_{cR} V_k [G_{km} \sin(\delta_{cR} - \theta_k) - B_{km} \cos(\delta_{cR} - \theta_k)] \\ &\quad + V_{cR} V_m [G_{mm} \sin(\delta_{cR} - \theta_m) - B_{mm} \cos(\delta_{cR} - \theta_m)]; \end{aligned} \quad (5.55)$$

shunt converter:

$$P_{vR} = -V_{vR}^2 G_{vR} + V_{vR} V_k [G_{vR} \cos(\delta_{vR} - \theta_k) + B_{vR} \sin(\delta_{vR} - \theta_k)], \quad (5.56)$$

$$Q_{vR} = V_{vR}^2 B_{vR} + V_{vR} V_k [G_{vR} \sin(\delta_{vR} - \theta_k) - B_{vR} \cos(\delta_{vR} - \theta_k)]. \quad (5.57)$$

Assuming loss-less converter valves, the active power supplied to the shunt converter,  $P_{vR}$ , equals the active power demanded by the series converter,  $P_{cR}$ ; that is,

$$P_{vR} + P_{cR} = 0. \quad (5.58)$$

Furthermore, if the coupling transformers are assumed to contain no resistance then the active power at bus  $k$  matches the active power at bus  $m$ . Accordingly,

$$P_{vR} + P_{cR} = P_k + P_m = 0. \quad (5.59)$$

The UPFC power equations, in linearised form, are combined with those of the AC network. For the case when the UPFC controls the following parameters: (1) voltage magnitude at the shunt converter terminal (bus  $k$ ), (2) active power flow from bus  $m$  to bus  $k$ , and (3) reactive

power injected at bus  $m$ , and taking bus  $m$  to be a  $PQ$  bus, the linearised system of equations is as follows:

$$\begin{bmatrix} \Delta P_k \\ \Delta P_m \\ \Delta Q_k \\ \Delta Q_m \\ \Delta P_{mk} \\ \Delta Q_{mk} \\ \Delta P_{bb} \end{bmatrix} = \begin{bmatrix} \frac{\partial P_k}{\partial \theta_k} & \frac{\partial P_k}{\partial \theta_m} & \frac{\partial P_k}{\partial V_{vR}} V_{vR} & \frac{\partial P_k}{\partial V_m} V_m & \frac{\partial P_k}{\partial \delta_{cR}} & \frac{\partial P_k}{\partial V_{cR}} V_{cR} & \frac{\partial P_k}{\partial \delta_{vR}} \\ \frac{\partial P_m}{\partial \theta_k} & \frac{\partial P_m}{\partial \theta_m} & 0 & \frac{\partial P_m}{\partial V_m} V_m & \frac{\partial P_m}{\partial \delta_{cR}} & \frac{\partial P_m}{\partial V_{cR}} V_{cR} & 0 \\ \frac{\partial Q_k}{\partial \theta_k} & \frac{\partial Q_k}{\partial \theta_m} & \frac{\partial Q_k}{\partial V_{vR}} V_{vR} & \frac{\partial Q_k}{\partial V_m} V_m & \frac{\partial Q_k}{\partial \delta_{cR}} & \frac{\partial Q_k}{\partial V_{cR}} V_{cR} & \frac{\partial Q_k}{\partial \delta_{vR}} \\ \frac{\partial Q_m}{\partial \theta_k} & \frac{\partial Q_m}{\partial \theta_m} & 0 & \frac{\partial Q_m}{\partial V_m} V_m & \frac{\partial Q_m}{\partial \delta_{cR}} & \frac{\partial Q_m}{\partial V_{cR}} V_{cR} & 0 \\ \frac{\partial P_{mk}}{\partial \theta_k} & \frac{\partial P_{mk}}{\partial \theta_m} & 0 & \frac{\partial P_{mk}}{\partial V_m} V_m & \frac{\partial P_{mk}}{\partial \delta_{cR}} & \frac{\partial P_{mk}}{\partial V_{cR}} V_{cR} & 0 \\ \frac{\partial Q_{mk}}{\partial \theta_k} & \frac{\partial Q_{mk}}{\partial \theta_m} & 0 & \frac{\partial Q_{mk}}{\partial V_m} V_m & \frac{\partial Q_{mk}}{\partial \delta_{cR}} & \frac{\partial Q_{mk}}{\partial V_{cR}} V_{cR} & 0 \\ \frac{\partial P_{bb}}{\partial \theta_k} & \frac{\partial P_{bb}}{\partial \theta_m} & \frac{\partial P_{bb}}{\partial V_{vR}} V_{vR} & \frac{\partial P_{bb}}{\partial V_m} V_m & \frac{\partial P_{bb}}{\partial \delta_{cR}} & \frac{\partial P_{bb}}{\partial V_{cR}} V_{cR} & \frac{\partial P_{bb}}{\partial \delta_{vR}} \end{bmatrix} \begin{bmatrix} \Delta \theta_k \\ \Delta \theta_m \\ \frac{\Delta V_{vR}}{V_{vR}} \\ \frac{\Delta V_m}{V_m} \\ \Delta \delta_{cR} \\ \frac{\Delta V_{cR}}{V_{cR}} \\ \Delta \delta_{vR} \end{bmatrix}, \tag{5.60}$$

where  $\Delta P_{bb}$  is the power mismatch given by Equation (5.58).

If voltage control at bus  $k$  is deactivated, the third column of Equation (5.60) is replaced by partial derivatives of the bus and UPFC mismatch powers with respect to the bus voltage magnitude  $V_k$ . Moreover, the voltage magnitude increment of the shunt source,  $\Delta V_{vR}/V_{vR}$  is replaced by the voltage magnitude increment at bus  $k$ ,  $\Delta V_k/V_k$ .

If both buses,  $k$  and  $m$ , are  $PQ$  the linearised system of equations is as follows:

$$\begin{bmatrix} \Delta P_k \\ \Delta P_m \\ \Delta Q_k \\ \Delta Q_m \\ \Delta P_{mk} \\ \Delta Q_{mk} \\ \Delta P_{bb} \end{bmatrix} = \begin{bmatrix} \frac{\partial P_k}{\partial \theta_k} & \frac{\partial P_k}{\partial \theta_m} & \frac{\partial P_k}{\partial V_k} V_k & \frac{\partial P_k}{\partial V_m} V_m & \frac{\partial P_k}{\partial \delta_{cR}} & \frac{\partial P_k}{\partial V_{cR}} V_{cR} & \frac{\partial P_k}{\partial \delta_{vR}} \\ \frac{\partial P_m}{\partial \theta_k} & \frac{\partial P_m}{\partial \theta_m} & \frac{\partial P_m}{\partial V_k} V_k & \frac{\partial P_m}{\partial V_m} V_m & \frac{\partial P_m}{\partial \delta_{cR}} & \frac{\partial P_m}{\partial V_{cR}} V_{cR} & 0 \\ \frac{\partial Q_k}{\partial \theta_k} & \frac{\partial Q_k}{\partial \theta_m} & \frac{\partial Q_k}{\partial V_k} V_k & \frac{\partial Q_k}{\partial V_m} V_m & \frac{\partial Q_k}{\partial \delta_{cR}} & \frac{\partial Q_k}{\partial V_{cR}} V_{cR} & \frac{\partial Q_k}{\partial \delta_{vR}} \\ \frac{\partial Q_m}{\partial \theta_k} & \frac{\partial Q_m}{\partial \theta_m} & \frac{\partial Q_m}{\partial V_k} V_k & \frac{\partial Q_m}{\partial V_m} V_m & \frac{\partial Q_m}{\partial \delta_{cR}} & \frac{\partial Q_m}{\partial V_{cR}} V_{cR} & 0 \\ \frac{\partial P_{mk}}{\partial \theta_k} & \frac{\partial P_{mk}}{\partial \theta_m} & \frac{\partial P_{mk}}{\partial V_k} V_k & \frac{\partial P_{mk}}{\partial V_m} V_m & \frac{\partial P_{mk}}{\partial \delta_{cR}} & \frac{\partial P_{mk}}{\partial V_{cR}} V_{cR} & 0 \\ \frac{\partial Q_{mk}}{\partial \theta_k} & \frac{\partial Q_{mk}}{\partial \theta_m} & \frac{\partial Q_{mk}}{\partial V_k} V_k & \frac{\partial Q_{mk}}{\partial V_m} V_m & \frac{\partial Q_{mk}}{\partial \delta_{cR}} & \frac{\partial Q_{mk}}{\partial V_{cR}} V_{cR} & 0 \\ \frac{\partial P_{bb}}{\partial \theta_k} & \frac{\partial P_{bb}}{\partial \theta_m} & \frac{\partial P_{bb}}{\partial V_k} V_k & \frac{\partial P_{bb}}{\partial V_m} V_m & \frac{\partial P_{bb}}{\partial \delta_{cR}} & \frac{\partial P_{bb}}{\partial V_{cR}} V_{cR} & \frac{\partial P_{bb}}{\partial \delta_{vR}} \end{bmatrix} \begin{bmatrix} \Delta \theta_k \\ \Delta \theta_m \\ \frac{\Delta V_k}{V_k} \\ \frac{\Delta V_m}{V_m} \\ \Delta \delta_{cR} \\ \frac{\Delta V_{cR}}{V_{cR}} \\ \Delta \delta_{vR} \end{bmatrix} \tag{5.61}$$

In this case,  $V_{vR}$  is maintained at a fixed value within prescribed limits,  $V_{vR \min} \leq V_{vR} \leq V_{vR \max}$ . The Jacobian terms in Equations (5.60) and (5.61) are given in Appendix A, Section A.4.

## 5.6.2 Unified Power Flow Controller Computer Program in Matlab® Code

Program 5.6 incorporates the UPFC model within the Newton–Raphson power flow program. The functions `PowerFlowsData`, `YBus`, and `PQflows` are also used here. In the main UPFC Newton–Raphson program, the function `UPFCData` is added to read the UPFC data, `UPFCNewtonRaphson` replaces `NewtonRaphson`, and `UPFCPQflows` is used to calculate power flows and losses in the UPFC.

PROGRAM 5.6 Program written in Matlab® to incorporate the unified power flow controller (UPFC) model within the Newton–Raphson power flow algorithm

```
% - - - Main UPFC Program

PowerFlowsData; %Function to read network data

UPFCdata; %Function to read the UPFC data

[YR, YI] = YBus(tlsend, tlrec, tlresis, tlreac, tlsuscep, tlcond, ntl, nbb);

[VM, VA, it, Vcr, Tcr, Vvr, Tvr] = UPFCNewtonRaphson(tol, itmax, ngn, nld, ...
nbb, bustype, genbus, loadbus, PGEN, QGEN, QMAX, QMIN, PLOAD, QLOAD, YR, YI, ...
VM, VA, NUPFC, UPFCsend, UPFCrec, Xcr, Xvr, Flow, Psp, PSta, Qsp, QSta, Vcr, ...
Tcr, VcrLo, VcrHi, Vvr, Tvr, VvrLo, VvrHi, VvrTar, VvrSta);

[PQsend, PQrec, PQloss, PQbus] = PQflows(nbb, ngn, ntl, nld, genbus, ...
loadbus, tlsend, tlrec, tlresis, tlreac, tlcond, tlsuscep, PLOAD, QLOAD, ...
VM, VA);

[UPFC_PQsend, UPFC_PQrec, PQcr, PQvr] = PQUPFCpower(nbb, VA, VM, NUPFC, ...
UPFCsend, UPFCrec, Xcr, Xvr, Vcr, Tcr, Vvr, Tvr);
%Print results
it           %Number of iterations
VM           %Nodal voltage magnitude (p.u.)
VA=VA*180/pi %Nodal voltage phase angles (deg)
Sources=[Vcr, Tcr*180/pi, Vvr, Tvr*180/pi] %Final source voltage para-
% meters
UPFC_PQsend  %Active and reactive powers in sending bus (p.u.)
UPFC_PQrec   %Active and reactive powers in receiving bus (p.u.)

%End of MAIN UPFC PROGRAM

%Carry out iterative solution using the Newton–Raphson method
function [VM, VA, it, Vcr, Tcr, Vvr, Tvr] = UPFCNewtonRaphson(tol, itmax, ...
ngn, nld, nbb, bustype, genbus, loadbus, PGEN, QGEN, QMAX, QMIN, PLOAD, ...
QLOAD, YR, YI, VM, VA, NUPFC, UPFCsend, UPFCrec, Xcr, Xvr, Flow, Psp, PSta, ...
Qsp, QSta, Vcr, Tcr, VcrLo, VcrHi, Vvr, Tvr, VvrLo, VvrHi, VvrTar, VvrSta);
```

## 204 POWER FLOW INCLUDING FACTS CONTROLLERS

```
% GENERAL SETTINGS
flag = 0;
it = 1;

% CALCULATE NET POWERS
[PNET,QNET] = NetPowers(nbb,ngn,nld,genbus,loadbus,PGEN,QGEN,...
PLOAD,QLOAD);

while ( it < itmax & flag==0 )
    % CALCULATED POWERS
    [PCAL,QCAL] = CalculatedPowers(nbb,VM,VA,YR,YI);

    % CALCULATED UPFC POWERS
    [PspQsend,PspQrec,PQcr,PQvr,PCAL,QCAL] = UPFCCalculatedpower...
    (nbb,VA,VM,NUPFC,UPFCsend,UPFCrec,Xcr,Xvr,Vcr,Tcr,Vvr,Tvr,PCAL,...
    QCAL);

    % POWER MISMATCHES
    [DPQ,DP,DQ,flag] = PowerMismatches(nbb,tol,bustype,flag,PNET,QNET,...
    PCAL,QCAL);

    % UPFC POWER MISMATCHES
    [DPQ,flag] = UPFCPowerMismatches(flag,tol,nbb,DPQ,VM,VA,NUPFC,Flow,...
    Psp,PSta,Qsp,QSta,PspQsend,PspQrec,PQcr,PQvr);
    if flag == 1
        break
    end

    % JACOBIAN FORMATION
    [JAC] = NewtonRaphsonJacobian(nbb,bustype,PCAL,QCAL,DPQ,VM,VA,YR,...
    YI);

    % MODIFICATION OF THE JACOBIAN FOR UPFC
    [JAC] = UPFCJacobian(nbb,JAC,VM,VA,NUPFC,UPFCsend,UPFCrec,Xcr,...
    Xvr,Flow,PSta,QSta,Vcr,Tcr,Vvr,Tvr,VvrSta);

    % SOLVE JOCOBIAN
    D = JAC\DPQ';

    % UPDATE THE STATE VARIABLES VALUES
    [VA,VM] = StateVariablesUpdating(nbb,D,VA,VM,it);

    % UPDATE THE TCSC VARIABLES
```

```

[VM,Vcr,Tcr,Vvr,Tvr] = UPFCUpdating(nbb,VM,D,NUPFC,UPFCsend,PSta,...
QSta,Vcr,Tcr,Vvr,Tvr,VvrTar,VvrSta);

%CHECK VOLTAGE LIMITS IN THE CONVERTERS
[Vcr,Vvr] = UPFCLimits(NUPFC,Vcr,VcrLo,VcrHi,Vvr,VvrLo,VvrHi);

it = it + 1;

end

%Function to calculate injected bus powers by the UPFC
function [UPFC_PQsend,UPFC_PQrec,PQcr,PQvr,PCAL,QCAL] = UPFCCalcula...
tedpower(nbb,VA,VM,NUPFC,UPFCsend,UPFCrec,Xcr,Xvr,Vcr,Tcr,Vvr,...
Tvr,PCAL,QCAL);
for ii = 1 : NUPFC
    Bkk = -1/Xcr(ii)-1/Xvr(ii);
    Bmm = -1/Xcr(ii);
    Bmk = 1/Xcr(ii);
    Bvr = 1/Xvr(ii);
    for kk = 1 : 2
        A1 = VA(UPFCsend(ii))-VA(UPFCrec(ii));
        A2 = VA(UPFCsend(ii))-Tcr(ii);
        A3 = VA(UPFCsend(ii))-Tvr(ii);
        % Computation of Conventional Terms
        Pkm = VM(UPFCsend(ii))*VM(UPFCrec(ii))*Bmk*sin(A1);
        Qkm = - VM(UPFCsend(ii))^2*Bkk - VM(UPFCsend(ii))*VM(UPFCrec(ii))...
        *Bmk*cos(A1);
        % Computation of Shunt Converters Terms
        Pvrk = VM(UPFCsend(ii))*Vvr(ii)*Bvr*sin(A3);
        Qvrk = - VM(UPFCsend(ii))*Vvr(ii)*Bvr*cos(A3);
        if kk == 1
            % Computation of Series Converters Terms
            Pcrk = VM(UPFCsend(ii))*Vcr(ii)*Bmk*sin(A2);
            Qcrk = - VM(UPFCsend(ii))*Vcr(ii)*Bmk*cos(A2);
            %Power in bus k
            Pk = Pkm + Pcrk + Pvrk;
            Qk = Qkm + Qcrk + Qvrk;
            UPFC_PQsend(ii) = Pk + Qk*i;
            PCAL(UPFCsend(ii)) = PCAL(UPFCsend(ii)) + Pk;
            QCAL(UPFCsend(ii)) = QCAL(UPFCsend(ii)) + Qk;
            %Power in Series Converter
            Pcr = Vcr(ii)*VM(UPFCsend(ii))*Bmk*sin(-A2);
            Qcr = - Vcr(ii)^2*Bmm - Vcr(ii)*VM(UPFCsend(ii))*Bmk*cos(-A2);
            %Power in Shunt Converter
            Pvr = Vvr(ii)*VM(UPFCsend(ii))*Bvr*sin(-A3);
            Qvr = Vvr(ii)^2*Bvr - Vvr(ii)*VM(UPFCsend(ii))*Bvr*cos(-A3);
            PQvr(ii) = Pvr + Qvr*i;
        end
    end
end

```

```

else
    % Computation of Series Converters Terms
    Pcrk = VM(UPFCsend(ii))*Vcr(ii)*Bkk*sin(A2);
    Qcrk = - VM(UPFCsend(ii))*Vcr(ii)*Bkk*cos(A2);
    %Power in bus m
    Pcal = Pkm + Pcrk;
    Qcal = Qkm + Qcrk;
    UPFC_PQrec(ii) = Pcal + Qcal*i;
    PCAL(UPFCsend(ii)) = PCAL(UPFCsend(ii)) + Pcal;
    QCAL(UPFCsend(ii)) = QCAL(UPFCsend(ii)) + Qcal;
    %Power in Series Converter
    Pcr = Pcr + Vcr(ii)*VM(UPFCsend(ii))*Bkk*sin(-A2);
    Qcr = Qcr - VM(UPFCsend(ii))*Vcr(ii)*Bkk*cos(-A2);
    PQcr(ii) = Pcr + Qcr*i;
end
send = UPFCsend(ii);
UPFCsend(ii) = UPFCrec(ii);
UPFCrec(ii) = send;
Beq = Bmm;
Bmm = Bkk;
Bkk = Beq;
end
end

```



```

%Function to compute power mismatches with UPFC
function [DPQ,flag] = UPFCPowerMismatches(flag,tol,nbb,DPQ,VM,VA,...
NUPFC,Flow,Psp,PSta,Qsp,QSta,UPFC_PQsend,UPFC_PQrec,PQcr,PQvr);
iii = 0;
for ii = 1 : NUPFC
    index = 2*(nbb + ii) + iii;
    if PSta(ii) == 1
        if Flow(ii) == 1
            DPQ(index-1) = Psp(ii) - real(UPFC_PQsend(ii));
        else
            DPQ(index-1) = - Psp(ii) - real(UPFC_PQrec(ii));
        end
    else
        DPQ(index-1) = 0;
    end

    if QSta(ii) == 1
        if Flow(ii) == 1
            DPQ(index) = Qsp(ii) - imag(UPFC_PQrec(ii));
        else
            DPQ(index) = - Qsp(ii) - imag(UPFC_PQrec(ii));
        end
    end
end

```

```

else
    DPQ(index) = 0;
end

DPQ(index + 1) = - real(PQcr(ii) + PQvr(ii));
iii=iii+1;
end
% Check for convergence
if ( abs(DPQ) < tol )
    flag = 1;
end

%Function to add the UPFC elements to the Jacobian matrix
function [JAC] = UPFCJacobian(nbb,JAC,VM,VA,NUPFC,UPFCsend,...
UPFCrece,Xcr,Xvr,Flow,PSta,QSta,Vcr,Tcr,Vvr,Tvr,VvrSta);
iii = 0;

for ii = 1 : NUPFC
    indexQ=2*(nbb + ii) + iii;
    indexP=indexQ-1;
    indexL=indexQ + 1;
    if VvrSta(ii) == 1
        JAC(:,2*UPFCsend(ii)) = 0.0;
    end
    Bmm = - 1/Xcr(ii)-1/Xvr(ii);
    Bkk = -1/Xcr(ii);
    Bmk = 1/Xcr(ii);
    Bvr = 1/Xvr(ii);
    for kk = 1 : 2
        A1 = VA(UPFCsend(ii))-VA(UPFCrece(ii));
        A2 = VA(UPFCsend(ii))-Tcr(ii);
        A3 = VA(UPFCsend(ii))-Tvr(ii);
        % Computation of Conventional Terms
        Hkm = - VM(UPFCsend(ii))*VM(UPFCrece(ii))*Bmk*cos(A1);
        Nkm = VM(UPFCsend(ii))*VM(UPFCrece(ii))*Bmk*sin(A1);
        % Computation of Shunt Converters Terms
        Hvr = -VM(UPFCsend(ii))*Vvr(ii)*Bvr*cos(A3);
        Nvr = VM(UPFCsend(ii))*Vvr(ii)*Bvr*sin(A3);
        % Computation of Series Converters Terms
        if kk == 1
            Hcr = - VM(UPFCsend(ii))*Vcr(ii)*Bmk*cos(A2);
            Ncr = VM(UPFCsend(ii))*Vcr(ii)*Bmk*sin(A2);
        else
            Hcr = - VM(UPFCsend(ii))*Vcr(ii)*Bkk*cos(A2);

```

```

Ncr = VM(UPFCsend(ii))*Vcr(ii)*Bkk*sin(A2);
end
if kk == 1
    JAC(2*UPFCsend(ii)-1,2*UPFCsend(ii)-1) = JAC(2*UPFCsend...
(ii)-1, 2*UPFCsend(ii)-1) - VM(UPFCsend(ii))^2*Bmm;
    if VvrSta(ii) == 1
        JAC(2*UPFCsend(ii)-1,2*UPFCsend(ii)) = Nvr;
        JAC(2*UPFCsend(ii),2*UPFCsend(ii)) = Hvr;
    else
        JAC(2*UPFCsend(ii)-1,2*UPFCsend(ii)) = JAC(2*UPFCsend(ii)-1,...
2*UPFCsend(ii)) - Nkm + Nvr;
        JAC(2*UPFCsend(ii),2*UPFCsend(ii)) = JAC(2*UPFCsend...
(ii),2*UPFCsend(ii)) - Hkm + Hvr + 2*VM(UPFCsend(ii))^2*Bmk;
    end
    JAC(2*UPFCsend(ii)-1,indexL) = Hvr;
    JAC(2*UPFCsend(ii),indexL) = - Nvr;
else
    JAC(2*UPFCsend(ii)-1,2*UPFCsend(ii)-1) = JAC(2*UPFCsend...
(ii)-1,2*UPFCsend(ii)-1) + VM(UPFCsend(ii))^2*Bmk;
    JAC(2*UPFCsend(ii),2*UPFCsend(ii)) = JAC(2*UPFCsend(ii),...
2*UPFCsend(ii)) + VM(UPFCsend(ii))^2*Bmk;

    JAC(2*UPFCsend(ii)-1,indexL) = 0.0;
    JAC(2*UPFCsend(ii),indexL) = 0.0;
end

JAC(2*UPFCsend(ii)-1,2*UPFCrece(ii)-1) = JAC(2*UPFCsend(ii)-1,...
2*UPFCrece(ii)-1) + Hkm;
JAC(2*UPFCsend(ii),2*UPFCrece(ii)-1) = JAC(2*UPFCsend(ii),...
2*UPFCrece(ii)-1) - Nkm;
if VvrSta(ii) == 1 & kk == 2
    JAC(2*UPFCsend(ii)-1,2*UPFCrece(ii)) = 0.0;
    JAC(2*UPFCsend(ii),2*UPFCrece(ii)) = 0.0;
else
    JAC(2*UPFCsend(ii)-1,2*UPFCrece(ii)) = JAC(2*UPFCsend(ii)-1,...
2*UPFCrece(ii)) + Nkm;
    JAC(2*UPFCsend(ii),2*UPFCrece(ii)) = JAC(2*UPFCsend(ii),...
2*UPFCrece(ii)) + Hkm;
end

% Computation of Active Power Controlled Jacobian's Terms
if PSta(ii) == 1
    if (Flow(ii) == 1 & kk == 1) | (Flow(ii) == -1 & kk == 2)
        if kk == 1
            JAC(indexP, 2*UPFCsend(ii)-1) = - Hkm - Hcr - Hvr;
            JAC(indexP, 2*UPFCsend(ii)) = - Nkm + Ncr;

```

```

JAC(indexP, 2*UPFCrece(ii)-1) = - Hkm;
if VvrSta(ii) == 1
    JAC(indexP, 2*UPFCrece(ii)) = 0.0;
else
    JAC(indexP, 2*UPFCrece(ii)) = Nkm;
end
JAC(indexP, indexP) = Hcr;
if QSta(ii) == 1
    JAC(indexP, indexQ) = Ncr;
else
    JAC(indexP, indexQ) = 0.0;
end
else
    JAC(indexP, 2*UPFCsend(ii)-1) = - Hkm - Hcr;
    JAC(indexP, 2*UPFCsend(ii)) = Nkm + Ncr;
    JAC(indexP, 2*UPFCrece(ii)-1) = Hkm;
    if VvrSta(ii) == 1
        JAC(indexP, 2*UPFCrece(ii)) = 0.0;
    else
        JAC(indexP, 2*UPFCrece(ii)) = Nkm;
    end
    JAC(indexP, indexP) = Hcr;
    if QSta(ii) == 1
        JAC(indexP, indexQ) = Ncr;
    else
        JAC(indexP, indexQ) = 0.0;
    end
    JAC(indexP, indexL) = 0.0;
end
end
JAC(2*UPFCsend(ii)-1, indexP) = + Hcr;
JAC(2*UPFCsend(ii), indexP) = - Ncr;
else
    JAC(indexP, indexP) = 1.0;
end
% Computation of Rective Power Controlled Jacobian's Terms
if QSta(ii) == 1
    if (Flow(ii) == 1 & kk == 1) | (Flow(ii) == -1 & kk == 2)
        if kk == 1
            JAC(indexQ, 2*UPFCsend(ii)-1) = - Nkm + Ncr;
            JAC(indexQ, 2*UPFCsend(ii)) = - 2*VM(UPFCsend(ii))^2*Bmm - ...
            Hkm + Hcr;
            JAC(indexQ, 2*UPFCrece(ii)-1) = Nkm;
            JAC(indexQ, indexQ) = Hcr;
            if VvrSta(ii) == 1
                JAC(indexQ, 2*UPFCrece(ii)) = 0.0;
            end
        end
    end
end

```

```

else
    JAC(indexQ, 2*UPFCrece(ii)) = Hkm;
end
if PSta(ii) == 1
    JAC(indexQ, indexP) = - Ncr;
else
    JAC(indexQ, indexP) = 0.0;
end
else
    JAC(indexQ, 2*UPFCsend(ii)-1) = Nkm + Ncr;
    JAC(indexQ, 2*UPFCsend(ii)) = - 2*VM(UPFCsend(ii)) ...
    ^2*Bkk + Hkm + Hcr;
    JAC(indexQ, 2*UPFCrece(ii)-1) = - Nkm;
    JAC(indexQ, indexQ) = Hcr;
    if VvrSta(ii) == 1
        JAC(indexQ, 2*UPFCrece(ii)) = 0.0;
    else
        JAC(indexQ, 2*UPFCrece(ii)) = Hkm;
    end
    if PSta(ii) == 1
        JAC(indexQ, indexP) = - Ncr;
    else
        JAC(indexQ, indexP) = 0.0;
    end
end
end
end
JAC(2*UPFCsend(ii)-1, indexQ) = Ncr;
JAC(2*UPFCsend(ii), indexQ) = Hcr;
else
    JAC(indexQ, indexQ) = 1.0;
end
temp = UPFCsend(ii);
UPFCsend(ii) = UPFCrece(ii);
UPFCrece(ii) = temp;
end
A1 = Tcr(ii) - VA(UPFCsend(ii));
A2 = Tcr(ii) - VA(UPFCrece(ii));
A3 = Tvr(ii) - VA(UPFCsend(ii));

Hcrk = - Vcr(ii)*VM(UPFCsend(ii))*Bmk*cos(A1);
Ncrk = Vcr(ii)*VM(UPFCsend(ii))*Bmk*sin(A1);
Hcrm = Vcr(ii)*VM(UPFCrece(ii))*Bmk*cos(A2);
Ncrm = - Vcr(ii)*VM(UPFCrece(ii))*Bmk*sin(A2);
Hvrk = - Vvr(ii)*VM(UPFCsend(ii))*Bvr*cos(A3);
Nvrk = Vvr(ii)*VM(UPFCsend(ii))*Bvr*sin(A3);

JAC(indexL, 2*UPFCsend(ii)-1) = Hcrk + Hvrk;
if VvrSta == 1

```

```

    JAC(indexL, 2*UPFCsend(ii)) = Nvrk;
else
    JAC(indexL, 2*UPFCsend(ii)) = Nvrk + Ncrk;
end
JAC(indexL, 2*UPFCrece(ii)-1) = Hcrm;
JAC(indexL, 2*UPFCrece(ii)) = Ncrm;
JAC(indexL, indexL) = - Hvrk;
if PSta == 1
    JAC(indexL, indexP) = - Hcrk - Hcrm;
else
    JAC(indexL, indexP) = 0.0;
end
if QSta == 1
    JAC(indexL, indexQ) = Ncrk + Ncrm;
else
    JAC(indexL, indexP) = 0.0;
end
    iii = iii + 1;
end

```

%Function to update the UPFC state variables

```

function [VM,Vcr,Tcr,Vvr,Tvr] = UPFCUpdating(nbb,VM,D,NUPFC,...
UPFCsend,PSta, QSta,Vcr,Tcr,Vvr,Tvr,VvrTar,VvrSta);
    iii = 0;
for ii = 1 : NUPFC
    indexQ=2*(nbb + ii) + iii;
    indexP=indexQ-1;
    indexL=indexQ + 1;

    if PSta(ii) == 1
        Tcr(ii) = Tcr(ii) + D(indexP);
    end
    if QSta(ii) == 1
        Vcr(ii) = Vcr(ii) + D(indexQ)*Vcr(ii);
    end
    if VvrSta(ii) == 1
        Vvr(ii) = Vvr(ii) + D(2*UPFCsend(ii),1)*Vvr(ii);
        VM(UPFCsend(ii)) = VvrTar(ii);
    end
    Tvr(ii) = Tvr(ii) + D(indexL);
    iii = iii +1;
end

```

%Function to check the voltage sources limits in the UPFC

```

function [Vcr,Vvr] = UPFCLimits(NUPFC,Vcr,VcrLo,VcrHi,Vvr,VvrLo,...
VvrHi);

```

```

for ii = 1 : NUPFC
    % Check Magnitude Voltage Limits
    if abs(Vcr(ii)) < VcrLo(ii) | abs(Vcr(ii)) > VcrHi(ii)
        if abs(Vcr(ii)) < VcrLo(ii)
            Vcr(ii) = VcrLo(ii);
        elseif abs(Vcr(ii)) > VcrHi(ii)
            Vcr(ii) = VcrHi(ii);
        end
    end
end
if abs(Vvr(ii)) < VvrLo(ii) | abs(Vvr(ii)) > VvrHi(ii)
    if abs(Vvr(ii)) < VvrLo(ii)
        Vvr(ii) = VvrLo(ii);
    elseif abs(Vvr(ii)) > VvrHi(ii)
        Vvr(ii) = VvrHi(ii);
    end
end
end

%Function to calculate the power flows in the UPFC controller
function [UPFC_PQsend,UPFC_PQrec,PQcr,PQvr] = PQUPFCpower(nbb,...
VA,VM, NUPFC,UPFCsend,UPFCrec,Xcr,Xvr,Vcr,Tcr,Vvr,Tvr);
for ii = 1 : NUPFC
    Bkk = - 1/Xcr(ii)-1/Xvr(ii);
    Bmm = -1/Xcr(ii);
    Bmk = 1/Xcr(ii);
    Bvr = 1/Xvr(ii);
    for kk = 1 : 2
        A1 = VA(UPFCsend(ii))-VA(UPFCrec(ii));
        A2 = VA(UPFCsend(ii))-Tcr(ii);
        A3 = VA(UPFCsend(ii))-Tvr(ii);
    % Computation of Conventional Terms
        Pkm = VM(UPFCsend(ii))*VM(UPFCrec(ii))*Bmk*sin(A1);
        Qkm = - VM(UPFCsend(ii))^2*Bkk - VM(UPFCsend(ii))...
            *VM(UPFCrec(ii))*Bmk*cos(A1);
    % Computation of Shunt Converters Terms
        Pvrk = VM(UPFCsend(ii))*Vvr(ii)*Bvr*sin(A3);
        Qvrk = - VM(UPFCsend(ii))*Vvr(ii)*Bvr*cos(A3);
        if kk == 1
    % Computation of Series Converters Terms
            Pcrk = VM(UPFCsend(ii))*Vcr(ii)*Bmk*sin(A2);
            Qcrk = - VM(UPFCsend(ii))*Vcr(ii)*Bmk*cos(A2);
    %Power in bus k
            Pk = Pkm + Pcrk + Pvrk;
            Qk = Qkm + Qcrk + Qvrk;
            UPFC_PQsend(ii) = Pk + Qk*i;
    %Power in Series Converter

```

```

Pcr = Vcr(ii)*VM(UPFCsend(ii))*Bmk*sin(-A2);
Qcr = - Vcr(ii)^2*Bmm - Vcr(ii)*VM(UPFCsend(ii))*Bmk*cos(-A2);
%Power in Shunt Converter
Pvr = Vvr(ii)*VM(UPFCsend(ii))*Bvr*sin(-A3);
Qvr = Vvr(ii)^2*Bvr - Vvr(ii)*VM(UPFCsend(ii))*Bvr*cos(-A3);
PQvr(ii) = Pvr + Qvr*i;
else
% Computation of Series Converters Terms
Pcrk = VM(UPFCsend(ii))*Vcr(ii)*Bkk*sin(A2);
Qcrk = - VM(UPFCsend(ii))*Vcr(ii)*Bkk*cos(A2);
%Power in bus m
Pcal = Pkm + Pcrk;
Qcal = Qkm + Qcrk;
UPFC_PQrec(ii) = Pcal + Qcal*i;
%Power in Series Converter
Pcr = Pcr + Vcr(ii)*VM(UPFCsend(ii))*Bkk*sin(-A2);
Qcr = Qcr - VM(UPFCsend(ii))*Vcr(ii)*Bkk*cos(-A2);
PQcr(ii) = Pcr + Qcr*i;
end
send = UPFCsend(ii);
UPFCsend(ii) = UPFCrec(ii);
UPFCrec(ii) = send;
Beq = Bmm;
Bmm = Bkk;
Bkk = Beq;
end
end
end

```

### 5.6.3 Numerical Example of Power Flow Control using One Unified Power Flow Controller

The five-bus network is modified to include one UPFC to compensate the transmission line linking bus Lake and bus Main. The modified network is shown in Figure 5.18. The UPFC is used to maintain active and reactive powers leaving the UPFC, towards Main, at 40 MW and 2 MVAR, respectively. Moreover, the UPFC shunt converter is set to regulate the nodal voltage magnitude at Lake at 1 p.u.

The starting values of the UPFC voltage sources are taken to be  $V_{cR} = 0.04$  p.u.,  $\delta_{cR} = 87.13^\circ$ ,  $V_{vR} = 1$  p.u., and  $\delta_{vR} = 0^\circ$ . Information on how to determine the starting values for these voltage sources is given in Section 5.8.1. The source impedances have values of  $X_{cR} = X_{vR} = 0.1$  p.u.

Convergence is obtained in five iterations to a power mismatch tolerance of  $1e-12$ . The UPFC upheld its target values. The power flow results are shown in Figure 5.18, and the bus voltages are given in Table 5.6.

The data given in function `PowerFlowsData` in Section 4.3.9 are modified to accommodate for the inclusion of the UPFC. Furthermore, function `UPFCData` is used to

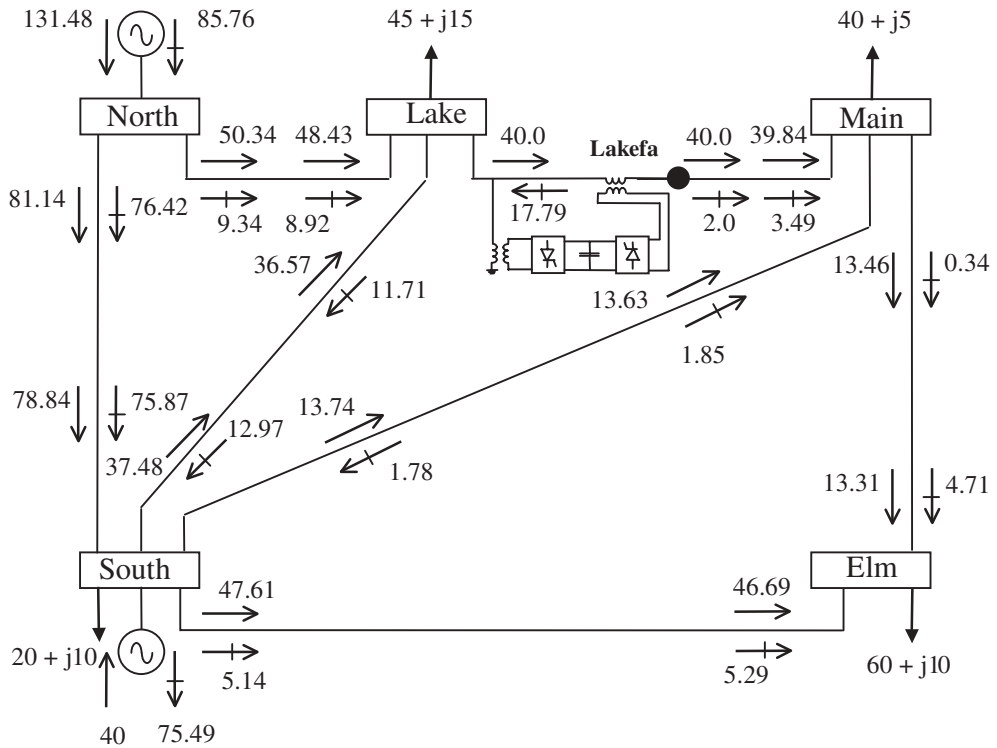


Figure 5.18 Five-bus test network with one unified power flow controller, and power flow result

Table 5.6 Bus voltages of modified network

Nodal voltage	System bus					
	North	South	Lake	Lakefa	Main	Elm
Magnitude (p.u.)	1.06	1.00	1.00	0.997	0.992	0.975
Phase angle (deg)	0	-1.77	-6.02	-2.51	-3.19	-4.97

enter UPFC data:

%This function is used exclusively to enter data for:

% UNIFIED POWER FLOW CONTROLLER

% NUPFC : Number of UPFC's

% UPFCsend : Shunt converter's bus and series converter' sending bus

% UPFCrec : Series converter' receiving bus

% Xcr : Inductive reactance of Shunt impedance (p.u.)

% Xvr : Inductive reactance of Series impedance (p.u.)

% Flow : Power flow direction : 1 is for sending to receiving bus

```

% -1 indicates opposite direction
% Psp : Target active power flow (p.u.)
% PSta : control status for active power : 1 is on; 0 is off
% Qsp : Target reactive power flow (p.u.)
% QSta : control status for reactive power : 1 is on; 0 is off
% Vcr : Initial condition for the series source voltage magnitude (p.u.)
% Tcr : Initial condition for the series source voltage angle (rad.)
% VcrLo : Lower limit of series source voltage magnitude (p.u.)
% VcrHi : Higher limit of series source voltage magnitude (p.u.)
% Vvr : Initial condition to the shunt source voltage magnitude (p.u.)
% Tvr : Initial condition to the shunt source voltage angle (rad.)
% VvrLo : Lower limit of shunt source voltage magnitude (p.u.)
% VvrHi : Higher limit of shunt source voltage magnitude (p.u.)
% VvrTar : Target nodal voltage magnitude to be controlled by shunt ...
% branch (p.u.)
% VvrSta : Control status for nodal voltage magnitude: 1 is on; 0 is off

NUPFC=1;
UPFCsend(1)=3; UPFCrec(1)=6; Xcr(1)=0.1; Xvr(1)=0.1;
Flow(1)=-1; Psp(1)=0.4; PSta(1)=1; Qsp(1)=0.02; QSta(1)=1;
Vcr(1)=0.04; Tcr(1)=-87.13/57.3; VcrLo(1)=0.001; VcrHi(1)=0.2;
Vvr(1)=1.0; Tvr(1)=0.0; VvrLo(1)=0.9; VvrHi(1)=1.1;
VvrTar(1)=1.0; VvrSta(1)=1;
    
```

As expected, the power flows in the UPFC-upgraded network differ with respect to the original case. The most noticeable changes are as follows: there is a 32% increase of active power flowing towards Lake through transmission lines North–Lake and South–Lake. The increase is in response to the large amount of active power demanded by the UPFC series converter. The maximum amount of active power exchanged between the UPFC and the AC system will depend on the robustness of the UPFC shunt bus, Lake. Since the UPFC generates its own reactive power, the generator at North decreases its reactive power generation by 5.6%, and the generator connected at South increases its absorption of reactive power by 22.6%.

The maximum absolute power mismatches in the system buses and UPFC are shown in Table 5.7. It must be noted that the selected UPFC initial conditions are very good

**Table 5.7** Maximum power mismatches in the bus system and unified power flow controller (UPFC)

Iteration	Buses		UPFC		
	$\Delta P$	$\Delta Q$	$\Delta P_{mk}$	$\Delta Q_{mk}$	$P_{cR} + P_{vR}$
1	7.745e-1	1.401e-1	5.0e-04	4.0e-02	0
2	1.89e-2	1.001e-2	5.1e-03	6.5e-02	5.7e-03
3	3.8e-03	5.1e-04	3.7e-03	5.0e-04	8.6e-05
4	1.2e-07	1.6e-06	1.2e-07	1.6e-6	1.2e-07
5	1.3e-12	1.9e-13	1.2e-12	1.8e-13	1.3e-14

estimates, since the UPFC mismatches have small values from the outset of the iterative process.

For completeness Table 5.8 shows the variation of the controllable voltage sources during the iterative process.

**Table 5.8** Variation of ideal source voltages

Iteration	Series source		Shunt source	
	$V_{cR}$ (p.u.)	$\theta_{cR}$ (deg)	$V_{vR}$ (p.u.)	$\theta_{vR}$ (deg)
1	0.04	-87.12	1	0
2	0.1004	-97.54	1.0134	-5.8882
3	0.1009	-92.71	1.0174	-6.0051
4	0.1013	-92.73	1.0173	-6.0055
5	0.1013	-92.73	1.0173	-6.0055

### 5.7 HIGH-VOLTAGE DIRECT-CURRENT-BASED VOLTAGE SOURCE CONVERTER

From the principles of HVDC-VSC operation outlined in Chapter 2 it may be argued that for the purpose of fundamental frequency analysis each converter station may be adequately represented by a complex voltage source  $V_{vR}$  behind its transformer reactance  $X_{vR}$  (impedance  $Z_{vR}$ ). Similar to the case for the STATCOM, and UPFC, the synchronous voltage sources represent the fundamental Fourier series component of the switched voltage waveforms at the AC converter terminals of the HVDC-VSC.

The two voltage sources work in a coordinated fashion, and this fact is taken into account by the mismatch power equation in the equivalent circuit shown in Figure 5.19. This circuit is used to derive the mathematical model of the HVDC-VSC for inclusion in the power flow Newton–Raphson algorithm.

The complex voltage sources representing the two VSC stations in the HVDC-VSC are:

$$E_{vR1} = V_{vR1} (\cos \delta_{vR1} + j \sin \delta_{vR1}), \tag{5.62}$$

$$E_{vR2} = V_{vR2} (\cos \delta_{vR1} + j \sin \delta_{vR2}). \tag{5.63}$$

In the current application, the voltage sources have the following voltage magnitudes and phase angle limits:  $0 \leq V_{vR1} \leq V_{vR1 \max}$ ;  $0 \leq \delta_{vR1} \leq 2\pi$ ;  $0 \leq V_{vR2} \leq V_{vR2 \max}$ ;  $0 \leq \delta_{vR2} \leq 2\pi$ .

The constraining power equation for the back-to-back HVDC-VSC (i.e.  $R_{dc} = 0$ ) is

$$\text{Re}\{V_{vR1} I_{vR1}^* + V_{vR2} I_{vR2}^*\} = 0, \tag{5.64}$$

and for the case when both VSC stations are linked by a DC cable (i.e.  $R_{dc} > 0$ ) is

$$\text{Re}\{V_{vR1} I_{vR1}^* + V_{vR2} I_{vR2}^* + P_{DC, \text{loss}}\} = 0. \tag{5.65}$$

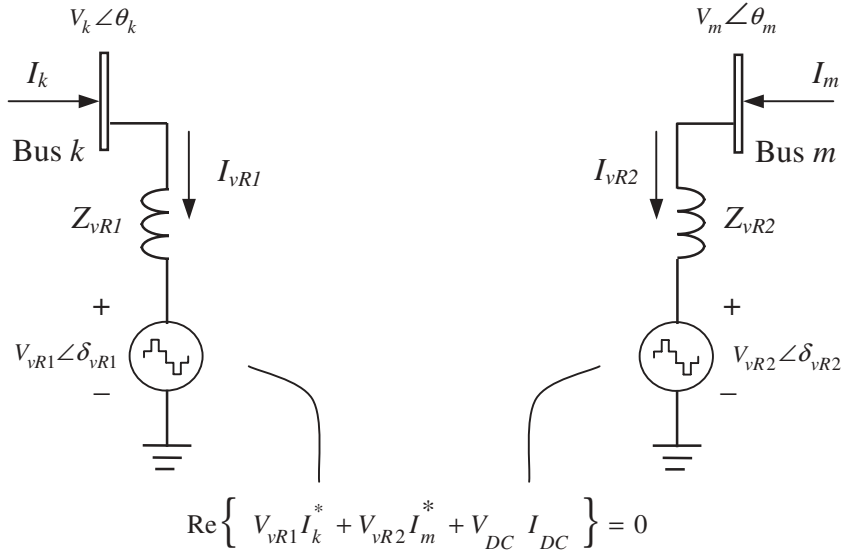


**Figure 5.19** High-voltage direct-current based voltage source converter equivalent circuit

### 5.7.1 Power Equations

If it is assumed that the power flows from the station connected at bus  $k$  (rectifier) to the station connected at bus  $m$  (inverter), the power flow equations injected at bus  $k$  are:

$$P_k = V_k^2 G_{vR1} + V_k V_{vR1} [G_{vR1} \cos(\theta_k - \delta_{vR1}) + B_{vR1} \sin(\theta_k - \delta_{vR1})], \quad (5.66)$$

$$Q_k = -V_k^2 B_{vR1} + V_k V_{vR1} [G_{vR1} \sin(\theta_k - \delta_{vR1}) - B_{vR1} \cos(\theta_k - \delta_{vR1})]. \quad (5.67)$$

The powers flowing into the rectifier are described by the following equations:

$$P_{vR1} = V_{vR1}^2 G_{vR1} + V_{vR1} V_k [G_{vR1} \cos(\delta_{vR1} - \theta_k) + B_{vR1} \sin(\delta_{vR1} - \theta_k)], \quad (5.68)$$

$$Q_{vR1} = -V_{vR1}^2 B_{vR1} + V_{vR1} V_k [G_{vR1} \sin(\delta_{vR1} - \theta_k) - B_{vR1} \cos(\delta_{vR1} - \theta_k)]. \quad (5.69)$$

The power equations for bus  $m$  and for the inverter are obtained by exchanging the subscripts  $k$  and  $vR1$  for  $m$  and  $vR2$ , respectively.

Moreover, one further equation is required to represent the power constraint given in the form of either Equation (5.64) or Equation (5.65), depending on the application. For the case of the full HVDC-VSC, the relevant power equation is:

$$P_{vR1} + P_{vR2} + P_{DC} = 0. \quad (5.70)$$

It should be remarked that for the purpose of power flow studies the equivalent circuit of one leg of the HVDC-VSC shown in Figure 5.19 is closely related to the equivalent circuit of the STATCOM (see Section 5.5.1).

As described in Chapter 4, an  $n$ -bus power network with no voltage and power flow regulation provisions is described by a  $2 \times (n - 1)$  nonlinear system of equations.

Moreover, for each HVDC-VSC that exists in the power network the  $2 \times (n - 1)$  system of equations is augmented by up to five equations to take account of the two converter stations and the power constraint equation that exists on the dc side of the converters. The solution of the combined system of nonlinear equations is carried out by iteration using the Newton–Raphson method, enabling quadratic convergent solutions.

Both converter stations are capable of controlling the amount of active power injected at their respective AC buses. In a given power flow solution, one of the converters is designated to be the master station, with the other converter being the slave station. Moreover, both stations have control over either voltage magnitude or reactive power injected at their connecting buses.

For the HVDC-VSC, when active power is regulated at the rectifier end and voltage magnitude is regulated at the inverter end, the linearised system of equations has the following structure:

$$\begin{bmatrix} \Delta P_k \\ \Delta Q_k \\ \Delta P_{vR} \\ \Delta Q_{vR} \\ \Delta P_{HVDC} \end{bmatrix} = \begin{bmatrix} \frac{\partial P_k}{\partial \theta_k} & \frac{\partial P_k}{\partial V_k} V_k & \frac{\partial P_k}{\partial \delta_{vR1}} & \frac{\partial P_k}{\partial V_{vR1}} V_{vR1} & 0 \\ \frac{\partial Q_k}{\partial \theta_k} & \frac{\partial Q_k}{\partial V_k} V_k & \frac{\partial Q_k}{\partial \delta_{vR1}} & \frac{\partial Q_k}{\partial V_{vR1}} V_{vR1} & 0 \\ \frac{\partial P_{vR1}}{\partial \theta_k} & \frac{\partial P_{vR1}}{\partial V_k} V_k & \frac{\partial P_{vR1}}{\partial \delta_{vR1}} & \frac{\partial P_{vR1}}{\partial V_{vR1}} V_{vR1} & 0 \\ \frac{\partial Q_{vR1}}{\partial \theta_k} & \frac{\partial Q_{vR1}}{\partial V_k} V_k & \frac{\partial Q_{vR1}}{\partial \delta_{vR1}} & \frac{\partial Q_{vR1}}{\partial V_{vR1}} V_{vR1} & 0 \\ \frac{\partial P_{HVDC}}{\partial \theta_k} & \frac{\partial P_{HVDC}}{\partial V_k} V_k & \frac{\partial P_{HVDC}}{\partial \delta_{vR1}} & \frac{\partial P_{HVDC}}{\partial V_{vR1}} V_{vR1} & \frac{\partial P_{HVDC}}{\partial \delta_{vR2}} \end{bmatrix} \begin{bmatrix} \Delta \theta_k \\ \frac{\Delta V_k}{V_k} \\ \Delta \delta_{vR1} \\ \frac{\Delta V_{vR1}}{V_{vR1}} \\ \Delta \delta_{vR2} \end{bmatrix}, \tag{5.71}$$

where  $\Delta P_{HVDC}$ , given by

$$\Delta P_{HVDC} = \Delta P_{vR1} - \Delta P_{vR2},$$

is the active power flow mismatch for the DC link. Notice that, since active power is regulated at the rectifier end (i.e.  $\Delta P_{vR1} = P_{vR1}^{spec} - P_{vR1}^{calc}$ ), the corresponding active power equations of the inverter become redundant (i.e.  $\Delta P_{vR2}$  and  $\Delta P_m$ ) and are not used in Equation (5.71). Moreover, since the voltage magnitude at bus  $m$  is kept constant the reactive power equations of the inverter also become redundant (i.e.  $\Delta Q_{vR2}$  and  $\Delta Q_{P_m}$ ). The relevant Jacobian elements are given in Appendix A, Section A.5.

### 5.7.2 High-voltage Direct-current-based Voltage Source Converter Computer Program in Matlab® Code

Program 5.7 incorporates the HVDC model within the Newton–Raphson power flow program. The functions `PowerFlowsData`, `YBus`, and `PQflows` are also used here. In the main HVDC Newton–Raphson program, the function `HVDCData` is added to read the HVDC data, `HVDCNewtonRaphson` replaces `NewtonRaphson`, and `HVDCPQflows` is used to calculate power flows and losses in the HVDC.

PROGRAM 5.7 Program written in Matlab<sup>®</sup> to incorporate the high-voltage direct-current (HVDC) model within the Newton–Raphson power flow algorithm.

```
% - - - Main HVDC Program

PowerFlowsData;

HVDCdata;

[YR, YI] = YBus(tlsend, tlrec, tlresis, tlreac, tlsuscep, tlcond, ntl, nbb);

[VM, VA, it, Vvr1, Tvr1, Vvr2, Tvr2] = HVDCNewtonRaphson(tol, itmax, ngn, ...
nld, nbb, bustype, genbus, loadbus, PGEN, QGEN, QMAX, QMIN, PLOAD, QLOAD, YR, ...
YI, VM, VA, NHVDC, HVDCsend, HVDCrec, Xvr1, Xvr2, Rcd, TarVol1, VSta1, Qsp1, ...
QSta1, TarVol2, VSta2, Qsp2, QSta2, Psp, Vvr1, Tvr1, Vvr2, Tvr2, VvrHi, ...
VvrLo);

[PQsend, PQrec, PQloss, PQbus] = PQflows(nbb, ngn, ntl, nld, genbus, ...
loadbus, tlsend, tlrec, tlresis, tlreac, tlcond, tlsuscep, PLOAD, QLOAD, ...
VM, VA);

[HVDC_PQsend, HVDC_PQrec] = HVDCPQpower(nbb, VA, VM, NHVDC, HVDCsend, ...
HVDCrec, Xvr1, Xvr2, Vvr1, Tvr1, Vvr2, Tvr2);

%Print results
it           %Number of iterations
VM           %Nodal voltage magnitude (p.u)
VA=VA*180/pi %Nodal voltage phase angles (deg)
Sources=[Vv1, Tvr1*180/pi, Vvr2, Tvr2*180/pi] %Final source voltage
% parameters
HVDC_PQsend %Active and reactive powers in sending bus (p.u.)
HVDC_PQrec  %Active and reactive powers in receiving bus (p.u.)

%End of MAIN HVDC PROGRAM

%Carry out iterative solution using the Newton–Raphson method
function [VM, VA, it, Vvr1, Tvr1, Vvr2, Tvr2] = NewtonRaphson(tol, itmax, ...
ngn, nld, nbb, bustype, genbus, loadbus, PGEN, QGEN, QMAX, QMIN, PLOAD, ...
QLOAD, YR, YI, VM, VA, NHVDC, HVDCsend, HVDCrecec, Xvr1, Xvr2, Rcd, TarVol1, ...
VSta1, Qsp1, QSta1, TarVol2, VSta2, Qsp2, QSta2, Psp, Vvr1, Tvr1, Vvr2, ...
Tvr2, VvrHi, VvrLo);

% GENERAL SETTINGS
flag = 0;
it = 1;

% CALCULATE NET POWERS
[PNET, QNET] = NetPowers(nbb, ngn, nld, genbus, loadbus, PGEN, QGEN, ...
PLOAD, QLOAD);
```

```

while ( it < itmax & flag==0 )
  % CALCULATED POWERS
  [PCAL,QCAL] = CalculatedPowers(nbb,VM,VA,YR,YI);

  %STATCOM CALCULATED POWERS
  [PCAL,QCAL,PHVDC,QHVDC] = HVDCCalculatePowers(PCAL,QCAL,VM,VA,...
  NHVDC, HVDCsend,HVDCrece,Xvr1,Xvr2,Vvr1,Tvr1,Vvr2,Tvr2);

  % POWER MISMATCHES
  [DPQ,DP,DQ,flag] = PowerMismatches(nbb,tol,bustype,flag,PNET,QNET,...
  PCAL,QCAL);

  %HVDC POWER MISMATCHES
  [DPQ,flag] = HVDCMismatches(flag,tol,DPQ,nbb,VM,VA,NHVDC, HVDCsend,...
  HVDCrece,TarVol1,VSta1,TarVol2,VSta2,Psp,Qsp1,QSta1,Qsp2,QSta2,...
  PHVDC, QHVDC);
  if flag == 1
    break
  end

  % JACOBIAN FORMATION
  [JAC] = NewtonRaphsonJacobian(nbb,bustype,PCAL,QCAL,DPQ,VM,VA,...
  YR,YI);

  % HVDC JACOBIAN
  [JAC] = HVDC_Jacobian(nbb,JAC,VM,VA,NHVDC,HVDCsend,HVDCrece,...
  Xvr1,Xvr2,Rcd,VSta1,VSta2,QSta1,QSta2,Vvr1,Tvr1,Vvr2,Tvr2);

  % SOLVE FOR THE STATE VARIABLES VECTOR
  D = JAC\DPQ';

  % UPDATE THE STATE VARIABLES VALUES, WITH TRUNCATED CORRECTIONS IF
  % NECESSARY (VM increments < +-0.1 p.u. and VA increments < +- 5 deg)
  [VA,VM] = StateVariablesUpdating(nbb,D,VA,VM,it);

  %UPDATE HVDC STATE VARIABLES
  [VM,Vvr1,Tvr1,Vvr2,Tvr2] = HVDC_Updating(nbb,D,VM,VA,NHVDC,...
  HVDCsend,HVDCrece,QSta1,QSta2,VSta1,TarVol1,TarVol2,VSta2,Vvr1,...
  Tvr1,Vvr2,Tvr2);
  %CHECK VOLTAGE CONVERTERS FOR LIMITS
  [Vvr1,Vvr2] = HVDCLimits(NHVDC,Vvr1,Vvr2,VvrLo,VvrHi);

```

```

it = it + 1;

end

%Function to calculate injected bus powers by the HVDC
function [PCAL,QCAL,PHVDC,QHVDC] = HVDCCalculatePowers(PCAL,QCAL,...
VM,VA,NHVDC,HVDCsend,HVDCrece,Xvr1,Xvr2,Vvr1,Tvr1,Vvr2,Tvr2);
for ii = 1 : NHVDC
    for kk = 1 : 2
        Bkk = -1/Xvr1(ii);
        Bvr = 1/Xvr1(ii);
        A = VA(HVDCsend(ii)) - Tvr1(ii);

        PHVDC(ii,kk) = VM(HVDCsend(ii))*Vvr1(ii)*Bvr*sin(A);
        QHVDC(ii,kk) = - VM(HVDCsend(ii))^2*Bkk - VM(HVDCsend(ii))...
        *Vvr1(ii)*Bvr*cos(A);

        PCAL(HVDCsend(ii)) = PCAL(HVDCsend(ii)) + PHVDC(ii,kk);
        QCAL(HVDCsend(ii)) = QCAL(HVDCsend(ii)) + QHVDC(ii,kk);

        HVDCsend(ii) = HVDCrece(ii);
        Xvr1(ii) = Xvr2(ii);
        Tvr1(ii) = Tvr2(ii);
        Vvr1(ii) = Vvr2(ii);
    end
end

%Function to compute power mismatches with HVDC
function [DPQ,flag] = HVDCMismatches(flag,tol,DPQ,nbb,VM,VA,NHVDC,...
HVDCsend,HVDCrece,TarVol1,VSta1,TarVol2,VSta2,Psp,Qsp1,QSta1,...
Qsp2,QSta2,PHVDC,QHVDC);
iii = 0;
for ii = 1 : NHVDC
    index= 2*(nbb + ii) + iii;
    DPQ(index-1) = Psp(ii) - PHVDC(ii,1);

    DPQ(index) = Qsp1(ii) - QHVDC(ii,1);

    DPQ(index + 1) = - Psp(ii) - PHVDC(ii,2);

    DPQ(index + 2) = Qsp2(ii) - QHVDC(ii,2);
    iii = iii + 2;
end
% Check for convergence

```

```

if ( abs(DPQ) < tol )
    flag = 1;
end

%Function to add up the HVDC elements to Jacobian matrix
function [JAC] = HVDC_Jacobian(nbb,JAC,VM,VA,NHVDC,HVDCsend,...
HVDCrecre, Xvr1,Xvr2,Rcd,VSta1,VSta2,QSta1,QSta2,Vvr1,Tvr1,Vvr2,Tvr2);
iii = 0;
for ii = 1 : NHVDC
    index= 2*(nbb + ii) + iii;
    for kk = 1 : 2
        if VSta1(ii) == 1
            JAC( : , 2*HVDCsend(ii) )=0;
        end
        JAC(index-1,index-1) = 1;
        JAC(index,index) = 1;

        Bvr = 1/Xvr1(ii);
        A1 = Tvr1(ii)-VA(HVDCsend(ii));
        A2 = VA(HVDCsend(ii))-Tvr1(ii);

        Pcal = - VM(HVDCsend(ii))*Vvr1(ii)*Bvr*sin(A2);
        Qcal = Vvr1(ii)*VM(HVDCsend(ii))*Bvr*cos(A2);
        Phvdc = - Vvr1(ii)*VM(HVDCsend(ii))*Bvr*sin(A1);
        Qhvdc = Vvr1(ii)*VM(HVDCsend(ii))*Bvr*cos(A1);

        JAC(2*HVDCsend(ii)-1,2*HVDCsend(ii)-1) = JAC(2*HVDCsend(ii)-1,...
        2*HVDCsend(ii)-1) + VM(HVDCsend(ii))^2*Bvr;
        if (QSta1(ii) == 1 )
            JAC(2*HVDCsend(ii),2*HVDCsend(ii)) = JAC(2*HVDCsend(ii),...
            2*HVDCsend(ii)) + VM(HVDCsend(ii))^2*Bvr;
        else
            JAC(2*HVDCsend(ii)-1,2*HVDCsend(ii)) = JAC(2*HVDCsend(ii)-1,...
            2*HVDCsend(ii)) + Phvdc;
            JAC(2*HVDCsend(ii),2*HVDCsend(ii)) = JAC(2*HVDCsend(ii),...
            2*HVDCsend(ii)) - Qhvdc;
            JAC(2*HVDCsend(ii),2*HVDCsend(ii)-1) = JAC(2*HVDCsend(ii),...
            2*HVDCsend(ii)-1) - Phvdc;
        end
        JAC(2*HVDCsend(ii)-1,index-1) = - Qcal;
        JAC(index-1,2*HVDCsend(ii)-1) = Qhvdc;
        JAC(index-1,2*HVDCsend(ii)) = Phvdc;
        JAC(index-1,index-1) = - Qhvdc;
        if (QSta1(ii) == 1)
            JAC(index-1,index) = Phvdc;
            JAC(2*HVDCsend(ii),index-1) = Pcal;
        end
    end
end

```

```

else
    JAC(index-1,index) = 0.0 ;
    JAC(2*HVDCsend(ii),index-1) = - Phvdc;
end
if (QSta1(ii) == 1)
    JAC(2*HVDCsend(ii)-1,index) = - Pcal;
    JAC(2*HVDCsend(ii),index) = - Qcal;
    JAC(index,2*HVDCsend(ii)-1) = - Phvdc;
    JAC(index,2*HVDCsend(ii)) = Qhvdc;
    JAC(index,index) = -2*Vvr1(ii)^2*Bvr + Qhvdc;
    JAC(index,index-1) = Phvdc;
end
HVDCsend(ii) = HVDCrecre(ii);
Xvr1(ii) = Xvr2(ii);
Vvr1(ii) = Vvr2(ii);
Tvr1(ii) = Tvr2(ii);
VSta1(ii) = VSta2(ii);
QSta1(ii) = QSta2(ii);
index = index + 2;
end
iii = iii + 2;
end

%Function to update HVDC state variables
function [VM,Vvr1,Tvr1,Vvr2,Tvr2] = HVDC_Updating(nbb,D,VM,VA,NHVDC,...
HVDCsend,HVDCrecre,QSta1,QSta2,VSta1,TarVol1,TarVol2,VSta2,Vvr1,...
Tvr1,Vvr2, Tvr2);
iii =0;
for ii = 1 : NHVDC
    index = 2*(nbb + ii) + iii;
    if (VSta1(ii) == 1)
        % Adjust the Volatge Magnitud target
        Vvr1(ii) = Vvr1(ii) + Vvr1(ii)*D(2*HVDCsend(ii));
        VM(HVDCsend(ii)) = TarVol1(ii);
        Tvr1(ii) = Tvr1(ii) + D(index-1);
    else
        Vvr1(ii) = Vvr1(ii) + Vvr1(ii)*D(index);
        Tvr1(ii) = VA(HVDCsend(ii));
    end
    if (VSta2(ii) == 1)
        % Adjust the Volatge Magnitud target
        Vvr2(ii) = Vvr2(ii) + Vvr1(ii)*D(2*HVDCrecre(ii));
        VM(HVDCsend(ii)) = TarVol2(ii);
        Tvr2(ii) = Tvr2(ii) + D(index + 2);
    else
        Vvr2(ii) = Vvr2(ii) + Vvr2(ii)*D(index + 2);
    end
end

```

```

    Tvr2(ii) = Tvr2(ii) + D(index + 1);
end
end

```

```

%Function to check voltagesources limits in HVDC controllers
function [Vvr1,Vvr2] = HVDCLimits(NHVDC,Vvr1,Vvr2,VvrLo,VvrHi);

```

```

for ii = 1 : NHVDC
    % Check Magnitude Voltage Limits
    for kk = 1 : 2
        if Vvr1(ii) < VvrLo(ii) | Vvr1(ii) > VvrHi(ii)
            if Vvr1(ii) < VvrLo(ii)
                Vvr1(ii) = VvrLo(ii);
            elseif Vvr1(ii) > VvrHi(ii)
                Vvr1(ii) = VvrHi(ii);
            end
        end
    end

    temp = Vvr1(ii);
    Vvr1(ii) = Vvr2(ii);
    Vvr2(ii) = temp;
end
end

```

```

%Function to calculate the power flows in HVDC controller
function [HVDC_PQsend,HVDC_PQrece] = HVDCPQpower(nbb,VA,VM,NHVDC,...
HVDCsend, HVDCrece,Xvr1,Xvr2,Vvr1,Tvr1,Vvr2,Tvr2);

```

```

for ii = 1: NHVDC
    for kk = 1: 2
        Bkk = -1/Xvr1(ii);
        Bvr = 1/Xvr1(ii);
        A = VA(HVDCsend(ii)) - Tvr1(ii);
        PHVDC(ii) = VM(HVDCsend(ii))*Vvr1(ii)*Bvr*sin(A);
        QHVDC(ii) = - VM(HVDCsend(ii))^2*Bkk - (HVDCsend(ii))*Vvr1(ii)...
        *Bvr*cos(A);

        if kk == 1
            HVDC_PQsend(ii) = PHVDC(ii) + i*QHVDC(ii);
        else
            HVDC_PQrece(ii) = PHVDC(ii) + i*QHVDC(ii);
        end

        HVDCsend(ii) = HVDCrece(ii);
        Xvr1(ii) = Xvr2(ii);
        Vvr1(ii) = Vvr2(ii);
        Tvr1(ii) = Tvr2(ii);
    end
end
end

```

### 5.7.3 Numerical Example of Power Flow Control using One HVDC-VSC

The five-bus system is used to illustrate the power flow control performance of the HVDC-VSC models. This power flow controller may be used to regulate the amount of power flow at their points of connection or even to reverse the direction of power flowing through the controller.

#### 5.7.3.1 HVDC-VSC back-to-back model

The original network is modified to include one back-to-back (BTB) HVDC model to regulate power flow at the points of connection. Take, for instance, the case when the UPFC is installed at the receiving end of line Lake–Main and is set to regulate active and reactive powers flowing from Lake to Main at 40 MW and 2 MVAR, respectively. The voltage magnitude at bus Lake is controlled at 1 p.u. The back-to-back HVDC model replaces the UPFC used in the test case described in Section 5.6.3. As expected, the power flow results for both cases are exactly the same.

#### 5.7.3.2 HVDC-VSC full model

A different situation arises when the full HVDC-VSC model replaces the combined UPFC–transmission-line model connected between Lake and Main since the DC cable will contain neither the inductance nor the capacitance of the transmission line. In this example, the cable resistance in the DC system is taken to have the same value as the transmission-line resistance in the AC system, which is 1 %. Figure 5.20 shows results for the case when the full HVDC-VSC is used to control active power flow at Lake at 40 MW, and Table 5.9 shows the nodal voltages in the modified network.

The data given in function `PowerFlowsData` in Section 4.3.9 is modified to accommodate for the inclusion of the HVDC. For HVDC-BTB the modification is as in Section 5.4.3, and for the HVDC-VSC the transmission line originally connected between Lake and Main is replaced by the HVDC-VSC. Function `HVDCData` is used to enter HVDC data:

```
%This function is used exclusively to enter data for :
%HIGH VOLTAGE DIRECT CURRENT (HVDC)

% NHVDC : Number of HVDC's
% HVDCsend : Shunt converter's sending bus
% HVDCrec : Shunt converter's receiving bus
% Rcd : DC cable's resistance for HVDC DC-Link model
% Psp : Target active power flow (p.u.)
% VvrLo : Lower limit for voltage sources magnitudes (p.u.)
% VvrHi : Higher limit for voltage sources magnitudes (p.u.)
% SENDING BUS
```

```

% Xvr1 : Inductive reactance of transformer-sending
% TarVol1 : Target nodal voltage magnitude (pu.)
% VSta1 : control status for nodal voltage magnitude: 1 is on; 0 is off
% Qsp1 : Target reactive power flow
% QSta1 : control status for reactive power: 1 is on; 0 is off
% Vvr1 : Initial condition for the shunt source voltage magnitude (p.u.)
% Tvr1 : Initial condition for the shunt source voltage phase angle (rad.)
  % RECEIVING BUS
% Xvr2 : Inductive reactance of transformer-receiving
% TarVol2 : Target nodal voltage magnitude (pu.)
% VSta2 : Control status for nodal voltage magnitude: 1 is on; 0 is off
% Qsp2 : Target reactive power flow
% QSta2 : Control status for reactive power: 1 is on; 0 is off
% Vvr2 : Initial condition for the shunt source voltage magnitude (p.u.)
% Tvr2 : Initial condition for the shunt source voltage angle (rad.)
NHVDC=1;
HVDCsend(1)=3; HVDCrec(1)=4; Xvr1(1)=0.1; Xvr2(1)=0.1; Rcd(1)=0.1;
TarVol1(1)=1.0; VSta1(1)=1; Qsp1(1)=0.02; QSta1(1)=0;
TarVol2(1)=1.0; VSta2(1)=0; Qsp2(1)=-0.02; QSta2(1)=1;
Psp(1)=0.4;
Vvr1(1)=1.0; Tvr1(1)=0.0; Vvr2(1)=1.0; Tvr2(1)=0.0;
VvrHi(1)=1.1; VvrLo(1)=0.9;
    
```

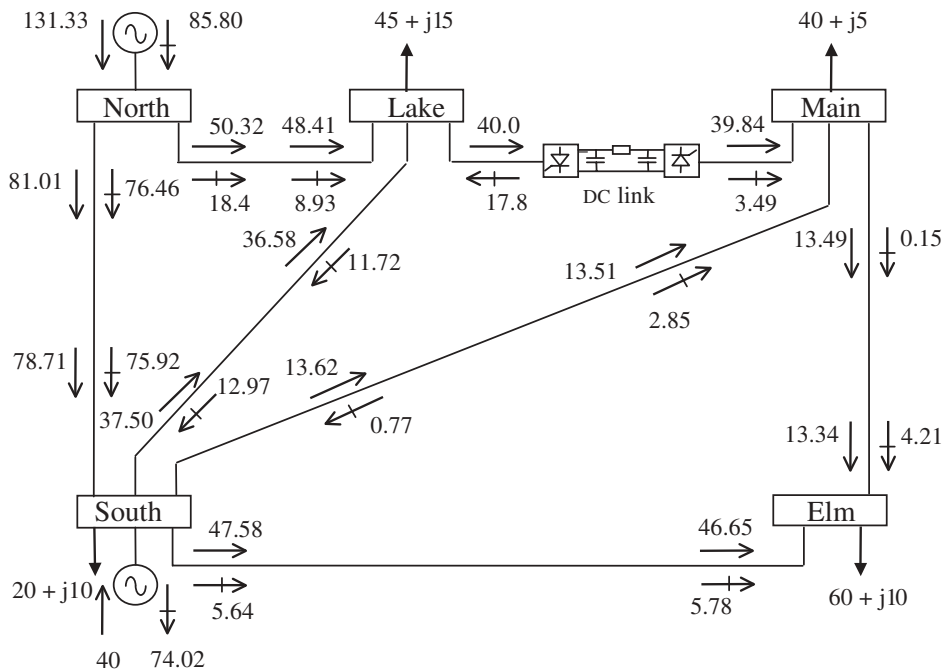


Figure 5.20 Power flow results in the five-bus network with one full high-voltage direct-current-based voltage source converter

**Table 5.9** Nodal voltages in the modified network

Nodal voltage	Network bus				
	North	South	Lake	Main	Elm
Magnitude (p.u.)	1.06	1	1	0.989	0.973
Phase angle (deg)	0	-1.76	-6.01	-3.14	-4.95

## 5.8 EFFECTIVE INITIALISATION OF FACTS CONTROLLERS

The modelling of FACTS controllers for application in power flow analysis results in highly nonlinear equations which should be suitably initialised to ensure quadratic convergent solutions when using the Newton–Raphson method. This section addresses such a problem and makes firm recommendations for the use of simple and effective initialisation procedures for all FACTS models in power flow and related studies.

### 5.8.1 Controllers Represented by Shunt Synchronous Voltage Sources

Extensive use of FACTS models represented by shunt voltage sources indicates that elements such as the STATCOM, the shunt source of the UPFC, and the two-shunt sources representing the HVDC-VSC are suitably initialised by selecting 1 p.u. voltage magnitudes and  $0^\circ$  phase angles.

### 5.8.2 Controllers Represented by Shunt Admittances

It has been found that the SVC is well initialised by selecting a firing-angle value that corresponds to the reactance resonant peak; this value is calculated by using Equation (5.40).

### 5.8.3 Controllers Represented by Series Reactances

The TCSC can be represented as an equivalent variable reactance, the ability of which either to generate or to absorb reactive power is a function of the thyristor firing angle,  $\alpha_{\text{TCSC}}$ . The adjustable reactance representing the TCSC module shown in Figure 5.11 is well described by Equations (5.31)–(5.35).

Normally, the active power flow through the TCSC is chosen to be the control variable, and  $\alpha_{\text{TCSC}}$  is chosen to be the state variable. Hence, good initial values for  $\alpha_{\text{TCSC}}$  become mandatory in order to ensure robust iterative solutions. To this end, an approximation of Equation (5.31) is used:

$$X_{\text{TCSC}(1)}(\alpha_{\text{TCSC}}) \approx -C_2 \cdot \varpi \cdot \tan[\varpi(\pi - \alpha_{\text{TCSC}})]. \quad (5.72)$$

Extensive testing carried out with a wide range of practical combination of values of  $X_C$  and  $X_L$  confirm that Expression (5.72) represents the most significant term of Equation (5.31) for the range of interest of TCSC operation.

Expression (5.72) is further altered to include the reactance of the compensated transmission line (i.e.  $X_{TCSC(1)} + X_{TL} = X_{TCSC(1)}$ ) and then solving for  $\alpha_{TCSC}$ ,

$$\alpha_{TCSC} = \pi - \frac{1}{\varpi} \arctan \left( \frac{-X_{TCSC(1)-TL}}{C_2 \varpi} \right). \quad (5.73)$$

It has been found that this expression yields very effective initialisations of  $\alpha_{TCSC}$  when the reactance contribution of the TCSC to  $X_{TCSC(1)-TL}$  is assumed to be nil. Hence,

$$\alpha_{TCSC} = \pi - \frac{1}{\varpi} \arctan \left( \frac{-X_{TL}}{C_2 \varpi} \right). \quad (5.74)$$

### 5.8.4 Controllers Represented by Series Synchronous Voltage Sources

Suitable initialisation of series voltage sources in power flow studies is mandatory to ensure robust solutions. Examples of power electronic controllers that use one or more series voltage sources are: the static synchronous series compensator (SSSC), UPFC, and the latest addition to the family of FACTS controllers, the interline power flow controller (IPFC).

Different equations exist for the purpose of initialising the series voltage source, depending on the operating condition exhibited by the controller. For example, for the case when active and reactive powers are specified at bus  $k$ , and assuming  $V_k = V_m = 1$  p.u., and  $\theta_k = \theta_m = 0$  in Equations (5.50) and (5.51), leads to the following simple expressions:

$$V_{cR} = X_{cR} (P_{msp}^2 + Q_{msp}^2)^{1/2}, \quad (5.75)$$

$$\theta_{cR} = \arctan \left( \frac{P_{msp}}{Q_{msp}} \right). \quad (5.76)$$

These equations are used to initialise the parameters of series voltage sources within the Newton–Raphson power flow solution. These parameters are referred to as  $V_{vR}^{(0)}$  and  $\theta_{vR}^{(0)}$ .

## 5.9 SUMMARY

This chapter has covered the topic of power flow models of FACTS controllers and assessed their role in network-wide applications. Key aspects of modelling implementation in power flow algorithms have received attention. Numerical examples have been included for each one of the FACTS controllers presented.

The nonlinear power flow equations of the various FACTS controllers have been linearised and included in a Newton–Raphson power flow algorithm. In this context, the state variables corresponding to the controllable devices have been combined simultaneously

with the state variables of the network in a single frame of reference for unified, iterative solutions. The robustness of the method has been illustrated by numerical examples.

Coordinated strategies have been developed to handle cases when more than one controller, either conventional or FACTS, regulates voltage magnitude at the same bus.

The starting values given to state variables of some FACTS controllers have proved to have a determining effect as to whether or not the power flow solution can be obtained. This is an implementation aspect of paramount importance and has been duly addressed. A set of analytical equations has been derived to give series synchronous voltage sources good initial conditions. The case of shunt synchronous voltage sources is not a critical issue. The variable series compensation representation based on firing angle is a highly nonlinear model, and use of the simple analytical equation presented in this chapter for initialisation purposes should be used.

## REFERENCES

- Acha, E., 1993, 'A Quasi-Newton Algorithm for the Load Flow Solution of Large Networks with FACTS Controlled Branches', in *Proceedings of the 28th Universities Power Engineering Conference 1993, Staffordshire University, Volume 1, 21–23 September, Stafford, UK*, pp. 153–156.
- Ambriz-Pérez, H., Acha, E., and Fuerte-Esquivel, C.R., 2000, 'Advanced SVC Models for Newton–Raphson Load Flow and Newton Optimal Power Flow Studies', *IEEE Trans. Power Systems* **15**(1) 129–136.
- Arrillaga, J., Arnold, C.P., 1990, *Computer Analysis of Power Systems*, John Wiley & Sons, Chichester.
- Chang, S.K., Brandwajn V., 1988, 'Adjusted Solutions in Fast Decoupled Load Flow', *IEEE Trans. Power Systems* **3**(2) 726–733.
- Erinmez, I.A. (Ed.), 1986, 'Static Var Compensators', Working Group 38-01, Task Force No. 2 on SVC, Conseil International des Grands Réseaux Electriques (CIGRÉ).
- Fuerte-Esquivel, C.R., Acha, E., 1996, 'Newton–Raphson Algorithm for the Reliable Solution of Large Power Networks with Embedded FACTS Devices', *IEE Proceedings : Generation, Transmission and Distribution* **143**(5) 447–454.
- Fuerte-Esquivel, C.R., Acha, E., 1997, 'The Unified Power Flow Controller: A Critical Comparison of Newton–Raphson UPFC Algorithms in Power Flow Studies' *IEE Proceedings : Generation, Transmission and Distribution* **144**(5) 437–444.
- Fuerte-Esquivel, C.R., Acha, E., Ambriz-Pérez, H., 2000a, 'Integrated SVC and Step-down Transformer Model for Newton–Raphson Load Flow Studies', *IEEE Power Engineering Review* **20**(2) 45–46.
- Fuerte-Esquivel, C.R., Acha, E., Ambriz-Pérez, H., 2000b, 'A Thyristor Controlled Series Compensator Model for the Power Flow Solution of Practical Power Networks', *IEEE Trans. Power Systems* **15**(1) 58–64.
- Fuerte-Esquivel, C.R., Acha, E., Ambriz-Pérez, H., 2000c, 'A Comprehensive UPFC Model for the Quadratic Load Flow Solution of Power Networks', *IEEE Trans. Power Systems* **15**(1) 102–109.
- Fuerte-Esquivel, C.R., Acha, E., Tan, S.G., Rico, J.J., 1998, 'Efficient Object Oriented Power System Software for the Analysis of Large-scale Networks Containing FACTS Controlled Branches', *IEEE Trans. Power System* **3**(2) 464–472.
- Grainger, J.J., Stevenson W.D. Jr., 1994, *Power System Analysis*, McGraw-Hill, New York.
- Hingorani, N.G., Gyugyi, L., 2000, *Understanding FACTS Concepts and Technology of Flexible AC Transmission Systems*, Institute of Electrical and Electronic Engineers, New York.
- IEEE/CIGRÉ: (Institute of Electrical and Electronic Engineers/Conseil International des Grands Réseaux Électriques), 1995, 'FACTS Overview', Special Issue, 95TP108, IEEE Service Center, Piscataway, NJ.

- IEEE SSCWG (Special Stability Controls Working Group), 1995, 'Static Var Compensator Models for Power Flow and Dynamic Performance Simulation', *IEEE Trans. Power Systems* **9**(1) 229–240.
- Kundur P.P., 1994, *Power System Stability and Control*, McGraw-Hill, New York.
- Nabavi-Niaki, A., Iravani, M.R., 1996, 'Steady-state and Dynamic Models of Unified Power Flow Controller (UPFC) for Power System Studies', *IEEE Trans. Power Delivery* **11**(4) 1937–1943.
- Noroozian M., Andersson G., 1993, 'Power Flow Control by Use of Controllable Series Components', *IEEE Trans. on Power Delivery* **8**(3) 1420–1429.
- Song, Y.H., Johns, A.T., 1999, *Flexible AC Transmission Systems (FACTS)*, Institution of Electric Engineers, London.
- Tinney W.F., Hart C.E., 1967, 'Power Flow Solution by Newton's Method', *IEEE Trans. Power Apparatus and Systems* **PAS-96**(11) 1449–1460.

# 6

## Three-phase Power Flow

### 6.1 INTRODUCTION

If no proper action is taken at the design stage, long-distance alternating-current (AC) transmission circuits introduce a significant amount of geometric unbalance, which in turn causes undesirable voltage, current, and power flow imbalances (Wasley and Shlash, 1974a, 1947b). Over the years, a number of anomalies have been traced to the existence of power system imbalances, such as increased power losses, heating of synchronous generators, misfiring of power converters and ill-tripping of protective relays (Arrillaga and Harker, 1978; Harker and Arrillaga, 1979). Quite often, transmission lines are cited as the sole, most important, reason for the existence of geometric imbalances (Hesse, 1966). In the past, line transpositions were a popular resource for restoring geometric balance, but nowadays the tendency is to avoid them on economic and design grounds. Under normal circumstances, other power plant equipment such as transformers, generators, and shunt and series banks of capacitors introduce little geometric unbalance and are no cause for concern. Moreover, bulk transmission loads tend to be balanced.

In low-voltage distribution systems, the opposite situation exists. Three-phase transmission lines and cables are short and tend to be geometrically balanced, but urban loads are mostly of the single-phase type, fed from single-phase feeders. In aggregate, at the distribution substation, they result in three-phase loads exhibiting a high degree of unbalance. The rapid growth of electrified railroads has also been cited as a contributing factor to distribution system imbalances (Zhang and Chen, 1994). In rural circuits, continuity of supply has sometimes been maintained by using two of the three single-phase transformers in the bank, following failure of one of the units. The resulting three-phase transformer connection is termed ‘open delta’ and, although not recommended for normal operation owing to its unbalanced nature, can be used as a last resort to maintain supply. Positive sequence power flows are not suitable for the study of power losses in systems exhibiting significant transmission imbalances. The alternative solution approach is to use a three-phase power flow algorithm, with all the relevant power plant equipment modelled in phase coordinates, as detailed in Chapter 3 (Chen and Dillon, 1974; Laughton, 1968). Comprehensive assessments of the impact of unbalanced loading and equipment on system operation are carried out with little effort using fully fledged three-phase power flow solutions

(Birt, Graffy, and McDonald, 1976; Chen *et al.*, 1990; Laughton and Saleh, 1985; Smith and Arrillaga, 1998).

Line transpositions are no longer regarded as the preferred option for keeping geometric imbalances under control. Instead, a new solution is emerging, based on the use of power electronics. If a thyristor-controlled series compensator (TCSC) is already available for the purpose of impedance compensation then the idea would be to operate it in an unbalanced manner so that geometric balance can be restored at the point of connection. The applicability of a static VAR compensator (SVC) to restore voltage balance, in addition to achieving its primary function of providing reactive power support, has been established at the simulation level. However, this is at the expense of injecting a substantial amount of third harmonic current into the AC system. An alternative solution is to use a static compensator (STATCOM) for which the harmonic generation pattern is not significantly influenced by terminal AC voltage conditions.

To carry out comprehensive studies of active and reactive power flows in unbalanced transmission systems, and to determine the role that FACTS controllers may play in reducing transmission imbalances, it is mandatory to have a three-phase power flow computer program with FACTS equipment modelling capability (Angeles-Camacho, 2000; Venegas and Fuerte-Esquivel, 2001). This is the object of this chapter, where the theory of three-phase power flow is presented. It builds on the strength of the material presented in Chapters 2–5. Chapters 2 and 3 addressed the modelling of FACTS controllers and conventional power systems plant in phase coordinates, respectively. Chapters 4 and 5 studied the theory of conventional and FACTS power flow using the Newton–Raphson method, respectively.

## 6.2 POWER FLOW IN THE PHASE FRAME OF REFERENCE

The starting point for developing nodal power equations suitable for three-phase power flow solutions using the Newton–Raphson method is to establish a relationship between injected bus currents and bus voltages. This may be achieved by using an approach similar to that followed in Section 4.2.1 for the case of positive sequence power flows.

With reference to the three-phase transmission circuit shown in Figure 3.2, and redrawn for convenience in Figure 6.1 in a slightly modified form, the three-phase currents and

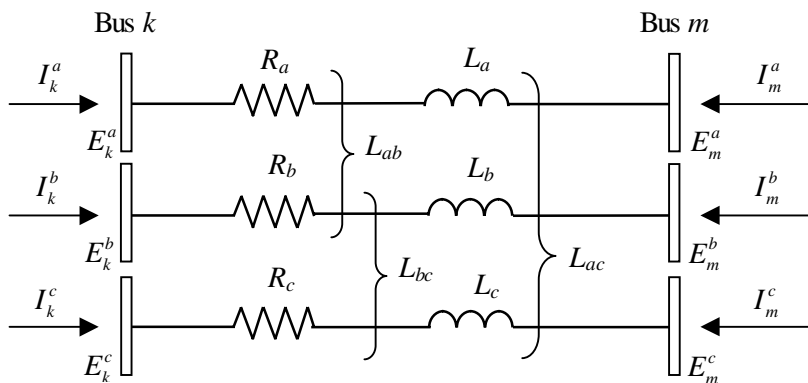


Figure 6.1 Three-phase branch

voltages are related by the transfer admittance matrix of the branch:

$$\begin{bmatrix} \mathbf{I}_k^{\text{abc}} \\ \mathbf{I}_m^{\text{abc}} \end{bmatrix} = \begin{bmatrix} \mathbf{Y}_{kk}^{\text{abc}} & \mathbf{Y}_{km}^{\text{abc}} \\ \mathbf{Y}_{mk}^{\text{abc}} & \mathbf{Y}_{mm}^{\text{abc}} \end{bmatrix} \begin{bmatrix} \mathbf{E}_k^{\text{abc}} \\ \mathbf{E}_m^{\text{abc}} \end{bmatrix}, \quad (6.1)$$

where

$$\mathbf{Y}_{kk}^{\text{abc}} = \mathbf{G}_{kk}^{\text{abc}} + j\mathbf{B}_{kk}^{\text{abc}} = \begin{bmatrix} R_{km}^{aa-g} + j\omega L_{km}^{aa-g} & R_{km}^{ab-g} + j\omega L_{km}^{ab-g} & R_{km}^{ac-g} + j\omega L_{km}^{ac-g} \\ R_{km}^{ba-g} + j\omega L_{km}^{ba-g} & R_{km}^{bb-g} + j\omega L_{km}^{bb-g} & R_{km}^{bc-g} + j\omega L_{km}^{bc-g} \\ R_{km}^{ca-g} + j\omega L_{km}^{ca-g} & R_{km}^{cb-g} + j\omega L_{km}^{cb-g} & R_{km}^{cc-g} + j\omega L_{km}^{cc-g} \end{bmatrix}^{-1}, \quad (6.2)$$

$$\begin{aligned} \mathbf{Y}_{kk}^{\text{abc}} &= \mathbf{Y}_{mm}^{\text{abc}} = -\mathbf{Y}_{km}^{\text{abc}} = -\mathbf{Y}_{mk}^{\text{abc}}, \\ \mathbf{E}_k^{\text{abc}} &= [E_k^a \ E_k^b \ E_k^c]^t = [V_k^a e^{j\theta_k^a} \ V_k^b e^{j\theta_k^b} \ V_k^c e^{j\theta_k^c}]^t, \\ \mathbf{E}_m^{\text{abc}} &= [E_m^a \ E_m^b \ E_m^c]^t = [V_m^a e^{j\theta_m^a} \ V_m^b e^{j\theta_m^b} \ V_m^c e^{j\theta_m^c}]^t, \\ \mathbf{I}_k^{\text{abc}} &= [I_k^a \ I_k^b \ I_k^c]^t, \\ \mathbf{I}_m^{\text{abc}} &= [I_m^a \ I_m^b \ I_m^c]^t, \end{aligned} \quad (6.3)$$

and where t is the transpose of the matrix or vector. Notice that the impedance parameters in Equation (6.2) are assumed to include the impedance contribution due to ground return loops.

### 6.2.1 Power Flow Equations

Expressions for active and reactive power injected at the three-phase buses  $k$  and  $m$  of Figure 6.1 may be derived from the following complex power expression:

$$\begin{bmatrix} \mathbf{S}_k^{\text{abc}} \\ \mathbf{S}_m^{\text{abc}} \end{bmatrix} = \begin{bmatrix} \mathbf{P}_k^{\text{abc}} + j\mathbf{Q}_k^{\text{abc}} \\ \mathbf{P}_m^{\text{abc}} + j\mathbf{Q}_m^{\text{abc}} \end{bmatrix} = \begin{bmatrix} \mathbf{E}_k^{\text{abc}} \mathbf{I}_k^{\text{abc}*} \\ \mathbf{E}_m^{\text{abc}} \mathbf{I}_m^{\text{abc}*} \end{bmatrix}. \quad (6.4)$$

After some arduous algebra, the expressions for active and reactive powers injected at phases  $a$ ,  $b$ , and  $c$  of bus  $k$  are arrived at:

$$P_k^\rho = V_k^\rho \left\{ \sum_{i=k,m} \sum_{j=a,b,c} V_i^j [G_{ki}^{\rho j} \cos(\theta_k^\rho - \theta_i^j) + B_{ki}^{\rho j} \sin(\theta_k^\rho - \theta_i^j)] \right\}, \quad (6.5)$$

$$Q_k^\rho = V_k^\rho \left\{ \sum_{i=k,m} \sum_{j=a,b,c} V_i^j [G_{ki}^{\rho j} \sin(\theta_k^\rho - \theta_i^j) - B_{ki}^{\rho j} \cos(\theta_k^\rho - \theta_i^j)] \right\}, \quad (6.6)$$

where the superscript  $\rho$  is used to denote phases  $a$ ,  $b$ , and  $c$ .

As expected, the expressions for calculating the active and reactive powers injected at bus  $m$  are of the same form as Equations (6.5) and (6.6), with the subscript  $m$  replacing  $k$ , and vice versa:

$$P_m^\rho = V_m^\rho \left\{ \sum_{i=m,k} \sum_{j=a,b,c} V_i^j [G_{mi}^{\rho j} \cos(\theta_m^\rho - \theta_i^j) + B_{mi}^{\rho j} \sin(\theta_m^\rho - \theta_i^j)] \right\}, \quad (6.7)$$

$$Q_m^\rho = V_m^\rho \left\{ \sum_{i=m,k} \sum_{j=a,b,c} V_i^j [G_{mi}^{\rho j} \sin(\theta_m^\rho - \theta_i^j) - B_{mi}^{\rho j} \cos(\theta_m^\rho - \theta_i^j)] \right\}. \quad (6.8)$$

### 6.2.2 Newton–Raphson Power Flow Algorithm

Solution of the positive sequence nodal power equations using the Newton–Raphson method has shown strong reliability towards convergence. Building on experience, the Newton–Raphson technique has been adopted to solve the three-phase nodal power equations.

The power expressions Equations (6.5)–(6.8) are linearised around a base operating point, as illustrated in Section 4.3.2 for the case of positive sequence power flow. In the three-phase application, mismatch powers and state variables terms become vectors of order  $3 \times 1$ , and individual Jacobian terms become matrices of order  $3 \times 3$ . The resulting linearised equation, suitable for iterative solutions, becomes:

$$\begin{bmatrix} \Delta \mathbf{P}_\ell^\rho \\ \Delta \mathbf{Q}_\ell^\rho \end{bmatrix}^{(i)} = \begin{bmatrix} \frac{\partial \mathbf{P}_\ell^\rho}{\partial \boldsymbol{\theta}_j^\rho} & \frac{\partial \mathbf{P}_\ell^\rho}{\partial \mathbf{V}_j^\rho} \mathbf{V}_j^\rho \\ \frac{\partial \mathbf{Q}_\ell^\rho}{\partial \boldsymbol{\theta}_j^\rho} & \frac{\partial \mathbf{Q}_\ell^\rho}{\partial \mathbf{V}_j^\rho} \mathbf{V}_j^\rho \end{bmatrix}^{(i)} \begin{bmatrix} \Delta \boldsymbol{\theta}_j^\rho \\ \frac{\Delta \mathbf{V}_j^\rho}{\mathbf{V}_j^\rho} \end{bmatrix}^{(i)}, \quad (6.9)$$

where  $\ell = k, m, j = k, m$ , and  $(i)$  is the iteration number.

The vector terms take the following form:

$$\Delta \mathbf{P}_\ell^\rho = [\Delta P_k^a \ \Delta P_k^b \ \Delta P_k^c \ \Delta P_m^a \ \Delta P_m^b \ \Delta P_m^c]^t, \quad (6.10)$$

$$\Delta \mathbf{Q}_\ell^\rho = [\Delta Q_k^a \ \Delta Q_k^b \ \Delta Q_k^c \ \Delta Q_m^a \ \Delta Q_m^b \ \Delta Q_m^c]^t, \quad (6.11)$$

$$\Delta \boldsymbol{\theta}_j^\rho = [\Delta \theta_k^a \ \Delta \theta_k^b \ \Delta \theta_k^c \ \Delta \theta_m^a \ \Delta \theta_m^b \ \Delta \theta_m^c]^t, \quad (6.12)$$

$$\frac{\Delta \mathbf{V}_j^\rho}{\mathbf{V}_j^\rho} = \left[ \frac{\Delta V_k^a}{V_k^a} \ \frac{\Delta V_k^b}{V_k^b} \ \frac{\Delta V_k^c}{V_k^c} \ \frac{\Delta V_m^a}{V_m^a} \ \frac{\Delta V_m^b}{V_m^b} \ \frac{\Delta V_m^c}{V_m^c} \right]^t. \quad (6.13)$$

The Jacobian terms are:

$$\frac{\partial \mathbf{P}_\ell^\rho}{\partial \boldsymbol{\theta}_j^\rho} = \begin{bmatrix} \frac{\partial P_\ell^a}{\partial \theta_j^a} & \frac{\partial P_\ell^a}{\partial \theta_j^b} & \frac{\partial P_\ell^a}{\partial \theta_j^c} \\ \frac{\partial P_\ell^b}{\partial \theta_j^a} & \frac{\partial P_\ell^b}{\partial \theta_j^b} & \frac{\partial P_\ell^b}{\partial \theta_j^c} \\ \frac{\partial P_\ell^c}{\partial \theta_j^a} & \frac{\partial P_\ell^c}{\partial \theta_j^b} & \frac{\partial P_\ell^c}{\partial \theta_j^c} \end{bmatrix}, \quad (6.14)$$

$$\frac{\partial \mathbf{P}_\ell^\rho}{\partial \mathbf{V}_j^\rho} \mathbf{V}_j^\rho = \begin{bmatrix} \frac{\partial P_\ell^a}{\partial V_j^a} V_j^a & \frac{\partial P_\ell^a}{\partial V_j^b} V_j^b & \frac{\partial P_\ell^a}{\partial V_j^c} V_j^c \\ \frac{\partial P_\ell^b}{\partial V_j^a} V_j^a & \frac{\partial P_\ell^b}{\partial V_j^b} V_j^b & \frac{\partial P_\ell^b}{\partial V_j^c} V_j^c \\ \frac{\partial P_\ell^c}{\partial V_j^a} V_j^a & \frac{\partial P_\ell^c}{\partial V_j^b} V_j^b & \frac{\partial P_\ell^c}{\partial V_j^c} V_j^c \end{bmatrix}, \quad (6.15)$$

$$\frac{\partial \mathbf{Q}_\ell^\rho}{\partial \boldsymbol{\theta}_j^\rho} = \begin{bmatrix} \frac{\partial Q_\ell^a}{\partial \theta_j^a} & \frac{\partial Q_\ell^a}{\partial \theta_j^b} & \frac{\partial Q_\ell^a}{\partial \theta_j^c} \\ \frac{\partial Q_\ell^b}{\partial \theta_j^a} & \frac{\partial Q_\ell^b}{\partial \theta_j^b} & \frac{\partial Q_\ell^b}{\partial \theta_j^c} \\ \frac{\partial Q_\ell^c}{\partial \theta_j^a} & \frac{\partial Q_\ell^c}{\partial \theta_j^b} & \frac{\partial Q_\ell^c}{\partial \theta_j^c} \end{bmatrix}, \quad (6.16)$$

$$\frac{\partial \mathbf{Q}_\ell^\rho}{\partial \mathbf{V}_j^\rho} \mathbf{V}_j^\rho = \begin{bmatrix} \frac{\partial Q_\ell^a}{\partial V_j^a} V_j^a & \frac{\partial Q_\ell^a}{\partial V_j^b} V_j^b & \frac{\partial Q_\ell^a}{\partial V_j^c} V_j^c \\ \frac{\partial Q_\ell^b}{\partial V_j^a} V_j^a & \frac{\partial Q_\ell^b}{\partial V_j^b} V_j^b & \frac{\partial Q_\ell^b}{\partial V_j^c} V_j^c \\ \frac{\partial Q_\ell^c}{\partial V_j^a} V_j^a & \frac{\partial Q_\ell^c}{\partial V_j^b} V_j^b & \frac{\partial Q_\ell^c}{\partial V_j^c} V_j^c \end{bmatrix}. \quad (6.17)$$

It should be noted that the linearised Equation (6.9) applies to only one three-phase transmission line connected between buses  $k$  and  $m$ . However, the result may be readily extended to the more practical case, involving  $n_l$  transmission lines connected between  $n_b$  generic buses  $\ell$  and  $j$ , where  $\ell = 1, \dots, k, m, \dots, n_b - 1$ , and  $j = 1, \dots, k, m, \dots, n_b - 1$ . Note that only  $n_b - 1$  buses are considered since the contribution of the slack bus is not explicitly represented in the linearised system of equations.

Consider the  $\ell$ th element connected between buses  $k$  and  $m$  in Equation (6.9), for which the self and mutual Jacobian terms are explicitly given below, with the help of two phase superscripts  $\rho_1$  and  $\rho_2$  used to denote  $a$ ,  $b$ , and  $c$ , respectively.

For  $k = m$ , and  $\rho_1 = \rho_2$ :

$$\frac{\partial P_{k,l}^{\rho_1}}{\partial \theta_{k,l}^{\rho_1}} = -Q_k^{\rho_1 \text{ cal}} - (V_k^{\rho_1})^2 B_{kk}^{\rho_1 \rho_1}, \quad (6.18)$$

$$\frac{\partial P_{k,l}^{\rho_1}}{\partial V_{k,l}^{\rho_1}} V_{k,l}^{\rho_1} = P_k^{\rho_1 \text{ cal}} + (V_k^{\rho_1})^2 G_{kk}^{\rho_1 \rho_1}, \quad (6.19)$$

$$\frac{\partial Q_{k,l}^{\rho_1}}{\partial \theta_{k,l}^{\rho_1}} = P_k^{\rho_1 \text{ cal}} - (V_k^{\rho_1})^2 G_{kk}^{\rho_1 \rho_1}, \quad (6.20)$$

$$\frac{\partial Q_{k,l}^{\rho_1}}{\partial V_{k,l}^{\rho_1}} V_{k,l}^{\rho_1} = Q_k^{\rho_1 \text{ cal}} - (V_k^{\rho_1})^2 B_{kk}^{\rho_1 \rho_1}. \quad (6.21)$$

For  $k = m$ , and  $\rho_1 \neq \rho_2$ :

$$\frac{\partial P_{k,l}^{\rho_1}}{\partial \theta_{k,l}^{\rho_2}} = V_k^{\rho_1} V_k^{\rho_2} \left[ G_{kk}^{\rho_1 \rho_2} \sin(\theta_k^{\rho_1} - \theta_k^{\rho_2}) - B_{kk}^{\rho_1 \rho_2} \cos(\theta_k^{\rho_1} - \theta_k^{\rho_2}) \right], \quad (6.22)$$

$$\frac{\partial P_{k,l}^{\rho_1}}{\partial V_{k,l}^{\rho_2}} V_{k,l}^{\rho_2} = V_k^{\rho_1} V_k^{\rho_2} \left[ G_{kk}^{\rho_1 \rho_2} \cos(\theta_k^{\rho_1} - \theta_k^{\rho_2}) + B_{kk}^{\rho_1 \rho_2} \sin(\theta_k^{\rho_1} - \theta_k^{\rho_2}) \right], \quad (6.23)$$

$$\frac{\partial Q_{k,l}^{\rho_1}}{\partial \theta_{k,l}^{\rho_2}} = -V_k^{\rho_1} V_k^{\rho_2} \left[ G_{kk}^{\rho_1 \rho_2} \cos(\theta_k^{\rho_1} - \theta_k^{\rho_2}) + B_{kk}^{\rho_1 \rho_2} \sin(\theta_k^{\rho_1} - \theta_k^{\rho_2}) \right], \quad (6.24)$$

$$\frac{\partial Q_{k,l}^{\rho_1}}{\partial V_{k,l}^{\rho_2}} V_{k,l}^{\rho_2} = V_k^{\rho_1} V_k^{\rho_2} \left[ G_{kk}^{\rho_1 \rho_2} \sin(\theta_k^{\rho_1} - \theta_k^{\rho_2}) - B_{kk}^{\rho_1 \rho_2} \cos(\theta_k^{\rho_1} - \theta_k^{\rho_2}) \right]. \quad (6.25)$$

For  $k \neq m$ :

$$\frac{\partial P_{k,l}^{\rho_1}}{\partial \theta_{m,l}^{\rho_2}} = V_k^{\rho_1} V_m^{\rho_2} \left[ G_{km}^{\rho_1 \rho_2} \sin(\theta_k^{\rho_1} - \theta_m^{\rho_2}) - B_{km}^{\rho_1 \rho_2} \cos(\theta_k^{\rho_1} - \theta_m^{\rho_2}) \right], \quad (6.26)$$

$$\frac{\partial P_{k,l}^{\rho 1}}{\partial V_{m,l}^{\rho 2}} V_{m,l}^{\rho 2} = V_k^{\rho 1} V_m^{\rho 2} \left[ G_{km}^{\rho 1 \rho 2} \cos(\theta_k^{\rho 1} - \theta_m^{\rho 2}) + B_{km}^{\rho 1 \rho 2} \sin(\theta_k^{\rho 1} - \theta_m^{\rho 2}) \right], \quad (6.27)$$

$$\frac{\partial Q_{k,l}^{\rho 1}}{\partial \theta_{m,l}^{\rho 2}} = -V_k^{\rho 1} V_m^{\rho 2} \left[ G_{km}^{\rho 1 \rho 2} \cos(\theta_k^{\rho 1} - \theta_m^{\rho 2}) + B_{km}^{\rho 1 \rho 2} \sin(\theta_k^{\rho 1} - \theta_m^{\rho 2}) \right], \quad (6.28)$$

$$\frac{\partial Q_{k,l}^{\rho 1}}{\partial V_{m,l}^{\rho 2}} V_{m,l}^{\rho 2} = V_k^{\rho 1} V_m^{\rho 2} \left[ G_{km}^{\rho 1 \rho 2} \sin(\theta_k^{\rho 1} - \theta_m^{\rho 2}) - B_{km}^{\rho 1 \rho 2} \cos(\theta_k^{\rho 1} - \theta_m^{\rho 2}) \right]. \quad (6.29)$$

The iterative solution of the three-phase power flow equations using the Newton–Raphson method requires similar considerations to those applied in the case of positive sequence solutions regarding state variable initialisation and generator reactive power limit checking, as presented in Sections 4.3.3 and 4.3.4, respectively. However, note that in the three-phase application the voltage phase angles of phases *a*, *b*, and *c* are initialised at values of 0,  $-2\pi/3$ , and  $2\pi/3$ , respectively.

### 6.2.3 Matlab<sup>®</sup> Code of a Power Flow Program in the Phase Frame of Reference

The Matlab<sup>®</sup> computer program, given in Section 4.3.6, has been extended to cater for the power flow solution of three-phase networks. The function `TLParameters` is used to furnish transmission-line data in phase coordinates, starting from positive, negative, and zero sequence information. This information is widely available in utility data bases since it is used for the purpose of short-circuit current calculations, even though its usefulness is of somewhat limited applicability in three-phase power flow studies, as it assumes that transmission lines are geometrically balanced. The relevant theory is covered in Section 3.2.13. If more realistic representation of transmission lines are required then the function `LongLine` given in Sections 3.2.7 and function `TransmissionLineData` given in Section 3.2.11 can be used, and the ensuing transmission-line parameters supplied to the three-phase power flow application.

Generators are represented as three-phase active power injections and adjustable reactive power injections to meet specified nodal voltage magnitudes at their terminals. If a more realistic synchronous generator representation is required then the three-phase model derived in Section 3.4 should be implemented in the power flow program. Note that this is a very comprehensive model which caters for saliency and has explicit representation of the generator load angle.

To keep the length and complexity of the current program (Program 6.1) within bounds, it does not contain provisions for three-phase transformer representation. However, implementation of three-phase transformer banks with a wide range of connections can be implemented with ease. The most popular transformer connections are detailed in Section 3.3.4, where emphasis is placed on transformer complex tap modelling.

Loads are taken to be constant sinks of active and reactive power in the program but, again, voltage dependency can be incorporated by using the relevant models provided in Section 3.5.

Program 6.1 Program written in Matlab<sup>®</sup> to carry out power flow calculations in the three-phase frame of reference using the Newton–Raphson method

```

PowerFlowsData3Ph; % read threephasedata

[TLImpedInv,TLAdmit]=TLParameters(ntl,tlresisp,tlreacp,tlcondp,...
tlsuscepp,tlresisz,tlreacz,tlcondz,tlsuscepz);

[YR,YI]=YBus3Ph(nbb,ntl,tlsend,tlrec,TLImpedInv,TLAdmit,nsh,...
shbus,shresis,shreac);

[VM,VA,it]=NewtonRaphson3Ph(nmax,tol,itmax,ngn,ntl,tlsend,tlrec,...
nld,nbb,bustype,genbus,loadbus,PGEN,QGEN,QMAX,QMIN,PLOAD,QLOAD,...
YR,YI,TLImpedInv,TLAdmit,VM,VA);

[PQsend,PQrec,PQloss]=PowerFlows3Ph(nbb,ntl,tlsend,tlrec,VM,VA,...
TLImpedInv,TLAdmit);

% END of main three-phase program

function [TLImpedInv,TLAdmit]=TLParameters(ntl,tlresisp,tlreacp,...
tlcondp,tluscepp,tlresisz,tlreacz,tlcondz,tluscepz)
% Transmission line parameters
TLImpedInv=zeros(3,3,ntl);
TLAdmit=zeros(3,3,ntl);
for kk=1:ntl
    Zself=((tlresisz(kk)+tlreacz(kk)*i)+2*(tlresisp(kk)+tlreacp...
(kk)*i))/3;
    Zmutual=((tlresisz(kk)+tlreacz(kk)*i)-(tlresisp(kk)+tlreacp...
(kk)*i))/3;
    Yself=((tlcondz(kk)+tluscepz(kk)*i)+2*(tlcondp(kk)+...
tluscepp(kk)*i))/3;
    Ymutual=((tlcondz(kk)+tluscepz(kk)*i)-(tlcondp(kk)+tluscepp...
(kk)*i))/3;
    for ii=1:3
        for jj=1:3
            if ii==jj
                TLImpedInv(ii,jj,kk)=Zself;
                TLAdmit(ii,jj,kk)=Yself;
            else
                TLImpedInv(ii,jj,kk)=Zmutual;
            end
        end
    end
end

```

```

        TLAdmit(ii,jj,kk)=Ymutual;
    end
end
end
imped=TLImpedInv(1:3,1:3,kk);
imped2=inv(imped);
TLImpedInv(1:3,1:3,kk)=imped2;
end

```

```

function [YR,YI]=YBus3Ph(nbb,ntl,tlsend,tlrec,TLImpedInv,...
    TLAdmit,nsh,shbus,shresis,shreac)
% Set up YY
YY=zeros(nbb*3,nbb*3);
% Transmission lines contribution
for kk=1:ntl
    ii=(tlsend(kk)-1)*3+1;
    jj=(tlrec(kk)-1)*3+1;
    YY(ii:ii+2,ii:ii+2)=YY(ii:ii+2,ii:ii+2)+...
        TLImpedInv(:,,kk)+0.5*TLAdmit(:,,kk);
    YY(ii:ii+2,jj:jj+2)=YY(ii:ii+2,jj:jj+2)-TLImpedInv(:,,kk);
    YY(jj:jj+2,ii:ii+2)=YY(jj:jj+2,ii:ii+2)-TLImpedInv(:,,kk);
    YY(jj:jj+2,jj:jj+2)=YY(jj:jj+2,jj:jj+2)+...
        TLImpedInv(:,,kk)+0.5*TLAdmit(:,,kk);
end
% Shunt elements contribution
for kk=1:nsh
    SHAdmit=zeros(3,3);
    jj=shbus(kk)*3;
    for ii=1:3
        SHAdmit(ii,ii)=1/(shresis(kk,ii)+shreac(kk,ii)*i);
    end
    YY(jj-2:jj,jj-2:jj)=YY(jj-2:jj,jj-2:jj)+SHAdmit(:,,);
end
YR=real(YY);
YI=imag(YY);

function [VM,VA,it]=NewtonRaphson3Ph(nmax,tol,itmax,ngn,ntl,...
    tlsend,tlrec,nld,nbb,bustype,genbus,loadbus,PGEN,QGEN,QMAX,QMIN,...
    PLOAD,QLOAD,YR,YI,TLImpedInv,TLAdmit,VM,VA)
% GENERAL SETTINGS
D=zeros(1,nmax*3);
flag=0;
it=1;
% CALCULATE NET POWERS

```

```

[PNET,QNET]=NetPowers3Ph(nbb,ngn,nld,genbus,loadbus,PGEN,QGEN,...
PLOAD,QLOAD);

while ( it <= itmax & flag==0 )
% CALCULATED POWERS
  [PCAL,QCAL]=CalculatedPowers3Ph(nbb,ntl, tsend,tlrec,VM,VA,...
  TLImpedInv,TLAdmit);
% POWER MISMATCHES
  [DPQ,flag]=PowerMismatches3Ph(nmax,nbb,tol,bustype,flag,PNET,...
  QNET, PCAL,QCAL);
  if flag==1;
    break;
  end

% JACOBIAN FORMATION
  [JAC]=NewtonRaphsonJacobian3Ph(nmax,nbb,bustype,PCAL,QCAL,VM,...
  VA,YR, YI);

% SOLVE FOR THE STATE VARIABLES VECTOR
  D=JAC\DPQ';

% UPDATE STATE VARIABLES
  [VA,VM]=StateVariablesUpdates3Ph(nbb,D,VA,VM);

  it=it+1;
end

function [PNET,QNET]=NetPowers3Ph(nbb,ngn,nld,genbus,loadbus,...
PGEN,QGEN, PLOAD,QLOAD);
% CALCULATE NET POWERS
PNET=zeros(1,nbb*3);
QNET=zeros(1,nbb*3);
for ii=1:ngn
  for jj=1:3
    PNET((genbus(ii)-1)*3+jj)=PNET((genbus(ii)-1)*3+jj)+...
    PGEN(ii,jj);
    QNET((genbus(ii)-1)*3+jj)=QNET((genbus(ii)-1)*3+jj)+...
    QGEN(ii,jj);
  end
end
for ii=1:nld
  for jj=1:3
    PNET((loadbus(ii)-1)*3+jj)=PNET((loadbus(ii)-1)*3+jj)-...
    PLOAD(ii,jj);
  end
end

```

```

    QNET((loadbus(ii)-1)*3 + jj) = QNET((loadbus(ii)-1)*3 + jj) - ...
    QLOAD(ii,jj);
end
end

function [PCAL,QCAL] = CalculatedPowers3Ph(nbb,ntl,tlsend,tlrec,...
VM,VA, TLImpedInv,TLAdmit);
% Include all entries
PQsend = zeros(ntl,3);
PQrec = zeros(ntl,3);
PQloss = zeros(ntl,3);
for iii = 1 : ntl
    Vsend = ( VM(tlsend(iii),:).*cos(VA(tlsend(iii),:)) + ...
    VM(tlsend(iii),:).*sin(VA(tlsend(iii),:))*i );
    Vrec = ( VM(tlrec(iii),:).*cos(VA(tlrec(iii),:))...
    VM(tlrec(iii),:).*sin(VA(tlrec(iii),:))*i );
    for jj = 1 : 5
        if jj < 4
            PQsend(iii,jj) = Vsend(1,jj)*(conj(-TLImpedInv(jj,:,iii)) *...
            (Vrec(1,:))' + conj(TLImpedInv(jj,:,iii) + 0.5*...
            TLAdmit(jj,:,iii))*(Vsend(1,:))');
            PQrec(iii,jj) = Vrec(1,jj)*(-conj(TLImpedInv(jj,:,iii))*...
            (Vsend(1,:))' + conj(TLImpedInv(jj,:,iii) + 0.5*...
            TLAdmit(jj,:,iii))*(Vrec(1,:))');
        elseif jj == 4
            PQsend(iii,jj) = tlsend(iii);
            PQrec(iii,jj) = tlrec(iii);
        else
            PQsend(iii,jj) = tlrec(iii);
            PQrec(iii,jj) = tlsend(iii);
        end
        PQloss = PQsend - PQrec;
    end
end
PCAL1 = zeros(nbb,3);
for ii = 1 : nbb
    for jj = 1:ntl
        if PQsend(jj,4) == ii
            PCAL1(ii,:) = PCAL1(ii,:) + PQsend(jj,1:3);
        end
        if PQrec(jj,4) == ii
            PCAL1(ii,:) = PCAL1(ii,:) + PQrec(jj,1:3);
        end
    end
end
end
for ii = 1 : nbb

```

```

    PCAL2(1,3*ii-2:ii*3)=PCAL1(ii,:);
end
PCAL = real(PCAL2);
QCAL = imag(PCAL2);

function [DPQ,flag]=PowerMismatches3Ph(nmax,nbb,tol,bustype,...
flag,PNET,QNET,PCAL,QCAL);
% POWER MISMATCHES
DPQ=zeros(1,nmax);
DP=PNET - PCAL;
DQ=QNET - QCAL;
% To remove the active and reactive powers contributions of the slack
% bus and reactive power of all PV buses
kk=1;
for ii=1 : nbb
    for jj=1 : 3
        if (bustype(ii)==1 )
            DP(kk)=0;
            DQ(kk)=0;
        elseif (bustype(ii)==2 )
            DQ(kk)=0;
        end
        kk=kk + 1;
    end
end
% Re-arrange mismatch entries
kk=1;
for ii=1 : nbb
    for jj=1 : 3
        DPQ((ii-1)*3 + kk)=DP(kk);
        DPQ((ii-1)*3 + kk + 3)=DQ(kk);
        kk=kk+1;
    end
end
% Check for convergence
for ii=1 : nbb*6
    if (abs(DPQ) < tol)
        flag=1;
    end
end

function [JAC]=NewtonRaphsonJacobian(nmax,nbb,bustype,PCAL,QCAL,...
VM,VA, YR,YI);
% JACOBIAN FORMATION - Include all entries
JAC = zeros(nmax,nmax);

```

```

iii=1;
for ii=1 : nbb
    kk=(ii-1)*3 + 1;
    jjj=1;
    for jj=1 : nbb
        ll=(jj-1)*3 + 1;
        if ii==jj
            for mm=1:3;
                for nn=1:3;
                    if nn==mm
                        JAC(iii + mm-1, jjj + nn-1) = - QCAL(kk + mm-1) - VM(ii,mm)...
                        ^2*YI(kk + mm-1, kk + mm-1);
                        JAC(iii + mm-1, 3 + jjj + nn-1) = PCAL(kk + mm-1) + ...
                        VM(ii,mm)^2*YR(kk + mm-1, kk + mm-1);
                        JAC(iii + 3 + mm-1, jjj + nn-1) = PCAL(kk + mm-1) - VM(ii,mm)...
                        ^2*YR(kk + mm-1, kk + mm-1);
                        JAC(iii + 3 + mm-1, jjj + 3 + nn-1) = QCAL(kk + mm-1) - ...
                        VM(ii,mm)^2*YI(kk + mm-1, kk + mm-1);
                    else
                        JAC(iii + mm-1, jjj + nn-1) = VM(ii,mm)*VM(ii,nn)*(YR(kk + ...
                        mm-1, kk + nn-1)*sin(VA(ii,mm)-VA(ii,nn))-YI(kk + mm-1, ...
                        kk + nn-1)*cos(VA(ii,mm)-VA(ii,nn)));
                        JAC(iii + mm-1, 3 + jjj + nn-1) = VM(ii,mm)*VM(ii,nn)*...
                        (YR(kk + mm-1, kk + nn-1)*cos(VA(ii,mm)-VA(ii,nn)) + YI(kk + ...
                        mm-1, kk + nn-1)*sin(VA(ii,mm)-VA(ii,nn)));
                        JAC(iii + 3 + mm-1, jjj + nn-1) = -VM(ii,mm)*VM(ii,nn)*...
                        (YR(kk + mm-1, kk + nn-1)*cos(VA(ii,mm)-VA(ii,nn)) + YI(kk + ...
                        mm-1, kk + nn-1)*sin(VA(ii,mm)-VA(ii,nn)));
                        JAC(iii + 3 + mm-1, jjj + 3 + nn-1) = VM(ii,mm)*VM(ii,nn)...
                        *(YR(kk + mm-1, kk + nn-1)*sin(VA(ii,mm)-VA(ii,nn))-YI...
                        (kk + mm-1, kk + nn-1)*cos(VA(ii,mm)-VA(ii,nn)));
                    end
                end
            end
        end
    else
        for mm=1:3;
            for nn=1:3;
                JAC(iii + mm-1, jjj + nn-1) = VM(ii,mm)*VM(jj,nn)*(YR(kk + ...
                mm-1, ll + nn-1)*sin(VA(ii,mm)-VA(jj,nn)) - YI(kk + mm-1, ll + ...
                nn-1)*cos(VA(ii,mm)-VA(jj,nn)));
                JAC(iii + mm-1, 3 + jjj + nn-1) = VM(ii,mm)*VM(jj,nn)*(YR(kk + ...
                mm-1, ll + nn-1)*cos(VA(ii,mm)-VA(jj,nn)) + YI(kk + mm-1, ll + ...
                nn-1)*sin(VA(ii,mm)-VA(jj,nn)));
                JAC(iii + 3 + mm-1, jjj + nn-1) = -VM(ii,mm)*VM(jj,nn)*(YR(kk + ...
                mm-1, ll + nn-1)*cos(VA(ii,mm)-VA(jj,nn)) + YI(kk + mm-1, ll + ...
                nn-1)*sin(VA(ii,mm)-VA(jj,nn)));
                JAC(iii + 3 + mm-1, jjj + 3 + nn-1) = VM(ii,mm)*VM(jj,nn)...

```



```

    iii=iii+1;
end
end

function [PQsend,PQrec,PQloss]=PowerFlows3Ph(nbb,ntl,tlsend,...
tlrec,VM,VA,TLImpedInv,TLAdmit);
% Include all entries
PQsend=zeros(ntl,3);
PQrec=zeros(ntl,3);
PQloss=zeros(ntl,3);
for iii=1:ntl
    Vsend=( VM(tlsend(iii),:).*cos(VA(tlsend(iii),:))+...
    VM(tlsend(iii),:).*sin(VA(tlsend(iii),:))*i );
    Vrec=( VM(tlrec(iii),:).*cos(VA(tlrec(iii),:))+...
    VM(tlrec(iii),:).*sin(VA(tlrec(iii),:))*i );
    for jj=1:5
        if jj<4
            PQsend(iii,jj)=Vsend(1,jj)*(conj(-TLImpedInv(jj,:,iii))...
            *(Vrec(1,:))'+conj(TLImpedInv(jj,:,iii))+...
            0.5*TLAdmit(jj,:,iii) *(Vsend(1,:))');
            PQrec(iii,jj)=Vrec(1,jj)*(-conj(TLImpedInv(jj,:,iii))*...
            (Vsend(1,:))'+conj(TLImpedInv(jj,:,iii))+...
            0.5*TLAdmit(jj,:,iii) *(Vrec(1,:))');
        elseif jj==4
            PQsend(iii,jj)=tlsend(iii);
            PQrec(iii,jj)=tlrec(iii);
        else
            PQsend(iii,jj)=tlrec(iii);
            PQrec(iii,jj)=tlsend(iii);
        end
        PQloss=PQsend - PQrec;
    end
end
end

```

### 6.2.4 Numerical Example of a Three-phase Network

The five-bus network shown in Section 4.3.9 is used as the basis for illustrating how the three-phase power flow performs under balanced and unbalanced operating conditions. The file `threephasedata` contains all the required data for the power flow solution. Notice that voltage information is provided explicitly for the three phases, where a balanced set of three-phase voltages means equal voltage magnitude and phase angles between adjacent phases separated by  $2\pi/3$  radians, with the following rotation:  $0, -2\pi/3, 2\pi/3$ .

In this application, transmission lines require zero sequence information for resistance, reactance, susceptance, and conductance, in addition to the corresponding positive sequence parameters. Negative sequence parameters are not explicitly required since they are equal to

positive sequence parameters in transmission lines. It should be mentioned that in the original five-bus network, aimed at the testing of positive sequence power flow algorithms, no information exists for zero sequence transmission-line parameters. For the purpose of the current exercise, zero sequence transmission-line parameters have been taken to be three times the positive sequence values.

The function `threephasedata` for the balanced test case is as follows:

```
% Bubars data
nbb=5;
bustype(1)=1; VM(1,1)=1.06; VA(1,1)=0*pi/180;
VM(1,2)=1.06; VA(1,2)=240*pi/180; VM(1,3)=1.06; VA(1,3)=120*pi/180;
bustype(2)=2; VM(2,1)=1.00; VA(2,1)=0*pi/180;
VM(2,2)=1.00; VA(2,2)=240*pi/180; VM(2,3)=1; VA(2,3)=120*pi/180;
bustype(3)=3; VM(3,1)=1.00; VA(3,1)=0*pi/180;
VM(3,2)=1.00; VA(3,2)=240*pi/180; VM(3,3)=1; VA(3,3)=120*pi/180;
bustype(4)=3; VM(4,1)=1.00; VA(4,1)=0*pi/180;
VM(4,2)=1.00; VA(4,2)=240*pi/180; VM(4,3)=1; VA(4,3)=120*pi/180;
bustype(5)=3; VM(5,1)=1.00; VA(5,1)=0*pi/180;
VM(5,2)=1.00; VA(5,2)=240*pi/180; VM(5,3)=1; VA(5,3)=120*pi/180;

% Generators data
ngn=2;
genbus(1)=1; PGEN(1,1)=0.0; QGEN(1,1)=0; PGEN(1,2)=0.0;
QGEN(1,2)=0; PGEN(1,3)=0.0; QGEN(1,3)=0; QMAX(1)=9; QMIN(1)=-9;
genbus(2)=2; PGEN(2,1)=0.4; QGEN(2,1)=0.0; PGEN(2,2)=0.4;
QGEN(2,2)=0.0; PGEN(2,3)=0.4; QGEN(2,3)=0.0; QMAX(2)=9;
QMIN(2)=-9;

% Transmission lines data
ntl=7;
tlsen(1)=1; tlrec(1)=2; tlresisp(1)=0.02; tlreacp(1)=0.06;
tlcondp(1)=0; tlsuscepp(1)=0.060; tlresisz(1)=0.06;
tlreacz(1)=0.18; tlcondz(1)=0; tlsuscepz(1)=0.18;
tlsen(2)=1; tlrec(2)=3; tlresisp(2)=0.08; tlreacp(2)=0.24;
tlcondp(2)=0; tlsuscepp(2)=0.050; tlresisz(2)=0.24;
tlreacz(2)=0.72; tlcondz(2)=0; tlsuscepz(2)=0.15;
tlsen(3)=2; tlrec(3)=3; tlresisp(3)=0.06; tlreacp(3)=0.18;
tlcondp(3)=0; tlsuscepp(3)=0.040; tlresisz(3)=0.18;
tlreacz(3)=0.54; tlcondz(3)=0; tlsuscepz(3)=0.12;
tlsen(4)=2; tlrec(4)=4; tlresisp(4)=0.06; tlreacp(4)=0.18;
tlcondp(4)=0; tlsuscepp(4)=0.040; tlresisz(4)=0.18;
tlreacz(4)=0.54; tlcondz(4)=0; tlsuscepz(4)=0.12;
tlsen(5)=2; tlrec(5)=5; tlresisp(5)=0.04; tlreacp(5)=0.12;
tlcondp(5)=0; tlsuscepp(5)=0.030; tlresisz(5)=0.12;
tlreacz(5)=0.36; tlcondz(5)=0; tlsuscepz(5)=0.09;
tlsen(6)=3; tlrec(6)=4; tlresisp(6)=0.01; tlreacp(6)=0.03;
```

```

tlcondp(6)=0; tlsuscepp(6)=0.020; tlresisz(6)=0.03;
tlreacz(6)=0.09; tlcondz(6)=0; tlsuscepz(6)=0.06;
tlsend(7)=4; tlrec(7)=5; tlresisp(7)=0.08; tlreacp(7)=0.24;
tlcondp(7)=0; tlsuscepp(7)=0.050; tlresisz(7)=0.24;
tlreacz(7)=0.72; tlcondz(7)=0; tlsuscepz(7)=0.15;

% Loads data
nld=4;
loadbus(1)=2; PLOAD(1,1)=0.20; QLOAD(1,1)=0.10; PLOAD(1,2)=0.20;
QLOAD(1,2)=0.10; PLOAD(1,3)=0.20; QLOAD(1,3)=0.10;
loadbus(2)=3; PLOAD(2,1)=0.45; QLOAD(2,1)=0.15; PLOAD(2,2)=0.45;
QLOAD(2,2)=0.15; PLOAD(2,3)=0.45; QLOAD(2,3)=0.15;
loadbus(3)=4; PLOAD(3,1)=0.40; QLOAD(3,1)=0.05; PLOAD(3,2)=0.40;
QLOAD(3,2)=0.05; PLOAD(3,3)=0.40; QLOAD(3,3)=0.05;
loadbus(4)=5; PLOAD(4,1)=0.60; QLOAD(4,1)=0.10; PLOAD(4,2)=0.60;
QLOAD(4,2)=0.10; PLOAD(4,3)=0.60; QLOAD(4,3)=0.10;

% General parameters
itmax=10;
tol=1e-12;
nmax=6*nbb;

```

As expected, the solution given by the three-phase program essentially agrees with that provided by the positive sequence power flow program, given in Table 4.1. More specifically, the nodal voltage magnitudes and phase angles for phase *a* of the network coincide with those for the positive sequence. The voltage magnitude for phases *a*, *b*, and *c* have equal values, with the phase angles for phases *b* and *c* displaced by 240° and 120°, respectively, with respect to those of phase *a*. Table 6.1 summarises the results for the balanced three-phase solution. Convergence was achieved in 5 iterations to a power mismatch tolerance of 1e-12.

Since this is a case of balanced operation and design parameters – all loads are taken to be balanced – neither negative nor zero sequence voltages exist.

**Table 6.1** Three-phase nodal voltages for the balanced case

Voltage	Phase	Network bus				
		North	South	Lake	Main	Elm
Magnitude (p.u.)	<i>a</i>	1.06	1.00	0.9872	0.9841	0.9717
	<i>b</i>	1.06	1.00	0.9872	0.9841	0.9717
	<i>c</i>	1.06	1.00	0.9872	0.9841	0.9717
Phase angle (deg)	<i>a</i>	0	-2.06	-4.63	-4.95	-5.76
	<i>b</i>	240	237.93	235.36	235.04	234.23
	<i>c</i>	120	117.93	115.36	115.04	114.23

An altogether different situation arises if imbalances are introduced into the test network, say in the system load. This requires only a straightforward change in the data file, with the file `unbalthreephasedata` reflecting these changes – at each bus, active and reactive power loads have been altered arbitrarily by  $\pm 15\%$  with respect to the base, balanced case:

```
%Loads data with 15 unbalance

nld=4;

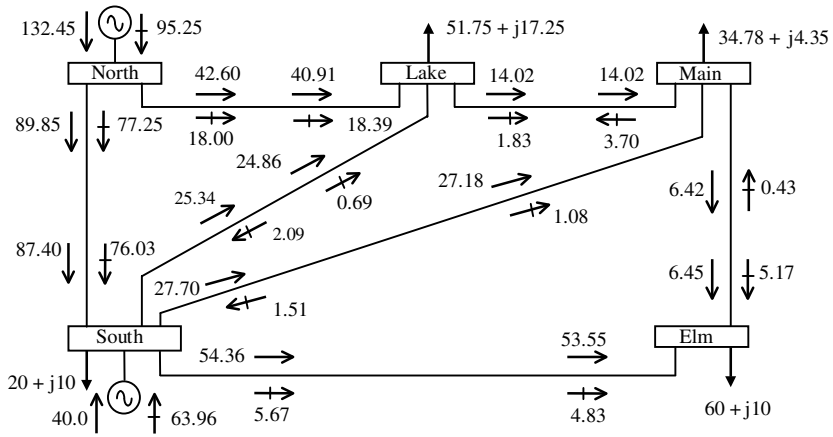
loadbus(1)=2;   PLOAD(1,1)=0.20;   QLOAD(1,1)=0.10;
PLOAD(1,2)=0.1739;   QLOAD(1,2)=0.08695;   PLOAD(1,3)=0.23;
QLOAD(1,3)=0.115;   loadbus(2)=3;
PLOAD(2,1)=0.5175;   QLOAD(2,1)=0.1725;
PLOAD(2,2)=0.45;   QLOAD(2,2)=0.15;   PLOAD(2,3)=0.3913;
QLOAD(2,3)=0.1304;   loadbus(3)=4;
PLOAD(3,1)=0.3478;   QLOAD(3,1)=0.0435;
LOAD(3,2)=0.46;   QLOAD(3,2)=0.0575;   PLOAD(3,3)=0.40;
QLOAD(3,3)=0.05;   loadbus(4)=5;
PLOAD(4,1)=0.60;   QLOAD(4,1)=0.10;
PLOAD(4,2)=0.5217;   QLOAD(4,2)=0.087;   PLOAD(4,3)=0.69;
QLOAD(4,3)=0.115;
```

Table 6.2(a) shows the three-phase voltage solution for unbalanced loading. The solution was achieved in 5 iterations to a power mismatch tolerance of  $1e-12$ .

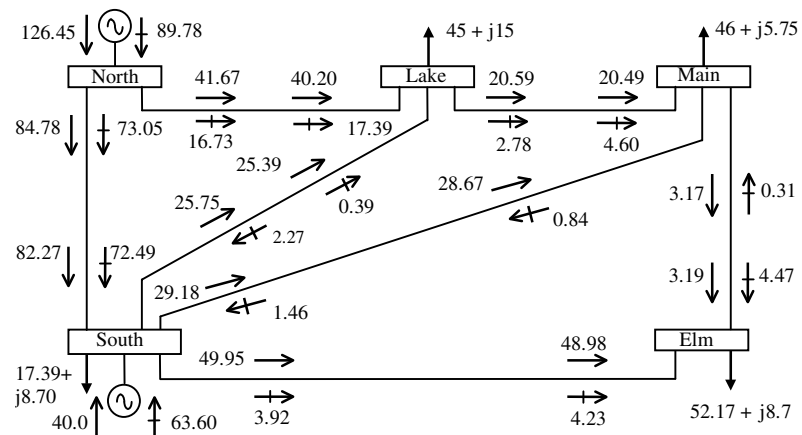
The impact of unbalanced loading on system performance can be appreciated by comparing the results given in Table 6.2(b), where small amounts of negative and zero

**Table 6.2** Three-phase nodal voltages in the unbalanced network: (a) phase voltages and (b) sequence voltages

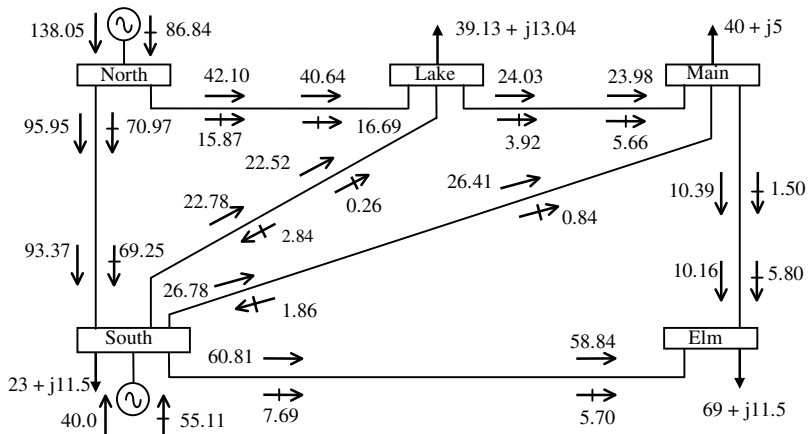
Voltage	Phase	Network bus				
		North	South	Lake	Main	Elm
(a) Phase voltages						
Magnitude (p.u.)	<i>a</i>	1.06	1.00	0.9820	0.9811	0.9789
	<i>b</i>	1.06	1.00	0.9881	0.9831	0.9755
	<i>c</i>	1.06	1.00	0.9908	0.9872	0.9599
Phase angle (deg)	<i>a</i>	0	-2.02	-4.67	-4.84	-5.96
	<i>b</i>	240	238.16	235.26	234.95	235.26
	<i>c</i>	120	117.58	115.38	114.88	113.23
(b) Sequence voltages						
Magnitude (p.u.)	Negative	0.00	0.0030	0.0032	0.0027	0.0148
	Positive	1.06	1.0000	0.9870	0.9838	0.9713
	Zero	0.00	0.0030	0.0020	0.0017	0.0070



(a)



(b)



(c)

Figure 6.2 Three-phase power flows: (a) phase a, (b) phase b, and (c) phase c

sequence voltages are now evident. Power system loss increased by nearly 2 % with respect to the balanced case. It can be seen from the power flow results in Figures 6.2(a)–6.2(c) that the power flows in all three phases are unbalanced.

It has been stated in the introduction of this chapter that FACTS controllers intended for nodal voltage control could perform the role of restoring voltage magnitude balance at the point of connection. It was also argued that a series compensator could provide a useful role in balancing out power flows at the point of compensation. Such use of FACTS controllers is assessed in the following sections.

### 6.3 STATIC VAR COMPENSATOR

In order to assess the role of SVC operation in unbalanced three-phase power systems it is necessary to develop a more detailed model of the SVC than the one developed in Section 5.3 for the case of positive sequence power flows. The new SVC power flow model is developed in the frame of reference afforded by the phases, building on its admittance matrix representation derived in Section 2.3.2.

The model corresponds to a three-phase, delta-connected thyristor-controlled reactor (TCR) placed in parallel with a three-phase bank of capacitors connected in star configuration, with its star point floating. Figure 6.3 shows the SVC equivalent circuit used to derive the three-phase power flow equations. The individual branches are adjusted individually, by controlling the firing angles of the thyristors, in order to achieve specified nodal voltage magnitudes while satisfying the constraint power equations. Two distinct SVC power flow models are described in this section: one uses controllable susceptances as state variables whereas the other uses the firing angles of the thyristors.

It is illustrated in Figure 6.3 that the three-phase, star-connected capacitor bank has an alternative representation in the form of a delta-connected equivalent circuit. Equation (6.30) describes the three-phase SVC model, which is obtained by the simple addition of

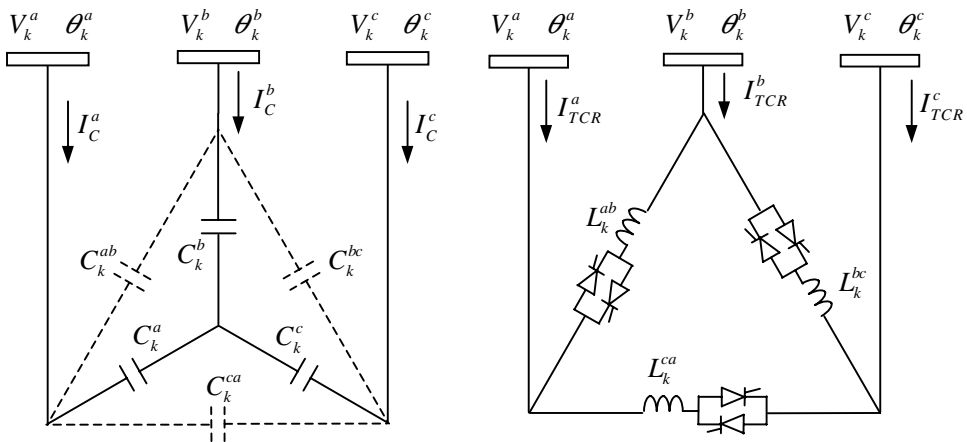


**Figure 6.3** Three-phase model of the static VAR compensator (SVC) in phase coordinates

Equations (2.10) and (2.14):

$$\begin{bmatrix} I_k^a \\ I_k^b \\ I_k^c \end{bmatrix} = \frac{1}{3} \begin{bmatrix} jB_{SVC}^{aa} & -jB_{SVC}^{ab} & -jB_{SVC}^{ac} \\ -jB_{SVC}^{ba} & jB_{SVC}^{bb} & -jB_{SVC}^{bc} \\ -jB_{SVC}^{ca} & -jB_{SVC}^{cb} & jB_{SVC}^{cc} \end{bmatrix} \begin{bmatrix} V_k^a \\ V_k^b \\ V_k^c \end{bmatrix}. \quad (6.30)$$

In this matrix expression, two different kinds of terms exist, namely, self and mutual terms:

$$B_{SVC}^{\rho_1 \rho_2} = \begin{cases} \frac{B_C^{\rho_1}}{\Delta B_C} \sum_{\substack{j=a,b,c \\ j \neq \rho_1}} B_C^j - \sum_{\substack{j=a,b,c \\ j \neq \rho_1}} B_{TCR}^{\rho_1 j}, & \text{for } \rho_1 = \rho_2; \\ -\frac{B_C^{\rho_1} B_C^{\rho_2}}{\Delta B_C} + B_{TCR}^{\rho_1 \rho_2}, & \text{for } \rho_1 \neq \rho_2; \end{cases} \quad (6.31)$$

where

$$B_{TCR}^{\rho_1 \rho_2} = \frac{2(\pi - \alpha_{TCR}^{\rho_1 \rho_2}) - \sin 2\alpha_{TCR}^{\rho_1 \rho_2}}{\pi \omega L_{TCR}^{\rho_1 \rho_2}}, \quad (6.32)$$

$$B_C^{\rho_1} = \omega C_C^{\rho_1}, \quad (6.33)$$

$$\Delta B_C = \sum_{j=a,b,c} B_C^j. \quad (6.34)$$

The superscripts  $\rho_1$ ,  $\rho_2$ , and  $j$  take values  $a$ ,  $b$ , and  $c$ . Note that parameters with double superscripts,  $\rho_1$  and  $\rho_2$ , correspond to branch parameters connected between phases  $\rho_1$  and  $\rho_2$ .

### 6.3.1 Variable Susceptance Model

The three-phase power flow equations for the SVC may be derived with reference to the equivalent circuit in Figure 6.3 and using the variable susceptances  $B_{SVC}^{\rho_1 \rho_2}$  as state variables. The three susceptance values are adjusted automatically by the iterative algorithm in order to constrain the nodal voltage magnitude at the specified value. The final values of susceptance represent the line susceptances in the delta-connected SVC equivalent circuit.

With reference to Figure 6.3, and using the SVC transfer admittance matrix of Equation (6.30), the three-phase power flow equations for the SVC are as follows:

$$P_k^\rho = -V_k^\rho \sum_{\substack{j=a,b,c \\ j \neq \rho}} V_k^j B_{SVC}^{\rho j} \sin(\theta_k^\rho - \theta_k^j), \quad (6.35)$$

$$Q_k^\rho = -(V_k^\rho)^2 B_{SVC}^{\rho \rho} + V_k^\rho \sum_{\substack{j=a,b,c \\ j \neq \rho}} V_k^j B_{SVC}^{\rho j} \cos(\theta_k^\rho - \theta_k^j), \quad (6.36)$$

where the variables  $\rho$  and  $j$  take values  $a$ ,  $b$ , and  $c$ .

Taking the partial derivatives of the power flow Equations (6.35) and (6.36), with respect to the equivalent susceptances (state variables), we arrive at the following

linearised equation:

$$\begin{bmatrix} \Delta P_k^a \\ \Delta P_k^b \\ \Delta P_k^c \\ \Delta Q_k^a \\ \Delta Q_k^b \\ \Delta Q_k^c \end{bmatrix}^{(i)} = \begin{bmatrix} \frac{\partial P_k^a}{\partial \theta_k^a} & \frac{\partial P_k^a}{\partial \theta_k^b} & \frac{\partial P_k^a}{\partial \theta_k^c} & \frac{\partial P_k^a}{\partial B_{SVC}^{ab}} B_{SVC}^{ab} & 0 & \frac{\partial P_k^a}{\partial B_{SVC}^{ca}} B_{SVC}^{ca} \\ \frac{\partial P_k^b}{\partial \theta_k^a} & \frac{\partial P_k^b}{\partial \theta_k^b} & \frac{\partial P_k^b}{\partial \theta_k^c} & \frac{\partial P_k^b}{\partial B_{SVC}^{ab}} B_{SVC}^{ab} & \frac{\partial P_k^b}{\partial B_{SVC}^{bc}} B_{SVC}^{bc} & 0 \\ \frac{\partial P_k^c}{\partial \theta_k^a} & \frac{\partial P_k^c}{\partial \theta_k^b} & \frac{\partial P_k^c}{\partial \theta_k^c} & 0 & \frac{\partial P_k^c}{\partial B_{SVC}^{bc}} B_{SVC}^{bc} & \frac{\partial P_k^c}{\partial B_{SVC}^{ca}} B_{SVC}^{ca} \\ \frac{\partial Q_k^a}{\partial \theta_k^a} & \frac{\partial Q_k^a}{\partial \theta_k^b} & \frac{\partial Q_k^a}{\partial \theta_k^c} & \frac{\partial Q_k^a}{\partial B_{SVC}^{ab}} B_{SVC}^{ab} & 0 & \frac{\partial Q_k^a}{\partial B_{SVC}^{ca}} B_{SVC}^{ca} \\ \frac{\partial Q_k^b}{\partial \theta_k^a} & \frac{\partial Q_k^b}{\partial \theta_k^b} & \frac{\partial Q_k^b}{\partial \theta_k^c} & \frac{\partial Q_k^b}{\partial B_{SVC}^{ab}} B_{SVC}^{ab} & \frac{\partial Q_k^b}{\partial B_{SVC}^{bc}} B_{SVC}^{bc} & 0 \\ \frac{\partial Q_k^c}{\partial \theta_k^a} & \frac{\partial Q_k^c}{\partial \theta_k^b} & \frac{\partial Q_k^c}{\partial \theta_k^c} & 0 & \frac{\partial Q_k^c}{\partial B_{SVC}^{bc}} B_{SVC}^{bc} & \frac{\partial Q_k^c}{\partial B_{SVC}^{ca}} B_{SVC}^{ca} \end{bmatrix}^{(i)} \begin{bmatrix} \Delta \theta_k^a \\ \Delta \theta_k^b \\ \Delta \theta_k^c \\ \frac{\Delta B_{SVC}^{ab}}{B_{SVC}^{ab}} \\ \frac{\Delta B_{SVC}^{bc}}{B_{SVC}^{bc}} \\ \frac{\Delta B_{SVC}^{ca}}{B_{SVC}^{ca}} \end{bmatrix}^{(i)} \quad (6.37)$$

The new Jacobian entries in the linearised expression have the following form:

$$\frac{\partial P_k^\rho}{\partial B_{SVC}^{\rho j}} B_{SVC}^{\rho j} = -V_k^\rho V_k^j B_{SVC}^{\rho j} \sin(\theta_k^\rho - \theta_k^j), \quad (6.38)$$

$$\frac{\partial Q_k^\rho}{\partial B_{SVC}^{\rho j}} B_{SVC}^{\rho j} = -2(V_k^\rho)^2 B_{SVC}^{\rho j} + V_k^\rho V_k^j B_{SVC}^{\rho j} \cos(\theta_k^\rho - \theta_k^j). \quad (6.39)$$

The terms corresponding to partial derivatives of active and reactive powers with respect to nodal voltage phase angles have the same form as Equations (6.18), (6.20), (6.22), (6.24), (6.26), and (6.28), respectively.

Once the SVC linearised equation has been evaluated at a given iteration,  $(i)$ , it is then combined with the linearised expression representing the overall external system – Equation (6.9) – and a new set of state variables is obtained. The SVC susceptances are updated by using the following expression:

$$B_{SVC}^{\rho j (i)} = B_{SVC}^{\rho j (i-1)} + \left( \frac{\Delta B_{SVC}^{\rho j}}{B_{SVC}^{\rho j}} \right)^{(i)} B_{SVC}^{\rho j (i-1)}. \quad (6.40)$$

This calculation completes iteration  $(i)$ , and the three-phase mismatch power equations are calculated and checked for convergence. If the convergence criterion has not been satisfied, a new iteration is carried out.

### 6.3.2 Firing-angle Model

An alternative SVC model is realised by using the firing angles of the thyristors as state variables, rather than equivalent susceptances. In this situation, the new SVC linearised

equation takes the form:

$$\begin{bmatrix} \Delta P_k^a \\ \Delta P_k^b \\ \Delta P_k^c \\ \Delta Q_k^a \\ \Delta Q_k^b \\ \Delta Q_k^c \end{bmatrix}^{(i)} = \begin{bmatrix} \frac{\partial P_k^a}{\partial \theta_k^a} & \frac{\partial P_k^a}{\partial \theta_k^b} & \frac{\partial P_k^a}{\partial \theta_k^c} & \frac{\partial P_k^a}{\partial \alpha_{SVC}^{ab}} & 0 & \frac{\partial P_k^a}{\partial \alpha_{SVC}^{ca}} \\ \frac{\partial P_k^b}{\partial \theta_k^a} & \frac{\partial P_k^b}{\partial \theta_k^b} & \frac{\partial P_k^b}{\partial \theta_k^c} & \frac{\partial P_k^b}{\partial \alpha_{SVC}^{ab}} & \frac{\partial P_k^b}{\partial \alpha_{SVC}^{bc}} & 0 \\ \frac{\partial P_k^c}{\partial \theta_k^a} & \frac{\partial P_k^c}{\partial \theta_k^b} & \frac{\partial P_k^c}{\partial \theta_k^c} & 0 & \frac{\partial P_k^c}{\partial \alpha_{SVC}^{bc}} & \frac{\partial P_k^c}{\partial \alpha_{SVC}^{ca}} \\ \frac{\partial Q_k^a}{\partial \theta_k^a} & \frac{\partial Q_k^a}{\partial \theta_k^b} & \frac{\partial Q_k^a}{\partial \theta_k^c} & \frac{\partial Q_k^a}{\partial \alpha_{SVC}^{ab}} & 0 & \frac{\partial Q_k^a}{\partial \alpha_{SVC}^{ca}} \\ \frac{\partial Q_k^b}{\partial \theta_k^a} & \frac{\partial Q_k^b}{\partial \theta_k^b} & \frac{\partial Q_k^b}{\partial \theta_k^c} & \frac{\partial Q_k^b}{\partial \alpha_{SVC}^{ab}} & \frac{\partial Q_k^b}{\partial \alpha_{SVC}^{bc}} & 0 \\ \frac{\partial Q_k^c}{\partial \theta_k^a} & \frac{\partial Q_k^c}{\partial \theta_k^b} & \frac{\partial Q_k^c}{\partial \theta_k^c} & 0 & \frac{\partial Q_k^c}{\partial \alpha_{SVC}^{bc}} & \frac{\partial Q_k^c}{\partial \alpha_{SVC}^{ca}} \end{bmatrix}^{(i)} \begin{bmatrix} \Delta \theta_k^a \\ \Delta \theta_k^b \\ \Delta \theta_k^c \\ \Delta \alpha_{SVC}^{ab} \\ \Delta \alpha_{SVC}^{bc} \\ \Delta \alpha_{SVC}^{ca} \end{bmatrix}^{(i)}. \quad (6.41)$$

The new Jacobian entries in the linearised expression have the following form:

$$\frac{\partial P_k^p}{\partial \alpha_{SVC}^{ab}} = -V_k^p V_k^j \sin(\theta_k^p - \theta_k^j) \frac{\partial B_{SVC}^{pj}}{\partial \alpha_{SVC}^{ab}}, \quad (6.42)$$

$$\frac{\partial Q_k^p}{\partial \alpha_{SVC}^{ab}} = -\left[ (V_k^p)^2 - V_k^p V_k^j \cos(\theta_k^p - \theta_k^j) \right] \frac{\partial B_{SVC}^{pj}}{\partial \alpha_{SVC}^{ab}}, \quad (6.43)$$

$$\frac{\partial B_{SVC}^{pj}}{\partial \alpha_{SVC}^{ab}} = -\frac{2}{\pi X_L} \left[ 1 + \cos 2\alpha_{SVC}^{pj} \right]. \quad (6.44)$$

The terms corresponding to partial derivatives of active and reactive powers with respect to nodal voltage phase angles are the same terms referred to in Equation (6.37).

Upon solution of the combined Equations (6.9) and (6.41), a new set of state variable increments is obtained. The increments are used to update the state variable values – among them the SVC firing angles – using the following expression:

$$(\alpha_{SVC}^{pj})^{(i)} = (\alpha_{SVC}^{pj})^{(i-1)} + (\Delta \alpha_{SVC}^{pj})^{(i)}. \quad (6.45)$$

This calculation completes iteration (i), and the three-phase mismatch power equations are calculated and checked for convergence.

### 6.3.3 Numerical Example: Static VAR Compensator Voltage Magnitude Balancing Capability

A three-phase SVC is added to the unbalanced five-bus network in Section 6.2.4 in order to explore the capability of the SVC to restore geometric balance at the point of connection while at the same time providing effective voltage magnitude regulation. The SVC is assumed to be connected at Elm, and the voltage magnitude is set at 0.98 p.u. The study is conducted using the SVC reactance model, and convergence is achieved in 5 iterations to satisfy a power mismatch tolerance of  $1e - 12$ .

**Table 6.3** Nodal voltage in the three-phase unbalanced network with a static VAR compensator: (a) phase voltages and (b) sequence voltages

Voltage	Phase	Network bus				
		North	South	Lake	Main	Elm
(a) Phase voltages						
Magnitude (p.u.)	<i>a</i>	1.06	1.00	0.9822	0.9810	0.98
	<i>b</i>	1.06	1.00	0.9888	0.9974	0.98
	<i>c</i>	1.06	1.00	0.9947	0.9923	0.98
Phase angle (deg)	<i>a</i>	0	-2.04	-4.64	-4.79	-5.76
	<i>b</i>	240	238.16	235.17	234.84	234.81
	<i>c</i>	120	117.60	115.37	114.86	113.09
(b) Sequence voltages						
Magnitude (p.u.)	Zero	0.00	0.0028	0.0047	0.0050	0.0087
	Positive	1.06	1.0000	0.9886	0.9859	0.9799
	Negative	0.00	0.0028	0.0025	0.0022	0.0086

The three-phase nodal voltage magnitudes and phase angles are given in Table 6.3(a), in which it is shown that the SVC is effective in regulating and balancing nodal voltage magnitude at Elm. As expected, the phase angles at that bus are still unbalanced. It should be mentioned that power losses now stand at 1.01 %, a result that compares favourably with the unbalanced case where no SVC is used and where power losses stand at 2 %. Note that negative sequence voltages have also reduced in magnitude [Table 6.3(b)].

## 6.4 THYRISTOR-CONTROLLED SERIES COMPENSATOR

Based on the nodal admittance representation of the TCSC, derived in Chapter 2, two quite useful positive sequence power flow models were developed in Section 5.4. One model uses an adjustable reactance as the state variable and the other uses the thyristor firing angle. The same idea is now extended to the case of the TCSC power flow models in phase coordinates.

### 6.4.1 Variable Susceptance Model

The three-phase TCSC representation is simply obtained by using three independent TCSC modules, as shown in Figure 2.12. The changing susceptance, shown in Figure 6.4, represents the fundamental frequency equivalent susceptance of each series module making up the three-phase TCSC. The value of  $B_{TCSC}$  is determined by using the Newton–Raphson method to regulate active power flow through the three branches to a specified value.

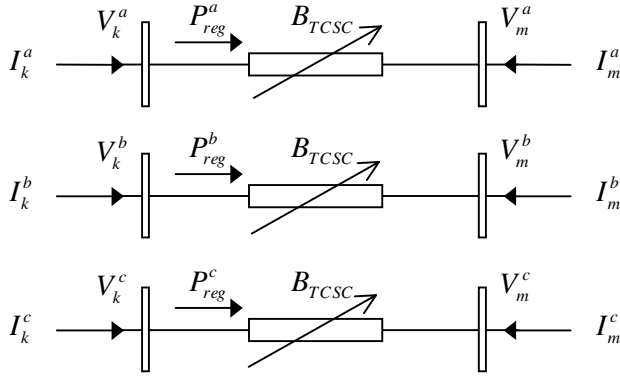


Figure 6.4 Three-phase variable series susceptance

The transfer admittance of the TCSC may be derived from visual inspection of the equivalent circuit shown in Figure 6.4. Assuming that  $\rho$  takes the values  $a, b, c$ :

$$\begin{bmatrix} \mathbf{I}_k^\rho \\ \mathbf{I}_m^\rho \end{bmatrix} = \begin{bmatrix} \mathbf{jB}_{kk}^\rho & \mathbf{jB}_{km}^\rho \\ \mathbf{jB}_{mk}^\rho & \mathbf{jB}_{mm}^\rho \end{bmatrix} \begin{bmatrix} \mathbf{V}_k^\rho \\ \mathbf{V}_m^\rho \end{bmatrix}. \quad (6.46)$$

In Equation (6.46) the terms  $\mathbf{B}_{kk}^\rho, \mathbf{B}_{km}^\rho, \mathbf{B}_{mk}^\rho$ , and  $\mathbf{B}_{mm}^\rho$  are diagonal matrices since the three TCSC modules are electromagnetically decoupled:

$$\mathbf{B}_{kk}^\rho = \mathbf{B}_{mm}^\rho = \mathbf{B}_{TCSC}^\rho = -\frac{1}{X^\rho}, \quad (6.47)$$

$$\mathbf{B}_{km}^\rho = \mathbf{B}_{mk}^\rho = -\mathbf{B}_{TCSC}^\rho = \frac{1}{X^\rho}, \quad (6.48)$$

where  $X^\rho$  represents the fundamental frequency equivalent reactance of the  $\rho$ th series modules making up the TCSC.

With reference to Figure 6.4 and using the transfer admittance matrix in Equation (6.46), the three-phase nodal power injections at bus  $k$  are:

$$P_k^\rho = V_k^\rho V_m^\rho \mathbf{B}_{km}^\rho \sin(\theta_k^\rho - \theta_m^\rho), \quad (6.49)$$

$$Q_k^\rho = -(V_k^\rho)^2 \mathbf{B}_{kk}^\rho - V_k^\rho V_m^\rho \mathbf{B}_{km}^\rho \cos(\theta_k^\rho - \theta_m^\rho). \quad (6.50)$$

Power equations at bus  $m$  are obtained by replacing the subscript  $k$  with  $m$ , and vice versa, in Equations (6.49) and (6.50).

The first partial derivatives of the power equations with respect to  $X^\rho$  are:

$$\frac{\partial P_k^\rho}{\partial X^\rho} X^\rho = -P_k^\rho, \quad (6.51)$$

$$\frac{\partial Q_k^\rho}{\partial X^\rho} X^\rho = -Q_k^\rho. \quad (6.52)$$

When the TCSC is controlling active power flowing from  $k$  to  $m$ , at specified value, the set of linearised power flow equations is

$$\begin{bmatrix} \Delta P_k^\rho \\ \Delta P_m^\rho \\ \Delta Q_k^\rho \\ \Delta Q_m^\rho \\ \Delta P_{km}^{\rho,X} \end{bmatrix}^{(i)} = \begin{bmatrix} \frac{\partial P_k^\rho}{\partial \theta_k^\rho} & \frac{\partial P_k^\rho}{\partial \theta_m^\rho} & \frac{\partial P_k^\rho}{\partial V_k^\rho} V_k^\rho & \frac{\partial P_k^\rho}{\partial V_m^\rho} V_m^\rho & \frac{\partial P_k^\rho}{\partial X^\rho} X^\rho \\ \frac{\partial P_m^\rho}{\partial \theta_k^\rho} & \frac{\partial P_m^\rho}{\partial \theta_m^\rho} & \frac{\partial P_m^\rho}{\partial V_k^\rho} V_k^\rho & \frac{\partial P_m^\rho}{\partial V_m^\rho} V_m^\rho & \frac{\partial P_m^\rho}{\partial X^\rho} X^\rho \\ \frac{\partial Q_k^\rho}{\partial \theta_k^\rho} & \frac{\partial Q_k^\rho}{\partial \theta_m^\rho} & \frac{\partial Q_k^\rho}{\partial V_k^\rho} V_k^\rho & \frac{\partial Q_k^\rho}{\partial V_m^\rho} V_m^\rho & \frac{\partial Q_k^\rho}{\partial X^\rho} X^\rho \\ \frac{\partial Q_m^\rho}{\partial \theta_k^\rho} & \frac{\partial Q_m^\rho}{\partial \theta_m^\rho} & \frac{\partial Q_m^\rho}{\partial V_k^\rho} V_k^\rho & \frac{\partial Q_m^\rho}{\partial V_m^\rho} V_m^\rho & \frac{\partial Q_m^\rho}{\partial X^\rho} X^\rho \\ \frac{\partial P_{km}^{\rho,X}}{\partial \theta_k^\rho} & \frac{\partial P_{km}^{\rho,X}}{\partial \theta_m^\rho} & \frac{\partial P_{km}^{\rho,X}}{\partial V_k^\rho} V_k^\rho & \frac{\partial P_{km}^{\rho,X}}{\partial V_m^\rho} V_m^\rho & \frac{\partial P_{km}^{\rho,X}}{\partial X^\rho} X^\rho \end{bmatrix}^{(i)} \begin{bmatrix} \Delta \theta_k^\rho \\ \Delta \theta_m^\rho \\ \frac{\Delta V_k^\rho}{V_k^\rho} \\ \frac{\Delta V_m^\rho}{V_m^\rho} \\ \frac{\Delta X^\rho}{X^\rho} \end{bmatrix}^{(i)}, \quad (6.53)$$

where  $\Delta P_{km}^{\rho,X}$ , given by

$$\Delta P_{km}^{\rho,X} = P_{km}^{\rho,X,Reg} - P_{km}^{\rho,X,cal},$$

is the active power flow mismatch for the TCSC.  $\Delta X^\rho$  is the incremental change in the total series TCSC reactance, and the superscript  $(i)$  indicates iteration number.

### 6.4.2 Firing-angle Model

The TCSC structure shown in Figure 2.12 is extended to account for the three phases as shown in Figure 6.5. This is used as the basis for deriving the three-phase power flow model,

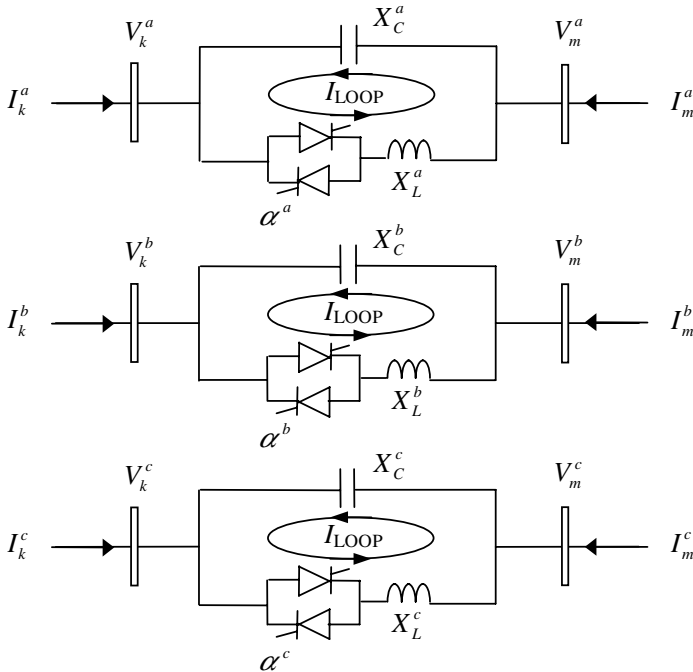


**Figure 6.5** Three thyristor-controlled series compensator modules

where the TCSC firing angle is used as state variable (Venegas and Fuerte-Esquivel, 2001). The three TCSC branches are assumed to be electrically and magnetically decoupled.

The fundamental frequency TCSC equivalent reactance, as a function of TCSC firing angle, is given by Equation (2.52). It follows that the extension to three phases is quite straightforward, owing to the decoupled nature of the three modules:

$$X_{\text{TCSC}(1)}^\rho = -X_C^\rho + C_1^\rho \{2(\pi - \alpha^\rho) + \sin[2(\pi - \alpha^\rho)]\} - C_2^\rho \cos^2(\pi - \alpha^\rho) \times \{\omega \tan[\omega(\pi - \alpha^\rho)] - \tan(\pi - \alpha^\rho)\}, \quad (6.54)$$

where

$$X_{\text{LC}}^\rho = \frac{X_C^\rho X_L^\rho}{X_C^\rho - X_L^\rho}, \quad (6.55)$$

$$C_1^\rho = \frac{X_C^\rho + X_{\text{LC}}^\rho}{\pi}, \quad (6.56)$$

$$C_2^\rho = \frac{4(X_{\text{LC}}^\rho)^2}{X_L^\rho \pi}. \quad (6.57)$$

The transfer admittance matrices of both TCSC representations are identical, given by Equations (6.46)–(6.48). Moreover, the TCSC nodal power equations also coincide. The TCSC power equations with respect to the firing angle are:

$$\frac{\partial B_{\text{TCSC}(1)}^\rho}{\partial \alpha^\rho} = \left( B_{\text{TCSC}(1)}^\rho \right)^2 \frac{\partial X_{\text{TCSC}(1)}^\rho}{\partial \alpha^\rho}, \quad (6.58)$$

$$\frac{\partial P_k^\rho}{\partial \alpha^\rho} = P_k^\rho B_{\text{TCSC}(1)}^\rho \frac{\partial X_{\text{TCSC}(1)}^\rho}{\partial \alpha^\rho}, \quad (6.59)$$

$$\frac{\partial Q_k^\rho}{\partial \alpha^\rho} = Q_k^\rho B_{\text{TCSC}(1)}^\rho \frac{\partial X_{\text{TCSC}(1)}^\rho}{\partial \alpha^\rho}, \quad (6.60)$$

where

$$\begin{aligned} \frac{\partial X_{\text{TCSC}(1)}^\rho}{\partial \alpha^\rho} &= -2C_1^\rho [1 + \cos(2\alpha^\rho)] + C_2^\rho \sin(2\alpha^\rho) \{ \omega \tan[\omega(\pi - \alpha^\rho)] - \tan \alpha^\rho \} \\ &+ C_2^\rho \left( \omega^2 \frac{\cos^2(\pi - \alpha^\rho)}{\cos^2[\omega(\pi - \alpha^\rho)]} - 1 \right). \end{aligned} \quad (6.61)$$

When the TCSC module is controlling the active power flowing from buses  $k$  to  $m$ , at a specified value, the set of linearised power flow equations is:

$$\begin{bmatrix} \Delta P_k^\rho \\ \Delta P_m^\rho \\ \Delta Q_m^\rho \\ \Delta Q_m^\rho \\ \Delta P_{km}^{\rho,\alpha} \end{bmatrix}^{(i)} = \begin{bmatrix} \frac{\partial P_k^\rho}{\partial \theta_k^\rho} & \frac{\partial P_k^\rho}{\partial \theta_m^\rho} & \frac{\partial P_k^\rho}{\partial V_k^\rho} V_k^\rho & \frac{\partial P_k^\rho}{\partial V_m^\rho} V_m^\rho & \frac{\partial P_k^\rho}{\partial \alpha^\rho} \\ \frac{\partial P_m^\rho}{\partial \theta_k^\rho} & \frac{\partial P_m^\rho}{\partial \theta_m^\rho} & \frac{\partial P_m^\rho}{\partial V_k^\rho} V_k^\rho & \frac{\partial P_m^\rho}{\partial V_m^\rho} V_m^\rho & \frac{\partial P_m^\rho}{\partial \alpha^\rho} \\ \frac{\partial Q_k^\rho}{\partial \theta_k^\rho} & \frac{\partial Q_k^\rho}{\partial \theta_m^\rho} & \frac{\partial Q_k^\rho}{\partial V_k^\rho} V_k^\rho & \frac{\partial Q_k^\rho}{\partial V_m^\rho} V_m^\rho & \frac{\partial Q_k^\rho}{\partial \alpha^\rho} \\ \frac{\partial Q_m^\rho}{\partial \theta_k^\rho} & \frac{\partial Q_m^\rho}{\partial \theta_m^\rho} & \frac{\partial Q_m^\rho}{\partial V_k^\rho} V_k^\rho & \frac{\partial Q_m^\rho}{\partial V_m^\rho} V_m^\rho & \frac{\partial Q_m^\rho}{\partial \alpha^\rho} \\ \frac{\partial P_{km}^{\rho,\alpha}}{\partial \theta_k^\rho} & \frac{\partial P_{km}^{\rho,\alpha}}{\partial \theta_m^\rho} & \frac{\partial P_{km}^{\rho,\alpha}}{\partial V_k^\rho} V_k^\rho & \frac{\partial P_{km}^{\rho,\alpha}}{\partial V_m^\rho} V_m^\rho & \frac{\partial P_{km}^{\rho,\alpha}}{\partial \alpha^\rho} \end{bmatrix}^{(i)} \begin{bmatrix} \Delta \theta_k^\rho \\ \Delta \theta_m^\rho \\ \frac{\Delta V_k^\rho}{V_k^\rho} \\ \frac{\Delta V_m^\rho}{V_m^\rho} \\ \Delta \alpha^\rho \end{bmatrix}^{(i)}, \quad (6.62)$$

where  $\Delta P_{km}^{\rho,\alpha}$

$$\Delta P_{km}^{\rho,\alpha} = P_{km}^{\rho,\alpha,Reg} - P_{km}^{\rho,\alpha,cal},$$

and  $P_{km}^{\rho,\alpha,cal}$ ,  $P_k^\rho$ , are the active power flow mismatches for the three-phase TCSC module, and  $\alpha^{\rho(i)}$ , given by

$$\alpha^{\rho(i)} = \alpha^{\rho(i-1)} + \Delta\alpha^{\rho(i)},$$

is the incremental change in the TCSC firing angle. The superscript (*i*) indicates iteration number.

### 6.4.3 Numerical Example: Power Flow Control using One Thyristor-controlled Series Compensator

In order to show the flexibility of the TCSC model in the phase domain, a three-phase power flow study is carried out. The TCSC is added to the unbalanced five-bus network, connected between buses Lake and Main. The aim of this example is to balance out the amount of active power through the TCSC at 21 MW. The increase of active power in phase *a* is almost 50 % and in phase *b* 5 %; in phase *c* it decreases by 14 % with respect to the unbalanced case in Section 6.2.4. The three-phase nodal voltage magnitudes and phase angles are given in Table 6.4(a), whereas Table 6.4(b) gives the nodal voltage magnitudes in the sequence domain. The power flows are shown in Figure 6.6.

**Table 6.4** Nodal voltages in the three-phase unbalanced network with a thyristor-controlled series compensator (TCSC): (a) phase voltages and (b) sequence voltages

Voltage	Phase	Network bus					
		North	South	Lake	Main	Elm	LakeTCSC
(a) Phase voltages							
Magnitude (p.u.)	<i>a</i>	1.06	1.00	0.9839	0.9797	0.9788	0.9800
	<i>b</i>	1.06	1.00	0.9884	0.9823	0.9751	0.9871
	<i>c</i>	1.06	1.00	0.9912	0.9866	0.9593	0.9902
Phase angle (deg)	<i>a</i>	0.00	-1.87	-5.28	-3.86	-5.54	-3.48
	<i>b</i>	240.00	238.14	235.36	234.80	235.21	235.07
	<i>c</i>	120.00	117.52	115.58	114.51	113.05	114.94
(b) Sequence voltages							
Magnitude (p.u.)	Zero	0.00	0.0035	0.0046	0.0097	0.0147	0.0098
	Positive	1.06	1.0000	0.9878	0.9828	0.9710	0.9857
	Negative	0.00	0.0035	0.0052	0.0079	0.0092	0.0086

## 6.5 STATIC COMPENSATOR

With reference to the single-phase equivalent circuit shown in Figure 2.18(b), and assuming that the three Thévenin equivalents representing a three-phase STATCOM are decoupled, the equivalent circuit is shown in Figure 6.7.

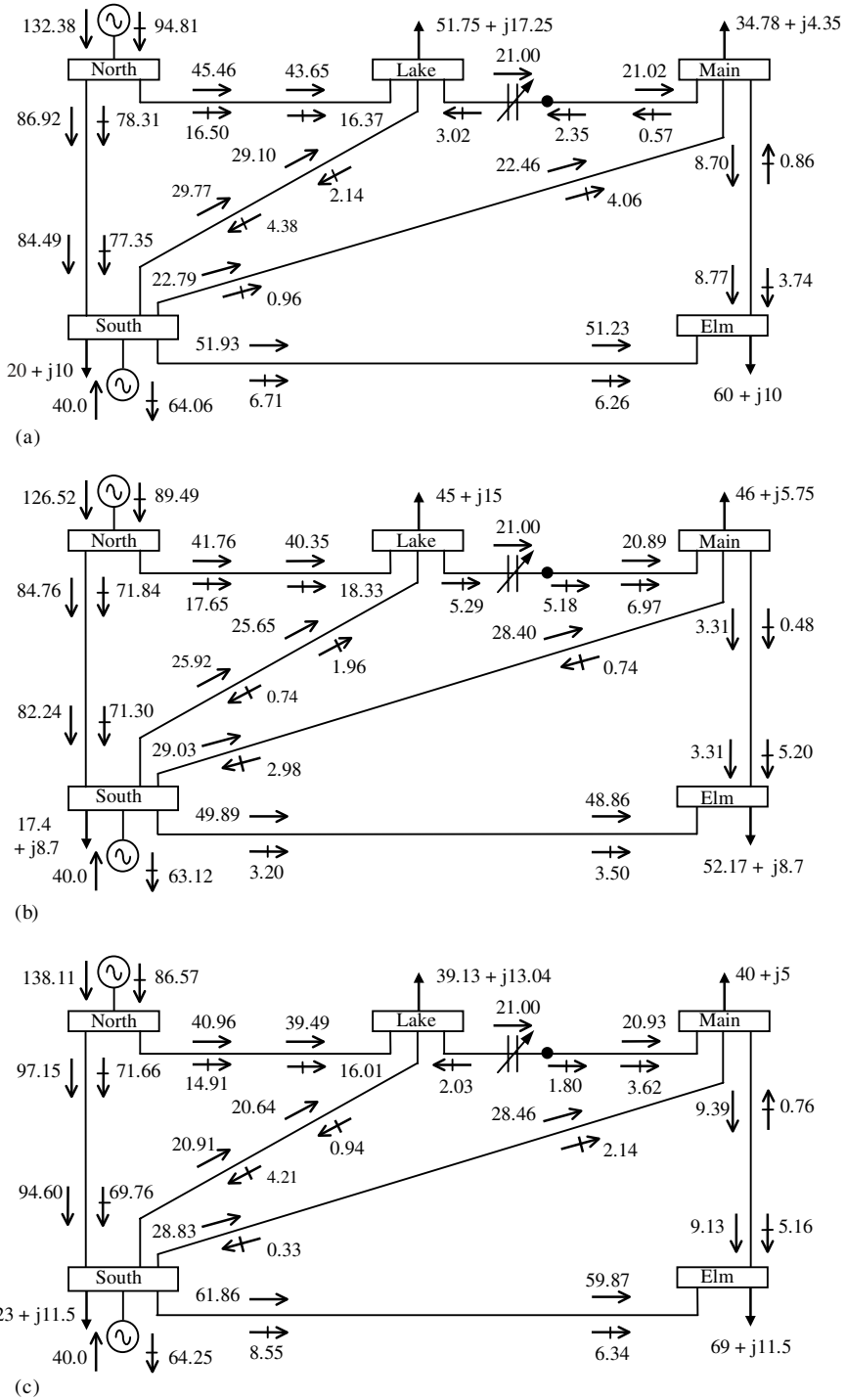


**Figure 6.6** Five-bus network with thyristor-controlled series compensator: (a) phase *a*, (b) phase *b*, and (c) phase *c*

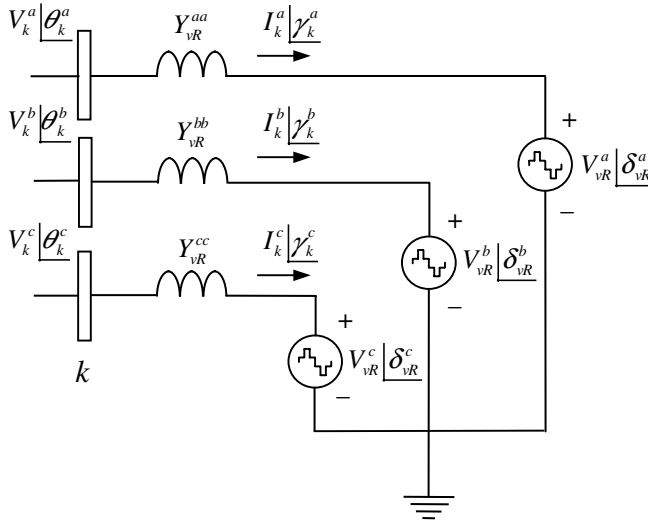


**Figure 6.7** Three-phase static compensator equivalent circuit

Based on this equivalent circuit, and the three-phase transfer admittance Equation (2.65), the following expressions for active and reactive power injections at bus  $k$  may be written:

$$P_k^\rho = (V_k^\rho)^2 G_{vR}^{\rho\rho} + V_k^\rho V_{vR}^\rho [G_{vR}^{\rho\rho} \cos(\theta_k^\rho - \delta_{vR}^\rho) + B_{vR}^{\rho\rho} \sin(\theta_k^\rho - \delta_{vR}^\rho)], \quad (6.63)$$

$$Q_k^\rho = -(V_k^\rho)^2 B_{vR}^{\rho\rho} + V_k^\rho V_{vR}^\rho [G_{vR}^{\rho\rho} \sin(\theta_k^\rho - \delta_{vR}^\rho) - B_{vR}^{\rho\rho} \cos(\theta_k^\rho - \delta_{vR}^\rho)]. \quad (6.64)$$

The corresponding expressions for the three sources are:

$$P_{vR}^\rho = (V_{vR}^\rho)^2 G_{vR}^{\rho\rho} + V_{vR}^\rho V_k^\rho [G_{vR}^{\rho\rho} \cos(\delta_{vR}^\rho - \theta_k^\rho) + B_{vR}^{\rho\rho} \sin(\delta_{vR}^\rho - \theta_k^\rho)], \quad (6.65)$$

$$Q_{vR}^\rho = -(V_{vR}^\rho)^2 B_{vR}^{\rho\rho} + V_{vR}^\rho V_k^\rho [G_{vR}^{\rho\rho} \sin(\delta_{vR}^\rho - \theta_k^\rho) - B_{vR}^{\rho\rho} \cos(\delta_{vR}^\rho - \theta_k^\rho)], \quad (6.66)$$

where  $\rho$  refers to phases  $a$ ,  $b$ , and  $c$  at bus  $k$  and at the terminals of the source.

Derivation of these power equations with respect to the STATCOM state variables  $V_{vR}^\rho$  and  $\delta_{vR}^\rho$  yields the following linearised equation:

$$\begin{bmatrix} \Delta P_k^\rho \\ \Delta Q_k^\rho \\ \Delta P_{vR}^\rho \\ \Delta Q_{vR}^\rho \end{bmatrix} = \begin{bmatrix} \frac{\partial P_k^\rho}{\partial \theta_k^\rho} & \frac{\partial P_k^\rho}{\partial V_k^\rho} V_k^\rho & \frac{\partial P_k^\rho}{\partial \delta_{vR}^\rho} & \frac{\partial P_k^\rho}{\partial V_{vR}^\rho} V_{vR}^\rho \\ \frac{\partial Q_k^\rho}{\partial \theta_k^\rho} & \frac{\partial Q_k^\rho}{\partial V_k^\rho} V_k^\rho & \frac{\partial Q_k^\rho}{\partial \delta_{vR}^\rho} & \frac{\partial Q_k^\rho}{\partial V_{vR}^\rho} V_{vR}^\rho \\ \frac{\partial P_{vR}^\rho}{\partial \theta_k^\rho} & \frac{\partial P_{vR}^\rho}{\partial V_k^\rho} V_k^\rho & \frac{\partial P_{vR}^\rho}{\partial \delta_{vR}^\rho} & \frac{\partial P_{vR}^\rho}{\partial V_{vR}^\rho} V_{vR}^\rho \\ \frac{\partial Q_{vR}^\rho}{\partial \theta_k^\rho} & \frac{\partial Q_{vR}^\rho}{\partial V_k^\rho} V_k^\rho & \frac{\partial Q_{vR}^\rho}{\partial \delta_{vR}^\rho} & \frac{\partial Q_{vR}^\rho}{\partial V_{vR}^\rho} V_{vR}^\rho \end{bmatrix} \begin{bmatrix} \Delta \theta_k^\rho \\ \frac{\Delta V_k^\rho}{V_k^\rho} \\ \Delta \delta_{vR}^\rho \\ \frac{\Delta V_{vR}^\rho}{V_{vR}^\rho} \end{bmatrix}. \quad (6.67)$$

The Jacobian elements created for this application are as follows:

$$\frac{\partial P_k^\rho}{\partial \theta_k^\rho} = -Q_k^\rho - (V_k^\rho)^2 G_{vR}^\rho, \quad (6.68)$$

$$\frac{\partial P_k^\rho}{\partial V_k^\rho} V_k^\rho = P_k^\rho + (V_k^\rho)^2 G_{vR}^\rho, \quad (6.69)$$

$$\frac{\partial P_k^\rho}{\partial \delta_{vR}^\rho} = \frac{\partial Q_{vR}^\rho}{\partial V_k^\rho} V_k^\rho = V_{vR}^\rho V_k^\rho [G_{vR}^\rho \cos(\delta_{vR}^\rho - \theta_k^\rho) + B_{vR}^\rho \sin(\delta_{vR}^\rho - \theta_k^\rho)], \quad (6.70)$$

$$\frac{\partial P_k^\rho}{\partial V_{vR}^\rho} V_{vR}^\rho = -\frac{\partial Q_{vR}^\rho}{\partial \theta_k^\rho} = V_k^\rho V_{vR}^\rho [G_{vR}^\rho \cos(\theta_k^\rho - \delta_{vR}^\rho) + B_{vR}^\rho \sin(\theta_k^\rho - \delta_{vR}^\rho)], \quad (6.71)$$

$$\frac{\partial Q_k^\rho}{\partial \theta_k^\rho} = P_k^\rho - (V_k^\rho)^2 G_{vR}^\rho, \quad (6.72)$$

$$\frac{\partial Q_k^\rho}{\partial V_k^\rho} V_k^\rho = Q_k^\rho - (V_k^\rho)^2 B_{vR}^\rho, \quad (6.73)$$

$$\frac{\partial Q_k^\rho}{\partial \delta_{vR}^\rho} = -\frac{\partial P_{vR}^\rho}{\partial V_k^\rho} V_k^\rho = -V_k^\rho V_{vR}^\rho [G_{vR}^\rho \cos(\theta_k^\rho - \delta_{vR}^\rho) + B_{vR}^\rho \sin(\theta_k^\rho - \delta_{vR}^\rho)], \quad (6.74)$$

$$\frac{\partial Q_k^\rho}{\partial V_{vR}^\rho} V_{vR}^\rho = \frac{\partial P_{vR}^\rho}{\partial \theta_k^\rho} = V_k^\rho V_{vR}^\rho [G_{vR}^\rho \sin(\theta_k^\rho - \delta_{vR}^\rho) - B_{vR}^\rho \cos(\theta_k^\rho - \delta_{vR}^\rho)], \quad (6.75)$$

$$\frac{\partial P_{vR}^\rho}{\partial \delta_{vR}^\rho} = -Q_{vR}^\rho - (V_{vR}^\rho)^2 B_{vR}^\rho, \quad (6.76)$$

$$\frac{\partial P_{vR}^\rho}{\partial V_{vR}^\rho} V_{vR}^\rho = P_{vR}^\rho + (V_{vR}^\rho)^2 G_{vR}^\rho, \quad (6.77)$$

$$\frac{\partial Q_{vR}^\rho}{\partial \delta_{vR}^\rho} = P_{vR}^\rho - (V_{vR}^\rho)^2 G_{vR}^\rho, \quad (6.78)$$

$$\frac{\partial Q_{vR}^\rho}{\partial V_{vR}^\rho} V_{vR}^\rho = Q_{vR}^\rho - (V_{vR}^\rho)^2 B_{vR}^\rho. \quad (6.79)$$

Solution of the linearised Equation (6.67) yields information on the state variable increments. The increments are, in turn, used to update the state variables. Voltage magnitude limits are checked at the end of each iterative step and if one or more limits are violated the voltage magnitude is fixed at the violated limit.

### 6.5.1 Static Compensator Three-phase Numerical Example

The three-phase STATCOM model is used to balance voltage magnitude at Elm at 0.98 p.u. This is, in essence, the same case study carried out with the SVC model in Section 6.3.3.

The source impedances are  $X_{vR} = 0.1$  p.u. per phase. The power flow results indicate that the STATCOM generates 4.81 MVAR, 8.47 MVAR and 15.25 MVAR in phases  $a$ ,  $b$  and  $c$ , respectively, in order to achieve the three-phase voltage magnitude target. The STATCOM parameters associated with this amount of reactive power generation are:  $V_{vR} = 0.9849$ , 0.9886 and 0.9955 p.u. for phases  $a$ ,  $b$  and  $c$ , respectively. As expected power flows results coincide with those obtained using the SVC model in Section 6.3.3. Nodal voltage magnitudes and phase angles are given in Table 6.3(a), and sequence domain voltage magnitudes are given in Table 6.3(b).

### 6.6 UNIFIED POWER FLOW CONTROLLER

The UPFC schematic representation and its operational control were presented in Section 2.4.4, and a positive sequence power flow model was developed in Section 5.6. However, in order to assess the role of the UPFC operating under unbalanced conditions it is necessary to develop the model in phase coordinates.

Assuming that the equivalent circuit of a three-phase UPFC consist of three single-phase UPFC equivalent circuits, with no couplings between them, as shown in Figure 6.8, the

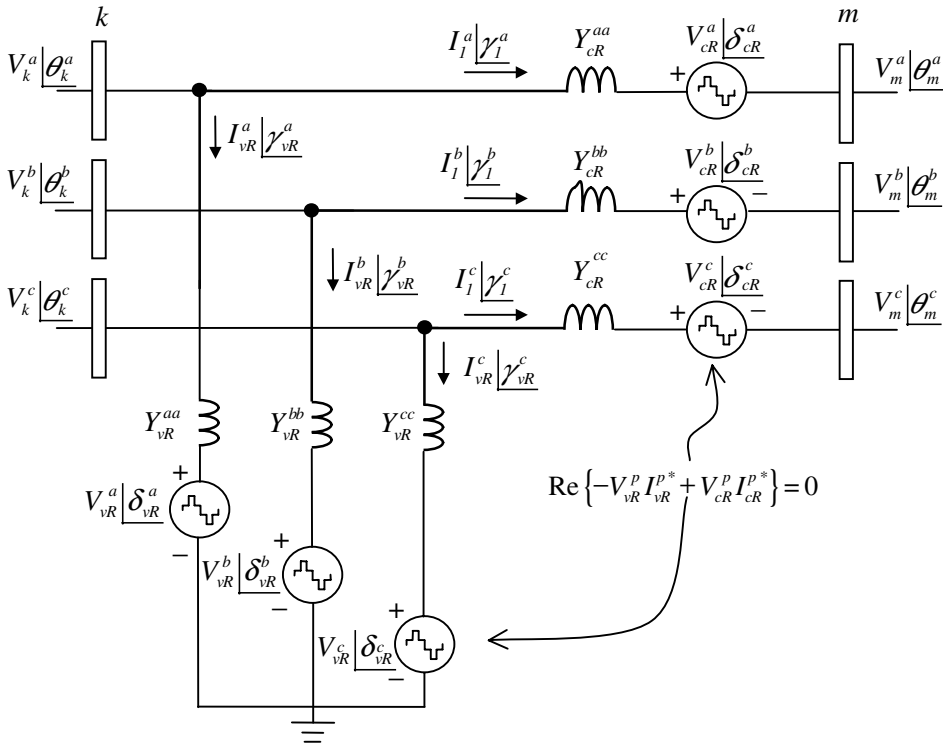


Figure 6.8 Three-phase unified power flow controller equivalent circuit

three-phase power flow equations are as follows:

$$\begin{aligned}
 P_k^\rho &= (V_k^\rho)^2 G_{kk}^{\rho\rho} + V_k^\rho V_m^\rho [G_{km}^{\rho\rho} \cos(\theta_k^\rho - \theta_m^\rho) + B_{km}^{\rho\rho} \sin(\theta_k^\rho - \theta_m^\rho)] \\
 &\quad + V_k^\rho V_{cR}^\rho [G_{km}^{\rho\rho} \cos(\theta_k^\rho - \delta_{cR}^\rho) + B_{km}^{\rho\rho} \sin(\theta_k^\rho - \delta_{cR}^\rho)] \\
 &\quad + V_k^\rho V_{vR}^\rho [G_{vR}^{\rho\rho} \cos(\theta_k^\rho - \delta_{vR}^\rho) + B_{vR}^{\rho\rho} \sin(\theta_k^\rho - \delta_{vR}^\rho)], \tag{6.80}
 \end{aligned}$$

$$\begin{aligned}
 Q_k^\rho &= -(V_k^\rho)^2 B_{kk}^{\rho\rho} + V_k^\rho V_m^\rho [G_{km}^{\rho\rho} \sin(\theta_k^\rho - \theta_m^\rho) - B_{km}^{\rho\rho} \cos(\theta_k^\rho - \theta_m^\rho)] \\
 &\quad + V_k^\rho V_{cR}^\rho [G_{km}^{\rho\rho} \sin(\theta_k^\rho - \delta_{cR}^\rho) - B_{km}^{\rho\rho} \cos(\theta_k^\rho - \delta_{cR}^\rho)] \\
 &\quad + V_k^\rho V_{vR}^\rho [G_{vR}^{\rho\rho} \sin(\theta_k^\rho - \delta_{vR}^\rho) - B_{vR}^{\rho\rho} \cos(\theta_k^\rho - \delta_{vR}^\rho)]. \tag{6.81}
 \end{aligned}$$

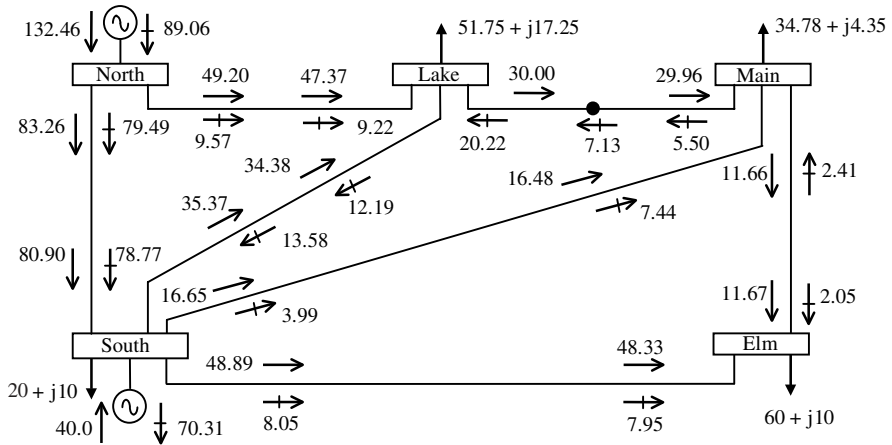
Equations (6.80) and (6.81) are the three-phase counterparts of Equations (5.50) and (5.51). Equations for bus  $m$ , and the series and shunt converters are also obtained by direct extensions of Equations (5.52)–(5.57) into phase coordinates.

In this situation, the active power supplied to the shunt converter,  $\text{Re}\{V_{vR}^\rho I_{vR}^{\rho*}\}$  satisfies the active power demanded by the series converter,  $\text{Re}\{V_{cR}^\rho I_m^{\rho*}\}$ . The impedance of the series and shunt transformers,  $Z_{cR}^{\rho\rho}$  and  $Z_{vR}^{\rho\rho}$ , are included explicitly in the model.

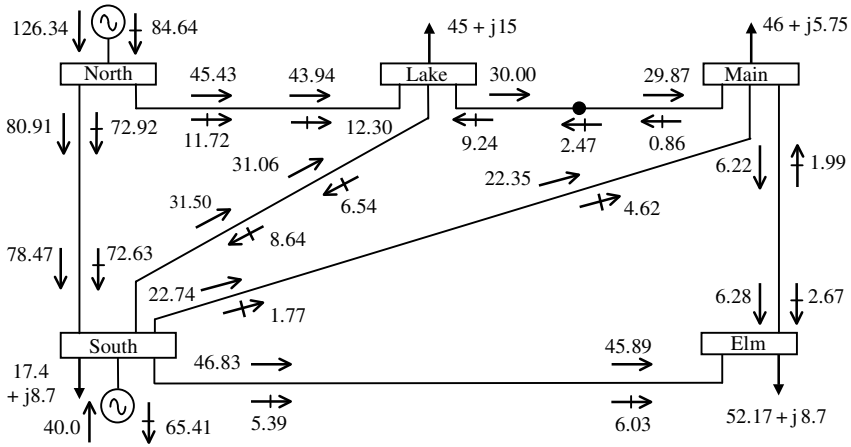
The UPFC power equations, in linearised form, are combined with those of the AC network. For the case when the UPFC controls the following parameters: (1) voltage magnitude at the shunt converter terminal (bus  $k$ ), (2) active power flowing from bus  $m$  to bus  $k$ , and (3) reactive power injected at bus  $m$ , and taking bus  $m$  to be a  $PQ$  bus, the linearised system of equations is as follows:

$$\begin{bmatrix} \Delta P_k^\rho \\ \Delta P_m^\rho \\ \Delta Q_k^\rho \\ \Delta Q_m^\rho \\ \Delta P_{mk}^\rho \\ \Delta Q_{mk}^\rho \\ \Delta P_{bb}^\rho \end{bmatrix} = \begin{bmatrix} \frac{\partial P_k^\rho}{\partial \theta_k^\rho} & \frac{\partial P_k^\rho}{\partial \theta_m^\rho} & \frac{\partial P_k^\rho}{\partial V_k^\rho} V_k^\rho & \frac{\partial P_k^\rho}{\partial V_m^\rho} V_m^\rho & \frac{\partial P_k^\rho}{\partial \delta_{cR}^\rho} & \frac{\partial P_k^\rho}{\partial V_{cR}^\rho} V_{cR}^\rho & \frac{\partial P_k^\rho}{\partial \delta_{vR}^\rho} \\ \frac{\partial P_m^\rho}{\partial \theta_k^\rho} & \frac{\partial P_m^\rho}{\partial \theta_m^\rho} & \frac{\partial P_m^\rho}{\partial V_k^\rho} V_k^\rho & \frac{\partial P_m^\rho}{\partial V_m^\rho} V_m^\rho & \frac{\partial P_m^\rho}{\partial \delta_{cR}^\rho} & \frac{\partial P_m^\rho}{\partial V_{cR}^\rho} V_{cR}^\rho & 0 \\ \frac{\partial Q_k^\rho}{\partial \theta_k^\rho} & \frac{\partial Q_k^\rho}{\partial \theta_m^\rho} & \frac{\partial Q_k^\rho}{\partial V_k^\rho} V_k^\rho & \frac{\partial Q_k^\rho}{\partial V_m^\rho} V_m^\rho & \frac{\partial Q_k^\rho}{\partial \delta_{cR}^\rho} & \frac{\partial Q_k^\rho}{\partial V_{cR}^\rho} V_{cR}^\rho & \frac{\partial Q_k^\rho}{\partial \delta_{vR}^\rho} \\ \frac{\partial Q_m^\rho}{\partial \theta_k^\rho} & \frac{\partial Q_m^\rho}{\partial \theta_m^\rho} & \frac{\partial Q_m^\rho}{\partial V_k^\rho} V_k^\rho & \frac{\partial Q_m^\rho}{\partial V_m^\rho} V_m^\rho & \frac{\partial Q_m^\rho}{\partial \delta_{cR}^\rho} & \frac{\partial Q_m^\rho}{\partial V_{cR}^\rho} V_{cR}^\rho & 0 \\ \frac{\partial P_{mk}^\rho}{\partial \theta_k^\rho} & \frac{\partial P_{mk}^\rho}{\partial \theta_m^\rho} & \frac{\partial P_{mk}^\rho}{\partial V_k^\rho} V_k^\rho & \frac{\partial P_{mk}^\rho}{\partial V_m^\rho} V_m^\rho & \frac{\partial P_{mk}^\rho}{\partial \delta_{cR}^\rho} & \frac{\partial P_{mk}^\rho}{\partial V_{cR}^\rho} V_{cR}^\rho & 0 \\ \frac{\partial Q_{mk}^\rho}{\partial \theta_k^\rho} & \frac{\partial Q_{mk}^\rho}{\partial \theta_m^\rho} & \frac{\partial Q_{mk}^\rho}{\partial V_k^\rho} V_k^\rho & \frac{\partial Q_{mk}^\rho}{\partial V_m^\rho} V_m^\rho & \frac{\partial Q_{mk}^\rho}{\partial \delta_{cR}^\rho} & \frac{\partial Q_{mk}^\rho}{\partial V_{cR}^\rho} V_{cR}^\rho & 0 \\ \frac{\partial P_{bb}^\rho}{\partial \theta_k^\rho} & \frac{\partial P_{bb}^\rho}{\partial \theta_m^\rho} & \frac{\partial P_{bb}^\rho}{\partial V_k^\rho} V_k^\rho & \frac{\partial P_{bb}^\rho}{\partial V_m^\rho} V_m^\rho & \frac{\partial P_{bb}^\rho}{\partial \delta_{cR}^\rho} & \frac{\partial P_{bb}^\rho}{\partial V_{cR}^\rho} V_{cR}^\rho & \frac{\partial P_{bb}^\rho}{\partial \delta_{vR}^\rho} \end{bmatrix} \begin{bmatrix} \Delta \theta_k^\rho \\ \Delta \theta_m^\rho \\ \frac{\Delta V_k^\rho}{V_k^\rho} \\ \frac{\Delta V_m^\rho}{V_m^\rho} \\ \Delta \delta_{cR}^\rho \\ \frac{\Delta V_{cR}^\rho}{V_{cR}^\rho} \\ \Delta \delta_{vR}^\rho \end{bmatrix}. \tag{6.82}$$

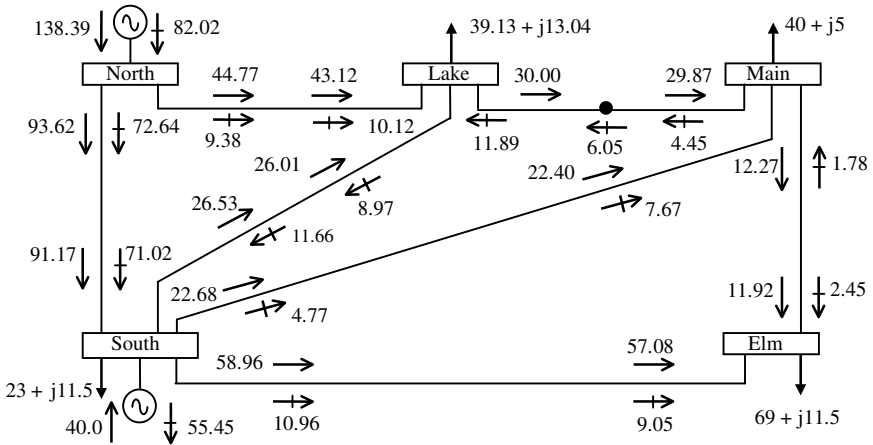
The Jacobian entries, which are  $3 \times 3$  matrices, are derived in a similar way to those of the STATCOM in Section 6.5. The linearised equation (6.82) is solved for the vector of state variables increments, and this information is used to update the state variables. If the convergence criterion has not been satisfied then a new iteration is started using the latest, state variables information available.



(a)



(b)



(c)

Figure 6.9 Unified power flow controller upgraded test network and power flow

### 6.6.1 Numerical Example of Power Flow Control using One Unified Power Flow Controller

In order to assess the effectiveness of UPFC controllers to regulate active and reactive power flow and to control voltage magnitude in one of the UPFC connecting buses, the five-bus network is modified to include a three-phase UPFC model to compensate and to balance the transmission line linking buses Lake and Main. The modified network is shown in Figure 6.9. The UPFC is used to maintain active power leaving the UPFC, towards Main, at 30 MW in each phase; reactive power towards Main is selected in such a manner that balanced voltage magnitudes of 0.98 p.u. are obtained at the bus connecting the UPFC and compensated transmission line; the reactive power injections are set at 7.13 MVAR, 2.47 MVAR, and 6.05 MVAR for phases *a*, *b*, and *c*, respectively; voltage magnitudes at bus Lake are fixed at 1 p.u. The three-phase nodal voltage magnitudes and phase angles are given in Table 6.5(a), where it is shown that the UPFC is effective in regulating voltage magnitude in both of the connecting buses. Figure 6.9 shows the power flow results when the UPFC regulates reactive power at the above values. It is clear that the UPFC is an effective device for restoring power balance. Table 6.5(b) shows the nodal voltage magnitudes in the sequence domain.

**Table 6.5** Nodal voltages in the three-phase unbalanced network with a unified power flow controller: (a) phase voltages and (b) sequence voltages

Voltage	Phase	Network bus					
		North	South	Lake	Main	Elm	LakeUPFC
(a) Phase voltages							
Magnitude (p.u.)	<i>a</i>	1.06	1.00	1.00	0.980	0.979	0.98
	<i>b</i>	1.06	1.00	1.00	0.977	0.973	0.98
	<i>c</i>	1.06	1.00	1.00	0.978	0.957	0.98
Phase angle (deg)	<i>a</i>	0.00	-1.74	-6.05	-3.04	-5.19	-2.49
	<i>b</i>	240.00	238.27	234.80	235.90	235.67	236.41
	<i>c</i>	120.00	117.65	114.83	115.36	113.39	115.98
(b) Sequence voltages							
Magnitude (p.u.)	Zero	0.00	0.0036	0.0050	0.0087	0.0161	0.0077
	Positive	1.06	1.0000	1.0000	0.9782	0.9695	0.9799
	Negative	0.00	0.0036	0.0050	0.0073	0.0090	0.0078

## 6.7 SUMMARY

In the first part of this chapter we presented the theory of power flow in phase coordinates using the Newton–Raphson method. This enables the reliable solution of three-phase power systems exhibiting any degree of geometric and operational imbalance. To illustrate the

additional flexibility introduced by the phase coordinates modelling, the five-bus network was solved for cases of balanced and unbalanced system load, and comparisons were drawn. A three-phase power flow function written in Matlab<sup>®</sup> code was provided to enable a hands-on application of the theory. It used the Newton–Raphson method and is suitable for solving small and medium-sized networks with balanced and unbalanced system loads. The function is quite general, but modelling capability has been kept at a relatively low level to avoid cumbersome and lengthy code. Nevertheless, incorporation of advanced power plant models, such as those studied in Chapter 3, is quite a straightforward programming exercise.

The second part of the chapter focused on developing three-phase models of key FACTS controllers, such as the SVC, STATCOM, TCSC, and UPFC. The first two controllers are shunt-connected, and the test cases presented emphasise the fact that, at least in principle, these controllers are capable of restoring voltage magnitude at the point of connection, in addition to fulfilling their basic function of providing reactive power support. The TCSC and UPFC are series-connected controllers and, in their respective numerical examples, they are set to enable balanced active power flows in the compensated transmission line. This is achieved by contributing unbalanced compensation, a fact that does not dent the quadratic convergence characteristic of the three-phase power flow Newton–Raphson method. Incorporation of these FACTS controller models into the Matlab<sup>®</sup> function given in this chapter is a more cumbersome exercise than the incorporation of conventional power plant models.

## REFERENCES

- Angeles-Camacho, C., 2000, *Modelado en Estado Estacionario del Controlador Unificado de Flujo de Potencia para el Análisis Trifásico de Sistemas Eléctricos*, MSc thesis, Instituto Tecnológico de Morelia, México.
- Arrillaga, J., Harker B.J., 1978, ‘Fast Decoupled Three-phase Load Flow’, *Proceedings of the IEE* **125**(8) 734–740.
- Birt, K.A., Graffy, J.J., McDonald J.D., 1976, ‘Three-phase Load Flow Program’, *IEEE Trans. on Power Apparatus and Systems* **PAS-95**(1) 59–65.
- Chen, B.K., Chen, M.S., Shoults, R.R., Liang, C.C., 1990, ‘Hybrid Three-phase Load Flow’, *IEE Proceedings on Generation, Transmission and Distribution, Part C* **137**(3) 177–185.
- Chen, M.S., Dillon, W.E., 1974, ‘Power System Modelling’, *Proceedings of the IEE* **62**(7) 901–915.
- Harker, B.J., Arrillaga, J., 1979, ‘3-phase a.c./d.c. Load Flow’, *Proceedings of the IEE* **126**(12) 1275–1281.
- Hesse, M.H., 1966, ‘Circulating Currents in Parallel Untransposed Multicircuits Lines’, *IEEE Trans. Power Apparatus and Systems* **PAS-85**(July) 802–820.
- Laughton, M.A., 1968, ‘Analysis of Unbalanced Polyphase Networks by the Method of Phase Coordinates’, *Proceedings of the IEE* **115**(8) 1163–1172.
- Laughton, M.A., Saleh, A.O.M., 1985, ‘Unified Phase Coordinate Load-flow and Fault Analysis of Polyphase Networks’, *Electrical Power & Energy Systems* **2**(4) 2805–2814.
- Smith, B.C., Arrillaga, J., 1998, ‘Improved Three-phase Load Flow using Phase and Sequence Components’, *IEE Proceedings on Generation, Transmission and Distribution, Part C* **145**(3) 245–250.

- Venegas, T., Fuerte-Esquivel, C.R., 2001, 'Steady-state Modelling of an Advanced Series Compensator for Power Flow Analysis of Electric Networks in Phase Co-ordinates', *IEEE Trans. on Power Systems* **16**(4) 758–765.
- Wasley, R.G., Shlash, M.A., 1974a, 'Newton–Raphson Algorithm for 3-phase Load Flow', *Proceedings of the IEE* **121**(7) 630–638.
- Wasley, R.G., Shlash, M.A., 1974b, 'Steady-state Phase-variable Model of the Synchronous Machine for Use in 3-phase Load-flow Studies', *Proceedings of the IEE*, **121**(10) 1155–1164.
- Zhang, X.P., Chen, H., 1994, 'Asymmetrical Three-phase Load-flow Study based on Symmetrical Component Theory', *IEE Proceedings on Generation, Transmission and Distribution, Part C* **141**(3) 248–252.

# 7

## Optimal Power Flow

### 7.1 INTRODUCTION

Electric power systems have experienced continuous growth in all three sectors of the business, namely, generation, transmission, and distribution. In the past, transmission systems were characterised by a low degree of interconnection, hence, it was uncomplicated to share the load among several generating units. The increase in load sizes and operational complexity brought about by widespread interconnection of transmission systems, some encompassing continental distances, introduced major difficulties into the operation of electrical power networks. It became necessary for many electrical utilities to operate their systems closer to the system operating capacity. It became impractical to determine appropriate operating strategies based only on observation and the experience of the operator. The operating philosophy had to be revised, and new concepts based on economic considerations were adopted. Optimal power flow (OPF) solution methods have been developed over the years to meet this very practical requirement of power system operation (Alsac *et al.*, 1990; Dommel and Tinney, 1968; El-Hawary and Tsang, 1986; Happ, 1977; Huneault and Galiana, 1991; Maria and Findlay, 1987; Monticelli and Liu, 1992; Sasson, 1969; Sasson, Vilorio, and Aboites, 1973; Sun *et al.*, 1984; Tinney and Hart, 1967; Wood and Wollenberg, 1984)

Optimal power flows can be more easily understood if one thinks in terms of conventional power flows, where the objective is to determine the steady-state operating conditions of the power network. Voltage magnitudes and angles at all buses of the network corresponding to specified levels of load and generation are determined first. Power flows throughout the network are calculated afterwards. It is most likely that this solution, although feasible, will not yield the most economic generating schedule or an operating point where minimum losses are incurred. The OPF solution, in contrast, includes an objective function that is optimised without violating the system operating constraints. These include the network equations, loading conditions, and physical limits on active and reactive power generation. The selection of the objective function depends on the operating philosophy of each power system. A common objective function concerns the active power generation cost. The economic dispatch problem is a particular case of the OPF problem (Wood and Wollenberg, 1984).

## 7.2 OPTIMAL POWER FLOW USING NEWTON'S METHOD

### 7.2.1 General Formulation

OPF solutions are carried out to determine the optimum operating state of a power network subjected to physical and operational constraints. An objective function, which may incorporate economic, security, or environmental aspects of the power system, is formulated and solved using a suitable optimisation algorithm, such as Newton's method. The constraints are physical laws that govern power generation and transmission system availability, the design limits of the electrical equipment, and operating strategies. This kind of problem is usually expressed as a static, nonlinear programming problem, with the objective function represented as a nonlinear equation and the constraints represented by nonlinear or linear equations.

More often than not, the objective function is taken to be the cost of generation, reflecting the economic aspects of the electrical power system (Dommel and Tinney, 1968; Maria and Findlay, 1987; Monticelli and Liu, 1992; Sun *et al.*, 1984). Hence, the mathematical formulation minimises active power generation cost by suitable adjustment of the control parameters.

The OPF problem can be formulated as follows:

$$\text{Minimise } f(\mathbf{x}) \text{ subject to } h(\mathbf{x}) = 0 \text{ and } g(\mathbf{x}) \leq 0. \quad (7.1)$$

In this expression,  $\mathbf{x}$  is the vector of state variables,  $f(\mathbf{x})$  is the objective function to be optimised,  $h(\mathbf{x})$  represents the power flow equations, and  $g(\mathbf{x})$  consists of state variable limits and functional operating constraints.

In general, the aim is to optimise an objective function with the solution satisfying a number of equality and inequality constraints. Any solution point that satisfies all the constraints is said to be a feasible solution. A local minimum is a feasible solution point where the objective function is minimised within a neighbourhood. The global minimum is a local minimum with the lowest value in the complete feasible region (Bertsekas, 1982; Luenberger, 1984).

#### 7.2.1.1 Variables

Variables that can be adjusted in pursuit of the optimal solution are termed control variables, such as active power generation, taps and phase angles in tap-changing and phase-shifting transformers, respectively, and voltage magnitudes at the generator buses. The control parameters are taken to be continuous quantities. Such a representation is well handled by the OPF formulation and provides a suitable representation of controls with small discrete steps.

Dependent variables are those that depend on the control variables. They can take any value, within limits, as dictated by the solution algorithm. Examples of dependent variables are voltage phase angles at all buses, except the slack bus; voltage magnitudes at all load buses; reactive power at all generation buses; active power generation costs; and active and reactive power flows (network losses) in transmission lines and transformers.

In addition to control and dependent variables, active and reactive power loads and network topology and data form a set of fixed parameters that must be specified at the outset of the study.

### 7.2.1.2 Objective function

The main aim of the OPF solution is to determine the control settings and system state variables that optimise the value of the objective function. The selection of the objective function should be based on careful analysis of the power system security and economy. Arguably, power generation cost is the most popular objective function in OPF studies, where the thermal generation unit costs are generally represented by a nonlinear, second-order function (Luenberger, 1984; Sun *et al.*, 1984):

$$F_T = \sum_{k=1}^{n_g} F_k(P_{gk}), \quad (7.2)$$

where  $F_k$  is the fuel cost of unit  $k$ ,  $P_{gk}$  is the active power generated by unit  $k$ , and  $n_g$  is the number of generators in the system, including the slack generator. More specifically,

$$F_k(P_{gk}) = a_k + b_k P_{gk} + c_k P_{gk}^2, \quad (7.3)$$

where  $a_k$ ,  $b_k$ , and  $c_k$  are the cost coefficients of unit  $k$ .

It should be noted that it is crucial to include the slack generator contribution in the OPF formulation, Equation (7.1), otherwise the minimisation process will dispatch all the generating units at their minimum capacity while assigning the rest of the required generation to the slack generator, which would be seen by the optimisation procedure as having zero generation cost and infinite generation capacity.

### 7.2.1.3 Equality constraints

The power flow equations provide a means for calculating the power balance that exists in the network during steady-state operation. They must be satisfied, unconditionally, if a feasible solution is to exist (Dommel and Tinney, 1968; Sun *et al.*, 1984), otherwise the OPF problem is said to be infeasible, with attempts being made to find a limited but still useful solution by relaxing some of the network constraints.

The power flow equations represent the link between the control variables and the dependent variables,

$$P_k(V, \theta) + P_{dk} - P_{gk} = 0, \quad (7.4)$$

$$Q_k(V, \theta) + Q_{dk} - Q_{gk} = 0, \quad (7.5)$$

where  $P_k$  and  $Q_k$  are, respectively, the active and reactive power injections at bus  $k$ ;  $P_{dk}$  and  $Q_{dk}$  are, respectively, the active and reactive power loads at bus  $k$ ;  $P_{gk}$  and  $Q_{gk}$  are, respectively, the scheduled active and reactive power generations at bus  $k$ ;  $V$  and  $\theta$  are, respectively, the nodal voltage magnitudes and angles.

A generic bus including generation, load, and a transmission line is shown in Figure 7.1. It should be noted that all equality constraints in the power network are nonlinear. However, they are incorporated in a linearised form within the OPF formulation (Luenberger, 1984).

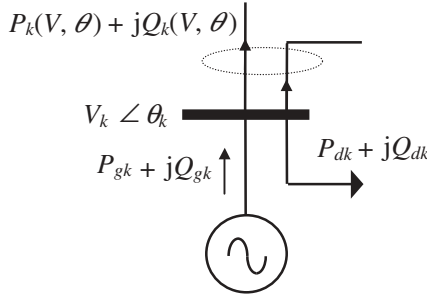


Figure 7.1 A generic bus of the electrical power network

### 7.2.1.4 Inequality constraints

All variables have upper and lower limits that must be satisfied in the optimal solution. Constraints on control variables reflect the bounds of the operating conditions of the equipment used for power dispatch. Arguably, limits on the generated active power and voltage magnitude at the generating units are the most important of such bounds.

Functional constraints result from the application of limits on control variables, with constraints on voltage magnitudes at load buses and on active and reactive power flows in transmission lines being the most popular:

$$P_{gk}^{\min} \leq P_{gk} \leq P_{gk}^{\max}, \quad k = 1, \dots, n_g; \tag{7.6}$$

$$Q_{gk}^{\min} \leq Q_{gk} \leq Q_{gk}^{\max}, \quad k = 1, \dots, n_g; \tag{7.7}$$

$$V_k^{\min} \leq V_k \leq V_k^{\max}, \quad k = 1, \dots, n_b; \tag{7.8}$$

where  $n_b$  is the total number of buses,  $n_g$  is the total number of generation buses, and

$$Q_{gk} = Q_k(V, \theta) + Q_{dk}. \tag{7.9}$$

If a reactive power limit violation takes place in a generator bus, it changes to a load bus, with associated voltage constraints.

It should be mentioned that functional constraints are normally relaxed under system emergency conditions in order to obtain suboptimal but still technically feasible solutions.

## 7.2.2 Application of Newton's Method to Optimal Power Flow

The first step towards solving the constrained optimisation problem using Newton's method is to convert the problem into an unconstrained optimisation problem. This is achieved by constructing an augmented Lagrangian function for Equation (7.1), which in generic form may be written as:

$$L(\mathbf{x}, \boldsymbol{\lambda}) = f(\mathbf{x}) + \boldsymbol{\lambda}^T h(\mathbf{x}) + \psi[g(\mathbf{x}), \boldsymbol{\mu}], \tag{7.10}$$

where  $\boldsymbol{\lambda}$  and  $\boldsymbol{\mu}$  are Lagrange multiplier vectors for equality and inequality constraints, respectively,  $\psi[g(\mathbf{x}), \boldsymbol{\mu}]$  is the penalty function of the inequality constraints, and a superscript

t indicates the transpose. In Equation (7.10) there are as many Lagrange multipliers as number of active constraints. The method for handling functional inequality constraints is addressed in Section 7.2.6.

In OPF using Newton's method, the Lagrangian function for active and reactive power flows is modelled as an equality constraint, given by the following equation (Luenberger, 1984):

$$L_{\text{system}}(\mathbf{x}, \boldsymbol{\lambda}) = F_T + \sum_{k=1}^{n_b} \lambda_{pk} [P_k(V, \theta) + P_{dk} - P_{gk}] + \sum_{k=1}^{n_b} \lambda_{qk} [Q_i(V, \theta) + Q_{dk} - Q_{gk}], \quad (7.11)$$

where  $F_T$  is the objective function, the summations are for the  $n_b$  buses specified in the study, and  $\lambda_{pk}$  and  $\lambda_{qk}$  are the Lagrange multipliers for the active and reactive power equations, respectively.

### 7.2.3 Linearised System Equations

Solution of the Lagrangian function of Equation (7.11) may be efficiently achieved by solving, by iteration, the following system of linearised equations,

$$[\mathbf{W}] \begin{bmatrix} \Delta \mathbf{x} \\ \Delta \boldsymbol{\lambda} \end{bmatrix} = \begin{bmatrix} \nabla \mathbf{x} \\ \nabla \boldsymbol{\lambda} \end{bmatrix}. \quad (7.12)$$

Sometimes, it is more convenient to express the system of Equations (7.12) as follows:

$$\mathbf{W} \Delta \mathbf{z} = -\mathbf{g}, \quad (7.13)$$

where

$$\mathbf{W} = \begin{bmatrix} \mathbf{H} & \mathbf{J}^t \\ \mathbf{J} & \mathbf{0} \end{bmatrix}, \quad (7.14)$$

$$\Delta \mathbf{z} = [\Delta \mathbf{x} \ \Delta \boldsymbol{\lambda}]^t, \quad (7.15)$$

$$\mathbf{g} = [\nabla \mathbf{x} \ \nabla \boldsymbol{\lambda}]^t, \quad (7.16)$$

$$\nabla \mathbf{x} = [\nabla \mathbf{P}_g \ \nabla \boldsymbol{\theta} \ \nabla \mathbf{V}]^t, \quad (7.17)$$

$$\nabla \boldsymbol{\lambda} = [\nabla \lambda_p \ \nabla \lambda_q]^t, \quad (7.18)$$

$$\Delta \mathbf{x} = [\Delta \mathbf{P}_g \ \Delta \boldsymbol{\theta} \ \Delta \mathbf{V}]^t, \quad (7.19)$$

$$\Delta \boldsymbol{\lambda} = [\Delta \lambda_p \ \Delta \lambda_q]^t. \quad (7.20)$$

Matrix  $\mathbf{W}$  contains the second partial derivatives of the Lagrangian function  $L(\mathbf{x}, \boldsymbol{\lambda})$  with respect to the state variables  $\mathbf{x}$  and Lagrange multipliers  $\boldsymbol{\lambda}$ . Some derivative terms give rise to the Hessian  $\mathbf{H}$  whereas others give rise to the Jacobian  $\mathbf{J}$  or its transposed matrix  $\mathbf{J}^t$ . Matrix  $\mathbf{W}$  is symmetric and has a null submatrix,  $\mathbf{0}$ , at its lower right-hand corner, since the second partial derivatives of the form  $\partial^2 L(\mathbf{x}, \boldsymbol{\lambda}) / \partial \lambda_k \partial \lambda_m$  do not exist.

The gradient vector  $\mathbf{g}$  is  $\nabla L(\mathbf{x}, \boldsymbol{\lambda})$ , and the first partial derivatives of  $\mathbf{g}$  are the second partial derivatives of the Lagrangian function  $L(\mathbf{x}, \boldsymbol{\lambda})$ . The Lagrange multipliers are the incremental costs for active and reactive powers,  $\lambda_p$  and  $\lambda_q$ , respectively.  $\Delta \mathbf{z}$  is the vector of correction terms. The state variables are the active power generations, the nodal voltage magnitudes, and phase angles,  $P_g$ ,  $V$ , and  $\theta$ , respectively.

The derivative terms associated with the inequality constraints,  $\psi[\mathbf{g}(\mathbf{x}), \boldsymbol{\mu}]$ , are not included at the beginning of the iterative solution. They are incorporated into the linearised system of Equations (7.12) only after limits become enforced; hence, the Hessian and Jacobian terms are:

$$\mathbf{H} = \frac{\partial^2 L(\mathbf{x}, \boldsymbol{\lambda})}{\partial \mathbf{x}^2} = \frac{\partial^2 f(\mathbf{x})}{\partial \mathbf{x}^2} + \left[ \frac{\partial^2 h(\mathbf{x})}{\partial \mathbf{x}^2} \right]^t \boldsymbol{\lambda}, \quad (7.21)$$

$$\mathbf{J} = \frac{\partial^2 L(\mathbf{x}, \boldsymbol{\lambda})}{\partial \mathbf{x} \partial \boldsymbol{\lambda}} = \frac{\partial h(\mathbf{x})}{\partial \mathbf{x}}. \quad (7.22)$$

A key property of submatrices  $\mathbf{H}$ ,  $\mathbf{J}$ , and  $\mathbf{J}^t$  is that they all have the same sparsity structure as the nodal admittance matrix (Wood and Wollenberg, 1984).

#### 7.2.4 Optimality Conditions for Newton's Method

In general, conditions for global optimality ( $\mathbf{x}^{\text{opt}}$ ,  $\boldsymbol{\lambda}^{\text{opt}}$ ) can be checked by assessing the positiveness of matrix  $\mathbf{W}$ . However, it is computationally too expensive for large-scale problems to verify that matrix  $\mathbf{W}$  is positive definite, and this test is skipped in most practical problems. Other optimality tests performed involve checking that the gradient vector is zero and that the Lagrange multipliers for the binding inequalities pass their sign test (Bertsekas, 1982; Luenberger, 1984).

In practical OPF solutions the following tests are carried out (Sun *et al.*, 1984).

- all power mismatches are within a prescribed tolerance;
- the inequality constraints are satisfied;
- the vector gradient is zero;
- further reductions in the objective function are possible only if constraints are violated.

It should be emphasised that in general optimisation problems, the solution has to satisfy a number of equality and inequality constraints. Inequality constraints are made active by changing them into equality constraints. Hence, the general optimisation problem is to find the optimum of a function subjected to a set of equality constraints.

#### 7.2.5 Conventional Power Plant Modelling in Optimal Power Flow

Superposition is used to construct the linearised system of Equations (7.12) at each iterative step. The plant components of the power system are modelled independently and their individual entries placed in  $\mathbf{W}$  and  $\mathbf{g}$ . The bus number to which the plant component is connected determines the location of the individual Hessian and Jacobian terms in the overall  $\mathbf{W}$  and  $\mathbf{g}$  structures.

### 7.2.5.1 Transmission lines

The positive sequence representation of the nominal  $\pi$ -circuit shown in Figure 3.1 is used to derive the transmission line power flow equations required by the OPF formulation in a similar manner to the procedure carried out in Section 4.2.1 for the case of a series impedance.

The Lagrangian function associated with the power mismatch equations at buses  $k$  and  $m$  is:

$$L = L_{\text{trans-line}}(\mathbf{x}, \boldsymbol{\lambda}) = \lambda_{pk}(P_k + P_{dk} - P_{gk}) + \lambda_{qk}(Q_k + Q_{dk} - Q_{gk}) \\ + \lambda_{pm}(P_m + P_{dm} - P_{gm}) + \lambda_{qm}(Q_m + Q_{dm} - Q_{gm}). \quad (7.23)$$

The first partial derivatives of the Lagrangian function in Equation (7.23), with respect to the voltage magnitudes and phase angles at buses  $k$  and  $m$ , and the four Lagrange multipliers, are used as entries in the gradient vector  $\mathbf{g}$ . The individual entries of matrix  $\mathbf{W}$  are the second derivative terms of the Lagrangian function with respect to voltage magnitudes and phase angles at buses  $k$  and  $m$ , and the four Lagrange multipliers in Equation (7.23). These terms are given explicitly in Appendix B, Section B.1.

The contribution of a transmission line to the overall linearised system of Equations (7.12) is:

$$\begin{bmatrix} \mathbf{W}_{kk} & \mathbf{W}_{km} \\ \mathbf{W}_{mk} & \mathbf{W}_{mm} \end{bmatrix} \begin{bmatrix} \Delta \mathbf{z}_k \\ \Delta \mathbf{z}_m \end{bmatrix} = - \begin{bmatrix} \mathbf{g}_k \\ \mathbf{g}_m \end{bmatrix} \quad (7.24)$$

where

$$\mathbf{W}_{kk} = \begin{bmatrix} \frac{\partial^2 L}{\partial \theta_k^2} & \frac{\partial^2 L}{\partial \theta_k \partial V_k} & \frac{\partial P_k}{\partial \theta_k} & \frac{\partial Q_k}{\partial \theta_k} \\ \frac{\partial^2 L}{\partial V_k \partial \theta_k} & \frac{\partial^2 L}{\partial V_k^2} & \frac{\partial P_k}{\partial V_k} & \frac{\partial Q_k}{\partial V_k} \\ \frac{\partial P_k}{\partial \theta_k} & \frac{\partial P_k}{\partial V_k} & 0 & 0 \\ \frac{\partial Q_k}{\partial \theta_k} & \frac{\partial Q_k}{\partial V_k} & 0 & 0 \end{bmatrix}, \quad (7.25)$$

$$\mathbf{W}_{km} = \begin{bmatrix} \frac{\partial^2 L}{\partial \theta_k \partial \theta_m} & \frac{\partial^2 L}{\partial \theta_k \partial V_m} & \frac{\partial P_m}{\partial \theta_k} & \frac{\partial Q_m}{\partial \theta_k} \\ \frac{\partial^2 L}{\partial V_k \partial \theta_m} & \frac{\partial^2 L}{\partial V_k \partial V_m} & \frac{\partial P_m}{\partial V_k} & \frac{\partial Q_m}{\partial V_k} \\ \frac{\partial P_k}{\partial \theta_m} & \frac{\partial P_k}{\partial V_m} & 0 & 0 \\ \frac{\partial Q_k}{\partial \theta_m} & \frac{\partial Q_k}{\partial V_m} & 0 & 0 \end{bmatrix}, \quad (7.26)$$

$$\mathbf{W}_{mk} = \begin{bmatrix} \frac{\partial^2 L}{\partial \theta_m \partial \theta_k} & \frac{\partial^2 L}{\partial \theta_m \partial V_k} & \frac{\partial P_k}{\partial \theta_m} & \frac{\partial Q_k}{\partial \theta_m} \\ \frac{\partial^2 L}{\partial V_m \partial \theta_k} & \frac{\partial^2 L}{\partial V_m \partial V_k} & \frac{\partial P_k}{\partial V_m} & \frac{\partial Q_k}{\partial V_m} \\ \frac{\partial P_m}{\partial \theta_k} & \frac{\partial P_m}{\partial V_k} & 0 & 0 \\ \frac{\partial Q_m}{\partial \theta_k} & \frac{\partial Q_m}{\partial V_k} & 0 & 0 \end{bmatrix}, \quad (7.27)$$

$$\mathbf{W}_{mm} = \begin{bmatrix} \frac{\partial^2 L}{\partial \theta_m^2} & \frac{\partial^2 L}{\partial \theta_m \partial V_m} & \frac{\partial P_m}{\partial \theta_m} & \frac{\partial Q_m}{\partial \theta_m} \\ \frac{\partial^2 L}{\partial V_m \partial \theta_m} & \frac{\partial^2 L}{\partial V_m^2} & \frac{\partial P_m}{\partial V_m} & \frac{\partial Q_m}{\partial V_m} \\ \frac{\partial P_m}{\partial \theta_m} & \frac{\partial P_m}{\partial V_m} & 0 & 0 \\ \frac{\partial Q_m}{\partial \theta_m} & \frac{\partial Q_m}{\partial V_m} & 0 & 0 \end{bmatrix}, \quad (7.28)$$

$$\Delta \mathbf{z}_k = [\Delta \theta_k \ \Delta V_k \ \Delta \lambda_{pk} \ \Delta \lambda_{qk}]^t, \quad (7.29)$$

$$\Delta \mathbf{z}_m = [\Delta \theta_m \ \Delta V_m \ \Delta \lambda_{pm} \ \Delta \lambda_{qm}]^t, \quad (7.30)$$

$$\mathbf{g}_k = [\nabla \theta_k \ \nabla V_k \ \nabla \lambda_{pk} \ \nabla \lambda_{qk}]^t, \quad (7.31)$$

$$\mathbf{g}_m = [\nabla \theta_m \ \nabla V_m \ \nabla \lambda_{pm} \ \nabla \lambda_{qm}]^t. \quad (7.32)$$

These terms are systematically placed in  $\mathbf{W}$  and  $\mathbf{g}$  to make them correspond to the locations of buses  $k$  and  $m$ .

### 7.2.5.2 Shunt elements

In electrical power systems, nodal voltages are markedly affected by load variations and by network topology changes. The voltage drops when the network operates under heavy loading, and, conversely, when the load level is low overvoltages can arise owing to the capacitive effect of transmission lines. Such voltage variations are not conducive to good operation, and voltage regulation is enforced by controlling the production or absorption of reactive power at key locations in the network. Shunt capacitors and shunt reactors are used for such a purpose. Shunt compensators are either permanently connected to the network or are switched on or off according to requirements (Wood and Wollenberg, 1984).

A way to include a purely reactive shunt element in the OPF formulation is shown below. If the shunt element is connected at bus  $k$ , the Lagrangian function is given by:

$$L = L_{\text{shunt}}(\mathbf{x}, \boldsymbol{\lambda}) = \lambda_{qk}(Q_{\text{shunt},k}) = \lambda_{qk}(-V_k^2 B_{\text{shunt}}). \quad (7.33)$$

The shunt element contribution to the overall linearised system of equations is:

$$\begin{bmatrix} -2\lambda_{qk}B_{\text{shunt}} & -2V_kB_{\text{shunt}} \\ -2V_kB_{\text{shunt}} & 0 \end{bmatrix} \begin{bmatrix} \Delta V_k \\ \Delta\lambda_{qk} \end{bmatrix} = - \begin{bmatrix} -2\lambda_{qk}V_kB_{\text{shunt}} \\ -V_k^2B_{\text{shunt}} \end{bmatrix}. \quad (7.34)$$

### 7.2.5.3 Synchronous generators

In addition to providing the active power demanded by the system, synchronous generators also control the production or absorption of reactive power, aimed at maintaining a constant voltage magnitude at their terminals. In the OPF formulation, the active power–cost characteristics of steam generators are included in the problem formulation whereas hydro generators are assumed to operate at a fixed active power generation while contributing fully to the production or absorption of reactive power.

The generator representation in the OPF formulation may be based on a quadratic expression of the active power–cost characteristic. The Lagrangian function of a generator supplying active power to a bus  $k$  is given by:

$$L = L_{\text{gen}}(\mathbf{x}, \boldsymbol{\lambda}) = a_k + b_k P_{gk} + c_k P_{gk}^2. \quad (7.35)$$

Its contribution to the overall linearised system of equations is:

$$\begin{bmatrix} 2c_k & -1 \\ -1 & 0 \end{bmatrix} \begin{bmatrix} \Delta P_{gk} \\ \Delta\lambda_{pk} \end{bmatrix} = - \begin{bmatrix} b_k + 2c_k P_{gk} - \lambda_{pk} \\ 0 \end{bmatrix}. \quad (7.36)$$

## 7.2.6 Handling of Inequality Constraints

The set of equality constraints included in the Lagrangian function at any stage of the iterative process is called the active set (Bertsekas, 1982; Luenberger, 1984). The set of inequality constraints that are active when the optimum is reached is called the binding set, and the optimal solution does not necessarily require all the inequality constraints to be binding. The binding set is not known a priori, and it is the task of the optimisation algorithm to determine it as well as to enforce it. The inequalities that become active during the solution process are changed to equalities and included in the active set. The problem is then to minimise the Lagrangian function for the newly updated active set.

### 7.2.6.1 Handling of inequality constraints on variables

The inequality constraints are handled in the OPF formulation by means of the multiplier method, as opposed to the penalty function method (Bertsekas, 1982; Luenberger, 1984). The inequality constraints, when made active, are changed to equality constraints. This has the effect of a restraining force that pulls the inadmissible points back into the admissible region. In the multiplier method, a penalty term is added to the Lagrangian function  $L(\mathbf{x}, \boldsymbol{\lambda})$ , thus forming an augmented Lagrangian function, given by Equation (7.10). The minimisation of the Lagrangian function is carried out by using Newton's method only for the primal variables (state variables). The dual variables,  $\boldsymbol{\mu}$ , are updated at the end of

each global iteration. Multipliers (dual variables) are checked for limit violations, and variables within bounded limits are ignored.

The inequality constraints used in Equation (7.10) are handled by using the following generic form:

$$\Psi_k[\mathbf{g}_k(\mathbf{x}), \mu_k] = \begin{cases} \mu_k[\mathbf{g}_k(\mathbf{x}) - \bar{\mathbf{g}}_k] + \frac{c}{2}[\mathbf{g}_k(\mathbf{x}) - \bar{\mathbf{g}}_k]^2, & \text{if } \mu_k + c[\mathbf{g}_k(\mathbf{x}) - \bar{\mathbf{g}}_k] \geq 0; \\ \mu_k[\mathbf{g}_k(\mathbf{x}) - \underline{\mathbf{g}}_k] + \frac{c}{2}[\mathbf{g}_k(\mathbf{x}) - \underline{\mathbf{g}}_k]^2, & \text{if } \mu_k + c[\mathbf{g}_k(\mathbf{x}) - \underline{\mathbf{g}}_k] \leq 0; \\ 0 & \text{otherwise;} \end{cases} \quad (7.37)$$

where  $\bar{\mathbf{g}}$  and  $\underline{\mathbf{g}}$  are limits on state variables as well as functional constraints.

At a given iteration,  $(i + 1)$ , the multipliers are adjusted according to the following criteria:

$$\mu_k^{(i+1)} = \begin{cases} \mu_k^{(i)} + c^{(i)}[\mathbf{g}_k(\mathbf{x}^{(i)}) - \bar{\mathbf{g}}_k], & \text{if } \mu_k^{(i)} + c^{(i)}[\mathbf{g}_k(\mathbf{x}^{(i)}) - \bar{\mathbf{g}}_k] \geq 0; \\ \mu_k^{(i)} + c^{(i)}[\mathbf{g}_k(\mathbf{x}^{(i)}) - \underline{\mathbf{g}}_k], & \text{if } \mu_k^{(i)} + c^{(i)}[\mathbf{g}_k(\mathbf{x}^{(i)}) - \underline{\mathbf{g}}_k] \leq 0; \\ 0 & \text{otherwise;} \end{cases} \quad (7.38)$$

where  $0 < c^{(i)} < c^{(i+1)}$ .

Upon convergence,  $\boldsymbol{\mu}$  satisfies the optimality conditions as given by Kuhn and Tucker (Bertsekas, 1982; Luenberger, 1984). In such a case, all the state variable increments are smaller than a pre-specified tolerance and no limit violations occur.

The multiplier method provides an efficient way to handle the binding and nonbinding constraints. After moving a variable to one of its limits, the algorithm holds it there for as long as it is required, otherwise the variable is freed.

Equation (7.37) satisfies the Kuhn and Tucker conditions (Bertsekas, 1982; Luenberger, 1984):

$$\mu \mathbf{g}(\mathbf{x}) = 0; \quad \mu \geq 0. \quad (7.39)$$

For any given constraint, if the product  $\mu \mathbf{g}(\mathbf{x})$  is equal to zero, either  $\mu$  is equal to zero or  $\mathbf{g}(\mathbf{x})$  is nonbinding; if  $\mu > 0$ , then  $\mathbf{g}(\mathbf{x})$  must be zero. Equation (7.37) provides a means to indicate whether or not a constraint is binding.

At the end of each iteration, all variables are checked according to Equation (7.37) and updated according to Equation (7.38). Equation (7.37) is used to evaluate the gradient vector and matrix  $\mathbf{W}$ . Hence, the first and second derivatives of Equation (7.37) are required. The first derivative is added to the gradient vector  $\mathbf{g}$  and the second derivative to matrix  $\mathbf{W}$ . It should be noted that when a variable is within limits, the derivatives are null.

Successful initialisation and updating of the penalty parameter  $c$  is largely dependent on the kind of system being solved and on experience, but the following practical conditions should be observed:

- the initial parameter  $c^{(0)}$  should not be too large to the point that the unconstrained minimisation becomes ill-conditioned;
- the parameter  $c^{(i)}$  should not be increased too fast to the point that the unconstrained minimisation becomes numerically unstable;
- the parameter  $c^{(i)}$  should not be increased too slowly to the extent that the multiplier iterations have a poor rate of convergence.

Experience shows that an effective evaluation of the penalty parameter is achieved by giving  $c^{(0)}$  a value determined by experimentation, with subsequent evaluations of  $c^{(i)}$  based on the following monotonic increases:  $c^{(i+1)} = \beta c^{(i)}$ , where  $\beta$  is a scalar greater than one.

### 7.2.6.2 Handling of inequality constraints on functions

Arguably, the most important functional inequality constraints are those corresponding to controllable sources of reactive power (Wood and Wollenberg, 1984). Reactive power generator limits are checked at the end of each global iteration. It should be pointed out that there are computational advantages gained by including explicitly the reactive power equation of a generator in matrix  $\mathbf{W}$ . If the generator operates within reactive power limits, a large number in the diagonal element associated with  $\lambda_q$  is used to nullify the reactive power equation. However, the large number is removed when the functional inequality constraint becomes activated, in order to enforce either an upper or a lower reactive power limit.

The penalty function technique may be used either to activate or to deactivate the equations corresponding to generator buses. Quadratic penalty functions are used since they have first and second derivatives. The form of the penalty function for the reactive power constraint at a generator bus  $k$  is (Bertsekas, 1982; Luenberger, 1984):

$$E_{qk} = \frac{1}{2} S \lambda_{qk}^2. \quad (7.40)$$

The first and second derivatives are:

$$\frac{dE_{qk}}{d\lambda_{qk}} = S \lambda_{qk}, \quad (7.41)$$

$$\frac{d^2 E_{qk}}{d^2 \lambda_{qk}} = S, \quad (7.42)$$

where  $S$  is a large, positive penalty weighting factor.

Adding the first and second derivatives of the penalty function to the elements associated with  $\lambda_{qk}$  in  $\mathbf{g}$  and  $\mathbf{W}$  deactivates the reactive power flow equation of the generator bus  $k$ . In such a situation,  $\lambda_{qk}$  has a zero value. When one of the reactive power limits is violated, the derivatives are removed from  $\mathbf{W}$  and  $\mathbf{g}$ , and the bus changes from being a generator bus to a load bus. Hence,  $\lambda_{qk}$  changes its value from zero to nonzero.

The sign in  $\lambda_{qk}$  indicates whether or not the reactive power has returned within limits as indicated by the criteria given in Table 7.1.

**Table 7.1** Constraints on reactive power injections

Limit	$\lambda_{qk} < 0$	$\lambda_{qk} > 0$
Upper	Add penalty term	Remove penalty term
Lower	Remove penalty term	Add penalty term

### 7.3 IMPLEMENTATION OF OPTIMAL POWER FLOW USING NEWTON'S METHOD

The mathematical formulation for active power optimisation has been dealt with above (Bertsekas, 1982; Luenberger, 1984). Practical aspects of computer implementation are now presented, with three main steps identified in the flow diagram of Figure 7.2: (1) initialisation of control variables; (2) the outer (main) iteration loop; and (3) the inner iteration loop, which corresponds to the actual Newton process (Ambriz-Pérez, 1998).

The first step comprises initialisation of variables and a lossless economic dispatch (Wood and Wollenberg, 1984). In the main iterative loop, the state variables  $x$  are checked to assess

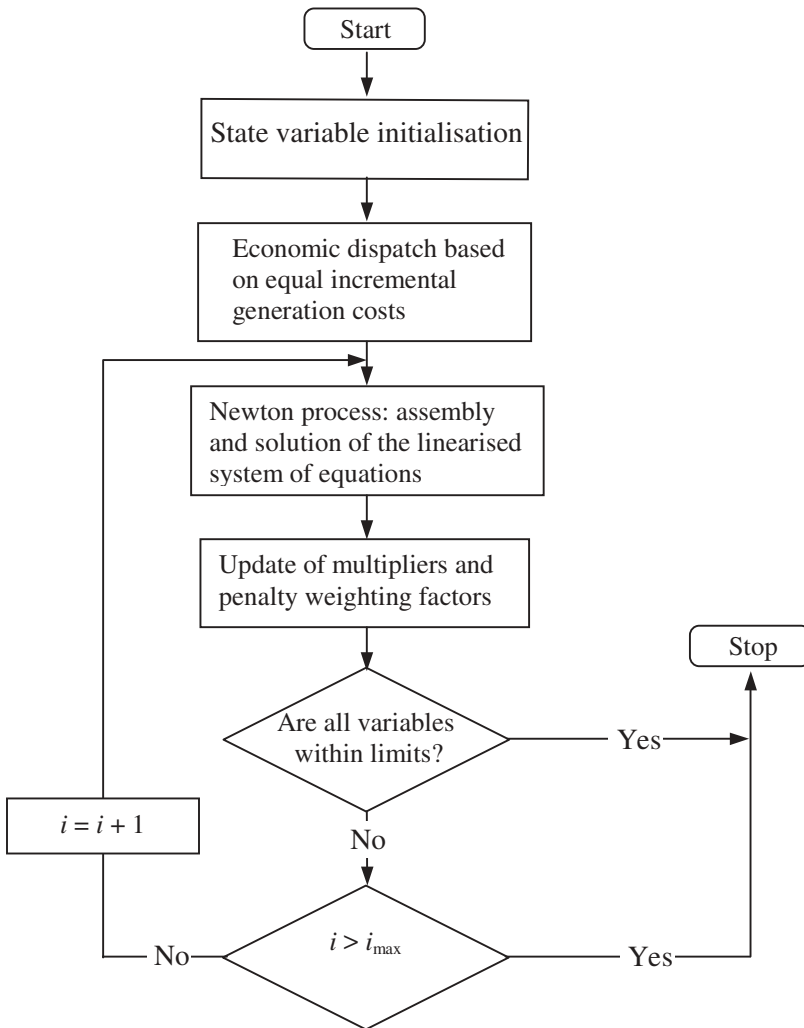


Figure 7.2 Flowchart for active power optimisation

whether or not they are within bounds. The inequality constraints either are activated or inactivated according to the criteria established in Equation (7.37). The multipliers and penalty weighting factors are updated by using Equation (7.38). At a given iteration, ( $i$ ), if no change in the inequality constraint set takes place at the end of the main loop then the optimisation process terminates.

The Newton process takes place in the inner iteration loop, a process characterised by fixed values of the multipliers and penalty weighting factors. The linearised system of equations for minimising the active power generation cost is solved in this loop. Once the linearised system of equations has been assembled then a sparsity-oriented solution is carried out. This process is repeated until a small, prespecified, tolerance is reached. Normally, a tight convergence criterion is adopted for the mismatch gradient vector (i.e.  $1e - 12$ ).

### 7.3.1 Initial Conditions in Optimal Power Flow Solutions

All the state variables and Lagrange multipliers must be given an initial value at the beginning of the solution procedure. The initial values should be selected by following good engineering judgement in order to ensure an acceptable rate of convergence. In this application, nodal voltages are initialised in a way similar to that of the power flow problem [i.e. 1 p.u. magnitude and  $0^\circ$  phase angle for all buses]. This provides a suitable starting condition. Engineering experience indicates that, for most problems, departure from the unitary voltage magnitude and zero phase angle is not too large (i.e.  $0.95 \leq V_k \leq 1.05$ , and  $-10^\circ \leq \theta_k \leq 10^\circ$ ).

### 7.3.2 Active Power Schedule

A lossless economic dispatch, as opposed to a power flow solution, is used to provide good starting conditions for the OPF application. The equal incremental cost criterion may be used for this purpose. Different variants of the method are available in the open literature, but the one recommended here is to take the generator limits into consideration, since this yields more realistic starting conditions (Wood and Wollenberg, 1984).

The Lagrangian of the lossless economic dispatch may be expressed by

$$L = L_{\text{gen}}(\mathbf{x}, \boldsymbol{\lambda}) = F_T + \lambda \left( P_d - \sum_{k=1}^{n_g} P_{gk} \right). \quad (7.43)$$

Necessary conditions to minimise active power generation cost is that the first derivative of the cost function, with respect to each one of the variables involved, is zero and that the balance between the generation and the demand be met:

$$\frac{\partial L}{\partial P_{gk}} = \frac{dF_k(P_{gk})}{dP_{gk}} - \lambda_{pk} = 0, \quad (7.44)$$

$$\sum_{k=1}^{n_g} P_{gk} = P_d. \quad (7.45)$$

Moreover, the inequality constraints given by Expression (7.6) have to be satisfied. If this is not the case, an economic dispatch is carried out and the inequality constraints are handled by means of the multiplier method.

The following set of equations is formed when Newton’s method is applied to the lossless economic dispatch problem.

$$\begin{bmatrix} \frac{d^2 F_1}{dP_1^2} & 0 & \cdots & 0 & -1 \\ 0 & \frac{d^2 F_2}{dP_2^2} & \cdots & 0 & -1 \\ \vdots & \vdots & \ddots & \vdots & \vdots \\ 0 & 0 & \cdots & \frac{d^2 F_{n_g}}{dP_{n_g}^2} & -1 \\ -1 & -1 & \cdots & -1 & 0 \end{bmatrix} \begin{bmatrix} \Delta P_1 \\ \Delta P_2 \\ \vdots \\ \Delta P_{n_g} \\ \Delta \lambda \end{bmatrix} = - \begin{bmatrix} \frac{\partial L}{\partial P_{g1}} \\ \frac{\partial L}{\partial P_{g2}} \\ \vdots \\ \frac{\partial L}{\partial P_{n_g}} \\ P_d - \sum_{k=1}^{n_g} P_{gk} \end{bmatrix}. \quad (7.46)$$

If only quadratic cost functions are used and no limits violations take place then the optimal solution is reached in just one iteration. Otherwise, if generation limits are violated then such limits are enforced and a new iteration is started.

### 7.3.3 Lagrange Multipliers

The Lagrange multipliers for active and reactive power flow mismatch equations are initialised at the  $\lambda_p$  value given by the lossless economic dispatch and  $\lambda_q$  equal to zero, respectively. Experience shows that these values give rise to very robust iterative solutions.

### 7.3.4 Penalty Weighting Factors

There is general agreement that the multiplier method is more effective than the penalty function method to deal with inequality constraints (Bertsekas, 1982; Luenberger, 1984). The former is a less empirical method, but a great deal of experimentation is still needed to select suitable values for the weighting parameter  $c$ . For instance, a value of  $c^{(0)} = 1000$  is recommended for voltage magnitude constraints, whereas for active power constraints a good value to choose is the largest quadratic coefficient of the cost curves multiplied by 1000 (Ambriz-Pérez, 1998).

In subsequent iterations, the parameter  $c^{(i)}$  is increased by a constant factor  $\beta$ . Values of  $\beta = 1.3$  produce reliable solutions. Larger values of  $\beta$  may lead to ill-conditioned situations whereas smaller values of  $\beta$  may lead to a slow rate of convergence.

The weighting factor  $S$  in Equations (7.40)–(7.42) is a positive parameter as large as  $1e + 10$ . It provides an effective enforcement of the functional inequality constraints for controllable sources of reactive power.

### 7.3.5 Conjugated Variables

The voltage magnitude and reactive power generation at a given bus are strongly interlinked. If a pair of such variables is simultaneously outside limits during the solution process, only

one of them will be made active in the first instance. The voltage magnitude is bounded first, that is, reactive power generation is not made active if its associated voltage magnitude is outside limits. Likewise, if these variables are bounded and they are about to be released at the end of a main iteration, only one of them will be released at the time (Ambriz-Pérez, 1998).

### 7.3.6 An Optimal Power Flow Numerical Example

The five-bus test network (Stagg and El-Abiad, 1968) used in Section 4.3.9 to illustrate the use of the conventional power flow Newton–Raphson method is also used in this section to illustrate the use of the Matlab<sup>®</sup> OPF computer program and associated data, given in Appendix C.

The maximum and minimum voltage magnitude limits at all buses are taken to be 0.9 p.u. and 1.1 p.u., respectively, except at North, where the maximum limit is set at 1.5 p.u. The cost coefficients of the two generating units are taken to be:  $a = 60 \text{ \$ h}^{-1}$ ,  $b = 3.4 \text{ \$ MW}^{-1} \text{ h}^{-1}$ , and  $c = 0.004 \text{ \$ MW}^{-2} \text{ h}^{-1}$ . The maximum and minimum generator active power limits are set at 200 MW and 10 MW, respectively, whereas the maximum and minimum reactive power limits are set at 300 MVAR and  $-300 \text{ MVAR}$ , respectively.

The resulting power flows are shown in Figure 7.3, and the nodal voltages and Lagrange multipliers at the optimum operating point are given in Table 7.2.

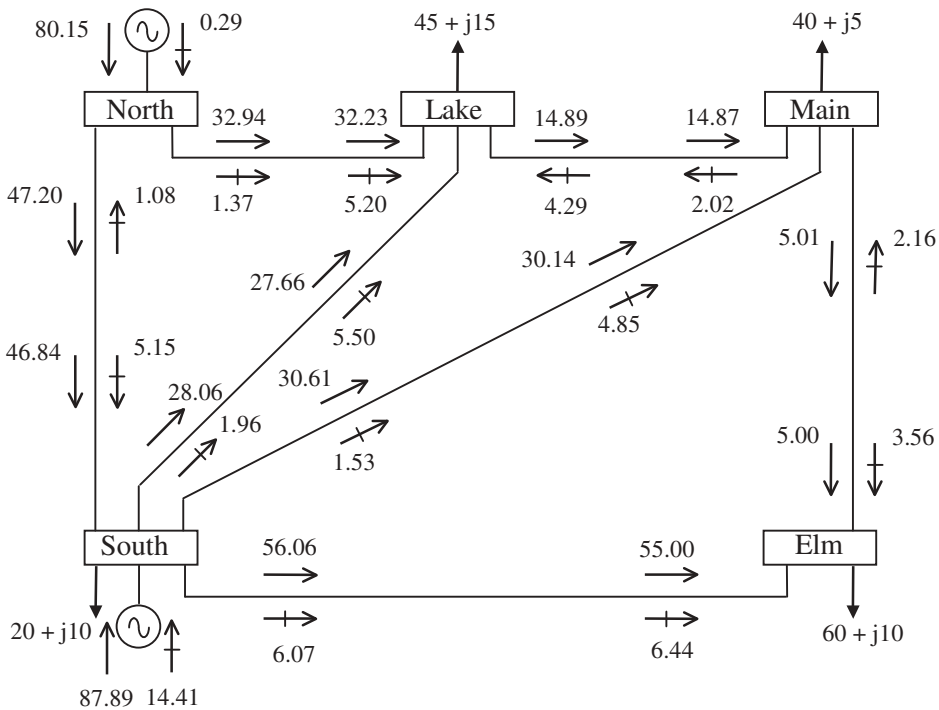


Figure 7.3 Five-bus test network and optimal power flow results

**Table 7.2** Nodal parameters for the five-bus system

	Bus				
	Elm	Main	Lake	South	North
Voltage:					
Magnitude (p.u.)	1.0726	1.0779	1.0784	1.1000	1.1096
Phase angle (deg)	-4.42	-3.85	-3.62	-1.31	0.00
$\lambda_p$ (\$ MW <sup>-1</sup> h <sup>-1</sup> )	4.2639	4.2341	4.2232	4.1032	4.0412

It can be observed from the results presented in Table 7.2 that all nodal voltages edge towards the high side. However, they serve the purpose of the OPF solution in this example, where limit violations take place during the iterative process and the multiplier method handles the violations very efficiently. For example, the voltage magnitude in South is bounded at its upper limit of 1.1 p.u. at the end of the solution process. All other nodal voltages are well within their permitted range. It should be mentioned that selection of a more stringent voltage range (e.g.  $100 \pm 6\%$ ) poses no problem in Newton's method.

The results in Table 7.2 also show that the largest nodal Lagrange multiplier is at Elm, which, incidentally, is the most remote bus in the network. The nodal Lagrange multipliers are closely connected with the cost of supplying nodal load (Ambriz-Pérez, 1998).

It may be argued that the active power flows shown in Figure 7.3 are not markedly different from those given by the conventional power flow solution, presented in the numerical example in Section 4.3.9, except for the active and reactive power flows in line North–South. It was remarked in Section 4.3.9 that these power flows were quite high and that the line incurred high power losses: 2.5 MW and 1.12 MVAR. This is in contrast to the values provided by the OPF solution, where the new active power flow is 47.2 MW and the transmission line generates reactive power. The active power loss reduces to 0.36 MW.

The powers produced by the two generators in the OPF solution are very different from those obtained in the conventional power flow solution. In the case of the OPF solution the production or absorption of reactive power is an intrinsic function of the optimisation algorithm, thus avoiding the undesirable situation that arises in the case of the conventional power flow solution, where one generator is set to generate a large amount of reactive power only for the second generator to absorb slightly more than 60% of that power. In the OPF solution of this example, the two generators tend to share as evenly as possible the system active power requirements because both generators have been given equal cost functions.

Table 7.3 summarises the key parameters generated by the OPF solution, such as active power generation cost and active power loss.

**Table 7.3** Optimal power flow solution for the five-bus system

Quantity	Value
Active power generation cost (\$ h <sup>-1</sup> )	747.98
Active power loss (MW)	3.05
Active power generation (MW)	168.05
Reactive power generation (MVAR)	14.71

## 7.4 POWER SYSTEM CONTROLLER REPRESENTATION IN OPTIMAL POWER FLOW STUDIES

Building on the basic theory and practice of OPF using Newton's method, covered in Section 7.2, extensions are now made to study the representation of controllable equipment found in electrical power networks, such as the well-established tap-changing transformer and the new breed of power electronic controllers generically known as FACTS equipment (IEEE/CIGRÉ, 1995).

The following controllers are studied in the remainder of the chapter: the tap changer, the phase shifter, the static VAR compensator (SVC), the thyristor-controlled series compensator (TCSC), and the unified power flow controller (UPFC). The nature and control characteristics of each of these controllers differ from one another, and their modelling within the OPF solution reflects these facts; hence, they are addressed separately.

In general, an augmented Lagrangian function is established for each controller, in the form of Equation (7.11), which serves the basis for establishing a linearised equation, in the form of the system of Equation (7.12). The state variables of a given power system controller are combined with the network nodal voltage magnitudes and phase angles in a single frame of reference for a unified optimal solution using Newton's method. The controller state variables are adjusted automatically to satisfy specified power flows, voltage magnitudes, and optimality conditions, as given by Kuhn and Tucker (Bertsekas, 1982; Wood and Wollenberg, 1984).

Once the equation has been assembled and combined with matrix  $\mathbf{W}$  and gradient vector  $\mathbf{g}$  of the entire network, a sparsity-oriented solution is carried out. This process is repeated until a small, prespecified, tolerance is reached for all the variables involved.

## 7.5 LOAD TAP-CHANGING TRANSFORMER

Load tap-changing (ltc) transformers regulate nodal voltage magnitude by varying automatically the transformer tap ratio under load. Their representation in system application studies is a matter of paramount importance that has received a great deal of research attention over many years. Nowadays, the problem is well understood and a variety of ltc models are available in the literature (Acha, Ambriz-Pérez, and Fuerte-Esquivel, 2000). A case in point is the simple and yet flexible power flow ltc model derived in Section 4.4.1. We now turn our attention to the more involved problem of load tap changer representation in OPF studies.

### 7.5.1 Load Tap-changing Lagrangian Function

The nodal power equations required in this OPF application are the same as those derived in Section 4.4.1 for the power flow ltc model, namely, Equations (4.52)–(4.55). These equations are used in the Lagrangian function associated with the active and reactive power mismatches at buses  $k$  and  $m$ , which can be expressed by:

$$L_{\text{ltc}}(\mathbf{x}, \boldsymbol{\lambda}) = \lambda_{pk}(P_k + P_{dk} - P_{gk}) + \lambda_{qk}(Q_k + Q_{dk} - Q_{gk}) \\ + \lambda_{pm}(P_m + P_{dm} - P_{gm}) + \lambda_{qm}(Q_m + Q_{dm} - Q_{gm}). \quad (7.47)$$

In this expression,  $\lambda$  is the vector of Lagrange multipliers, and the state variable vector  $\mathbf{x}$  includes  $P_g, V, \theta$ , and  $T_k$ . If the tapping facilities are on the secondary winding, as opposed to the primary winding, then  $U_m$  replaces  $T_k$  as state variable.

### 7.5.2 Linearised System of Equations

Representation of the ltc transformer in the OPF algorithm requires that matrix  $\mathbf{W}$  be augmented by one row and one column. Furthermore,  $T_k$  or  $U_m$  becomes an extra state variable in the OPF formulation.

Application of Newton’s method to the case when the LTC taps are on the primary winding yields the following linearised system of equations:

$$\begin{bmatrix} \mathbf{W}_{kk} & \mathbf{W}_{km} & \mathbf{W}_{kT} \\ \mathbf{W}_{mk} & \mathbf{W}_{mm} & \mathbf{W}_{mT} \\ \mathbf{W}_{Tk} & \mathbf{W}_{Tm} & \mathbf{W}_{TT} \end{bmatrix} \begin{bmatrix} \Delta \mathbf{z}_k \\ \Delta \mathbf{z}_m \\ \Delta \mathbf{z}_T \end{bmatrix} = - \begin{bmatrix} \mathbf{g}_k \\ \mathbf{g}_m \\ \mathbf{g}_T \end{bmatrix}. \quad (7.48)$$

In this expression, the structure of the matrix and vector terms:  $\mathbf{W}_{kk}, \mathbf{W}_{km}, \mathbf{W}_{mk}, \mathbf{W}_{mm}, \Delta \mathbf{z}_k, \Delta \mathbf{z}_m, \mathbf{g}_k$ , and  $\mathbf{g}_m$  is given by Equations (7.24)–(7.32), respectively. The additional matrix terms in Equation (7.48) reflect the contribution of  $T_k$ , the ltc state variable. These terms are giving explicitly by the following matrix and vector terms:

$$\mathbf{W}_{kT}^t = \mathbf{W}_{Tk} = \begin{bmatrix} \frac{\partial^2 L}{\partial \theta_k \partial T_k} & \frac{\partial^2 L}{\partial V_k \partial T_k} & \frac{\partial P_k}{\partial T_k} & \frac{\partial Q_k}{\partial T_k} \end{bmatrix}, \quad (7.49)$$

$$\mathbf{W}_{mT}^t = \mathbf{W}_{Tm} = \begin{bmatrix} \frac{\partial^2 L}{\partial \theta_m \partial T_k} & \frac{\partial^2 L}{\partial V_m \partial T_k} & \frac{\partial P_m}{\partial T_k} & \frac{\partial Q_m}{\partial T_k} \end{bmatrix}, \quad (7.50)$$

$$\mathbf{W}_{TT} = \begin{bmatrix} \frac{\partial^2 L}{\partial T_k^2} \end{bmatrix}, \quad (7.51)$$

$$\Delta \mathbf{z}_T = [\Delta T_k], \quad (7.52)$$

$$\mathbf{g}_T = [\nabla T_k]. \quad (7.53)$$

If the LTC taps are on the secondary winding rather than the primary winding the state variable  $U_m$  replaces  $T_k$  in Equations (7.49)–(7.53).

It should be noted that the first and second partial derivatives for the various entries in Equation (7.48) are derived from the Lagrangian function of Equation (7.47), given in Appendix B, Section B.1.2. The derivative terms corresponding to inequality constraints are entered into matrix  $\mathbf{W}$  only if limits are enforced as a result of one or more state variable having violated limits.

If the LTC is set to control voltage magnitude at a specified value at either bus  $k$  or bus  $m$  then  $\mathbf{W}_{TT}$  in Equation (7.51) is modified by adding the second derivative term of a large quadratic penalty function. Furthermore, the first derivative term of the quadratic penalty function is entered into the gradient element  $\mathbf{g}_T$  in Equation (7.53).

The initial values of the primary and secondary taps are set to 1. The experience gained with the OPF using Newton’s method indicates that the algorithm is highly reliable towards convergence (Ambriz-Pérez, 1998).

### 7.5.3 Load Tap-changing Transformer Test Cases

The five-bus test network used in the numerical example in Section 7.3.6 is modified to include LTC-1 in series with transmission line Lake–Main, and LTC-2 and LTC-3, in parallel, connected in series with transmission line Elm–Main. Two dummy buses, namely LakeLTC and ElmLTC, are used to connect the three LTCs. The topology of the upgraded network is shown in Figure 7.4, where none of the three LTCs is set to maintain voltage magnitude at a specified value. The LTC taps are assumed to be on the primary windings and are initiated at 1 p.u. The impedances are taken to be on the secondary winding, having zero resistance and 0.05 p.u. inductive reactance. The OPF algorithm takes four iterations to converge.

The nodal voltages and active and reactive powers dispatched by the generators and Lagrange multiplier at each bus are given in Table 7.4. The power flows and tap positions as a function of iteration number are shown in Figure 7.4 and Table 7.5, respectively. It should be noted that the algorithm updates the taps of both parallel LTCs identically, something expected as these two LTCs have identical parameters. Experience with the OPF algorithm shows that Newton’s method can handle any number of parallel transformers with ease (Ambriz-Pérez, 1998). This applies whether or not the transformers have different parameters or tap position limits. If an LTC hits one of its limits then the multiplier method is used to enforce that limit (Bertsekas, 1982; Wood and Wollenberg, 1984).

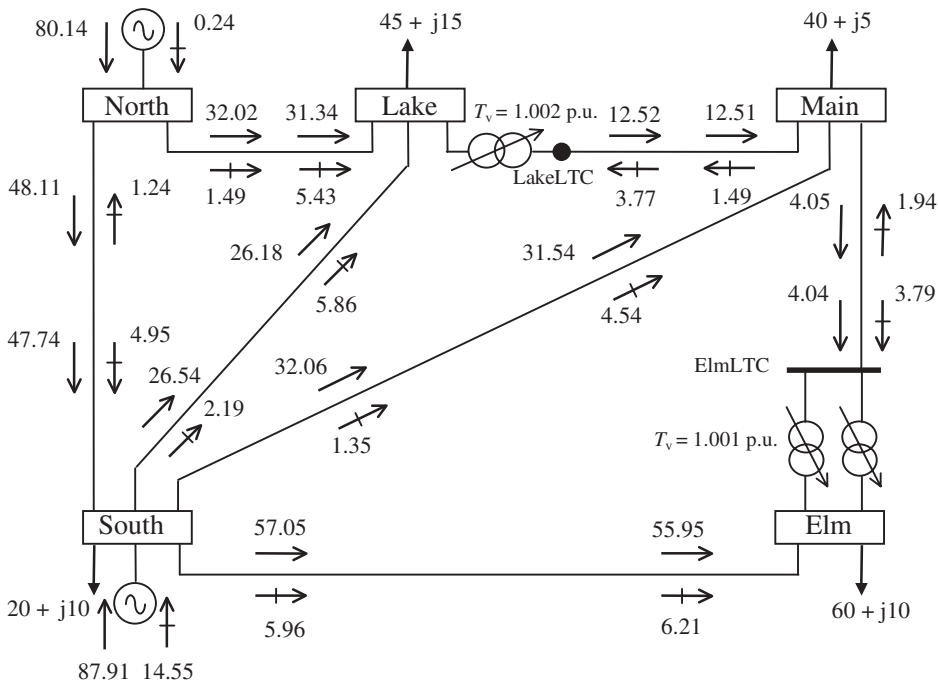


**Figure 7.4** Modified five-bus system with three load tap changers (LTCs) and the optimal power flow solution

**Table 7.4** Nodal voltages in the modified five-bus system with three load tap changers (LTCs)

	Bus						
	LakeLTC	ElmLTC	Elm	Main	Lake	South	North
Voltage:							
Magnitude (p.u.)	1.077	1.072	1.072	1.077	1.078	1.100	1.109
Phase angle (deg)	-3.815	-4.457	-4.508	-4.013	-3.505	-1.332	0.000
$\lambda_p$ (\$ MW <sup>-1</sup> h <sup>-1</sup> )	4.2247	4.2640	4.2645	4.2352	4.2222	4.1033	4.0411

**Table 7.5** Load tap changer (LTC) tap positions in the five-bus system

Iteration	LTC-1	LTC-2	LTC-3
0	1.000	1.000	1.000
1	1.007	1.007	1.007
2	1.001	0.998	0.998
3	1.003	1.001	1.001
4	1.002	1.001	1.001

It may be observed that this OPF solution changes little compared with the base OPF case presented in Section 7.3.6, where no LTCs are used. This may be explained by the fact that the solution achieved in Section 7.3.6 was already a very good solution and that the OPF is fixing the taps of all three LTCs to be fairly close to their nominal value of 1 p.u. (i.e. the three LTCs are operating as conventional transformers).

## 7.6 PHASE-SHIFTING TRANSFORMER

The OPF implementation of the advanced transformer model derived in Section 3.3.4, with reference to its phase-shifting capability, is addressed in this section. The OPF uses Newton’s method as its optimisation engine, enabling an OPF phase-shifter model that is both flexible and robust towards convergence (Acha, Ambriz-Pérez, and Fuerte-Esquivel, 2000). It can be set to simulate a wide range of operating modes with ease. The power flow Equations (4.76)–(4.79) provide the starting point for the derivation of the phase-shifter OPF formulation.

### 7.6.1 Lagrangian Function

The main aim of the optimisation algorithm described in this chapter is to minimise the active power generation cost in the power system by adjusting suitable controllable

parameters. For a phase-shifter model with phase-shifting facilities in the primary winding, the Lagrangian function may be expressed by:

$$L(\mathbf{x}, \boldsymbol{\lambda}) = f(P_g) + \boldsymbol{\lambda}^t h(P_g, V, \theta, \phi_t). \quad (7.54)$$

In this expression,  $f(P_g)$  is the objective function to be optimised; the term  $h(P_g, V, \theta, \phi_t)$  represents the power flow equations;  $\mathbf{x}$  is the vector of state variables,  $\boldsymbol{\lambda}$  is the vector of Lagrange multipliers for equality constraints; and  $P_g, V, \theta,$  and  $\phi_t$  are the active power generation, voltage magnitude, voltage phase angle, and phase-shifter angle for tapping position  $t$ , respectively. The inequality constraints,  $h(P_g, V, \theta, \phi_t) < 0$ , are not shown in Equation (7.54) because they are included only when variables are outside limits.

The Lagrangian function of the power flow mismatch equations at buses  $k$  and  $m$  is incorporated into the OPF formulation as an equality constraint, given by the following equation:

$$\begin{aligned} L_{km}(\mathbf{x}, \boldsymbol{\lambda}) = & \lambda_{pk}(P_k + P_{dk} - P_{gk}) + \lambda_{qk}(Q_k + Q_{dk} - Q_{gk}) \\ & + \lambda_{pm}(P_m + P_{dm} - P_{gm}) + \lambda_{qm}(Q_m + Q_{dm} - Q_{gm}). \end{aligned} \quad (7.55)$$

In this expression,  $P_{dk}, P_{dm}, Q_{dk},$  and  $Q_{dm}$  are the active and reactive power loads at buses  $k$  and  $m$ ;  $P_{gk}, P_{gm}, Q_{gk},$  and  $Q_{gm}$  are scheduled active and reactive power generations at buses  $k$  and  $m$ ; and  $\lambda_{pk}, \lambda_{pm}, \lambda_{qk},$  and  $\lambda_{qm}$  are Lagrange multipliers for active and reactive powers at buses  $k$  and  $m$ .

A key function of the phase-shifting transformer is to regulate the amount of active power that flows through it, say  $P_{km}$ . In the OPF formulation this operating condition is expressed as an equality constraint, represented by the following Lagrangian function:

$$L_{\text{flow}}(\mathbf{x}, \boldsymbol{\lambda}) = \lambda_{\text{flow-}km}(P_{km} - P_{\text{specified}}). \quad (7.56)$$

In this expression,  $\lambda_{\text{flow-}km}$  is the Lagrange multiplier associated with the active power flowing from bus  $k$  to bus  $m$ ;  $P_{\text{specified}}$  is the required amount of active power flow through the phase-shifter transformer.

The overall Lagrangian function of the phase shifter, encompassing the individual contributions, is:

$$L_{\text{ps}}(\mathbf{x}, \boldsymbol{\lambda}) = L_{km}(\mathbf{x}, \boldsymbol{\lambda}) + L_{\text{flow}}(\mathbf{x}, \boldsymbol{\lambda}). \quad (7.57)$$

## 7.6.2 Linearised System of Equations

Representation of the phase-shifting transformer in the OPF algorithm requires that matrix  $\mathbf{W}$  be augmented by one row and one column, with  $\phi_t$  becoming the state variable. Furthermore, if the phase shifter is set to control active power flow then the dimension of matrix  $\mathbf{W}$  is increased further by one row and one column. Hence, for each phase shifter involved in the OPF solution the dimension of  $\mathbf{W}$  is increased by up to two rows and columns, depending on operational requirements.

If the two-winding transformer has phase-shifting facilities in the primary winding, the linearised system of equations for minimising the Lagrangian function using Newton's method is:

$$\begin{bmatrix} \mathbf{W}_{kk} & \mathbf{W}_{km} & \mathbf{W}_{k\phi} \\ \mathbf{W}_{mk} & \mathbf{W}_{mm} & \mathbf{W}_{m\phi} \\ \mathbf{W}_{\phi k} & \mathbf{W}_{\phi m} & \mathbf{W}_{\phi\phi} \end{bmatrix} \begin{bmatrix} \Delta \mathbf{z}_k \\ \Delta \mathbf{z}_m \\ \Delta \mathbf{z}_\phi \end{bmatrix} = - \begin{bmatrix} \mathbf{g}_k \\ \mathbf{g}_m \\ \mathbf{g}_\phi \end{bmatrix}. \quad (7.58)$$

In this expression, the structure of matrix and vector terms  $\mathbf{W}_{kk}$ ,  $\mathbf{W}_{km}$ ,  $\mathbf{W}_{mk}$ ,  $\mathbf{W}_{mm}$ ,  $\Delta\mathbf{z}_k$ ,  $\Delta\mathbf{z}_m$ ,  $\mathbf{g}_k$ , and  $\mathbf{g}_m$  is given by Equations (7.24)–(7.32), respectively. The additional matrix terms in Equation (7.58) reflect the contribution of  $\phi_t$ , the phase shifter state variable. These terms are given explicitly by:

$$\mathbf{W}_{k\phi}^t = \mathbf{W}_{\phi k} = \begin{bmatrix} \frac{\partial^2 L}{\partial\theta_k\partial\phi_t} & \frac{\partial^2 L}{\partial V_k\partial\phi_t} & \frac{\partial P_k}{\partial\phi_t} & \frac{\partial Q_k}{\partial\phi_t} \\ \frac{\partial^2 L}{\partial\theta_k\partial\lambda_\phi} & \frac{\partial^2 L}{\partial V_k\partial\lambda_\phi} & 0 & 0 \end{bmatrix}, \quad (7.59)$$

$$\mathbf{W}_{m\phi}^t = \mathbf{W}_{\phi m} = \begin{bmatrix} \frac{\partial^2 L}{\partial\theta_m\partial\phi_t} & \frac{\partial^2 L}{\partial V_m\partial\phi_t} & \frac{\partial P_m}{\partial\phi_t} & \frac{\partial Q_m}{\partial\phi_t} \\ \frac{\partial^2 L}{\partial\theta_m\partial\lambda_\phi} & \frac{\partial^2 L}{\partial V_m\partial\lambda_\phi} & 0 & 0 \end{bmatrix}, \quad (7.60)$$

$$\mathbf{W}_{\phi\phi} = \begin{bmatrix} \frac{\partial^2 L}{\partial\phi_t^2} & \frac{\partial^2 L}{\partial\phi_t\partial\lambda_\phi} \\ \frac{\partial^2 L}{\partial\lambda_\phi\partial\phi_t} & 0 \end{bmatrix}, \quad (7.61)$$

$$\Delta\mathbf{z}_\phi = [\Delta\phi_t \ \Delta\lambda_\phi]^t, \quad (7.62)$$

$$\mathbf{g}_\phi = [\nabla\phi_t \ \nabla\lambda_\phi]^t. \quad (7.63)$$

If the phase-shifting mechanism is on the secondary winding rather than the primary winding, the state variable  $\phi_u$  replaces  $\phi_t$  in Equations (7.59)–(7.63).

It should be noted that the first and second partial derivatives for the various entries in Equation (7.58) are derived from the Lagrangian function of Equation (7.57), and given in Appendix B, Section B.2. The derivative terms corresponding to inequality constraints are entered into matrix  $\mathbf{W}$  only if limits are enforced as a result of one or more state variables having violated limits.

The procedure described by Equations (7.58)–(7.63) corresponds to a situation where the phase shifter is set to control active power flowing from buses  $k$  to  $m$ , which is the phase-shifter standard control mode. However, in OPF solutions the phase shifter variables are normally adjusted automatically during the solution process in order to reach the best operating point of the electrical power system. In such a situation, the phase shifter is not set to control a fixed amount of active power flowing from buses  $k$  to  $m$ , and matrix  $\mathbf{W}$  is suitably modified to reflect this operating condition. This is done by adding the second partial derivative term of a large (infinite), quadratic penalty function to the diagonal location in the matrix in Equation (7.61) corresponding to the Lagrange multiplier  $\lambda_{km}$ . The first derivative term of the function is added to the corresponding gradient element in Equation (7.63).

The initial conditions given to all variables involved in the study impact significantly the convergence pattern. Experience has shown that the phase-shifter model is very robust towards convergence when the phase-shifting angle is initialised at  $0^\circ$ . State variables are initialised similarly to the power flow problem (i.e. 1 p.u. voltage magnitude and  $0^\circ$  voltage angle for all buses). The Lagrange multiplier for the power flow constraint,  $\lambda_{\text{flow-}km}$ , is set to zero. These values enable very robust iterative solutions (Ambriz-Pérez, 1998).

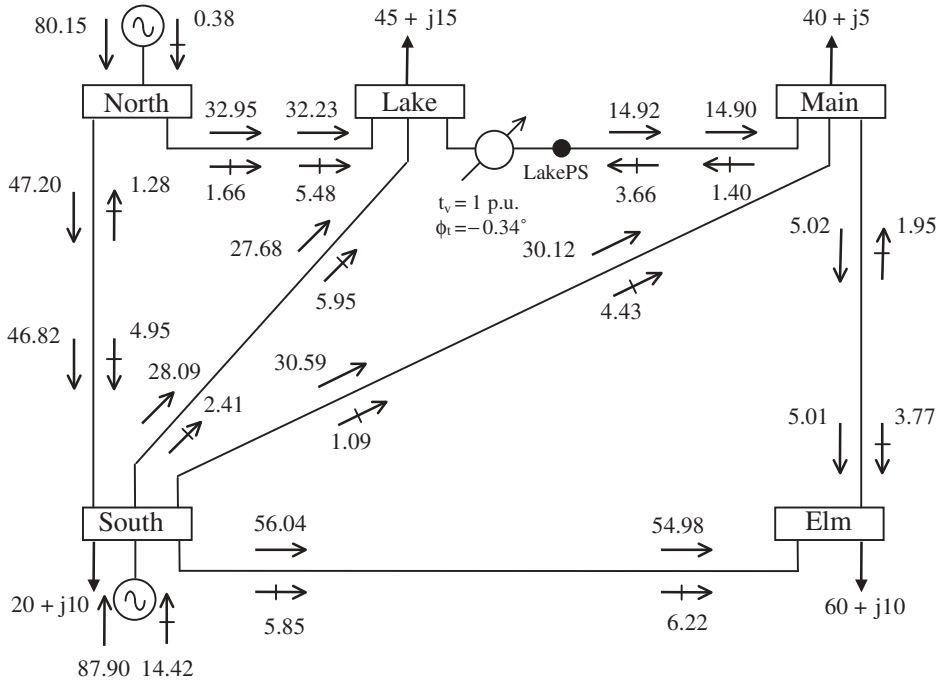


Figure 7.5 Five-bus network with one phase shifter, and optimal power flow solution

### 7.6.3 Phase-shifting Transformer Test Cases

The five-bus system given in Section 7.3.6 is used to illustrate the performance of the phase-shifter model. One phase shifter is connected in series with the transmission line Lake–Main. An additional bus, termed LakePS, is used for the purpose of incorporating the phase shifter, as shown in Figure 7.5. Two different modes of phase-shifter operation are considered in this test case: (1) no active power flow regulation and (2) active power flow regulation at LakePS.

The phase-shifter primary and secondary windings contain no resistance, and  $0.05$  p.u. inductive reactance. The phase-shifting control is assumed to be located in the primary winding and having phase angle limits of  $\pm 10^\circ$ . For both test cases, the primary complex tap is initialised at  $1\angle 0^\circ$ , and convergence is obtained in four iterations to a tolerance of  $1e - 9$ .

#### 7.6.3.1 Case 1: no active power flow regulation

The OPF solution for the unregulated case is shown in Figure 7.5. This case enables the OPF solution to find the optimum amount of power transfer between buses Lake and Main, which is calculated to be  $14.92$  MW. This power flow value yields minimum fuel cost and active power system losses (i.e.  $747.98$   $\$/h$ , and  $3.052$  MW, respectively). The voltage magnitudes and phase angles, active and reactive powers dispatched by the generators, and Lagrange multipliers are given in Table 7.6.

**Table 7.6** Nodal voltages in the five-bus network with one phase shifter: case 1 (no active power flow regulation)

	Bus					
	LakePS	Elm	Main	Lake	South	North
Voltage:						
Magnitude (p.u.)	1.079	1.072	1.078	1.077	1.100	1.109
Phase angle (deg)	-3.632	-4.424	-3.864	-3.610	-1.306	0.000
$\lambda_p$ (\$ MW <sup>-1</sup> h <sup>-1</sup> )	4.223	4.26	4.234	4.223	4.103	4.041

It should be noted that, in this case, the OPF solution forces the phase angle of the phase-shifter transformer to be small, yielding a very similar power flow distribution to that produced when no phase shifter is used in the network, which is the case presented in Section 7.3.6. The slight differences between the two solutions can be traced to the fact that, in the modified network, the inductive reactance of the original transmission line Lake–Main may be seen as having increased by approximately 10 %.

### 7.6.3.2 Case 2: active power flow regulation at LakePS

Information similar to that given for case 1 is presented in Table 7.7 for the case when the phase shifter is set to regulate active power flow through LakePS at 25 MW.

The phase shifter is set to control active power flow at a level different from the one that yields an optimum solution; hence, the fuel cost and network losses are bound to increase. The solution given by the OPF algorithm gives an active power generation cost of 748.33 \$ h<sup>-1</sup>, and transmission losses are 3.143 MW.

It is interesting to note that the 40 % increase in active power flow through LakePS is achieved with a relatively modest increase in total cost, calculated to be below 0.05 %, but the active power loss increases more markedly, calculated to be just under 3 %. This test case indicates that the great operational flexibility brought about by power system controllers may come at a price. It should be remarked, however, that this is a small network

**Table 7.7** Nodal voltages in the five-bus network with one phase shifter: case 2 (active power flow regulation at LakePS)

	Bus					
	LakePS	Elm	Main	Lake	South	North
Voltage:						
Magnitude (p.u.)	1.079	1.073	1.079	1.076	1.100	1.109
Phase angle (deg)	-2.705	-4.097	-3.102	-4.098	-1.193	0.000
$\lambda_p$ (\$ MW <sup>-1</sup> h <sup>-1</sup> )	4.182	4.251	4.201	4.251	4.101	4.044

**Table 7.8** Phase-shifter angles in the five-bus test system

Iterations	$\phi_t$ (deg)	
	Case 1	Case 2
0	0.000	0.000
1	-0.325	-1.874
2	-0.363	-2.122
3	-0.346	-2.009
4	-0.346	-2.010

Note: case 1, no active power flow regulation; case 2, active power flow regulation at LakePS.

and no general conclusions can be drawn for practical utility networks, but this comparative study does indicate that copious OPF studies and trade-offs may become necessary when dealing with large-scale power systems and a large number of power system controllers.

The phase-shifter angles for both test cases are shown in Table 7.8, highlighting the strong convergence characteristics of OPF using Newton’s method. Owing to the two very different operational requirements on the phase shifter, its phase angles reach quite distinct values (i.e.  $-0.346^\circ$  and  $-2.01^\circ$ ). The larger value corresponds to the regulated case, where a larger amount of active power passes through the phase-shifter transformer.

## 7.7 STATIC VAR COMPENSATOR

This section focuses on SVC models suitable for OPF solutions using Newton’s method (Ambriz-Pérez, Acha, and Fuerte-Esquivel, 2000). The modelling approach taken is to assume that the SVC acts as a continuous, variable shunt susceptance, which adjusts automatically in order to ensure that a target nodal voltage magnitude at the SVC terminal is met, while satisfying network constraint conditions.

Two different ‘flavours’ of the SVC model are presented in this section: (1) the firing-angle model and (2) the shunt susceptance model.

A linearised SVC model suitable for OPF iterative solutions using Newton’s method is described below. The SVC state variable is combined with the network state variables for a unified, optimal solution using Newton’s method (Ambriz-Pérez, 1998).

### 7.7.1 Lagrangian Function

The constrained optimisation problem stated in Equation (7.1) is transformed into an unconstrained optimisation problem by forming the augmented Lagrangian function of an SVC model expressed in the form of an adjustable shunt susceptance:

$$L(\mathbf{x}, \lambda) = f(P_g) + \lambda^t h[P_g, V, \theta, B(\alpha)]. \tag{7.64}$$

In this expression,  $f(P_g)$  is the objective function;  $h(P_g, V, \theta, B(\alpha))$  represents the power flow equations;  $\mathbf{x}$  is the vector of state variables;  $\lambda$  is the vector of Lagrange multipliers for equality constraints;  $P_g, V, \theta$ , and  $B(\alpha)$  are the active power generation, voltage magnitude, voltage phase angle, and SVC shunt susceptance, respectively. The inequality constraint  $g[P_g, V, \theta, B(\alpha)] < 0$  is not shown in Equation (7.64) because it is added to  $L(\mathbf{x}, \lambda)$  only when variables go outside limits.

The SVC susceptance,  $B(\alpha)$ , may be expressed as either an equivalent susceptance,  $B_{\text{svc}}$ , or a susceptance that is an explicit function of the SVC firing angle,  $\alpha$ . Both parameters may be used as state variables and, respectively, form the basis of the two SVC models addressed in this section.

The contribution of the SVC to the Lagrangian function is explicitly represented in Newton’s method as an equality constraint given by the following equation:

$$L_{\text{svc}}(\mathbf{x}, \lambda) = \lambda_{qk} Q_k. \tag{7.65}$$

In this expression,  $\mathbf{x}$  is the vector of state variables,  $[V_k B(\alpha)]^t$ ;  $Q_k$  is the reactive power injected or absorbed by the SVC at bus  $k$ , as given in Equation (5.5); and  $\lambda$  is the vector of Lagrange multipliers, with  $\lambda_{qk}$  being the Lagrange multiplier at bus  $k$  associated with the reactive power balance equation. The variable  $B(\alpha)$  is either  $B_{\text{svc}}$  or  $\alpha$ , depending on the SVC model used in the OPF study.

### 7.7.2 Linearised System of Equations

Representation of the SVC controller into the OPF algorithm using Newton’s method requires that for each SVC present in the network, matrix  $\mathbf{W}$  be augmented by one row and one column. Either  $\alpha$  or  $B_{\text{svc}}$ , depending on the SVC models selected, enters as an extra state variable in the OPF formulation.

Application of Newton’s method to the SVC firing-angle model is given by the following linearised equation:

$$\begin{bmatrix} \frac{\partial^2 L}{\partial V_k^2} & \frac{\partial Q_k}{\partial V_k} & \frac{\partial^2 L}{\partial V_k \partial \alpha} \\ \frac{\partial Q_k}{\partial V_k} & 0 & \frac{\partial Q_k}{\partial \alpha} \\ \frac{\partial^2 L}{\partial \alpha \partial V_k} & \frac{\partial Q_k}{\partial \alpha} & \frac{\partial^2 L}{\partial \alpha^2} \end{bmatrix} \begin{bmatrix} \Delta V_k \\ \Delta \lambda_{qk} \\ \Delta \alpha \end{bmatrix} = - \begin{bmatrix} \nabla V_k \\ \nabla \lambda_{qk} \\ \nabla \alpha \end{bmatrix}. \tag{7.66}$$

The entries in Equation (7.66) are obtained by deriving Equation (7.65) with respect to the relevant state variables and Lagrange multipliers. These terms are given in explicit form in Appendix B, Section B.3. The derivative terms corresponding to inequality constraints are not required at the beginning of the iterative solution; they are introduced into matrix Equation (7.66) after limits become enforced in response to limits violations.

An alternative OPF model for the SVC is readily established by choosing the SVC equivalent susceptance,  $B_{\text{svc}}$ , to be the state variable rather than the firing angle,  $\alpha$ . The

linearised system of equations describing the alternative SVC OPF model is:

$$\begin{bmatrix} \frac{\partial^2 L}{\partial V_k^2} & \frac{\partial Q_k}{\partial V_k} & \frac{\partial^2 L}{\partial V_k \partial B_{\text{svc}}} \\ \frac{\partial Q_k}{\partial V_k} & 0 & \frac{\partial Q_k}{\partial B_{\text{svc}}} \\ \frac{\partial^2 L}{\partial B_{\text{svc}} \partial V_k} & \frac{\partial Q_k}{\partial B_{\text{svc}}} & 0 \end{bmatrix} \begin{bmatrix} \Delta V_k \\ \Delta \lambda_{qk} \\ \Delta B_{\text{svc}} \end{bmatrix} = - \begin{bmatrix} \nabla V_k \\ \nabla \lambda_{qk} \\ \nabla B_{\text{svc}} \end{bmatrix}. \quad (7.67)$$

The entries in Equation (7.67) are obtained by deriving Equation (7.65) with respect to the relevant state variables and Lagrange multipliers. These terms are given in explicit form in Appendix B, Section B.3.

In OPF studies it is normal to assume that voltage magnitudes at SVC terminals are controlled within limits (e.g. 0.95–1.05 p.u.). However, more stringent voltage magnitude requirements are met with ease in Newton's method. For instance, to control the voltage magnitude at bus  $k$  at a fixed value, it is necessary only to add the second derivative term of a large, quadratic, penalty factor to the second derivative term of the Lagrangian function with respect to the voltage magnitude  $V_k$  (i.e.  $\partial^2 L / \partial V_k^2$ ). Also, the first derivative term of the quadratic penalty function is added to the corresponding gradient element (i.e.  $\partial L / \partial V_k$ ). Hence, in Equations (7.66) and (7.67) the diagonal elements corresponding to voltage magnitude  $V_k$  will have a very large (infinite) value, resulting in a null voltage increment  $\Delta V_k$ .

The SVC is well initialised by selecting a firing-angle value corresponding to the equivalent reactance resonance peak, which can be calculated using Equation (5.39). The SVC Lagrange multiplier,  $\lambda_{qk}$ , is initialised at zero value. These initial values give rise to very robust iterative solutions (Ambriz-Pérez, 1998).

### 7.7.3 Static VAR Compensator Test Cases

The five-bus system in Section 7.3.6 is modified to include one SVC at Main, as shown in Figure 7.6. The objective is to minimise its active power generation cost. The SVC capacitive and inductive reactance are  $X_C = 0.9375$  p.u., and  $X_L = 0.1625$  p.u., respectively. The lower and upper limits for the firing angle are  $90^\circ$  and  $180^\circ$ , respectively. The initial firing angle is given a value  $\alpha = 145^\circ$ .

Four case studies are carried out: cases A and B use the SVC model based on the firing-angle concept, whereas cases C and D use the model based on the equivalent variable susceptance. Moreover, cases A and C consider the voltage magnitude at Main to be allowed to take any value in the range 0.95–1.1 p.u.; cases B and D consider the voltage magnitude at Main to be fixed at 1.1 p.u.

#### 7.7.3.1 Firing-angle model

In the firing-angle model, two cases are simulated:

- Case A: the voltage magnitude at Main is allowed to take any value in the range 0.95–1.1 p.u.;
- Case B: the voltage magnitude at Main is fixed at 1.1 p.u.

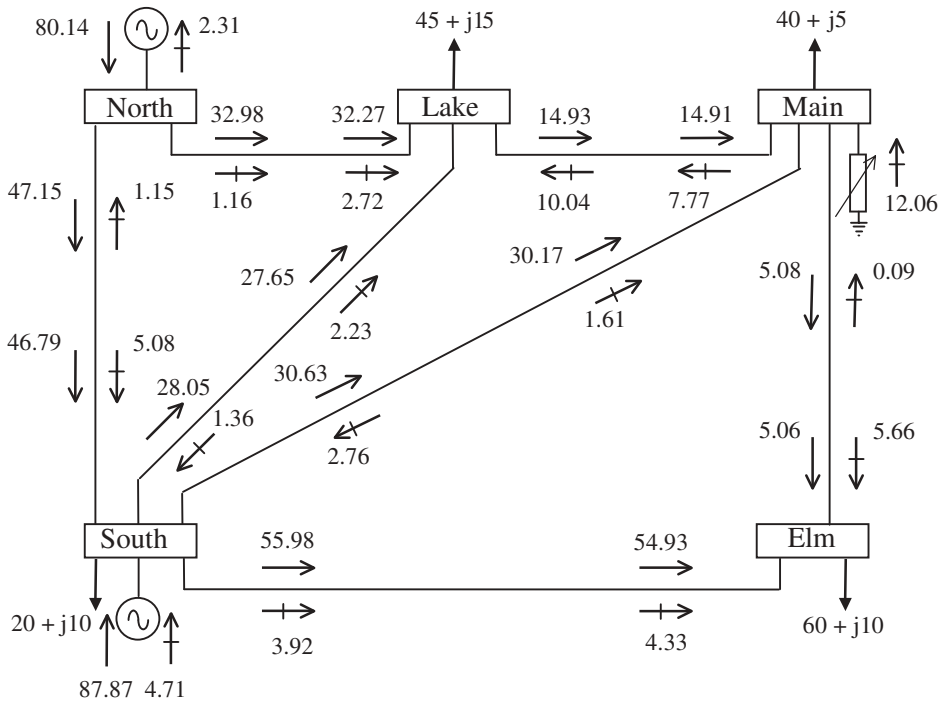


**Figure 7.6** Modified five-bus network with one static VAR compensator, and optimal power flow solution

The power flow results are shown in Figure 7.6. The voltage magnitudes and phase angles and Lagrange multipliers are given in Table 7.9. Similar results are given for case B in Table 7.10. The SVC susceptance values and reactive power injections are shown in Table 7.11.

As expected, active power generation cost and active power loss increase in case B. The OPF results are 748.339 \$ h<sup>-1</sup>, 3.14226 MW, and 37.13 MVAR. In this case there are relatively large flows of reactive power from bus Main to other buses, thus increasing network losses.

**Table 7.9** Nodal voltages in the modified network: case A (use of static VAR compensator model based on the firing-angle concept, with voltage magnitude at Main allowed to take any value in the range 0.95–1.1 p.u.)

	Bus				
	Elm	Main	Lake	South	North
Voltage:					
Magnitude (p.u.)	1.075	1.085	1.083	1.100	1.109
Phase angle (deg)	-4.450	-3.962	-3.701	-1.304	0.000
$\lambda_p$ (\$ MW <sup>-1</sup> h <sup>-1</sup> )	4.2625	4.2324	4.2217	4.1030	4.0411

**Table 7.10** Nodal voltages in the modified network: case B (use of static VAR compensator model based on the firing-angle concept, with voltage magnitude at Main fixed at 1.1 p.u.)

	Bus				
	Elm	Main	Lake	South	North
Voltage:					
Magnitude (p.u.)	1.080	1.100	1.095	1.100	1.111
Phase angle (deg)	-4.471	-4.148	-3.836	-1.2613	0.000
$\lambda_p$ (\$MW <sup>-1</sup> h <sup>-1</sup> )	4.2650	4.2431	4.2299	4.1024	4.0426

**Table 7.11** Static VAR compensator parameters at each iteration: firing-angle model, cases A and B

Iteration	Case A			Case B		
	$\alpha$ (deg)	$B_{eq}$ (p.u.)	$Q$ (MVAR)	$\alpha$ (deg)	$B_{eq}$ (p.u.)	$Q$ (MVAR)
0	145.000	0.514	-51.420	145.000	0.514	-51.420
1	136.627	0.056	-7.231	136.598	0.054	-6.630
2	137.819	0.131	-14.534	144.712	0.501	-60.640
3	137.234	0.095	-11.213	140.832	0.306	-37.130
4	137.347	0.102	-12.061	-	-	-

- Iteration not required; model has converged.

The results in Table 7.11 indicate that in order to maintain the voltage magnitude at Main at 1.1 p.u. it is necessary for the SVC to inject more reactive power. It should be noted that the minus sign indicates injection of reactive power. These results illustrate the strong convergence of the SVC OPF algorithm, with solutions achieved in 4 and 3 iterations, respectively.

### 7.7.3.2 Susceptance model

The SVC modelled in the form of a susceptance replaces the SVC firing-angle-based model used in the two test cases above (cases A and B). The initial SVC susceptance value is set at  $B_{svc} = 0.514$  p.u., which corresponds to  $\alpha = 145^\circ$ . Two cases are simulated:

- Case C: the voltage magnitude at Main is allowed to take any value in the range 0.95–1.1 p.u.;
- Case D: the voltage magnitude at Main is fixed at 1.1 p.u.

Convergence is obtained in four and three iterations for cases C and D, respectively. As expected, the solution for voltage magnitude, voltage phase angle, active and reactive power generation, and Lagrange multipliers coincide with those presented in Tables 7.9 and 7.10.

**Table 7.12** Equivalent static VAR compensator susceptances for cases C and D

Iteration	Case C		Case D	
	$B_{svc}$ (p.u.)	$Q$ (MVAR)	$B_{svc}$ (p.u.)	$Q$ (MVAR)
0	0.514	-51.420	0.514	-51.420
1	0.056	-7.204	0.054	-6.594
2	0.131	-14.534	0.501	-60.641
3	0.095	-11.213	0.306	-37.130
4	0.102	-12.061	-	-

- Iteration not required; model has converged.

The equivalent susceptance values taken by the SVC model during the iterative process are shown in Table 7.12. It can be observed from Tables 7.11 and 7.12 that both sets of SVC susceptances coincide with each other.

## 7.8 THYRISTOR-CONTROLLED SERIES COMPENSATOR

This section studies the topic of OPF TCSC modelling and simulation (Acha and Ambriz-Pérez, 1999). This is done within the context of Newton’s method in which the TCSC is modelled as an adjustable, nonlinear series reactance which is a function of the TCSC firing angle.

### 7.8.1 Lagrangian Function

The constrained optimisation problem, stated in generic form in Equation (7.1), is converted into an unconstrained problem. This involves formulating a suitable Lagrangian function for the TCSC controller, which may take the following form:

$$L(\mathbf{x}, \boldsymbol{\lambda}) = f(P_g) + \boldsymbol{\lambda}^t h[P_g, V, \theta, X(\alpha)]. \tag{7.68}$$

In this expression,  $f(P_g)$  is the objective function;  $h[P_g, V, \theta, X(\alpha)]$  represents the power flow equations;  $\mathbf{x}$  is the vector of state variables;  $\boldsymbol{\lambda}$  is the vector of Lagrange multipliers for equality constraints; and  $P_g, V, \theta,$  and  $X(\alpha)$  are the active power generation, voltage magnitude, voltage phase angle, and TCSC reactance, respectively. The reactance,  $X(\alpha)$ , is an explicit function of the TCSC firing angle,  $\alpha$ . The inequality constraint  $g[P_g, V, \theta, X(\alpha)] < 0$  is not shown in Equation (7.68) because it is added to  $L(\mathbf{x}, \boldsymbol{\lambda})$  only when variables go outside limits.

The power flow mismatch equations at buses  $k$  and  $m$  are explicitly modelled in the Lagrangian function as an equality constraint given by the following equation:

$$L_{tcsc}(\mathbf{x}, \boldsymbol{\lambda}) = \lambda_{pk}(P_k + P_{dk} - P_{gk}) + \lambda_{qk}(Q_k + Q_{dk} - Q_{gk}) + \lambda_{pm}(P_m + P_{dm} - P_{gm}) + \lambda_{qm}(Q_m + Q_{dm} - Q_{gm}). \tag{7.69}$$

In this expression,  $P_{dk}, P_{dm},$  and  $Q_{dk}, Q_{dm}$  are the active and reactive power loads at buses  $k$  and  $m$ ;  $P_{gk}, P_{gm}, Q_{gk},$  and  $Q_{gm}$  are the scheduled active and reactive power generations at buses  $k$  and  $m$ ; and  $\lambda_{pk}, \lambda_{pm}, \lambda_{qk},$  and  $\lambda_{qm}$  are Lagrange multipliers at buses  $k$  and  $m$ .

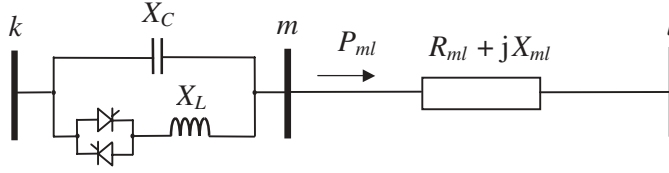


**Figure 7.7** Compensated transmission line

As shown in Figure 7.7, the active power flow across branch  $m-l$ ,  $P_{ml}$ , is controlled by the TCSC connected between buses  $k$  and  $m$ . In the OPF formulation this operating condition is expressed as an equality constraint, which remains active throughout the iterative process unless one expressly wishes this constraint to be deactivated.

The Lagrangian function,  $L$ , of the total branch  $k-l$ , may be expressed by:

$$L = L_{\text{tcsc}}(\mathbf{x}, \boldsymbol{\lambda}) + L_{\text{flow}}(\mathbf{x}, \boldsymbol{\lambda}), \quad (7.70)$$

where

$$L_{\text{flow}} = \lambda_{ml}(P_{ml} - P_{\text{specified}}). \quad (7.71)$$

In this expression,  $\lambda_{ml}$  is the Lagrange multiplier for the active power flow in branch  $m-l$ , and  $P_{\text{specified}}$  is the target active power flow through the TCSC controller.

## 7.8.2 Linearised System of Equations

Incorporation of the TCSC controller into the OPF algorithm using Newton's method requires that for each TCSC present in the network, matrix  $\mathbf{W}$  be augmented by two rows and two columns when the aim is to exert active power flow control. However, if the TCSC is not controlling active power flow then matrix  $\mathbf{W}$  is augmented only by one row and one column. The former case uses the Lagrange multiplier,  $\lambda_{ml}$ , to account for the contribution of the power flow through branch  $m-l$ , and  $\alpha$  enters as an extra state variable in the OPF formulation.

Application of Newton's method to the TCSC firing-angle model is given by the following linearised equation:

$$\begin{bmatrix} \mathbf{W}_{kk} & \mathbf{W}_{km} & \mathbf{0} & \mathbf{W}_{k\alpha} \\ \mathbf{W}_{mk} & \mathbf{W}_{mm} & \mathbf{W}_{ml} & \mathbf{W}_{m\alpha} \\ \mathbf{0} & \mathbf{W}_{ml} & \mathbf{W}_{ll} & \mathbf{W}_{l\alpha} \\ \mathbf{W}_{\alpha k} & \mathbf{W}_{\alpha m} & \mathbf{W}_{\alpha l} & \mathbf{W}_{\alpha\alpha} \end{bmatrix} \begin{bmatrix} \Delta \mathbf{z}_k \\ \Delta \mathbf{z}_m \\ \Delta \mathbf{z}_l \\ \Delta \mathbf{z}_\alpha \end{bmatrix} = - \begin{bmatrix} \mathbf{g}_k \\ \mathbf{g}_m \\ \mathbf{g}_l \\ \mathbf{g}_\alpha \end{bmatrix}. \quad (7.72)$$

In this expression, the structure of matrix and vector terms  $\mathbf{W}_{kk}$ ,  $\mathbf{W}_{km}$ ,  $\mathbf{W}_{mk}$ ,  $\mathbf{W}_{mm}$ ,  $\Delta \mathbf{z}_k$ ,  $\Delta \mathbf{z}_m$ ,  $\mathbf{g}_k$ , and  $\mathbf{g}_m$  is given by Equations (7.25)–(7.32), respectively. The additional matrix terms in Equation (7.72) reflect the contribution of  $\alpha$ , the TCSC state variable. These terms are given explicitly by:

$$\mathbf{W}_{\alpha k} = \mathbf{W}_{k\alpha}^t = \begin{bmatrix} \frac{\partial^2 L}{\partial \theta_k \partial \alpha} & \frac{\partial^2 L}{\partial V_k \partial \alpha} & \frac{\partial P_k}{\partial \alpha} & \frac{\partial Q_k}{\partial \alpha} \\ 0 & 0 & 0 & 0 \end{bmatrix}, \quad (7.73)$$

$$\mathbf{W}_{lm} = \mathbf{W}_{ml}^t = \begin{bmatrix} \frac{\partial^2 L}{\partial \theta_m \partial \theta_l} & \frac{\partial^2 L}{\partial \theta_m \partial V_l} & \frac{\partial P_l}{\partial \theta_m} & \frac{\partial Q_l}{\partial \theta_m} \\ \frac{\partial^2 L}{\partial V_m \partial \theta_l} & \frac{\partial^2 L}{\partial V_m \partial V_l} & \frac{\partial P_l}{\partial V_m} & \frac{\partial Q_l}{\partial V_m} \\ \frac{\partial P_m}{\partial \theta_l} & \frac{\partial P_m}{\partial V_l} & 0 & 0 \\ \frac{\partial Q_m}{\partial \theta_l} & \frac{\partial Q_m}{\partial V_l} & 0 & 0 \end{bmatrix}, \quad (7.74)$$

$$\mathbf{W}_{\alpha m} = \mathbf{W}_{m\alpha}^t = \begin{bmatrix} \frac{\partial^2 L}{\partial \theta_m \partial \alpha} & \frac{\partial^2 L}{\partial V_m \partial \alpha} & \frac{\partial P_m}{\partial \alpha} & \frac{\partial Q_m}{\partial \alpha} \\ \frac{\partial P_{ml}}{\partial \theta_m} & \frac{\partial P_{ml}}{\partial V_m} & 0 & 0 \end{bmatrix}, \quad (7.75)$$

$$\mathbf{W}_{ll} = \begin{bmatrix} \frac{\partial^2 L}{\partial \theta_l^2} & \frac{\partial^2 L}{\partial \theta_l \partial V_l} & \frac{\partial P_l}{\partial \theta_l} & \frac{\partial Q_l}{\partial \theta_l} \\ \frac{\partial^2 L}{\partial V_l \partial \theta_l} & \frac{\partial^2 L}{\partial V_l^2} & \frac{\partial P_l}{\partial V_l} & \frac{\partial Q_l}{\partial V_l} \\ \frac{\partial P_l}{\partial \theta_l} & \frac{\partial P_l}{\partial V_l} & 0 & 0 \\ \frac{\partial Q_l}{\partial \theta_l} & \frac{\partial Q_l}{\partial V_l} & 0 & 0 \end{bmatrix}, \quad (7.76)$$

$$\mathbf{W}_{\alpha l} = \mathbf{W}_{l\alpha}^t = \begin{bmatrix} 0 & 0 & 0 & 0 \\ \frac{\partial P_{ml}}{\partial \theta_l} & \frac{\partial P_{ml}}{\partial V_l} & 0 & 0 \end{bmatrix}, \quad (7.77)$$

$$\mathbf{W}_{\alpha\alpha} = \begin{bmatrix} \frac{\partial^2 L}{\partial \alpha^2} & 0 \\ 0 & 0 \end{bmatrix}, \quad (7.78)$$

$$\Delta \mathbf{z}_l = [\Delta \theta_l \quad \Delta V_l \quad \Delta \lambda_{pl} \quad \Delta \lambda_{ql}]^t, \quad (7.79)$$

$$\mathbf{g}_l = [\nabla \theta_l \quad \nabla V_l \quad \nabla \lambda_{pl} \quad \nabla \lambda_{ql}]^t, \quad (7.80)$$

$$\Delta \mathbf{z}_\alpha = [\Delta \alpha \quad \Delta \lambda_{ml}]^t, \quad (7.81)$$

$$\mathbf{g}_\alpha = [\nabla \alpha \quad \nabla \lambda_{ml}]^t. \quad (7.82)$$

The first and second partial derivatives for the various entries in Equation (7.72) are derived from the Lagrangian function of Equation (7.70) and are given in Appendix B, Section B.4. The derivative terms corresponding to inequality constraints are entered into matrix  $\mathbf{W}$  only if limits are enforced as a result of one or more state variable having violated

limits. It should be noted that the procedure in Equation (7.72) corresponds to the case when the TCSC is controlling active power flowing through branch  $m-l$  (standard control mode).

In OPF applications, minimum-cost solutions are obtained when the OPF algorithm itself selects the optimum level of power flow through the TCSC. However, any change in the TCSC operating mode is easily accommodated in the OPF formulation given in Equation (7.72). For instance, if the TCSC is not controlling active power flow then matrix  $\mathbf{W}$  and vector  $\mathbf{g}$  are suitably modified to reflect this operating mode. This can be achieved by adding the second derivative term of a large (infinite) quadratic penalty factor to the diagonal element of the matrix in Equation (7.78) corresponding to multiplier  $\lambda_{ml}$ , thus forcing this multiplier to be zero for the whole of the iterative process. The first derivative term of the quadratic penalty function is added to the corresponding element in Equation (7.80).

The Lagrange multipliers for active and reactive power flow mismatch equations are initialised at the  $\lambda_p$  value given by the lossless economic dispatch solutions and at  $\lambda_q$  equal to 0, respectively. For TCSC Lagrange multipliers the initial value of  $\lambda_{ml}$  is set to zero. Experience shows that these values give rise to very robust iterative solutions (Ambriz-Pérez, 1998). The main factor affecting the OPF rate of convergence of TCSC-upgraded networks is the initial firing angle,  $\alpha$ . Good starting conditions are required to prevent the solution diverging or arriving at some anomalous value. Good initial conditions for the TCSC firing angle were established in Section 5.8.3. Use of Equations (5.72)–(5.73) invariably leads to good OPF solutions for TCSC-upgraded networks.

### 7.8.3 Thyristor-controlled Series Compensator Test Cases

The five-bus test system of Section 7.3.6 is used to study the impact of the TCSC on the network. The TCSC is added in series with transmission line Lake–Main, and the dummy bus LakeTCSC is added to enable such a connection to take place.

The OPF solution is achieved in five iterations to a mismatch tolerance of  $1e - 9$  and starting from a TCSC firing-angle value equal to  $150^\circ$ . The TCSC optimises the active power flow level in transmission line Lake–Main to a value of 14.97 MW. Moreover, the OPF solution yields the following minimum active power generation cost and network losses:  $747.975 \text{ \$ h}^{-1}$  and 3.05 MW, respectively. The TCSC capacitive and inductive reactance values required to achieve the result are:  $X_C = 0.9375 \%$  and  $X_L = 0.1625 \%$ , respectively, using a base voltage of 400 kV. The optimal power flows are shown in Figure 7.8. The nodal voltage magnitudes and phase angles and the Lagrange multipliers are given in Table 7.13.

It can be observed that the OPF solution changes little compared with the base OPF case presented in Section 7.3.6 when no TCSC is used. This may be explained by the fact that the solution achieved in Section 7.3.6 is already a very good solution and that the OPF is fixing the level of compensation afforded by the TCSC to be fairly small.

The TCSC firing angles, per iteration, are shown in Table 7.14, highlighting the very strong convergence characteristics of OPF using Newton’s method and the importance of selecting good initial conditions. For completeness, the equivalent TCSC reactance is also provided.

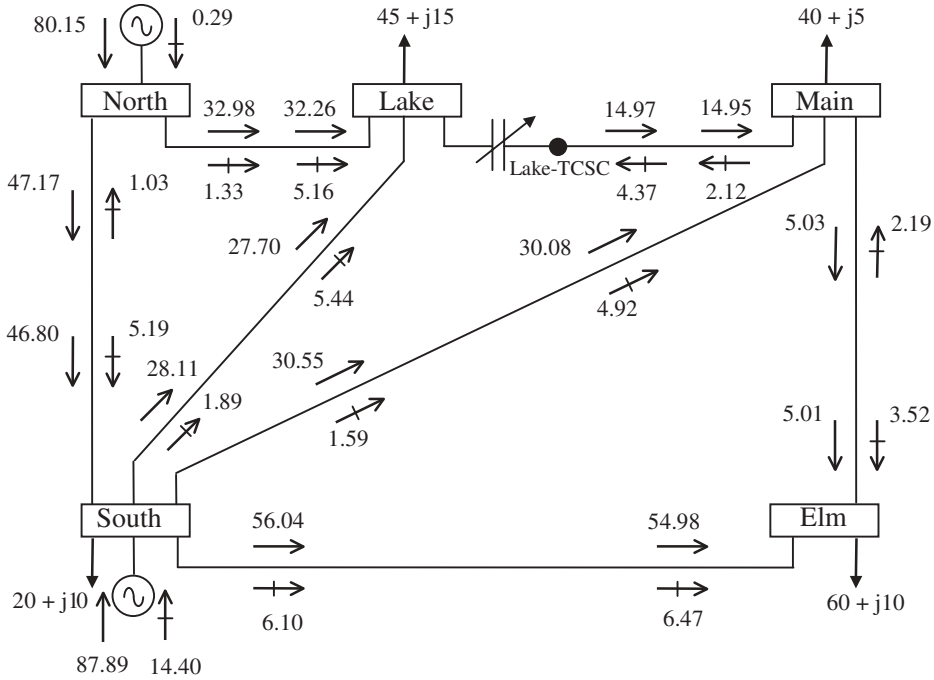


Figure 7.8 Modified five-bus system, and optimal power flow solution

Table 7.13 Nodal voltages in TCSC-upgraded network

	Bus					
	LakeTCSC	Elm	Main	Lake	South	North
Voltage:						
Magnitude (p.u.)	1.078	1.072	1.077	1.078	1.100	1.109
Phase angle (deg)	-3.534	-4.417	-3.846	-3.622	-1.303	0.000
$\lambda_p$ (\$ MW <sup>-1</sup> h <sup>-1</sup> )	4.2232	4.2639	4.2341	4.2232	4.1031	4.0412

Table 7.14 Thyristor-controlled series compensator (TCSC) parameters

Iteration	TCSC parameters	
	$\alpha$ (deg)	$X_{TCSC}$ (p.u.)
0	150.000	-0.0180
1	150.587	-0.0169
2	162.845	-0.0101
3	154.328	-0.0130
4	156.399	-0.0119
5	156.407	-0.0119

## 7.9 UNIFIED POWER FLOW CONTROLLER

The UPFC OPF model presented in this section enables very flexible and reliable power system optimisation studies to be carried out (Ambriz-Pérez *et al.*, 1998). The flexibility stems from the generality of the UPFC model and the robustness from the strong convergence exhibited by the OPF solution using Newton's method. The UPFC model may be set to control active and reactive powers simultaneously as well as nodal voltage magnitude, at either the sending or the receiving end bus. Alternatively, the UPFC model may be set to control one or more of the parameters above in any combination or to control none of them.

### 7.9.1 Unified Power Flow Controller Lagrangian Function

Based on the equivalent circuit shown in Figure 5.17 and Equations (5.50)–(5.59), the Lagrangian function for the UPFC may be written as:

$$L(\mathbf{x}, \boldsymbol{\lambda}) = f(P_g) + \boldsymbol{\lambda}^t h(P_g, V, \theta, \delta_{cR}, V_{cR}, \delta_{vR}, V_{vR}). \quad (7.83)$$

In this expression,  $f(P_g)$  is the objective function to be optimised;  $h(P_g, V, \theta, V_{cR}, \delta_{cR}, V_{vR}, \delta_{vR})$  represents the power flow equations;  $\mathbf{x}$  is the vector of state variables;  $\boldsymbol{\lambda}$  is the vector of Lagrange multipliers for equality constraints; and  $P_g, V,$  and  $\theta$  are the active power generation, voltage magnitude, and voltage phase angle, respectively. The UPFC control variables are  $\delta_{cR}, V_{cR}, \delta_{vR},$  and  $V_{vR}$ . The inequality constraints  $g(P_g, V, \theta, V_{cR}, \delta_{cR}, V_{vR}, \delta_{vR}) < 0$  are not shown in Equation (7.83) because it is added only to  $L(\mathbf{x}, \boldsymbol{\lambda})$  when there are variables outside limits.

The Lagrangian function,  $L_{km}(\mathbf{x}, \boldsymbol{\lambda})$ , corresponding to the power flow mismatch equations at buses  $k$  and  $m$ , is given by the following equation:

$$\begin{aligned} L_{km}(\mathbf{x}, \boldsymbol{\lambda}) = & \lambda_{pk}(P_k + P_{dk} - P_{gk}) + \lambda_{qk}(Q_k + Q_{dk} - Q_{gk}) \\ & + \lambda_{pm}(P_m + P_{dm} - P_{gm}) + \lambda_{qm}(Q_m + Q_{dm} - Q_{gm}). \end{aligned} \quad (7.84)$$

In this expression  $P_{dk}, P_{dm}, Q_{dk},$  and  $Q_{dm}$  are the active and reactive power loads at buses  $k$  and  $m$ ;  $P_{gk}, P_{gm}, Q_{gk},$  and  $Q_{gm}$  are the scheduled active and reactive power generations at buses  $k$  and  $m$ ; and  $\lambda_{pk}, \lambda_{pm}, \lambda_{qk},$  and  $\lambda_{qm}$  are Lagrange multipliers at buses  $k$  and  $m$ . The vector of state variables  $\mathbf{x}$  is  $[\mathbf{V} \ \boldsymbol{\delta}]^t$ , where  $\mathbf{V}$  and  $\boldsymbol{\delta}$  include both nodal voltages and UPFC voltage sources.

### 7.9.2 Direct-current Link Lagrangian Function

A fundamental premise in the UPFC model is that the active power supplied to the shunt converter,  $P_{vR}$ , must satisfy the active power demanded by the series converter,  $P_{cR}$ . This condition must be met throughout the solution process. In the OPF formulation this condition is expressed as an equality constraint,

$$L_{\text{sh-se}}(\mathbf{x}, \boldsymbol{\lambda}) = \lambda_{\text{sh-se}}(P_{vR} + P_{cR}), \quad (7.85)$$

where  $\lambda_{\text{sh-se}}$  is the Lagrange multiplier associated with the shunt and series power converters.

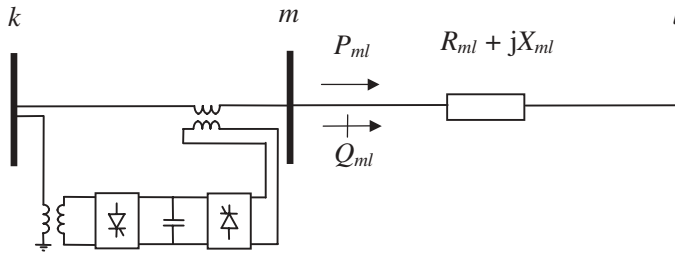


Figure 7.9 Unified power flow controller power flow constraint at bus  $m$

### 7.9.3 Unified Power Flow Controller Power Flow Constraints

The power injected at bus  $m$  by the UPFC, as illustrated in Figure 7.9, can be formulated as a power flow constraint in the branch connecting buses  $m$  and  $l$ . We may write:

$$L_{ml}(\mathbf{x}, \boldsymbol{\lambda}) = \lambda_{p\ ml}(P_{ml} - P_{\text{specified}}) + \lambda_{q\ ml}(Q_{ml} - Q_{\text{specified}}), \quad (7.86)$$

where  $\lambda_{p\ ml}$  and  $\lambda_{q\ ml}$  are, respectively, the Lagrange multipliers associated with the active and reactive power injections at bus  $m$ ; and  $P_{\text{specified}}$  and  $Q_{\text{specified}}$  are, respectively, the specified active and reactive powers leaving bus  $m$ .

In conventional OPF formulations, such constraints are enforced only if power flow limits have been exceeded. However, in this particular application this constraint may remain active throughout the iterative solution.

The UPFC Lagrangian function comprising the individual contributions presented above is as follows:

$$L_{\text{upfc}}(\mathbf{x}, \boldsymbol{\lambda}) = L_{km}(\mathbf{x}, \boldsymbol{\lambda}) + L_{\text{sh-se}}(\mathbf{x}, \boldsymbol{\lambda}) + L_{ml}(\mathbf{x}, \boldsymbol{\lambda}). \quad (7.87)$$

### 7.9.4 Linearised System of Equations

Incorporation of the UPFC controller into the OPF algorithm using Newton’s method requires that, for each UPFC, matrix  $\mathbf{W}$  be augmented by up to eleven rows and columns. This procedure corresponds to the case where the UPFC is operated in standard control mode (i.e. it is controlling the nodal voltage magnitude at bus  $k$ , active power flowing from buses  $m$  to  $l$ , and reactive power injected at bus  $m$ ). The linearised system of equations for minimising the UPFC Lagrangian function of Equation (7.87), using Newton’s method is:

$$\begin{bmatrix} \mathbf{W}_{kk} & \mathbf{W}_{km} & \mathbf{W}_{kcR} & \mathbf{W}_{kvR} & \mathbf{W}_{ksh-se} & \mathbf{0} & \mathbf{0} \\ \mathbf{W}_{mk} & \mathbf{W}_{mm} & \mathbf{W}_{mcR} & \mathbf{W}_{mvR} & \mathbf{W}_{msh-se} & \mathbf{W}_{ml} & \mathbf{W}_{m\ m-1} \\ \mathbf{W}_{cRk} & \mathbf{W}_{cRm} & \mathbf{W}_{cRcR} & \mathbf{W}_{cRvR} & \mathbf{W}_{cRsh-se} & \mathbf{0} & \mathbf{0} \\ \mathbf{W}_{vRk} & \mathbf{W}_{vRm} & \mathbf{W}_{vRcR} & \mathbf{W}_{vRvR} & \mathbf{W}_{vRsh-se} & \mathbf{0} & \mathbf{0} \\ \mathbf{W}_{sh-se\ k} & \mathbf{W}_{sh-se\ m} & \mathbf{W}_{sh-se\ cR} & \mathbf{W}_{sh-se\ vR} & \mathbf{0} & \mathbf{0} & \mathbf{0} \\ \mathbf{0} & \mathbf{W}_{1m} & \mathbf{0} & \mathbf{0} & \mathbf{0} & \mathbf{W}_{1l} & \mathbf{W}_{1\ m-1} \\ \mathbf{0} & \mathbf{W}_{m-1m} & \mathbf{0} & \mathbf{0} & \mathbf{0} & \mathbf{W}_{m-1l} & \mathbf{0} \end{bmatrix} \begin{bmatrix} \Delta \mathbf{z}_k \\ \Delta \mathbf{z}_m \\ \Delta \mathbf{z}_{cR} \\ \Delta \mathbf{z}_{vR} \\ \Delta \mathbf{z}_{sh-se} \\ \Delta \mathbf{z}_l \\ \Delta \mathbf{z}_{m-1} \end{bmatrix} = \begin{bmatrix} -\mathbf{g}_k \\ -\mathbf{g}_m \\ -\mathbf{g}_{cR} \\ -\mathbf{g}_{vR} \\ -\mathbf{g}_{sh-se} \\ -\mathbf{g}_l \\ -\mathbf{g}_{m-1} \end{bmatrix}. \quad (7.88)$$

In this expression, the structure of matrix and vector terms  $\mathbf{W}_{kk}$ ,  $\mathbf{W}_{km}$ ,  $\mathbf{W}_{mk}$ ,  $\mathbf{W}_{mm}$ ,  $\mathbf{\Delta z}_k$ ,  $\mathbf{\Delta z}_m$ ,  $\mathbf{g}_k$ , and  $\mathbf{g}_m$  is given by Equations (7.25)–(7.32), respectively. Also,  $\mathbf{W}_{ml}$ ,  $\mathbf{W}_{lm}$ ,  $\mathbf{W}_{ll}$ ,  $\mathbf{\Delta z}_l$ , and  $\mathbf{g}_l$  are given by Equations (7.74), (7.76), (7.79), and (7.80), respectively. The additional matrix terms in Equation (7.88) reflect the contribution of  $\theta_{cR}$ ,  $V_{cR}$ ,  $\theta_{vR}$ , and  $V_{vR}$ , the UPFC state variables. These terms are given explicitly by:

$$\mathbf{W}_{cRk} = \mathbf{W}_{kcR}^t = \begin{bmatrix} \frac{\partial^2 L}{\partial \theta_k \partial \delta_{cR}} & \frac{\partial^2 L}{\partial V_k \partial \delta_{cR}} & \frac{\partial P_k}{\partial \delta_{cR}} & \frac{\partial Q_k}{\partial \delta_{cR}} \\ \frac{\partial^2 L}{\partial \theta_k \partial V_{cR}} & \frac{\partial^2 L}{\partial V_k \partial V_{cR}} & \frac{\partial P_k}{\partial V_{cR}} & \frac{\partial Q_k}{\partial V_{cR}} \end{bmatrix}, \quad (7.89)$$

$$\mathbf{W}_{vRk} = \mathbf{W}_{kvR}^t = \begin{bmatrix} \frac{\partial^2 L}{\partial \theta_k \partial \delta_{vR}} & \frac{\partial^2 L}{\partial V_k \partial \delta_{vR}} & \frac{\partial P_k}{\partial \delta_{vR}} & \frac{\partial Q_k}{\partial \delta_{vR}} \\ \frac{\partial^2 L}{\partial \theta_k \partial V_{vR}} & \frac{\partial^2 L}{\partial V_k \partial V_{vR}} & \frac{\partial P_k}{\partial V_{vR}} & \frac{\partial Q_k}{\partial V_{vR}} \end{bmatrix}, \quad (7.90)$$

$$\mathbf{W}_{sh-sek} = \mathbf{W}_{ksh-se}^t = \begin{bmatrix} \frac{\partial P_{sh-se}}{\partial \theta_k} & \frac{\partial P_{sh-se}}{\partial V_k} & 0 & 0 \end{bmatrix}, \quad (7.91)$$

$$\mathbf{W}_{cRm} = \mathbf{W}_{mcR}^t = \begin{bmatrix} \frac{\partial^2 L}{\partial \theta_m \partial \delta_{cR}} & \frac{\partial^2 L}{\partial V_m \partial \delta_{cR}} & \frac{\partial P_m}{\partial \delta_{cR}} & \frac{\partial Q_m}{\partial \delta_{cR}} \\ \frac{\partial^2 L}{\partial \theta_m \partial V_{cR}} & \frac{\partial^2 L}{\partial V_m \partial V_{cR}} & \frac{\partial P_m}{\partial V_{cR}} & \frac{\partial Q_m}{\partial V_{cR}} \end{bmatrix}, \quad (7.92)$$

$$\mathbf{W}_{vRm} = \mathbf{W}_{mvR}^t = \begin{bmatrix} \frac{\partial^2 L}{\partial \theta_m \partial \delta_{vR}} & \frac{\partial^2 L}{\partial V_m \partial \delta_{vR}} & \frac{\partial P_m}{\partial \delta_{vR}} & \frac{\partial Q_m}{\partial \delta_{vR}} \\ \frac{\partial^2 L}{\partial \theta_m \partial V_{vR}} & \frac{\partial^2 L}{\partial V_m \partial V_{vR}} & \frac{\partial P_m}{\partial V_{vR}} & \frac{\partial Q_m}{\partial V_{vR}} \end{bmatrix}, \quad (7.93)$$

$$\mathbf{W}_{sh-sem} = \mathbf{W}_{msh-se}^t = \begin{bmatrix} \frac{\partial P_{sh-se}}{\partial \theta_m} & \frac{\partial P_{sh-se}}{\partial V_m} & 0 & 0 \end{bmatrix}, \quad (7.94)$$

$$\mathbf{W}_{m-lm} = \mathbf{W}_{lmm-1}^t = \begin{bmatrix} \frac{\partial P_{ml}}{\partial \theta_m} & \frac{\partial P_{ml}}{\partial V_m} & 0 & 0 \\ \frac{\partial Q_{ml}}{\partial \theta_m} & \frac{\partial Q_{ml}}{\partial V_m} & 0 & 0 \end{bmatrix}, \quad (7.95)$$

$$\mathbf{W}_{cRcR} = \begin{bmatrix} \frac{\partial^2 L}{\partial \delta_{cR}^2} & \frac{\partial^2 L}{\partial \delta_{cR} \partial V_{cR}} \\ \frac{\partial^2 L}{\partial V_{cR} \partial \delta_{cR}} & \frac{\partial^2 L}{\partial V_{cR}^2} \end{bmatrix}, \quad (7.96)$$

$$\mathbf{W}_{cRvR} = \mathbf{W}_{vRcR}^t = \begin{bmatrix} \frac{\partial^2 L}{\partial \delta_{cR} \partial \delta_{vR}} & \frac{\partial^2 L}{\partial \delta_{cR} \partial V_{vR}} \\ \frac{\partial^2 L}{\partial V_{cR} \partial \delta_{vR}} & \frac{\partial^2 L}{\partial V_{cR} \partial V_{vR}} \end{bmatrix}, \quad (7.97)$$

$$\mathbf{W}_{sh-se\ cR} = \mathbf{W}_{cR\ sh-se}^t = \begin{bmatrix} \frac{\partial P_{sh-se}}{\partial \delta_{cR}} & \frac{\partial P_{sh-se}}{\partial V_{cR}} & 0 & 0 \end{bmatrix}, \quad (7.98)$$

$$\mathbf{W}_{vR\ vR} = \begin{bmatrix} \frac{\partial^2 L}{\partial \delta_{vR}^2} & \frac{\partial^2 L}{\partial \delta_{vR} \partial V_{vR}} \\ \frac{\partial^2 L}{\partial V_{vR} \partial \delta_{vR}} & \frac{\partial^2 L}{\partial V_{vR}^2} \end{bmatrix}, \quad (7.99)$$

$$\mathbf{W}_{sh-se\ vR} = \mathbf{W}_{vR\ sh-se}^t = \begin{bmatrix} \frac{\partial P_{sh-se}}{\partial \delta_{vR}} & \frac{\partial P_{sh-se}}{\partial V_{vR}} \end{bmatrix}, \quad (7.100)$$

$$\mathbf{W}_{lm-1} = \mathbf{W}_{m-1l}^t = \begin{bmatrix} \frac{\partial P_{ml}}{\partial \theta_l} & \frac{\partial P_{ml}}{\partial V_l} & 0 & 0 \\ \frac{\partial Q_{ml}}{\partial \theta_l} & \frac{\partial Q_{ml}}{\partial V_l} & 0 & 0 \end{bmatrix}, \quad (7.101)$$

$$\Delta \mathbf{z}_{cR} = [\Delta \delta_{cR} \quad \Delta V_{cR}]^t, \quad (7.102)$$

$$\Delta \mathbf{z}_{vR} = [\Delta \delta_{vR} \quad \Delta V_{vR}]^t, \quad (7.103)$$

$$\Delta \mathbf{z}_{sh-se} = [\Delta \lambda_{sh-se}], \quad (7.104)$$

$$\Delta \mathbf{z}_{m-1} = [\Delta \lambda_{pml} \quad \Delta \lambda_{qml}]^t, \quad (7.105)$$

$$\mathbf{g}_{cR} = [\nabla \delta_{cR} \quad \nabla V_{cR}]^t, \quad (7.106)$$

$$\mathbf{g}_{vR} = [\nabla \delta_{vR} \quad \nabla V_{vR}]^t, \quad (7.107)$$

$$\mathbf{g}_{sh-se} = [\nabla \lambda_{sh-se}], \quad (7.108)$$

$$\mathbf{g}_{m-1} = [\nabla \lambda_{pml} \quad \nabla \lambda_{qml}]^t. \quad (7.109)$$

The elements of matrix  $\mathbf{W}$  are given explicitly in Appendix B, Section B.5. The derivative terms corresponding to inequality constraints are not required at the beginning of the iterative process; they are introduced into matrix Equation (7.88) only after limits become enforced.

The representation given in Equation (7.88) corresponds to a situation where the UPFC is operated in standard control mode. However, if different UPFC operating modes are required then matrix  $\mathbf{W}$  and multipliers  $\lambda$  are modified with ease to reflect the new operating mode.

For instance, if buses  $m$  and  $k$  are  $PQ$  type and the UPFC is not controlling active power flowing from buses  $m$  to  $l$  and reactive power is not injected at bus  $m$  then matrix  $\mathbf{W}$  and gradient vector  $\mathbf{g}$  are modified as follows: (1) the second derivative term of a large (infinite), quadratic penalty factor is added to the diagonal elements of matrix  $\mathbf{W}_{ll}$ , corresponding to the multipliers  $\lambda_{pml}$  and  $\lambda_{qml}$ ; (2) the first derivative terms of the quadratic penalty functions are evaluated and added to the corresponding gradient elements in  $\mathbf{g}_l$ . Alternatively, if only one operating constraint is released, say reactive power injected at bus  $m$ , then only the diagonal element of matrix  $\mathbf{W}_{ll}$  corresponding to multiplier  $\lambda_{qml}$  is penalised.

The Lagrange multipliers for active and reactive power flow mismatch equations are initialised at the  $\lambda_p$  value given by the lossless economic dispatch solution and  $\lambda_q$  equal to zero, respectively. For UPFC Lagrange multipliers, the initial value of  $\lambda_{sh-se}$  is set to  $\lambda_p$ , and  $\lambda_p$   $m-l$  and  $\lambda_q$   $m-l$  are set equal to zero. Experience has shown that these values give rise to very robust iterative solutions. Equations for initialising the voltage magnitudes and phase angles of the series and shunt sources are given in Section 5.8.4.

### 7.9.5 Unified Power Flow Controller Test Cases

One UPFC is added to the five-bus system of Figure 7.3, in series with the transmission line Lake–Main. A dummy bus, termed LakeUPFC, is added to enable the UPFC model to be connected, as shown in Figure 7.10. The UPFC is used to maintain active and reactive power at 25 MW and  $-6$  MVAR, respectively, at the sending end of transmission line LakeUPFC–Main. The shunt converter is used to maintain Lake’s nodal voltage magnitude at 1 p.u.

The two UPFC voltage sources are initialised with reference to equations and guidelines given in Section 5.8.4, resulting in the following values:  $V_{cR} = 0.025$  p.u.,  $\delta_{cR} = 76.5^\circ$ ,  $V_{vR} = 1.0$  p.u., and  $\delta_{vR} = 0^\circ$ ; The resistances of the coupling transformers are ignored and their inductive reactances are taken to be  $X_{cR} = X_{vR} = 0.1$  p.u.. The voltage magnitude  $V_{cR}$  varies in the range 0.001–0.6 p.u., and  $V_{vR}$  in the range 0.9–1.1 p.u.

This is a case of regulated UPFC operation, and the OPF solution, albeit optimal, is not expected to be the one that yields minimum cost. This point will be addressed further, by

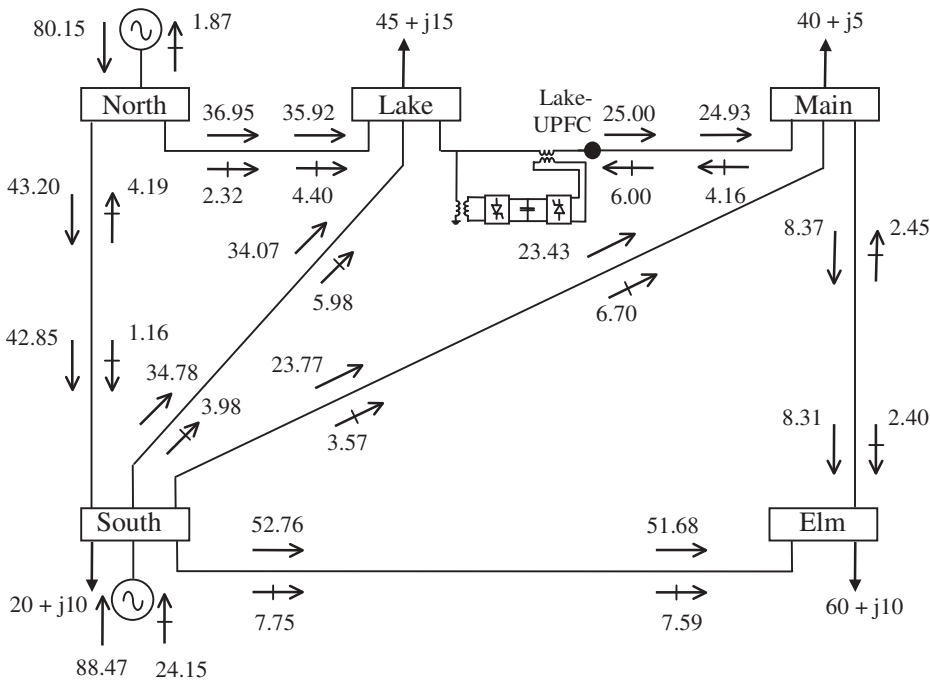


Figure 7.10 UPFC-upgraded five-bus system, and optimal power flow solution

**Table 7.15** Nodal voltages in the UPFC-upgraded network

	Bus					
	LakeUPFC	Elm	Main	Lake	South	North
Voltage:						
Magnitude (p.u.)	1.007	0.999	1.006	1.000	1.029	1.036
Phase angle (deg)	-3.128	-4.722	-3.580	-4.685	-1.402	0.000
$\lambda_p$ (\$ MW <sup>-1</sup> h <sup>-1</sup> )	4.2680	4.2823	4.2246	4.2680	4.1077	4.0412

numerical example, in Section 7.9.6. The cost and active power losses given by the OPF solution in this test case are: 750.357 \$ h<sup>-1</sup>, and 3.631 MW, respectively. The optimal power flow results are shown in Figure 7.10; the voltage magnitudes and phase angles, and the Lagrange multipliers are given in Table 7.15.

Compared with the base case shown in Figure 7.3, larger active power flows in transmission lines North–Lake and South–Lake take place in order to meet the demand imposed by the UPFC power constraints. By comparing both OPF solutions, it can be observed that in the UPFC-upgraded system there are increases in active and reactive power generation of 0.5 MW and 7.015 MVAR. Furthermore, the generation cost and the network losses increased by 2.027 \$ h<sup>-1</sup> and 0.5 MW, respectively. The reason for the higher generation cost and power loss can be explained in terms of a reduced number of control variables available to the OPF solution; the UPFC is set to regulate active and reactive power flows and voltage magnitude.

It may be argued, with reference to the voltage information shown in Table 7.15, that the nodal voltage regulation imposed by the UPFC at Lake yields a much improved voltage profile than that achieved by the base OPF solution, shown in Table 7.2, where nodal voltage magnitudes edged on the high side. Conversely, the  $\lambda_p$  values tend to be higher in the present test case than in the base OPF case, where no UPFC is used. This may be explained in terms of the slightly higher cost incurred by the regulating action of the UPFC controller.

The voltage magnitudes and phase angles of the UPFC series and shunt voltage sources are shown in Table 7.16, highlighting the strong convergence characteristic of the OPF using Newton’s method and the all-important point of selecting good initial conditions for the two UPFC voltage sources.

**Table 7.16** Parameters of unified power flow controller voltage sources

Iteration	Series source		Shunt source	
	$V_{cR}$ (p.u.)	$\delta_{cR}$ (deg)	$V_{vR}$ (p.u.)	$\delta_{vR}$ (deg)
0	0.025	-76.500	1.000	0.000
1	0.052	-94.102	0.998	-4.718
2	0.052	-94.876	0.997	-4.705

**Table 7.17** Unified power flow controller (UPFC) operating modes

Operating mode	Number of iterations	Generation cost (\$ h <sup>-1</sup> )	Power loss (MW)
Normal UPFC operation	2	750.357	3.631
Fixed voltage (at bus Lake)	2	749.928	3.519
Fixed $P$ and $Q$	3	748.236	3.119
All constraints deactivated	3	747.828	3.015

### 7.9.6 Unified Power Flow Controller Operating Modes

In order to illustrate the behaviour of the various UPFC operating modes, its functional constraints are freed in sequence. The normal UPFC operating mode (all constraints activated) is compared with cases where active and reactive power flows are freed, and the voltage magnitude remains fixed; the voltage magnitude is freed, and active and reactive power flows are fixed; all three constraints are freed. Table 7.17 presents a summary of the results.

As expected, the case of normal UPFC operation gives the most expensive solution, whereas the case where all the constraints are deactivated gives the minimum cost solution. The former case was studied in Section 7.9.5, and the latter case is very much in line with the results obtained in the base OPF solution, where no UPFC is used. However, it may be argued that one of the main purposes of installing a UPFC controller in the first place is, to have the ability to regulate power flows and voltage magnitude at the point of UPFC deployment.

## 7.10 SUMMARY

The OPF algorithm studied in this chapter is a direct application of Newton's method to the minimisation of a multivariable, nonlinear function. An iteration of the OPF algorithm consists of the simultaneous solution of all the unknown variables involved in the problem using Lagrange functions. Second partial derivatives of the Lagrange function with respect to all the variables and the Lagrange multipliers are determined and the resultant terms are suitably accommodated in matrix  $\mathbf{W}$ . This matrix has a block matrix structure where each block stores 12 nonzero elements per bus.

The OPF solution gives the optimum operational state of a power network where a specific objective has been met, and the network is subjected to physical and operational constraints. Active power generation cost is the most popular objective function used today.

An OPF computer program is an effective tool to conduct power system studies. It provides a realistic and effective way to obtain a minimum production cost of active power dispatch within the specified plant and transmission network operating limits. The optimal redistribution of generated active power results in a significant reduction in the active power generation cost and active power transmission losses.

FACTS controller models have been developed for an OPF algorithm using first principles. The models have been linearised and included in the frame of reference afforded

by Newton's method. The extended OPF Newton algorithm is a very powerful tool capable of solving FACTS-upgraded power networks very reliably, using a minimum of iterative steps. The computational efficiency of the algorithm is further increased by employing the multiplier method to handle the binding set.

The FACTS controller models have been shown to be very flexible; they take into account their various operating modes as well as their interactions with the network and other controllable plant components. Flexibility has been achieved without adversely affecting the efficiency of the solution. In general, the solution of networks with and without FACTS controllers has been achieved in the same number of iterations. The effect of the initial conditions on convergence has also been studied. Improper selection of initial conditions may degrade convergence or, more seriously, cause the solution to diverge.

## REFERENCES

- Acha, E., Ambriz-Pérez, H., 1999, 'FACTS Device Modelling in Optimal Power Flows Using Newton's Method', *Proceedings of the 13th Power System Computation Conference, Trondheim, Norway, June–July 1999*, pp. 1277–1284.
- Acha, E., Ambriz-Pérez, H., Fuerte-Esquivel, C.R., 2000, 'Advanced Transformer Control Modelling in an Optimal Power Flow Using Newton's Method', *IEEE Trans. Power Systems* **15**(1) 290–298.
- Alsac, O., Bright, J., Prais, M., Stott, B., 1990, 'Further Developments in LP-based Optimal Power Flow', *IEEE Trans. Power Systems* **5**(3) 697–711.
- Ambriz-Pérez, H., 1998, *Flexible AC Transmission Systems Modelling in Optimal Power Flows Using Newton's Method*, PhD Thesis, Department of Electronics and Electrical Engineering, University of Glasgow, Glasgow.
- Ambriz-Pérez, H., Acha, E., Fuerte-Esquivel, C.R., De la Torre, A., 1998, 'Incorporation of a UPFC model in an Optimal Power Flow using Newton's Method', *IEE Proceedings on Generation, Transmission and Distribution* **145**(3) 336–344.
- Ambriz-Pérez, H., Acha, E., Fuerte-Esquivel, C.R., 2000, 'Advanced SVC Models for Newton–Raphson Load Flow and Newton Optimal Power Flow Studies', *IEEE Trans. Power Systems* **15**(1) 129–136.
- Bertsekas, D.P., 1982, *Constrained Optimization and Lagrange Multiplier Methods*, Academic Press, New York.
- Dommel, H.W., Tinney, W.F., 1968, 'Optimal Power Flow Solutions', *IEEE Trans. Power Apparatus and Systems* **PAS-87**(10) 1866–1876.
- El-Hawary, M.E., Tsang, D.H., 1986, 'The Hydro-thermal Optimal Power Flow, A Practical Formulation and Solution Technique using Newton's Approach', *IEEE Trans. Power Systems* **PWRS-1**(3) 157–167.
- Happ, H.H., 1977, 'Optimal Power dispatch – A Comprehensive Survey', *IEEE Trans. Power Apparatus and Systems* **PAS-96**(3) 841–854.
- Huneault, M., Galiana, F.D., 1991, 'A Survey of the Optimal Power Flow Literature', *IEEE Trans. Power Systems* **6**(2) 762–770.
- IEEE/CIGRÉ (Institute of Electrical and Electronic Engineers/Conseil International des Grands réseaux Electriques), 1995, 'FACTS Overview', Special Issue, 95TP108, IEEE Service Centre Piscataway, NJ.
- Luenberger, D.G., 1984, *Introduction to Linear and Nonlinear Programming*, 2nd edn, Addison-Wesley, New York.
- Maria, G.A., Findlay, J.A., 1987, 'A Newton Optimal Power Flow Program for Ontario Hydro EMS', *IEEE Trans. Power Systems* **PWRS-2**(3) 576–584.

- Monticelli, A., Liu, W.H.E., 1992, 'Adaptive Movement Penalty Method for the Newton Optimal Power Flow', *IEEE Trans. Power Systems* **7**(1) 334–342.
- Sasson, A.M., 1969, 'Nonlinear Programming Solutions for Load-flow, Minimum-loss, and Economic Dispatching Problems', *IEEE Trans. Power Apparatus and Systems* **PAS-88**(4) 399–409.
- Sasson, A.M., Vilorio, F., Aboites, F., 1973, 'Optimal Load Flow Solution Using the Hessian Matrix', *IEEE Trans. Power Apparatus and Systems* **PAS-92**(1) 31–41.
- Stagg, G.W., El-Abiad, A.H., 1968, *Computer Methods in Power Systems Analysis*, McGraw-Hill, New York.
- Sun, D.I., Ashley, B., Brewer, B., Hughes, A., Tinney W.F., 1984, 'Optimal Power Flow By Newton Approach', *IEEE Trans. Power Apparatus and Systems* **PAS-103**(10) 2864–2880.
- Tinney, W.F., Hart, C.E., 1967, 'Power Flow Solution by Newton's Method', *IEEE Trans. Power Apparatus and Systems* **PAS-96**(11) 1449–1460.
- Wood, A.J., Wollenberg, B., 1984, *Power Generation, Operation and Control*, 2nd edn, John Wiley & Sons, Chichester.





# 8



## Power Flow Tracing

### 8.1 INTRODUCTION

Deregulation and unbundling of transmission services in the electricity supply industry worldwide has given rise to a new area of operation known as ‘electrical energy trading’. Since the late 1980s, the time of privatisation of the UK supply industry, several proposals for the operation of the power network have been put forward in various parts of the world. Arguably, the concept of virtual direct access through a voluntary wholesale pool (Secretary of State for Energy, 1988) was the first workable market-oriented operating philosophy, but it is not in operation any more; it has been superseded by the New Energy Trading Agreement (NETA), which is in operation in England and Wales (Saunders and Boag, 2001). Furthermore, the NETA operating philosophy will soon be extended to encompass Scotland, becoming the British Electricity Trading and Transmission Arrangements (BETTA) (OFGEM, 2003). The ‘Pool’ concept served well the needs of the newly established market but its management attracted criticism for being too complex to operate and for being open to market distortions.

In academic circles, a major criticism of the ‘pool’ was that it did not address crucial issues such as the use of system charges and power transmission losses on a sound engineering basis. It was also argued that this operating philosophy was limiting business opportunities, such as the provision of ancillary services. The ‘pool’ was born out of the inability to trace individual generator power contributions in the network. Indeed, at the time of privatisation, the issue was deemed as too complicated to have a viable solution. The electricity pool rules state that “with an integrated system it is not possible to trace electricity from a particular generator to a particular supplier” (EPEW, 1993). Nevertheless, it was shown in the mid-1990s that the tracing of power flows from generators to suppliers was indeed possible, and algorithms, based on the concepts of dominant power flows and proportional sharing, were put forward to solve such an outstanding issue. Independent, basic research at the University of Manchester Institute of Science and Technology (UMIST; Kirschen and Strbac, 1999; Kirschen, Allan, and Strbac, 1997), Durham University (Bialek, 1996, 1997, 1998), and University of Glasgow (Acha, Fuerte-Esquivel, and Chua, 1996; Acha *et al.*, 1997) led to similar outcomes. Earlier work had addressed the plausibility of such a solution, but this work was confined to solving dominant power flows in radial systems (Macqueen, 1993) as opposed to general, interconnected networks. More recently,

variations and further applications of the basic algorithms have been published (Acha, 1998; Reta and Vargas, 2001), including the incorporation of FACTS equipment models (Acha *et al.*, 2003; Laguna-Velasco *et al.*, 2001). The notion of proportional sharing has been shown to be mathematically demonstrable (Laguna-Velasco, 2002).

In this chapter, the power flow tracing algorithm put forward in an earlier publication (Acha *et al.*, 2003) is first detailed. It should be mentioned that power flow tracing is only a mechanism for tracing generation costs and allocating charges for use of line. The algorithm is in fact an electricity auditing procedure and answers all questions relating to individual generator contributions to optimal power flows, power losses, and costs in each plant component of the power network. A distinction is made between generation costs, possibly attributable to fuel burning, and costs incurred for use of ‘wires’. The contribution of FACTS equipment to reactive power flows and losses is discussed.

### 8.2 BASIC ASSUMPTIONS

As successfully argued by Reta and Vargas (2000), the power tracing algorithms are based only on electric circuit concepts and hence, at their core, they use the proportional sharing principle (Bialek, 1996, 1997, 1998). This is explained with reference to the simple radial transmission system shown in Figure 8.1, consisting of three buses, two generators, two

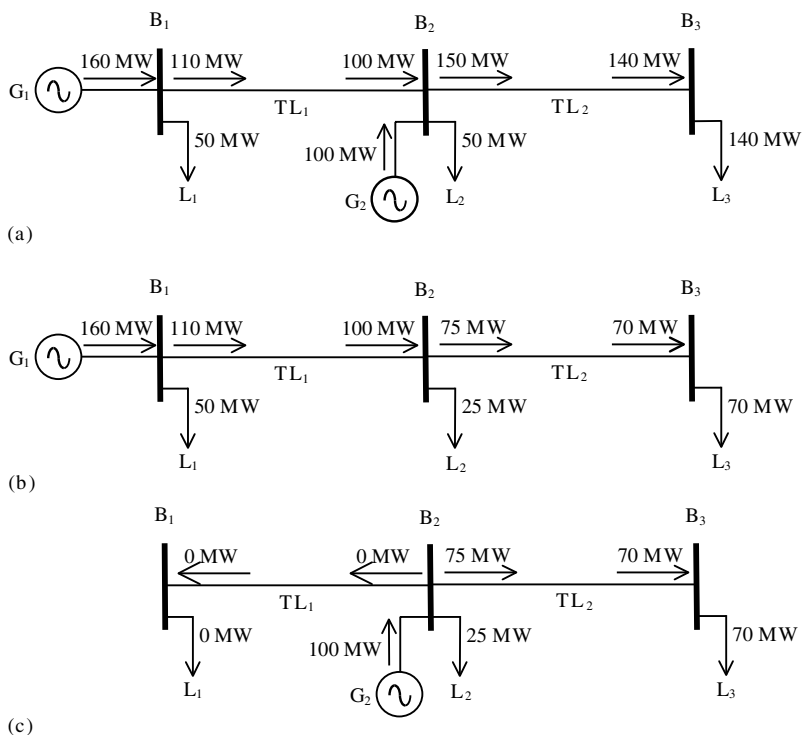


**Figure 8.1** Individual power flows in a simple radial system: (a) power solution; (b) contribution of generator  $G_1$ , and (c) contribution of generator  $G_2$

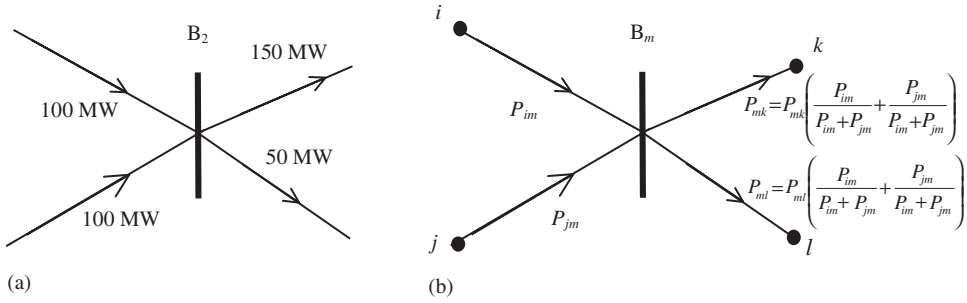


**Figure 8.2** The proportional sharing principle: intuitive appeal: (a) The situation at bus  $B_2$  and (b) the situation at bus  $B_m$

transmission lines, and three loads. The power flow solution is given in Figure 8.1(a), where it is appreciated that the combined generation of 260 MW by generators,  $G_1$  and  $G_2$ , go to supply the system load of 240 MW. Each transmission line in this contrived system incurs power losses of 10 MW. Figure 8.1(b) shows the contribution of generator  $G_1$  to the power flows at the sending and receiving ends of transmission lines  $TL_1$  and  $TL_2$  and to loads  $L_1$ ,  $L_2$ , and  $L_3$ . By the same token, Figure 8.1(c) shows the contribution of generator  $G_2$  to the power flows at the sending and receiving end of transmission line  $TL_2$  and to loads  $L_2$  and  $L_3$ . Notice that there is no contribution of generator  $G_2$  to load  $L_1$  and that it causes no power loss in transmission line  $TL_1$ . Hence, the 10 MW loss in  $TL_1$  is due entirely to  $G_1$ , whereas the 10 MW loss in  $TL_2$  is shared equally by  $G_1$  and  $G_2$ .

As appreciated from Figure 8.1(b), generator  $G_1$  contributes to power flows in branches  $TL_1$  and  $TL_2$  and to loads  $L_1$ ,  $L_2$ , and  $L_3$ ; it is also clear that, in this case, the entire system falls within the dominion of generator  $G_1$ . Similarly, as appreciated from Figure 8.1(c), generator  $G_2$  contributes only to the power flow in branches  $TL_2$  and to loads  $L_2$  and  $L_3$ . Hence, the dominion of generator  $G_2$  is more restricted than that of generator  $G_1$ . Furthermore, there is an overlap between the dominions of generators  $G_1$  and  $G_2$ .

Of particular interest are the power inflows and outflows in bus  $B_2$ , where the principle of proportional sharing is self-evident. An anatomy of this bus may be drawn: Figure 8.2(a) represents the situation prevailing in bus  $B_2$  in Figure 8.1(a), and Figure 8.2(b) is a more generic expansion of the concept involved.

In Figure 8.2(b), the expressions  $P_{mk}P_{im}/(P_{im} + P_{jm})$  and  $P_{mk}P_{jm}/(P_{im} + P_{jm})$  represent the contributions of inflows  $P_{im}$  and  $P_{jm}$  to outflow  $mk$ , respectively. Similarly, the expressions  $P_{ml}P_{im}/(P_{im} + P_{jm})$  and  $P_{ml}P_{jm}/(P_{im} + P_{jm})$  represent the contributions of inflows  $P_{im}$  and  $P_{jm}$  to outflow  $ml$ , respectively.

### 8.3 MATHEMATICAL JUSTIFICATION OF THE PROPORTIONAL SHARING PRINCIPLE

The following justification is drawn from Laguna-Velasco (2002). With reference to Figure 8.2, the voltage at bus  $m$  may be expressed as a function of the branch impedance  $Z_{mk}$  and its current flow  $I_{mk}$ , or of  $Z_{ml}$  and  $I_{ml}$ :

$$V_m = Z_{mk}I_{mk} = Z_{ml}I_{ml}. \tag{8.1}$$

Alternatively, it may be expressed as the product of the equivalent impedance, as seen from bus  $m$ , and the total injected current into bus  $m$ :

$$V_m = \left( \frac{Z_{mk}Z_{ml}}{Z_{mk} + Z_{ml}} \right) I_T, \quad (8.2)$$

where

$$I_T = I_{im} + I_{jm}. \quad (8.3)$$

Combining Equations (8.1) and (8.2), and solving for  $I_{mk}$  and  $I_{ml}$ , gives:

$$I_{mk} = \left( \frac{Z_{ml}}{Z_{mk} + Z_{ml}} \right) I_T, \quad (8.4)$$

$$I_{ml} = \left( \frac{Z_{mk}}{Z_{mk} + Z_{ml}} \right) I_T. \quad (8.5)$$

An expression for the power flow in branch  $mk$  may be derived as a function of the powers contributed by inflows  $im$  and  $jm$ :

$$\begin{aligned} S_{mk} &= V_m I_{mk}^* \\ &= V_m \left( \frac{Z_{ml}^*}{Z_{mk}^* + Z_{ml}^*} \right) (I_{im}^* + I_{jm}^*) \\ &= \left( \frac{Z_{ml}^*}{Z_{mk}^* + Z_{ml}^*} \right) (S_{im} + S_{jm}), \end{aligned} \quad (8.6)$$

where

$$S_{im} = V_m I_{im}^*, \quad (8.7)$$

$$S_{jm} = V_m I_{jm}^*. \quad (8.8)$$

By the same token, the power flow in branch  $ml$  is:

$$S_{ml} = \left( \frac{Z_{mk}^*}{Z_{mk}^* + Z_{ml}^*} \right) (S_{im} + S_{jm}). \quad (8.9)$$

Equations (8.6) and (8.9) can be given in terms of only complex powers as opposed to powers and impedances by making use of the relations

$$Z_{mk} = V_m^2 / S_{mk}^*$$

and  $Z_{ml} = V_m^2 / S_{ml}^*$ :

$$S_{mk} = \left( \frac{S_{mk}}{S_{mk} + S_{ml}} \right) S_{im} + \left( \frac{S_{mk}}{S_{mk} + S_{ml}} \right) S_{jm}, \quad (8.10)$$

$$S_{ml} = \left( \frac{S_{ml}}{S_{ml} + S_{mk}} \right) S_{im} + \left( \frac{S_{ml}}{S_{ml} + S_{mk}} \right) S_{jm}. \quad (8.11)$$

It should be noted that the following power conservation relation:

$$S_{im} + S_{jm} = S_{mk} + S_{ml}$$

can be used instead in Equations (8.10) and (8.11):

$$S_{mk} = \left( \frac{S_{im}}{S_{im} + S_{jm}} + \frac{S_{jm}}{S_{im} + S_{jm}} \right) S_{mk}, \quad (8.12)$$

$$S_{ml} = \left( \frac{S_{im}}{S_{im} + S_{jm}} + \frac{S_{jm}}{S_{im} + S_{jm}} \right) S_{ml}. \quad (8.13)$$

Separation of the real and imaginary components in Equations (8.12) and (8.13) leads to useful expressions for active and reactive powers:

$$P_{mk} = \left( \frac{P_{im}}{P_{im} + P_{jm}} + \frac{P_{jm}}{P_{im} + P_{jm}} \right) P_{mk}, \quad (8.14)$$

$$Q_{mk} = \left( \frac{Q_{im}}{Q_{im} + Q_{jm}} + \frac{Q_{jm}}{Q_{im} + Q_{jm}} \right) Q_{mk}, \quad (8.15)$$

$$P_{ml} = \left( \frac{P_{im}}{P_{im} + P_{jm}} + \frac{P_{jm}}{P_{im} + P_{jm}} \right) P_{ml}, \quad (8.16)$$

$$Q_{ml} = \left( \frac{Q_{im}}{Q_{im} + Q_{jm}} + \frac{Q_{jm}}{Q_{im} + Q_{jm}} \right) Q_{ml}. \quad (8.17)$$

Note that the expressions for active power are those derived intuitively in Section 8.3, appearing in Figure 8.2(b). They are generalised in Sections 8.5–8.6 for the case of  $n$  inflows and loads.

## 8.4 DOMINIONS

The concept of dominion is at the centre of the power tracing algorithm. In its most basic form it may be seen as a directed graph consisting of one source, and one or more sinks. The set of branches linking source and buses are related to transmission components present in the network, such as lines, transformers, high-voltage direct-current (HVDC) links and series FACTS equipment. The directions of the branches are dictated by the power flow or the optimal power flow (OPF) solution upon which the tracing study is based.

There are several ways of carrying out the actual implementation of the algorithm used for determining the sources dominions. Kirschen, Allan, and Strbac (1997) give one possible course of action, where the concepts of ‘commons’ and ‘links’ are used. A ‘common’ is defined as a set of contiguous buses supplied by the same source. Branches within a common are termed internal branches’, and the set of external branches linking two commons is termed the ‘link’. The analysis is conducted at the common and link level first. Once the power contribution to each common is known then all buses, loads, and branches within the common are allocated a share of the power flowing into that common.

An alternative algorithm is detailed in this section. It is a lower-level algorithm in which the concepts of source dominions and common branches are used (Bialek, 1997), as opposed to commons and links (Kirschen, Allan, and Strbac, 1997).

The source dominions are determined as follows:

- Select the first source and, starting from the source bus, check all the branches with a connection to the bus.

- Branches in which the power flows away from the bus (i.e. outflows) are included as part of the dominion along with the bus at the receiving end of the branch. Conversely, branches in which the power flows into the bus (i.e. inflows) do not form part of the dominion of the source. The procedure is repeated for each new bus as soon as it becomes part of the dominion of the source.
- After no further buses can be reached, the process comes to a halt, resulting in a directed subgraph containing only branches that carry power pertaining to the source currently under analysis.
- The above procedure is repeated for the second source of the network, the third, and so on.
- If the dominion of a source contains no branches, then the dominion is a *degenerated dominion*, and the source will contribute power only to the local load.

The use of the branch–node incidence matrix offers a systematic way for implementing this algorithm. This matrix is highly sparse and yields very efficient solutions.

By way of example, Figure 8.3 shows the five-bus system with active and reactive power flows, which correspond to the optimal power flow solution as opposed to a conventional power flow solution. Figures 8.4(a) and 8.4.2(b) show the active power dominions, and Figure 8.5(a) and 8.5(b) show the reactive power dominions.

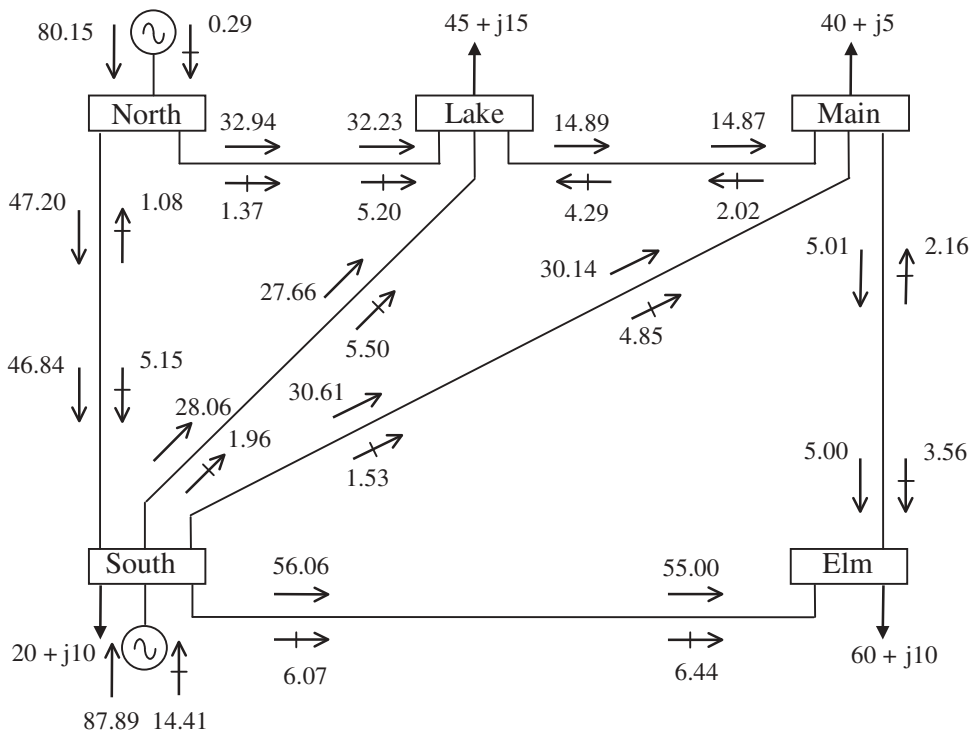
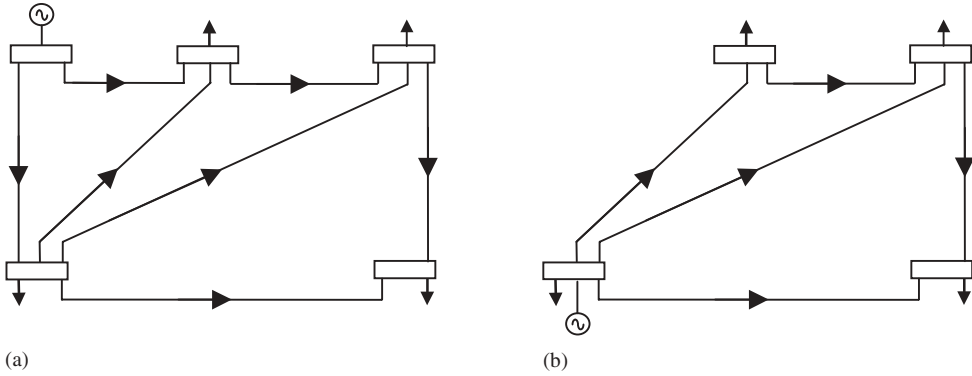
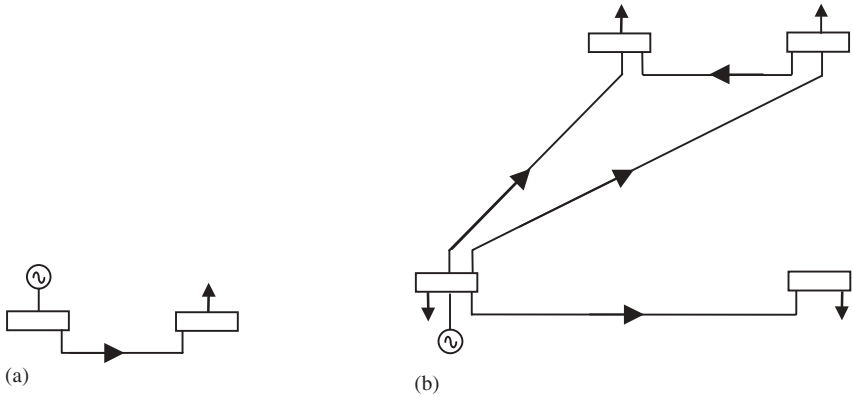


Figure 8.3 Optimal power flow solution



**Figure 8.4** The active dominion of the generators: (a) Gen-North and (b) Gen-South



**Figure 8.5** The reactive dominion of the generators: (a) Gen-North and (b) Gen-South

### 8.4.1 Dominion Contributions to Active Power Flows

Building on the ideas advanced in Section 8.2, the two-inflow, two-outflow system shown in Figure 8.2 is modified, as shown in Figure 8.6, to include  $n$  inflows, with one of the outflows being a transmission line and the other a load.

The active and reactive power contribution of each dominion or generator to the branch and load is determined by using the proportional sharing principle demonstrated in Section 8.3. In this section the issue of active power is addressed, and Figure 8.6 reflects this point.

The power flow at the sending end of line  $m$  is made up of the contribution of the  $n$  inflows and the generator. Similarly, the load  $P_L$  is fed by the contribution of the  $n$  inflows and the generator.

Expanding on the result given in Equation (8.14) to encompass  $n$  inflows but restricted to branch  $mk$  (the load will be treated separately in Section 8.4.3), the following equations

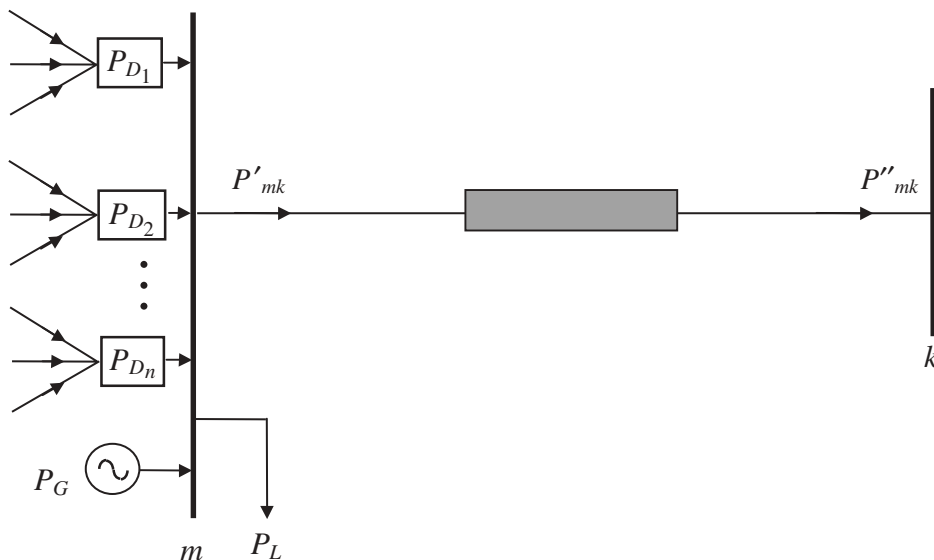


Figure 8.6 Contributions of active power dominions to branch  $mk$

apply at the sending end of the branch:

$$P'_{mk} = P'_{D_1} + P'_{D_2} + \dots + P'_{D_n} + P'_G, \tag{8.18}$$

$$P'_{D_i} = P_{D_i} \times C'_{P_{mk}}, \tag{8.19}$$

$$P'_G = P_G \times C'_{P_{mk}}, \tag{8.20}$$

$$C'_{P_{mk}} = \frac{P'_{mk}}{P_{D_1} + P_{D_2} + \dots + P_{D_n} + P_G}, \tag{8.21}$$

where  $i = 1, 2, \dots, n$ , and single primes indicate the sending end.

As an extension, the contribution of the  $n$  inflows at the receiving end of branch  $mk$  is determined by the following expressions:

$$P''_{mk} = P''_{D_1} + P''_{D_2} + \dots + P''_{D_n} + P''_G, \tag{8.22}$$

$$P''_{D_i} = P_{D_i} \times C''_{P_{mk}}, \tag{8.23}$$

$$P''_G = P_G \times C''_{P_{mk}}, \tag{8.24}$$

$$C''_{P_{mk}} = \frac{P''_{mk}}{P_{D_1} + P_{D_2} + \dots + P_{D_n} + P_G}, \tag{8.25}$$

where  $i = 1, 2, \dots, n$ , and double primes indicate the receiving end.

In these expressions,  $P_{D_i}$  are the power contributions of dominion  $D_i$  to bus  $m$ . The contribution of each dominion will contain inflows from every one of its branches. If bus  $m$  is the starting point then the bus inflow will be  $P_G$  as opposed to  $P_{D_i}$ .  $C_{P_m}$  are contribution coefficients.

### 8.4.2 Dominion Contributions to Reactive Power Flows

In each branch, the reactive power contribution of each dominion, and any source of reactive power connected directly to the bus, is also determined by using the proportional sharing principle. The circuit representation in Figure 8.6 is suitably modified to accommodate the slightly more involved situation prevailing in reactive power applications, where sources of reactive power may come in a variety of forms: namely, as synchronous generators, shunt and series compensation, FACTS equipment, and long transmission lines. This situation is illustrated in Figure 8.7.

In Figure 8.7,  $Q_L$  is a reactive power load, and  $Q_S$  is a reactive power sink. The sink caters for the possibility of generator or FACTS equipment connected at bus  $m$  and drawing reactive power from the bus. Also,  $Q_{TL}$  is the reactive power contribution from the capacitive effects of transmission lines, and  $Q_{D_1}, \dots, Q_{D_n}$  are the reactive power contributions of dominions 1,  $\dots$ ,  $n$  to bus  $m$ . If bus  $m$  is the starting point of the dominion then the bus inflow will be  $Q_G$  or  $Q_F$  as opposed to  $Q_{D_1}, \dots, Q_{D_n}$ .  $Q_G$  would correspond to a generator, and  $Q_F$  to FACTS equipment.

Based on Figure 8.7, the contributions from the dominion are obtained by using the following equations.

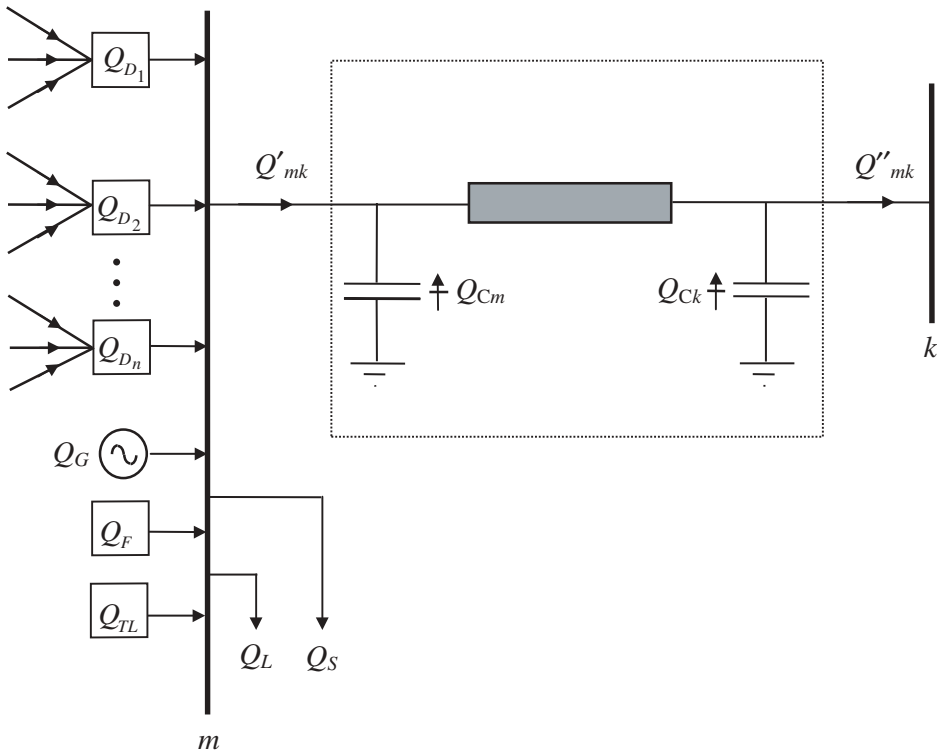


Figure 8.7 Contribution of reactive power dominions to branch  $mk$

Sending end of line  $mk$ :

$$Q'_{mk} = Q'_{D_1} + Q'_{D_2} + \dots + Q'_{D_n} + Q'_G + Q'_F + Q'_{TL}, \quad (8.26)$$

$$Q'_{D_i} = Q_{D_i} \times C'_{Qmk}, \quad (8.27)$$

$$Q'_G = Q_G \times C'_{Qmk}, \quad (8.28)$$

$$Q'_F = Q_F \times C'_{Qmk}, \quad (8.29)$$

$$Q'_{TL} = Q_{TL} \times C'_{Qmk}, \quad (8.30)$$

$$C'_{Qmk} = \frac{Q'_{mk}}{Q_{D_1} + Q_{D_2} + \dots + Q_{D_n} + Q_G + Q_F + Q_{TL}}, \quad (8.31)$$

where  $i = 1, 2, \dots, n$ .

Receiving end of line  $mk$ :

$$Q''_{mk} = Q''_{D_1} + Q''_{D_2} + \dots + Q''_{D_n} + Q''_G + Q''_F + Q''_{TL}, \quad (8.32)$$

$$Q''_{D_i} = Q'_{D_i} \times C''_{Qkm}, \quad (8.33)$$

$$Q''_G = Q'_G \times C''_{Qkm}, \quad (8.34)$$

$$Q''_F = Q'_F \times C''_{Qkm}, \quad (8.35)$$

$$C''_{Qmk} = \frac{Q''_{mk} - Q_{Ck}}{Q_{D_1} + Q_{D_2} + \dots + Q_{D_n} + Q_G + Q_F + Q_{TL} - Q_{Cm}}, \quad (8.36)$$

$$Q''_{TL} = (Q'_{TL} + Q_{Cm}) \times C''_{Qmk} + Q_{Ck}, \quad (8.37)$$

where  $i = 1, 2, \dots, n$ .

### 8.4.3 Dominion Contributions to Loads and Sinks

The proportional sharing principle is also used for finding the dominion and source contributions to the load connected at bus  $m$ . Based on Figure 8.8, the following equations apply for the case of active power:

$$P_L = P'_{D_1} + P'_{D_2} + \dots + P'_{D_n} + P'_G, \quad (8.38)$$

$$P'_{D_i} = P_{D_i} \times C_{PL}, \quad (8.39)$$

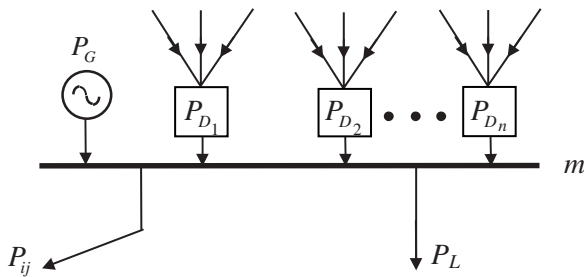


Figure 8.8 Active dominions contributions to load L

$$P'_G = P_G \times C_{PL}, \quad (8.40)$$

$$C_{PL} = \frac{P_L}{P_{D_1} + P_{D_2} + \cdots + P_{D_n} + P_G}, \quad (8.41)$$

where  $i = 1, 2, \dots, n$ . For the case of reactive power, the variable  $Q$  replaces  $P$  in Equations (8.38)–(8.41). Note also that reactive power contributions from  $Q_F$  and  $Q_{TL}$  may exist.

## 8.5 TRACING ALGORITHM

The general algorithm for tracing power flows is summarised in Figure 8.9. Note that the algorithm differs slightly for the cases of active and reactive powers.

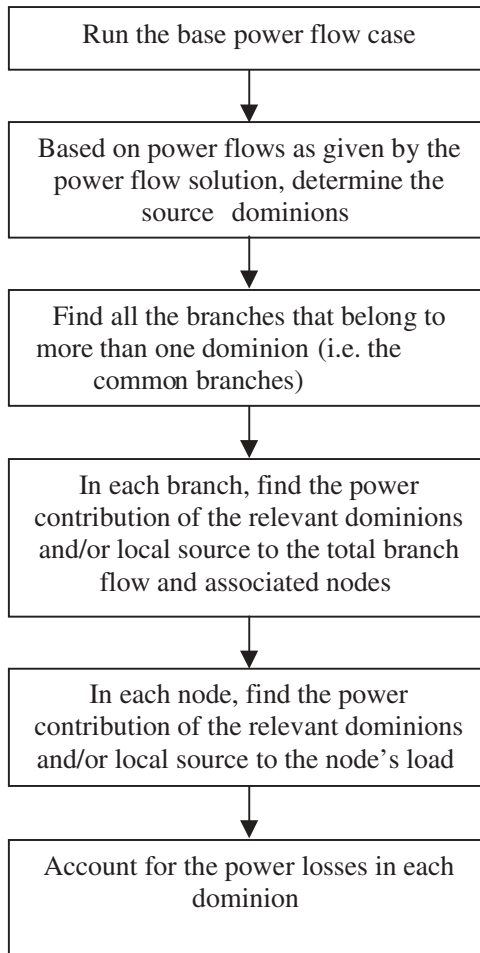


**Figure 8.9** Flowchart for the tracing algorithm

### 8.6 NUMERICAL EXAMPLES

This section is concerned with the application of the power tracing algorithm to solve a number of test cases of varying degrees of complexity. The first example (Section 8.6.1) corresponds to a simple radial network, which serves rather well the purpose of illustrating the application of the theory to active power concerns. The second example (Section 8.6.2) addresses the case of active power in a meshed network, which is still a fairly simple network. The motivation for solving this test case is that it enables a direct comparison between the power tracing methodology presented in this chapter and an alternative tracing methodology (Bialek, 1996, 1997, 1998). The third test case (Section 8.6.3) deals with reactive power, as opposed to active power, and includes the contribution of FACTS equipment to reactive power generation. The tracing of reactive power in a large power network is quantified in the fourth test case (Section 8.6.4). The last case (Section 8.6.5) corresponds to the tracing of active power contributed by one wind generator and one conventional generator in a meshed network.

#### 8.6.1 Simple Radial Network

The tracing algorithm is applied first to the case of active power in the test system shown in Figure 8.1, which is a radial network. In addition to finding the individual power contributions of generators  $G_1$  and  $G_2$  to power flows in transmission lines  $TL_1$  and  $TL_2$ , and to system loads  $L_1$ ,  $L_2$ , and  $L_3$ , the individual contributions of the generators to transmission loss becomes readily available. If information exists on charges for use of line then it is a straightforward matter to allocate charges to each generator per transmitted or lost megawatt. It is assumed in this example that there is a charge of £1 per lost megawatt in  $TL_1$  and  $TL_2$ .

The dominions of generators  $G_1$  and  $G_2$  were identified by inspection in Section 8.2; however, for the purpose of computer implementation it is essential to have a systematic approach. In this section the branch–bus incidence matrix is used for the purpose of dominion identification. The branch–bus incidence matrix of this network is given in Figure 8.10, together with the branch searches for the dominions of generators  $G_1$  and  $G_2$ .

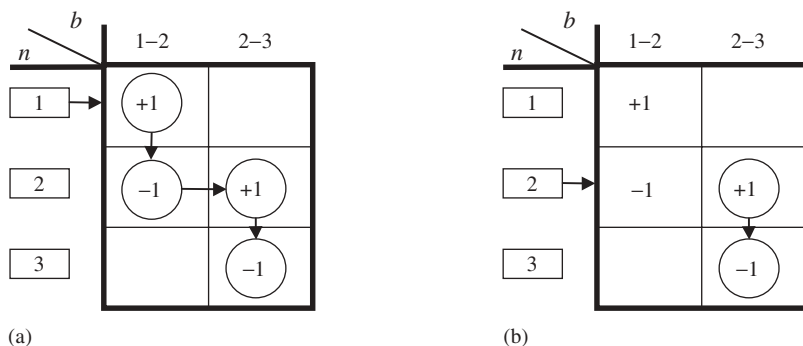


**Figure 8.10** Branch–bus incidence matrices and branch searches for the dominions of (a) generator  $G_1$  and (b) generator  $G_2$

Generator  $G_1$  is connected to bus 1. This entry provides the starting point for establishing the dominion of  $G_1$ . The +1 in location (1, 1) of the matrix indicates that line 1–2 belongs to the dominion of  $G_1$ . One additional line belongs to this dominion and, from the branch–bus incidence matrix, it is found as follows: the sending end of line 1–2 is bus 1, and the receiving bus is bus 2, as given by +1 and –1 in locations (1, 1) and (2, 1) of the matrix, respectively. There is a +1 entry in the row corresponding to the receiving end of line 1–2. This indicates that bus 2 contains inflows, and the search is moved from column 1 to column 2 of the matrix. This makes line 2–3 part of the dominion of  $G_1$ . There is no +1 found in the row corresponding to the receiving end of line 2–3. Hence, bus 3 contains no outflows, and the search stops at bus 3.

Using the same line of reasoning,  $G_2$  is connected to bus 2. This entry provides the starting point for establishing the dominion of  $G_2$ . The +1 in location (2, 2) of the matrix indicates that line 2–3 belongs to the dominion of  $G_2$ . There is no +1 found in the row corresponding to the receiving end of line 2–3. Hence, bus 3 contains no outflows, and the search stops at bus 3.

The dominion contributions to system loads and power losses in transmission lines are determined quite straightforwardly by using Equations (8.18)–(8.25).

In transmission line  $TL_1$ :

$$P'_{G_1} = P_{G_1} \times C'_{12} = 160 \times 0.6875 = 110,$$

$$P''_{G_1} = P_{G_1} \times C''_{12} = 160 \times 0.625 = 100,$$

with

$$C'_{12} = \frac{P_{12}}{P_{G_1}} = \frac{110}{160} = 0.6875,$$

$$C''_{12} = \frac{P'_{12}}{P_{G_1}} = \frac{100}{160} = 0.625.$$

In transmission line  $TL_2$ :

$$P'_{D_1} = P_{D_1} \times C'_{23} = 100 \times 0.75 = 75,$$

$$P''_{D_1} = P_{D_1} \times C''_{23} = 100 \times 0.7 = 70,$$

$$P'_{G_2} = P_{G_2} \times C'_{23} = 100 \times 0.75 = 75,$$

$$P''_{G_2} = P_{G_2} \times C''_{23} = 100 \times 0.7 = 70,$$

with

$$C'_{23} = \frac{P_{23}}{P_{D_1} + P_{G_1}} = \frac{150}{100 + 100} = 0.75,$$

$$C''_{23} = \frac{P'_{23}}{P_{D_1} + P_{G_2}} = \frac{140}{100 + 100} = 0.7.$$

This information is summarised in Table 8.1, and Table 8.2 presents a breakdown of the power loss and charge for use of line for generators  $G_1$  and  $G_2$ .

From this simple example, it is interesting to note that generator  $G_2$  contributes no power flow to transmission line  $TL_1$  and, quite correctly, is not charged for the use of  $TL_1$ . Similarly, both generators contribute in equal measure to power flow and power loss in transmission line  $TL_2$  and are charged equally.

**Table 8.1** Contributions to active power flows

Branch	Sending end			Receiving end		
	$C'$ (%)	$P'_{D_1}$ (MW)	$P'_{D_2}$ (MW)	$C''$ (%)	$P''_{D_1}$ (MW)	$P''_{D_2}$ (MW)
1-2	68.75	110	0	62.5	100	0
2-3	75	75	75	70	70	70

**Table 8.2** Contributions to power loss and charges for use of line for dominions  $D_1$  and  $D_2$

Branch	Power loss (W)		Charge for use of lines (£)	
	$D_1$	$D_2$	$D_1$	$D_2$
1-2	10	0	10	0
2-3	5	5	5	5
Total	15	5	15	5

Note: The charge for use of line is set at £1 per megawatt.

### 8.6.2 Simple Meshed Network: Active Power

The test system used by Bialek (1996, 1997, 1998) forms the basis of the example presented in this section. As shown in Figure 8.11, it is a simple power network comprising four buses, linked together by five transmission lines. Generation is available at buses  $B_1$  and  $B_2$ , and loads are connected at buses  $B_3$  and  $B_4$ .

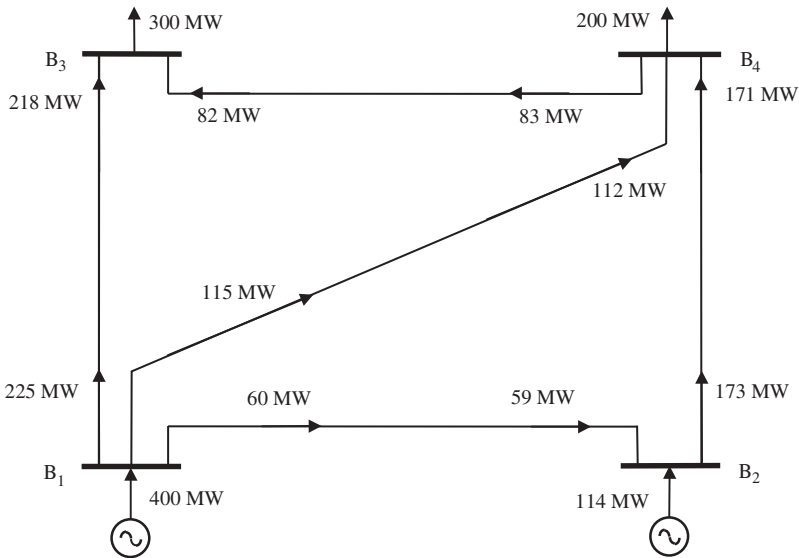


**Figure 8.11** Power flows in a small, meshed network

**Table 8.3** Charges for use of line

Line	1-2	1-3	1-4	2-4	4-3
Charge (£)	12.75	6	11.7	3.5	5.75

Table 8.3 gives information on applied charges for use of line, which have been taken to be equal to the branch resistances (Bialek, 1996, 1997, 1998). The power flows, as given by a power flow solution, are shown in Figure 8.11. Based on these trajectories, the two domains of the network are determined, one domain per generator.

The branch–bus incidence matrix of this network is given in Figure 8.12 together with the branch search for the dominion of generator  $G_1$ . Generator  $G_1$  is connected to bus  $B_1$ . This entry provides the starting point for establishing the dominion of generator  $G_1$ . A +1 at locations (1, 1), (1, 2), and (1, 3) of the matrix indicates that lines 1-3, 1-2, and 1-4 belong to the dominion of generator 1. Additional lines belong to this dominion, and they will be found as follows:

- The sending end of line 1-3 is bus  $B_1$ , and the receiving end is bus  $B_3$ , as given by the +1 and -1 in locations (1, 1) and (3, 1) of the matrix, respectively. There is no +1 entry in the row corresponding to the receiving end of line 1-3. This indicates that bus  $B_3$  contains no outflows. Therefore, the search stops at bus  $B_3$  for this route.
- The row corresponding to the receiving end of line 1-2 contains +1s. Thus, the search is moved from column 2 to column 4 of the matrix. This makes line 2-4 part of the dominion of generator  $G_1$ . Applying the same line of reasoning, we move the search on from column 4 to column 5, and line 4-3 is incorporated into the dominion of generator  $G_1$ . No +1 is found in the row corresponding to the receiving end of line 4-3. Hence, bus  $B_3$  contains no outflows, and the search stops at bus  $B_3$  for this route.
- The row corresponding to the receiving end of line 1-4 contains a +1 in column 5. Accordingly, the search is moved on from column 3 to column 5 of the matrix. This makes line 4-3 part of the dominion of generator  $G_1$ . It must be noted that this line has

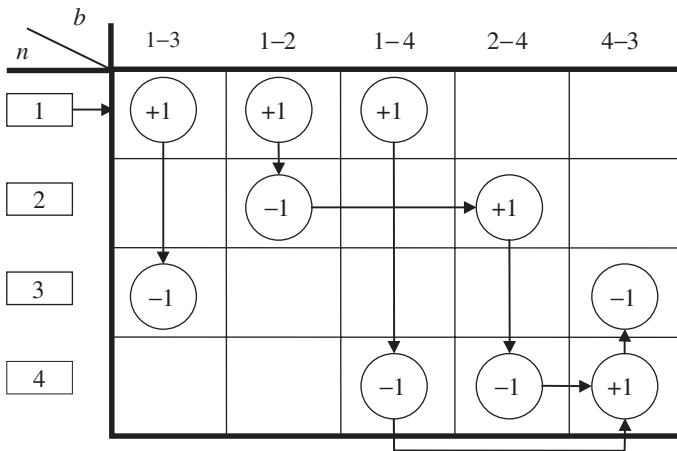


**Figure 8.12** Branch–bus incidence matrix and branch search for the dominion of generator  $G_1$

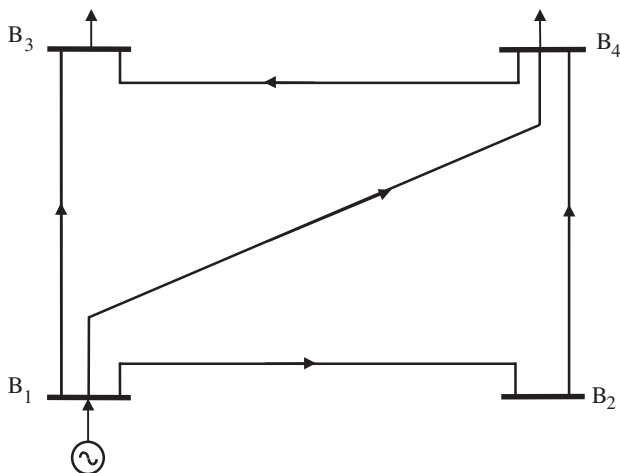


Figure 8.13 Dominion of generator  $G_1$

already been added to the dominion of generator  $G_1$ , and it should not be incorporated twice in the dominion. No +1 is found in the row corresponding to the receiving end of line 4-3.

- Since we have exhausted all the +1 entries in row 1 of the matrix then we are satisfied that we have completed the search for all branches belonging to the dominion of generator  $G_1$ . It must be noted that, in this case, the entire network belongs to the dominion of generator  $G_1$ .

The directed subgraph of dominion  $D_1$  is shown in Figure 8.13.

The branch-bus incidence matrix of the network shown in Figure 8.11 together with the branch search process for the dominion of generator  $G_2$  are shown in Figure 8.14. Generator  $G_2$  is connected to bus  $B_2$ . This entry provides the starting point for establishing the dominion of generator  $G_2$ . A +1 entry in location (2, 4) of the matrix indicates that line 2-4 belongs to the dominion of generator  $G_2$ . Additional lines belonging to this dominion will

$n \backslash b$	1-3	1-2	1-4	2-4	4-3
1	(+1)	(+1)	(+1)		
2		(-1)		(+1)	
3	(-1)				(-1)
4			(-1)	(-1)	(+1)

Figure 8.14 Branch-bus incidence matrix and branch search for the dominion of generator  $G_2$

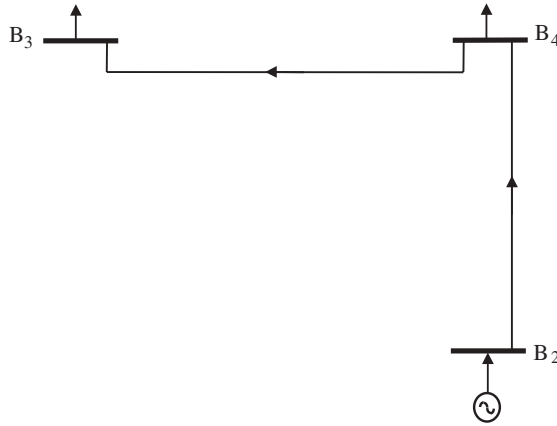


**Figure 8.15** Dominion of generator  $G_2$

be found as follows:

- The row corresponding to the receiving end of line 2–4 contains +1 entries. Accordingly, the search is moved on from column 4 to column 5 of the matrix. This makes line 4–3 part of the dominion of generator  $G_2$ . We move the search on from column 4 to column 5 of the matrix and line 4–3 is incorporated into the dominion of generator  $G_2$ . No +1 entries are found in the row corresponding to the receiving end of line 4–3. Bus  $B_3$  contains no outflows.
- We have exhausted all the +1 entries in row 2 of the matrix and this indicates that we have completed the search for all branches belonging to the dominion of generator  $G_2$ . At this point we have also completed the search for all the dominions available in this network.

The directed subgraph of dominion 2 is shown in Figure 8.15.

Branch 2–4 and branch 4–3 are both common to dominions  $D_1$  and  $D_2$ . Hence, the power tracing algorithm is used to calculate the contributions of each dominion to common branches 2–4 and 4–3. This information is presented in Table 8.4.

By way of example, the power flow contribution of dominion  $D_1$  at the sending and receiving ends of transmission line 2–4 are calculated as follow:

$$C'_{24} = \frac{173}{59 + 114} = 1, \quad P'_{D_1} = 1 \times 59 = 59;$$

$$C''_{24} = \frac{171}{59 + 114} = 0.988444, \quad P''_{D_1} = 0.988444 \times 59 = 58.317919.$$

**Table 8.4** Contribution of dominions  $D_1$  and  $D_2$  to branches 2–4 and 4–3

Branch	Sending end			Receiving end		
	$C'$ (%)	$P'_{D_1}$ (MW)	$P'_{D_2}$ (MW)	$C''$ (%)	$P''_{D_1}$ (MW)	$P''_{D_2}$ (MW)
2–4	100	59	114	98.8439	58.3179	112.6821
4–3	29.3286	49.9519	33.0481	28.9753	49.3501	32.6499

**Table 8.5** System power losses (sending end) and charges for use of line for dominions D<sub>1</sub> and D<sub>2</sub>

Branch	Power loss (MW)		Charge for use of lines (p.u.)		
	D <sub>1</sub>	D <sub>2</sub>	Per line	D <sub>1</sub>	D <sub>2</sub>
1–2	1	0	12.75	12.75	0
1–3	7	0	6	6	0
1–4	3	0	11.7	11.7	0
2–4	0.6821	1.3179	3.5	1.1937	2.3063
4–3	0.6018	0.3982	5.75	3.4604	2.2896
Total	12.2839	1.7161	N.A.	35.1041	4.5959

N.A. Not applicable.

The contributions of dominions D<sub>1</sub> and D<sub>2</sub> to active power losses in branch 2–4 become readily available from the above result. Table 8.5 gives the power losses and charges for use of line.

The charge, *E*, for use of line in line 2–4 is calculated as follows:

$$E_{D_1} = \left( \frac{3.5}{0.6821 + 1.3179} \right) \times 0.6821 = 1.1937 \text{ p.u.},$$

$$E_{D_2} = \left( \frac{3.5}{0.6821 + 1.3179} \right) \times 1.3179 = 2.3063 \text{ p.u.}$$

The charge for use of line in line 4–3 is:

$$E_{D_1} = \left( \frac{5.75}{0.6018 + 0.3982} \right) \times 0.6018 = 3.4604 \text{ p.u.},$$

$$E_{D_2} = \left( \frac{5.75}{0.6018 + 0.3982} \right) \times 0.3982 = 2.2896 \text{ p.u.}$$

It is important to remark that a number of methodologies exist for calculating charges for use of line. For instance, Table 8.6 gives the charges for use of line as calculated by three

**Table 8.6** Comparison of charges (p.u.) for use of line by three different methods for dominions D<sub>1</sub> and D<sub>2</sub>: (a) the tracing algorithm (presented in this chapter), (b) the generalised factor algorithm (Ng, 1980), and (c) the topological factor method (Bialek, 1996, 1997, 1998)

Branch	(a) Tracing		(b) Generalised factor		(c) Topological factor	
	D <sub>1</sub>	D <sub>2</sub>	D <sub>1</sub>	D <sub>2</sub>	D <sub>1</sub>	D <sub>2</sub>
1–2	12.75	0	12.75	0	12.75	0
1–3	6	0	5.22	0.78	6	0
1–4	11.7	0	11.7	0	11.7	0
2–4	1.1937	2.3063	1.77	1.73	1.21	2.29
4–3	3.4604	2.2896	3.06	2.69	3.48	2.27
Total	35.1041	4.5959	34.5	5.2	35.14	4.56

different methods. The tracing algorithm presented in this chapter is compared with the method of topological factors (Bialek, 1996, 1997, 1998) and the method of generalised factors detailed by Ng (1980). It is brought to the reader's attention that in this example some of the generalised factors are negative and would produce negative charges for use of line (i.e. a generator would be compensated for using a transmission facility; Bialek, 1996, 1997, 1998). In actual applications all negative factors and costs are set to zero (Ng, 1980).

The charges based on topological factors compare very well with the charges given by the tracing algorithm. In contrast, some differences are observed with respect to the charges given by the generalised factor algorithm. Perhaps the most suspect results are the charges made to generator  $G_2$  for the use of branch 1–3, and the undercharge to generator  $G_1$ . It must be noted that branch 1–3 is not part of the dominion of generator  $G_1$ . This fact is correctly recognised by the topological factor algorithm. Also, important differences exist in the charges made to generators  $G_1$  and  $G_2$  for the use of line 2–4.

### 8.6.3 Meshed Network with FACTS Controllers: Reactive Power

In this case, two FACTS devices are included: one unified power flow controller (UPFC) in branch Lake–Main and one static compensator (STATCOM) in node Elm. The reactive power flows throughout the network are shown in Figure 8.16. The dominions of the

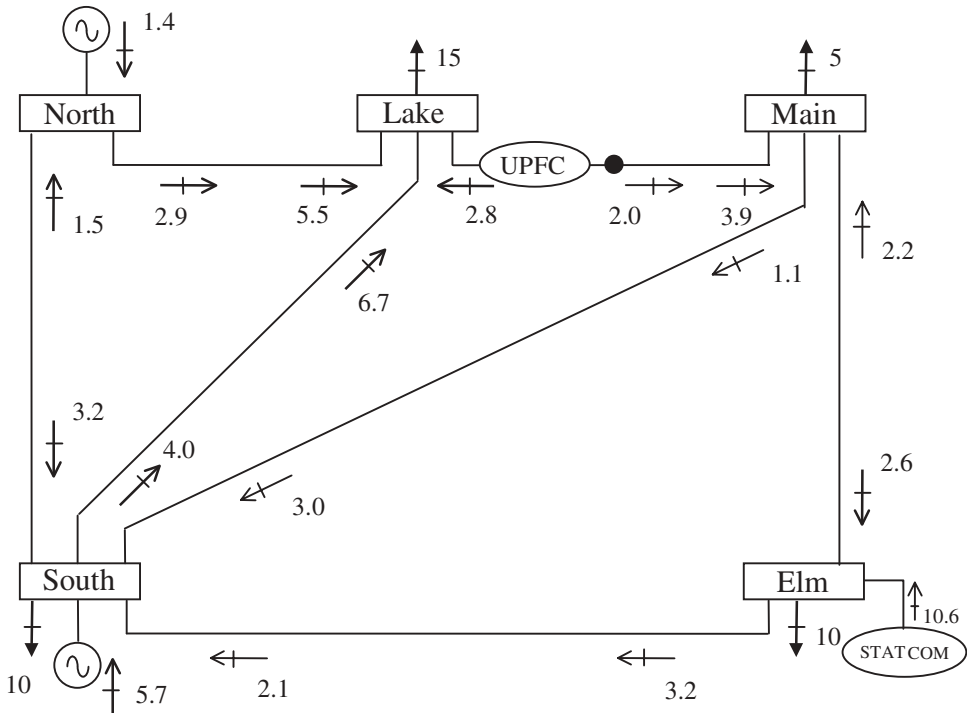


**Figure 8.16** Five-node system with unified power flow controller (UPFC) and static compensator (STATCOM)

**Table 8.7** Reactive dominions of generators, FACTS, and transmission lines (TLs)

	Transmission line	Loads and sinks
Gen–North	North–Lake	Lake
Gen–South	South–Lake	South, Lake
UPFC	Lake–Main, Main–South, South–Lake	Lake, Main, South
STATCOM	Elm–South, South–Lake	Elm, South, Lake
TL: North–Lake	None	Lake
TL: South–Lake	None	Lake
TL: North–South	North–Lake, South–Lake	South, Lake
TL: Main–South	South–Lake	South, Lake
TL: Lake–Main	Main–South, South–Lake	Main, South, Lake
TL: Main–Elm	Elm–South, Main–South, South–Lake	Main, Elm, South, Lake

Note: UPFC, unified power flow controller; STATCOM, static compensator.

reactive source’s dominions are given in Table 8.7. The dominions of generators and FACTS equipments are as shown in Figure 8.17.

The reactive dominion of Gen–North reduces to line North–Lake, and this generator contributes only to the reactive load connected at Lake. Six transmission lines become

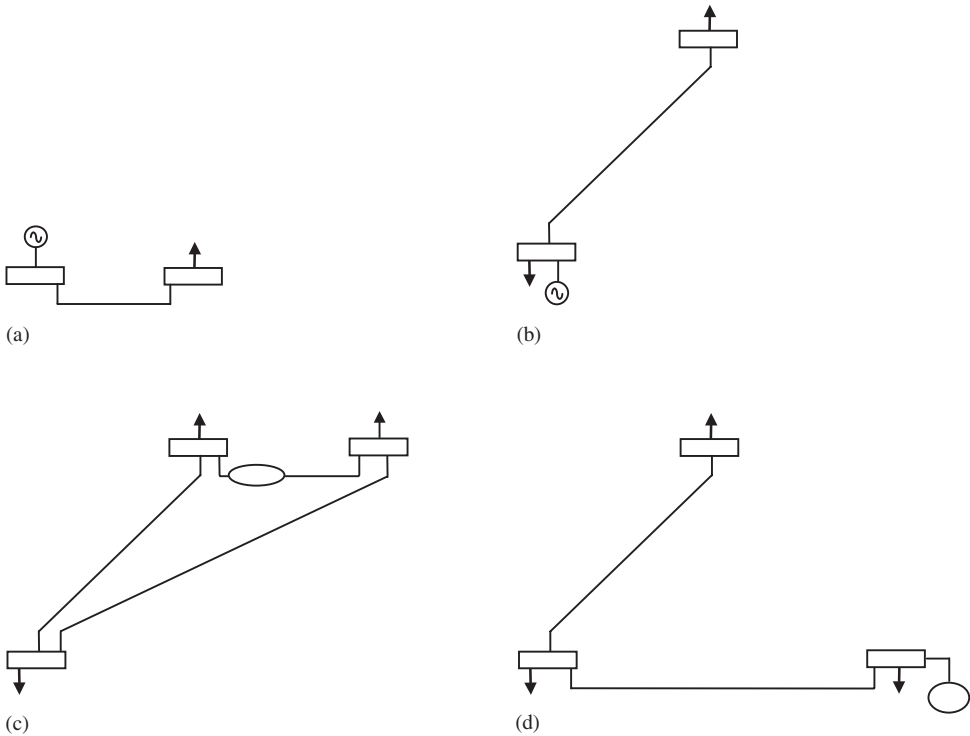


**Figure 8.17** Reactive dominions: (a) Gen–North, (b) Gen–South, (c) unified power flow converter, and (d) static compensator

**Table 8.8** Dominion contributions to system loads

	South	Elm	Main	Lake
Gen–North	0.0	0.0	0.0	1.4
Gen–South	4.1	0.0	0.0	1.6
UPFC	0.3	0.0	1.6	2.9
STATCOM	1.2	8.0	0.0	0.5
TL: North–Lake	0.0	0.0	0.0	2.6
TL: South–Lake	0.0	0.0	0.0	2.7
TL: North–South	2.3	0.0	0.0	2.4
TL: Main–South	1.4	0.0	0.0	0.5
TL: Lake–Main	0.1	0.0	1.6	0.2
TL: Main–Elm	0.6	2.0	1.8	0.2
Total load at node	10	10	5	15

Note: STATCOM, static compensator; UPFC, unified power flow controller; TL, transmission line; TL: South–Elm is absorbing MVAR.

sources of reactive power but they also form part of various dominions. Table 8.8 shows the contributions of the various sources to the individual reactive system loads.

### 8.6.4 Large Network

In order to show how the tracing algorithm works with a larger power system, the New Zealand South Island 220 kV system illustrated in Figure 8.18 is used to carry out this study. The system data are given in Arrillaga and Watson (2001).

From the power flow solution, it emerges that there are two machines that contribute substantial reactive power injections into their connecting nodes. These synchronous machines are the one connected at Islington–220 and the one connected at Benmore–016.

The synchronous machine's dominion connected to Islington–220 is depicted schematically in Figure 8.19 together with the system contribution to reactive power flow in this particular dominion.

In this case, the transformers complex taps have been set to nominal values (i.e. the transformer equivalent circuits do not contain shunt admittances).

Information on the Islington–220 dominion is shown in Table 8.9. The reactive power absorption of each line is depicted in Table 8.10.

### 8.6.5 Tracing the Power Output of a Wind Generator

With the ongoing deregulation of the electricity supply industry, the opportunity has arisen for the widespread incorporation of renewable sources of electricity into the power network. In the United Kingdom, for instance, wind generation is a form of renewable generation that is set to experience unprecedented growth, in particular, offshore wind generation.

Among the pressing problems that the industry will have to solve, if electricity generation from the wind is to become commercially successful in a deregulated environment,

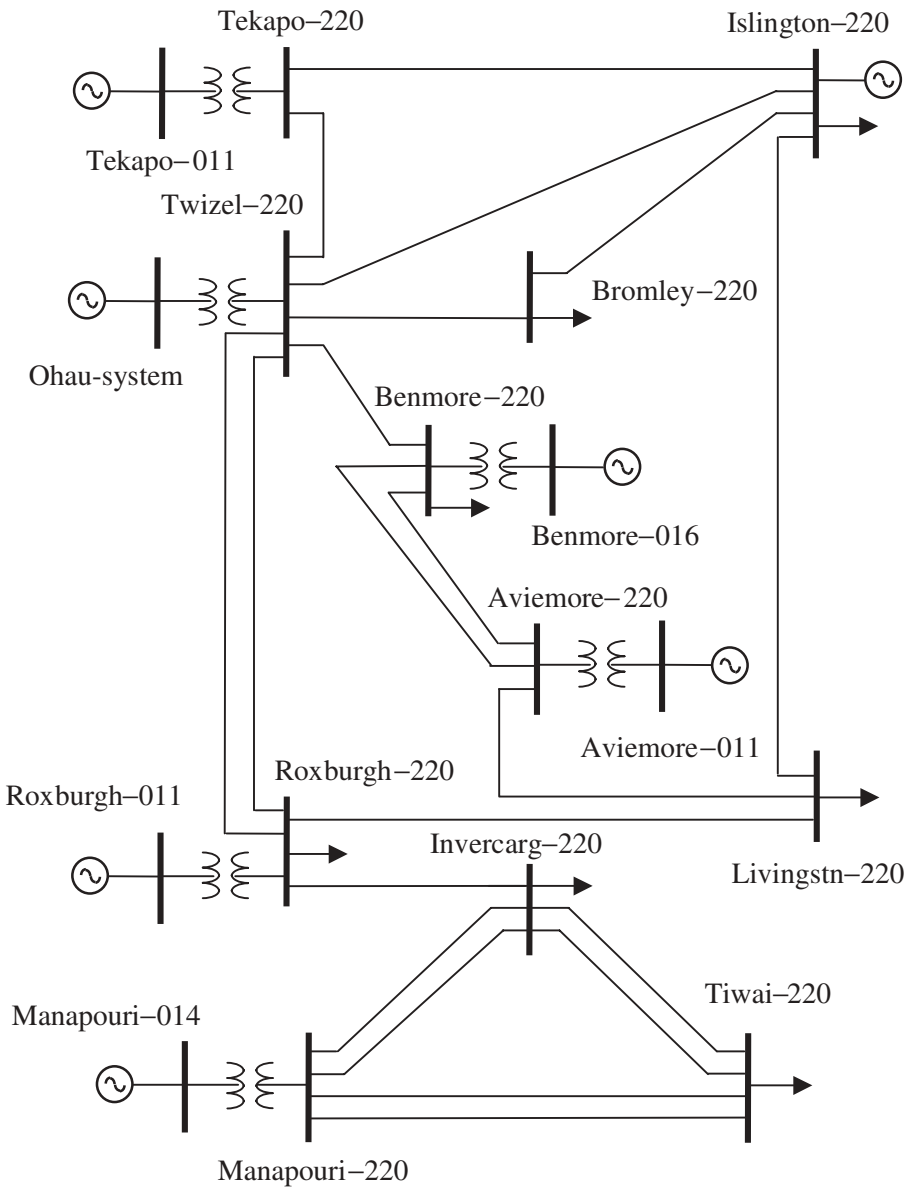


**Figure 8.18** The New Zealand South Island 220 kV system. Reproduced by permission of John Wiley & Sons Ltd from J. Arrillaga and N.R. Watson, 2001, *Computer Modelling of Electrical Power System*, 2nd edn

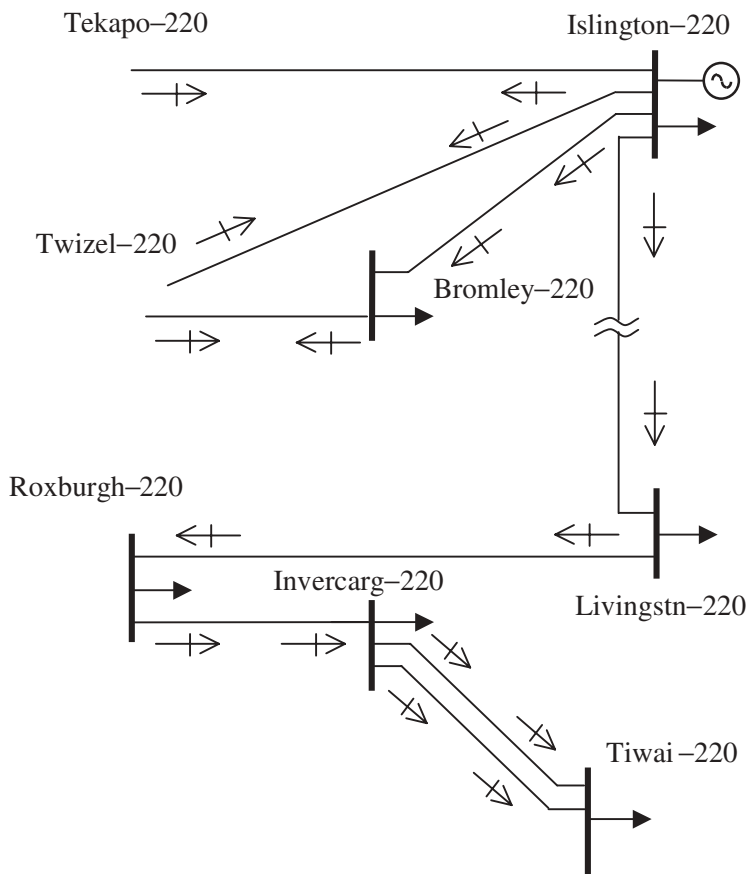


**Figure 8.19** Islington-220 reactive power dominion

**Table 8.9** Islington-220 dominion: general data

Index	Sending end	Receiving end	Q absorbed (MVAR)
TL1	Islington-220	Tekapo-220	42.5108
TL2	Islington-220	Twizel-220	40.7907
TL3	Islington-220	Bromley-220	0.8010
TL4	Bromley-220	Twizel-220	38.2211
TL5	Islington-220	Livingstn-220	19.1111
TL6	Livingstn-220	Roxburgh-220	74.0988
TL7	Roxburgh-220	Invercarg-220	5.6353
TL8	Invercarg-220	Tiwai-220	0.4756
TL9	Invercarg-220	Tiwai-220	0.4756

**Table 8.10** Line contributions to reactive power absorption

Index	Q (MVAR)			Contribution coefficients
	Outflow	Inflow	Contributed	
TL1:				
dominion	17.0548	0.0000	17.0548	0.4012
system	17.5000	-7.9559	25.4560	0.5988
TL2:				
dominion	12.0992	0.0000	12.0992	0.2966
system	22.5000	-6.1915	28.6915	0.7034
TL3:				
dominion	62.3661	61.5959	0.7701	0.9615
system	2.5000	2.4691	0.0309	0.0385
TL4:				
dominion	6.0533	0.0000	6.0532	0.1584
system	22.7513	-9.41658	32.1678	0.8416
TL5:				
dominion	25.3950	14.0807	11.3143	0.5920
system	17.5000	9.70321	7.7968	0.4080
TL6:				
dominion	7.78264	0.7990	6.9836	0.0942
system	26.6437	2.7355	23.9082	0.3226
TL7:				
dominion	0.3232	0.2860	0.0372	0.0066
system	28.3145	25.0573	3.2572	0.5780
TL8:				
dominion	0.0873	0.0863	0.0010	0.0021
system	22.0149	21.7640	0.2501	0.5277
TL9:				
dominion	0.0873	0.0863	0.0010	0.0021
system	22.0149	21.7640	0.2501	0.5277

is to develop an understanding of the impact that large, random blocks of electricity will have on the power network. For instance, how much electricity can a wind-generating company, under obligation to supply, afford to contract to supply given its ‘fuel’ supply uncertainty?

An equally critical issue that needs addressing concerns the ability to trace the power output of one or more wind farms within an interconnected network. This has a direct bearing on the aspirations of a growing number of consumers keen on being supplied with electricity that has been produced with little damage to the environment. The power tracing methodology offers a realistic possibility of achieving this goal and one that should encourage providers of clean energy.

The numerical example presented in this section addresses one way in which the tracing methodology can be applied in the area of delivery of clean power. This requires a simulation environment similar to the one shown in Figure 8.20, where the interaction of the

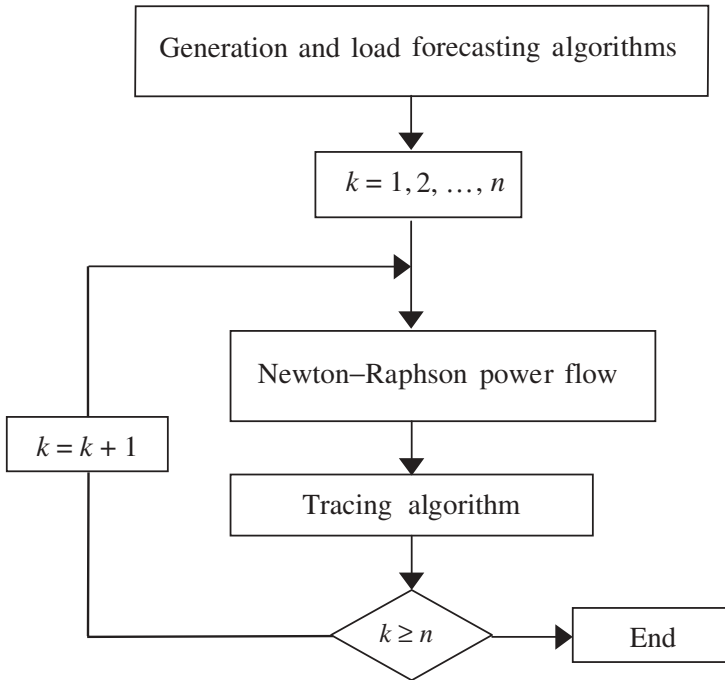


**Figure 8.20** Power flow simulation environment

forecasting, power flow, and power tracing algorithms is illustrated. This simulation environment offers a simple and yet comprehensive way of modelling time-dependent generators and loads.

### 8.6.5.1 The wind generator model

Wind generators slaved to the power network are mostly of the induction type. During high winds, when the rotor speed supersedes the synchronous speed, active power is injected into the grid. In the presence of low winds there is an automatic cutout to prevent motoring from happening. During normal conditions, the turbine operates at nearly constant frequency. The induction wind generator achieves its operation at the expense of consuming reactive power. From the power flow point of view, it makes engineering sense to treat the generator bus as a  $PQ$  bus with a positive active power injection and a negative reactive power injection.

However, these power injections must be time-dependent to reflect the stochastic nature of the prime mover (i.e. the wind). Figure 8.21 shows the active power output of a typical wind farm for a period of 54 hours, where very large variations between measurements are observed; for example, the generator goes from zero power output at 16 hours, to 1.8 MW at 18 hours (Johansson *et al.*, 1992). For cases of wind farms of low capacity, their reactive power requirements can be met locally. Moreover, if suitable power electronics equipment is

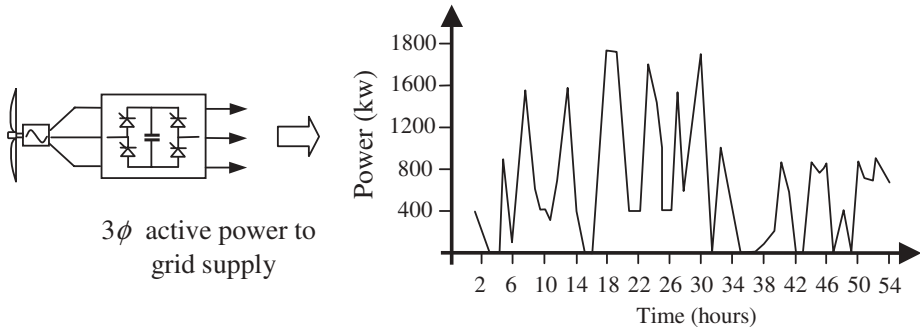


**Figure 8.21** Wind generator model for power flow studies that caters for time dependency

used in tandem with the wind generator set then the reactive power compensation can be met adaptively.

### 8.6.5.2 Numerical example

This numeric example illustrates how the simulation environment of Figure 8.20 works. The example relates to the power network shown in Figure 8.22, where only active power flows are shown. In this example all the power flows are expressed in kilowatts. Generator  $G_2$  is a wind generator with the power generation profile shown in Figure 8.21. The output of generator  $G_3$  and loads are taken to remain constant. Generator  $G_1$  is the slack generator. By

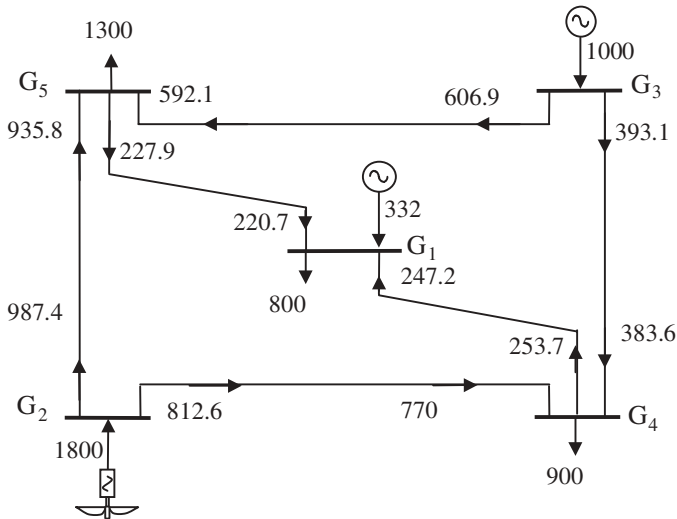


**Figure 8.22** Power flows (in kilowatts) when the wind generator injects maximum active power (i.e. 1.8 MW)

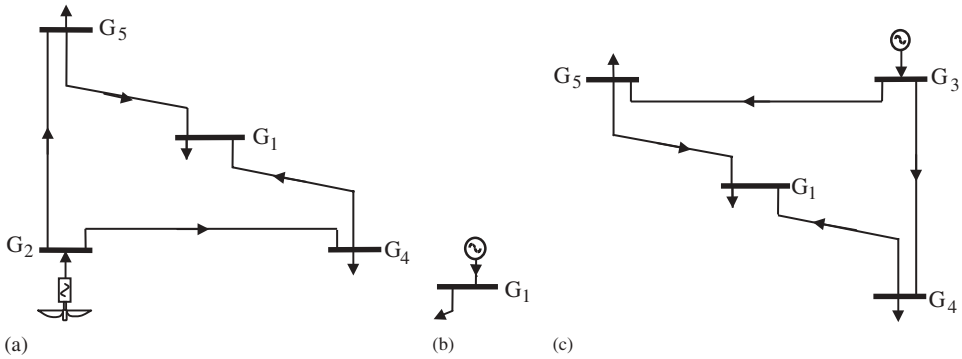


**Figure 8.23** Dominions of (a) generator G<sub>2</sub>, (b) generator G<sub>1</sub>, and (c) generator G<sub>3</sub>

way of example, two cases are considered below: (1) at 18 hours when the wind generator is injecting maximum power (i.e. 1.8 MW) and (2) at 36 hours when it is injecting zero power.

*The wind generator injects maximum power*

Figure 8.22 shows the power flows for the case when the wind generator is injecting 1.8 MW. Based on these power flows, three network dominions are determined. Figure 8.23 shows the dominions of generators G<sub>1</sub>–G<sub>3</sub>.

It can be observed in Figure 8.23 that branches 4–1 and 5–1 are common to the dominions of generator 2 and generator 3. Using the tracing algorithm, the contribution of both dominions to each element of the network are calculated. Active power losses and charges for use of line associated with each dominion are then established. This information is summarised in Table 8.11.

The charge for use of line to dominion *k*, in branch *ij*, is calculated as follows:

$$E_{D_k} = \left( \frac{x_{ij}}{L_{Total}} \right) L_{D_k}, \tag{8.42}$$

where *x<sub>ij</sub>* is the company charge assigned to the use of branch *ij*.

*The wind generator contributes no active power*

Figure 8.24(a) shows the power flows for the case when the wind generator contributes no active power. The directed subgraphs for the two dominions are shown in Figures 8.24(b) and 8.24(c). The contribution of dominions D<sub>1</sub> and D<sub>3</sub> to active power losses throughout the network become readily available. Table 8.12 gives the power losses and charges for use of line.

**Table 8.11** System power losses and charges for use of line to dominions D<sub>2</sub> and D<sub>3</sub>

Branch	Sending end			Receiving end			Power loss				
	$C'$	$P'_{D_2}$ (KW)	$P'_{D_3}$ (KW)	$C''$	$P''_{D_2}$ (KW)	$P''_{D_3}$ (KW)	D <sub>2</sub>	D <sub>3</sub>	Charge (p.u.)	E <sub>D<sub>2</sub></sub> (p.u.)	E <sub>D<sub>3</sub></sub> (p.u.)
3-5	0.6069	0	606.9	0.5921	0	592.1	0	14.8	$x_{35}$	0	$x_{55}$
3-4	0.3931	0	393.1	0.3836	0	383.6	0	9.5	$x_{34}$	0	$x_{14}$
4-1	0.2199	169.3	84.4	0.2143	165.0	82.2	4.3	2.2	$x_{41}$	0.6615 $x_{41}$	0.3384 $x_{41}$
5-1	0.1492	139.6	88.3	0.1444	135.2	85.5	4.4	2.8	$x_{51}$	0.6111 $x_{51}$	0.3889 $x_{51}$
2-4	0.5486	812.6	0	0.5206	770.0	0	42.6	0	$x_{24}$	$x_{24}$	0
2-5	0.4514	987.4	0	0.4278	935.8	0	51.8	0	$x_{25}$	$x_{25}$	0

Note:  $x_{ij}$ , company charge assigned to use of branch  $ij$ .

**Table 8.12** System power losses and charges for use of line to dominions D<sub>1</sub> and D<sub>3</sub>

Branch	Sending end			Receiving end			Power loss				
	$C'$	$P'_{D_1}$ (kW)	$P'_{D_3}$ (kW)	$C''$	$P''_{D_1}$ (kW)	$P''_{D_3}$ (kW)	D <sub>1</sub>	D <sub>3</sub>	Charge (p.u.)	E <sub>D<sub>1</sub></sub> (p.u.)	E <sub>D<sub>3</sub></sub> (p.u.)
3-5	0.6295	0	629.5	0.6134	0	613.14	0	16.1	$x_{35}$	0	$x_{35}$
3-4	0.3705	0	370.5	0.3620	0	362.0	0	7.5	$x_{34}$	0	$x_{34}$
4-1	0.2761	566.1	0	0.2809	576.1	0	10	0	$x_{41}$	$x_{41}$	0
5-1	0.3223	661.0	0	0.3290	674.6	0	13.6	0	$x_{51}$	$x_{51}$	0
2-4	0.0291	16.47	10.53	0.0303	17.14	10.96	0.67	0.43	$x_{24}$	0.6091 $x_{24}$	0.3909 $x_{24}$
2-5	1	16.47	10.53	0.9481	15.62	9.98	0.85	0.55	$x_{25}$	0.6072 $x_{25}$	0.3928 $x_{25}$

Note: See Table 8.11.

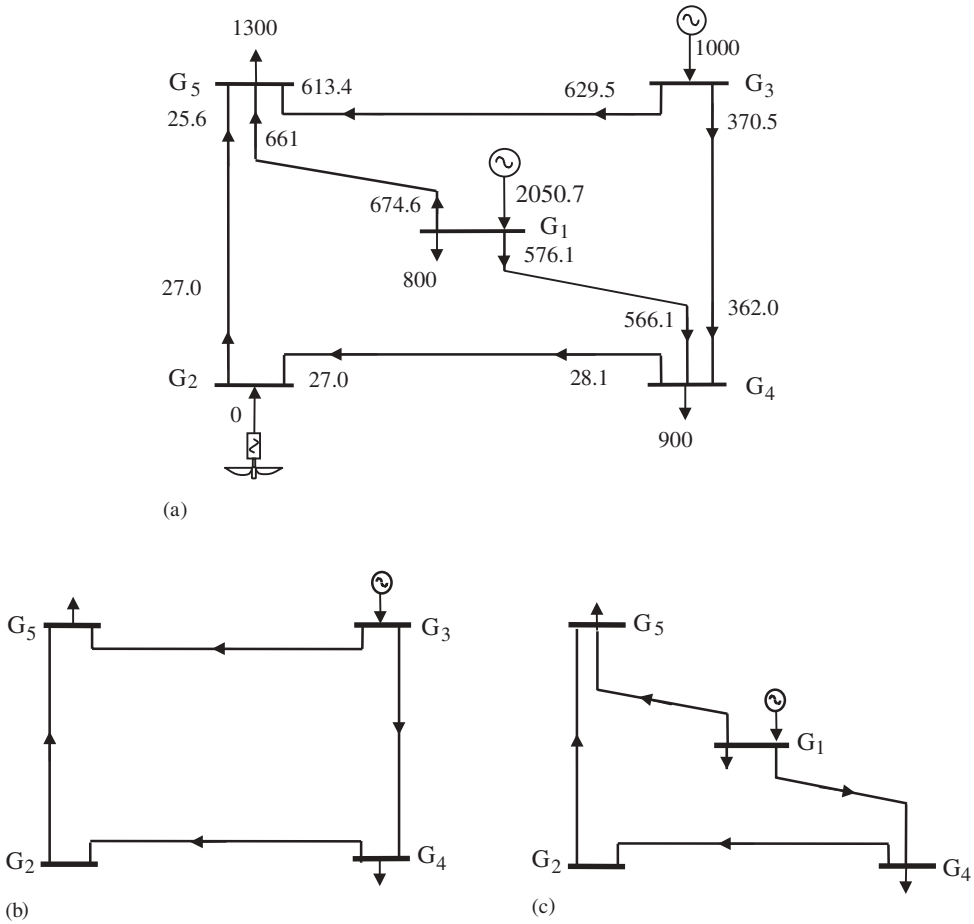


**Figure 8.24** (a) Power flows in the test network for the case when the wind generator,  $G_2$ , contributes no active power (i.e. 0 MW); directed subgraph for (b) dominion  $D_1$  and (c) dominion  $D_3$

### 8.7 SUMMARY

The relentless trend towards deregulation and unbundling of transmission services in the electricity supply industry has provided the motivation for developing methodologies that trace the output of each generator throughout a power system, whether it is a simple radial network or an interconnected network of national or even continental dimensions. Over the last few years a great deal of progress has been made in this direction, and methods based on the principle of proportional sharing are well regarded in academic circles. Several alternative algorithms have appeared in the open literature since 1996, with a large proportion of these papers devoted to economic issues. However, other applications are beginning to emerge such as the tracing of power contributed by ‘green’ generators and distortion power contributed by harmonic sources.

The tracing algorithm we have detailed in this chapter is the one we developed at Glasgow, but the application cases contained in this chapter can equally be solved by using any of the alternative methodologies found in the open literature. The algorithm may serve the purpose of auditing the individual generator contributions to system loading, power flows, transmission losses, generation costs, and charges for use of lines. The algorithm is independently applied to the tracing of active, reactive, and distortion powers. The algorithm is accurate and comprehensive. In fact, power flow tracing is only a mechanism for tracing, for instance, generation costs and allocating charges for use of line. These two basic capabilities of the algorithm have been compared with results corresponding to a simple case available in the open literature. Also, a larger study involving a subsection of an interconnected power network has been conducted.

## REFERENCES

- Acha, E., 1998, 'Tracing Wind Power in a Pooled Transmission System', EPSOM'98, Zurich, Switzerland, September 1998, pp. 23–25.
- Acha, E., Fuente-Esquivel, C.R., Chua C.S., 1996, 'On the Auditing of Individual Generator Contributions to Power Flows and Losses in Meshed Power Networks', RVP 96-SIS-10, Reunion de Verano de Potencia, IEEE Sección México, Acapulco Gro., Mexico, July 1996, pp. 170–173.
- Acha, E. Ambriz-Perez, H., Fuente-Esquivel, C.R., Chua, C.S., 1997, 'On the Auditing of Individual Generator Contributions to Optimal Power Flows, Losses and Costing of Large, Interconnected Power Networks', *IPEC'97 Proc., Volume II, Nanyang University, Singapore, May 1997*, pp. 22–24.
- Acha, E., Tortelli, O.L., Angeles-Camacho, C., Santos Jr, A., 2003, 'Reactive Power Tracking in FACS Upgraded Power Networks', IASTED, Proceedings of The Third IASTED International Conference on Power and Energy Systems, Marbella, Spain, September 2003.
- Arrillaga, J., Watson, N.R., 2001, *Computer Modelling of Electrical Power System*. 2nd edn, John Wiley & Sons, Chichester.
- Bialek, J., 1996, 'Tracing the Flow Electricity', *IEE Proc.* **143**(4) 313–320.
- Bialek, J., 1997, 'Topological Generation and Load Distribution Factors for Supplemental Charge Allocation in Transmission Open Access', *IEEE Trans. on Power Systems* **12**(3) 1185–1193.
- Bialek, J., 1998, 'Allocation of Transmission Supplementary Charges to Real and Reactive Loads', *IEEE Trans. on Power Systems* **13**(3) 749–754.
- EPEW, 1993, 'An Introduction to Pool Rules', April 1993, Electric Pool of England and Wales, London.
- Johansson, T.B., Kelly, H., Reddy, A.K.N., Willians, R.H., 1992, *Renewable Energy: Sources for Fuel and Electricity*, Earthscan Publications London.
- Kirschen, D., Strbac, G., 1999, 'Tracing Active and Reactive Power between Generators and Loads Using Real and Imaginary Currents', *IEEE Trans. on Power Systems* **14**(4) 1312–1319.
- Kirschen, D., Allan, R.N., Strbac, G., 1997, 'Contributions of Individual Generators to Loads and Flows', *IEEE Trans. on Power Systems* **12**(1) 52–60.
- Laguna-Velasco, R., 2002, *Asignación de cargos por el porteo de flujos de potencia activa y reactiva en los sistemas de transmisión basada en el método de rastreo de la electricidad*, MSc thesis (in Spanish), Centro de Investigación Avarzada del Instituto Politécnico Nacional, Unidad Guadalajara, Mexico.
- Laguna-Velasco, R., Fuente-Esquivel, C.R., Acha, E., Ambriz-Perez, H., 2001, 'On the Auditing of Individuals Generator Contributions to Reactive Power Flows in Power Networks', paper presented at the IEEE Powertech Conference, Porto, Portugal, September 2001.

- Macqueen, C.N., 1993, *Time-based Load Flow Analysis and Loss Costing in Electrical Distribution System*, PhD thesis, School of Engineering, University of Durham, Durham.
- Ng, W.Y., 1981, 'Generalised Generation Distribution Factors for Power Systems Security Evaluations', *IEEE Trans. Power App. Systems* **PAS-100**(3) 1001–1005.
- 'Recovery of Cost under BETTA and Ofgem/DTI Conclusions Document', July 2003, OFGEM (Office of Gas and Electricity Markets), London.
- Reta, R., Vargas, A., 2001, 'Electricity Tracing and Loss Allocation Methods Based on Electric Concepts', *IEE Proc. on Gener. Transm. Distrib.* **148**(6) 518–522.
- Saunders, B., Boag M., 2001, 'NETA: A Dramatic Change', Conseil International des Grands Reseaux Électriques (CIGRÉ), *Electra* No. 199, 14–23.
- Secretary of State for Energy, 1988, *Privatising Electricity – The Government's Proposals for the Privatisation of the Electric Supply Industry in England and Wales*, February 1988, Her Majesty's Stationary Office, London.



# Appendix A: Jacobian Elements for FACTS Controllers in Positive Sequence Power Flow

## A.1 TAP-CHANGING TRANSFORMER

The partial derivatives of the power equations with respect to the primary tap of the two winding transformer are:

$$\begin{aligned} \frac{\partial P_k}{\partial T_v} T_v &= \frac{2V_k^2 T_v^2}{\Delta} [R_m(U_v^2 + R_1) + X_m R_2 - 2G_{kk}(R_m F_1 + X_m F_2)] + V_k V_m [G_{km} \cos(\delta_1) \\ &\quad + B_{km} \sin(\delta_1)] \left[ 1 - \frac{4T_v^2}{\Delta} (R_m F_1 + X_m F_2) \right] + \frac{2V_k V_m T_v^3 U_v}{\Delta} [X_m \sin(\delta_1 - \phi_1) \\ &\quad - R_m \cos(\delta_1 - \phi_1)], \\ \frac{\partial Q_k}{\partial T_v} T_v &= \frac{2V_k^2 T_v^2}{\Delta} [2B_{kk}(R_m F_1 + X_m F_2) - R_m R_2 + X_m (U_m^2 + R_1)] + V_k V_m [G_{km} \sin(\delta_1) \\ &\quad - B_{km} \cos(\delta_1)] \left[ 1 - \frac{4T_v^2}{\Delta} (R_m F_1 + X_m F_2) \right] \\ &\quad - \frac{2V_k V_m T_v^3 U_v}{\Delta} [R_m \sin(\delta_1 - \phi_1) + X_m \cos(\delta_1 - \phi_1)]. \end{aligned}$$

The partial derivatives of the power equations with respect to the secondary tap of the two winding transformer are:

$$\begin{aligned} \frac{\partial P_k}{\partial U_v} U_v &= \frac{2V_k^2 U_v^2}{\Delta} [R_m(U_v^2 + R_1) + X_k R_2 + F_1 - 2G_{kk}(R_k F_1 + X_k F_2)] \\ &\quad + V_k V_m [G_{km} \cos(\delta_1) + B_{km} \sin(\delta_1)] \left[ 1 - \frac{4U_v^2}{\Delta} (R_k F_1 + X_k F_2) \right] \\ &\quad + \frac{2V_k V_m U_v^3 T_v}{\Delta} [X_k \sin(\delta_1 - \phi_1) - R_k \cos(\delta_1 - \phi_1)], \end{aligned}$$

$$\begin{aligned} \frac{\partial Q_k}{\partial U_v} U_v &= \frac{2V_k^2 U_v^2}{\Delta} [2B_{kk}(R_k F_1 + X_k F_2) - R_k R_2 + X_k (U_v^2 + R_1 + F_2)] \\ &\quad + V_k V_m [G_{km} \sin(\delta_1) - B_{km} \cos(\delta_1)] \left[ 1 - \frac{4U_v^2}{\Delta} (R_k F_1 + X_k F_2) \right] \\ &\quad - \frac{2V_k V_m U_v^3 T_v}{\Delta} [R_k \sin(\delta_1 - \phi_1) + X_k \cos(\delta_1 - \phi_1)], \end{aligned}$$

where

$$\begin{aligned} F_1 &= T^2 R_s + U_v^2 R_p + R_{eq1}, \\ F_2 &= T_v^2 X_s + U_v^2 X_p + X_{eq1}, \\ R_{eq1} &= (R_p R_s - X_p X_s) G_o - (R_p X_s + R_s X_p) B_o, \\ X_{eq1} &= (R_p R_s - X_p X_s) B_o + (R_p X_s + R_s X_p) G_o, \\ R_1 &= R_s G_o - X_s B_o, \\ R_2 &= R_s B_o + X_s G_o, \\ R_3 &= R_p G_o - X_p B_o, \\ R_4 &= R_p B_o + X_p G_o, \\ \phi_1 &= \phi_{tv} - \phi_{uv}, \\ \phi_2 &= \phi_{uv} - \phi_{tv}, \\ \Delta &= F_1^2 + F_2^2, \\ \delta_1 &= \theta_k - \theta_m. \end{aligned}$$

## A.2 THYRISTOR-CONTROLLED SERIES COMPENSATOR

Partial derivatives of the variable series impedance model are:

$$\begin{aligned} \frac{\partial P_k}{\partial X} X &= -V_k V_m B_{km} \sin(\theta_k - \theta_m), \\ \frac{\partial Q_k}{\partial X} X &= V_k^2 B_{kk} + V_k V_m B_{km} \cos(\theta_k - \theta_m), \\ \frac{\partial P_{km}^X}{\partial X} X &= \frac{\partial P_k}{\partial X} X. \end{aligned}$$

Partial derivatives of the firing angle model:

$$\begin{aligned} \frac{\partial P_k}{\partial \alpha} &= P_k B_{TCSC(1)} \frac{\partial X_{TCSC(1)}}{\partial \alpha}, \\ \frac{\partial Q_k}{\partial \alpha} &= Q_k B_{TCSC(1)} \frac{\partial X_{TCSC(1)}}{\partial \alpha}, \\ \frac{\partial B_{TCSC(1)}}{\partial \alpha} &= B_{TCSC(1)}^2 \frac{\partial X_{TCSC(1)}}{\partial \alpha}, \\ \frac{\partial X_{TCSC(1)}}{\partial \alpha} &= -2C_1 [1 + \cos(2\alpha)] + C_2 \sin(2\alpha) \{ \varpi \tan[\varpi(\pi - \alpha)] - \tan \alpha \} \\ &\quad + C_2 \left\{ \varpi^2 \frac{\cos^2(\pi - \alpha)}{\cos^2[\varpi(\pi - \alpha)]} - 1 \right\}. \end{aligned}$$

### A.3 STATIC SYNCHRONOUS COMPENSATOR

Partial derivatives for the static compensator (STATCOM) model are:

$$\begin{aligned}
 \frac{\partial P_k}{\partial \theta_k} &= -Q_k - V_k^2 G_{vR}, \\
 \frac{\partial P_k}{\partial \delta_{vR}} &= V_k V_{vR} [G_{vR} \sin(\theta_k - \delta_{vR}) - B_{vR} \cos(\theta_k - \delta_{vR})], \\
 \frac{\partial P_{vR}}{\partial \delta_{vR}} &= -Q_{vR} - V_{vR}^2 B_{vR}, \\
 \frac{\partial P_{vR}}{\partial \theta_k} &= V_{vR} V_k [G_{vR} \sin(\delta_{vR} - \theta_k) - B_{vR} \cos(\delta_{vR} - \theta_k)], \\
 \frac{\partial P_k}{\partial V_k} V_k &= P_k + V_k^2 G_{vR}, \\
 \frac{\partial P_k}{\partial V_{vR}} V_{vR} &= V_k V_{vR} [G_{vR} \cos(\theta_k - \delta_{vR}) + B_{vR} \sin(\theta_k - \delta_{vR})], \\
 \frac{\partial P_{vR}}{\partial V_{vR}} V_{vR} &= P_{vR} + V_{vR}^2 G_{vR}, \\
 \frac{\partial P_{vR}}{\partial V_k} V_k &= V_{vR} V_k [G_{vR} \cos(\delta_{vR} - \theta_k) + B_{vR} \sin(\delta_{vR} - \theta_k)], \\
 \frac{\partial Q_k}{\partial \theta_k} &= P_k - V_k^2 G_{vR}, \\
 \frac{\partial Q_k}{\partial \delta_{vR}} &= -V_k V_{vR} [G_{vR} \cos(\theta_k - \delta_{vR}) + B_{vR} \sin(\theta_k - \delta_{vR})], \\
 \frac{\partial Q_{vR}}{\partial \delta_{vR}} &= P_{vR} - V_{vR}^2 G_{vR}, \\
 \frac{\partial Q_{vR}}{\partial \theta_k} &= -V_{vR} V_k [G_{vR} \cos(\delta_{vR} - \theta_k) + B_{vR} \sin(\delta_{vR} - \theta_k)], \\
 \frac{\partial Q_k}{\partial V_k} V_k &= Q_k - V_k^2 B_{vR}, \\
 \frac{\partial Q_k}{\partial V_{vR}} V_{vR} &= V_k V_{vR} [G_{vR} \sin(\theta_k - \delta_{vR}) - B_{vR} \cos(\theta_k - \delta_{vR})], \\
 \frac{\partial Q_{vR}}{\partial V_{vR}} V_{vR} &= Q_{vR} - V_{vR}^2 B_{vR}, \\
 \frac{\partial Q_{vR}}{\partial V_k} V_k &= -V_{vR} V_k [G_{vR} \sin(\delta_{vR} - \theta_k) - B_{vR} \cos(\delta_{vR} - \theta_k)].
 \end{aligned}$$

### A.4 UNIFIED POWER FLOW CONTROLLER

Partial derivatives for the unified power flow controller (UPFC) at bus  $k$  are:

$$\begin{aligned}
 \frac{\partial P_k}{\partial \theta_k} &= -Q_k - V_k^2 B_{kk}, \\
 \frac{\partial Q_k}{\partial \theta_k} &= P_k - V_k^2 G_{kk},
 \end{aligned}$$

$$\begin{aligned}
\frac{\partial P_k}{\partial \theta_m} &= V_k V_m [G_{km} \sin(\theta_k - \theta_m) - B_{km} \cos(\theta_k - \theta_m)], \\
\frac{\partial Q_k}{\partial \theta_m} &= -N_{km}, \\
\frac{\partial P_k}{\partial V_k} V_k &= P_k + V_k^2 G_{kk}, \\
\frac{\partial Q_k}{\partial V_m} V_m &= H_{km}, \\
\frac{\partial P_k}{\partial V_m} V_m &= V_k V_m [G_{km} \cos(\theta_k - \theta_m) + B_{km} \sin(\theta_k - \theta_m)], \\
\frac{\partial Q_k}{\partial V_k} V_k &= Q_k - V_k^2 B_{kk}, \\
\frac{\partial P_k}{\partial \delta_{cR}} &= V_k V_{cR} [G_{km} \sin(\theta_k - \delta_{cR}) - B_{km} \cos(\theta_k - \delta_{cR})], \\
\frac{\partial Q_k}{\partial \theta_{cR}} &= -N_{kcR}, \\
\frac{\partial P_k}{\partial V_{cR}} V_{cR} &= V_k V_{cR} [G_{km} \cos(\theta_k - \delta_{cR}) + B_{km} \sin(\theta_k - \delta_{cR})], \\
\frac{\partial Q_k}{\partial V_{cR}} V_{cR} &= H_{kcR}, \\
\frac{\partial P_k}{\partial \theta_{vR}} &= V_k V_{vR} [G_{vR} \sin(\theta_k - \delta_{vR}) - B_{vR} \cos(\theta_k - \delta_{vR})], \\
\frac{\partial Q_k}{\partial \theta_{vR}} &= -N_{kvR}, \\
\frac{\partial P_k}{\partial V_{vR}} V_{vR} &= V_k V_{vR} [G_{vR} \cos(\theta_k - \delta_{vR}) + B_{vR} \sin(\theta_k - \delta_{vR})], \\
\frac{\partial Q_k}{\partial V_{vR}} V_{vR} &= H_{kvR}.
\end{aligned}$$

Partial derivatives at the receiving bus  $m$  are:

$$\begin{aligned}
H_{mk} &= \frac{\partial P_m}{\partial \theta_k} = V_m V_k [G_{mk} \sin(\theta_m - \theta_k) - B_{mk} \cos(\theta_m - \theta_k)], \\
\frac{\partial Q_m}{\partial \theta_k} &= -N_{mk}, \\
H_{mm} &= \frac{\partial P_m}{\partial \theta_m} = -Q_m - V_m^2 B_{mm}, \\
\frac{\partial Q_m}{\partial \theta_m} &= P_m - V_m^2 G_{mm}, \\
N_{mk} &= \frac{\partial P_m}{\partial V_k} V_k = V_m V_k [G_{mk} \cos(\theta_m - \theta_k) + B_{mk} \sin(\theta_m - \theta_k)], \\
\frac{\partial Q_m}{\partial V_k} V_k &= H_{mk},
\end{aligned}$$

$$\begin{aligned}
N_{mm} &= \frac{\partial P_m}{\partial V_m} V_m = P_m + V_m^2 G_{mm}, \\
\frac{\partial Q_m}{\partial V_m} V_m &= Q_m - V_m^2 B_{mm}, \\
H_{mcR} &= \frac{\partial P_m}{\partial \theta_{cR}} = V_m V_{cR} [G_{mm} \sin(\theta_m - \delta_{cR}) - B_{mm} \cos(\theta_m - \delta_{cR})], \\
\frac{\partial Q_m}{\partial \theta_{cR}} &= -N_{mcR}, \\
N_{mcR} &= \frac{\partial P_m}{\partial V_{cR}} V_{cR} = V_m V_{cR} [G_{mm} \cos(\theta_m - \delta_{cR}) - B_{mm} \sin(\theta_m - \delta_{cR})], \\
\frac{\partial Q_m}{\partial V_{cR}} V_{cR} &= H_{mcR}.
\end{aligned}$$

The partial derivatives at the UPFC series converter are:

$$\begin{aligned}
\frac{\partial P_{cR}}{\partial \theta_k} &= V_{cR} V_k [G_{km} \sin(\delta_{cR} - \theta_k) - B_{km} \cos(\delta_{cR} - \theta_k)], \\
\frac{\partial P_{cR}}{\partial \delta_{cR}} &= -Q_{cR} - V_{cR}^2 B_{mm}, \\
\frac{\partial P_{cR}}{\partial \theta_m} &= V_{cR} V_m [G_{mm} \sin(\delta_{cR} - \theta_m) - B_{mm} \cos(\delta_{cR} - \theta_m)], \\
\frac{\partial P_{cR}}{\partial V_{cR}} V_{cR} &= P_{cR} + V_{cR}^2 G_{mm}, \\
\frac{\partial P_{cR}}{\partial V_k} V_k &= V_{cR} V_k [G_{km} \cos(\delta_{cR} - \theta_k) + B_{km} \sin(\delta_{cR} - \theta_k)], \\
\frac{\partial P_{cR}}{\partial V_m} V_m &= V_{cR} V_m [G_{mm} \cos(\delta_{cR} - \theta_m) + B_{mm} \sin(\delta_{cR} - \theta_m)].
\end{aligned}$$

The partial derivatives for the UPFC shunt converter are:

$$\begin{aligned}
\frac{\partial P_{vR}}{\partial \theta_k} &= V_{vR} V_k [G_{vR} \sin(\delta_{vR} - \theta_k) - B_{vR} \cos(\delta_{vR} - \theta_k)], \\
\frac{\partial P_{vR}}{\partial \delta_{vR}} &= -Q_{vR} - V_{vR}^2 B_{vR}, \\
\frac{\partial P_{vR}}{\partial V_k} V_k &= V_{vR} V_k [G_{vR} \cos(\delta_{vR} - \theta_k) + B_{vR} \sin(\delta_{vR} - \theta_k)], \\
\frac{\partial P_{vR}}{\partial V_{vR}} V_{vR} &= P_{vR} + V_{vR}^2 G_{vR}.
\end{aligned}$$

## A.5 HIGH-VOLTAGE DIRECT-CURRENT-BASED VOLTAGE SOURCE CONVERTER

Partial derivatives for the rectifier and inverter stations of the high-voltage direct-current-based voltage source converter (HVDC-SVC) are:

$$\frac{\partial P_k}{\partial \theta_k} = -Q_k - V_k^2 G_{vR1},$$

$$\frac{\partial P_k}{\partial \delta_{vR1}} = -V_k V_{vR1} [G_{vR1} \sin(\theta_k - \delta_{vR1}) - B_{vR1} \cos(\theta_k - \delta_{vR1})],$$

$$\frac{\partial P_k}{\partial V_k} V_k = P_k + V_k^2 G_{vR1},$$

$$\frac{\partial P_k}{\partial V_{vR1}} V_{vR1} = -V_k V_{vR1} [G_{vR1} \cos(\theta_k - \delta_{vR1}) + B_{vR1} \sin(\theta_k - \delta_{vR1})],$$

$$\frac{\partial Q_k}{\partial \theta_k} = P_k - V_k^2 G_{vR1},$$

$$\frac{\partial Q_k}{\partial \delta_{vR1}} = V_k V_{vR1} [G_{vR1} \cos(\theta_k - \delta_{vR1}) + B_{vR1} \sin(\theta_k - \delta_{vR1})],$$

$$\frac{\partial Q_k}{\partial V_k} V_k = Q_k - V_k^2 B_{vR1},$$

$$\frac{\partial Q_k}{\partial V_{vR1}} V_{vR1} = -V_k V_{vR1} [G_{vR1} \sin(\theta_k - \delta_{vR1}) - B_{vR1} \cos(\theta_k - \delta_{vR1})],$$

$$\frac{\partial P_{vR1}}{\partial \delta_{vR1}} = -Q_{vR1} - V_{vR1}^2 B_{vR1},$$

$$\frac{\partial P_{vR1}}{\partial \theta_k} = -V_{vR1} V_k [G_{vR1} \sin(\delta_{vR1} - \theta_k) - B_{vR1} \cos(\delta_{vR1} - \theta_k)],$$

$$\frac{\partial P_{vR1}}{\partial V_{vR1}} V_{vR1} = P_{vR1} + V_{vR1}^2 G_{vR1},$$

$$\frac{\partial P_{vR1}}{\partial V_k} V_k = -V_{vR1} V_k [G_{vR1} \cos(\delta_{vR1} - \theta_k) + B_{vR1} \sin(\delta_{vR1} - \theta_k)],$$

$$\frac{\partial Q_{vR1}}{\partial \delta_{vR1}} = P_{vR1} - V_{vR1}^2 G_{vR1},$$

$$\frac{\partial Q_{vR1}}{\partial \theta_k} = V_{vR1} V_k [G_{vR1} \cos(\delta_{vR1} - \theta_k) + B_{vR1} \sin(\delta_{vR1} - \theta_k)],$$

$$\frac{\partial Q_{vR1}}{\partial V_{vR1}} V_{vR1} = Q_{vR1} - V_{vR1}^2 B_{vR1},$$

$$\frac{\partial Q_{vR1}}{\partial V_k} V_k = -V_{vR1} V_k [G_{vR1} \sin(\delta_{vR1} - \theta_k) - B_{vR1} \cos(\delta_{vR1} - \theta_k)],$$

$$\frac{\partial P_{HVDC}}{\partial \theta_k} = -Q_k - V_k^2 G_{vR1},$$

$$\frac{\partial P_{HVDC}}{\partial \delta_{vR1}} = -V_k V_{vR1} [G_{vR1} \sin(\theta_k - \delta_{vR1}) - B_{vR1} \cos(\theta_k - \delta_{vR1})],$$

$$\frac{\partial P_{HVDC}}{\partial V_k} V_k = P_k + V_k^2 G_{vR1},$$

$$\frac{\partial P_{HVDC}}{\partial V_{vR1}} V_{vR1} = -V_k V_{vR1} [G_{vR1} \cos(\theta_k - \delta_{vR1}) + B_{vR1} \sin(\theta_k - \delta_{vR1})],$$

$$\frac{\partial P_{HVDC}}{\partial \delta_{vR2}} = -Q_{vR2} - V_{vR2}^2 B_{vR2}.$$

# Appendix B: Gradient and Hessian Elements for Optimal Power Flow Newton's Method

## B.1 FIRST AND SECOND PARTIAL DERIVATIVES FOR TRANSMISSION LINES

### B.1.1 The Gradient Vector

The first partial derivatives with respect to the state variables at bus  $k$  are:

$$\begin{aligned}\frac{\partial L}{\partial \theta_k} &= \lambda_{pk} \frac{\partial P_k}{\partial \theta_k} + \lambda_{qk} \frac{\partial Q_k}{\partial \theta_k} + \lambda_{pm} \frac{\partial P_m}{\partial \theta_k} + \lambda_{qm} \frac{\partial Q_m}{\partial \theta_k}, \\ \frac{\partial L}{\partial \lambda_{pk}} &= P_k + P_{dk} - P_{gk}, \\ \frac{\partial L}{\partial V_k} &= \lambda_{pk} \frac{\partial P_k}{\partial V_k} + \lambda_{qk} \frac{\partial Q_k}{\partial V_k} + \lambda_{pm} \frac{\partial P_m}{\partial V_k} + \lambda_{qm} \frac{\partial Q_m}{\partial V_k}, \\ \frac{\partial L}{\partial \lambda_{qk}} &= Q_k + Q_{dk} - Q_{gk}.\end{aligned}$$

The first partial derivatives with respect to the state variables at bus  $m$  are:

$$\begin{aligned}\frac{\partial L}{\partial \theta_m} &= \lambda_{pk} \frac{\partial P_k}{\partial \theta_m} + \lambda_{qk} \frac{\partial Q_k}{\partial \theta_m} + \lambda_{pm} \frac{\partial P_m}{\partial \theta_m} + \lambda_{qm} \frac{\partial Q_m}{\partial \theta_m}, \\ \frac{\partial L}{\partial \lambda_{pm}} &= P_m + P_{dm} - P_{gm}, \\ \frac{\partial L}{\partial V_m} &= \lambda_{pk} \frac{\partial P_k}{\partial V_m} + \lambda_{qk} \frac{\partial Q_k}{\partial V_m} + \lambda_{pm} \frac{\partial P_m}{\partial V_m} + \lambda_{qm} \frac{\partial Q_m}{\partial V_m}, \\ \frac{\partial L}{\partial \lambda_{qm}} &= Q_m + Q_{dm} - Q_{gm}.\end{aligned}$$

### B.1.2 The Matrix $W$

The second partial derivatives with respect to the state variables at bus  $k$  are (diagonal blocks):

$$\begin{aligned}
 \frac{\partial^2 L}{\partial \theta_k^2} &= \lambda_{pk} \frac{\partial^2 P_k}{\partial \theta_k^2} + \lambda_{qk} \frac{\partial^2 Q_k}{\partial \theta_k^2} + \lambda_{pm} \frac{\partial^2 P_m}{\partial \theta_k^2} + \lambda_{qm} \frac{\partial^2 Q_m}{\partial \theta_k^2}, \\
 \frac{\partial^2 L}{\partial \theta_k \partial \lambda_{pk}} &= \frac{\partial^2 L}{\partial \lambda_{pk} \partial \theta_k} = \frac{\partial P_k}{\partial \theta_k}, \\
 \frac{\partial^2 L}{\partial \theta_k \partial V_k} &= \frac{\partial^2 L}{\partial V_k \partial \theta_k} = \lambda_{pk} \frac{\partial^2 P_k}{\partial \theta_k \partial V_k} + \lambda_{qk} \frac{\partial^2 Q_k}{\partial \theta_k \partial V_k} + \lambda_{pm} \frac{\partial^2 P_m}{\partial \theta_k \partial V_k} + \lambda_{qm} \frac{\partial^2 Q_m}{\partial \theta_k \partial V_k}, \\
 \frac{\partial^2 L}{\partial \theta_k \partial \lambda_{qk}} &= \frac{\partial^2 L}{\partial \lambda_{qk} \partial \theta_k} = \frac{\partial Q_k}{\partial \theta_k}, \\
 \frac{\partial^2 L}{\partial V_k^2} &= \lambda_{pk} \frac{\partial^2 P_k}{\partial V_k^2} + \lambda_{qk} \frac{\partial^2 Q_k}{\partial V_k^2} + \lambda_{pm} \frac{\partial^2 P_m}{\partial V_k^2} + \lambda_{qm} \frac{\partial^2 Q_m}{\partial V_k^2}, \\
 \frac{\partial^2 L}{\partial V_k \partial \lambda_{pk}} &= \frac{\partial^2 L}{\partial \lambda_{pk} \partial V_k} = \frac{\partial P_k}{\partial V_k}, \\
 \frac{\partial^2 L}{\partial V_k \partial \lambda_{qk}} &= \frac{\partial^2 L}{\partial \lambda_{qk} \partial V_k} = \frac{\partial Q_k}{\partial V_k}.
 \end{aligned}$$

The second partial derivatives with respect to the state variables at buses  $k$  and  $m$  are (off-diagonal blocks):

$$\begin{aligned}
 \frac{\partial^2 L}{\partial \theta_k \partial \theta_m} &= \frac{\partial^2 L}{\partial \theta_m \partial \theta_k} = \lambda_{pk} \frac{\partial^2 P_k}{\partial \theta_k \partial \theta_m} + \lambda_{qk} \frac{\partial^2 Q_k}{\partial \theta_k \partial \theta_m} + \lambda_{pm} \frac{\partial^2 P_m}{\partial \theta_k \partial \theta_m} + \lambda_{qm} \frac{\partial^2 Q_m}{\partial \theta_k \partial \theta_m}, \\
 \frac{\partial^2 L}{\partial \theta_k \partial \lambda_{pm}} &= \frac{\partial^2 L}{\partial \lambda_{pm} \partial \theta_k} = \frac{\partial P_m}{\partial \theta_k}, \\
 \frac{\partial^2 L}{\partial \theta_k \partial V_m} &= \frac{\partial^2 L}{\partial V_m \partial \theta_k} = \lambda_{pk} \frac{\partial^2 P_k}{\partial \theta_k \partial V_m} + \lambda_{qk} \frac{\partial^2 Q_k}{\partial \theta_k \partial V_m} + \lambda_{pm} \frac{\partial^2 P_m}{\partial \theta_k \partial V_m} + \lambda_{qm} \frac{\partial^2 Q_m}{\partial \theta_k \partial V_m}, \\
 \frac{\partial^2 L}{\partial \theta_k \partial \lambda_{qm}} &= \frac{\partial^2 L}{\partial \lambda_{qm} \partial \theta_k} = \frac{\partial Q_m}{\partial \theta_k}, \\
 \frac{\partial^2 L}{\partial V_k \partial \theta_m} &= \frac{\partial^2 L}{\partial \theta_m \partial V_k} = \lambda_{pk} \frac{\partial^2 P_k}{\partial V_k \partial \theta_m} + \lambda_{qk} \frac{\partial^2 Q_k}{\partial V_k \partial \theta_m} + \lambda_{pm} \frac{\partial^2 P_m}{\partial V_k \partial \theta_m} + \lambda_{qm} \frac{\partial^2 Q_m}{\partial V_k \partial \theta_m}, \\
 \frac{\partial^2 L}{\partial V_k \partial \lambda_{pm}} &= \frac{\partial^2 L}{\partial \lambda_{pm} \partial V_k} = \frac{\partial P_m}{\partial V_k}, \\
 \frac{\partial^2 L}{\partial V_k \partial V_m} &= \frac{\partial^2 L}{\partial V_m \partial V_k} = \lambda_{pk} \frac{\partial^2 P_k}{\partial V_k \partial V_m} + \lambda_{qk} \frac{\partial^2 Q_k}{\partial V_k \partial V_m} + \lambda_{pm} \frac{\partial^2 P_m}{\partial V_k \partial V_m} + \lambda_{qm} \frac{\partial^2 Q_m}{\partial V_k \partial V_m}, \\
 \frac{\partial^2 L}{\partial V_k \partial \lambda_{qm}} &= \frac{\partial^2 L}{\partial \lambda_{qm} \partial V_k} = \frac{\partial Q_m}{\partial V_k}, \\
 \frac{\partial^2 L}{\partial \lambda_{pk} \partial \theta_m} &= \frac{\partial^2 L}{\partial \theta_m \partial \lambda_{pk}} = \frac{\partial P_k}{\partial \theta_m},
 \end{aligned}$$

$$\begin{aligned}\frac{\partial^2 L}{\partial \lambda_{qk} \partial \theta_m} &= \frac{\partial^2 L}{\partial \theta_m \partial \lambda_{qk}} = \frac{\partial Q_k}{\partial \theta_m}, \\ \frac{\partial^2 L}{\partial \lambda_{pk} \partial V_m} &= \frac{\partial^2 L}{\partial V_m \partial \lambda_{pk}} = \frac{\partial P_k}{\partial V_m}, \\ \frac{\partial^2 L}{\partial \lambda_{qk} \partial V_m} &= \frac{\partial^2 L}{\partial V_m \partial \lambda_{qk}} = \frac{\partial Q_k}{\partial V_m}.\end{aligned}$$

The second partial derivatives with respect to the state variables at bus  $m$  are (diagonal block):

$$\begin{aligned}\frac{\partial^2 L}{\partial \theta_m^2} &= \lambda_{pk} \frac{\partial^2 P_k}{\partial \theta_m^2} + \lambda_{qk} \frac{\partial^2 Q_k}{\partial \theta_m^2} + \lambda_{pm} \frac{\partial^2 P_m}{\partial \theta_m^2} + \lambda_{qm} \frac{\partial^2 Q_m}{\partial \theta_m^2}, \\ \frac{\partial^2 L}{\partial \theta_m \partial \lambda_{pm}} &= \frac{\partial^2 L}{\partial \lambda_{pm} \partial \theta_m} = \frac{\partial P_m}{\partial \theta_m}, \\ \frac{\partial^2 L}{\partial \theta_m \partial V_m} &= \frac{\partial^2 L}{\partial V_m \partial \theta_m} = \lambda_{pk} \frac{\partial^2 P_k}{\partial \theta_m \partial V_m} + \lambda_{qk} \frac{\partial^2 Q_k}{\partial \theta_m \partial V_m} + \lambda_{pm} \frac{\partial^2 P_m}{\partial \theta_m \partial V_m} + \lambda_{qm} \frac{\partial^2 Q_m}{\partial \theta_m \partial V_m}, \\ \frac{\partial^2 L}{\partial \theta_m \partial \lambda_{qm}} &= \frac{\partial^2 L}{\partial \lambda_{qm} \partial \theta_m} = \frac{\partial Q_m}{\partial \theta_m}, \\ \frac{\partial^2 L}{\partial V_m^2} &= \lambda_{pk} \frac{\partial^2 P_k}{\partial V_m^2} + \lambda_{qk} \frac{\partial^2 Q_k}{\partial V_m^2} + \lambda_{pm} \frac{\partial^2 P_m}{\partial V_m^2} + \lambda_{qm} \frac{\partial^2 Q_m}{\partial V_m^2}, \\ \frac{\partial^2 L}{\partial V_m \partial \lambda_{pm}} &= \frac{\partial^2 L}{\partial \lambda_{pm} \partial V_m} = \frac{\partial P_m}{\partial V_m}, \\ \frac{\partial^2 L}{\partial V_m \partial \lambda_{qm}} &= \frac{\partial^2 L}{\partial \lambda_{qm} \partial V_m} = \frac{\partial Q_m}{\partial V_m}.\end{aligned}$$

The second partial derivatives of active and reactive power flow equations are:

$$\begin{aligned}\frac{\partial^2 P_k}{\partial \theta_m \partial \theta_k} &= V_k V_m [G_{km} \cos(\theta_k - \theta_m) + B_{km} \sin(\theta_k - \theta_m)], \\ \frac{\partial^2 Q_k}{\partial \theta_m \partial \theta_k} &= V_k V_m [G_{km} \sin(\theta_k - \theta_m) - B_{km} \cos(\theta_k - \theta_m)], \\ \frac{\partial^2 P_k}{\partial \theta_m \partial V_k} &= V_m [G_{km} \sin(\theta_k - \theta_m) - B_{km} \cos(\theta_k - \theta_m)], \\ \frac{\partial^2 Q_k}{\partial \theta_m \partial V_k} &= -V_m [G_{km} \cos(\theta_k - \theta_m) + B_{km} \sin(\theta_k - \theta_m)], \\ \frac{\partial^2 P_k}{\partial \theta_m \partial V_m} &= V_k [G_{km} \sin(\theta_k - \theta_m) - B_{km} \cos(\theta_k - \theta_m)], \\ \frac{\partial^2 Q_k}{\partial \theta_m \partial V_m} &= -V_k [G_{km} \cos(\theta_k - \theta_m) + B_{km} \sin(\theta_k - \theta_m)], \\ \frac{\partial^2 P_k}{\partial \theta_k \partial V_k} &= -V_m [G_{km} \sin(\theta_k - \theta_m) - B_{km} \cos(\theta_k - \theta_m)],\end{aligned}$$

$$\begin{aligned}
\frac{\partial^2 Q_k}{\partial \theta_k \partial V_k} &= V_m [G_{km} \cos(\theta_k - \theta_m) + B_{km} \sin(\theta_k - \theta_m)], \\
\frac{\partial^2 P_k}{\partial \theta_k \partial V_m} &= -V_k [G_{km} \sin(\theta_k - \theta_m) - B_{km} \cos(\theta_k - \theta_m)], \\
\frac{\partial^2 Q_k}{\partial \theta_k \partial V_m} &= V_k [G_{km} \cos(\theta_k - \theta_m) + B_{km} \sin(\theta_k - \theta_m)], \\
\frac{\partial^2 P_k}{\partial V_k \partial V_m} &= [G_{km} \cos(\theta_k - \theta_m) + B_{km} \sin(\theta_k - \theta_m)], \\
\frac{\partial^2 Q_k}{\partial V_k \partial V_m} &= [G_{km} \sin(\theta_k - \theta_m) - B_{km} \cos(\theta_k - \theta_m)], \\
\frac{\partial^2 P_k}{\partial \theta_m^2} &= -V_k V_m [G_{km} \cos(\theta_k - \theta_m) + B_{km} \sin(\theta_k - \theta_m)], \\
\frac{\partial^2 Q_k}{\partial \theta_m^2} &= -V_k V_m [G_{km} \sin(\theta_k - \theta_m) - B_{km} \cos(\theta_k - \theta_m)], \\
\frac{\partial^2 P_k}{\partial \theta_k^2} &= -V_k V_m [G_{km} \cos(\theta_k - \theta_m) + B_{km} \sin(\theta_k - \theta_m)], \\
\frac{\partial^2 Q_k}{\partial \theta_k^2} &= -V_k V_m [G_{km} \sin(\theta_k - \theta_m) - B_{km} \cos(\theta_k - \theta_m)], \\
\frac{\partial^2 P_k}{\partial V_k^2} &= 2G_{kk}, \\
\frac{\partial^2 Q_k}{\partial V_k^2} &= -2B_{kk}, \\
\frac{\partial^2 P_k}{\partial V_m^2} &= 0, \\
\frac{\partial^2 Q_k}{\partial V_m^2} &= 0.
\end{aligned}$$

To obtain the partial derivatives of  $P_m$  and  $Q_m$  it is only necessary to exchange subscripts  $k$  and  $m$  in the above equations.

## B.2 PHASE SHIFTER TRANSFORMER

The first partial derivatives making up the gradient are not given here since they coincide with the elements of the phase shifter (PS) Jacobian already given in Section 4.4.2.

The second partial derivatives of active and reactive power with respect to the phase shifter angle  $\phi_{tv}$  and phase angle voltages are:

$$\begin{aligned}
\frac{\partial^2 P_k}{\partial \phi_{tv} \partial \theta_k} &= V_k V_m (G_{km} \cos \delta_1 + B_{km} \sin \delta_1), \\
\frac{\partial^2 Q_k}{\partial \phi_{tv} \partial \theta_m} &= V_k V_m (G_{km} \sin \delta_1 - B_{km} \cos \delta_1),
\end{aligned}$$

$$\begin{aligned}
\frac{\partial^2 P_k}{\partial \phi_{tv} \partial \delta_m} &= -V_k V_m (G_{km} \cos \delta_1 + B_{km} \sin \delta_1), \\
\frac{\partial^2 Q_k}{\partial \phi_{tv} \partial \theta_m} &= -V_k V_m (G_{km} \sin \delta_1 - B_{km} \cos \delta_1), \\
\frac{\partial^2 P_m}{\partial \phi_{tv} \partial \theta_m} &= -V_m V_k (G_{mk} \cos \delta_2 + B_{mk} \sin \delta_2), \\
\frac{\partial^2 Q_m}{\partial \phi_{tv} \partial \theta_m} &= -V_m V_k (G_{mk} \sin \delta_2 - B_{mk} \cos \delta_2), \\
\frac{\partial^2 P_m}{\partial \phi_{tv} \partial \theta_k} &= V_m V_k (G_{mk} \cos \delta_2 + B_{mk} \sin \delta_2), \\
\frac{\partial^2 Q_m}{\partial \phi_{tv} \partial \theta_k} &= V_m V_k (G_{mk} \sin \delta_2 - B_{mk} \cos \delta_2).
\end{aligned}$$

The second partial derivatives of active and reactive power at buses  $k$  and  $m$  with respect to the phase shifter angle  $\phi_{tv}$  and voltages magnitudes are:

$$\begin{aligned}
\frac{\partial^2 P_k}{\partial \phi_{tv} \partial V_k} &= V_m (G_{km} \sin \delta_1 - B_{km} \cos \delta_1), \\
\frac{\partial^2 Q_k}{\partial \phi_{tv} \partial V_k} &= -V_m (G_{km} \cos \delta_1 + B_{km} \sin \delta_1), \\
\frac{\partial^2 P_k}{\partial \phi_{tv} \partial V_m} &= V_k (G_{km} \sin \delta_1 - B_{km} \cos \delta_1), \\
\frac{\partial^2 Q_k}{\partial \phi_{tv} \partial V_m} &= -V_k (G_{km} \cos \delta_1 + B_{km} \sin \delta_1), \\
\frac{\partial^2 P_m}{\partial \phi_{tv} \partial V_k} &= -V_m (G_{mk} \sin \delta_2 - B_{mk} \cos \delta_2), \\
\frac{\partial^2 Q_m}{\partial \phi_{tv} \partial V_k} &= V_m (G_{mk} \cos \delta_2 + B_{mk} \sin \delta_2), \\
\frac{\partial^2 P_m}{\partial \phi_{tv} \partial V_m} &= -V_k (G_{mk} \sin \delta_2 - B_{mk} \cos \delta_2), \\
\frac{\partial^2 Q_m}{\partial \phi_{tv} \partial V_k} &= V_k (G_{mk} \cos \delta_2 + B_{mk} \sin \delta_2).
\end{aligned}$$

The second partial derivatives with respect to the phase shifter angle  $\phi_{tv}$  are:

$$\begin{aligned}
\frac{\partial^2 P_k}{\partial^2 \phi_{tv}} &= V_k V_m \left( \sin \delta_1 \frac{\partial G_{km}}{\partial \phi_{tv}} - \cos \delta_1 \frac{\partial B_{km}}{\partial \phi_{tv}} \right), \\
\frac{\partial^2 Q_k}{\partial^2 \phi_{tv}} &= V_k V_m \left( \cos \delta_1 \frac{\partial G_{km}}{\partial \phi_{tv}} + \sin \delta_1 \frac{\partial B_{km}}{\partial \phi_{tv}} \right), \\
\frac{\partial^2 P_m}{\partial^2 \phi_{tv}} &= -V_m V_k \left( \sin \delta_2 \frac{\partial G_{mk}}{\partial \phi_{tv}} - \cos \delta_2 \frac{\partial B_{mk}}{\partial \phi_{tv}} \right),
\end{aligned}$$

$$\begin{aligned}
\frac{\partial^2 Q_m}{\partial \phi_{rv}^2} &= V_m V_k \left( \cos \delta_2 \frac{\partial G_{mk}}{\partial \phi_{rv}} + \sin \delta_2 \frac{\partial B_{mk}}{\partial \phi_{rv}} \right), \\
\frac{\partial G_{km}}{\partial \phi_{rv}} &= \frac{T_v U_v}{A_2} (F_1 \sin \phi_1 - F_2 \cos \phi_1), \\
\frac{\partial B_{km}}{\partial \phi_{rv}} &= -\frac{T_v U_v}{A_2} (F_2 \sin \phi_1 + F_1 \cos \phi_1), \\
\frac{\partial G_{mk}}{\partial \phi_{rv}} &= -\frac{T_v U_v}{A_2} (F_1 \sin \phi_2 - F_2 \cos \phi_2), \\
\frac{\partial B_{mk}}{\partial \phi_{rv}} &= \frac{T_v U_v}{A_2} (F_2 \sin \phi_2 + F_1 \cos \phi_2).
\end{aligned}$$

The second partial derivatives of active and reactive power with respect to the phase shifter angle  $\phi_{uv}$  and phase angle voltages are:

$$\begin{aligned}
\frac{\partial^2 P_k}{\partial \phi_{uv} \partial \theta_k} &= -V_k V_m (G_{mk} \cos \delta_1 + B_{mk} \sin \delta_1), \\
\frac{\partial^2 Q_k}{\partial \phi_{uv} \partial \theta_k} &= -V_k V_m (G_{km} \sin \delta_1 - B_{km} \cos \delta_1), \\
\frac{\partial^2 P_k}{\partial \phi_{uv} \partial \theta_m} &= V_k V_m (G_{km} \cos \delta_1 + B_{km} \sin \delta_1), \\
\frac{\partial^2 Q_k}{\partial \phi_{uv} \partial \theta_m} &= V_k V_m (G_{km} \sin \delta_1 - B_{km} \cos \delta_1), \\
\frac{\partial^2 P_m}{\partial \phi_{uv} \partial \theta_m} &= V_m V_k (G_{mk} \cos \delta_2 + B_{mk} \sin \delta_2), \\
\frac{\partial^2 Q_m}{\partial \phi_{uv} \partial \theta_m} &= V_m V_k (G_{mk} \sin \delta_2 - B_{mk} \cos \delta_2), \\
\frac{\partial^2 P_m}{\partial \phi_{uv} \partial \theta_k} &= -V_m V_k (G_{mk} \cos \delta_2 + B_{mk} \sin \delta_2), \\
\frac{\partial^2 Q_m}{\partial \phi_{uv} \partial \theta_k} &= -V_m V_k (G_{mk} \sin \delta_2 - B_{mk} \cos \delta_2).
\end{aligned}$$

The second partial derivatives of active and reactive power with respect to the phase-shifter angle  $\phi_{uv}$  and voltage magnitudes are:

$$\begin{aligned}
\frac{\partial^2 P_k}{\partial \phi_{uv} \partial V_k} &= -V_m (G_{km} \sin \delta_1 - B_{km} \cos \delta_1), \\
\frac{\partial^2 Q_k}{\partial \phi_{uv} \partial V_k} &= V_m (G_{km} \cos \delta_1 + B_{km} \sin \delta_1), \\
\frac{\partial^2 P_k}{\partial \phi_{uv} \partial V_m} &= -V_k (G_{km} \sin \delta_1 - B_{km} \cos \delta_1), \\
\frac{\partial^2 Q_k}{\partial \phi_{uv} \partial V_m} &= V_k (G_{km} \cos \delta_1 + B_{km} \sin \delta_1),
\end{aligned}$$

$$\begin{aligned}\frac{\partial^2 P_m}{\partial \phi_{uv} \partial V_k} &= V_m (G_{mk} \sin \delta_2 - B_{mk} \cos \delta_2), \\ \frac{\partial^2 Q_m}{\partial \phi_{uv} \partial V_k} &= -V_m (G_{mk} \cos \delta_2 + B_{mk} \sin \delta_2), \\ \frac{\partial^2 P_m}{\partial \phi_{uv} \partial V_m} &= V_m (G_{mk} \sin \delta_2 - B_{mk} \cos \delta_2), \\ \frac{\partial^2 Q_m}{\partial \phi_{uv} \partial V_m} &= -V_m (G_{mk} \cos \delta_2 + B_{mk} \sin \delta_2).\end{aligned}$$

The second partial derivatives of active and reactive power with respect to the phase-shifter angle  $\phi_{uv}$  are:

$$\begin{aligned}\frac{\partial^2 P_m}{\partial^2 \phi_{uv}} &= V_m V_k \left( \sin \delta_2 \frac{\partial G_{mk}}{\partial \phi_{uv}} - \cos \delta_2 \frac{\partial B_{mk}}{\partial \phi_{uv}} \right), \\ \frac{\partial^2 Q_k}{\partial^2 \phi_{uv}} &= V_k V_m \left( \cos \delta_1 \frac{\partial G_{km}}{\partial \phi_{uv}} + \sin \delta_1 \frac{\partial B_{km}}{\partial \phi_{uv}} \right), \\ \frac{\partial^2 P_k}{\partial^2 \phi_{uv}} &= -V_k V_m \left( \sin \delta_1 \frac{\partial G_{km}}{\partial \phi_{uv}} - \cos \delta_1 \frac{\partial B_{km}}{\partial \phi_{uv}} \right), \\ \frac{\partial^2 Q_m}{\partial^2 \phi_{uv}} &= -V_m V_k \left( \cos \delta_2 \frac{\partial G_{mk}}{\partial \phi_{uv}} + \sin \delta_2 \frac{\partial B_{mk}}{\partial \phi_{uv}} \right), \\ \frac{\partial G_{mk}}{\partial \phi_{uv}} &= \frac{T_v U_v}{A_2} (F_1 \sin \phi_2 - F_2 \cos \phi_2), \\ \frac{\partial B_{mk}}{\partial \phi_{uv}} &= \frac{T_v U_v}{A_2} (F_2 \sin \phi_1 + F_2 \cos \phi_1), \\ \frac{\partial G_{km}}{\partial \phi_{uv}} &= -\frac{T_v U_v}{A_2} (F_1 \sin \phi_1 - F_2 \cos \phi_1), \\ \frac{\partial B_{mk}}{\partial \phi_{uv}} &= -\frac{T_v U_v}{A_2} (F_1 \cos \phi_2 + F_2 \sin \phi_2).\end{aligned}$$

### B.3 STATIC VAR COMPENSATOR

The first and second partial derivative making up the static VAR compensator (SVC) gradient are not given here; they correspond to Equations (5.6) and (5.9) for variable susceptance and the firing-angle SVC model, respectively.

The second partial derivative terms for the SVC reactive power are:

$$\begin{aligned}\frac{\partial^2 Q_k}{\partial V_k^2} &= -2B_{\text{SVC}}, \\ \frac{\partial^2 Q_k}{\partial V_k^2} &= \frac{2}{X_C X_L} \left\{ X_L - \frac{X_C}{\pi} [2(\pi - \alpha) + \sin(2\alpha)] \right\},\end{aligned}$$

$$\begin{aligned}
\frac{\partial^2 Q_k}{\partial V_k \partial B_{\text{SVC}}} &= -2V_k, \\
\frac{\partial^2 Q_k}{\partial \alpha^2} &= -\frac{4V_k \sin(2\alpha)}{\pi X_L}, \\
\frac{\partial^2 Q_k}{\partial \alpha \partial V_k} &= \frac{4V_k [\cos(2\alpha) - 1]}{\pi X_L}, \\
B_{\text{SVC}} &= -\frac{1}{X_C X_L} \left\{ X_L - \frac{X_C}{\pi} [2(\pi - \alpha) + \sin(2\alpha)] \right\}.
\end{aligned}$$

#### B.4 THYRISTOR-CONTROLLED SERIES COMPENSATOR

The first partial derivatives of the power equations with respect to the controllable reactance are given in Appendix A. These terms are used to assemble the thyristor-controlled series compensator (TCSC) gradient.

The second partial derivatives of active and reactive power equations with respect to the controllable reactance are:

$$\begin{aligned}
\frac{\partial^2 P_k}{\partial X_{\text{TCSC}} \partial V_k} &= -V_m \sin(\theta_k - \theta_m) \frac{1}{X_{\text{TCSC}}^2}, \\
\frac{\partial^2 Q_k}{\partial X_{\text{TCSC}} \partial V_k} &= [-2V_k + V_m \cos(\theta_k - \theta_m)] \frac{1}{X_{\text{TCSC}}^2}, \\
\frac{\partial^2 P_k}{\partial X_{\text{TCSC}} \partial V_m} &= -V_m \sin(\theta_k - \theta_m) \frac{1}{X_{\text{TCSC}}^2}, \\
\frac{\partial^2 Q_k}{\partial X_{\text{TCSC}} \partial V_m} &= V_k \cos(\theta_k - \theta_m) \frac{1}{X_{\text{TCSC}}^2}, \\
\frac{\partial^2 P_k}{\partial X_{\text{TCSC}} \partial \theta_k} &= -V_k V_m \cos(\theta_k - \theta_m) \frac{1}{X_{\text{TCSC}}^2}, \\
\frac{\partial^2 Q_k}{\partial X_{\text{TCSC}} \partial \theta_k} &= -V_k V_m \sin(\theta_k - \theta_m) \frac{1}{X_{\text{TCSC}}^2}, \\
\frac{\partial^2 P_k}{\partial X_{\text{TCSC}} \partial \theta_m} &= V_k V_m \cos(\theta_k - \theta_m) \frac{1}{X_{\text{TCSC}}^2}, \\
\frac{\partial^2 Q_k}{\partial X_{\text{TCSC}} \partial \theta_m} &= V_k V_m \sin(\theta_k - \theta_m) \frac{1}{X_{\text{TCSC}}^2}, \\
\frac{\partial^2 P_k}{\partial X_{\text{TCSC}}^2} &= V_k V_m \sin(\theta_k - \theta_m) \frac{2}{X_{\text{TCSC}}^3}, \\
\frac{\partial^2 Q_k}{\partial X_{\text{TCSC}}^2} &= [V_k^2 - V_k V_m \cos(\theta_k - \theta_m)] \frac{2}{X_{\text{TCSC}}^3}.
\end{aligned}$$

The equations for bus  $m$  are simply obtained by exchanging subscripts  $k$  and  $m$  in the above set of equations.

The second partial derivative terms of active and reactive power with respect to the firing angle are:

$$\begin{aligned}
 \frac{\partial^2 P_k}{\partial \alpha \partial V_k} &= -V_m \sin(\theta_k - \theta_m) B_{\text{TCSC}}^2 \frac{\partial X_{\text{TCSC}}}{\partial \alpha}, \\
 \frac{\partial^2 Q_k}{\partial \alpha \partial V_k} &= [-2V_k + V_m \cos(\theta_k - \theta_m)] B_{\text{TCSC}}^2 \frac{\partial X_{\text{TCSC}}}{\partial \alpha}, \\
 \frac{\partial^2 P_k}{\partial \alpha \partial V_m} &= -V_k \sin(\theta_k - \theta_m) B_{\text{TCSC}}^2 \frac{\partial X_{\text{TCSC}}}{\partial \alpha}, \\
 \frac{\partial^2 Q_k}{\partial \alpha \partial V_m} &= V_k \cos(\theta_k - \theta_m) B_{\text{TCSC}}^2 \frac{\partial X_{\text{TCSC}}}{\partial \alpha}, \\
 \frac{\partial^2 P_k}{\partial \alpha \partial \theta_k} &= -V_k V_m \cos(\theta_k - \theta_m) B_{\text{TCSC}}^2 \frac{\partial X_{\text{TCSC}}}{\partial \alpha}, \\
 \frac{\partial^2 Q_k}{\partial \alpha \partial \theta_k} &= -V_k V_m \sin(\theta_k - \theta_m) B_{\text{TCSC}}^2 \frac{\partial X_{\text{TCSC}}}{\partial \alpha}, \\
 \frac{\partial^2 P_k}{\partial \alpha \partial \theta_m} &= V_k V_m \cos(\theta_k - \theta_m) B_{\text{TCSC}}^2 \frac{\partial X_{\text{TCSC}}}{\partial \alpha}, \\
 \frac{\partial^2 Q_k}{\partial \alpha \partial \theta_m} &= V_k V_m \sin(\theta_k - \theta_m) B_{\text{TCSC}}^2 \frac{\partial X_{\text{TCSC}}}{\partial \alpha}, \\
 \frac{\partial^2 P_k}{\partial \alpha^2} &= -V_k V_m \sin(\theta_k - \theta_m) \left( B_{\text{TCSC}}^2 \frac{\partial^2 X_{\text{TCSC}}}{\partial \alpha^2} + \frac{\partial X_{\text{TCSC}}}{\partial \alpha} \frac{\partial B_{\text{TCSC}}^2}{\partial \alpha} \right), \\
 \frac{\partial^2 Q_k}{\partial \alpha^2} &= [-V_k^2 + V_k V_m \cos(\theta_k - \theta_m)] \left( B_{\text{TCSC}}^2 \frac{\partial^2 X_{\text{TCSC}}}{\partial \alpha^2} + \frac{\partial X_{\text{TCSC}}}{\partial \alpha} \frac{\partial B_{\text{TCSC}}^2}{\partial \alpha} \right), \\
 \frac{\partial^2 B_{\text{TCSC}}}{\partial \alpha^2} &= B_{\text{TCSC}}^2 \frac{\partial^2 X_{\text{TCSC}}}{\partial \alpha^2} + \frac{\partial X_{\text{TCSC}}}{\partial \alpha} \frac{\partial B_{\text{TCSC}}^2}{\partial \alpha}, \\
 \frac{\partial B_{\text{TCSC}}^2}{\partial \alpha} &= -\frac{2}{X_{\text{TCSC}}^3} \frac{\partial X_{\text{TCSC}}}{\partial \alpha}, \\
 \frac{\partial^2 X_{\text{TCSC}}}{\partial \alpha^2} &= -4C_1 \sin[2(\pi - \alpha)] + C_2 \varpi^2 \left\{ \frac{2 \cos^2[\varpi(\pi - \alpha)] \cos(\pi - \alpha) \sin(\pi - \alpha)}{\cos^4[\varpi(\pi - \alpha)]} \right\} \\
 &\quad - C_2 \varpi^2 \left\{ \frac{2 \varpi \cos^2(\pi - \alpha) \cos[\varpi(\pi - \alpha)] \sin[\varpi(\pi - \alpha)]}{\cos^4[\varpi(\pi - \alpha)]} \right\} \\
 &\quad + C_2 \varpi \left\{ 2 \tan[\varpi(\pi - \alpha)] \cos[2(\pi - \alpha)] + \frac{\varpi \sin[2(\pi - \alpha)]}{\cos^2[\varpi(\pi - \alpha)]} \right\} \\
 &\quad - C_2 \left\{ 2 \tan(\pi - \alpha) \cos[2(\pi - \alpha)] + \frac{\sin[2(\pi - \alpha)]}{\cos^2(\pi - \alpha)} \right\}.
 \end{aligned}$$

## B.5 UNIFIED POWER FLOW CONTROLLER

The first partial derivatives of active and reactive power with respect to the voltage magnitude and phase angles are given in Appendix A. These terms are used to assemble the unified power flow controller (UPFC) gradient.

The second partial derivatives of active and reactive power flow equations at bus  $k$  are:

$$\begin{aligned}
\frac{\partial^2 P_k}{\partial \theta_k^2} &= -V_k V_m [G_{km} \cos(\theta_k - \theta_m) + B_{km} \sin(\theta_k - \theta_m)] - V_k V_{cR} [G_{km} \cos(\theta_k - \delta_{cR}) \\
&\quad + B_{km} \sin(\theta_k - \delta_{cR})] - V_k V_{vR} [G_{vR} \cos(\theta_k - \delta_{vR}) + B_{vR} \sin(\theta_k - \delta_{vR})], \\
\frac{\partial^2 Q_k}{\partial \theta_k^2} &= -V_k V_r [G_{km} \sin(\theta_k - \theta_m) - B_{km} \cos(\theta_k - \theta_m)] - V_k V_{cR} [G_{km} \sin(\theta_k - \delta_{cR}) \\
&\quad - B_{km} \cos(\theta_k - \delta_{cR})] - V_k V_{vR} [G_{vR} \sin(\theta_k - \delta_{vR}) - B_{vR} \cos(\theta_k - \delta_{vR})], \\
\frac{\partial^2 P_k}{\partial \theta_k \partial \theta_m} &= V_k V_m [G_{km} \cos(\theta_k - \theta_m) + B_{km} \sin(\theta_k - \theta_m)], \\
\frac{\partial^2 Q_k}{\partial \theta_k \partial \theta_m} &= V_k V_m [G_{km} \sin(\theta_k - \theta_m) - B_{km} \cos(\theta_k - \theta_m)], \\
\frac{\partial^2 P_k}{\partial \theta_k \partial \delta_{cR}} &= V_k V_{cR} [G_{km} \cos(\theta_k - \delta_{cR}) + B_{km} \sin(\theta_k - \delta_{cR})], \\
\frac{\partial^2 Q_k}{\partial \theta_k \partial \delta_{cR}} &= V_k V_{cR} [G_{km} \sin(\theta_k - \delta_{cR}) - B_{km} \cos(\theta_k - \delta_{cR})], \\
\frac{\partial^2 P_k}{\partial \theta_k \partial \delta_{vR}} &= V_k V_{vR} [G_{vR} \cos(\theta_k - \delta_{vR}) + B_{vR} \sin(\theta_k - \delta_{vR})], \\
\frac{\partial^2 Q_k}{\partial \theta_k \partial \delta_{vR}} &= V_k V_{vR} [G_{vR} \sin(\theta_k - \delta_{vR}) - B_{vR} \cos(\theta_k - \delta_{vR})], \\
\frac{\partial^2 P_k}{\partial \theta_k \partial V_k} &= -V_m [G_{km} \sin(\theta_k - \theta_m) - B_{km} \cos(\theta_k - \theta_m)] - V_{cR} [G_{km} \sin(\theta_k - \delta_{cR}) \\
&\quad - B_{km} \cos(\theta_k - \delta_{cR})] - V_{vR} [G_{vR} \sin(\theta_k - \delta_{vR}) - B_{vR} \cos(\theta_k - \delta_{vR})], \\
\frac{\partial^2 Q_k}{\partial \theta_k \partial V_k} &= V_{vR} [G_{km} \cos(\theta_k - \theta_m) + B_{km} \sin(\theta_k - \theta_m)] + V_{cR} [G_{km} \cos(\theta_k - \delta_{cR}) \\
&\quad + B_{km} \sin(\theta_k - \delta_{cR})] + V_{vR} [G_{vR} \cos(\theta_k - \delta_{vR}) + B_{vR} \sin(\theta_k - \delta_{vR})], \\
\frac{\partial^2 P_k}{\partial \theta_k \partial V_m} &= -V_k [G_{km} \sin(\theta_k - \theta_m) - B_{km} \cos(\theta_k - \theta_m)], \\
\frac{\partial^2 Q_k}{\partial \theta_k \partial V_m} &= V_k [G_{km} \cos(\theta_k - \theta_m) + B_{km} \sin(\theta_k - \theta_m)], \\
\frac{\partial^2 P_k}{\partial \theta_k \partial V_{cR}} &= -V_k [G_{km} \sin(\theta_k - \delta_{cR}) - B_{km} \cos(\theta_k - \delta_{cR})], \\
\frac{\partial^2 Q_k}{\partial \theta_k \partial V_{cR}} &= V_k [G_{km} \cos(\theta_k - \delta_{cR}) + B_{km} \sin(\theta_k - \delta_{cR})], \\
\frac{\partial^2 P_k}{\partial \theta_k \partial V_{vR}} &= -V_k [G_{vR} \sin(\theta_k - \delta_{vR}) - B_{vR} \cos(\theta_k - \delta_{vR})], \\
\frac{\partial^2 Q_k}{\partial \theta_k \partial V_{vR}} &= V_k [G_{vR} \cos(\theta_k - \delta_{vR}) + B_{vR} \sin(\theta_k - \delta_{vR})], \\
\frac{\partial^2 P_k}{\partial \theta_m^2} &= -V_k V_m [G_{km} \cos(\theta_k - \theta_m) + B_{km} \sin(\theta_k - \theta_m)],
\end{aligned}$$

$$\begin{aligned}
\frac{\partial^2 Q_k}{\partial \theta_m^2} &= -V_k V_m [G_{km} \sin(\theta_k - \theta_m) - B_{km} \cos(\theta_k - \theta_m)], \\
\frac{\partial^2 P_k}{\partial \theta_m \partial V_k} &= V_m [G_{km} \sin(\theta_{km} - \theta_{km}) - B_{km} \cos(\theta_k - \theta_m)], \\
\frac{\partial^2 Q_k}{\partial \theta_m \partial V_k} &= -V_m [G_{km} \cos(\theta_k - \theta_m) + B_{km} \sin(\theta_k - \theta_m)], \\
\frac{\partial^2 P_k}{\partial \theta_m \partial V_m} &= V_k [G_{km} \sin(\theta_k - \theta_m) - B_{km} \cos(\theta_k - \theta_m)], \\
\frac{\partial^2 Q_k}{\partial \theta_m \partial V_m} &= -V_k [G_{km} \cos(\theta_k - \theta_m) + B_{km} \sin(\theta_k - \theta_m)], \\
\frac{\partial^2 P_k}{\partial \delta_{cR}} &= -V_k V_{cR} [G_{km} \cos(\theta_k - \delta_{cR}) + B_{km} \sin(\theta_k - \delta_{cR})], \\
\frac{\partial^2 Q_k}{\partial \delta_{cR}^2} &= -V_k V_{cR} [G_{km} \sin(\theta_k - \delta_{cR}) - B_{km} \cos(\theta_k - \delta_{cR})], \\
\frac{\partial^2 P_k}{\partial \delta_{cR} \partial V_k} &= V_{cR} [G_{km} \sin(\theta_k - \delta_{cR}) - B_{km} \cos(\theta_k - \delta_{cR})], \\
\frac{\partial^2 Q_k}{\partial \delta_{cR} \partial V_k} &= -V_{cR} [G_{km} \cos(\theta_k - \delta_{cR}) + B_{km} \sin(\theta_k - \delta_{cR})], \\
\frac{\partial^2 P_k}{\partial \delta_{cR} \partial V_{cR}} &= V_k [G_{km} \sin(\theta_k - \delta_{cR}) - B_{km} \cos(\theta_k - \delta_{cR})], \\
\frac{\partial^2 Q_k}{\partial \delta_{cR} \partial V_{cR}} &= -V_k [G_{km} \cos(\theta_k - \delta_{cR}) + B_{km} \sin(\theta_k - \delta_{cR})], \\
\frac{\partial^2 P_k}{\partial \delta_{vR}^2} &= -V_k V_{vR} [G_{vR} \cos(\theta_k - \delta_{vR}) + B_{vR} \sin(\theta_k - \delta_{vR})], \\
\frac{\partial^2 Q_k}{\partial \delta_{vR}^2} &= -V_k V_{vR} [G_{vR} \sin(\theta_k - \delta_{vR}) - B_{vR} \cos(\theta_k - \delta_{vR})], \\
\frac{\partial^2 P_k}{\partial \delta_{vR} \partial V_k} &= V_{vR} [G_{vR} \sin(\theta_k - \delta_{vR}) - B_{vR} \cos(\theta_k - \delta_{vR})], \\
\frac{\partial^2 Q_k}{\partial \delta_{vR} \partial V_k} &= -V_{vR} [G_{vR} \cos(\theta_k - \delta_{vR}) + B_{vR} \sin(\theta_k - \delta_{vR})], \\
\frac{\partial^2 P_k}{\partial \delta_{vR} \partial V_{vR}} &= V_k [G_{vR} \sin(\theta_k - \delta_{vR}) - B_{vR} \cos(\theta_k - \delta_{vR})], \\
\frac{\partial^2 Q_k}{\partial \delta_{vR} \partial V_{vR}} &= -V_k [G_{vR} \cos(\theta_k - \delta_{vR}) + B_{vR} \sin(\theta_k - \delta_{vR})], \\
\frac{\partial^2 P_k}{\partial V_k^2} &= 2G_{kk}, \\
\frac{\partial^2 Q_k}{\partial V_k^2} &= -2B_{kk},
\end{aligned}$$

$$\begin{aligned}
\frac{\partial^2 P_k}{\partial V_k \partial V_m} &= [G_{km} \cos(\theta_k - \theta_m) + B_{km} \sin(\theta_k - \theta_m)], \\
\frac{\partial^2 Q_k}{\partial V_k \partial V_m} &= [G_{km} \sin(\theta_k - \theta_m) - B_{km} \cos(\theta_k - \theta_m)], \\
\frac{\partial^2 P_k}{\partial V_k \partial V_{cR}} &= [G_{km} \cos(\theta_k - \delta_{cR}) + B_{km} \sin(\theta_k - \delta_{cR})], \\
\frac{\partial^2 Q_k}{\partial V_k \partial V_{cR}} &= [G_{km} \sin(\theta_k - \delta_{cR}) - B_{km} \cos(\theta_k - \delta_{cR})], \\
\frac{\partial^2 P_k}{\partial V_k \partial V_{vR}} &= [G_{vR} \cos(\theta_k - \delta_{vR}) + B_{vR} \sin(\theta_k - \delta_{vR})], \\
\frac{\partial^2 Q_k}{\partial V_k \partial V_{vR}} &= [G_{vR} \sin(\theta_k - \delta_{vR}) - B_{vR} \cos(\theta_k - \delta_{vR})].
\end{aligned}$$

The second partial derivatives of active and reactive power flow equations at bus  $m$  are:

$$\begin{aligned}
\frac{\partial^2 P_m}{\partial \theta_k^2} &= -V_m V_k [G_{mk} \cos(\theta_m - \theta_k) + B_{km} \sin(\theta_m - \theta_k)], \\
\frac{\partial^2 Q_m}{\partial \theta_k^2} &= -V_m V_k [G_{km} \sin(\theta_m - \theta_k) - B_{km} \cos(\theta_m - \theta_k)], \\
\frac{\partial^2 P_m}{\partial \theta_k \partial \theta_m} &= V_m V_k [G_{km} \cos(\theta_m - \theta_k) + B_{km} \sin(\theta_m - \theta_k)], \\
\frac{\partial^2 Q_m}{\partial \theta_k \partial \theta_m} &= V_k V_m [G_{km} \sin(\theta_m - \theta_k) - B_{km} \cos(\theta_m - \theta_k)], \\
\frac{\partial^2 P_m}{\partial \theta_k \partial V_k} &= V_m [G_{km} \sin(\theta_m - \theta_k) - B_{km} \cos(\theta_m - \theta_k)], \\
\frac{\partial^2 Q_m}{\partial \theta_k \partial V_k} &= -V_m [G_{km} \cos(\theta_m - \theta_k) + B_{km} \sin(\theta_m - \theta_k)], \\
\frac{\partial^2 P_m}{\partial \theta_k \partial V_m} &= V_k [G_{km} \sin(\theta_m - \theta_k) - B_{km} \cos(\theta_m - \theta_k)], \\
\frac{\partial^2 Q_m}{\partial \theta_k \partial V_m} &= -V_k [G_{km} \cos(\theta_m - \theta_k) + B_{km} \sin(\theta_m - \theta_k)], \\
\frac{\partial^2 P_m}{\partial \theta_m^2} &= -V_m V_k [G_{km} \cos(\theta_m - \theta_k) + B_{km} \sin(\theta_m - \theta_k)] - V_m V_{cR} [G_{mm} \cos(\theta_m - \delta_{cR}) \\
&\quad + B_{mm} \sin(\theta_m - \delta_{cR})], \\
\frac{\partial^2 Q_m}{\partial \theta_m^2} &= -V_m V_k [G_{km} \sin(\theta_m - \theta_k) - B_{km} \cos(\theta_m - \theta_k)] - V_m V_{cR} [G_{mm} \sin(\theta_m - \delta_{cR}) \\
&\quad - B_{mm} \cos(\theta_m - \delta_{cR})], \\
\frac{\partial^2 P_m}{\partial \theta_m \partial \delta_{cR}} &= V_m V_{cR} [G_{mm} \cos(\theta_m - \delta_{cR}) + B_{mm} \sin(\theta_m - \delta_{cR})],
\end{aligned}$$

$$\frac{\partial^2 Q_m}{\partial \theta_m \partial \delta_{cR}} = V_m V_{cR} [G_{mm} \sin(\theta_m - \delta_{cR}) - B_{mm} \cos(\theta_m - \delta_{cR})],$$

$$\frac{\partial^2 P_m}{\partial \theta_m \partial V_k} = -V_m [G_{km} \sin(\theta_m - \theta_k) - B_{km} \cos(\theta_m - \theta_k)],$$

$$\frac{\partial^2 Q_m}{\partial \theta_m \partial V_k} = V_m [G_{km} \cos(\theta_m - \theta_k) + B_{km} \sin(\theta_m - \theta_k)],$$

$$\begin{aligned} \frac{\partial^2 P_m}{\partial \theta_m \partial V_m} = & -V_k [G_{km} \sin(\theta_m - \theta_k) - B_{km} \cos(\theta_m - \theta_s)] - V_{cR} [G_{mm} \sin(\theta_m - \delta_{cR}) \\ & - B_{mm} \cos(\theta_m - \delta_{cR})], \end{aligned}$$

$$\begin{aligned} \frac{\partial^2 Q_m}{\partial \theta_m \partial V_m} = & V_k [G_{km} \cos(\theta_m - \theta_k) + B_{km} \sin(\theta_m - \theta_k)] + V_{cR} [G_{mm} \cos(\theta_m - \delta_{cR}) \\ & + B_{mm} \sin(\theta_m - \delta_{cR})], \end{aligned}$$

$$\frac{\partial^2 P_m}{\partial \theta_m \partial V_{cR}} = -V_m [G_{mm} \sin(\theta_m - \delta_{cR}) - B_{mm} \cos(\theta_m - \delta_{cR})],$$

$$\frac{\partial^2 Q_m}{\partial \theta_m \partial V_{cR}} = V_m [G_{mm} \cos(\theta_m - \delta_{cR}) + B_{mm} \sin(\theta_m - \delta_{cR})],$$

$$\frac{\partial^2 P_m}{\partial \delta_{cR}^2} = -V_m V_{cR} [G_{mm} \cos(\theta_m - \delta_{cR}) + B_{mm} \sin(\theta_m - \delta_{cR})],$$

$$\frac{\partial^2 Q_m}{\partial \delta_{cR}^2} = -V_m V_{cR} [G_{mm} \sin(\theta_m - \delta_{cR}) - B_{mm} \cos(\theta_m - \delta_{cR})],$$

$$\frac{\partial^2 P}{\partial \delta_{cR} \partial V_m} = V_{cR} [G_{mm} \sin(\theta_m - \delta_{cR}) - B_{mm} \cos(\theta_m - \delta_{cR})],$$

$$\frac{\partial^2 Q_m}{\partial \delta_{cR} \partial V_m} = -V_{cR} [G_{mm} \cos(\theta_m - \delta_{cR}) + B_{mm} \sin(\theta_m - \delta_{cR})],$$

$$\frac{\partial^2 P_m}{\partial \delta_{cR} \partial V_{cR}} = V_m [G_{mm} \sin(\theta_m - \delta_{cR}) - B_{mm} \cos(\theta_m - \delta_{cR})],$$

$$\frac{\partial^2 Q_m}{\partial \delta_{cR} \partial V_{cR}} = -V_m [G_{mm} \cos(\theta_m - \delta_{cR}) + B_{mm} \sin(\theta_m - \delta_{cR})],$$

$$\frac{\partial^2 P_m}{\partial V_k \partial V_m} = [G_{km} \cos(\theta_m - \theta_k) + B_{km} \sin(\theta_m - \theta_k)],$$

$$\frac{\partial^2 Q_m}{\partial V_k \partial V_m} = [G_{km} \sin(\theta_m - \theta_k) - B_{km} \cos(\theta_m - \theta_k)],$$

$$\frac{\partial^2 P_m}{\partial V_m^2} = 2G_{mm},$$

$$\frac{\partial^2 Q_m}{\partial V_m^2} = -2B_{mm},$$

$$\frac{\partial^2 P_m}{\partial V_m \partial V_{cR}} = [G_{mm} \cos(\theta_m - \delta_{cR}) + B_{mm} \sin(\theta_m - \delta_{cR})],$$

$$\frac{\partial^2 Q_m}{\partial V_m \partial V_{cR}} = [G_{mm} \sin(\theta_m - \delta_{cR}) - B_{mm} \cos(\theta_m - \delta_{cR})].$$

The second partial derivatives of active power flow equations for the series converter are:

$$\frac{\partial^2 P_{cR}}{\partial \theta_k^2} = -V_{cR} V_k [G_{km} \cos(\delta_{cR} - \theta_k) + B_{km} \sin(\delta_{cR} - \theta_k)],$$

$$\frac{\partial^2 P_{cR}}{\partial \theta_m^2} = -V_{cR} V_m [G_{mm} \cos(\delta_{cR} - \theta_m) + B_{mm} \sin(\delta_{cR} - \theta_m)],$$

$$\frac{\partial^2 P_{cR}}{\partial \theta_k \partial \delta_{cR}} = V_{cR} V_k [G_{km} \cos(\delta_{cR} - \theta_k) + B_{km} \sin(\delta_{cR} - \theta_k)],$$

$$\frac{\partial^2 P_{cR}}{\partial \theta_m \partial \delta_{cR}} = V_{cR} V_m [G_{mm} \cos(\delta_{cR} - \theta_m) + B_{mm} \sin(\delta_{cR} - \theta_m)],$$

$$\frac{\partial^2 P_{cR}}{\partial \theta_k \partial V_k} = V_{cR} [G_{km} \sin(\delta_{cR} - \theta_k) + B_{km} \cos(\delta_{cR} - \theta_k)],$$

$$\frac{\partial^2 P_{cR}}{\partial \theta_m \partial V_m} = V_{cR} [G_{mm} \sin(\delta_{cR} - \theta_m) + B_{mm} \cos(\delta_{cR} - \theta_m)],$$

$$\frac{\partial^2 P_{cR}}{\partial \theta_k \partial V_{cR}} = V_k [G_{km} \sin(\delta_{cR} - \theta_k) + B_{km} \cos(\delta_{cR} - \theta_k)],$$

$$\frac{\partial^2 P_{cR}}{\partial \theta_m \partial V_{cR}} = V_m [G_{mm} \sin(\delta_{cR} - \theta_m) + B_{mm} \cos(\delta_{cR} - \theta_m)],$$

$$\frac{\partial^2 P_{cR}}{\partial \delta_{cR} \partial \theta_k} = V_{cR} V_k [G_{km} \cos(\delta_{cR} - \theta_k) + B_{km} \sin(\delta_{cR} - \theta_k)],$$

$$\frac{\partial^2 P_{cR}}{\partial \delta_{cR} \partial V_m} = -V_{cR} [G_{mm} \sin(\delta_{cR} - \theta_m) - B_{mm} \cos(\delta_{cR} - \theta_m)],$$

$$\frac{\partial^2 P_{cR}}{\partial \delta_{cR} \partial \theta_m} = V_{cR} V_m [G_{mm} \cos(\delta_{cR} - \theta_m) + B_{mm} \sin(\delta_{cR} - \theta_m)],$$

$$\frac{\partial^2 P_{cR}}{\partial \delta_{cR} \partial V_{cR}} = -V_m [G_{mm} \sin(\delta_{cR} - \theta_m) - B_{mm} \cos(\delta_{cR} - \theta_m)] - V_k [G_{km} \sin(\delta_{cR} - \theta_k) - B_{km} \cos(\delta_{cR} - \theta_k)],$$

$$\frac{\partial^2 P_{cR}}{\partial \delta_{cR}^2} = -V_{cR} V_m [G_{mm} \cos(\delta_{cR} - \theta_m) + B_{mm} \sin(\delta_{cR} - \theta_m)] - V_{cR} V_k [G_{km} \cos(\delta_{cR} - \theta_k) + B_{km} \sin(\delta_{cR} - \theta_k)],$$

$$\frac{\partial^2 P_{cR}}{\partial V_k \partial V_{cR}} = [G_{km} \cos(\delta_{cR} - \theta_k) + B_{km} \sin(\delta_{cR} - \theta_k)],$$

$$\frac{\partial^2 P_{cR}}{\partial \delta_{cR} \partial V_k} = -V_{cR} [G_{km} \sin(\delta_{cR} - \theta_k) - B_{km} \cos(\delta_{cR} - \theta_k)],$$

$$\frac{\partial^2 P_{cR}}{\partial V_m \partial V_{cR}} = [G_{mm} \cos(\delta_{cR} - \theta_m) + B_{mm} \sin(\delta_{cR} - \theta_m)],$$

$$\frac{\partial^2 P_{cR}}{\partial V_{cR}^2} = 2G_{mm}.$$

The second partial derivatives of active power flow equations for the shunt converters are:

$$\frac{\partial^2 P_{vR}}{\partial \theta_k^2} = -V_{vR} V_k [G_{vR} \cos(\delta_{vR} - \theta_k) + B_{vR} \sin(\delta_{vR} - \theta_k)],$$

$$\frac{\partial^2 P_{vR}}{\partial \delta_{vR}^2} = -V_{vR} V_k [G_{vR} \cos(\delta_{vR} - \theta_k) + B_{vR} \sin(\delta_{vR} - \theta_k)],$$

$$\frac{\partial^2 P_{vR}}{\partial \theta_k \partial \delta_{vR}} = V_{vR} V_k [G_{vR} \cos(\delta_{vR} - \theta_k) + B_{vR} \sin(\delta_{vR} - \theta_k)],$$

$$\frac{\partial^2 P_{vR}}{\partial \delta_{vR} \partial V_k} = -V_{vR} [G_{vR} \sin(\delta_{vR} - \theta_k) + B_{vR} \cos(\delta_{vR} - \theta_k)],$$

$$\frac{\partial^2 P_{vR}}{\partial \theta_k \partial V_k} = V_{vR} [G_{vR} \sin(\delta_{vR} - \theta_k) + B_{vR} \cos(\delta_{vR} - \theta_k)],$$

$$\frac{\partial^2 P_{vR}}{\partial \delta_{vR} \partial V_{vR}} = -V_k [G_{vR} \sin(\delta_{vR} - \theta_k) - B_{vR} \cos(\delta_{vR} - \theta_k)],$$

$$\frac{\partial^2 P_{vR}}{\partial \theta_k \partial V_{vR}} = V_k [G_{vR} \sin(\delta_{vR} - \theta_k) + B_{vR} \cos(\delta_{vR} - \theta_k)],$$

$$\frac{\partial^2 P_{vR}}{\partial V_k \partial V_{vR}} = [G_{vR} \cos(\delta_{vR} - \theta_k) + B_{vR} \sin(\delta_{vR} - \theta_k)],$$

$$\frac{\partial^2 P_{vR}}{\partial V_{vR}^2} = -2G_{vR}.$$





# Appendix C: Matlab<sup>®</sup> Computer Program for Optimal Power Flow Solutions using Newton's Method

A computer program suitable for the optimal power flow (OPF) solution of small and medium size power systems is given below. The program is general, as far as the topology of the network is concerned, and caters for any number of  $PV$  and  $PQ$  buses. The slack bus is the first generator bus in the data file. Notice that active and reactive power limits should be given to the slack generator. No transformers are represented in this base program and no sparsity techniques are incorporated.

```
%%***- - - - Main Program

%% *****
%% Input data *
%% *****
opfdata;
%% *****
%% Definition of auxiliary vectors and matrices *
%% *****
%%Nodes
VOLTAGE=zeros(nbb,1);ANGLE=zeros(nbb,1);LAMBDAQ=zeros(nbb,1);
LAMBDAQ=zeros(nbb,1);PGENERATED=zeros(nbb,1);
StatusVoltage = ones(nbb,1);
Violation=zeros(nbb,1);Kindexvol=zeros(nbb,1);MiuBus=zeros(nbb,1);
StatV=ones(nbb,1);ActivedV=zeros(nbb,1);

%%Generators
statusgen=ones(ngn,1);StatP=ones(ngn,1);StatQ=ones(ngn,1);
```

```

ActivedP=zeros(ngn,1);ActivedQ=zeros(ngn,1);Kindexgen=zeros(ngn,1);
IndGenQ=zeros(ngn,1);MiuGen=zeros(ngn,1);

ChangeStat=0;Kindex=0;cost=0;Ckg=0;MaxDz=0;
%%SetGenQ=0;GenViolado=0;Optimo=0;

%% *****
%% The elements of Ybus are calculated here *
%% *****
[GKK,BKK,GKM,BKM] = YBus(tlsend,tlrec,tlresis,tlreac,tlsuscep,...
tlcond, ntl,nbb);

%% *****
%%                               Initial dispatch *
%% *****
[PGEN,Ckg,LambdaP] = InitialDispatch(nbb,ngn,A,B,C,PLOAD, PGEN, PMIN,...
PMAx,Ckg,LambdaP);
Ckg=Ckg*10000;

%% *****
%%                               Main iteration starts here *
%% *****
[ cost ] = CostGeneration(cost,A,B,C,PGEN,ngn);

for(iterOpf = 1: IterOpfTot)

%% *****
%% Calculated powers in buses and generators *
%% *****
[Pbus,Qbus] = CalculatedPowers(nbb,VM,VA,GKK,BKK,GKM,BKM,ntl,...
tlsend,tlrec);
[QGEN]=ReactivePowerGenerators(QGEN,ngn,Qbus,QLOAD,genbus,bustype);

%% *****
%% Check reactive power of generators, including the slack *
%% generator. Remove penalty factors from Lagrangian multiplier *
%% LambdaQ in buses with reactive power limits *
%% violations *
%% *****
SetGenQ=0;
[Violation,ActivedQ,statusgen,SetGenQ,IndGenQ] = Voltage(nbb,ngn,...
genbus,QGEN,QLOAD,Violation,ActivedQ,vmin,vmax,TolVoltage,VM,Qbus,...
statusgen,bustype,QMAX,QMIN,SetGenQ,IndGenQ,iterOpf);

%% *****
%% Copy data from solution vector to auxiliary vector *
%% *****

```

```

[ANGLE,VOLTAGE,LAMBDA P,LAMBDA Q,PGENERATED]=VectorAux(nbb,ngn,VM,...
VA,LambdaP,LambdaQ,PGEN,vmax,vmin,ANGLE,VOLTAGE,LAMBDA P,LAMBDA Q,...
PGENERATED);

%% *****
%%                               Internal iterations                               *
%% *****
for( IntIter = 1: NIntIter)

%% *****
%% The Matrix W and gradient vector are calculated                             *
%% *****
if(IntIter == 1)
    [Hessian,grad] = MatrixW(nbb,bustype,ngn,GKK, BKK,GKM,BKM,...
    tlsend,tlrec,LambdaP,LambdaQ,VM,VA,ntl);

%% Generators
    [Hessian,grad]=MatrixWGen(nbb,ntl,ngn,genbus,B,C,LambdaP,PGEN,...
    Hessian,grad);

%% Mismatch of nodal powers
    [Hessian,grad] = Mismatch(nbb,ngn,genbus,PGEN,QGEN,PLOAD,QLOAD,...
    Pbus,Qbus,Hessian,grad);
end

%% *****
%%                               Penalize generators with no reactive           *
%%                               power limits violations                         *
%% *****
if(SetGenQ>0)
    AuxBigNumber=(10e+10)/2;
    [Hessian,grad] = PenaltyFunctionQ(nbb,AuxBigNumber,Hessian,...
    grad,genbus,IndGenQ,SetGenQ,LambdaQ,ActivatedQ);
end

%% *****
%% Penalize the voltage magnitude and phase angle of slack bus                 *
%%                               the phase angle must be 0                       *
%% *****
[Hessian,grad] = Convexificacion(nbb,Hessian,grad,Cc,vmax,...
vmin,VOLTAGE,StatusVoltage,VM);

%% *****
%% It holds activated variables in w-matrix,                                  *
%%                               after exiting internal iterations                *
%% *****
[Hessian,grad,ActivatedV,ActivatedP] = AugmentedLagrangian(nbb,...

```

```
Hessian,grad,Ckv,Ckg,vmax,vmin,VOLTAGE,StatusVoltage,VM,ActivedV,...
MiuBus, ngn,ActivedP,PGEN,StatP,MiuGen,PMAX,PMIN);
```

```
%% *****
%%          Solves the system, of equations          *
%% *****
Hessian=full(Hessian);
Dz = Hessian\grad;

%% *****
%%          Updates phase angles, voltages magnitudes,          *
%%          and multipliers lambdap and lambdaq          *
%% *****
if(iterOpf==1 & IntIter<20), Alfa=Alfa+0.025; end
Dz=Alfa*Dz;
[Dz,VA,VM,LambdaP,LambdaQ,PGEN] = Actualisation(Dz,nbb,VA,...
VM,LambdaP,LambdaQ,bustype,ngn,PGEN);

%% *****
%%          Reset calculated powers in buses, w-matrix and gradient          *
%% *****
[Hessian,grad] = Reset_Hessian_grad(Hessian,grad,ngn,nbb);

%% *****
%%          Calculated Powers in buses and generators (second time)          *
%% *****
[Pbus,Qbus] = CalculatedPowers(nbb,VM,VA,GKK,BKK,GKM,BKM,...
ntl,tlsend,tlrec);
[QGEN] = ReactivePowerGenerators(QGEN,ngn,Qbus,QLOAD,genbus,...
bustype);

%% *****
%%          The gradient vector is calculated (second time).          *
%%          Convergence is checked          *
%% *****
[Hessian,grad] = MatrixW(nbb,bustype,ngn,GKK,BKK,GKM,BKM,...
tlsend,tlrec,LambdaP,LambdaQ,VM,VA,ntl);
%% Generators
[Hessian,grad] = MatrixWGen(nbb,ntl,ngn,genbus,B,C,LambdaP,...
PGEN,Hessian,grad);
%% Mismatch of nodal powers
[Hessian,grad]=Mismatch(nbb,ngn,genbus,PGEN,QGEN,PLOAD,QLOAD,...
Pbus,Qbus,Hessian,grad);

Optimo=0; %%Flag
[Optimo] = ReviewNodes(Optimo,grad,nbb,bustype,ActivedV,Tol2);
```

```

[Optimo] = ReviewGen(Optimo,grad,ngn,ActivatedP,Toll,nbb);
[MaxDz] = Norma(MaxDz,grad,nbb,ngn);
if(Optimo==0),break, end;
end %%      End of internal iteration

%% *****
%%          Select the active set for the next iteration          *
%% *****
NumNode=zeros(nbb,1);
ValueVoltage= zeros(nbb,1);
NumGenerator=zeros(ngn,1);
ValueGenerator=zeros(ngn,1);
%% Identify candidates for addition to active set
SetVol=0;
[StatusVoltage,SetVol,NumNode,ValueVoltage] = Check_Limits_V...
(nbb, TolVoltage,vmin,vmax,VM,StatusVoltage,Dz,SetVol,NumNode,...
ValueVoltage, ActivatedV);

SetGenP=0;
if(iterOpf>=0)
    [StatP,SetGenP,NumGenerator,ValueGenerator] = Check_Limits_P...
(ngn,TolPower,PMIN,PMAX,PGEN,StatP,SetGenP,NumGenerator,...
ValueGenerator, ActivatedP);
end

%% *****
%%          Looking for the maximum index          *
%% *****
MaxVol=0;
if(SetVol>0)
    MaxVol=ValueVoltage(1);
    for(ii = 1: SetVol)
        if(ValueVoltage(ii)>MaxVol),MaxVol=ValueVoltage(ii);end
    end
end

MaxGen=0;
if(SetGenP>0)
    MaxGen=ValueGenerator(1);
    for(ii = 1: SetGenP)
        if(ValueGenerator(ii)>MaxGen),MaxGen=ValueGenerator(ii);end
    end
end

%% *****
%%          Adding new inequality constraints to the active set.          *
%%          They must be >= Tolerance          *
%% *****

```

```

if(SetVol>0)
    [Hessian,grad,ActivatedV] = AugmentedLagrangianV(nbb,Hessian,...
    grad,Ckv,vmax,vmin,StatusVoltage,VM,ActivatedV,MiuBus,SetVol,...
    NumNode,ValueVoltage,MaxVol,EnforceTol);
end

if(SetGenP>0)
    [Hessian,grad,ActivatedP] = AugmentedLagrangianG(ngn,nbb,Hessian,...
    rad,Ckg,PMIN,PMAX,StatP,PGEN,ActivatedP,MiuGen,SetGenP,...
    NumGenerator,ValueGenerator,MaxGen,EnforceTol);
end

%% *****
%%          Select candidate, constraints to be removed          *
%%          from the active set                                  *
%% *****
NumMiu_V=zeros(nbb,1);
ValMiu_V=zeros(nbb,1);
NumMiu_P=zeros(ngn,1);
ValMiu_P=zeros(ngn,1);
RelVol=0;
for(ii = 1: nbb)
    if(ActivatedV(ii)==2)
        [Hessian,grad,ActivatedV]=AugmentedLagrangian_IV(nbb,Hessian,...
        grad,Ckv,vmax,vmin,StatusVoltage,VM,ActivatedV,MiuBus,ii);
        [MiuBus,NumMiu_V,ValMiu_V,RelVol] = IdentifyMiuBus...
        (StatusVoltage, MiuBus,Ckv,VM,vmax,vmin,ActivatedV,RelVol,...
        NumMiu_V,ValMiu_V,ii);
    end
end

RelGen=0;
for(ii = 1: ngn)
    if(ActivatedP(ii)==2)
        [Hessian,grad,ActivatedP] = AugmentedLagrangian_IG(ngn,...
        Hessian,grad,Ckg,PMIN,PMAX,StatP,PGEN,ActivatedP,MiuGen,ii);
        [MiuGen,NumMiu_P,ValMiu_P,RelGen] = IdentifyMiuGen(StatP,...
        MiuGen,Ckg,PGEN,PMAX,PMIN,ActivatedP,RelGen,NumMiu_P,ValMiu_P,ii);
    end
end

%% *****
%%          It looks for the maximum index                      *
%% *****
MaxVol=0;

```

```

if(RelVol>0)
    MaxVol=ValMiu_V(1);
    for(ii = 1: RelVol)
        if(ValMiu_V(ii)>MaxVol),MaxVol=ValMiu_V(ii);end
    end
end

MaxGen=0;
if(RelGen>0)
    MaxGen=ValMiu_P(1);
    for(ii = 1: RelGen)
        if(ValMiu_P(ii)>MaxGen),MaxGen=ValMiu_P(ii);end
    end
end

%% *****
%%          Releasing inequality constraints from the active          *
%%          set. They must be >= Tolerance                            *
%% *****
if(RelVol>0)
    for(ii = 1:RelVol)
        if(((ValMiu_V(ii)/MaxVol)>=RelTol)&(ValMiu_V(ii)>...
            (Fraction*MaxVol)))
            send=NumMiu_V(ii);
            [Hessian,grad,ActivatedV,StatusVoltage] = ...
            ReleasingAumentedLagrangianV(VM,vmax,vmin,StatusVoltage,MiuBus,...
            Hessian, grad,Ckv,ActivatedV,StatusVoltage,send);
        end
    end
end

if(RelGen>0)
    for(ii= 1:RelGen)
        if(((ValMiu_P(ii)/MaxGen)>=RelTol)&(ValMiu_P(ii)>...
            (Fraction*MaxGen)))
            send=NumMiu_P(ii);
            [Hessian,grad,ActivatedP,StatP] = ...
            ReleasingAumentedLagrangianG(PGEN,PMAX,PMIN,StatP,MiuGen,...
            Hessian, grad,Ckg,ActivatedP,StatP,send);
        end
    end
end

%% *****
%%          Compute the initial values of MiuBUS                    *
%%          and MiuGEN                                              *
%% *****
[MiuBus] = MultiplierBus(nbb,Ckv,MiuBus,VM,vmax,vmin);

```

```

[MiuGen] = MultiplierGen(ngn,Ckg,MiuGen,PGEN,PMAX,PMIN);

[ANGLE,VOLTAGE,LAMBDA_P,LAMBDA_Q,PGENERATED] = VectorAux(nbb,ngn,...
VM,VA,LambdaP,LambdaQ,PGEN,vmax,vmin,ANGLE,VOLTAGE,LAMBDA_P,...
LAMBDA_Q,PGENERATED);
Ckv=1.3*Ckv;
Ckg=1.3*Ckg;

%% *****
%%      It changes the status of 'Activated' variables from 1 to 2,      *
%%      to enable values to be identified at the following iteration:    *
%%          0 can be analyzed, 1 recently activated,                      *
%%          2 it is already active and checks its lambda.                *
%% *****
for(ii= 1: nbb)
    if(ActivatedV(ii)==1),ActivatedV(ii)=2;end
end
for(ii = 1: ngn)
    if(ActivatedP(ii)==1),ActivatedP(ii)=1;end
end

%% *****
%%      It checks whether or not there are changes                        *
%%      in the active set. Changes in Generators                          *
%% *****
in0=0;
for(ii = 1: ngn)
    [ChangeStat,Kindex1,statusgen,LambdaQ,ActivatedQ,bustype] =...
    IdentifyConstQ(ChangeStat,genbus,statusgen,LambdaQ,...
    ActivatedQ,bustype,ii);
    if(ChangeStat~=0),in0=1;end
end
GenViolado=0;
for(ii= 1: ngn)
    [GenViolado]=CheckQGenLimits(GenViolado,QLOAD,Qbus,QMIN,...
    QMAX,genbus,TolPower,ii);
    if(GenViolado==1),break;end
end
if(GenViolado==1),Optimo=1;end

%% *****
%%      It checks whether or not there are changes in the                *
%%      multipliers. Changes in generators                                *
%% *****
in1=0;in2=0;
for(ii = 1: nbb)
    [in1,in2]=MatrixWVVoltageMiu(in1,in2,TolVoltage,VM,vmax,vmin,...

```

```

MiuBus, ActivedV, StatusVoltage, ii);
if(in1==1 | in2==1), break; end
end
in3=0; in4=0;
for( ii = 1: ngn)
    [in3, in4] = MatrixWGenMiu(in3, in4, TolPower, PGEN, PMAX, PMIN, ...
    MiuGen, ActivedP, StatP, ii);
    if(in3==1 | in4==1), break; end
end

[ cost ] = CostGeneration( cost, A, B, C, PGEN, ngn );
[ suma ] = CheckConvexification( nbb, Cc, VM, VOLTAGE );

%% *****
%%                If the total cost is within tolerance                *
%%                and the optimality conditions are satisfied, then      *
%%                the process can be stopped.                            *
%% *****

if((in0==0)&(in1==0)&(in2==0)&(in3==0)&(in4==0)&(RelVol==0)& ...
(RelGen==0))
    eps=LastCost-cost;
    if(eps<0), eps=-eps; end
    if(TolEps==1e-8)
        if(eps<TolEps), Optimo=0; end
    end
end

LastCost=cost;

if((in0==0)&(in1==0)&(in2==0)&(in3==0)&(in4==0)&(RelVol==0)...
&(RelGen==0)&(Optimo==0))
    VM
    VA=VA*180/pi
    PGEN
    LambdaP
    LambdaQ
    fprintf( '\n=== Objective Function Value ===' );
    fprintf( '\n f = %%12.8f $/hr ', cost );
    fprintf( '\n' );
    fprintf( '\n' );
    fprintf( '\n*****' );
    fprintf( '\n*      End of main iteration      *' );
    fprintf( '\n*                               *' );
    fprintf( '\n*****' );
    break; %% This instruction breaks the main iterations loop
end

```

```

%% *****
%%           It checks for the Dz being too small. If true then           *
%%           Ckv=const, Ckg=const and IntIter=30                          *
%% *****
    if((MaxDz<0.00001)&(in1==0)&(in2==0)&(in3==0)&(in4==0)&...
       (RelVol==0)&(RelGen==0))
        NIntIter==30;
        Ckv=Ckv/1.3;
        Ckg=Ckg/1.3;
    end

end %% End of the Main PROGRAM

function [GKK,BKK,GKM,BKM] = YBus(tlsend,tlrec,tlresis,tlreac,...
    tlsuscep,tlcond,ntl,nbb);
%% Transmission lines contribution

GKK=zeros(ntl,1);
BKK=zeros(ntl,1);
GKM=zeros(ntl,1);
BKM=zeros(ntl,1);
for ii = 1: ntl
    denom = tlresis(ii)^2+tlreac(ii)^2;
    GKK(ii) = GKK(ii) + tlresis(ii)/denom + 0.5*tlcond(ii);
    BKK(ii) = BKK(ii) - tlreac(ii)/denom + 0.5*tlsuscep(ii);
    GKM(ii) = GKM(ii) - tlresis(ii)/denom;
    BKM(ii) = BKM(ii) + tlreac(ii)/denom;
end
return; %% End of Ybus

function [PGEN,Ckg,LAMBDA P] = InitialDispatch(nbb,ngn,A,B,C,PLOAD,...
    PGEN,PMIN,PMAX,Ckg,LambdaP);
sum1=0.0;sum2=0.0;sum3=0.0;sum4=0;sum5=0;
lambda=0.0;
Ckg=0;
for(ii= 1:ngn)
    sum1=sum1+B(ii)/C(ii);
    sum2=sum2+1/C(ii);
    if(C(ii)>=Ckg),Ckg=C(ii);end
end
for(ii= 1:nbb)
    sum3=sum3+PLOAD(ii);
end
sum3=1.03*sum3;

```

```

for( ii=1:ngn)
    sum4=sum4+PMIN(ii);
    sum5=sum5+PMAX(ii);
end
if(sum3>sum5|sum3<sum4)
    fprintf('\n*****');
    fprintf('\n*           THERE IS NO SOLUTION           *');
    fprintf('\n*           LOAD<PMIN OR LOAD>PMAX           *');
    fprintf('\n*                                           *');
    fprintf('\n*****');
end

lambda=(2*sum3+sum1)/sum2;
for(ii= 1:nbb)
    LambdaP(ii)=lambda;
end
for(ii= 1:ngn)
    sum1=1.0/(2*C(ii))*(lambda-B(ii));
    PGEN(ii)=sum1;
end
return;    %%End of InitialDispatch

```

```

function [cost] = CostGeneration(cost,A,B,C,PGEN,ngn)
cost=0.0;
for( ii = 1: ngn)
    cost=cost+A(ii)+B(ii)*PGEN(ii)+C(ii)*PGEN(ii)*PGEN(ii);
end
return;    %%End of CostGeneration function

```

```

function [Pbus,Qbus] = CalculatedPowers(nbb,VM,VA,GKK,BKK,GKM,BKM,
ntl,tlsend,tlrec);
Pbus= zeros(nbb,1);
Qbus = zeros(nbb,1);
V=zeros(2,1);
A=zeros(2,1);
for ii = 1: ntl
    send = tlsend(ii);    rece = tlrec(ii);
    V(1)= VM(send);      V(2)= VM(rece);
    A(1)= VA(send);      A(2)= VA(rece);
    angle=A(1)-A(1);
    Pbus(send)=Pbus(send)+V(1)*V(1)*(GKK(ii)*cos(angle)+...
    BKK(ii)*sin(angle));
    Qbus(send)=Qbus(send)+V(1)*V(1)*(GKK(ii)*sin(angle)-BKK(ii)...
    *cos(angle));angle=A(1)-A(2);

```

```

Pbus(send)=Pbus(send)+V(1)*V(2)*(GKM(ii)*cos(angle)+...
BKM(ii)*sin(angle));
Qbus(send)=Qbus(send)+V(1)*V(2)*(GKM(ii)*sin(angle)-BKM(ii)...
*cos(angle));
angle=A(2)-A(2);
Pbus(rece)=Pbus(rece)+V(2)*V(2)*(GKK(ii)*cos(angle)+...
BKK(ii)*sin(angle));
Qbus(rece)=Qbus(rece)+V(2)*V(2)*(GKK(ii)*sin(angle)-BKK(ii)...
*cos(angle));
angle=A(2)-A(1);
Pbus(rece)=Pbus(rece)+V(2)*V(1)*(GKM(ii)*cos(angle)+...
BKM(ii)*sin(angle));
Qbus(rece)=Qbus(rece)+V(2)*V(1)*(GKM(ii)*sin(angle)-BKM(ii)...
*cos(angle));
end
return; %%End of CalculatedPowers function

function [QGEN] = ReactivePowerGenerators(QGEN,ngn,Qbus,QLOAD,...
genbus,bustype);
for ii = 1: ngn
    bgen=genbus(ii);
    if(bustype(bgen)==1 | bustype(bgen)==2)
        QGEN(ii)=Qbus(bgen)+QLOAD(bgen);
    end
end
return; %%End of ReactivePowerGenerators function

function [Violation,ActivatedQ,statusgen,SetGenQ,IndGenQ] = Voltage...
(nbb,ngn,genbus,QGEN,QLOAD,Violation,ActivatedQ,vmin,vmax,TolVoltage,...
VM, Qbus,statusgen,bustype,QMAX,QMIN,SetGenQ,IndGenQ,iterOpf);
if (iterOpf >=2)
    for ii = 1: ngn
        bgen=genbus(ii);
        if(ActivatedQ(ii)==1)
            bgen=bgen;
        else
            Violation(bgen)=1;
            if(((vmin(bgen)-TolVoltage)<VM(bgen)) & (VM(bgen)<(vmax(bgen)+...
TolVoltage)))
                Violation(bgen)=0;
            end
        end
        if((VM(bgen)<0.5)|(VM(bgen)>1.5))
            fprintf('\n*****');
            fprintf('\n*                               *');
            fprintf('\n*          UNFEASIBLE SOLUTION          *');
            fprintf('\n*                               *');
            fprintf('\n*****');
        end
    end
end

```

```

if(Violation(bgen)==0)
    Rpower=QLOAD(bgen)+Qbus(bgen);
    if(statusgen(ii)==1)
        if((Rpower>(QMAX(ii)+0.001) |(Rpower<(QMIN(ii)...
        -0.001)))
            QGEN(ii)=-QGEN(ii);
            bustype(bgen)=3; %% load bus
            if(Rpower>QMAX(ii))
                QGEN(ii)=QMAX(ii);
                statusgen(ii)=0;
            else
                QGEN(ii)=QMIN(ii);
                statusgen(ii)=2;
            end
        end
    end
end
end
end
if(bustype(bgen)==1 | bustype(bgen)==2)
    SetGenQ=SetGenQ+1;
    IndGenQ(SetGenQ)=ii;
end
end
else
    for(ii = 1: ngn )
        SetGenQ=SetGenQ+1;
        IndGenQ(SetGenQ)=ii;
    end
end
return; %% End of Voltage function

function [ANGLE,VOLTAGE,LAMBDAQ,LAMBDAQ,PGENERATED] = VectorAux(nbb,...
ngn,VM,VA,LambdaP,LambdaQ,PGEN,vmax,vmin,ANGLE,VOLTAGE,LAMBDAQ,...
LAMBDAQ,PGENERATED);
for ii = 1: nbb
    ANGLE(ii)=VA(ii);
    VOLTAGE(ii)=VM(ii);
    LAMBDAQ(ii)=LambdaP(ii);
    LAMBDAQ(ii)=LambdaQ(ii);
    if(VM(ii) >=vmax(ii))
        VOLTAGE(ii)=vmax(ii);
    elseif(VM(ii)<=vmin(ii))
        VOLTAGE(ii)=vmin;
    end
end
end
for ii = 1: ngn

```

```

    PGENERATED(ii)=PGEN(ii);
end
return; %%End of VectorAux function

function [Hessian,grad] = MatrixW(nbb,bustype,ngn,GKK,BKK,GKM,BKM,...
    tlsend,tlrec,LambdaP,LambdaQ,VM,VA,ntl);
Hessian = zeros(4*nbb+ngn,4*nbb+ngn);
grad = zeros(4*nbb+ngn,1);
for jj = 1: ntl
    send= tlsend(jj);
    rece= tlrec(jj);
    %% Load-Load
    if(bustype(send)== 3 & bustype(rece)==3)
        nb=nbb;
        i1=1;
        i2=2;

        for ii = 1: 2
            v1= VM(send);      v2= VM(rece);
            A1= VA(send);      A2= VA(rece);
            LP1=LambdaP(send);    LP2=LambdaP(rece);
            LQ1=LambdaQ(send);    LQ2=LambdaQ(rece);
            difAng12=A1-A2;
            difAng21=A2-A1;
            G12=GKM(jj); B12=BKM(jj); G11=GKK(jj); B11=BKK(jj);
            G21=G12; B21=B12; G22=G11; B22=B11;
            Hkm=(G12*sin(difAng12)-B12*cos(difAng12));
            Nkm=(G12*cos(difAng12)+B12*sin(difAng12));
            Hmk=(G21*sin(difAng21)-B21*cos(difAng21));
            Nmk=(G21*cos(difAng21)+B21*sin(difAng21));

            %% Diagonal element
            Hessian(send,send)=Hessian(send,send)-LP1*v1*v2*Nkm-LP2*v1...
            *v2*Nmk -LQ1*v1*v2*Hkm-LQ2*v1*v2*Hmk;
            Hessian(send,1*nb+send)=Hessian(send,1*nb+send)-...
            LP1*v2*Hkm+LP2*v2*Hmk+LQ1*v2*Nkm-LQ2*v2*Nmk;
            Hessian(send,2*nb+send)=Hessian(send,2*nb+send)-v1*v2*Hkm;
            Hessian(send,3*nb+send)=Hessian(send,3*nb+send)+v1*v2*Nkm;

            Hessian(nb+send,send)=Hessian(nb+send,send)-...
            LP1*v2*Hkm+LP2*v2*Hmk+LQ1*v2*Nkm-LQ2*v2*Nmk;
            Hessian(nb+send,nb+send)=Hessian(nb+send,nb+send)...
            +LP1*2*G11-LQ1*2*B11;
            Hessian(nb+send,2*nb+send)=Hessian(nb+send,2*nb+send)...
            +2*v1*G11+v2*Nkm;

```

```

Hessian(nb+send,3*nb+send)=Hessian(nb+send,3*nb+send)-...
2*v1*B11+v2*Hkm;

Hessian(2*nb+send,send)=Hessian(2*nb+send,send)-v1*v2*Hkm;
Hessian(2*nb+send,nb+send)=Hessian(2*nb+send,nb+send)+2*v1*G11...
+v2*Nkm;
Hessian(2*nb+send,2*nb+send)=Hessian(2*nb+send,2*nb+send);
Hessian(2*nb+send,3*nb+send)=Hessian(2*nb+send,3*nb+send);

Hessian(3*nb+send,send)=Hessian(3*nb+send,send)+v1*v2*Nkm;
Hessian(3*nb+send,nb+send)=Hessian(3*nb+send,nb+send)-...
2*v1*B11+v2*Hkm;
Hessian(3*nb+send,2*nb+send)=Hessian(3*nb+send,2*nb+send);
Hessian(3*nb+send,3*nb+send)=Hessian(3*nb+send,3*nb+send);

%% Off diagonal element
Hessian(send,rece)=Hessian(send,rece)+LP1*v1*v2*Nkm+...
LP2*v1*v2*Nmk+LQ1*v1*v2*Hkm+LQ2*v1*v2*Hmk;
Hessian(send,nb+rece)=Hessian(send,nb+rece)-...
LP1*v1*Hkm+LP2*v1*Hmk+LQ1*v1*Nkm-LQ2*v1*Nmk;
Hessian(send,2*nb+rece)=Hessian(send,2*nb+rece)+v1*v2*Hmk;
Hessian(send,3*nb+rece)=Hessian(send,3*nb+rece)-v1*v2*Nmk;

Hessian(nb+send,rece)=Hessian(nb+send,rece)+LP1*v2...
*Hkm-LP2*v2*Hmk-LQ1*v2*Nkm+LQ2*v2*Nmk;
Hessian(nb+send,nb+rece)=Hessian(nb+send,nb+rece)+LP1*Nkm+...
LP2*Nmk+LQ1*Hkm+LQ2*Hmk;
Hessian(nb+send,2*nb+rece)=Hessian(nb+send,2*nb+rece)+v2*Nmk;
Hessian(nb+send,3*nb+rece)=Hessian(nb+send,3*nb+rece)+v2*Hmk;

Hessian(2*nb+send,rece)=Hessian(2*nb+send,rece)+v1*v2*Hkm;
Hessian(2*nb+send,nb+rece)=Hessian(2*nb+send,nb+rece)+v1*Nkm;
Hessian(2*nb+send,2*nb+rece)=Hessian(2*nb+send,2*nb+rece);
Hessian(2*nb+send,3*nb+rece)=Hessian(2*nb+send,3*nb+rece);

Hessian(3*nb+send,rece)=Hessian(3*nb+send,rece)-v1*v2*Nkm;
Hessian(3*nb+send,nb+rece)=Hessian(3*nb+send,nb+rece)+v1*Hkm;
Hessian(3*nb+send,2*nb+rece)=Hessian(3*nb+send,2*nb+rece);
Hessian(3*nb+send,3*nb+rece)=Hessian(3*nb+send,3*nb+rece);

grad(send)=grad(send)-(-LP1*v1*v2*Hkm+LP2*v1*v2*Hmk+LQ1*v1*v2...
*Nkm-LQ2*v1*v2*Nmk);
grad(nb+send)=grad(nb+send)-...
(+LP1*(2*v1*G11+v2*Nkm)+LP2*v2*Nmk+LQ1*(2*v1*B11+v2*Hkm)...
+LQ2*v2*Hmk);

```

```

grad(2*nb+send)=0.0;
grad(3*nb+send)=0.0;

    itemp=send;    send=rece;    rece=itemp;
    itemp=i1;     i1=i2;     i2=itemp;
    rtemp=A1;     A1=A2;     A2=rtemp;
end
end

%% PV-load buses or Slack-load buses
if((bustype(send)==2 & bustype(rece)==3) | ...
    (bustype(send)==3 & bustype(rece)==2) | ...
    (bustype(send)==1 & bustype(rece)==3) | ...
    (bustype(send)==3 & bustype(rece)==1))
    nb=nb+1;
    i1=1;
    i2=2;

    for ii = 1:2
        v1=VM(send);    v2=VM(rece);
        A1=VA(send);    A2=VA(rece);
        LP1=LambdaP(send);    LP2=LambdaP(rece);
        LQ1=LambdaQ(send);    LQ2=LambdaQ(rece);
        difAng12=A1-A2;    difAng21=A2-A1;
        G12=GKM(jj); B12=BKM(jj); G11=GKK(jj); B11=BKK(jj);
        G21=G12;    B21=B12;    G22=G11;    B22=B11;

        Hkm=(G12*sin(difAng12)-B12*cos(difAng12));
        Nkm=(G12*cos(difAng12)+B12*sin(difAng12));
        Hmk=(G21*sin(difAng21)-B21*cos(difAng21));
        Nmk=(G21*cos(difAng21)+B21*sin(difAng21));

        if(bustype(send)==2 | bustype(rece)==1)
            LQ1=0;
        else
            LQ2=0;
        end

        %% Diagonal elements
        Hessian(send,send) = Hessian(send,send)-LP1*v1*v2...
        *Nkm-LP2*v1*v2*Nmk-LQ1*v1*v2*Hkm-LQ2*v1*v2*Hmk;
        Hessian(send,1*nb+send) = Hessian(send,1*nb+send)-...
        LP1*v2*Hkm+LP2*v2*Hmk+LQ1*v2*Nkm-LQ2*v2*Nmk;
        Hessian(send,2*nb+send) = Hessian(send,2*nb+send)-v1*v2*Hkm;
    end
end

```

```

Hessian(send,3*nb+send) = Hessian(send,3*nb+send)+v1*v2*Nkm;
Hessian(nb+send,send) = Hessian(nb+send,send)-...
LP1*v2*Hkm+LP2*v2*Hmk+LQ1*v2*Nkm-LQ2*v2*Nmk;
Hessian(nb+send,nb+send) = Hessian(nb+send,nb+send)+...
LP1*2*G11-LQ1*2*B11;
Hessian(nb+send,2*nb+send) = Hessian(nb+send,2*nb+send)+...
2*v1*G11+v2*Nkm;
Hessian(nb+send,3*nb+send) = Hessian(nb+send,3*nb+send)-...
2*v1*B11+v2*Hkm;

Hessian(2*nb+send,send) = Hessian(2*nb+send,send)-v1*v2*Hkm;
Hessian(2*nb+send,nb+send) = Hessian(2*nb+send,nb+send)+...
2*v1*G11+v2*Nkm;
Hessian(2*nb+send,2*nb+send)=Hessian(2*nb+send,2*nb+send);
Hessian(2*nb+send,3*nb+send)=Hessian(2*nb+send,3*nb+send);

Hessian(3*nb+send,send)=Hessian(3*nb+send,send)+v1*v2*Nkm;
Hessian(3*nb+send,nb+send)=Hessian(3*nb+send,nb+send)-...
2*v1*B11+v2*Hkm;
Hessian(3*nb+send,2*nb+send)=Hessian(3*nb+send,2*nb+send);
Hessian(3*nb+send,3*nb+send)=Hessian(3*nb+send,3*nb+send);

%% Off-Diagonal elements
Hessian(send,rece)=Hessian(send,rece)+LP1*v1*v2*Nkm+LP2*v1*v2*...
Nmk+LQ1*v1*v2*Hkm+LQ2*v1*v2*Hmk;
Hessian(send,nb+rece)=Hessian(send,nb+rece)-...
LP1*v1*Hkm+LP2*v1*Hmk+LQ1*v1*Nkm-LQ2*v1*Nmk;
Hessian(send,2*nb+rece)=Hessian(send,2*nb+rece)+v1*v2*Hmk;
Hessian(send,3*nb+rece)=Hessian(send,3*nb+rece)-v1*v2*Nmk;

Hessian(nb+send,rece)=Hessian(nb+send,rece)+LP1*v2...
*Hkm-LP2*v2*Hmk-LQ1*v2*Nkm+LQ2*v2*Nmk;
Hessian(nb+send,nb+rece)=Hessian(nb+send,nb+rece)+LP1*Nkm+LP2*...
Nmk+LQ1*Hkm+LQ2*Hmk;
Hessian(nb+send,2*nb+rece)=Hessian(nb+send,2*nb+rece)+v2*Nmk;
Hessian(nb+send,3*nb+rece)=Hessian(nb+send,3*nb+rece)+v2*Hmk;

Hessian(2*nb+send,rece)=Hessian(2*nb+send,rece)+v1*v2*Hkm;
Hessian(2*nb+send,nb+rece)=Hessian(2*nb+send,nb+rece)+v1*Nkm;
Hessian(2*nb+send,2*nb+rece)=Hessian(2*nb+send,2*nb+rece);
Hessian(2*nb+send,3*nb+rece)=Hessian(2*nb+send,3*nb+rece);

Hessian(3*nb+send,rece)=Hessian(3*nb+send,rece)-v1*v2*Nkm;
Hessian(3*nb+send,nb+rece)=Hessian(3*nb+send,nb+rece)+v1*Hkm;
Hessian(3*nb+send,2*nb+rece)=Hessian(3*nb+send,2*nb+rece);

```

```

Hessian(3*nb+send,3*nb+rece)=Hessian(3*nb+send,3*nb+rece);

grad(send)=grad(send)-(-LP1*v1*v2*Hkm+LP2*v1*v2*Hmk+ ...
LQ1*v1*v2*Nkm-LQ2*v1*v2*Nmk);
grad(nb+send)=grad(nb+send)+(LP1*(2*v1*G11+v2*Nkm)+LP2*v2*Nmk+...
LQ1*(-2*v1*B11+v2*Hkm)+LQ2*v2*Hmk);
grad(2*nb+send)=0.0;
grad(3*nb+send)=0.0;

    itemp=send;    send=rece;    rece=itemp;
    itemp=i1;      i1=i2;        i2=itemp;
    rtemp=A1;      A1=A2;        A2=rtemp;
end
end
%% Slack-PV or PV-PV
if((bustype(send)==1 & bustype(rece)==2)|...
(bustype(send)==2 & bustype(rece)==1)|...
(bustype(send)==2 & bustype(rece)==2))
nb=nbb;
i1=1;
i2=2;
for ii = 1:2
    v1=VM(send);    v2=VM(rece);
    A1=VA(send);    A2=VA(rece);
    LP1=LambdaP(send);    LP2=LambdaP(rece);
    LQ1=0;    LQ2=0;
    difAng12=A1-A2;    difAng21=A2-A1;
    G12=GKM(jj);    B12=BKM(jj);    G11=GKK(jj);    B11=BKK(jj);
    G21=G12;    B21=B12;    G22=G11;    B22=B11;
    Hkm=(G12*sin(difAng12)-B12*cos(difAng12));
    Nkm=(G12*cos(difAng12)+B12*sin(difAng12));
    Hmk=(G21*sin(difAng21)-B21*cos(difAng21));
    Nmk=(G21*cos(difAng21)+B21*sin(difAng21));

%% Diagonal elements
Hessian(send,send)=Hessian(send,send)-LP1*v1*v2*Nkm-LP2*v1*v2*...
Nmk-LQ1*v1*v2*Hkm-LQ2*v1*v2*Hmk;
Hessian(send,1*nb+send)=Hessian(send,1*nb+send)-...
LP1*v2*Hkm+LP2*v2*Hmk+LQ1*v2*Nkm-LQ2*v2*Nmk;
Hessian(send,2*nb+send)=Hessian(send,2*nb+send)-v1*v2*Hkm;
Hessian(send,3*nb+send)=Hessian(send,3*nb+send)+v1*v2*Nkm;

Hessian(nb+send,send)=Hessian(nb+send,send)-...
LP1*v2*Hkm+LP2*v2*Hmk+LQ1*v2*Nkm-LQ2*v2*Nmk;
Hessian(nb+send,nb+send)=Hessian(nb+send,nb+send)+LP1*2*G11-...
LQ1*2*B11;

```

```

Hessian(nb+send,2*nb+send)=Hessian(nb+send,2*nb+send)+2*v1*G11...
+v2*Nkm;
Hessian(nb+send,3*nb+send)=Hessian(nb+send,3*nb+send)-...
2*v1*B11+v2*Hkm;

Hessian(2*nb+send,send)=Hessian(2*nb+send,send)-v1*v2*Hkm;
Hessian(2*nb+send,nb+send)=Hessian(2*nb+send,nb+send)+2*v1*G11...
+v2*Nkm;
Hessian(2*nb+send,2*nb+send)=Hessian(2*nb+send,2*nb+send);
Hessian(2*nb+send,3*nb+send)=Hessian(2*nb+send,3*nb+send);

Hessian(3*nb+send,send)=Hessian(3*nb+send,send)+v1*v2*Nkm;
Hessian(3*nb+send,nb+send)=Hessian(3*nb+send,nb+send)...
-2*v1*B11+v2*Hkm;
Hessian(3*nb+send,2*nb+send)=Hessian(3*nb+send,2*nb+send);
Hessian(3*nb+send,3*nb+send)=Hessian(3*nb+send,3*nb+send);

%% off-diagonal elements
Hessian(send,rece)=Hessian(send,rece)+LP1*v1*v2*Nkm+...
LP2*v1*v2*Nkm+LQ1*v1*v2*Hkm+LQ2*v1*v2*Hmk;
Hessian(send,nb+rece)=Hessian(send,nb+rece)-...
LP1*v1*Hkm+LP2*v1*Hmk+LQ1*v1*Nkm-LQ2*v1*Nmk;
Hessian(send,2*nb+rece)=Hessian(send,2*nb+rece)+v1*v2*Hmk;
Hessian(send,3*nb+rece)=Hessian(send,3*nb+rece)-v1*v2*Nmk;

Hessian(nb+send,rece)=Hessian(nb+send,rece)+LP1*v2...
*Hkm-LP2*v2*Hmk-LQ1*v2*Nkm+LQ2*v2*Nmk;
Hessian(nb+send,nb+rece)=Hessian(nb+send,nb+rece)+LP1...
*Nkm+LP2*Nmk+LQ1*Hkm+LQ2*Hmk;
Hessian(nb+send,2*nb+rece)=Hessian(nb+send,2*nb+rece)+v2*Nmk;
Hessian(nb+send,3*nb+rece)=Hessian(nb+send,3*nb+rece)+v2*Hmk;

Hessian(2*nb+send,rece)=Hessian(2*nb+send,rece)+v1*v2*Hkm;
Hessian(2*nb+send,nb+rece)=Hessian(2*nb+send,nb+rece)+v1*Nkm;
Hessian(2*nb+send,2*nb+rece)=Hessian(2*nb+send,2*nb+rece);
Hessian(2*nb+send,3*nb+rece)=Hessian(2*nb+send,3*nb+rece);

Hessian(3*nb+send,rece)=Hessian(3*nb+send,rece)-v1*v2*Nkm;
Hessian(3*nb+send,nb+rece)=Hessian(3*nb+send,nb+rece)+v1*Hkm;
Hessian(3*nb+send,2*nb+rece)=Hessian(3*nb+send,2*nb+rece);
Hessian(3*nb+send,3*nb+rece)=Hessian(3*nb+send,3*nb+rece);

grad(send)=grad(send)-(-LP1*v1*v2*Hkm+LP2*v1*v2*Hmk+LQ1*v1*v2...
*Nkm-LQ2*v1*v2*Nmk);
grad(nb+send)=grad(nb+send)-(+LP1*(2*v1*G11+v2*Nkm)+...

```

```

LP2*v2*Nmk+LQ1*(-2*v1*B11+v2*Hkm)+LQ2*v2*Hmk);
grad(2*nb+send)=0.0;
grad(3*nb+send)=0.0;

itemp=send;      send=rece;      rece=itemp;
itemp=i1;        i1=i2;         i2=itemp;
rtemp=A1;        A1=A2;         A2=rtemp;
end
end
end
return; %%End of MatrixW function

function [Hessian,grad] = MatrixWGen(nbb,ntl,ngn,genbus,B,C,LambdaP,...
PGEN,Hessian,grad);
for jj = 1: ngn
    Gbus=genbus(jj);
    Hessian(4*nbb+jj,4*nbb+jj)=Hessian(4*nbb+jj,4*nbb+jj)+2*C(jj);
%% // - - - - Out of Diagonal
    Hessian(4*nbb+jj,2*nbb+Gbus)=Hessian(4*nbb+jj,2*nbb+Gbus)-1.0;
    Hessian(2*nbb+Gbus,4*nbb+jj)=Hessian(2*nbb+Gbus,4*nbb+jj)-1.0;
    LP1=LambdaP(Gbus);
    PGenI=PGEN(jj);
    grad(4*nbb+jj)= grad(4*nbb+jj)-(B(jj)+2*C(jj)*PGenI-LP1);
end
return; %%End of MatrixWGen function

function [Hessian,grad] = Mismatch(nbb,ngn,genbus,PGEN,QGEN,PLOAD,...
QLOAD,Pbus,Qbus,Hessian,grad);
AUXP = zeros(nbb,1);
AUXQ = zeros(nbb,1);
for jj = 1: ngn
    AUXP(genbus(jj)) = PGEN(jj);
    AUXQ(genbus(jj)) = QGEN(jj);
end
for ii= 1: nbb
    grad(2*nbb+ii)=0;
    grad(3*nbb+ii)=0;
    grad(2*nbb+ii)=grad(2*nbb+ii)-(Pbus(ii)-AUXP(ii)+PLOAD(ii));
    grad(3*nbb+ii)=grad(3*nbb+ii)-(Qbus(ii)-AUXQ(ii)+QLOAD(ii));
end
return; %%End of Mismatch function

function [Hessian,grad] = PenaltyFunctionQ(nbb,BigNumber,Hessian,...
grad,genbus,IndGenQ,SetGenQ,LambdaQ,ActivedQ);
for(ii = 1: SetGenQ)
    in1=IndGenQ(ii);
    send=genbus(in1);

```

```

Hessian(3*nbb+send,3*nbb+send)=Hessian(3*nbb+send,3*nbb+send)+...
2*BigNumber;
ActivatedQ(in1)=2;
LQ1=LambdaQ(send);
grad(3*nbb+send)=grad(3*nbb+send)-2*BigNumber*LQ1;
end
return; %%End of PenaltyFunctionQ function

function [Hessian,grad] = Convexificacion(nbb,Hessian,grad,Cc,vmax,...
vmin,VOLTAGE,StatusVoltage,VM);
%% Slack bus must be the first node
Hessian(1,1)=Hessian(1,1)+10e10;
%% Voltage magnitudes
for ii= 1: nbb
    Vol=VM(ii);
    VOLD=VOLTAGE(ii);
    VolMax=vmax(ii);
    VolMin=vmin(ii);
    StatV=StatusVoltage(ii);
    Hessian(nbb+ii,nbb+ii)=Hessian(nbb+ii,nbb+ii)+Cc;
    if(StatV==0)
        grad(nbb+ii)=grad(nbb+ii)-(Cc*(Vol-VolMax));
    elseif(StatV==1)
        grad(nbb+ii)=grad(nbb+ii)-(Cc*(Vol-VOLD));
    elseif(StatV==2)
        grad(nbb+ii)=grad(nbb+ii)-(Cc*(Vol-VolMin));
    end
end
return; %%End of Convexification function

function [Hessian,grad,ActivatedV,ActivatedP] = AugmentedLagrangian(nbb,...
Hessian,grad,Ckv,Ckg,vmax,vmin,VOLTAGE,StatusVoltage,VM,ActivatedV,...
MiuBus,ngn,ActivatedP,PGEN,StatP,MiuGen,PMAX,PMIN);
%% NODES
for(ii= 1: nbb)
    if(ActivatedV(ii)~=0)
        Vol=VM(ii);
        VOLD=VOLTAGE(ii);
        VolMax=vmax(ii);
        VolMin=vmin(ii);
        StatV=StatusVoltage(ii);
        MiuB=MiuBus(ii);
        send= ii;
        Hessian(nbb+send,nbb+send)=Hessian(nbb+send,nbb+send)+Ckv;
        if(StatV==0)
            grad(nbb+send)=grad(nbb+send)-(MiuB+Ckv*(Vol-VolMax));
        end
    end
end

```

```

    if(StatV==2)
        grad(nbb+send)=grad(nbb+send)-(MiuB+Ckv*(Vol-VolMin));
    end
    if(ActivatedV(send)==0)
        ActivatedV(send)=1;
    end
end
end
end

%% GENERATORS
for(ii= 1: ngn)
    if(ActivatedP(ii)~=0)
        for (ii = 1: ngn)
            send=ii;
            PGenI=PGEN(ii);
            Stat=StatP(ii);
            MiuG= MiuGen(ii);
            Max_PGen=PMAX(ii);
            Min_PGen=PMIN(ii);
            Hessian(4*nbb+send,4*nbb+send) = Hessian(4*nbb+send,4*nbb...
+send)+Ckg;
            if(Stat==0)
                grad(4*nbb+send)=grad(4*nbb+send)-(MiuG+Ckg*...
(PGenI-Max_PGen));
            end
            if(Stat==2)
                grad(4*nbb+send)=grad(4*nbb+send)-(MiuG+Ckg*...
(PGenI-Min_PGen));
            end
            if(ActivatedP(ii)==0)
                ActivatedP(ii)=1;
            end
        end
    end
end
end
return; %%End of AugmentedLagrangian function

function [Dz,VA,VM,LambdaP,LambdaQ,PGEN] = Actualisation(Dz,nbb,VA,VM,...
LambdaP,LambdaQ,bustype,ngn,PGEN);
for(ii= 1: nbb)
    p1 = Dz(ii);
    p2 = Dz(nbb+ii);
    p3 = Dz(2*nbb+ii);
    p4 = Dz(3*nbb+ii);
    %% Load bus

```

```

if(bustype(ii)==3)
    VA(ii)=VA(ii)+p1;
    VM(ii)=VM(ii)+p2;
    LambdaP(ii)=LambdaP(ii)+p3;
    LambdaQ(ii)=LambdaQ(ii)+p4;
    %%%% Slack bus
elseif(bustype(ii)==1)
    VA(ii)=0.0; %%%% It must be zero
    VM(ii)=VM(ii)+p2;
    LambdaP(ii)=LambdaP(ii)+p3;
    LambdaQ(ii)=LambdaQ(ii)+0.0; %%%% It must be zero
    %%%% Generator bus
elseif(bustype(ii)==2)
    VA(ii)=VA(ii)+p1;
    VM(ii)=VM(ii)+p2;
    LambdaP(ii)=LambdaP(ii)+p3;
    LambdaQ(ii)=LambdaQ(ii)+0.0; %%%% It must be zero
end
end

for(ii= 1: ngn)
    PGEN(ii)=PGEN(ii)+Dz(4*nbb+ii);
end
return; %End of Actualisation function

function [Hessian,grad] = Reset_Hessian_grad(Hessian,grad,ngn,nbb);
for ii = 1: (4*nbb+ngn)
    for jj = 1: (4*nbb+ngn)
        Hessian(ii,jj)=0;
    end
    grad(ii)=0;
end
return; %End of Reset_Hessian_grad function

function [Optimo] =ReviewNodes(Optimo,grad,nbb,bustype,ActivatedV,TOL);
for (ii = 1: nbb)
    p1=grad(ii);
    p2=grad(nbb+ii);
    p3=grad(2*nbb+ii);
    p4=grad(3*nbb+ii);
    if(ActivatedV(ii)~=0)
        p2=1e-10;
    else
        p2=1e-10;
    end
end

```

```

    if(p1<0),p1=-p1;end
    if(p2<0),p2=-p2;end
    if(p3<0),p3=-p3;end
    if(p4<0),p4=-p4;end

    if(bustype(ii)==3) %%%% Load bus
        if(p1>TOL),Optimo=1;end
        if(p2>TOL),Optimo=1;end
        if(p3>TOL),Optimo=1;end
        if(p4>TOL),Optimo=1;end
    end
    if(bustype(ii)==1) %%%% Slack bus
        if(p1>TOL),Optimo=1;end
        if(p2>TOL),Optimo=1;end
        if(p3>TOL),Optimo=1;end
        if(p4>TOL),Optimo=1;end
    end
    if(bustype(ii)==2) %%%% Generator bus
        if(p1>TOL),Optimo=1;end
        if(p2>TOL),Optimo=1;end
        if(p3>TOL),Optimo=1;end
        if(p4>TOL),Optimo=1;end
    end
end
return; %%End of ReviewNodes function

function [Optimo] = ReviewGen(Optimo,grad,ngn,ActivatedP,TOL,nbb);
for (ii = 1: ngn)
    p1=grad(4*nbb+ii);
    if(ActivatedP(ii)~=0), p1=1e-10;end
    if(p1<0),p1=-p1;end
    if(p1>TOL)Optimo=1;end
end
return; %%End of ReviewGen function

function [MaxDz] = Norma(MaxDz,grad,nbb,ngn);
MaxDz=0;
for(ii = 1: nbb)
    value=grad(ii);
    if(value<0),value=-value;end
    if(value>MaxDz),MaxDz=value;end
end
for(ii = (2*nbb+1): (4*nbb+ngn))
    value=grad(ii);

```

```

    if(value<0),value=-value;end
    if(value>MaxDz),MaxDz=value;end
end
return; %%End of Norma function

```

```

function [StatusVoltage,SetVol,NumNode,ValueVoltage]...
= Check_Limits_V(nbb,TolVoltage,vmin,vmax,VM,StatusVoltage,Dz,...
SetVol,NumNode,ValueVoltage,ActivatedV);
for (ii = 1: nbb)
    if(ActivatedV(ii)==0)
        Movement=Dz(nbb+ii);
        Kindex=0.0;
        if(((vmin(ii)-TolVoltage)<VM(ii)) &(VM(ii)<(vmax(ii) + ...
TolVoltage)))
            StatusVoltage(ii)=1;
        end
        if(VM(ii)>(vmax(ii)+TolVoltage))
            StatusVoltage(ii)=0;
            Kindex=(VM(ii)-vmax(ii))/Movement;
            if(Kindex<0),Kindex=-Kindex;end
        end
        if(VM(ii)<(vmin(ii)-TolVoltage))
            StatusVoltage(ii)=2;
            Kindex=(vmin(ii)-VM(ii))/Movement;
            if(Kindex<0),Kindex=-Kindex;end
        end
        if(Kindex > 0)
            SetVol=SetVol+1;
            NumNode(SetVol)= ii;
            ValueVoltage(SetVol)=Kindex;
        end
    end
end
return; %%End of Check_Limits_V function

```

```

function [StatP,SetGenP,NumGenerator,ValueGenerator]...
= Check_Limits_P(ngn,TolPower,PMIN,PMAX,PGEN,StatP,SetGenP,...
NumGenerator,ValueGenerator,ActivatedP);
for (ii = 1: ngn)
    if(ActivatedP(ii)==0)
        Movement=1;
        Kindex=0.0;

```

```

    if(((PMIN(ii)-TolPower)<PGEN(ii)) &(PGEN(ii)<(PMAx(ii)...
+TolPower)))
        StatP(ii)=1;
    end
    if(PGEN(ii)>(PMAx(ii)+TolPower))
        StatP(ii)=0;
        Kindex=(PGEN(ii)-PMAx(ii))/Movement;
        if(Kindex<0),Kindex=-Kindex;end
    end
    if(PGEN(ii)<(PMIN(ii)-TolPower))
        StatP(ii)=2;
        Kindex=(PMIN(ii)-PGEN(ii))/Movement;
        if(Kindex<0),Kindex=-Kindex;end
    end
    if(Kindex > 0)
        SetGenP=SetGenP+1;
        NumGenerator(SetGenP)= ii;
        ValueGenerator(SetGenP)=Kindex;
    end
end
end
return; %%End of Check_Limits_P function

function [Hessian,grad,ActivatedV] = AugmentedLagrangianV(nbb,...
Hessian,grad,Ckv,vmax,vmin,StatusVoltage,VM,ActivatedV,MiuBus,...
SetVol,NumNode,ValueVoltage,MaxVol,EnforceTol);
for(jj = 1: SetVol)
    in1=NumNode(jj);
    if(((ValueVoltage(jj)/MaxVol)>=EnforceTol) | (VM(in1)<0.80)...
| (VM(in1)>1.20))
        ii=in1;
        Vol=VM(ii);
        VolMax=vmax(ii);
        VolMin=vmin(ii);
        StatV=StatusVoltage(ii);
        MiuB=MiuBus(ii);
        send= ii;
        Hessian(nbb+send,nbb+send)=Hessian(nbb+send,nbb+send)+Ckv;
        if(StatV==0)
            grad(nbb+send)=grad(nbb+send)-(MiuB+Ckv*(Vol-VolMax));
        end
        if(StatV==2)
            grad(nbb+send)=grad(nbb+send)-(MiuB+Ckv*(Vol-VolMin));
        end
        if(ActivatedV(send)==0)

```

```

        ActivedV(send)=1;
    end
end
end
return; %%End of AugmentedLagrangianV function

```

```

function[Hessian,grad,ActivatedP] = AugmentedLagrangianG(ngn,nbb,...
Hessian,grad,Ckg,PMIN,PMAX,StatP,PGEN,ActivatedP,MiuGen,SetGenP,...
NumGenerator,ValueGenerator,MaxGen,EnforceTol);
for(jj = 1: SetGenP)
    in1=NumGenerator(jj);
    if((ValueGenerator(jj)/MaxGen)>=EnforceTol)
        ii=in1;
        send=ii;
        PGenI=PGEN(ii);
        Stat=StatP(ii);
        MiuG= MiuGen(ii);
        Max_PGen=PMAX(ii);
        Min_PGen=PMIN(ii);
        Hessian(4*nbb+send,4*nbb+send)=Hessian(4*nbb+send,4*nbb+send)...
        +Ckg;
        if(Stat==0)
            grad(4*nbb+send)=grad(4*nbb+send)-(MiuG+Ckg*(PGenI- ...
            Max_Pgen));
        end
        if(Stat==2)
            grad(4*nbb+send)=grad(4*nbb+send)-(MiuG+Ckg*(PGenI-...
            Min_PGen));
        end
        if(ActivatedP(ii)==0)
            ActivedP(ii)=1;
        end
    end
end
return; %%End of AugmentedLagrangianG function

```

```

function [Hessian,grad,ActivatedV] = AugmentedLagrangian_IV(nbb,...
Hessian,grad,Ckv,vmax,vmin,StatusVoltage,VM,ActivatedV,MiuBus,ii);
Vol=VM(ii);
VolMax=vmax(ii);
VolMin=vmin(ii);
StatV=StatusVoltage(ii);
MiuB=MiuBus(ii);
send= ii;
Hessian(nbb+send,nbb+send)=Hessian(nbb+send,nbb+send)+Ckv;
if(StatV==0)

```

```

    grad(nbb+send)=grad(nbb+send)-(MiuB+Ckv*(Vol-VolMax));
end
if(StatV==2)
    grad(nbb+send)=grad(nbb+send)-(MiuB+Ckv*(Vol-VolMin));
end
if(ActivatedV(send)==0);ActivatedV(send)=1;end
return; %%End of AugmentedLagrangian_IV function

```

```

function [MiuBus,NumMiu_V,ValMiu_V,RelVol] = IdentifyMiuBus(...
StatusVoltage,MiuBus,Ckv,VM,vmax,vmin,ActivatedV,RelVol,NumMiu_V,...
ValMiu_V,ii);
Tolerance=0.0001;
StatV=StatusVoltage(ii);
if(MiuBus(ii)==0),Tolerance=0;end
temp=MiuBus(ii);
if(StatV==0)
    MiuBus(ii)=MiuBus(ii)+Ckv*(VM(ii)-vmax(ii)+Tolerance);
end
if(StatV==2)
    MiuBusS(ii)=MiuBus(ii)+Ckv*(VM(ii)-vmin(ii)-Tolerance);
end
Kindex=0.0;
Kindex1=0.0;
if(StatV==1),Kindex1=Kindex; end
if(ActivatedV(ii)==2)
    if(StatV==0)
        if(MiuBus(ii)<0),Kindex1=MiuBus(ii); end
        if(MiuBus(ii)>=0),Kindex1=0; end
        if(Kindex1<0),Kindex1=-Kindex1; end
    end
    if(StatV==2)
        if(MiuBus(ii)>0),Kindex1=MiuBus(ii); end
        if(MiuBus(ii)<=0),Kindex1=0; end
        if(Kindex1<0),Kindex1=-Kindex1; end
    end
end
MiuBus(ii)=temp;
if(Kindex1>0)
    RelVol=RelVol+1;
    NumMiu_V(RelVol)=ii;
    ValMiu_V(RelVol)=Kindex;
end
return; %%End of IdentifyMiuBus function

```

```

function [Hessian,grad,ActivatedP] = AugmentedLagrangian_IG(ngn,...
Hessian,grad,Ckg,PMIN,PMAX,StatP,PGEN,ActivatedP,MiuGen,ii);

```

```

send=ii;
PGenI=PGEN(ii);
Stat=StatP(ii);
MiuG=MiuGen(ii);
Max_PGen=PMAX(ii);
Min_PGen=PMIN(ii);

Hessian(4*nbb+send,4*nbb+send)=Hessian(4*nbb+send,4*nbb+send)+Ckg;
if(Stat==0)
    grad(4*nbb+send)=grad(4*nbb+send)-(MiuG+Ckg*(PGenI-Max_PGen));
end
if(Stat==2)
    grad(4*nbb+send)=grad(4*nbb+send)-(MiuG+Ckg*(PGenI-Min_PGen));
end

if(ActivatedP(ii)==0);ActivatedP(ii)=1;end
return; %%End of AugmentedLagrangian_IG function

function [MiuBus,NumMiu_P,ValMiu_P,RelGen] = IdentifyMiuGen...
(StatP,MiuGen,Ckg,PGEN,PMAX,PMIN,ActivatedP,RelGen,NumMiu_P,...
ValMiu_P,ii);
Tolerance=0.0000001;
Stat=StatP(ii);
if(MiuGen(ii)==0),Tolerance=0;end
temp=MiuGen(ii);
Kindex=0.0;
Kindex1=0.0;
if(Stat==0),MiuGen(ii)=MiuGen(ii)+Ckg*(PGen+Tolerance-Max_PGen);end
if(Stat==2),MiuGen(ii)=MiuGen(ii)+Ckg*(PGen-Tolerance-Min_PGen);end
if(Stat==1),Kindex1=Kindex;end
if(ActivatedP(ii)==2)
if(Stat==0)
    if(MiuGen(ii)<0),Kindex1=MiuGen(ii);end
    if(MiuGen(ii)>0),Kindex1=0;end
    if(Kindex1<0),Kindex1=-Kindex1;end
end
if(Stat==2)
    if(MiuGen(ii)>0),Kindex1=MiuGen(ii);end
    if(MiuGen(ii)<0),Kindex1=0;end
    if(Kindex1<0),Kindex1=-Kindex1;end
end
end
MiuGen(ii)=temp;
if(Kindex1>0)
    RelGen=RelGen+1;
    NumMiu_P(RelVol)=ii;

```



```

    ValMiu_P(RelVol)=Kindex;
end
return; %%End of IdentifyMiuGen function

```

```

function [Hessian,grad,ActivatedV,StatusVoltage] =...
ReleasingAumentedLagrangianV(VM,vmax,vmin,StatusVoltage,MiuBus,...
Hessian,grad,Ckv,ActivatedV,StatusVoltage,send);
Vol=VM(send);
VolMax=vmax(send);
VolMin=vmin(send);
StatV=StatusVoltage(send);
MiuB=MiuBus(send);
Hessian(nbb+send,nbb+send)=Hessian(nbb+send,nbb+send)-Ckv;
if(StatV==0),grad(nbb+send)=grad(nbb+send)+MiuB+Ckv*(Vol-VolMax);end
if(StatV==2),grad(nbb+send)=grad(nbb+send)+MiuB+Ckv*(Vol-VolMin);end
ActivatedV(send)=0;
StatusVoltage(send)=1;
return; %%End of ReleasingAumentedLagrangianV function

```

```

function [Hessian,grad,ActivatedP,StatP]=ReleasingAumentedLagrangianG...
(PGEN,PMAX,PMIN,StatP,MiuGen,Hessian, grad,Ckg,ActivatedP,StatP,send);
PGenI=PGEN(send);
Stat=StatP(send);
MiuG=MiuGen(send);
Hessian(4*nbb+send,4*nbb+send)=Hessian(4*nbb+send,4*nbb+send)-Ck;
if(Stat==0)
    grad(4*nbb+send)=grad(4*nbb+send)+MiuG+Ckg*(PGenI-PMAX(send));
end
if(Stat==2),
    grad(4*nbb+send)=grad(4*nbb+send)+MiuG+Ckg*(PGenI-PMIN(send));
end
ActivatedP(send)=0;
StatP(send)=1;
return; %%End of ReleasingAumentedLagrangianG function

```

```

function [MiuBus] = MultiplierBus(nbb,Ckv,MiuBus,VM,vmax,vmin);
TolVoltage=0.00000001;
for(ii = 1:nbb)
    if((MiuBus(ii)+Ckv*(VM(ii)-vmax(ii)+TolVoltage)) >= 0)
        MiuBus(ii)=MiuBus(ii)+Ckv*(VM(ii)-vmax(ii)+TolVoltage);
    elseif((MiuBus(ii)+Ckv*(VM(ii)-vmin(ii)-TolVoltage)) <= 0)
        MiuBus(ii)=MiuBus(ii)+Ckv*(VM(ii)-vmin(ii)-TolVoltage);
    end
end

```

```

else
    MiuBus(ii)=0;
end
end
return; %%End of MultiplierBus function

```

```

function [MiuGen] = MultiplierGen(ngn,Ckg,MiuGen,PGEN,PMAX,PMIN);
TolPower=0.0000001;
for(ii = 1:ngn)
    if((MiuGen(ii)+Ckg*(PGEN(ii)-PMAX(ii)+TolPower)) >= 0)
        MiuGen(ii)=MiuGen(ii)+Ckg*(PGEN(ii)-PMAX(ii)+TolPower);
    elseif((MiuGen(ii)+Ckg*(PGEN(ii)-PMIN(ii)-TolPower)) <= 0)
        MiuGen(ii)=MiuGen(ii)+Ckg*(PGEN(ii)-PMIN(ii)-TolPower);
    else
        MiuGen(ii)=0;
    end
end
return; %%End of MultiplierGen function

```

```

function [ChangeStat,Kindex1,statusgen,LambdaQ,ActivedQ,bustype] =...
IdentifyConstQ(ChangeStat,genbus,statusgen,LambdaQ,ActivedQ,...
bustype, ii);
send=genbus(ii);
ChangeStat=statusgen(ii);
Kindex1=0;
if(statusgen(ii)==0)
    if(LambdaQ(send)<0)
        ActivedQ(ii)=2;
        Kindex1=0;
        bustype(send)=2;
        statusgen(ii)=1;
        LambdaQ(send)=0;
    else
        ActivedQ(ii)=1;
        Kindex1=1;
    end
end
if(statusgen(ii)==2)
    if(LambdaQ(send)>0)
        ActivedQ(ii)=2;
        Kindex1=0;
        bustype(send)=2;
        statusgen(ii)=1;
        LambdaQ(ii)=0;
    end
end

```

```

else
    ActivedQ(ii)=1;
    Kindex1=1;
end
end
if(ChangeStat==statusgen(ii))
    ChangeStat=0;
else
    ChangeStat=1;
end
return; %%End of IdentifyConstQ function

```

```

function [GenViolado] = CheckQGenLimits(GenViolado,QLOAD,Qbus,...
QMIN,QMAX,genbus,TolPower,ii);
GenViolado=1;
Qpower=QLOAD(genbus(ii))+Qbus(genbus(ii));
if(((QMIN(genbus(ii))-TolPower)<Qpower)&(QMAX(genbus(ii))+TolPower)))
    GenViolado=0;
end
return; %%End of CheckQGenLimits function

```

```

function [in1,in2] = MatrixWVtoltageMiu(in1,in2,TolVoltage,VM,vmax,...
vmin,MiuBus,ActivatedV,StatusVoltage,ii);
if(((vmin(ii)-TolVoltage)<VM(ii))&(VM(ii)<(vmax(ii)+TolVoltage)))
    in1=0;
else
    in1=1;
end
if((VM(ii)<0.5)| (VM(ii)>1.5))
    fprintf('\n*****');
    fprintf('\n*                               *');
    fprintf('\n*          UNFEASIBLE SOLUTION          *');
    fprintf('\n*                               *');
    fprintf('\n*****');
end
delta=0;
if(ActivatedV(ii)~=0)
    if(StatusVoltage(ii)==0)
        delta=VM(ii)-vmax(ii);
        if(delta<0),delta=-delta; end
        if(delta>0.0001),in2=1; end
end
if(StatusVoltage(ii)==2)
    delta=VM(ii)-vmax(ii);

```

```

    if(delta<0),delta=-delta; end
    if(delta>0.0001),in2=1; end
    end
end
if(ActivatedV(ii)==0)
    if(MiuBus(ii)>0),in2=1;end
    if(MiuBus(ii)<0),in2=1;end
end
return; %%End of MatrixWVoltageMiu function

```

```

function [in3,in4] = MatrixWGenMiu(in3,in4,TolPower,PGEN,PMAX,PMIN,...
MiuGen,ActivatedP,StatP,ii);
if(((PMIN(ii)-TolPower)<PGEN(ii))(PMAX(ii)+TolPower))
    in3=0;
else
    in3=1;
end
delta=0;
if(ActivatedP(ii)~=0)
    if(StatP(ii)==0)
        delta=PGEN(ii)-PMAX(ii);
        if(delta<0),delta=-delta; end
        if(delta>0.0001),in4=1; end
    end
    if(StatP(ii)==2)
        delta=PGEN(ii)-PMAX(ii);
        if(delta<0),delta=-delta; end
        if(delta>0.0001),in4=1; end
    end
end
if(ActivatedP(ii)==0)
    if(MiuGen(ii)>0),in4=1;end
    if(MiuGen(ii)<0),in4=1;end
end
return; %%End of MatrixWGenMiu function

```

```

function [sum] = CheckConvexification(nbb,Cc,VM,VOLTAGE);
sum=0;
for( ii = 1: nbb)
    sum=sum+Cc*(VM(ii)-VOLTAGE(ii))*(VM(ii)-VOLTAGE(ii));
end
fprintf('\n=== Convexification Value ===');
fprintf('\n C = %%12.8f ', sum);
fprintf('\n');

return; %%End of CheckConvexification function

```



# Index

- a axis, 82
- d axis, 82, 84
- q axis, 83–4
  
- ABCD parameters, 62–3
- Active power, 3–4, 18, 28, 34–8, 40, 94, 96–7, 111, 118–9, 129, 131–3, 134, 140–4, 147, 150, 171–3, 178, 181–2, 187, 199–201, 215, 218, 225, 227, 237, 253, 255–7, 262, 264, 266, 268–70, 272, 275, 278–80, 282, 286–97, 299, 301–2, 304, 306–7, 315, 317, 318, 320, 322–3, 328, 335–7, 339
- Advanced series capacitor (ASC), 42
- Amplitude modulation ratio, 32
- Angular stability, 3
- Annular conductors, 47
  
- Bank of capacitors, 16–8, 231–49
- Bank of transformers, 89, 236
- Bulk power load, 87
- Bulk power supply, 28, 56
- Bundle conductors, 56, 59
  
- Carrier frequency, 30
- Carrier signal, 30, 32
- Compensated transmission line, 228, 264–5, 297
- Compensation, 3, 29, 33, 70, 159, 178, 232, 249, 265, 299, 336
  - Series, 4, 40, 43, 60–1, 63, 89, 178, 229, 319
  - Shunt, 5, 11, 44, 61, 63, 89, 104, 319
- Complex depth, 49
- Conduction angle, 12–3, 20
- Controllable reactance, 41
- Controllable susceptance, 5, 12, 149
- Control variables, 97, 301, 306, 268–70, 278
  
- Convergence, 6, 48, 94, 98, 101–2, 111, 129–31, 141, 415–6, 150, 154, 166, 170, 178, 188, 198, 213, 253, 234, 248, 251–2, 262, 265, 276, 279, 280, 284, 287, 288–9, 291, 295, 299, 301, 306, 308
- Converters, 4–5
- Current source converters, 29
- Custom power, 9–11
  
- Damper winding, 82, 84, 86
- DC-AC converters, 28–9, 231, 301
- DC capacitor, 5, 34–5,
- Delta-connected TCR, 14, 17, 249–50
- Delta-delta, 70, 76, 78–81
- Dependent variables, 147, 268–9
- Deregulation, 4, 93, 311, 331, 339
- Diode, 30
- Distribution, 1–2, 4, 9–11, 43–4, 47, 129, 153, 231, 267, 290, 307
- Double circuit transmission line, 54–5
- Dynamic stability, 2–3
  
- Economic dispatch, 267, 278–80, 299, 305
- Electrical length, 3, 10–1, 18, 20, 45
- Electricity supply industry, 1, 4, 41, 339
- Electromagnetic transients, 2–3
- EMF, 82, 86
- Equality constraints, 268–72, 275, 289, 292, 296, 301
- Equivalent  $\pi$ -circuit, 35, 44
  
- FACTS
  - Concepts, 2, 9
  - Controllers, 2–6, 9, 11, 150, 153–4, 227–9, 232, 249, 265, 307–8, 329

- Modelling, 6, 227, 232, 265, 308
- Series controllers, 143, 173
- Simulation, 6
- Technology, 2, 4, 6
- Fast decoupled, 111–3, 115, 117, 150
- Feasibility region, 140, 143
- Field winding, 82–4
- Filters, 11, 14
- Firing angle, 12–4, 16, 20, 22–3, 26, 155, 158–9, 162–3, 166–7, 169–71, 180, 182, 187–8, 190–1, 227, 229, 249, 251–3, 255–7, 291–7, 299
- First derivative, 293, 299, 304
- Fluctuating loads, 9
- Frame of reference, 15, 18, 19, 28, 41, 44, 61, 67, 79, 80, 83, 89, 90, 102, 154–5, 229, 232, 236–7, 249, 283, 307
- Frequency dependency, 45–8, 50, 52
- Frequency modulation ratio, 32
- Frequency switching, 28, 30, 33
- Fundamental frequency, 11–5, 19–20, 24–6, 30–4, 40–1, 44–5, 50, 60–1, 70, 89, 180, 189, 200, 216, 253–4, 256
- Gauss-Seidel, 98
- Generation, 3–4, 35, 43, 94, 96, 102, 118, 147, 153, 199, 215, 232, 261, 268–70, 272, 275, 279–82, 286–7, 290, 292–6, 299, 301, 306–7, 312–3, 322, 324, 331, 336, 340
- Generator PQ bus, 97, 102
- Generator PV bus, 97, 101–3, 121
- Geometric imbalances, 44, 46, 50, 60, 70, 89, 231–2, 236, 252, 264
- Geometric mean radius, 47, 52
- Global iteration, 276–7
- Global optimal, 268, 272
- Gradient, 272–3, 276, 279, 283–4, 288, 293, 304
- Ground return, 45–6, 48–50, 60, 70, 89
- Ground wires, 44, 50–5, 59, 79, 89
- GTO, 5, 28–9, 41
- Harmonic, 12, 14, 19, 20, 24, 30, 32–3, 41, 70, 87, 232, 239
- Harmonic cancellation, 14, 41
- Harmonic domain, 19
- Harmonic voltages, 9, 31–2
- Hessian, 271–2
- High current, 2, 4, 9
- High power, 9, 29, 30, 232
- High-speed control, 2, 6, 10
- High voltage, 2, 4, 5, 9, 11, 14, 16, 29, 30, 38–9, 43, 54, 111, 154, 156, 166, 216, 219, 225–6
- High-voltage transmission, 44, 54, 62, 70, 76, 89, 111–2
- HVDC, 5, 9–11, 29, 38, 40–1, 43, 154, 216–9, 225–7, 315
- IGBT, 28–30
- Induction motor, 87
- Inductive effects, 45–6
- Inequality constraints, 268, 270–2, 275, 277, 279–80, 284, 287–8, 292, 296, 298, 301, 304
- Interconnection, 1, 9, 267
- Internal impedances, 47–8
- IPC, 4, 5
- Iron core, 70–1
- Iteration, 19, 94, 98–102, 111–2, 117, 120, 122, 129–31, 133, 135, 141–2, 144, 146, 149–50, 154, 158, 162, 167, 170, 178, 182, 188–9, 198, 213, 251–6, 218, 234, 246–7, 251–2, 255, 257, 262, 271, 276–81, 285–6, 290–1, 295–6, 299, 300, 306–8
- Jacobian, 98–100, 102–4, 111–2, 117, 120, 122, 132–4, 144–5, 148, 150, 154–5, 157, 167, 173, 182, 191–2, 202, 218, 234–5, 251–2, 260, 262, 271–2
- Kayenta substation, 20, 24, 26, 189
- Kron's reduction, 52, 79, 80
- Kuhn and Tucker, 276, 283
- Lagrange multipliers, 270–4, 280–2, 284–5, 287, 289, 292–5, 297–9, 301–2, 305–7
- Lagrangian, 270–5, 279, 283–4, 286–8, 291–3, 296–8, 301–2
- Linear transformations, 15
- Line impedance control, 1, 5–6, 52
- Line transpose, 62
- Load angle, 90, 236
- Load flow analysis, 6, 82, 157–8, 166
- Load PQ bus, 97, 268, 270, 277
- Load tap changer (LTC), 2, 4, 72, 119–20, 122, 127, 130–1, 145–9, 154, 158, 283–7
- Loads, 1, 3, 5, 9, 11, 43–4, 56, 70, 86–90, 94, 97, 102, 156, 231, 236, 246–7, 265, 267–9, 274, 297, 301, 313, 315–7, 319–20, 322–4, 330–1, 335–6
- Long-distance, 1, 43, 60–1, 67, 231

- Long-line, 46, 60–1, 66, 89, 236, 319
- Low-voltage distribution, 9, 11, 44, 231
- Lumped parameters, 45, 61, 66
  
- Magnetic circuit, 70
- Magnetising branch, 73, 75, 119, 121, 132, 134
- Magnetising current, 70
- Matlab<sup>®</sup>, 56, 59, 61, 63, 66, 69, 89, 104, 112–3, 115, 122, 135, 150, 159, 162–3, 173, 182, 192, 203, 218–9, 236–7, 265, 281
- Multilimb transformers, 76
- Multiplier method, 275–6, 280, 282, 285, 308
- Mutual potential coefficients, 47
  
- Net active power, 96–7, 129
- Net reactive power, 96–7, 118, 129
- Network, 1–3, 5–6, 9–11, 13–4, 16, 20–1, 35, 37, 43–4, 55–6, 70, 93–4, 97, 101–2, 104, 112, 115, 118, 127, 129–30, 140, 145, 150, 153–5, 157, 169–70, 179, 187, 198–9, 201, 213, 215, 217–8, 225, 227–9, 244–7, 252–3, 257, 262, 264–5, 267–9, 274, 282–3, 285, 290–2, 294–5, 297, 299, 306–8, 311–12, 315–16, 322, 234–7, 329, 331, 334–7, 339–40
- Newton–Raphson, 1, 6, 98–9, 101–2, 104, 111–2, 115, 117, 122, 129, 135, 145, 150, 153–5, 157, 159, 162–3, 166, 171–3, 180, 182, 192, 203, 216, 218–9, 227–8, 232, 234, 236–7, 253, 264–5, 281, 335
- Newton’s method, 158, 268, 270–2, 275, 278, 280, 282–7, 291–3, 296–7, 299, 301–2, 306–8
- Nodal admittance, 15–6, 47, 75–6, 78, 112, 135, 144, 153, 272
- Nominal  $\pi$ -circuit, 45, 273
- Nonlinear loads, 9
  
- Objective function, 267–9, 271–2, 287, 292, 296, 301, 307
- One-line diagram, 9
- Open-circuit test, 70
- Operating frequencies, 9, 13, 29
- Optimality conditions, 272, 279, 283
  
- Partial conduction, 4, 12
- Partial derivatives, 98, 190, 202, 250–2, 254, 271–3, 284, 288, 298, 307
  
- Penalty function, 270, 275, 277, 280, 284, 288, 293, 299, 304
- Penalty weighting factors, 276–80
- Per-unit system, 55, 72
- Phase angle regulator, 2, 4, 35
- Phase coordinates, 15–6, 18, 35, 38, 76, 231–2, 236, 253, 261–2, 264–5
- Phase domain, 11, 15, 28, 41, 257
- Phase-shifting transformers, 3, 4, 35, 73, 75, 81, 89, 112, 119, 132–5, 140–1, 143, 145, 150, 154, 200, 268, 283, 286–7, 289–91
- Power converters, 4, 29, 231, 301
- Power electronics, 1, 2, 9, 10, 157, 232, 335
- Power flow, 1, 3, 6, 11, 33–5, 40–1, 44, 56, 70, 75, 90, 93–5, 97–9, 101, 105, 111–3, 115, 117, 119–22, 129, 132–4, 135, 140–3, 149–50, 153–4, 157, 159, 162–3, 167, 171, 173, 181–2, 187, 192, 198–9, 203, 215, 217–9, 225, 229, 231–4, 236, 244, 249, 250, 255, 257, 261–2, 264–5, 267–70, 272–3, 277–82, 285–90, 294, 296–7, 301, 305–7, 311–3, 315–7, 319, 321–3, 325, 329, 331, 335–7, 340
- Analysis, 6, 19, 26, 72, 87, 93, 98, 111, 145, 153, 155, 156, 191, 227–8, 236, 257, 283
- Control, 2, 3, 18, 34, 37, 41, 140, 143–4, 200, 213, 225, 257, 264, 297, 299
- Loops, 1
- Model, 119, 132, 154–5, 171, 178, 180, 189, 191, 201, 228, 249, 253, 255, 261
- Overvoltage, 4, 274
- Power interruptions, 9
- Powers Mismatch, 94, 96, 99, 101–3, 111, 129, 133, 141, 146, 150, 159, 163, 173, 178, 182, 188–9, 202, 213, 215–6, 218, 234, 246–7, 251–2, 255, 257, 272–3, 280, 283, 287, 296, 299, 301, 305
- Power quality, 2, 9, 41
- Power systems, 3, 5, 6, 9–11, 14, 20, 28–9, 33–4, 40–1, 43–5, 47, 49, 52, 70, 73, 83, 86, 89, 90, 93–4, 96–9, 101, 104, 111, 118, 144–5, 150, 153–4, 231–2, 249, 264, 267–9, 272, 274, 283, 286, 288–91, 301, 307, 331, 339
- Primary winding, 14, 73, 75–6, 121, 131, 134, 145, 148, 284–5, 287–9
- PS, 4, 6, 84, 148–54, 156, 161
- Pulse-width modulation (PWM), 33, 45
- PVT bus, 135, 145, 183

- Quadratic cost function, 280  
 Quadratic penalty function, 277, 284, 288, 293, 299, 304  
 Reactive limits, 104, 130–1  
 Reactive power, 1, 3–5, 9–10, 12–3, 16, 28–30, 33–8, 40–1, 56, 83, 93–4, 96–7, 99–103, 111, 118–9, 121, 129, 131, 146, 148, 150, 157–8, 167–9, 171–2, 178, 181, 191, 199, 201, 213, 215, 218, 225, 227–8, 232–3, 236, 247, 251–2, 259, 261–2, 264–5, 277, 280–3, 285, 287, 289, 292, 294–6, 299, 301–2, 204–7, 312, 315–6, 318–9, 321–2, 329, 331, 335–6  
 Resistive effects, 45, 60  
 Right of way, 89  
 RMS, 13, 14, 73, 86  
 Rotating load, 86–7  
 Rotor circuit, 83–4  
 Round rotor, 82  
 Saliency, 43, 83, 86, 90  
 Salient pole rotor, 86  
 Secondary winding, 14, 16, 71, 72, 73, 75, 119, 122, 132, 284–5, 288, 290  
 Second derivative, 273, 276–7, 284, 293, 299, 304  
 Self-potential coefficients, 47  
 Semiconductor device, 5, 28, 30, 41  
 Sequence domain, 11, 15, 28, 41, 44, 57, 67–9, 79, 80, 84, 89, 257, 261, 264  
 Sequence  
   Negative, 16, 18, 68, 70, 80–1, 85–6, 88, 236, 244, 246–7, 253  
   Positive, 2, 6, 8, 16, 18, 33, 41, 44, 56, 68, 70, 80–1, 85, 88, 90, 104, 113, 162, 191, 231–2, 234, 236, 244–6, 249, 253, 261, 273  
   Zero, 16, 18, 68–70, 80–1, 85, 88, 236, 244–7  
 Series capacitor bank, 10, 231  
 Series capacitors, 3, 11  
 Series compensation, 2–4, 11, 40, 43, 60–1, 63, 89, 172, 178, 200, 229, 249, 319  
 Series reactance, 5, 172–3, 180, 182, 188, 227  
 Series converters, 37, 200–1, 215, 262, 301  
 Series controllers, 173  
 Short line, 60, 66  
 Short-circuit level, 3, 10  
 Short-circuit test, 70–1, 76  
 Short-term interruptions, 93  
 Shunt admittances, 45–7, 56, 59–60, 227, 231  
 Shunt compensation, 5, 11, 43, 61, 63, 89, 104, 167, 274, 319  
 Shunt converters, 37, 200–1, 213, 262, 301, 305  
 Shunt susceptance, 155, 158–9, 170, 291–2  
 Skin effect, 47–8, 50  
 Slack bus, 97, 99, 101–4, 112, 145, 169, 235, 268  
 Slatt substation, 19  
 Solid-state controllers, 4  
 Sparsity, 104, 144–5, 272, 279, 283  
 SSSC, 5–6, 29, 35–6, 38, 40, 42, 44–5, 246  
 Stability, 1–3, 10, 19, 20, 93  
 Star-delta, 89–91  
 Star-star, 86, 88, 91  
 STATCOM, 4, 6, 11–2, 37–8, 42, 45, 169, 206–10, 213–5, 233–4, 238, 245, 250, 277, 279–82, 285, 358–60  
 State estimation, 2–3  
 State variables, 94, 97–8, 101–2, 120–1, 133–4, 145–6, 154–5, 158, 162, 168, 171, 173, 192, 227–9, 234, 236, 249–53, 256, 259–60, 262, 268–9, 261–2, 265–6, 278–9, 283–4, 287–8, 291–3, 296–8, 301, 303  
 Static load, 86–7, 90  
 Stator, 82–6  
 Steady-state, 2–6, 11–2, 19–21, 23, 34–5, 41, 44, 83–4, 86–7, 89, 93–4, 97, 150, 153–4, 200, 267, 269  
 Subsynchronous resonance, 4, 10  
 SVC, 6, 11–3, 17–9, 22, 31, 36–7, 44–5, 79, 169–86, 206, 245, 247, 250, 268–72, 280–1, 285, 306, 316–21, 336  
 Symmetrical components, 15–6, 18, 51, 67–8, 79–80, 88–9  
 Synchronous, 82–4, 191, 200, 216, 227–9, 331, 335  
   Condenser, 4, 34, 145–6, 331  
   Generator, 34, 43, 82–3, 89, 146, 168, 171, 231, 236, 275, 319  
   Motor, 86–7, 90  
   Compensator, 10, 191, 216  
 TCR, 4, 6, 13–7, 19, 21–3, 30, 45, 177, 182, 268–9  
 TCSC, 4, 6, 11, 13, 19, 21–4, 26–31, 45, 169, 177, 186–200, 202–6, 221, 245–6, 250, 272–5, 277, 285, 306, 321, 323, 325–6  
 Tertiary winding, 73, 75  
 THD, 22  
 Thermal limit, 1, 3, 5, 93

- Thévenin equivalent, 74
- Thyristor, 4–5, 9–12, 14, 16, 20–4, 28–9, 41, 159, 227, 249, 251, 253
- Transformation matrices, 53–4, 61, 77
- Transformers, 1, 5, 10, 14, 16, 30, 34, 38, 43–4, 56, 70–81, 89, 93–4, 102–4, 112, 119, 121, 131, 134, 148, 155–6, 166, 169–70, 201, 216, 231, 236, 262, 268, 286, 305, 315, 331
- Single-phase, 70, 76, 119, 132, 231
- Tap-changing, 4, 72–3, 75, 119, 121–2, 145, 148, 150, 154, 268, 283, 285
- Three-winding, 16, 73
- Two-winding, 70–2, 75, 121, 287
- Three-phase, 44, 75–7, 81, 89, 231, 236
- Transmission, 2–4, 6, 9–11, 28, 30, 38, 43–4, 51, 56, 60–1, 70, 76, 93, 96, 99–100, 111–2, 153–4, 231–2, 267–8, 307, 311–2, 315, 329, 339
- Transmission line, 1–6, 10–1, 18, 20, 43–8, 50–2, 54–6, 59–63, 66–70, 80, 89, 93, 102, 112, 115, 118, 127–8, 140–1, 143, 153, 171, 178–9, 187, 199, 213, 215, 225, 228, 231, 235–6, 244–5, 264–5, 268–70, 273–4, 282, 285, 289–90, 297, 299, 305–6, 313, 317, 319, 322–4, 327, 330
- Parameters, 44–5, 48, 50, 55–6, 59–61, 69, 89, 150, 245
- Losses, 1, 38, 43, 290, 307, 311, 322, 340
- Cost, 93
- UPFC, 6, 12, 32, 40–2, 44–6, 169, 216–7, 219–24, 228–33, 243, 245–8, 256, 281–2, 284–5, 306, 327, 329–32, 334–6, 358–60
- Voltage control, 3, 9, 32
- Linear, 32
- Overmodulation, 32
- Square-wave, 32
- Voltage, 2, 4, 9, 12–4, 20–4, 29–30, 32, 34–5, 37, 40–1, 43–5, 50–1, 53, 55–6, 62–3, 69–73, 76–8, 83–4, 87–9, 93–5, 97, 111–2, 121, 129, 153, 155–8, 166–7, 171, 191, 199–200, 202, 216–7, 231–3, 244, 247, 249, 270, 274, 293, 299, 306, 313
- Limits, 1, 5, 43, 55
- Magnitude, 3–6, 16, 35–7, 39–40, 72, 83, 88, 93–4, 97, 99–102, 111–2, 117, 119–21, 127–31, 141, 148–50, 154–5, 158, 166–9, 171, 178, 191–2, 198–9, 201–2, 213, 216, 218, 225, 227, 229, 236, 244, 246, 249–50, 252–3, 257, 260–2, 264–5, 267–70, 272–3, 275, 279–85, 287–9, 291–6, 299, 301–2, 305–7
- Phase angle, 6, 33, 36, 39, 93–4, 97, 99–101, 111–2, 141, 154–5, 192, 198, 200, 227, 236, 244, 246, 251, 253, 257, 264, 267–9, 272–3, 279, 283, 287–89, 292, 295–6, 299, 301, 305–6
- Source, 5, 29, 34–5, 38–9, 41, 191, 200, 213, 216, 227–9, 301, 305–6
- Nodal, 27, 37, 94–5, 102, 115, 117–22, 129, 131, 141, 145, 147, 157, 169, 178, 188, 225, 232, 247, 249, 274, 279, 281–2, 285, 301, 306
- Voltage source converters (VSC), 9, 10–2, 29, 32–40, 159, 217, 219, 225–6, 233–5, 243, 245
- Wave propagation equation, 61, 66
- Waveform, 13, 24, 29, 30, 93, 191, 200, 216

